ROLE OF INHIBITORS ON HOT CORROSION OF SUPERALLOYS IN Na_2SO_4-V_2O_5 ENVIRONMENT

A THESIS

Submitted in fulfilment of the
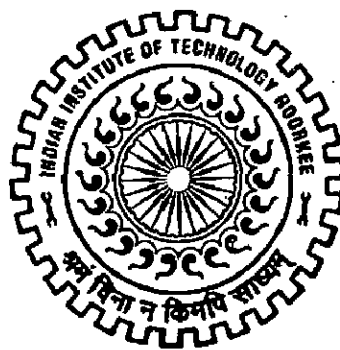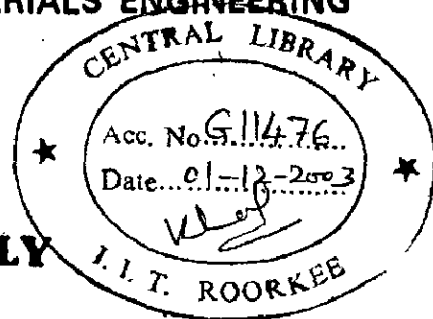*requirements for the award of the degree*

of

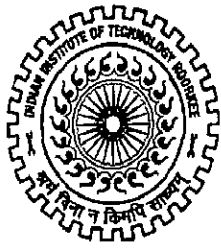DOCTOR OF PHILOSOPHY

in

METALLURGICAL AND MATERIALS ENGINEERING

by

GITANJALY

DEPARTMENT OF METALLURGICAL AND MATERIALS ENGINEERING
INDIAN INSTITUTE OF TECHNOLOGY ROORKEE
ROORKEE-247 667 (INDIA)

MARCH, 2003

INDIAN INSTITUTE OF TECHNOLOGY ROORKEE
ROORKEE

CANDIDATE'S DECLARATION

I hereby certify that the work which is being presented in the thesis, entitled "ROLE OF INHIBITORS ON HOT CORROSION OF SUPERALLOYS IN Na_2SO_4-V_2O_5 ENVIRONMENT" in fulfilment of the requirements for the award of the degree of Doctor of Philosophy and submitted in the Department of Metallurgical and Materials Engineering of the Institute, is an authentic record of my own work carried out during a period from July, 1998 to March, 2003 under the supervision of **Dr. Satya Prakash** and **Dr. Surendra Singh.**

The matter embodied in this thesis has not been submitted by me for the award of any other degree of this or any other University/Institute.

(GITANJALY)

Signature of the Candidate

This is to certify that the above statement made by the candidate is correct to the best of our knowledge.

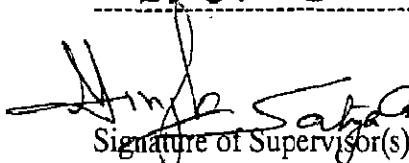Date: 02·03·03

(Dr. SATYA PRAKASH) (Dr. SURENDRA SINGH)

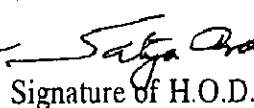Professor and Head Assoc. Professor

Department of Metallurgical and Materials Engineering
Indian Institute of Technology, Roorkee
Roorkee – 247 667, India

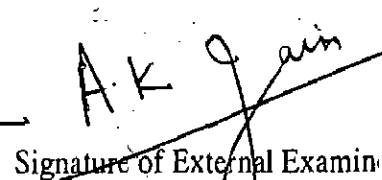The Ph.D. Viva-Voice examination of Gitanjaly, Research Scholar, has been held on

25·06·03

Signature of Supervisor(s) Signature of H.O.D. Signature of External Examin

i

ACKNOWLEDGEMENTS

ABSTRACT

Hot corrosion is an acute form of corrosion occurring at elevated temperature in the presence of an oxidizing gas and is associated with a thin electrolytic deposit (salt or ash) on alloy. The greatest corrosion is always associated with an ash composition corresponding to the sodium vanadyl vanadate ($Na_2O.V_2O_4.5V_2O_5$). Addition of Na_2O to liquid V_2O_5 causes an increase in the basicity of the melt with a corresponding increase in corrosivity with respect to the acidic oxides. Addition of Na_2O has also been shown to decrease the viscosity; the protective oxides become porous and non-adherent. The formation of binary and tertiary low melting eutectics increases the surface attack thereby reducing the useful life of the component.

For trouble free and continuous long service of power plants running at high temperatures, suitable materials should be selected after complete hot corrosion studies of alloys. Superalloys are used to resist oil ash corrosion and success is achieved to a considerable extent. There appears to be an advantage in using high chromium alloys. Thermal barrier coatings of alloys and ceramics have been tried to counter oil ash corrosion and they were found to be effective to some extent. Inhibitors and fuel additives have also been used with varying success to combat oil ash corrosion.

In the present investigation hot corrosion studies were carried out on Fe-base, Co-base and Ni-base superalloys procured from MIDHANI (Mishra Dhatu Nigham Ltd), Hyderabad (India) in Na_2SO_4-60% V_2O_5 with and without inhibitors.

Effect of oxide additives on the hot corrosion behaviour of superalloys Superfer 800H (alloy A), Superco 605 (alloy B), Superni 75 (alloy C), Superni 718 (alloy D) & Superni 601 (alloy E) have been studied in Na_2SO_4-60%V_2O_5 under cyclic conditions. The details of these alloys are given in Table 4.1 and those of the inhibitors employed are given in Table 4.2. MgO, CaO, MnO_2 and $ZnSO_4$ were mixed with Na_2SO_4-60%V_2O_5 and applied on the polished preheated samples whereas in case of CeO_2, SnO_2, Y_2O_3 and ZrO_2 first a coating of oxides was

applied; they were then heated to 900^0C for 8 hours to obtain the better adhesion of the oxide film. After 8 hours heating, a coating of Na_2SO_4-60%V_2O_5 was applied and then they were exposed to cyclic heating at 900^0C for 50 cycles (each cycle consisted of 1hour heating and 20 minutes cooling). Weight change measurement after each cycle was noted upto 0.1 mg accuracy by electronic balance.

Macrographs were taken to know the nature of corrosion product so formed. SEM, XRD and EPMA have been done for all the samples. EDAX of surface of the scale was done in few cases and in others cross-section have been analysed.

Hot corrosion products observed in the scale of these corroded alloys are mostly oxides of the elements present in the alloy. The presence of continuous Cr_2O_3 layer at the substrate /scale interface is predominantly revealed in most of the alloys where weight gain and scale thickness has been very less. Spinels of composition MCr_2O_4 have formed due to reaction of oxides of Fe, Ni and Co with Cr_2O_3 as XRD indicated the formation of such phases e.g. $FeCr_2O_4$, $NiCr_2O_4$ and $CoCr_2O_4$ in Fe-, Ni- and Co-base alloys respectively.

The weight gain values in Na_2SO_4-60%V_2O_5 environment have been found to be highest for Co-base alloys and lowest for Ni-base alloy Superni 75.
The general trend followed is:
Superco 605 (alloy B) > Superfer 800H (alloy A) > Superni 718 (alloy D)> Superni 601(alloy E)> Superni 75 (alloy C).
Scale thickness values measured after experimentation follow the sequence as given below:

Alloy B > Alloy A > Alloy D > Alloy E > Alloy C

After mixing MgO in Na_2SO_4-60%V_2O_5 (MgO/V_2O_5 ratio 3:1), the aggressiveness of the Na_2SO_4-60%V_2O_5 environment has been found to decrease in case of all the alloys except alloy D where the decrease is marginal. This may be attributed to the formation of a solid phase magnesium orthovanadate ($Mg_3V_2O_8$, m.p. 1190^0C), by reaction of V_2O_5 with MgO in preference to formation of liquid $NaVO_3$ and formation of above mentioned solid phase might have contributed to the decreased corrosion rate. X-ray diffraction analysis has identified the presence of $Mg_3V_2O_8$ phase in the scale developed on the surface of the alloys A, C and E

which has also been further confirmed from the EPMA micrographs as Mg, V and oxygen are co-existing in the scale.

Similar effect has been observed by adding of 20wt.% CaO to Na_2SO_4-60%V_2O_5 on the alloys A, B, C, D & E. Inhibiting behaviour of CaO may be owing to the formation of a protective uniform chromium enriched band present and also the formation of calcium vanadate, $Ca_3V_2O_8$ that was identified by XRD and EPMA. Effect in case of alloy C is distinct as a Cr enriched continuous band type scale is formed.

20wt% MnO_2 additions to Na_2SO_4-60% V_2O_5, has also been found to be beneficial in almost all the alloys. The extent of reduction in weight gain is more in alloy D & follows the trend as:

Alloy D > Alloy C> Alloy A> Alloy B> Alloy E.

A thick scale is indicated in case of alloys B & E and a thin irregular scale in alloy A & C whereas a continuous band type regular uniform scale is indicated in alloy D. Internal oxidation is indicated in alloys A, C, D & E. In case of alloy C & D, Cr is present throughout the scale where as in alloy D, it is present as a rich continuous band at the interface which is probably helping in reducing the rate of corrosion. Mn & V are coexisting in the scales of alloys B, C, D & E.

With addition of 10% $ZnSO_4$ in Na_2SO_4-60% V_2O_5, the scale formed is relatively very thick in case of alloys A and E. Due to severe sputtering experimentation had to be terminated after 8 cycles in case of alloy B and after 30 cycles in alloys A, C, D and E. $ZnSO_4$ is only marginally effective in all the alloys. In case of alloys A, C and D, very thin Cr_2O_3 layer has formed just above the substrate but internal oxidation is indicated.

In case of CeO_2 coated samples, a thick scale is indicated in alloy A where as it is of medium size in alloys B, C, D & E. But there is indication of overall reduction in the rate of corrosion for all the alloys. Formation of $CeVO_4$ is proposed on the basis of EPMA and EDAX analysis in case of alloys C & E. EDAX analysis of the corroded product of alloy A scanned along cross-section mainly indicated Cr, Ni and Fe and showed the presence of Ceria in small amounts near the substrate. EDAX of surface of the same scale confirmed the presence of Ce and

V in the scale. In case of alloy C, ceria is present in high concentration in the scale and is coexisting with V and also there is growth of Ni-rich crystals in Ce-enriched layer. Overall wt. change is very less as compared to that without CeO_2. But the scale of alloy D shows presence of Ce in pockets at few spots. Presence of Ti pockets near scale/substrate interface is indicated. Just above the interface, there is a thin layer rich in Cr where both Ni and Fe are absent. Presence of unreacted salt is also indicated. Very little change in weight was observed in case of alloy E.

Superficially applied Y_2O_3 seems to be most effective in combating aggressive environment of Na_2SO_4-60% V_2O_5 in case of alloy A as scale thickness was only 20μ. This scale is rich in Cr and is continuous. Alloy B has shown the formation of medium size scale rich in Cr and Co. Scale thickness is nearly 50% of that without Y_2O_3 barrier coating. In case of alloy C again a very thin scale is observed about 16.5μm in size and contains mainly Cr and Ni. Y is present as a thin layer along with V & S. A medium size scale has been formed in alloy D that is rich in Ni, Cr and Fe.

The scale thickness values in case of superficially applied Y_2O_3 follow the trend as:

Alloy C< Alloy D < Alloy A < Alloy B and Alloy E

In case of SnO_2 coated samples a thick scale is formed in alloys A, B & E whereas medium size scale in alloys C & D. There is a thick continuous Sn rich layer present at the top of the scale formed in alloys A, C & E indicating presence of unreacted SnO_2. V is indicated on the top of the scale and even above the thick tin layer which gives the possibility of the presence of some unreacted salt. Macrographs of the same samples indicate presence of unreacted salt on the surface, which has spalled off at many places. Percentage decrease in weight gain in alloys A, B, C, D and E with superficially applied SnO_2 is 17.2, 66, 50, 17 and 32 percent respectively after 30 cycles as compared to without inhibitor. The effectiveness of the SnO_2 is perhaps due to its non-reactive nature with the corroding species and high melting point (1630^0C).

With ZrO_2 superficial coating also, overall weight gain is less in case of alloys B, C, D & E. ZrO_2 is marginally effective in alloy A & B. A thick scale is observed in alloy A, rich in Cr, Ni,

Fe & V. Absence of protective continuous chromia layer and presence of less protective NiO is the main reason for more corrosion rate in alloy A. Similar can be the reason for thicker multilayered scale formed in alloy B where innermost layer is again Ni-rich. Presence of Cr in very high concentration just above the interface indicated by EPMA and EDAX and presence of Zr in the scale in the top and middle area detected by EDAX might have helped in providing some inhibiting effect. Scale of alloy C is very thin mainly consisting of Cr and Fe along with V, S & Zr in small percentages and weight gain is also reduced considerably. Scale of alloy D is slightly thicker and consists of mainly Cr with small amounts of nickel. Zr is present in the top most layer indicating presence of unreacted ZrO_2 on the surface which is even visible from the macrographs. ZrV_2O_7 might have formed and reduced the corrosion rate as Zr, V and oxygen are present in the scale at same areas as observed from the EDAX/EPMA. Chromium rich layer is present in both the alloys, which may perhaps be contributing to reduced reaction rates. But a single layer scale has been observed in case of alloy E which is rich in Cr, Fe and V. Various spinels and iron vanadate have been identified. Internal oxidation of Cr and Al is indicated by EPMA.

The role of all the inhibitors used in this study superficially applied or mixed with the aggressive environment is beneficial in decreasing the extent of corrosion attack under the given aggressive environment. The beneficial effect in most of the cases is found to be mainly due to formation of vanadates which could be solid at the given reaction temperature. The observance of a continuous band of Cr_2O_3 mostly along the interface between the scale and the substrate may be the other reason for providing protection to the alloy. In case of superalloys where the relatively higher extent of corrosion have been indicated, formation of vanadates and presence of exclusive continuous Cr_2O_3 band is not generally observed especially in case of alloy D in MgO, alloy B in MnO_2, alloy A in $ZnSO_4$, alloy E in SnO_2 and Alloy A in ZrO_2 whereas extent of reaction is still lower than that with inhibitor. From this it can be inferred that the formation of Cr_2O_3 rich band as well as solid vanadate gives the maximum protection to the alloys. In most of the cases this Cr_2O_3 layer has formed by diffusion of Cr from the substrate that is clearly marked by the depletion of Cr from the substrate.

PREFACE

The entire work has been presented in following seven chapters.

Chapter 1 deals with the general introduction of hot corrosion problem encountered in metals and alloys highlighting its relevance and importance.

Chapter 2 deals in hot corrosion mechanisms with the critical review of the hot corrosion studies on iron-, nickel and cobalt base alloys in Na_2SO_4-V_2O_5 environment and Na_2SO_4-60%V_2O_5 in particular, by various investigators. Behaviour of various oxides MgO, CaO, CeO_2, Y_2O_3, SnO_2, ZrO_2 in Na_2SO_4 and Na_2SO_4-V_2O_5 environment has been reviewed.

A review on literature about superficially applied oxides has also been done to understand their effects in enhancing the adhesion of chromia scale. Behaviour of metals and alloys in Na_2SO_4, combustion gases and other related environments have been presented in Table A.1 which is incorporated in the appendix.

Scope and aim of the present study has been highlighted in *Chapter 3*.

Chapter 4 gives the details of the experimental techniques and analytical procedures employed in the present investigation for characterization of the corrosion product formed.

Findings of the present investigation on Superalloys Superfer 800H (alloy A), Superco 605 (alloy B), Superni 75 (alloy C), Superni 718 (alloy D) and Superni 601(alloy E) ,which were procured from Mishra Dhatu Nigham Ltd. (MIDHANI), Hyderabad (India) have been summarized under various sections such as kinetic data giving plots between weight gain and number of cycles, visual observations showing macrographs of the samples after exposure, XRD analysis, SEM, EDAX and EPMA results in *Chapter 5*.

Chapter 6 presents the general discussion about the results obtained after experimentation under different subheadings. Schematic diagrams of possible mode of corrosion have been included wherever possible.

Chapter 7 summarizes the conclusions of the current study on the effect of various inhibitors on the hot corrosion behavior of Fe-, Co- & Ni-base superalloys in Na_2SO_4-60%V_2O_5 under cyclic conditions at 900^0C.

CONTENTS

CHAPTER 5　　RESULTS

LIST OF FIGURES

xvii

LIST OF TABLES

LIST OF RESEARCH PAPERS

1. "Effects of MgO & CaO on the Hot Corrosion of Fe - base Superalloy Superfer -800H in Na_2SO_4-60%V_2O_5 Environment", British Corrosion Journal, Vol.37, No.1, 2002, pp 56-62.

2. "Effect Of Superficially applied CeO_2 and Y_2O_3 on the Hot Corrosion behaviour of Fe-and Ni- base Superalloys in Na_2SO_4-60%V_2O_5" presented/published, Conference proceedings International Congress on Emerging Corrosion Control Strategies for the New Millennium held at India Habitat Centre, New Delhi., Feb.20-22, 2002.

3. "Effects of Additives on the Hot Corrosion behavior of Superalloy 800H"Presented in National Seminar on Advances in Materials & processing held on Nov. 9 to 10, 2001, Metallurgy & Materials Engg. Dept, I.I.T, Roorkee.

4. "Hot Corrosion —an Overview", presented in National Seminar on Advances in Materials & processing held on Nov. 9 to 10, 2001, Metallurgy & Materials Engg. Dept, I.I.T, Roorkee.

5. "Hot Corrosion of Fe-, Ni- & Co-base alloys in Na_2SO_4-V_2O_5 and Role of Inhibitors" Published in Conference Proceedings, International Symposium on Materials Ageing and Life Management. IGCAR Kalpakkam, Oct.3-6, 2000.

6. "Review on Effect of additives on the Hot Corrosion", 5th NACE, National Convention on Corrosion, Nov.22-24, 1999, New Delhi

ABBREVIATIONS

Alloy A	Superfer800H
Alloy B	Superco 605
Alloy C	Superni 75
Alloy D	Superni 718
Alloy E	Superni 601
BAL	Balance
BSEI	Back Scattered Electron Image
c .g	Combustion gas
EDAX	Energy Dispersive X-ray Analysis
EPMA	Electron Microprobe Analysis
kcs	Kilo cycles per second
m.p.	Melting Point
SEM	Scanning Electron Microscopy
Wt. %	Weight percentage
Wt. Gain	Weight Gain
XRD	X-ray Diffraction
.	Wave length

CHAPTER 1

INTRODUCTION

Hot corrosion is the degradation of materials caused by the presence of a deposit of salt or ash in a general sense. In a more restricted sense, hot corrosion is the degradation of metals and alloys owing to oxidation process, which are affected by a liquid salt deposit. In hot corrosion, metals and alloys are subject to degradation at much higher rates than in gaseous oxidation, with a porous, non-protective oxide scale formed at their surface, and sulfides in the substrate. It was first recognized as a serious problem in the 1940's in connection with the degradation of fireside boiler tubes in coal-fired steam generating plants and later with the severe attack of gas turbine air-foil materials (Rapp and Zhang, 1994). Hot corrosion is a serious problem in power generation equipment, in gas turbines for ships and aircraft and in other energy conversion and chemical process systems e.g. in boilers, internal combustion engines, fluidized bed combustion and industrial waste incinerators (Rapp, 2002; Rapp and Zhang, 1994 and Pettit and Giggins, 1987). A prime example is the attack of Ni-, Co- or Fe- base alloys by Na_2SO_4, which has served as a model for degradation process in gas turbines and other fossil-fueled devices.

The depletion of low sulphur fossil fuel has made it necessary to process high S containing fuels thereby making the environment more aggressive. The severity of hot corrosion in combustion processes can vary substantially and is significantly affected by the type of fuel and its impurity as well as the quality of the air supporting the combustion. In harnessing of geothermal energy high sulphurous environments are encountered at higher temperature (Prakash and Tewari, 1992).

Compounds of V, Na and S are invariably present in the heavy fractions of fuel oils, and subsequently the molten ash produced by their combustion has been recognized as a cause

of severe corrosion observed in boilers and gas turbines. Na_2SO_4 is the common or dominant component of the salt deposit involved in hot corrosion formed during combustion of certain low grade fossil fuels. Vanadium compounds such as $NaVO_3$ and V_2O_5 may also be deposited in the salt film. Thermodynamics of this deposition process was analysed by Luthra and Spacil (1982). Such corrosive oxyanion fused salts exhibit an acid /base chemistry with Na_2O, the basic component and SO_3, the acidic component for pure Na_2SO_4. Such salts are also usually ionically conducting electrolytes. Therefore, hot corrosion must be electrochemical in nature, and may involve fluxing of the protective metal oxides as either acidic or basic solutes in the fused salt. In some aspects, hot corrosion is similar to atmospheric corrosion of metals by thin aqueous films at ambient temperature though details with respect to the electroactive oxidant species and oxide dissolution etc. are different (Rapp, 2002).

An excellent review by Stringer covered work up to about 1976 (1977). Most of this work was aimed at developing improved alloys or aimed at understanding corrosion processes. Much of the mechanism work proposed during that period was focused on thermochemistry. Bornstein and DeCrescente (1969, 1971 and 1973) proposed a hot corrosion mechanism based on the basic dissolution of the protective oxide scale by a reaction involving Na_2O, the basic minority component of the fused salt. Goebel and Pettit (1970) at the same time also interpreted the hot corrosion of pure nickel in terms of a basic dissolution and re-precipitation of NiO in the fused salt film. Goebel et al (1973) extended this mechanism to include acidic fluxing and oxide reprecipitation to account for the catastrophic oxidation caused by pure Na_2SO_4 for alloys containing strong acid components such as vanadium or molybdenum. The next important step in the fluxing model was taken by Rapp and Goto (1981), who proposed that if the gradient in solubility of the protective oxide with distance into the salt layer was negative at the oxide/salt interface, accelerated attack could be sustained.

Superalloys have been developed for high temperature applications. These alloys need to be protected and the protection system must be practical, reliable and economically viable. No alloy is immune to hot-corrosion attack indefinitely although there are some alloy

compositions that require extremely long initiation time at which the hot corrosion process move from the initiation stage into the propagation stage.

Iron, nickel- and cobalt- base superalloys are the commercial alloys commonly used for the manufacture of components used in aggressive environments of gas turbines, steam boilers etc. Investigations have been carried out on the above alloys in various environments (solid, liquid & gaseous) at different temperatures (300 -1200^{0}C) for various time periods in isothermal and cyclic conditions without or under loads. Chromium is found to be the most important element in developing resistance to hot corrosion since it forms a protective oxide layer on the metal surface and inhibits the onset of attack regardless of the hot corrosion mechanism. Refractory metal concentration is also an important composition variable. It is necessary to keep its concentration low. However, higher concentrations of these elements can be used if the chromium concentration is also relatively increased. The molten salt deposits dissolve the protective oxide layer of either chromium or aluminium at the working temperature. The resistance to hot corrosion attack depends upon the amount and type of fluxing.

Knowledge of the solubilities of metal oxide in molten salts is important in evaluating corrosion resistance property of alloys. The solubilites of NiO, Co_3O_4 (Gupta and Rapp, 1980), iron oxides (Zhang and Rapp, 1985), Al_2O_3 (Jose, Gupta and Rapp, 1985), Cr_2O_3 (Zhang, 1986), Y_2O_3 (Deanhardt and Stern, 1982), Y_2O_3 and CeO_2 (Zhang and Rapp, 1987) have been reported as a function of melt basicity and oxygen activity for pure fused Na_2SO_4 at 1200K. Solubilites of Y_2O_3, HfO_2 and CeO_2 in a fused Na_2SO_4-30%$NaVO_3$ (Zhang and Rapp, 1987) salt solution have also been published. In the sulphate-vanadate melt, the conversion of the metavanadate to the orthovanadate solute drastically increased the acidic solubility for CeO_2 compared to that in pure Na_2SO_4. This mechanism and the resulting increase in acidic solubility are expected to be valid generally for all oxides in vanadate solutions. (Zhang and Rapp, 1987)

Protective coatings are frequently applied to structured alloys to achieve enhanced service lifetime. The purpose of these coatings is to form long-lived protective scales. But these coatings increase the material cost and proved uneconomical. Controlling the various process parameters (air/fuel ratio, temperature, pressure etc.) of the boiler and gas turbine

were also useful to some extent, but these can be controlled only within certain limits. There are numerous inhibitors commercially available that are intended to reduce the severity of oil ash corrosion such as Mg- & Mn-based additives, CaO, MnO_2, Al_2O_3, ZnO, BaO, PbO, SiO_2, BaO, $Ba(OH)_2$, $Ca(OH)_2$, $CaCO_3$, as well as oil soluble Ni, Al, Fe and other compounds. However in commercial practice Mg and Mn-based inhibitors have proven to be effective (Paul and Seeley, 1991).

Numerous investigations regarding the beneficial effect of rare-earth oxides by superficial coating have received special attention for more than a decade with a aim of imparting high-temperature oxidation resistance as well as providing improved scale adherence.

Thus hot corrosion problem of metals and alloys may be tackled by designing a suitable industrial alloy and selecting a proper composition of protective coating, process parameters, use of inhibitors and superficially applied oxides as per requirements in the given environment.

CHAPTER 2

LITERATURE REVIEW

Metals and alloys sometimes experience accelerated oxidation when their surfaces are covered with a thin film of fused salt in an oxidizing atmosphere at elevated temperatures. This mode of attack is called the "Hot Corrosion". Hot corrosion can be defined as deposit modified gas-induced degradation of materials at high temperature (Rapp and Zhang, 1994).

Alloys and ceramics may experience accelerated corrosion at high temperatures when their surfaces are coated by a thin film of fused salt in an oxidizing environment. Many very important engineering systems operating at high temperatures (650-1100^0C) involve contact of metallic or ceramic materials with combustion gases containing inorganic impurities, e.g. gas turbines, steam generators, incinerators and numerous petrochemical process vessels. As the gases are cooled, fused salt films may condense on the hardware to generate a highly corrosive condition analogous to aqueous atmospheric corrosion resulting in accelerated degradation known as hot corrosion (Rapp, 1990).

Hot corrosion became a topic of importance and popular interest in the late 60's as gas turbine engines of military aircraft suffered severe corrosion during the Viet Nam conflict in operation over seawater. Metallographic inspection of failed parts often showed sulphides of nickel and chromium, so the mechanism was initially called "sulphidation". Deposition of the condensed liquid film on the system hardware can result generally from one of the following processes: (1) chemical deposition: the vapour pressure of Na_2SO_4 in the vapour phase exceeds its equilibrium partial pressure for the substrate temperature, or (2) physical deposition: some solid or liquid salt could detach from an upstream component and attach to a hot substrate upon impact. Thus, in hot corrosion sulphide product is not formed by reaction with sulphur compounds in the gas phase, but rather from a metal-salt interaction (Rapp, 2002 and Rapp, 1986).

Because of its high thermodynamic stability in the mutual presence of sodium and sulphur impurities in the oxidizing gas, Na_2SO_4 is often found to be the common or dominant component of salt in the deposit. Sulphur is a principal impurity in fossil fuels and sodium is introduced into the combustion air usually in an aerosol originating from seawater. During combustion of certain low–grade fossil fuels, vanadium compounds such as $NaVO_3$ and V_2O_5 may also be deposited in the salt film (Rapp and Zhang, 1994).

Some other alkali or alkaline–earth sulphates may also exist in the deposit, depending upon the impurities contained in the fuel and in the intake air. Thus, thin liquid sulphate films may be deposited on the hardware either from the condensation of combustion products of fossil fuel or else from the direct impingement of liquid droplets from the hot gas stream.

There is a general agreement that condensed alkali metal salts notably, Na_2SO_4, are a prerequisite to hot corrosion (Beltran and Shores, 1972) The source of these salts may be

1. The direct ingestion of sea salt in a marine environment

2. The formation of Na_2SO_4 during the combustion of fuels containing both sodium and sulphur and

3. The formation of Na_2SO_4 during combustion from sodium-contaminated, air-borne dust and sulphur in the fuel

2.1   VANADATE-INDUCED HOT CORROSION

Kofstad (1988) has reported that fuel oils often contain vanadium impurities in the form of metal-organic complexes (porphyrins). The vanadium content depends on the source of the oil and during refining vanadium also becomes concentrated in the heavy distillates and residues and may then reach concentrations as high as 500 ppm.

Further he has proposed that during combustion the vanadium contaminants are oxidized to the higher valence vanadium oxides (V_2O_4 and V_2O_5) and sodium vanadates are formed by the reaction of vanadium oxides and sodium salts, e.g. Na_2SO_4. According to him the composition of the vanadates may in a simplified form be written as $(Na_2O)_xV_2O_5$, but the

detailed compositions of the individual vanadates may be more complex than this as part of the vanadium may be in the +IV state. The solid compounds comprise $(Na_2O)_xV_2O_4(V_2O_5)_{12-x}$ (often termed β bronze), $(Na_2O)_5(V_2O_4)_x(V_2O_5)_{12-x}$ (K bronze), $NaVO_3$ (sodium metavanadate), $Na_4V_2O_7$ (sodium pyrovanadate) and Na_3VO_4 (sodium orthovanadate). A notable feature of the vanadates is that they have relatively low melting points, which extend from 535^0C upwards. Furthermore, metal oxides dissolved in the vanadates may suppress the melting points and eutectic temperatures even further. He has quoted from a report that slags developed on valves in diesel engines are consisting predominantly of Na_2SO_4 and sodium vanadates and had a melting points as low as 400^0C.

Molten vanadates flux oxide ceramics. The solubilities of metal oxides may be high and are dependent on the Na:V ratio. The solubilities of Cr_2O_3 and Fe_2O_3 are highest at Na : V ratios close to 5 : 12 and amount to about 50 mol.%. For NiO the solubility is about 60 mol.% for Na : V = 3 : 2 and decreases to about 55 mol.% for Na : V = 5 : 12. As V_2O_5 is acidic, it will in general react with more basic oxides to form the corresponding vanadates.

Molten vanadates present as deposits on metal and alloy surfaces may cause highly accelerated corrosion due to the fluxing of the oxide scales and by increased diffusion of oxygen through the melt to the metal surface. Vanadates containing 10-20% Na_2O are reported to be the most corrosive.

The Na-V-S system has been studied by several other investigators (Niles & Sanders, 1962; Hancock, 1987). A phase equilibrium study, Fig 2.1 of the Na_2SO_4-V_2O_5 system (Otereo et al, 1987) shows that $NaVO_3.Na_2O.3V_2O_5$ and $Na_2O.6V_2O_5$ are the only compounds formed. These compounds were found to be essentially pure when the Na_2SO_4 / V_2O_5 ratios matched the formula molar ratio. X-ray diffraction identified $Na_2O.V_2O_4.5V_2O_5$ at ambient temperature. It is generally accepted that when $Na_2O.6V_2O_5$ is cooled to its freezing point, one atom of oxygen is evolved to give $Na_2O.V_2O_4.5V_2O_5$ at all temperatures. To verify the composition of the compounds, a study of the Na-V-S system was made by Niles and Sanders (1962) and compounds formed in the reactions were identified by X-ray diffraction.

Their results confirmed that only three Na-V compounds would form in the reactions of Na_2SO_4-V_2O_5 as follows:

$$Na_2SO_4 + V_2O_5 \rightarrow 2NaVO_3 + SO_3 \tag{1}$$

$$Na_2SO_4 + 3V_2O_5 \rightarrow Na_2O.3V_2O_5 + SO_3 \tag{2}$$

$$Na_2SO_4 + 6V_2O_5 \rightarrow Na_2O.6V_2O_5 + SO_3 \tag{3}$$
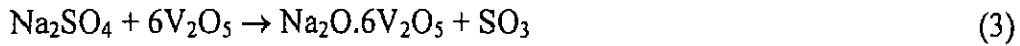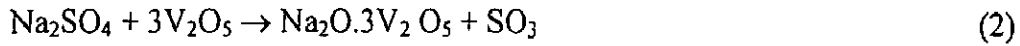
Products of reaction showed mixtures of $NaVO_3$ and $Na_2O_3.3V_2O_5$ when the ratio of V_2O_5 to Na_2SO_4 was greater than 1 but less than 3, and mixtures of $Na_2O.3V_2O_5$ and $Na_2O.6V_2O_5$ when the ratio was greater than 3 and less than 6, for example

$$2Na_2SO_4 + 4V_2O_5 \rightarrow 2NaVO_3 + Na_2O.3V_2O_5 + 2SO_3 \tag{4}$$

$$2Na_2SO_4 + 9V_2O_5 \rightarrow Na_2O.3V_2O_5 + Na_2O.6V_2O_5 + 2SO_3 \tag{5}$$
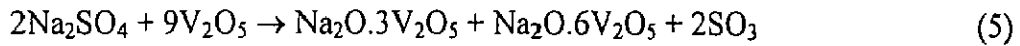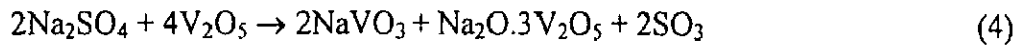
They concluded that the Na/V ratio plays an important role in deciding the reactions and their products.

Similar observations have been reported by Jones (1988 & 1991) and Jones & Williams (1987), where it is proposed that nondistillate petroleum fuels contain vanadium, which is oxidized to V_2O_5 in gas turbine combustion. Vanadium pentaoxide, an acidic oxide, reacts with Na_2O (a highly basic oxide derived from Na containing impurities ingested into gas turbine) to form a series of compounds of progressively lower acidic nature down to Na_3VO_4 (m.p. 1266^0C) which is essentially neutral.

$$Na_2O + 6V_2O_5 = Na_2V_{12}O_{31} \ (m.p.645^0C) \ (vanadium \ bronze \ I) \tag{1}$$

$$Na_2O + 3V_2O_5 = 2NaV_3O_8 \ (decomposes \ at \ 548^0C) \quad (vanadium \ bronze \ II) \tag{2}$$

$$Na_2O + V_2O_5 = 2NaVO_3 \ (m.p.610^0C) \ (sodium \ metavanadate) \tag{3}$$

$$2Na_2O + V_2O_5 = Na_4V_2O_7 \ (decomposes \ at \ 668^0C) \ (sodium \ pyrovanadate) \tag{4}$$

$$3Na_2O + V_2O_5 = 2Na_3VO_4 \ (m.p.1266^0C) \ (sodium \ orthovanadate) \tag{5}$$
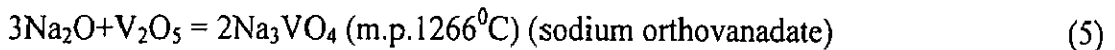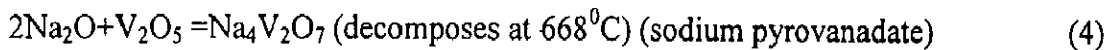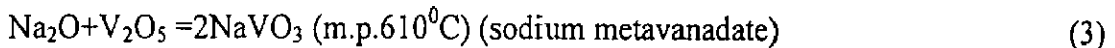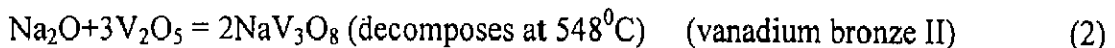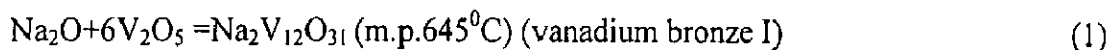
A characteristic V_2O_5 activity is associated with each of these compounds, with the V_2O_5 activity decreasing as the Na_2O content increases. When Na_2O, V_2O_5 and SO_3 are generated concurrently by combustion of Na, S and V contaminated fuel, the V_2O_5 and SO_3 compete for reaction with Na_2O, producing a mixed sodium vanadate/sulfate engine deposit

8
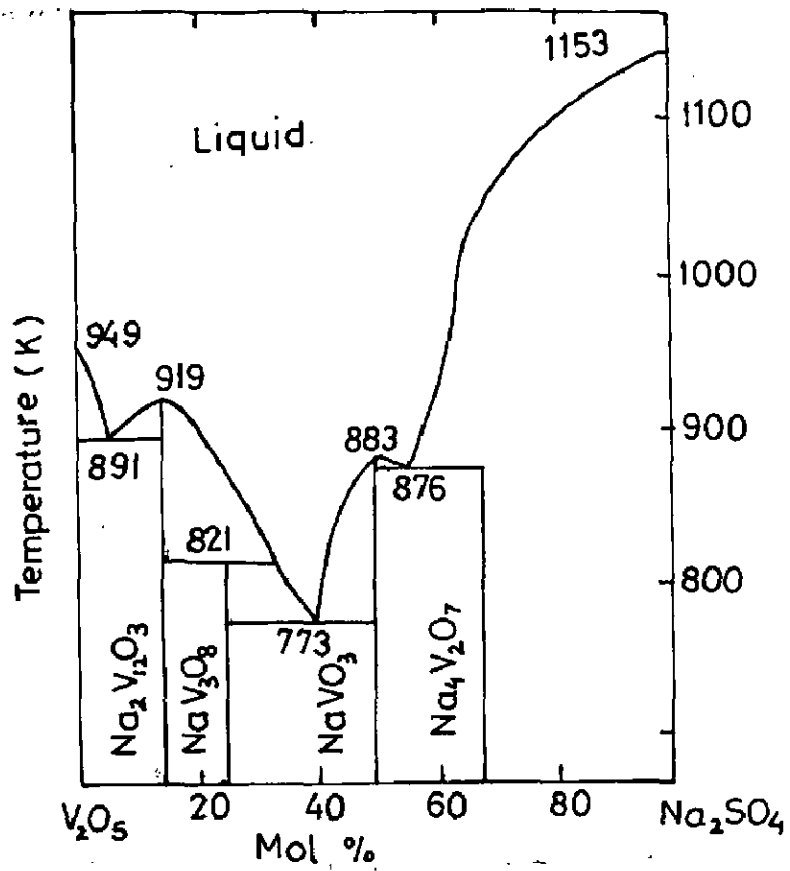
Fig.2.1:   Phase diagram for Na_2SO_4-V_2O_5 system (Otereo et al, 1987)

having certain equilibrium SO_3, V_2O_5 and Na_2O activities. It is these equilibrium oxide activities that are required to be known since they are the essential reagents causing corrosion of the oxide ceramics (Jones, 1990).

Vanadate-induced corrosion of high temperature alloys has been studied by thermogravimetry in laboratory furnaces (using a limited amount of vanadate deposit), in burner rigs (where small amounts of vanadates are continually being deposited on the surface), or by immersion of specimens in crucibles with molten salt. The reaction products formed during exposure in laboratory furnaces and in burner rigs are qualitatively the same, but the kinetics and reaction rates may differ considerably. The mechanisms are found to be complex (Beltran and Shores, 1972).

The kinetics of the reactions between $Na_2SO_4(x)$ and $V_2O_5(y)$ have been studied by Kolta et al (1972). It has been shown that the rate of reaction depends on both the temperature $(600-1300^0C)$ and the molar ratios X:Y. During the first 30 minutes and at a molar ratio 1:1, the reaction obeyed the second order. Under such conditions, the activation energy was reported to be 54.8 kcals mole^{-1}.

Phase equilibria in the $Na_2O-V_2O_5-SO_3$ system have been studied by Krasilni'kov et al (1987) using XRD and they inferred that the mixture of sodium sulphates with V_2O_5 has considerably higher melting points with lower thermal stability and they loose SO_3. Spontaneous reduction of V_2O_5 on heating occurred leading to the formation of sodium vanadate.

Hwang and Rapp (1989) have studied the solubilities of Al_2O_3, Cr_2O_3, CeO_2 and Y_2O_3 in the mixed sodium sulphate-vanadate solution containing 30mol.% vanadate. They concluded that the basicity of the melt, oxygen partial pressure and the proportion of V^{5+}/V^{4+} states of vanadate in the sulphate-vanadate decided the solubilities of oxides.

Zhang and Rapp (1994) measured the solubility of CeO_2 as a function of melt basicity in a Na_2SO_4-10mol.%NaVO$_3$ solution at 900^0C and 1 atm. oxygen. Comparison of the solubility in Na_2SO_4-10mol.%NaVO$_3$ with the solubilities in both pure Na_2SO_4 and in Na_2SO_4-30mol.%NaVO$_3$ was made. Their results indicated that CeO_2 dissolves in the salt solution either as a basic or as an acidic solute.

2.2 CHEMISTRY OF FORMATION OF SALT DURING COMBUSTION OF COAL/FUEL OILS (Khanna and Jha, 1998)

The sulphur present in coal and fuel oils yields SO_2 on combustion, which is partially oxidized to SO_3. The NaCl (either impurity in the fuel or in air) reacts with SO_3 and water vapour at combustion temperatures to yield Na_2SO_4.

$$2NaCl + SO_3 + H_2O \longrightarrow Na_2SO_4 + 2HCl\,(g)$$

Pure Na_2SO_4 has a m.p. of 884^0C, but with the dissolved salts e.g. NaCl or other metal sulphates, the melting point is lowered.

Na_2SO_4 is deposited on metal/alloy surfaces, and at sufficiently high temperatures is present as a liquid. At lower temperatures Na_2SO_4 can further react with SO_3 to form sodium pyrosulphate $Na_2S_2O_7$ with a m.p. of 401^0C .

$$Na_2SO_4 + SO_3 \longrightarrow Na_2S_2O_7$$
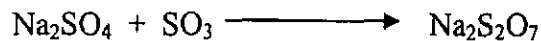
Small amounts of vanadium may be present in fuel oils, which on combustion forms V_2O_5. This may further react with Na_2SO_4 to form low melting sodium vanadates, which are highly corrosive.

$$xNa_2SO_4 + V_2O_5 \longrightarrow (Na_2O)_x.V_2O_5 + xSO_3$$
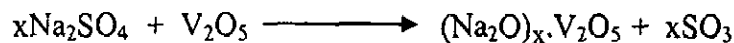
Thus metals and alloys in combustion gases are exposed to various corrosive agents such as O_2, SO_2/SO_3, molten salts, e.g. Na_2SO_4 or sulphate mixtures, sodium vanadates, NaCl etc.

2.3 THE HOT CORROSION DEGRADATION SEQUENCE

When superalloys under go hot corrosion degradation, this process almost always consists of two stages (Pettit and Giggins, 1987 & Pettit and Meier, 1984):

1. An initiation stage during which the alloys are behaving much as they would have behaved in the absence of the deposit and

2. Propagation stage where the deposit has caused the protective properties of the oxide scales to become significantly different from what they would have been had no deposit been present.

It effected the time for which the alumina or chromia scales are stable as protective scale upon the superalloys and it causes the properties of the corrosion product to be different. During the initiation stage of hot corrosion, superalloys are being degraded at rates similar to those that would have prevailed in the absence of the deposits. Elements in the alloy are oxidized and these are transferred from metallic atoms to the reducible substances in the deposit. Consequently, the reaction product barrier that forms beneath the deposit on the alloy surface usually exhibits primarily those features resulting from the gas–alloy reaction.

It is suggested that in some cases of hot corrosion, an increasing amount of sulfide particles become evident in the alloy beneath the protective reaction product barrier. In other small holes become evident in the protective reaction product barrier where the molten deposit begins to penetrate it. Eventually the protective barrier formed via selective oxidation is rendered ineffective and the hot corrosion process enters into the propagation stage. The hot corrosion degradation sequence is not always clearly evident, and the time for which protective reaction products are stable beneath the salt layer is influenced by a number of factors. The alloys must be depleted of certain elements before non-protective products can be formed or the composition of the deposits must change to prevent the formation of protective scales.

In case of Ni-30Cr-Al alloy which was cyclically oxidized with a Na_2SO_4 deposit, it was observed by Pettit and Meier (1984) that this alloy remained in the initiation stage for over 300 hours but after less than forty hours sulfides were detected in this alloy and the amount of sulfides in this alloy progressively increased with time. So they proposed that superalloys are being pre-conditioned by the deposits in a way that determines the time after which selective oxidation is no longer possible and which also determines the type of corrosion product scale that will be formed as the alloy enters the propagation stage. According to them this fact is responsible for the variety of hot corrosion processes that have been observed when superalloys are exposed to different environments. There are also cases where the initiation stage does not exist at all and the degradation process gets into the propagation stage as soon as the molten deposits come into contact with the alloy at elevated temperatures.

Numerous factors (Pettit & Giggins, 1987; Pettit & Meier, 1984 and Shores, 1981) affect the time at which the hot corrosion process moves from the initiation stage into the propagation stage and the time for which the protective scales are stable beneath the salt layer. These same factors also play the dominant role in determining the type of reaction product that is formed during the propagation stage. Alloy composition, gas composition, salt composition, salt composition rate, temperature, temperature cycles and erosion are some of the important factors.

The propagation stage of the hot corrosion sequence is the stage at which the superalloys must be removed from service since this stage always has much larger corrosion rates than for the same superalloy in the initiation stage.

2.4   SALT FLUXING

The processes by which the reaction product barrier becomes non-protective due to the formation of species, which are soluble in the liquid deposit, are called "fluxing" reactions. In a molten sulphate deposit, the following equilibrium can be used to define acidity or basicity:-

$$SO_4^{2-} = SO_3 + O^{2-}$$
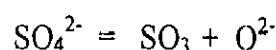
With the equilibrium constant, $K = P_{SO_3} \, a_{o^{2-}}$, where P_{SO_3} is the pressure of SO_3 and $a_{o^{2-}}$ is the activity of the oxide ions in the melt. Magnitude of K is determined by the standard free energies of formation for Na_2SO_4, SO_3 and Na_2O and $a_{o^{2-}}$ equals the activity of Na_2O in such melts.

In sulphate melts, the acidity is determined by the SO_3 pressure and the acidity increases as the SO_3 pressure is increased. The acidity need not only be controlled by the SO_3 pressure in the gas since there are other ingredients in some systems that may affect acidity.

For example V_2O_5 can react with Na_2SO_4 to increase the acidity of the melt via reaction: $Na_2SO_4 + V_2O_5 \longrightarrow 2NaVO_3 + SO_3$

Molybdenum and Tungsten in alloy can cause similar effects when their oxides are formed as corrosion products (Pettit and Giggins, 1987).

The initial concept of Basic Fluxing was first proposed by Bronstein and Decrescente (1969, 1971 and 1973) and then described in thermodynamics terms for the hot corrosion of nickel by Goebel and Petit (1970).

An essential feature of this process is that oxide ions are produced in the Na_2SO_4 deposit due to removal of oxygen and sulphur from the deposit via reaction with the alloy or metal. Furthermore, oxide scales (MO) that normally would form as protective barrier on the surface of these alloys can react with oxide ions via reaction such as:-

$$MO + O^{2-} \rightarrow MO_2^{2-}$$
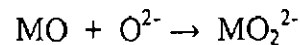
The protective oxide scales e.g. Al_2O_3 or Cr_2O_3 can react with O^{2-} ions to form soluble aluminates or chromate ions respectively:

$$Al_2O_3 + O^{2-} = 2AlO_2^{2-}$$

$$Cr_2O_3 + 2O^{2-} + \frac{3}{2} O_2 = 2CrO_4^{2-}$$
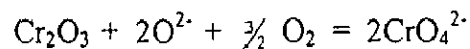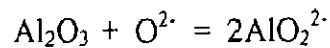
and their protective properties are destroyed. Such basic fluxing has a number of distinct features. Sulphides are usually found in the alloy substrate as a result of sulphur removal from Na_2SO_4 to produce oxide ions. The amount of attack depends upon the production of oxide ions by the melt. Hence a supply of Na_2SO_4 is necessary for the attack to continue and this type of fluxing is often not self-sustaining. This form of attack is usually restricted to high temperatures (above $\sim900^0C$) since the O^{2-} ion production is slow at lower temperatures, and is more likely to be important in gases without an acidic component (e.g. SO_3). However, according to Rapp and Goto (1981) basic fluxing can also occur in gases with acidic components.

They have proposed that protective scales on alloy could be made non-protective when the solubility gradients of the protective oxides in the molten deposit were negative since continuous dissolution and reprecipitation of oxide is then possible. The Rapp-Goto mechanism permits fluxing to be either basic or acidic, within the need for a source or sink for O^{2-} ions which mean that attack may continue without the additional supply of the deposit. But Shores.(1981) has examined the Rapp-Goto precipitation criteria for a variety of conditions and remarked that basic fluxing reactions are not always self sustaining. Further Otuska and Rapp (1990) have concluded from their

experimental studies that the negative solubility gradient for protective oxide can be taken as a criterion for continuity of hot corrosion.

Rapp and Goto (1981) proposed that, if the gradient in solubility of the protective oxide with distance into the salt layer was negative at the oxide /salt interface, accelerated attack could be sustained. This provided a quantitative expression of the earlier concepts of solubility gradients and oxide precipitation, that is, when

$$\left(\frac{d[\text{solubility of oxide}]}{dx} \right)_{x=0} < 0$$

Oxide can dissolve at the oxide/salt interface; migrate down a concentration gradient away from that site to a region of low solubility and precipitate. At steady state, oxide dissolves and is transferred away from the oxide/salt interface, just as fast as the oxide layer grows (Fig. 2.2 a & 2.2 b).

They recognized that such a gradient can be established across a thin salt film and that it need not be a consequence of the removal of sulfur from Na_2SO_4 or the introduction of acidic ions from the corrosion products as required by the Goebel and Pettit model (1970). When Rapp-Goto (1981) criterion for the oxide solubility is satisfied, fluxing is expected.

Solubility of an oxide depends on the acidity or basicity of the melt and in some cases, on p_{O_2} as well. In basic fluxing the solubility decreases with increasing p_{SO_3} (decreasing activity of O^{2-}). In acidic fluxing the solubility increases with increasing p_{SO_3} (decreasing activity of O^{2-}). Rapp and Goto suggested that the electrochemical reduction reaction should generally be expected to create a condition of local high basicity, because reduction reactions may generate oxide ions as reaction products. (Shores, 1981)

The acidic fluxing reactions involve the development of non-protective reaction products on superalloys as the result of a liquid deposit on the surface of the superalloy which has a deficiency of oxide ions. The deficiency of oxide ions in the Na_2SO_4 can arise due to an acidic component present in the gas or an acidic phase formed as an oxidation product upon

Metal   Oxide   Salt   Gas

Metal | Thin Oxide Film | ←Fused Salt→ film | Gas phase
Solubility of MO
O_2, SO_2, SO_3

Porous oxide Precipitate

Locally high (acidic or basic) solubility for MO   Locally low MO solubility

(a)   (b)
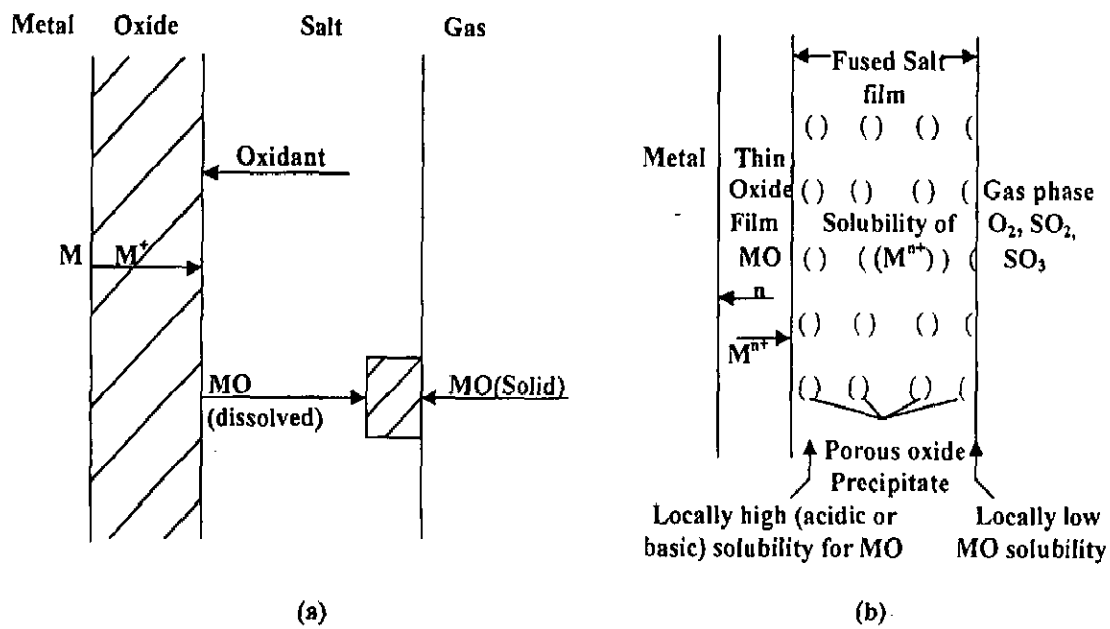
Fig. 2.2 (a):   Schematic diagram for fluxing. Metal oxide dissolves at the oxide/salt interface and migrates down a concentration gradient to a region of lower solubility, where MO precipitates. At steady state the oxide is dissolved and transported away just as fast as it grows. (Shores, 1981)

(b):   Precipitation of a porous MO oxide supported by the solubility gradient in a fused salt film. (Rapp & Zhang, 1994)

the superalloy. When the acidic component is present in the gas, the non-protective oxide scale ensues due to rapid transport of certain ionic species in the acidic melt.

If the melt becomes acidic due to formation of an oxide from an element in the superalloy, the attack becomes self-sustaining even with a small amount of Na_2SO_4. The refractory elements Mo, W and V form oxides that cause Na_2SO_4 to become acidic and hence these elements when oxidized in the presence of a Na_2SO_4 deposit on superalloys usually cause catastrophic self-sustaining hot corrosion via acidic fluxing (Pettit and Meier, 1984).

2.5 EFFECTS PRODUCED BY VARIOUS ALLOYING ELEMENTS ON THE HOT CORROSION

Alloying elements play significant role in the development of materials for hot corrosion resistance. Chromium inhibits the onset of basic fluxing in Ni-, Co- or Fe base alloys by causing O^{2-} ion concentration to be decreased to levels at which reaction with NiO, CaO and iron oxides is not feasible (Beltran and Shores, 1972).

For Ni-base alloys at least 19-20% Cr is needed for good resistance against basic fluxing, while for Fe- and Co-base alloys, the optimum range of Cr is 25-30%. More Cr is needed to establish a protective layer in Co-base alloys because diffusion coefficient for chromium in cobalt is about an order of magnitude less than that in nickel (Whittle, 1972).

It is reported that alumina forming Co- and Ni-base alloys are more susceptible to low temperature hot corrosion (600-850^{0}C) than chromia forming alloys. This is ascribed to the fact that Al_2O_3 formed in this temperature range does not consist of the highly protective α-Al_2O_3, rather of less protective γ-Al_2O_3. In addition chromium forms a more stable sulfide than aluminium and the oxidation of CrS yields a protective scale of Cr_2O_3. The chromium and aluminium are also beneficial for sulphur induced hot corrosion resistance. But Ni-base alloys (Al less than 6 wt %) are more susceptible to this attack than Co-base alloys when both chromium and aluminium are present (Khanna & Jha, 1998).

Titanium does not produce any significant effect on the degradation of Ni-, Co- or Fe-base alloys via basic fluxing (Pettit and Meier 1984). Pettit and Meier (1984) have stated that Ti and Pt are the only elements that produce beneficial effects for chlorine induced hot corrosion. Titanium when present often results in the formation of pervoksite ($NiTiO_3$). However, whether this is beneficial or not has not been clearly established (Whittle, 1972).

Mo, W & V all three of these elements produce similar effects. They do not inhibit the onset of basic fluxing, however the oxides of these elements are responsible for alloy induced acidic fluxing. These elements must be used with great care in any environment that can initiate hot corrosion attack. The characteristic features of the hot corrosion of molybdenum containing alloys (at least in the salt coating tests) are the catastrophic breakway and the development of characteristic, severe, hot corrosion morphology (Peters et al, 1976). The fact that superalloy containing Mo suffers catastrophic degradation has also been further reported by Pettit and Meier (1984); Fryburg et al (1984) and Misra (1986 A & B). It is proposed that the MoO_3 dissolves in the Na_2SO_4 melt, thus increasing the acidity of the salt leading to acidic fluxing. The MoO_3 gets incorporated into the Na_2SO_4 via the formation of compounds such as Na_2MoO_4, $Na_2MoO_4.MoO_3$ and $Na_2MoO_4.2MoO_4$. All these phases are liquid and have a high solubility for Al_2O_3, Cr_2O_3, NiO and CoO etc.

Ta & Nb: Ta has been reported to be having beneficial effects but there is a limited data available regarding the effect of Nb on the hot corrosion. This alloying element is not desirable when considering the oxidation resistance of superalloys (Pettit and Meier, 1984).

2.6 EFFECT OF REACTIVE ELEMENTS

Numerous investigations regarding the beneficial effect of rare-earth elements or their oxides either in the form of alloy additions or oxide dispersions in the alloys or simply by superficial coating of these oxides, have received special attention for more than a decade for imparting high-temperature–oxidation resistance as well as exhibiting improved scale adherence to the metal/alloy substrates (Mitra et al, 1992).

18

One of the beneficial effects of additions of reactive elements or dispersions of stable oxides is improvement in the adhesion of chromia and alumina scales. Many theories have been proposed (Smeggil, 1987 and Lees, 1987) to explain the improved adhesion which is produced by reactive elements and their oxide dispersions like

a)   Enhanced scale plasticity

b)   Presence of graded seal between the scale and the metal

c)   Modification of the growth mechanism of the scale

d)   The production of vacancy sinks

e)   The formation of oxide pegs

f)   Improved chemical bonding etc.

Lees (1987) in his "Sulphur Effects" theory proposed that elements such as sulphur segregate to the scale-metal interface, where they have a deleterious effect on the scale-metal adhesion and that reactive elements and dispersions of their oxides are beneficial because they prevent this segregation. They further reported that a fine dispersion of a stable oxide improves scale-metal adhesion, a coarse dispersion does not.

Reactive elements and dispersed oxides also affect the oxide growth mechanisms, and they appear to reduce the amount of cation diffusion (Weinbruch et al, 1999; Strawbridge and Rapp, 1994; Lagrange et al, 1984). Stott et al (1995) have also reported that the addition of reactive elements to alloy can influence very markedly the scale-growth mechanisms and especially can improve considerably the resistance of Cr_2O_3 and Al_2O_3 scales to mechanical failure.

Khanna et al (1989) have reported that deleterious effect of S can be checked by the addition of active elements such as Y, Ce or Hf and they found that Y was most effective in combating the negative effect of S. Chenbago and Yafang (1999) have reported that Y can slowdown the increment of the depth of diffusion layer formed during high temperature oxidation. Y improved the adherence of oxide scale to the substrate of alloy IC6. 0.2% of Y in Ni-Al-Cr_2C_2 alloy reduced the inward flux of oxygen in the alloy (Castello and Stott). Similar beneficial effect of Y addition to Fe-Ni-Cr-Al alloy has been investigated by Lagrange et al, 1984. They found that Y enhances oxidation resistance and improves oxide adherence. Zr when added

alone had little effect but produces an additional amelioration in spalling resistance when combined with Y.

Pandey et al have reported that 0.2% Zr addition is most effective in increasing oxidation resistance of Fe-15Cr-4Al alloy both under isothermal and cyclic oxidation conditions.

This is because the reactive element segregates to the oxide grain-boundaries where it blocks cation transport and possibly promotes oxygen transport (Lees, 1987 & Ecer and Meier, 1982).

2.7 HOT CORROSION OF IRON AND IRON BASE ALLOYS IN Na_2SO_4-V_2O_5 ENVIRONMENT

Harris et al (1955) in their study on the scaling resistance in moving air of some typical gas–turbine alloys with and without coatings of vanadium pentaoxide throughout their useful temperature range up to 1120 hrs in 70-hr cycles found that in all cases vanadium pentaoxide coatings have a deleterious effect. It is more pronounced for iron base alloys at temperatures above 750^0C.

Sachs (1958) studied accelerated high temperature corrosion of steels and stainless steel in V_2O_5 environment. They reported that oxidation of pure Cr in V_2O_5 occurs with a very rapid diffusion rate and so only the initial stages of the curve were supposed to be more important. Later slowing down of the oxidation rate was attributed mainly to the effect of scale thickening. Loose and spongy appearance of the scale was observed by them at the beginning of the process; V_2O_5 was present in excess and did dissolve the products of oxidation. According to them at the same point the liquid was saturated with the oxide which subsequently could get precipitated. The presence of various phases in a thin layer of scale would impose such severe strain on the film that cracking and exfoliation could be expected. This would permit liquid phase to reach the metal surface again and the conditions to form a spongy scale were seen to prevail. This mechanism would apply only to iron base alloys, which are susceptible to the catastrophic corrosion.

Fairman (1962) has studied some metal specimens in an ash mixture (V_2O_5 +10% Na_2SO_4) environment in air. The results showed that the corrosion was most severe at the ash/air or ash/atmosphere interface. He has observed that the attack was greatest where the concentration of oxygen and vanadium pentoxide are greatest, suggesting the transfer of oxygen atoms or ions by the pentaoxide to the metal surface: $2V_2O_5 \rightarrow 2V_2O_4 + 2O\downarrow$

According to him accelerated oxidation is a diffusion-controlled process of the incorporation of defects into the oxide scale. Accelerated attack by the slagging action of low melting point oxides constantly exposed fresh metal to the atmosphere. However, if this mechanism is valid, V_2O_5 can only have any effect when the ash is molten. Author opined that the mechanism of accelerated attack thus has been most satisfactorily explained by the catalytic action of V_2O_5 operating with an increase in the defect concentration of the scale.

Thilkan et al (1967) studied hot corrosion of nickel free austenitic stainless steel, Cr-Ni stainless steel and Inconel in oxygen atmosphere at different temperatures with vanadium-sodium slags of varying composition. They justified the use of saturated solution of Na_2SO_4 as the liquid medium because of its low gas solubility, vapor pressure and viscosity. Threshold temperature was found to lie between 700 and 800^0C. Above the threshold temperature the extent of attack initially increased but with increasing temperature either it became constant (as observed for Inconel) or decreased (for other alloys). Increasing amounts of Na_2SO_4 in mixtures with V_2O_5 first increased and then decreased the amount of oxidation at the temperature of 820-870^0C. At 950^0C, all Na_2SO_4 additions decreased the corrosive effect of V_2O_5. They observed that fluidity of slag was important in allowing diffusion of oxygen. At lower temperatures, the increase in fluidity might have a marked effect in increasing the attack. At higher temperatures, however, this may not have any effect on the corrosion rate as there may be negligible difference in the fluidity of fused V_2O_5 and V_2O_5-Na_2SO_4 mixture. They found an interesting observation that nickel free stainless steel has a high resistance to attack against V_2O_5-Na_2SO_4 mixture and under the experimental conditions showed a resistance superior to that of even Inconel at temperatures 850^0C specially in 70% V_2O_5-30% Na_2SO_4.

Valdes et al (1973), in study of AISI 446 stainless steel under V_2O_5 and $Na_2O.6V_2O_5$ environment in the temperature range 700-900^{0}C in air found that the oxide scale was mainly Cr_2O_3 with some vanadium oxide which acted as a moderate barrier to corrosion. Above 850^{0}C in V_2O_5, a breakaway corrosion reaction occurred. No Cr_2O_3 oxide barrier was present but there was a continuous oxide that comprised of Cr_2O_3, Fe_2O_3 and V_2O_5 at the metal/oxide interface from which a region of crystals grew. They suggested that the addition of Na_2O to V_2O_5 increased the oxide ion (O^{2-}) content of the melt and made it more aggressive to acidic oxides such as Cr_2O_3.

Kerby and Wilson (1972) have suggested that liquid vanadates increase the corrosion rate of metals by fluxing of the normally protective oxide layers present on the surface of the alloys and by providing a source of oxide ion for the corrosion reaction. The electrical conductivity increased with increase in temperature and with decreasing oxygen pressure. Incorporation of sodium into the V_2O_5 lattice structure caused a reduction in the valency of the vanadium atoms from V^{5+} to V^{4+} due to donation of the alkali metal valence electron to a vanadium atom.

Kerby and Wilson (1973) examined the rates of liquid vanadate corrosion of iron, nickel and several other Ni, Cr containing alloys and the rates of corrosion were found to depend on temperature, oxygen partial pressure, the composition, amount and turbulence of the liquid vanadates, composition of the metal or alloys in contact with the liquid vanadates and duration of the corrosion tests. They observed that the corrosion scales present on Armco iron specimens after cooling consisted of a thick, porous, outer oxide scale and a compact, slightly porous, inner oxide scale.

Tewari et al (1996) reported in their study on hot corrosion behaviour of Fe-base superalloy in Na_2SO_4-V_2O_5 environment that this alloy can be safely used for lower V/Na ratio (15% Na_2SO_4-85% V_2O_5) and for pure Na_2SO_4 environment upto 1100^{0}C.

Almerya et al (1998 A) carried out the electrochemical studies of steel SA 213-T22 and SA123-TP 347H in 80 wt % V_2O_5 + 20 wt % Na_2SO_4 at 540^{0}C–680^{0}C and found that the corrosion rate values obtained were around 0.58-7.14 mm/yr and there was increase in corrosion rate with time.

Almerya et al (1998 B) also carried electrochemical studies of hot corrosion of type 347H stainless steel in a mixture of 80 wt % V_2O_5 + 20 wt % Na_2SO_4 in the temperature range of 540 – 680^{0}C at intervals of 20K and found that with change in temperature from 540 to 680^{0}C the corrosion potential decreased.

Cuevas-Arteaga et al (2001), in their hot corrosion study of alloy 800 in Na_2SO_4-20% V_2O_5 reported that corrosion rate is slightly higher at 900^{0}C than at 700^{0}C as analyzed by both LPR (Linear Polarisation Resistance) and weight loss techniques. Using the above techniques, they reported that corrosion rates increased at the beginning of the experiment but decreased later on till they reached steady values.

2.8 HOT CORROSION OF NICKEL AND NICKEL-BASE ALLOYS IN Na_2SO_4-V_2O_5 ENVIRONMENT

Pantony and Vasu (1968 A) have explained the process of the fire side corrosion of boilers and gas turbines in the presence of vanadium pentaoxide with the help of a schematic diagram (Fig.2.3). They divided the process into six stages, any of which can be a rate-controlling. In the system, stages 1, 2 and 6 would be governed by the physical properties of the melt while stage 4 would be controlled by the physical nature and impurities of metal surface, together with the chemical properties of the metal and the melt. Stages 3 and 5 will be influenced by the physical and chemical properties of both the melt and products of corrosion to such an extent that the associated barrier may not exist at all. They mentioned that if any of the stages 1, 2, 3, 5 or 6 were rate controlling, the process was likely to be diffusion controlled with relatively low activation energy while if stage 4 was rate-controlling, then the whole process would be activation-controlled with relatively high activation energy. Pantony and Vasu (1968B) further mentioned that the vanadic corrosion could be viewed as a two-stage diffusion process, viz. an inward diffusion of oxygen and an outward diffusion of the corrosion products away from the surface. Kofstad (1990) has explained these diffusion

processes with the help of neat sketches shown in Fig. 2.4, which illustrates the growth of chromia scales in the presence or absence of oxygen active elements.

Bornstein et al (1972) found that the condensed vanadate alkali vanadates are like alkali sulphates, highly corrosive with respect to nickel base alloys. They further investigated that Na_2SO_4 must be present in the condensed state for sulphidation to occur. The presence of a liquid film can result in far greater adhesion between an ash particle and the metal surface. Liquid V_2O_5 has been proposed to be an excellent flux and easy path for oxygen diffusion (Bornstein et al 1975).

The corrosion caused by sodium sulphate, sodium vanadate mixtures has a complex mechanism as observed by Suito and Gaskell (1971). Nickel oxide in the oxide layer adjacent to the metal dissolved in the sulphate and precipitated as vanadate near the surface.

Kerby and Wilson (1973) have studied hot corrosion behavior of iron, nickel, alloys containing Fe, Ni, Cr and Inconel 600 by static and dynamic accelerated corrosion tests. They concluded that the presence of Fe and Na in the vanadate melts did not alter the rate controlling process of oxygen diffusion and oxygen sorption, but it increased the non stoichiometry and hence increased the oxygen diffusion. The rate of corrosion was reported to be affected by temperature, oxygen partial pressure and rotational speed, volume of liquid vanadate, composition of the metal and composition of the liquid vanadates. According to them, Inconel showed better corrosion resistance than stainless steels.

A 50Cr-50Ni commercial alloy had been corroded in pure V_2O_5 and in vanadate melts containing sodium sulphate and chloride in the temperature range 750 to 950^0C in a rotating disc apparatus by Dooley et al (1975). They concluded that in pure V_2O_5 chromium oxide scale formed on the alloy which dissolved only slowly into the liquid melt and was thus observed as a barrier layer. In $Na_2O.6V_2O_5$ this barrier layer was not observed. Marked internal oxidation of the Cr-rich α-phase occurred in chloride containing melts throughout the temperature range 750-950^0C.

```
Atmosphere          Melt           │ Diffusion or        Metal
   (1)               (2)           │ Barrier Layer
                ──────────────────►│    (3)
 Entry of    Diffusion of active species │ ───────────►
 oxygen      Through almost Pure V₂O₅    │                    (4)
 into melt                         │ Diffusion of agent through ► Chemical
                                   │ V₂O₅+ corrosion products    Reaction
                                   │    (5)
             ◄─────(6)──────────── │ ◄ Diffusion of
             Diffusion of corrosion products │ corrosion products
             through almost pure V₂O₅  │ through V₂O₅ +
                                   │ corrosion products
```
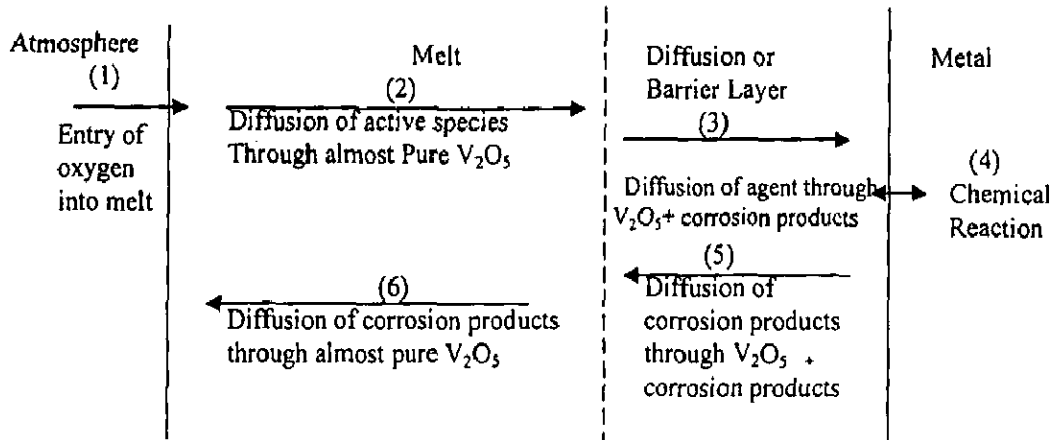
Fig. 2.3: Sequential steps in the vanadic corrosion of metals (Pantony & Vasu, 1968 A)
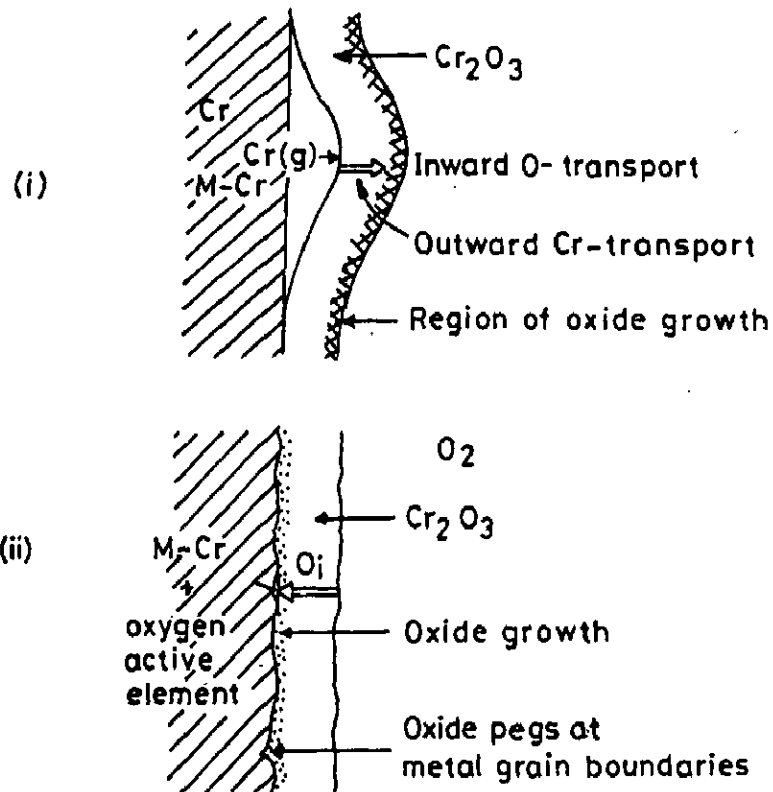
Fig. 2.4: Schematic illustration of the growth of chromia scales in (i) the absence of oxygen active element and with predominant outward transport of chromia through the scale, and (ii) the presence of oxygen active elements and with predominant inward transport of oxygen. (Kofstad, 1990)

Luthra and Spacil (1982) carried out a thermo-chemical analysis of impurity deposits in gas turbines for liquid fuels containing Na and V. They observed that the predominant species containing these elements were Na_2SO_4 and V_2O_5 in the condensed phase. The minimum concentrations of Na and V in the fuel above which deposition could occur were found to be 2.5×10^{-4} to 0.2 ppm and 3.5 to 259 ppm respectively.

The mechanisms of hot corrosion by molten sulphate-vanadate deposits were investigated by Sidky and Hocking (1987) by studying the corrosion of Ni-10Cr, Ni-30Cr, Ni-20Cr-3Al, Ni-21Cr-0.3Si, Ni-20Cr-5V and IN738 superalloys. The effect of adding Cr to Ni was found by them to be beneficial in the Na_2SO_4 melt, however, on increasing the VO_3^- concentration in the melt, this effect diminished, becoming harmful in pure $NaVO_3$ due to the formation of the non protective $CrVO_4$. According to them alloying element Al was found to be harmful in Na_2SO_4-$NaVO_3$ melts. Cr depletion was observed in rich VO_3^- melts but internal corrosion was more obvious in the SO_4^{2-} rich melts. Corrosion in rich VO_3^- melts was aggressive due to the fluxing action of the salt, which takes place along internally sulphidised areas. According to their study, IN738 suffered tremendous internal attack due to its γ precipitates those became sulphidation prone areas, which in turn were fluxed by the VO_3^- melt.

Thermogravimetric studies by simultaneous sulphate/vanadate induced corrosion at 650 to 800^0C have been performed by Seiersten and Kofstad (1987). NiCrAlY coatings with potassium sodium vanadyl vanadate deposits and the deposit alone have been exposed to oxygen containing 4% sulphur dioxide at 650-800^0C. They concluded that the solubility of SO_2 in fused Na-vanadate was observed to be higher than that expected from the literature values. The corrosion mechanism was found to change from initial vanadate induced to essentially sulphate induced hot corrosion as and when the SO_3 pressure was high enough. The phases Na_2SO_4, NiS, nickel oxides, nickel sulphate and nickel vanadates were identified by them.

Iyer et al (1987 A) have studied hot corrosion cracking behaviour of Nimonic 80A in flue gas atmosphere containing Na, S, V at 600-700^0C under tensile stress. Hot corrosion mechanism was explained by them on the basis that S reacts with chromium to form CrS at

600^0C which decomposes into Cr_2O_3 and SO_2 and then SO_2 escapes into atmosphere. In case of vanadium large quantities of oxides such as NiO, Cr_2O_3, $Ni(VO_3)_2$, $NiO.Cr_2O_3$ were formed. Fusion of these compounds is suggested to result in a spongy scale. Cr_2O_3 formed a non-protective sodium chromate (yellow stains) and hence further oxidation of Ni took place and the scale spalled off. The mechanism is not self sustaining at 600^0C and attack of S is not very severe, but they further observed that a eutectic of $Ni-Ni_3S_2$ formed at 650^0C that flowed along the grain boundaries at 700^0C resulting in severe attack which is self sustaining.

Iyer et al (1987 B) in their another investigation have studied hot corrosion behaviour of Nimonic 80A under tension using combustion gases environment at 600-700^0C and have shown that the oxide morphology had become irregular. Their X-ray examination indicated the presence of NiO, Cr_2O_3, $Ni(VO_3)_2$ and $NiO.Cr_2O_3$. Oxidation is reported to be very heavy and the scales were spongy. They have observed that the lowest melting liquid was formed even at 550^0C. They proposed that presence of stress will enhance the damage due to spalling off allowing fresh surface to be exposed to hot corrosion. It was proposed that as vanadium content increases some of the vanadium may participate in forming vanadates. So increasing vanadium beyond a certain level will not monotonically be aggressive. This critical level has been observed to be around 20 ppm vanadium. Also at high temperature, the stability of V_2O_5 would decrease resulting in critical level of V for the worst corrosion attack. They (Iyer et al, 1987C) have reported similar degradation mechanism for Superni-600 by vanadium at 700^0C and it has been attributed to the formation of two low melting eutectics ($NiO-V_2O_5-Cr_2O_3$, m.p. 550^0C & $V_2O_5-Cr_2O_3-Fe_2O_3$, m.p. 480^0C) and the presence of corrosive V_2O_5. Large quantities of oxides such as NiO, Cr_2O_3, Fe_2O_3, $NiO.Cr_2O_3$ and vanadates $Ni(VO_3)_2$ have been reported to be formed similar to Nimonic 80A.

(i)   Radial growth of sulphur rich particles dispersed into matrix.

(ii)   The acicular shaped vanadium rich phase and

(iii)   Idiomorphic Cr rich crystals which were formed from Cr of surface metal

They concluded that the substrate is depleted of Cr near to surface of alloy and with the increase in exposure time from 6 to 48 hrs there was a tendency of particles to take rounded shapes.

Using polarization resistance method Otero et al (1990) studied hot corrosion behavior of IN657 in 60%V_2O_5-40%Na_2SO_4. They observed that for duration less than 100 hrs the corrosion kinetics increased with temperature when the temperature was less than 1000 K. For temperatures > 1000 K, a decrease in corrosion rate was observed. Increase in corrosion rate with temperature observed during the initial stages of exposure was related to the higher fluidity of the molten salt mixture. At temperatures >1000 K, once the appropriate fluidity was achieved, corrosion rate decreased due to the decrease in the oxygen solubility in the molten salt. They also compared the gravimetric method with electrochemical data and confirmed that hot corrosion in molten salts is an electrochemical process.

The effects of chromate and vanadate anions on the hot corrosion of Ni by a thin fused Na_2SO_4 film in an SO_2-O_2 gas atmosphere at 900^0C were investigated by Otsuka and Rapp (1990). Their results showed that the inhibition of sulphidation may result from the precipitation of solid Cr_2O_3 from the melt and thereby partially sealing/plugging the crack defects and grain boundaries of the original protective oxide layer. It is proposed by them that vanadate anions enhanced the onset of the hot corrosion and sulphidation probably via rapid dissolution of the protective oxide scale at cracks/defects or grain boundaries.

A standard NiCrAlY and a silicon enriched alloys were studied by Lambert et al (1991) to investigate the effects of Si addition on their oxidation and hot corrosion behavior in Na_2SO-V_2O_5 environment. The chemical compositions (wt.%) of these alloys were Ni-17Cr-6Al-0.5Y and Ni-16Cr-5.7Al-0.47Y-5Si. They observed an outer layer of NiO developed on the surface of the standard alloy whereas a thin Al_2O_3 scale formed on the Si enriched alloy. Hot corrosion testing was carried out at 700^0C on specimens that were plasma spray coated with a corrosive mixture of Na_2SO_4-10wt.%V_2O_5. According to them, the development of protective oxide barrier was considerably affected by the corrosive coating, particularly in the Si enriched alloy. Ni, Cr, Al and Si complex oxides were detected in the inner oxide layer.

Laser glazing of gas flame sprayed NiCrAl, FeNiCrAl and NiCr alloys had a new surface composition and morphology. Hot corrosion tests by Longa and Takemoto (1992) in a mixed salt of 15% Na_2SO_4-V_2O_5 at 900^0C have shown that the modified coating offered

excellent corrosion resistance compared to the as sprayed coating because after laser modification the coatings achieved a more dense and homogenous structure without pores which supported the formation of continuous layers of Cr_2O_3 and Al_2O_3.

Swaminathan and Raghvan (1992) have reported that cracking and fluxing of the protective scales together with easier crack nucleation and growth at grain boundaries in the presence of liquid deposits of sodium metavanadate and sodium metavanadate plus 15wt% sodium sulphate at 650-750^{0}C account for the enhanced creep rates and reduced rupture life for Superni-600.

In their other study (Swaminathan and Raghvan, 1994) they have reported similar findings of enhanced creep damage in the presence of $NaVO_3$ and $NaVO_3$-15%Na_2SO_4 at all test temperatures of 650, 700 and 750^{0}C for Superni C-276. They have further reported that addition of sodium sulphate to sodium metavanadate increased the corrosivity of the deposit by lowering the melting point and by the formation of molten Ni-NiS_2 eutectic which initiates a self sustaining hot corrosion. The additional presence of molybdenum compounds Na_2MoO_4-MoO_3 enhanced the degradation.

Swaminathan et al (1993) studied the hot corrosion attack of Ni-base superalloy samples of Nimonic 80A, Hastealloy C-276 and Superni 600 coated with different amount of V_2O_5 by the wt. change measurement for a period of 100 hrs at 923, 973 and 1073 K in air.

Their results have shown that the hot corrosion kinetics obeyed a parabolic law with two regions at 973 and 1023 K, the corrosion rate falling with the formation of a solid $Ni_3V_2O_8$ layer. The rapid increase in weight at the initial hours was attributed to the ease in diffusion of nickel and oxygen ions in the molten V_2O_5. Once the compact solid vanadate layer was formed, the short circuit diffusion paths were blocked and diffusion became difficult for the oxygen ions to move towards the metal surface.

Longa et al (1996) in their study on LPPS (low pressure plasma sprayed) 80%Ni-20%Cr coating on 304 type stainless steel preoxidized for 3hr in air at 900^{0}C and tested in 0.7mol. fraction Na_2SO_4-0.3 mol. fraction $NaVO_3$ melt for 25hr (in 1% SO_2-O_2 at 900^{0}C)

observed that coating was penetrated by the fused salt upto -80 μm to 100 μm. They reported the formation of Ni and Cr vanadates such as $Ni_3(VO_4)_2$, $CrVO_4$ and nickel sulphides identified by them through EPMA and XRD techniques.

Deb et al (1996) in their study on the hot corrosion behaviour of a cast nickel base superalloy coated with 60% Na_2SO_4-30% $NaVO_3$-10% NaCl observed a thin layer of NiO and then a thick layer of $Ni_3(VO_4)_2$ and a inner porous duplex layer of oxides of Ni and Cr and CrS. They noticed that the corrosion rate decreases with time, which is due to the formation of refractory nickel vanadate layer over the surface.

2.9 HOT CORROSION OF COBALT-BASE ALLOYS IN Na_2SO_4-V_2O_5 ENVIRONMENT

The mechanism of hot corrosion by molten sulphate-vanadate deposits was investigated by Jones and Williams (1987) by studying the corrosion of Co-Cr-Al-Y gas turbine blade coating alloy by Na_3VO_4, $NaVO_3$, V_2O_5 and Na_2SO_4 or combinations thereof, in air or in controlled SO_3-air environments at 700^0C. They proposed that mixtures of 50%Na_2SO_4-V_2O_5 might produce greater corrosion than the pure vanadate product ($NaVO_3$) because of SO_3 liberated in the reaction Na_2SO_4 + V_2O_5 = $NaVO_3$ + SO_3. The mechanisms of $Co_2V_2O_7$ formation during vanadate-sulphate hot corrosion have been elucidated in depth with surface layers of $Co_2V_2O_7$ being shown to reduce the corrosion rate by acting as a barrier against SO_2 or O_2 inward diffusion and also possibly by reduction of V_2O_5 activity within the corrosion phase.

Tiwari et al (1997 A) have shown that in Na_2SO_4-60%V_2O_5 melt the degradation is due to the cracking of the protective scale under the influence of the fluxing action of the melt for both Fe-base alloy Superfer 800H and Cobalt base alloy Superco 605 and they further interpreted that presence of tungsten in form Na_2WO_4-WO_3 compound might have enhanced degradation. No oxidation and sulphidation into the substrate was observed by them in Co-base alloy as seen from X-ray mappings of the cross section taken by EPMA. Tewari (1997B)

has concluded that Co-base alloy has inferior corrosion resistance than Ni-base alloy in Na_2SO_4-60%V_2O_5 environment at 900^0C.

2.10 ROLE OF ADDITIVES /INHIBITORS

Modifying the physical or chemical characteristic of the deposit by adding various substances has been tried since corrosion and deposits first became a problem. Additives may be solid, liquid or gasses and they may be added to the fuel, injected into the combustor, sprayed onto heat-receiving surfaces or mixed with the products of combustion (Ch.7, Reid, 1971)

There are four main reasons of using additives:

1. To minimize the catalytic formation of SO_3 on hot surfaces.
2. To prevent formation of corrosive substances on heat-receiving surfaces.
3. To decrease the sintering tendency of high temperature deposits.
4. To neutralize acids normally condensing on cool surfaces.

Occasionally additives perform a double service, as in the injection of pulverized limestone or dolomite into boiler furnaces to remove SO_2 from the flue gas; these additives will minimize corrosion of super heaters and re-heaters, although they may add to the deposit problem.

As another example is addition of MgO to high vanadium residual fuel oil burnt in a central station power plant in USA, where it had been suggested that resulting deposit may be a saleable for recovering Vanadium (Ch.7, Reid, 1971).

Generally an appreciable quantity of materials must be added to modify the deposits. Trace amounts of additives seldom are useful, stochiometric quantities often being necessary to remove or inactivate undesirable substances.

The use of additives within furnaces is not wide spread as yet, and the industry is not convinced that additives are always worth while. Nevertheless, from the air-pollution stand point alone, since additives offer a mean of removing sulphur oxide from stack gasses, these modifying substances may be used much more widely in the future. There are numerous

inhibitors commercially available that are intended to reduce the severity of oil ash corrosion such as MgO, $MgSO_4$, CaO, MnO, Cr_2O_3, ZrO_2, Y_2O_3, In_2O_3, SnO_2, Al_2O_3, ZnO, BaO, PbO and SiO_2 etc. Some oil soluble Ni, Fe and Al and other compounds have also been tried with some success. However in commercial practice these inhibitors have not proven to be as effective as magnesium or manganese based inhibitors (Paul and Seeley, 1991).

Because of its effectiveness and relatively low cost, the most common fuel additives are based on limestone, dolomite and magnesia. Although magnesia is more expensive than limestone or dolomite it has been used widely as a corrosion-controlling additive in oil fired equipment. Both CaO and MgO react chemically with ash constituents. Both of these materials being active fluxes for coal ash at temperatures above 928^0C (Ch.7, Reid, 1971)

In 1943 Harlow (Ch.7, Reid, 1971) proposed that spraying superheaters periodically with $Ca(OH)_2$ during service would eliminate the catalytic formation of sulphuric acid in the flue gas. Keck was one of the first operators to use slurry spraying on a big scale in boiler furnaces. He applied water slurry of calcined magnesite periodically to the super-heater elements of an oil-fired utility boiler, using the conventional retractable soot blowers and manually controlled sprayers as the injection porI t. Keck reported that tube-wall thickness was not decreased, and tube sections showed no adverse effects after 39 months of slurry spraying in this installation.

Cotter in an unpublished review of Keck's system, confirmed that in another installation MgO slurry was applied once or twice a day on superheater and re-heater sections of an oil-fired boiler obtained equally favorable results. No gas-side plugging occurred, and the slurry was credited with stopping gas-side corrosion. Other methods of applying MgO to the tube surface include the injection of metallic magnesium directly into the furnace. Enough oxygen is always available to burn the metal to MgO, which is carried as extremely small particles to the flue gas to deposit as a thin film on heat-receiving surfaces. (Reid, 1971)

Metallic magnesium was being added continuously to the boilers at the March-wood station of CEGB in U.K, in 1963. Reese (1964) reported on similar procedures in the United States being used at various locations in large oil fired utility boiler where there had been problem of external corrosion.

Eric Blauenstein of Pentol GmbH, Rhein, West Germany studied in detail the effectiveness of incorporating magnesium oxide to overcome the serious corrosion problems due to use of high S low quality fuels . These fuels had 3-4% sulphur. The study was carried out at Ruein Station of the Intercom Utility system in Belgium. The technique used consisted of injecting magnesia into the upper fire box using 4 air atomizers of a proprietary design. The injection of dispersed magnesia Liquimag was found to affect the corrosion and deposits in both the furnace and the airheater. It also affected the stack emissions and boiler efficiency. They concluded that the additive increased the melting point and friability of the deposits while reducing their corrosiveness. The SO_3 emissions were also reduced significantly by additive injection i.e. 30 to 40 ppm to 20 to 25 ppm. Further it has been reported that proprietary additives based on ultrafine MgO dispersed in light weight oil has displaced the use of metallic magnesium where both cost and handling were a problem. It also allowed flexibility in adjusting the injected MgO amount in proportion to the quantity of S & V in the oil ash and there is a more uniform dispersion of MgO in the furnace gases.

2.10.1 Inhibition of Hot Corrosion by MgO Addition in Absence of Na_2SO_4

Fichera et al (1987) have evaluated the effectiveness of magnesium oxide as an additive to fuel oil. Fig. 2.5 shows the effect of addition of MgO on the melting point of fuel ash.

MgO directly reacts with V_2O_5 (Fig. 2.6) giving $2MgO.V_2O_5$ (magnesium pyrovanadate, melting point 835^0C) and $3MgO.V_2O_5$ (magnesium orthovanadate, melting point 1190^0C) as shown below:

$$2MgO + V_2O_5 \rightarrow 2MgO.V_2O_5$$

$$3MgO + V_2O_5 \rightarrow 3MgO.V_2O_5$$
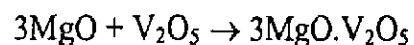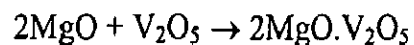
Increasing the melting points of the fuel ash constituents greatly increases the viscosity and reduces the diffusion of oxygen by up to an order of magnitude and counteracts the destruction of the protective oxide barrier film.

Work of Niles and Sanders (1962) suggests that the formation of these compounds is not a function of the magnesium concentration. When the molar ratio of MgO/V_2O_5 was less than 3:1 the reaction products contained $Mg_3V_2O_8$ and excess V_2O_5, while when the ratio exceeded 3:1 excess MgO was formed in the reaction products (Clark and Morley, 1976).

2.10.2 MgO Addition and Hot Corrosion Mechanism in Presence of Na_2SO_4

It is necessary to assume that, where sodium and vanadium are the major metal contaminants in a fuel, deposits will be composed principally of compounds of these two metals, and likewise, if an additive is used, it too will be a principal deposit component. The compound formed will depend upon the Na/V ratio (Niles and Sanders, 1962).

$$Na_2SO_4 \rightarrow Na_2O + SO_3$$
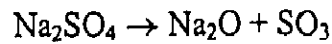
$$\Delta G^0 = -RT \ln K$$

where ΔG^0 is the standard Gibb's free energy for reaction at 900^0C and K is a equilibrium constant, $K = a_{Na_2O} p_{SO_3} / a_{Na_2SO_4}$, where a is the activity and p the partial pressure of the given species. Taking ΔG^0 from the literature (-388.928 kJ mol^{-1}) and setting the activity of Na_2SO_4 to unity gives $\log (a_{Na_2O}) + \log (P_{SO_3}) = \Delta G^0/2.303$ RT $= -17.3$ at 900^0C. By the dissociation of sodium sulphate, SO_3 is generated. When sufficient SO_3 is present the MgO can be sulphated to $MgSO_4$ (Rhys-Jones et al, 1983)

$$MgO + SO_3 \rightarrow MgSO_4 \ (K = -19.002 \ at \ 900^0C).$$
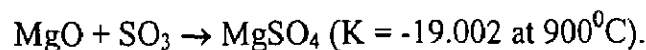
It is known that V_2O_5 competes with SO_3 for reaction with MgO when magnesium inhibitors are used with low quality fuel (Jones, 1992).

The $MgSO_4$ can then react with V_2O_5 to from magnesium pyrovanadate (melting point 835^0C) which may be molten on the surface of turbine blades.

$$MgSO_4 + V_2O_5 \rightarrow MgO.V_2O_5 + SO_3$$
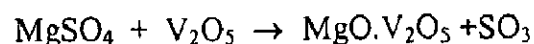
The reaction is likely to attain equilibrium in the porous deposits/scales present on gas turbine blades in a residual fuel fired system and is further catalyzed by V_2O_5.

34

2.10.3 Effect of SO₃

Tewari and Prakash (1998) reviewed that the presence of SO_3 is detrimental to MgO inhibition of hot ash corrosion as magnesium pyrovandate is more corrosive than V_2O_5. It has been further shown that the stability of these compounds, likely to be found in the gas turbine combustion zone, is function of P_{SO_3} (Rhys-Jones et al, 1983). If $P_{SO_3} \geq P_{SO_3}$ (equilibrium) then $Mg_3V_2O_8$ and MgO at unit activity are unstable and $MgSO_4$ is stable. However If $P_{SO_3} \leq P_{SO_3}$ (equilibrium) then $Mg_3V_2O_8$ and MgO are stable and $MgSO_4$ is unstable. Thus corrosion control in low grade or residual fuel oil depends upon the formation of these compounds and formation of these compounds is modified by the presence of SO_3.

Niles and Sanders (1962) have concluded from their test results that magnesium sulphate and magnesium vanadate, $2MgO.V_2O_5$, do not react at elevated temperatures. They may, however, interact in a mechanism involving corrosion products.

2.10.4 Effect of MgO Content

Regardless of the magnesium compound used, the corrosivity of magnesium vanadates decreased as excess magnesium was added. The amount of magnesium compound added in commercial practice is known to vary between 4:1 and 6:1 molar ratios of magnesium to vanadium to obtain acceptable corrosion protection at the operating temperature (825^0C). In steam boilers where P_{SO_3} is usually below equilibrium for $MgSO_4$ formation it has been shown that a 3 or 4:1 molar ratio (approximately 1.5–2:1 weight ratio) of magnesium to vanadium is often adequate for protection.

2.10.5 Inhibitor Efficiency

To express the effectiveness with which MgO inhibits vanadic corrosion, a term 'Inhibitor Efficiency' may be evaluated as follows (Rhys-Jones, 1983):

$$I = \frac{Corr\ I - Corr\ II}{Corr\ I} \times 100$$

I-The Inhibitor Efficiency.
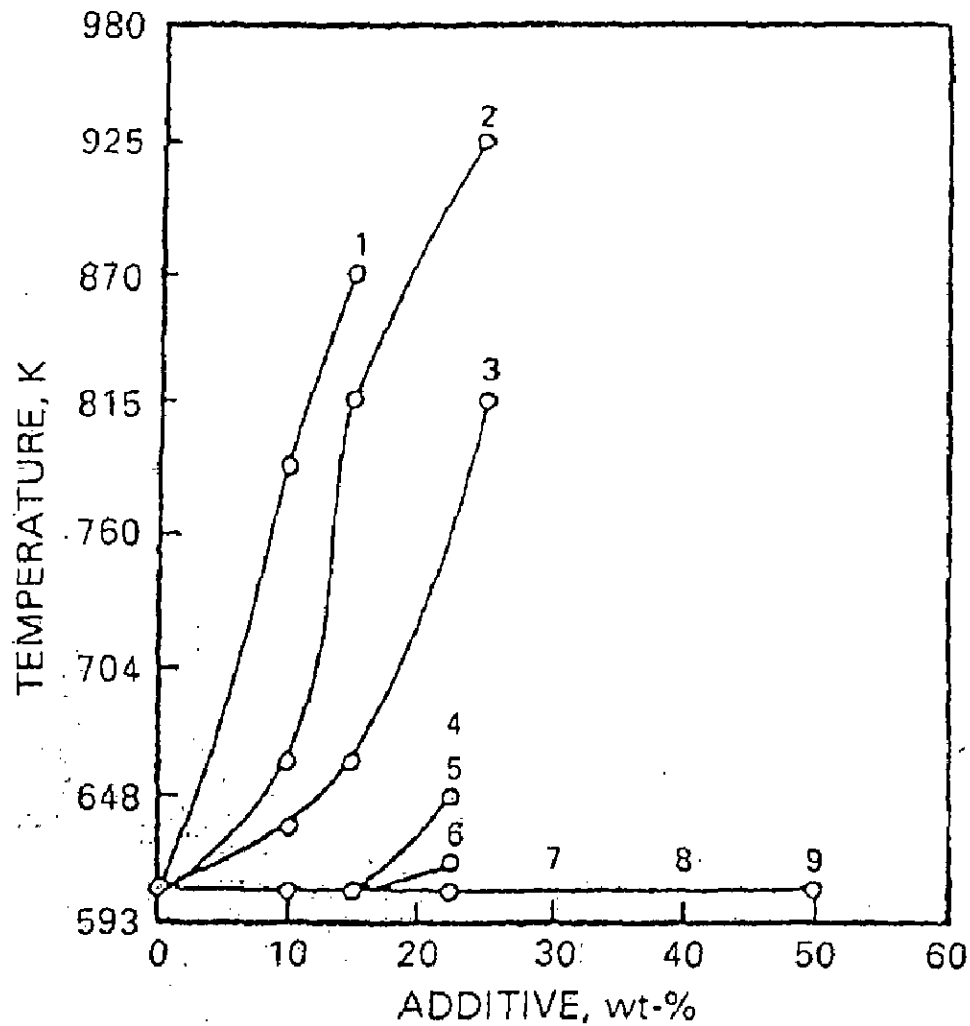
1: MgO, 2:CaO, 3:NiO, 4:Cr$_2$O$_3$, 5:ZrO, 6:TiO$_2$, 7:Al$_2$O$_3$, 8:SiO$_2$, 9:ZnO

Fig.2.5: Effect of various oxide additions on melting point of a typical crude oil ash: initial oil ash composition 60V$_2$O$_5$-15Na$_2$SO$_4$-10CaO-5PbO-5SiO$_2$-Fe$_2$O$_3$ (wt.%). (Reid, 1971)
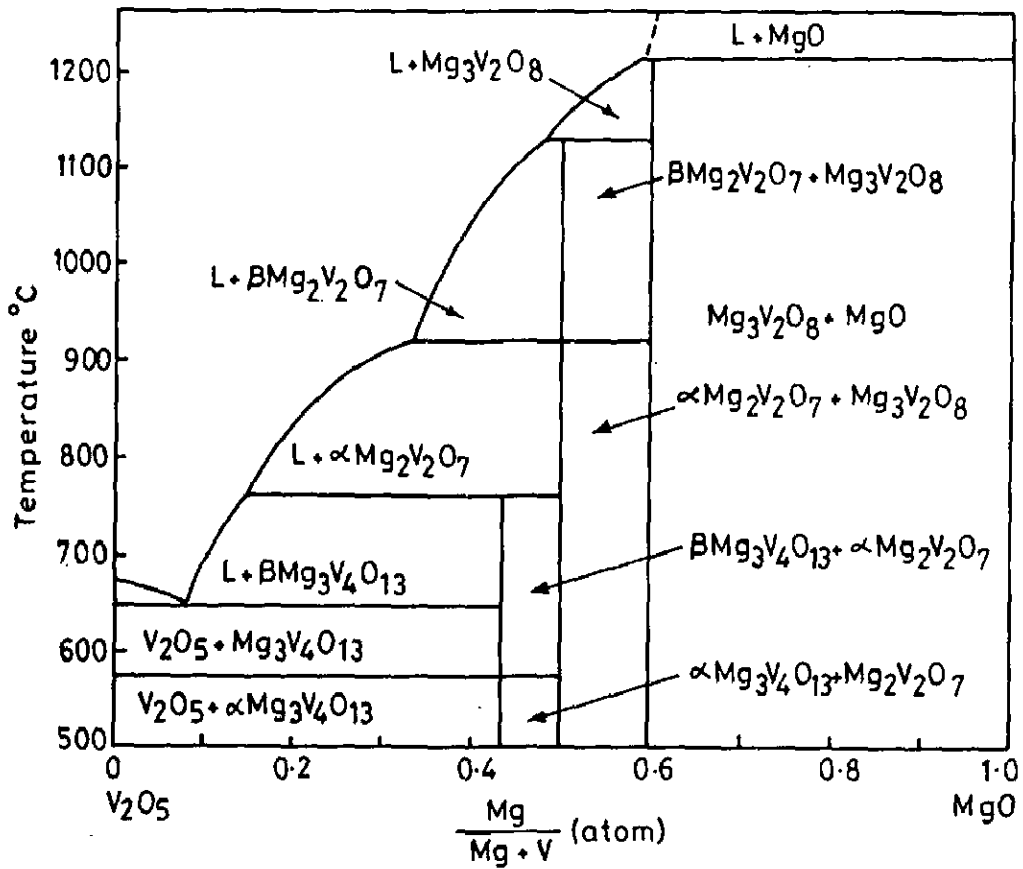
Fig.2.6: Phase diagram for MgO-V$_2$O$_5$ system (*Hancock, 1987*)

Corr I – in system alloy + V_2O_5 + air (mm/100 hr^{-1})

Corr II – in system, alloy + V_2O_5 +3 MgO + air (mm/100 hr^{-1})

100% efficiency will be achieved when Corr –II = 0 i.e. when all the corrosion due to the presence of V_2O_5 stopped by MgO i.e. when the measured corrosion rate is equal to that obtained in air oxidation. 85–90% efficiency can be realized in SO_2 free system.

The melting point of synthetic mixtures V_2O_5–Na_2SO_4 with increasing additions of MgO was also evaluated by Fichera et al (1989). To find out the minimum quantity of Mg/V ratio this leads to a 100^{0}C increase in the melting point. The mixtures tested were 13%V_2O_5– 87%Na_2SO_4 ii) 50%V_2O_5-50% Na_2SO_4 iii) 90%V_2O_5–10%Na_2SO_4.

They have concluded that

(i)   The melting points of the mixtures without additive range from 600 to 750^{0}C

(ii)   MgO additions lead to a m.p. between 800 and 900^{0}C

(iii)   0.8 Mg/V ratio is sufficient to guarantee a 100^{0}C increase in m.p. of deposits, even in complex mixtures.

Rhys-Jones et al (1983) studied the effect of various levels of V_2O_5 and V_2O_5 + MgO upon the higher temperature corrosion of Nimonic 90 and X-40 alloys in the absence and presence of SO_2/SO_3 at the temperature 850^{0}C in terms of metal loss. They have suggested that 3MgO:1V_2O_5 reduces the metal loss to a maximum extent.

Barboti et al (1988) studied the effect of $MgSO_4$ addition in depressing hot ash corrosion of stainless steel by carrying out wt. loss experiment. They have shown that $MgSO_4$ is stable upto 892^{0}C, where it decomposes into MgO and SO_3 at increasing rate. They have observed that in presence of V_2O_5, there was no influence of $MgSO_4$ in the temperature range 630-690^{0}C. They finally concluded that when $MgSO_4$ was added to ash in the ratio 1:1 the scale analysis showed Fe-Cr values of 0.12 which corresponded to a range of 77-82% inhibitor efficiency in the temperature range 600-800^{0}C.

Hancock (July, 1987) reported that when magnesium additives are used to combat vanadium, care must be taken to allow for sulphur contamination in the fuel, which reacts with the additive and reduces its efficiency.

Tewari (1997 B) reported that MgO as an inhibitor in the ratio of 3:1 $MgO:V_2O_5$ has proved to be effective in Fe, Ni & Co–base superalloys in Na_2SO_4-60%V_2O_5 at 900°C though the effect is more for Fe-base alloy (90.5%) and Co- base alloy (85.33%).

Thilkan et al (1969) studied the change in corrosion rate of Cr/Ni stainless steel (16.86%Cr, 11.24%Ni, 1.2%Mn, 0.21%Si and Bal Fe) in 90%V_2O_5-10%Na_2SO_4 mixture containing additives at 870°C. Few oxides were added (20%) to the ash mixture and the rates determined. CaO & MgO were found to give best inhibiting result (Fig. 2.7). They noticed that the major effect of the additives is to increase the period after which rapid oxidation starts. While the attack on the alloy was rapid most from the onset in a mixture without additives, the same was delayed to about ½ hour, ½ hour, 1 hour and 2½ hours when Al_2O_3, SiO_2, MnO_2 and MgO are respectively present as additives.

Detailed study was also made by them using increasing percentages of MnO_2 in the 90%V_2O_5-10%Na_2SO_4 mixture and it was observed that initial rate is reduced sharply and with progress of time. This decrease does not remain so marked, showing that the effect of additives in decreasing the extent of attack decreases with time, though increasing amount of additives considerably decreases the total attack.

Atul Kumar et al (1996) studied the hot corrosion behaviour of Ni-base alloys in the most corrosive vanadic environment 40% Na_2SO_4-60%V_2O_5 using $CaSO_4$ as an inhibitor in the ratio $3CaO:1V_2O_5$ at 700°C, 800°C and 900°C. It has proved beneficial by the formation of solid phase specially at temperatures 800°C and 900°C.

Similar beneficial effect of inhibitors MgO and CaO has been observed by Gitanjaly et al (2002) on the hot corrosion behaviour of superfer 800H in Na_2SO_4-60%V_2O_5 environment at 900°C. Formation of solid vanadates at test temperature, $Mg_3V_2O_8$ and $Ca_3V_2O_8$ have been reported in case of MgO & CaO coated samples respectively.

2.11 ROLE OF ZnSO₄ ADDITIONS

In 1980, the Canadian Armed Forces reported that the rate of attack on turbine components on Canadian warships was considerably less than that experienced by other
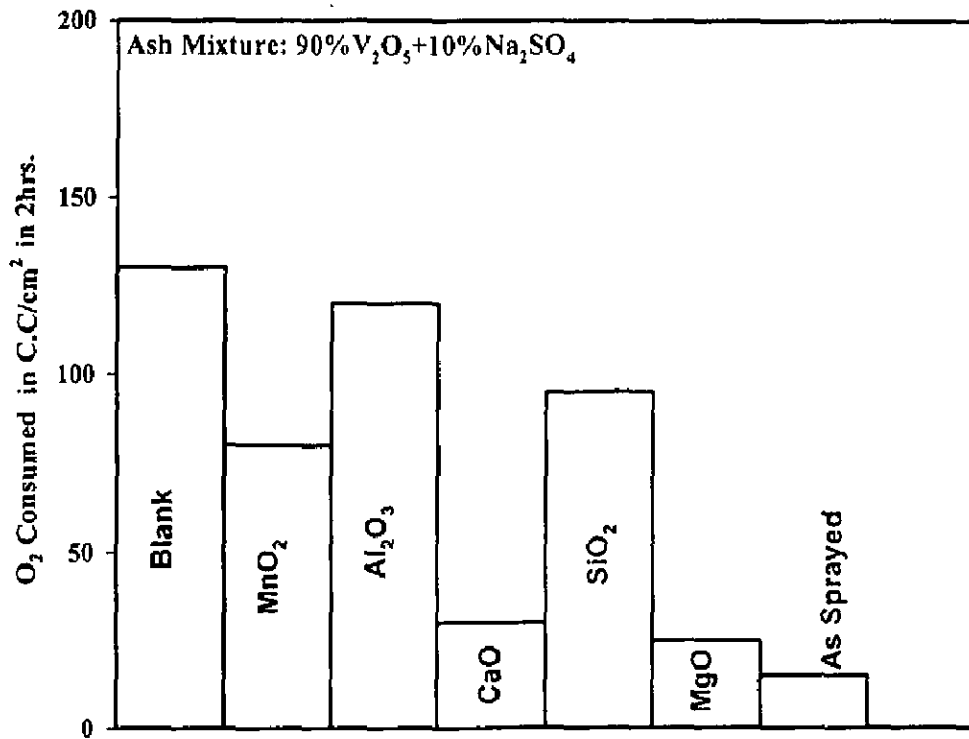
Fig.2.7: Effect of additives (20%) on corrosion of Cr/Ni stainless steel at 870^0C (Thilkan et al, 1969)
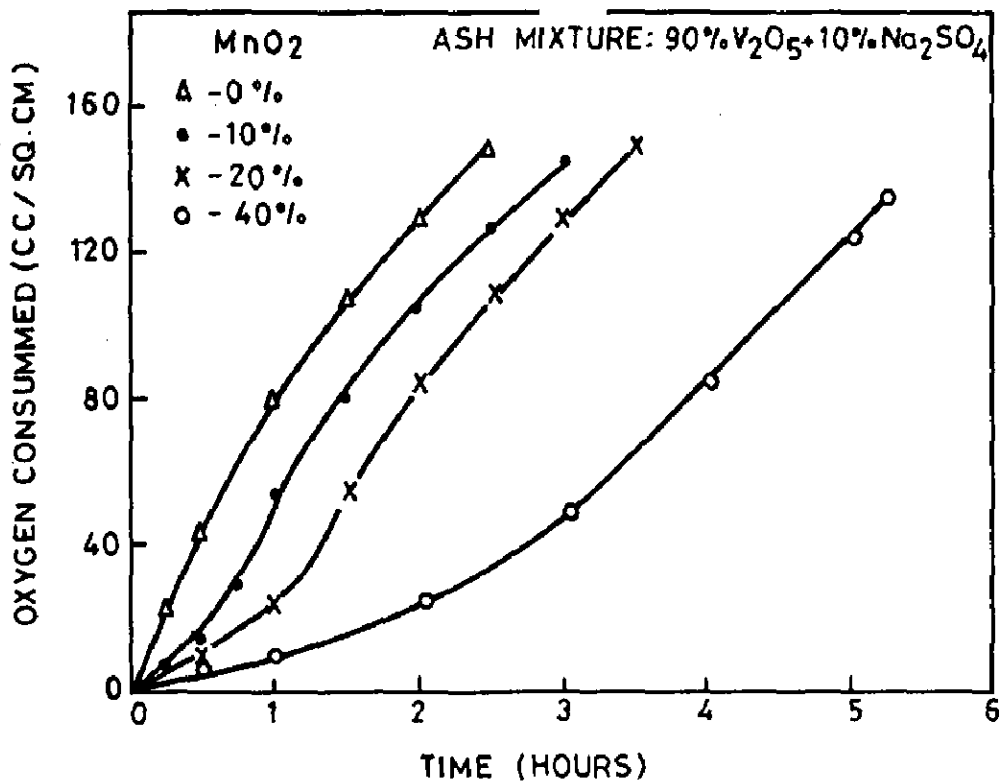
Fig.2.8: Effect of addition of MnO_2 on corrosion of Cr/Ni Stainless Steel at 870^0C (Thilkan et al, 1969)

navies using similar equipment (Hollingshead, 1980). Examination 1 of the turbine blades revealed the presence of zinc sulphate which was then traced to zinc based paint used to coat the inside of the turbine fuel tanks. It was found that fuel dissolved from 10 to 100 ppm zinc. This happening represented one of the rare occasions where a fuel additive to inhibit hot corrosion has been tested on an actual operating engine. The presence of the zinc sulphate apparently caused no harmful effects to the turbine.

The beneficial effect of zinc additions has been confirmed by a number of laboratory investigations. Hollingshead (1980) partially immersed specimens of superalloys S-816 and AMS 5385 in 10% NaCl-Na$_2$SO$_4$ salt mixtures containing various amounts of zinc sulphate. The alumina crucibles containing the salt and metal specimens were exposed to an air atmosphere at 900^{0}C for up to 80hr. The alloys suffered severe hot corrosion but when 1.5 and 5.0 wt.% ZnSO$_4$ was added to the salt mixture the same alloys were barely attacked.

Other investigators (Kanary et al, 1987) measured the rate of corrosion of a superalloy Nimocast 713 in a simulated gas turbine combustion atmosphere by observing the weight change. They partially immersed the alloy in 10% NaCl-Na$_2$SO$_4$ mixtures containing various amounts of ZnSO$_4$ at 900^0 and a gas stream containing O$_2$, N$_2$ and a P_{SO_3} of 750 Pa was passed over the metal-salt mixture. Their results confirmed that the rate of corrosion was significantly reduced by adding ZnSO$_4$, which reached a minimum in the presence of 10wt.% ZnSO$_4$ (Fig.2.9). Similar static corrosion tests on Nimocast 713 were carried by them at 700^{0}C (Hancock et al, 1985) and P_{SO_3} of 300 Pa and 750 Pa. They found that ZnSO$_4$ additions were equally effective in reducing low-temperature hot corrosion and the amount required varied according to the P_{SO_3}. At P_{SO_3} of 750 Pa the minimum amount of corrosion occurred when 10% ZnSO$_4$ was added. When P_{SO_3} was reduced to 300 Pa, the minimum corrosion occurred at higher concentrations of ZnSO$_4$ i.e. 20%. Reduced rates of corrosion were obtained by other investigators (Deadmore and Lowell, 1978) using a dynamic test method in which zinc was added to the combustion gases of a burner rig as an aqueous solution of Zn(NO$_3$)$_2$ to give 3 ppm zinc in the atmosphere. The tests were carried out at 900^{0}C for 100 hrs using various alloys

(Table 2.1) and the corrosion was measured by sectioning the test specimen. Fig. 2.10 shows that high chromium content improves the hot corrosion resistance of the alloys.

Table 2.1: Nominal composition of the superalloys referred in this review

Alloy Designation	Chromium	Cobalt	Nickel	Aluminium	Carbon
IN-100	10	15	Bal	5.5	0.18
Nimocast713	12	1	71	6.0	0.1
IN-792	12.7	9	Bal	3.2	0.2
U-700	14.2	15.5	Bal	4.2	0.06
IN-738	16	8.5	Bal	3.4	0.17
S-816	20	40min	20	-	0.35
MAR-M509	23	Bal	10	-	0.6
AMS-5385	27	67min	2.8	-	0.25

2.11.1 Zinc Additions in the Absence of NaCl (Hancock et al, 1989)

The mechanism of hot corrosion is believed to proceed in two phases; the initial phase is the penetration of the protective oxide coating which forms on superalloys at elevated temperatures. Usually, these oxides are either chromium oxide or aluminum oxide depending on the alloy composition. When the protective oxide has been removed, the metal then corrodes by an electro-chemical reaction in which the liquid salt deposits act as the electrolyte. The metal forms the anode of the corrosion cell, and SO_3 or O_2 in the atmosphere provides the cathode reaction (Hancock et al, 1989). The solubilities of some of the important metal oxides with respect to hot corrosion have been measured in sodium sulphate as a function of the activity of Na_2O using an electrochemical technique (Stroud and Rapp, 1978; Gupta and Rapp, 1980; Hancock, 1988). The solubilities were found to vary as predicted by the acid-base fluxing model. They concluded from Fig 2.11 that the solubility of zinc as ZnO is much higher than the solubility of NiO and Al_2O_3 and is similar to the solubility of Cr_2O_3, except that the minimum solubility occurs under more acid conditions, i.e. at lower activities of Na_2O or at a higher P_{SO_3}.

The ZnO dissolves under acid conditions as the double salt, $ZnO.2ZnSO_4$, according to following reaction,

$$3ZnO + 2Na_2SO_4 \rightarrow ZnO.2ZnSO_4 + 2Na_2O$$
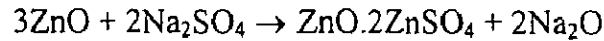
and under basic conditions as sodium zincate, Na_2ZnO_2, according to

$$ZnO + Na_2O \rightarrow Na_2ZnO_2$$
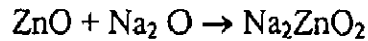
The equilibrium solubility measurements recorded in Fig.2.11, do not offer an explanation for the inhibiting effect of zinc additions to the salt mixture but Hancock (1988) noted that when zinc was present in the system it required very long intervals for the system to achieve equilibrium following changes in the P_{SO_3} or activity of Na_2O. This was explained by the higher solubility of zinc, which required the transport of larger amounts of SO_3 before equilibrium conditions could be satisfied. Since an essential feature of the acid - base fluxing theory for the mechanism of hot corrosion is the existence of a dynamic system, the sluggish behaviour caused by zinc would have an inhibiting effect on the rate of corrosion (Hancock, 1989).

The effect of zinc on the kinetics of the corrosion reaction itself i.e. the electrochemical oxidation of the alloy Nimocast 713 was studied by means of anodic polarization measurements (MacIsaac et al, 1988) with and without 10wt. % $ZnSO_4$ in the salt mixture 78 $LiSO_4$-13.5K_2SO_4-8.5 Na_2SO_4 in mol.% at 900^0C and P_{SO_3} =24 pa. The addition of $ZnSO_4$ changed the corrosion potential from -0.36 to - 0.15 V vs. a pure O_2 reference electrode and decreased the corrosion current from 3.8 x 10^4 nA cm^{-2} to 2.0 x 10^2 nA cm^{-2}.

The lower corrosion current confirms the inhibiting effect of additions of zinc. This change in electrode characteristics may be due to the effect of ZnO on solubility of various metals from alloy in sodium sulphate. The solubility of NiO, Al_2O_3 and Cr_2O_3 in liquid Na_2SO_4 saturated with ZnO at 900^0C has been observed to be significantly decreased e.g. The solubility of NiO was reduced by 88% in Na_2SO_4 saturated with ZnO where a_{Na_2O} was $10^{-12.3}$ (Hancock, 1988).

Hancock et al (1989) reviewed that in the absence of excess NaCl, the zinc provides a reservoir of reactive metal oxide in the deposit which makes the dissolution reactions, postulated in the acid-base fluxing theory, more sluggish and lowers the solubility of the protective metal oxides from the alloy in the salt mixture. Zinc also lowers the electrochemical potential of the corrosion reaction. In the presence of excess NaCl, the zinc readily reacts with the chloride ion and offers itself as a convenient substitute for other metals from the protective oxide layer which may dissolve by forming chlorides.

Foggo et al (1984) also observed that sulfation of Co_3O_4 and NiO in molten eutectic 50 mol.%$ZnSO_4$-Na_2SO_4 is substantially reduced as compared to their sulfation in the presence of an equivalent amount of Na_2SO_4 and this reduced sulfation appeared to be caused by decreased solubility of $CoSO_4$ and $NiSO_4$ in $ZnSO_4$-Na_2SO_4 as a result of solute –solute interactions with $ZnSO_4$ and/or formation of a barrier film on the metal oxide surface, which inhibits further sulfation of the remaining oxide. Although corrosion is not totally halted, the low temperature hot corrosion of CoCrAlY is inhibited by deposits of $ZnSO_4$-Na_2SO_4 for SO_3 concentrations upto 500 ppm.

2.12 EFFECTS OF SnO₂ ADDITIONS

Jones (1993) has reported that there is need for high temperature oxides that are resistant to reaction with molten vanadate or vanadate–sulphate phases. Such phases are found as deposits in engines burning fuels containing sodium, sulphur and vanadium impurities as well as in other areas of high temperature technology. SnO_2 has a listed melting point of 1630^0C and it is classed as a high temperature oxide ceramic. However, they suggested that SnO_2 is more readily reduced than such metal oxides as NiO and Fe_3O_4. SnO_2 has also relatively high volatility and it has been cited as being useful only in oxidizing atmosphere at temperatures below 1500^0C. Small additions of this might find a wider range of applications.

As shown in Fig. 2.12 there is essentially no difference in weight gain behaviour between $NaVO_3$ and the SnO_2-$NaVO_3$ mixtures. This indicates that SnO_2 does not undergo
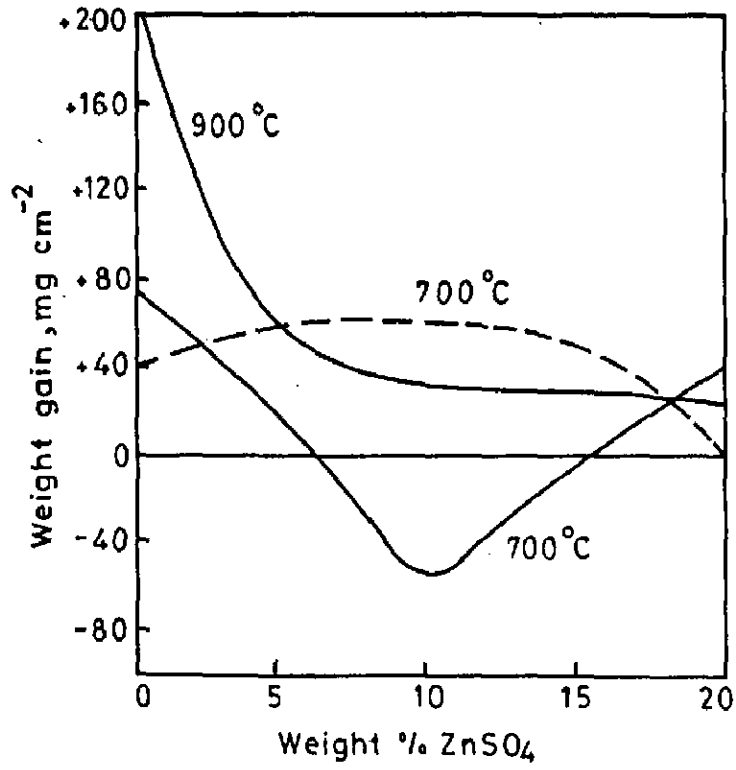
Fig.2.9: Weight change of Nimocast 713 in salt mixtures containing NaCl (10Wt.%)+Na₂SO₄ and various amounts of ZnSO₄ (Hancock, 1989)
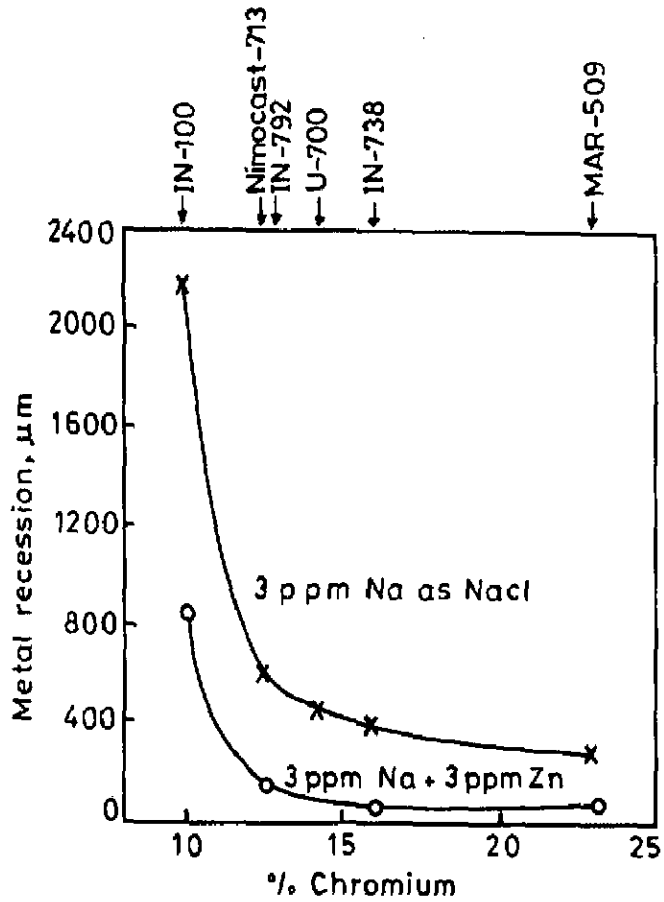
Fig.2.10: Burner rig corrosion tests on various alloys showing the effect of Zinc additions (Hancock, 1989)

45
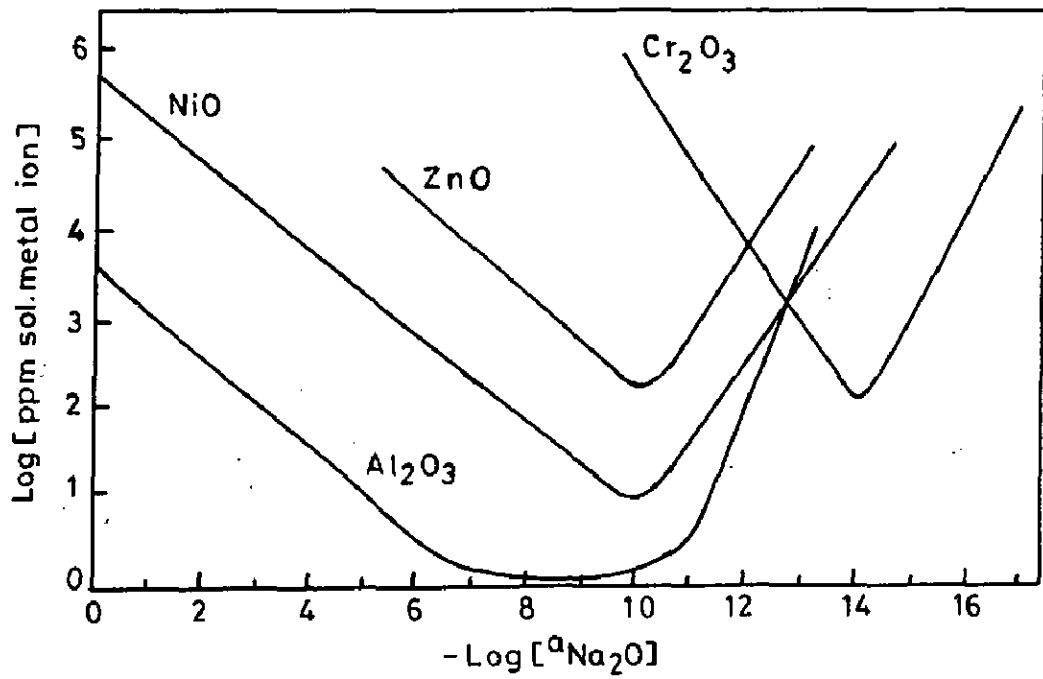
Fig.2.11: Solubility of various metal oxides in Na_2SO_4 as a function of a_{Na_2O} ka (Hancock, 1989)
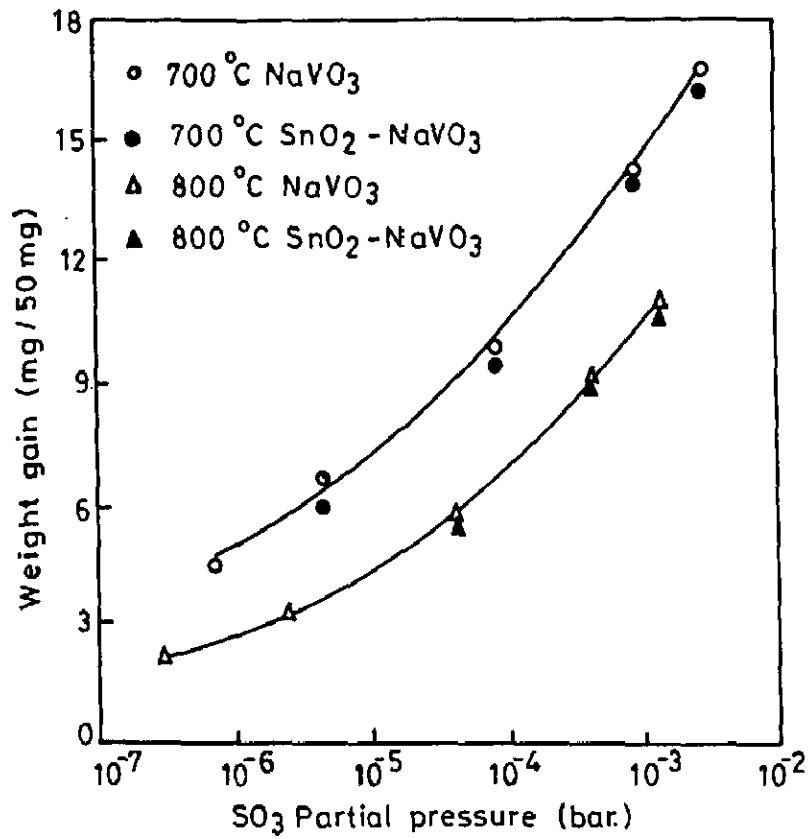
Fig. 2.12: Weight gain behaviour of SnO₂-NaVO₃ as a function of SO₃ partial pressure at 700°C and 800°C (Jones,1993)

chemical reaction at 700° C and 800°C with a melt system consisting of $NaVO_3$, Na_2SO_4 and V_2O_5 for SO_3 partial pressures as high as 5×10^{-2} bar (5 Kpa).

Jones (1991) studied the reaction between SnO_2, V_2O_5 and other sodium vanadates at 680°C and he found no reaction between SnO_2 and V_2O_5 and other Na-vandates with decreasing V_2O_5 activity. No reaction has been explained by close matching of Lewis acidity of SnO_2 and V_2O_5.

2.13 EFFECTS OF SURFACE APPLIED COATINGS ON OXIDATION IN AIR

Effects of surface-applied reactive element oxide films on the oxidation of alloys have recently attracted considerable attention. As early as 1945, a patent claimed that in the case of chromia–forming alloys, the reactive element effect (REE) could be achieved by a surface deposit of a reactive element oxide. (Yedong and Stott, 1996)

The effects of superficially applied CeO_2, mixed rare earth oxides, Co_3O_4, and Cr_2O_3 powders on the isothermal and cyclic oxidation of Ni-Cr alloys and the effects of CeO_2 and MgO powders on the isothermal oxidation of Fe-25wt.% Cr have been studied over the temperature range 940-1150°C in pure oxygen and dry air by Ecer et al (1982). They concluded that rates of oxidation of both the Ni-and Fe-base alloys were markedly reduced by the application of CeO_2 powder. The presence of CeO_2 also improved the scale adherence and resulted in marked changes in the oxidation morphology. The presence of Co_3O_4 or Cr_2O_3 powders on Ni-Cr alloys and MgO on Fe-Cr also produced changes in the oxidation morphology but did not decrease the rate of oxidation. These results are interpreted in terms of the influence of the oxide powders on the development of scale microstructure and their effectiveness in decreasing grain boundary transport.

Small alloy additions of rare-earth elements and other oxygen-active elements have been found to alter the oxidation resistance of Cr_2O_3-forming alloys. The effects of these additions usually include (i) formation of continuous Cr_2O_3 scales at low alloy Cr concentrations

(ii) reduction in the rate of Cr_2O_3 growth (iii) improved scale adhesion (iv) change in the primary growth mechanism of the oxide from outward cation migration to inward anion migration and (v) a reduction of the grain size in the Cr_2O_3 scale. Similar effects have also been observed when the oxygen-active elements are present as fine oxide dispersion in the alloys prior to oxidation.

The influence of Ce additions, which were the most effective in decreasing the scale growth rate and improving scale adherence, were proposed to be due to CeO_2 internal oxides serving as nucleation sites to produce a fine grained scale and Ce ions blocking grain boundary diffusion through the Cr_2O_3 scale.

Mitra et al (1993) studied the effect of superficially applied cerium-oxide coating on the isothermal oxidation behavior of AISI 304 stainless steel in dry air and analysed that the reactive oxide coating not only reduced the reaction rate but also facilitated scale adhesion to the alloy substrate.

Seal et al (1994) from their study of influence of superficially applied CeO_2 coatings on AISI-316,-321 and -304 reported that coating has remarkably decreased the reaction rates for all three grades of steel as well as facilitated scale adherence. Change in the scale-growth mechanism resulted in the presence of the coating from outward migration of cations to inward ingress of anions. Internal oxidation of Si was favoured and the internal-oxide stringers acted as pegs to provide better scale adhesion in the presence of superficially applied CeO_2 particles.

Seal et al (2001) further studied the beneficial effect of cerium oxide coating on the isothermal oxidation behaviour of 316, 321, 304 and 347 austenitic grade steels. Mechanically and electrolytically polished samples were coated with CeO_2 slurry and oxidation experiments were conducted in dry air in a vertically placed quartz tube at 1000^0C. It was observed by them that mechanically polished samples showed improved oxidation resistance as compared to electropolished samples.

This improvement has been attributed by them to the change in defect concentration within the material due to polishing conditions leading to enhanced diffusion through the distorted lattice structure as well as through grain boundaries to the alloy surface. According

to them XRD analysis of samples revealed the presence of simple, complex and mixed oxides (spinels) including Fe_2O_3, $NiCr_2O_4$, $FeCr_2O_4$, MoO_2, $NiFe_2O_4$, Fe-Ni-Cr spinels, $FeTiO_3$, TiO_2, Cr_2O_3, and $NiNb_2O_6$ for uncoated samples and CeO_2, Ce_2O_3, Fe_2O_3, $MnFe_xCr_{2-x}O_4$, $NiCr_2O_4$, $FeCr_2O_4$ and Fe_3O_4 for ceria coated samples. They concluded that in general, all grades of austenitic stainless steels receive protection against high temperature degradation due to the formation of a compact Cr_2O_3 healing layer which thickens slowly. The reduction in the rate of oxidation is due to the segregation of Ce^{3+} and Ce^{4+} ions at the oxide grain boundaries, causing hindrance to cation migration. This is attributed to the fine grained oxide layer formation that has taken place due to heterogeneous nucleation caused by the presence of a reactive–oxide particle. Other beneficial effects of ceria coating have been explained on the basis that scale adhesion may involve a reduction in compressive stress within the scale and enhancement in scale/substrate interface adhesion.

Similar beneficial effects of superficially applied CeO_2 coating on the high temperature oxidation behaviour of AISI 347 have been reported by Roy et al (1995). Reduced oxidation rate has been attributed to change over in rate controlling process from outward migration of cations to ingress of oxidant species by them.

Hou and Stringer (1987) studied the influence of surface–applied nitrate converted CaO, CeO_2, Y_2O_3, La_2O_3, HfO_2 and ZrO_2 on the oxidation behaviour of Co-15wt.% Cr, Co-25wt.% Cr and Ni-25wt.% Cr alloys at 1000 and 1100^0C in O_2 at 1atm. They found that none of the surface–applied oxides promoted Cr_2O_3 formation on the Co-15wt.% Cr alloy. Some (but not all) promoted Cr_2O_3 formation on Co-25wt%Cr at 1000^0C and this is ascribed to the surface–applied oxide acting as a physical barrier to O_2. Coated HfO_2 is seen to increase the rate but this effect decreased after longer periods of oxidation as observed with a 50h oxidation run. They reported that the rest of the surface–coated oxides reduced the oxidation rate to different degrees, with CaO being the most effective and Y_2O_3 and La_2O_3 better than CeO_2 and ZrO_2. Those surface coated Y_2O_3, La_2O_3 and CaO were found to be more resistant to spallation and it is noted that more beneficial surface coatings were those oxides that are

50
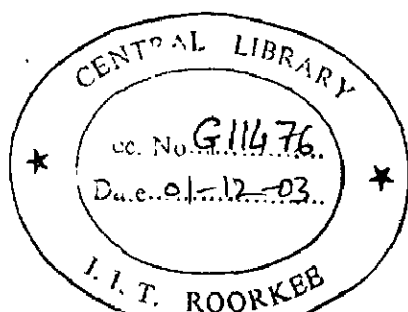
deposited with non-flaky morphologies. According to them the effects of the deposited oxides, whether CeO_2 or La_2O_3, strongly depended on the total amount of the deposition.

In case of Ni-25wt.% Cr alloy, CeO_2 is as effective as Y_2O_3 and La_2O_3. However, CaO with its usual morphology shows little beneficial effect. The surface deposited HfO_2 is again seen to increase the rate as well as the degree of spallation .The most effective applied oxides were those of yttrium, lanthanum and cerium, and the effectiveness is no longer dependent on the total coverage of the applied salt as for the Co-25wt.%Cr alloy. For Ni-25wt.%Cr alloy, some of the reactive oxides had a profound effect on the oxidation behaviour. The scale adhesion was greatly improved when the oxide growth direction was reversed and the growth rate of the oxide diminished.

Hou and Stringer (1987) concluded that reactive element oxides show no effect on the oxidation behaviour of non-Cr_2O_3 forming alloys. When the chromium concentration in the alloy is increased to a borderline Cr_2O_3 former, its oxidation behavior becomes sensitive to the ambient oxygen pressure. As a consequence, some of the applied coatings can act as a semiblocking layer and reduce the oxidation rate or even locally promote Cr_2O_3 formation. Surface applied CeO_2, Y_2O_3 and La_2O_3 were particularly very effective in reducing the growth rate of Cr_2O_3 scale and improving scale adhesion (Hou and Stringer, 1989). The extent of the beneficial effect greatly depends on the integrity of the applied oxide coatings. The most dense and continuous coatings seem to be the most effective.

Yedong and Stott (1994) studied the effects of surface-applied Y_2O_3, Al_2O_3 and Cr_2O_3 coatings or films on the selective oxidation of chromium in Ni-15Cr and Ni-10Cr in air at 1000^0C. They have observed that establishment of chromia scale can be promoted effectively by the presence of an Y_2O_3 film on Ni-15Cr and, at least locally on Ni-10Cr.Such a scale is only established locally and maintained for short periods on the two alloys in the presence of surface applied Al_2O_3 and Cr_2O_3 films. It subsequently breaks down and nickel oxide can then develop and grow. They concluded that the thin oxide films possibly influence the initial stages of oxidation in two ways, i.e. Al_2O_3 and Cr_2O_3 films act as diffusion barriers for oxygen, while all three films may provide preferential sites for oxide nucleation at the oxide film/alloy interface.

They suggested that a sintering process could be involved in the development of the oxide scale; this would be enhanced in the presence of a thin oxide film. It has been finally concluded by them that these effects result in a decrease in the critical amount of chromium required to form a selective chromia scale. They noticed that during subsequent oxidation, the thin oxide films are incorporated into the oxide scales on the alloys, where they may influence the transport mechanisms and stress conditions. In comparison with the cases of surface–deposited Al_2O_3 and Cr_2O_3 oxide films, the additional beneficial effect of the Y_2O_3 film in maintaining the selective oxidation of chromium is attributed to its ability to improve the oxide scale by affecting the transport mechanisms and stress conditions in the scale.

Yedong and Stott (1996) also studied the effects of thin surface applied Al_2O_3-Y_2O_3 composite films on the selective oxidation of chromium in Ni-10Cr in air at 1000^0C and they observed that an integral chromia scale was established on specimens coated with an Al_2O_3-Y_2O_3 film during oxidation for 100 hrs and the weight gains were almost two orders of magnitude lower than those of uncoated specimens.

Reduction in scaling rate and a noticeable change in oxide morphology has been reported by Strawbridge and Rapp (1994) during high temperature oxidation studies of pure nickel, iron, cobalt and copper coupons coated with thin superficial films ($100\text{-}500A^0$) of Ca, Sr or Ba .

2.14 REACTIONS OF CERAMIC OXIDES WITH VANADIUM COMPOUNDS

Jones, Williams and Jones (1986) have reported that the reactions of ceramic oxides with vanadium compounds are predominantly controlled by the Lux-Flood type of acid–base reactions and are explained in terms of the relative acid-base character of the oxides.

Lux-Flood acid-base, theory of molten salt/oxide reactions:-

Acid-base reactions of inorganic salts can be understood in terms of

$$Base \; = \; acid \; + \; O^{2-}$$

For example

$$SO_4^{2-} = SO_3^{2-} + O^{2-}$$

or equivalently

Na_2SO_4 (salt) = Na_2O (base) + SO_3 (acid)
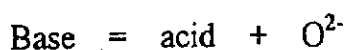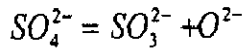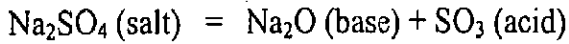
The various oxides all have a certain acid-base character and the more acidic oxide can displace less acidic oxide from combination with Na_2O. As it is commonly see in hot corrosion of superalloys containing Mo that MoO_3 formed by oxidation of Mo can displace SO_3 from sodium suplhate in the surface salt layer producing sodium molybdate.

$Na_2SO_4 + MoO_3 = Na_2MoO_4 + SO_3$
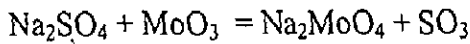
If the salt is sodium metavanadate the equation can be written as

$NaVO_3$ (salt) = Na_2O (base) + V_2O_5 (acid)
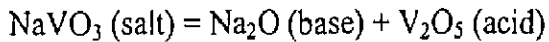
The oxide- vanadium compound reactions can be explained as follows:

Yttria is the most basic oxide and reacts with the acidic V_2O_5 component of $NaVO_3$ to form YVO_4, but it does not react with Na_3VO_4 where the V_2O_5 activity is lower, Ceria (less basic than Yttria) and Zirconia (in turn less basic than Ceria) do not react with Na_3VO_4 or $NaVO_3$ but still react with V_2O_5 to form $CeVO_4$ and ZrV_2O_7 (*Jones et al., 1986*).

Table 2.2: Reaction behaviour of ceramic oxides with vanadium compounds of increasing V_2O_5 activity showing products formed

	Na_3VO_4	$NaVO_3$	V_2O_5
Y_2O_3	NR	YVO_4	YVO_4
CeO_2	NR	NR	$CeVO_4$
ZrO_2	NR	NR	ZrV_2O_7 (but slowly)

Jones et al (1985 & 1986) have studied in detail the reactions of Vanadium Compounds with Y_2O_3, ZrO_2 & CeO_2 with Na_2SO_4 and without Na_2SO_4. These results are summarized in Table 2.3

Table 2.3   Reactions of ceramic oxides with vanadium compounds

Oxide	Conditions of Reaction	Reaction
Y_2O_3	1. Mixtures of 25 mole percent (m/o) Y_2O_3 in Na_3VO_4 heated at 850 (65h) and 900°C (24h).	No reaction
	2. 25 mol% Y_2O_3-$NaVO_3$ for only 4h at 700°C	YVO_4 formation
	3. ----Do---- Longer runs for up to 168h at 700°C	Confirmed YVO_4
	4. Mixtures of 50 m/o Y_2O_3 in V_2O_5 after 4h at 700°C.	Complete YVO_4 formation
CeO_2	1. 50 m/o CeO_2-Na_3VO_4 for 54h at 700°C	No reaction
	2. 35 m/o CeO_2- $NaVO_3$ for 92h at 700°C	No reaction
	3. 66m/o CeO_2 in V_2O_5 in 2h at 700°C,	$2CeO_2+V_2O_5 = 2CeVO_4 + 1/2\ O_2$
	4. 40 m/o CeO_2-20 m/o V_2O_5-40 m/o $NaVO_3$ heated for 24h at 700°C	$CeVO_4$ was formed
	5. 50 m/o CeO_2-25 m/o V_2O_5 -25 m/o Na_2SO_4 heated for 17h under air at 700°C	V_2O_5 reacted preferentially with CeO_2. Producing $CeVO_4$.
	6. 35 m/o CeO_2 in $NaVO_3$ and	Produced $CeVO_4$ in both cases:
	7. 20 m/o CeO_2-38 m/o $NaVO_3$-42 m/o Na_2SO_4 under 50$\pm$ 10 Pa of SO_3 in air at 700°C	$CeO_2 + NaVO_3$ (in Na_2SO_4) + SO_3 = $CeVO_4$
	*while CeO_2 and $NaVO_3$ do not react directly CeO_2 is converted to $CeVO_4$ if V_2O_5 is produced in the melt by the reaction of $NaVO_3$ and SO_3	
ZrO_2	1. 50 m/o ZrO_2-Na_3VO_4 and 35 m/o ZrO_2-$NaVO_3$ for more than 72h at 700°C	No evidence of ZrO_2 reaction.
	2. ZrO_2 with $NaVO_3$ or Na_3VO_4, at temperatures up to 950°C.	No reaction
	3. 50 m/o ZrO_2-V_2O_5 at 700°C, after 47h heating,	ZrV_2O_7 plus residual ZrO_2 and V_2O_5 being detected
	4. -------do----- after 168h of heating	Only ZrV_2O_7 (indicating complete conversion) being detected
	5. Heating of 35 m/o ZrO_2 in $NaVO_3$ for 93h under 110 $\pm$ 20 Pa of SO_3 in air	No discernible reaction of the ZrO_2.
	*These results suggest that ZrO_2 itself should be relatively resistant to degradation by Na, S and V contaminants in gas turbines.	(Because sufficient V_2O_5 activity to allow ZrO_2 reaction was not generated in the melt) $ZrO_2 + NaVO_3 + SO_3$ = No reaction

54

CHAPTER 3

FORMULATION OF THE PROBLEM

SCOPE

Hot corrosion can occur at high temperatures where the deposit is in the liquid state right from the beginning; or the solid deposit turns into liquid during the exposure as a result of reaction with the environment. The role of the liquid salt is to dissolve the protective oxide scale by the acid or the basic fluxing mechanism of the salt. The corrosion problem is more acute when the vanadium pentaoxide containing ash deposits on the metal surface is in molten condition which acts as a catalyst.

Power plants are one of the major industries suffering from severe corrosion problems resulting in the substantial losses. The problem is becoming more prominent as the plants are getting older. A survey around the globe confirmed that corrosion is responsible for losses amounting to approximately 5% of GDP of any nation. In a typical process plant, it has been reported across all industries that more than 55% of unscheduled downtime is directly attributed to the effects of corrosion. These are huge penalties for inadequate control, yet it has been notable that despite the efforts of scientists, researchers and engineers for past forty years, there has been little discernible improvement in overall corrosion prevention.

National Thermal Power Corporation (NTPC), India with an installed capacity of 17735 MW constitutes almost 19% of the total installed capacity of around 101,000 MW of this country (Bhaskaran, 2001). NTPC operates 19 coal and gas based power plants and uses mainly fossil fuels namely pulverized coal, natural gas /Naptha and HSD to operate

its plants. Gas based stations are combined cycle plants with gas turbines and steam turbine operated through waste heat recovery boilers.

Indian coals have high ash content. The corrosivity of coal is usually attributed to the non-silicate fraction of ash. Very little is known about the corrosive nature of Indian coals. Degradation in gas turbines has been a strong motivation for the continuous interest in sulphate induced hot corrosion over a period of more than thirty years (Sharma, 1996).

A new dawn is heralded in corrosion control technology; however the combination of modern sensor technologies, real time data acquisition and appraisal and low cost computer power at least enables meaningful measures to be taken in the battle to control corrosion. The traditional skills of material selection, inspection of coatings, cathodic protection and inhibitor treatment are still in demand.

Some investigations have been carried out on the hot corrosion of stainless steels, Fe-, Ni- and Co- base superalloys by V_2O_5, Na_2SO_4, Na_2SO_4-V_2O_5, Na_2SO_4-$NaVO_3$ mixtures. Most of the studies have been made in isothermal conditions. Relatively fewer studies are reported under actual working conditions, which actually simulate the working condition of boilers and gas turbines. In cyclic condition, high thermal stresses are developed but during cooling, the scale cracking takes place and fresh areas are exposed to corrosion. Cyclic hot corrosion studies have been made either with the help of a burner rig test or by using laboratory tube furnaces usually in the temperature range 600-1000^{0}C. Levy et al (1989) have concluded from their hot corrosion studies on Ni- base alloys that tube furnace tests can be used in place of burner rig tests to rank alloys, provided the tests are accompanied by detailed metallographic examination of the exposed specimen.

Modifying the physical or the chemical characteristic of the deposit by adding various substances has been tried since corrosion and deposits first became a problem. These additives may be incorporated in the fuel, injected into the combustor, sprayed onto heat-receiving surfaces or mixed with the products of combustion.

Use of additives is still not wide spread. It has been tried earlier as means of counteracting air pollution by removing SO_2 from the stack gases. Later on inhibitors and

fuel additives have been used with varying success to prevent oil ash corrosion (Paul and Seeley, 1991).

Recently the effects of thin surface-applied coatings of CeO_2, Y_2O_3, Al_2O_3 and Cr_2O_3 on the selective oxidation of chromium in Ni-15 Cr and Ni-10Cr in air at 1000^0C have been studied. It was shown that the establishment of a chromia scale can be promoted effectively by the presence of Y_2O_3 film on Ni-15Cr and, at least locally on Ni-10Cr. Such a scale was only established locally and maintained for short periods on the two alloys in the presence of surface-applied Al_2O_3 & Cr_2O_3 films. Thus it has been suggested that thin surface applied films have similar effects as oxide dispersions on the selective oxidation of alloys (Yedong and Stott, 1996).

AIM

In view of the fact that further investigations on the role of inhibitors and the effects of surface applied oxides on the hot corrosion of superalloys are needed, it was proposed to study the hot corrosion behaviour of some Fe-, Ni- and Co-base superalloys containing high chromium (15.5-23%) in one of the most aggressive environment i.e. Na_2SO_4-60%V_2O_5 (eutectic mixture with m.p. 550^0C) under cyclic conditions to simulate actual working environment of the plant. As it is learnt from literature that MgO, $MgSO_4$, CaO, MnO_2, Cr_2O_3, ZrO_2, Y_2O_3, In_2O_3, SnO_2, Al_2O_3, ZnO, BaO, PbO, SiO_2 etc. can be useful as inhibitors of hot corrosion and also the surface applied coating of CeO_2, Y_2O_3, Al_2O_3 and Cr_2O_3 are very beneficial in improving the oxidation resistance of stainless steels, Fe-, Ni- and Co-base alloys. So it has been proposed to study the effects of such oxides as MgO, CaO, MnO_2 and $ZnSO_4$ mixed with Na_2SO_4-60%V_2O_5 under cyclic conditions at 900^0C for maximum 50 cycles. The effect of other oxides like CeO_2, Y_2O_3, SnO_2 and ZrO_2 have been studied by pre-coating the alloy surface with these oxides (1-2mg/cm^2) and then exposing coated sample to Na_2SO_4-60%V_2O_5 at 900^0C for 50 cycles. It

is recommended in literature that $1mg/cm^2$ Na_2SO_4 is sufficient to undergo severe attack, therefore $3-5mg/cm^2$ of salt mixture was chosen in the form of thin applied film to create an aggressive environment.

It was also proposed to measure the weight change to study the corrosion kinetics and to use X-ray Diffraction (XRD), Scanning Electron Microscopy (SEM), Energy Dispersive X-ray Analysis (EDAX) and Electron Microprobe Analysis (EPMA) to characterize the corrosion products and to make an attempt to understand the effect of oxides in inhibiting the hot corrosion phenomenon.

CHAPTER 4

EXPERIMENTAL TECHNIQUES AND PROCEDURES

4.1 MATERIALS

High chromium (15.5-23.05%) containing Fe-, Ni- and Co-base superalloys namely Superfer 800H, Superco 605, Superni 75, Superni 718 and Superni 601 were procured from Mishra Dhatu Nigham Ltd. (MIDHANI), Hyderabad (India) for the present investigation. The alloys were in the rolled condition with varying thickness (1.4-4.0 mm). For convenience these alloys are marked as A, B, C, D and E respectively. Their chemical composition and other details are given in Table 4.1.

4.2 SPECIMEN PREPARATION AND COATING

The alloy sheets were cut into rectangular samples of size15mm x 20mm. The specimens were polished using silicon carbide papers upto 1200 grit and finally wheel polished with alumina powder (1μm). They were then washed with distilled water and cleaned with acetone. Their surface area was measured and weights were determined using an electronic balance to an accuracy of 0.01mg.

4.2.1 Coating of Samples

The samples were heated in the oven upto 250^0C and the salt mixture of Na_2SO_4-60% V_2O_5, Na_2SO_4-60%V_2O_5+MgO using MgO:V_2O_5 in the ratio of 3:1, Na_2SO_4-60%V_2O_5 +CaO (20wt.%), Na_2SO_4-60%V_2O_5+MnO_2 (20wt.%) and Na_2SO_4-60%V_2O_5+$ZnSO_4$ (10wt.%) were coated on the warm polished samples with a camel hair brush. The amount of the salt coating

varying from 3.0 -5.0 mg/cm^2, the coated samples were then dried (~110^{0}C) for 2 hours in the oven. The coatings of CeO$_2$, Y$_2$O$_3$, SnO$_2$ and ZrO$_2$ were applied in different manner. The samples were first coated with a thin layer of these oxides mixed in distilled water (1-2 mg/cm^2) and heated in the furnace at 900^{0}C for 8 hours to improve upon the adherence of the coating. A thin layer of Na$_2$SO$_4$-60%V$_2$O$_5$ was then applied on these coated warm samples, total amount of the coating ranging up to 5-6 mg/cm^2. These samples were also dried in the oven for 2-3 hours and then weighed. All these coated samples were subjected to cyclic heating.

4.3 HOT CORROSION STUDIES

The coated samples were kept in alumina boats and then transferred into the hot zone of a Silicon Carbide Horizontal Tube Furnace closed at both ends. A constant temperature was maintained at 900^{0}C with an accuracy of ±5^{0}C in air under cyclic conditions for maximum up-to-50 cycles (Each cycle of 1 hour heating and 20 minutes cooling). After each cycle the weight of the specimen was measured to obtain weight change value. Details of coatings and conditions of exposure are given in Table 4.2

4.4 INVESTIGATION OF CORROSION PRODUCTS

4.4.1 Thermogravimetric Studies

The weight change values were plotted with respect to number of cycles. The plots depict the effect of temperature and the salt mixture on the corrosion rate. The nature of the curves shows that in most of the cases a rapid rate of corrosion occurred during the first two cycles and then the rate decreased. In many cases spalling and scaling occurred and the scale could not be collected and incorporated in the weight change, due to which the weight has decreased with intermittent increase owing to further oxidation taking place.

4.4.2 Visual Observation

Visual examination was made after each cycle for their colour, lustre, adherence, spalling tendency and presence/absence of the unreacted salt etc. after heating of the samples is completed under cyclic conditions. The corroded specimens were visually examined and then their macrographs were taken.

4.4.3 Measurement of the Scale Thickness

Average scale thickness values of the specimens after exposure at 900^0C have been estimated from the BSE images of the well polished cross-section of the samples using Robinson Back Scattered Detector (RBSD) attached with Scanning Electron Microscope (LEO 430VP).

4.4.4 X-ray Diffractometry

For identification of the different phases formed during hot corrosion studies, X-ray diffractometry was carried out using Diffractometer PW1140/90 Phillips with copper target and nickel filter at a voltage of 35kV and a current of 15mA. The samples were scanned in the range (2θ), 20 to100 degree and recorded at a chart speed of 1 cm/min and the Goniometer speed 1^0/min. In most of the cases the scanning speed was kept at 1kcs (Kilo cycles per second) and in only few cases 2 Kcs. Diffractograms were analysed by adopting the following procedure:

1. d' values were calculated for all the prominent peaks in the usual manner using Bragg's law $2d\sin\theta = n\lambda$. Where, λ is the wave length of CuK_α radiation used for the diffraction and is taken as 1.54 Å. These calculated 'd' values are then used for identification of phases.

2. Assuming the height of the most prominent peak as 100%, the relative intensities were calculated for all the peaks.

3. The data so obtained was compared with ASTM data cards following the standard procedure for search and identification.

4. Finally the XRD profiles were drawn.

4.4.5 Scanning Electron Microscopy

Surfaces of the exposed specimens were examined using Scanning Electron Microscope LEO 435VP. Photographs have been taken at 640X mainly and at higher magnification in few cases to understand the nature of the scale formed.

4.4.6 EDAX Analysis

Point analysis was done of selected areas of the interest present in the scale formed on the alloy surface for 8 samples with an EDAX of Oxford make-model 6841 attached to Scanning Electron Microscope, JEOL (JSM-5800).

Point analysis along the cross-section through the oxide scale developed during exposure was done at IUC (Inter University Consortium for BARC), Indore using EDAX attachment, "Flex Scan 520" of Oxford Instruments with SEM (JEOL make) for 14 samples.

4.4.7 Electron Microprobe Analysis

Exposed samples were cut with the help of the diamond cutting wheel to examine the cross-section and these were mounted and polished for the EPMA analysis. This particular analysis has been conducted at three different places, few samples were analysed at DMRL (Defence Metallurgical Research Laboratory), Hyderabad using model JEOL 8600 and some samples at IGCAR, Kalpakkam with the help of Cameca–Micro Box. Fig. A.2 to A.8, present the EPMA analysis done at Kalpakkam. Rest of the samples have been analysed at IIC (Institute Instrumentation Centre), Indian Institute of Technology, Roorkee, again using the model JXA-8600M microprobe. The mounted samples were carbon coated before performing the EPMA analysis. The elements selected for X-ray mapping were as per the composition of base sample, type of coating and environment of study. X-ray maps showing the distribution of the elements (Ni, Fe, Cr, Co, Ti, S, V, Na and the coating element e.g Mg, Mn, Ca, Ce, Zr, Sn, Y, Zn and oxygen in few cases) have been taken using accelerated voltage of 15-20 KV.

Table 4.1: Nominal Composition of the Alloys Used

Alloy Nomen-clature	Alloy Midhani Grade (similar grade)	Chemical Composition (wt.%)												
		Fe	Ni	Co	Cr	Ti	Al	Mo	W	Mn	Si	Cu	Ta	C
A	Superfer 800H (Incoloy 800H)	Bal	32	-	21	0.3	0.3	-	-	1.5	1.0	-	-	0.1
B	Superco 605 (KC20WN/L 605)	3.0	10.0	Bal	20.0	-	-	-	15.0	1.5	0.3	-	-	0.08
C	Superni 75 (Nimonic 75)	3.0	Bal	-	19.5	0.3	-	-	-	-	-	-	-	0.1
D	Superni 718 (Inconel 718)	18.5	Bal	-	19.0	0.9	0.5	3.05	-	0.18	0.18	0.15	5.13	0.04
E	Superni 601 (Inconel 601)	Bal	62.6	-	23.05	-	1.4	-	-	0.1	0.37	0.1	-	0.025

Table 4.2: Environmental conditions of Hot Corrosion Studies

Condition of Test	Salt Mixture	Temperature(^{0}C)	Period of Tests	Environment
Cyclic (All Superalloys A, B, C, D & E mentioned in Table 4.1)	1. Na_2SO_4-60%V_2O_5 2. Na_2SO_4-60%V_2O_5+MgO (using MgO:V_2O_5 in the ratio of 3:1) 3. Na_2SO_4-60%V_2O_5+CaO (20wt.%) 4. Na_2SO_4-60%V_2O_5+MnO$_2$ (20wt.%) 5. Na_2SO_4-60%V_2O_5+ZnSO$_4$ (10wt.%) 6. Coated with CeO$_2$ & Na_2SO_4-60%V_2O_5 7. Coated with Y$_2$O$_3$ & Na_2SO_4-60%V_2O_5 8. Coated with SnO$_2$ & Na_2SO_4-60%V_2O_5 9. Coated with ZrO$_2$ & Na_2SO_4-60%V_2O_5	900^{0}C	Maximum 50 cycles (1 hr. heating, 20 min. cooling)	Air

CHAPTER 5

RESULTS

In this chapter the results of present investigation i.e behaviour of the given superalloys in Na_2SO_4-60%V_2O_5 environment under cyclic condition at 900^0C have been compiled. It is followed by the results obtained with incorporation of inhibitors like MgO, CaO, MnO_2 and $ZnSO_4$ by mixing with Na_2SO_4-60%V_2O_5 and superficially applied inhibitor oxides namely CeO_2, Y_2O_3, SnO_2 and ZrO_2 in Na_2SO_4-60% V_2O_5 environment at 900^0C under cyclic condition. The results have been reported in sub chapters and summarized for each individual alloy in Table A.31.

5.1 HOT CORROSION STUDIES IN Na_2SO_4-60%V_2O_5

5.1.1 Visual Observations

The samples were observed critically after every cycle for change in colour, luster, presence/absence of the salt on the surface of sample as well as and scaling and spalling tendency. Fig. A.1 shows the macrographs of the specimens of alloys A, B, C, D and E in Na_2SO_4- 60% V_2O_5 environment.

In case of alloy A, the scale was dull grey but adherent in the initial cycles. Loose scale was observed at few places on the surface after 5th cycle but there was no spalling. Little spalling started after 12th cycle and the colour of the scale changed to dark black. Loose and fragile scale was noticed on one corner after 17th cycle, which got separated in the subsequent experimentation. After 50 cycles the scale was shinning black in appearance.

For alloy B, the colour of the sample changed from dark brown to dark grey in the first two cycles. Fresh scale formation and spalling was observed throughout the experimentation. After 50 cycles the scale was dull grey with black patches on the surface.

For alloy C, colour of the sample changed to steel grey in the first cycle. The coating was compact and adherent upto 12 cycles with gradual increase in weight gain when suddenly spalling occurred. After spalling of the scale, the colour of the sample was black. In case of alloy D, a trend similar to alloy C was being followed, colour of the sample changed from reddish yellow to black, the scale formed was loose and had spalling tendency. In case of alloy E, the scale was dark black but adherent in nature. Very little spalling of black particles was observed.

5.1.2 Kinetic Data

The plots of weight change (expressed in mg/cm^2) as a function of time (expressed in number of cycles) for the Fe-base alloy A (Superfer 800H), Co-base alloy B (Superco 605) and Ni-base alloys C (Superni 75), D (Superni 718) & E (Superni 601) respectively in Na_2SO_4-60%V_2O_5 environment at 900^0C in air for maximum upto 50 cycles are shown along with the plots drawn for inhibitors used in the study like MgO, CaO, MnO_2, $ZnSO_4$, CeO_2 SnO_2, Y_2O_3 & ZrO_2. The tests have been confined to maximum 50 cycles, as beyond this it was difficult to carry out the experiment due to extensive spalling and sputtering. The plot for alloy A shows a rapid increase in weight gain during the first few cycles and then there is a negligible change. The plot for alloy B also shows a rapid increase in weight gain during the first two cycles and then rate of weight gain increases gradually till the 20th cycle but there is hardly any weight gain after that. Spalling was noticed during experimentation. The amount of the spalled scale has been incorporated in weight gain measurements to the extent possible.

In case of alloy C, the plot shows a gradual increase in weight gain during initial 10 cycles after which it is constant with some decrease in weight during the last few cycles. For alloy D there is a gradual increase in rate of weight gain upto 15 cycles after that only slight increase in weight is observed. But in case of alloy E, there is a continuous but gradual

increase in weight gain. The weight gain in case of alloys A, B, C, D & E is 9.5, 22, 7.4, 9.4 and 8 mg/cm^2 after exposure for 50 cycles.

5.1.3. X-ray Diffraction Analysis

The XRD of the corroded alloys A, B, C, D & E are compiled in Tables A.1, A.2 and A.3. The prominent phases identified in the alloy A are α-Fe$_2$O$_3$, Cr$_2$O$_3$, NiCr$_2$O$_4$, NiFe$_2$O$_4$ and FeV$_2$O$_4$ and in the scales of alloy B are Cr$_2$O$_3$, NiWO$_4$, Co$_3$O$_4$, NiO, CoCr$_2$O$_4$, NiCo$_2$O$_4$ & Co$_3$V$_2$O$_8$. In nickel base alloy C, the main phases identified are Ni(VO$_3$)$_2$, NiO, Cr$_2$O$_3$ & NiCr$_2$O$_4$, in alloy D are NiCr$_2$O$_4$, Cr$_2$O$_3$, NiO, Ni(VO$_3$)$_2$, NiCr$_2$O$_4$, α-Fe$_2$O$_3$ & FeV$_2$O$_4$ and in case of alloy E the main peaks of Ni(VO$_3$)$_2$, NiO, NiCr$_2$O$_4$ and FeV$_2$O$_4$ were identified. Other possible phases present in Ni-base alloy E are α-Fe$_2$O$_3$, FeS, (Cr,Fe)$_2$O$_3$, and NiFe$_2$O$_4$. The X-ray diffraction profiles are given in Fig.5.1, 5.2 & 5.3.

5.1.4. Scale Thickness Measurements

Scale thickness values after exposure to Na$_2$SO$_4$-60%V$_2$O$_5$ environment at 900^{0}C in air for maximum upto 50 cycles have been measured from the back scattered images for alloys A, B, C, D & E as shown in Fig. 5.4 The scale is having maximum thickness in case of alloy B and minimum in alloy C, the values measured are 62.5, 78, 38.5, 57.5 and 52 µm respectively.

5.1.5. SEM, EDAX and EPMA Results

SEM micrographs for the alloys A, B, C, D & E in Na$_2$SO$_4$-60%V$_2$O$_5$ without any additive are shown in Fig. 5.5. In case of alloys A, B, C & D, the scale appears to have fallen off leaving cavities on the surface. In case of alloy D there is also crystalline growth on the top surface. Micrograph of alloy E indicates fine grain dense scale with longitudinal cracks on the scale.

The X-ray maps of alloy A after exposure in Na$_2$SO$_4$-60%V$_2$O$_5$ shown in Fig. 5.6 indicate formation of a thick scale. Top layer of the scale is rich in Ni and Fe while the inner layer is mainly chromium. A nickel rich continuous layer depleted of iron is present at the scale/substrate

interface. No internal oxidation has been observed but horizontal cracks are visible in the scale. X-ray maps of alloy B, shown in Fig. 5.7 reveal the formation of a thick multilayer scale. Outer scale rich in Fe and Ni contains Co and Cr also. A thick scale having W follows it, containing Fe and Cr. But the areas rich in W are depleted of Cr. Vanadium is distributed throughout the scale. Higher concentration of S is indicated just above the substrate where Mn is also present in higher concentration indicating MnS formation, just below a tungsten rich scale.

EPMA for alloy C, Fig.5.8 indicates medium size scale which mainly contains a Cr-rich scale just above the substrate. In this scale, Ni and Fe are also occurring with Cr. V is present through out the scale indicating formation of various vanadates. Ti is present as a thin irregular layer just above the substrate where Fe and Ni are absent. S is indicated in the top layer.

Whereas in case of alloy D, Fig 5.9, the outer scale is rich in oxides of V, Cr, Fe, and Ni but the inner layer is mainly Cr_2O_3 and a thin layer of NiO is present at the interface between the scale and the substrate.

EPMA micrograph Fig.5.10, for alloy E indicates thick scale containing Fe, Cr and Ni distributed throughout the scale. Top scale is rich in Fe and middle scale contains more of Cr. The inner layer is rich in Ni and is depleted of Fe and Cr. Ni is also concentrated at few spots in the scale. V is present throughout the scale but more near the substrate and formation of Ni-vanadate is obvious from the X-ray maps for Ni and V as they are coexisting in the scale and near the substrate. The S is present in the substrate and the scale along with Mn indicating the formation of MnS. Internal sulphidation is thus indicated.
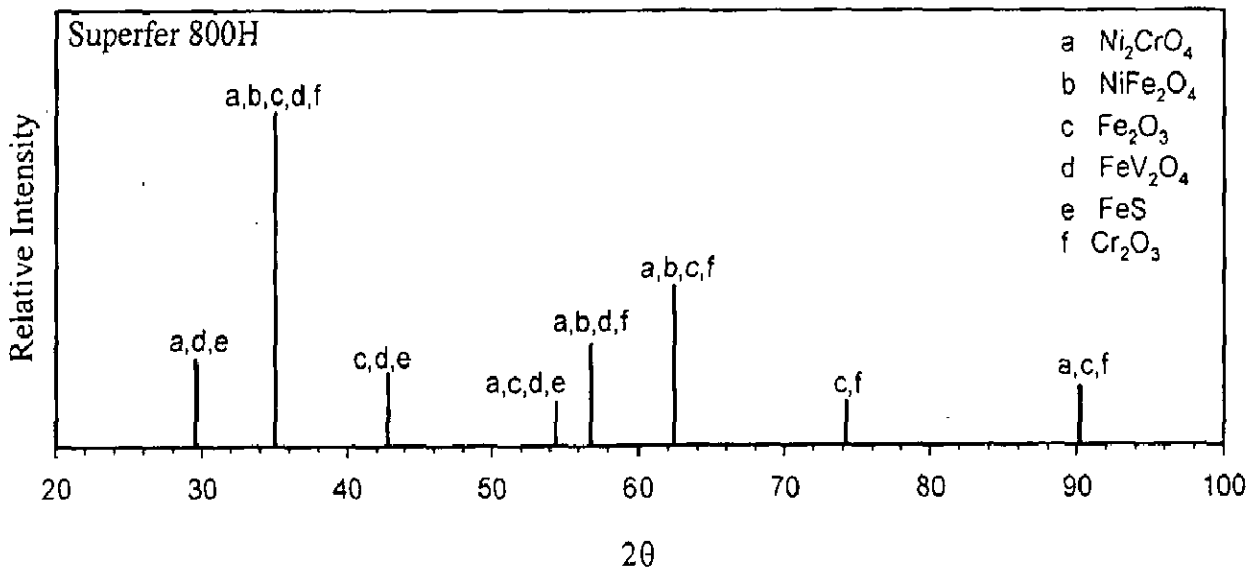
Fig. 5.1: X-ray diffraction profile for alloy A (Superfer 800H) after cyclic hot corrosion at 900^0C in Na_2SO_4-60% V_2O_5.
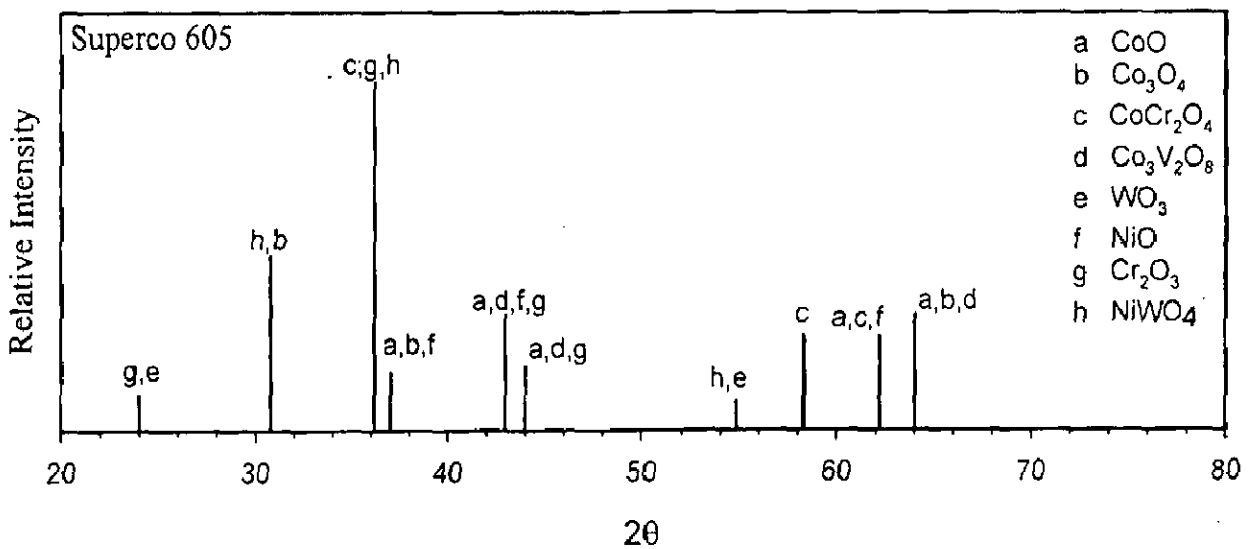
Fig. 5.2: X-ray diffraction profile for alloy B (Superco 605) after cyclic hot Corrosion at 900^0C in Na_2SO_4-60% V_2O_5.
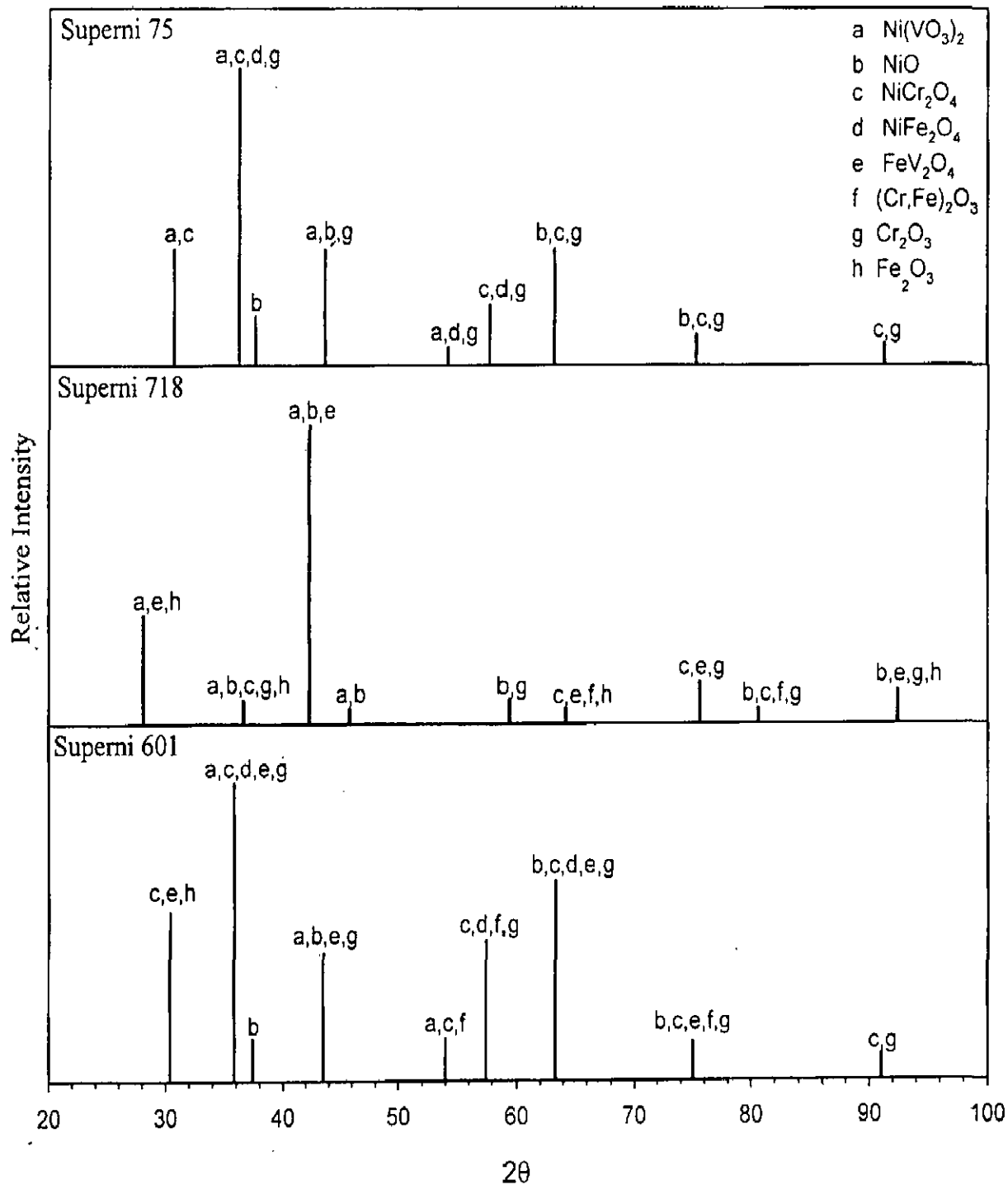
Fig. 5.3: X-ray diffraction profile for the nickel base alloys: alloy C (Superni 75), alloy D (Superni 718) and alloy E (Superni 601) after cyclic hot corrosion at 900°C in Na_2SO_4-60% V_2O_5

Fig . 5.4 :   BSE images of alloy A (Superfer 800H), alloy B (Superco 605), alloy C (Superni 75), alloy D (Superni 718) and alloy E (Superni 601) in Na_2SO_4-60%V_2O_5 environment after exposure at 900^{0}C in cyclic conditions.

71
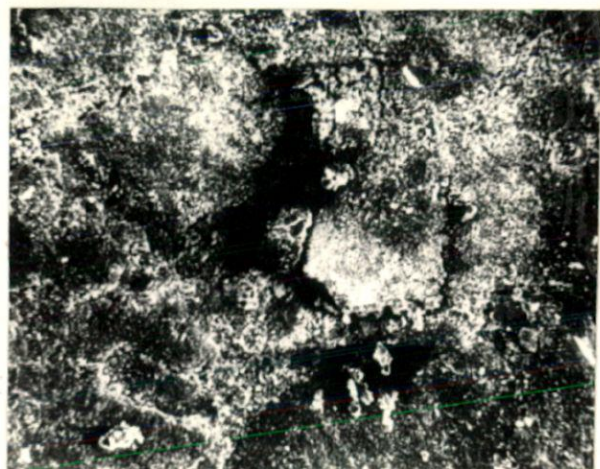
(a)
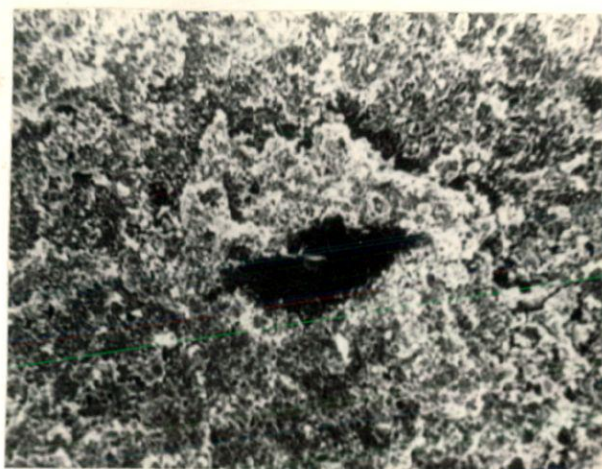
(b)

(c)

(d)

(e)

Fig. 5.5: Scanning Electron Micrographs after cyclic hot corrosion in Na_2SO_4-60%V_2O_5 of alloys:

a) Alloy A (Superfer 800H)   (X 640)
b) Alloy B (Superco 605)   (X 640)
c) Alloy C (Superni 75)   (X 640)
d) Alloy D (Superni 718)   (X 640)
e) Alloy E (Superni 601)   (X 640)
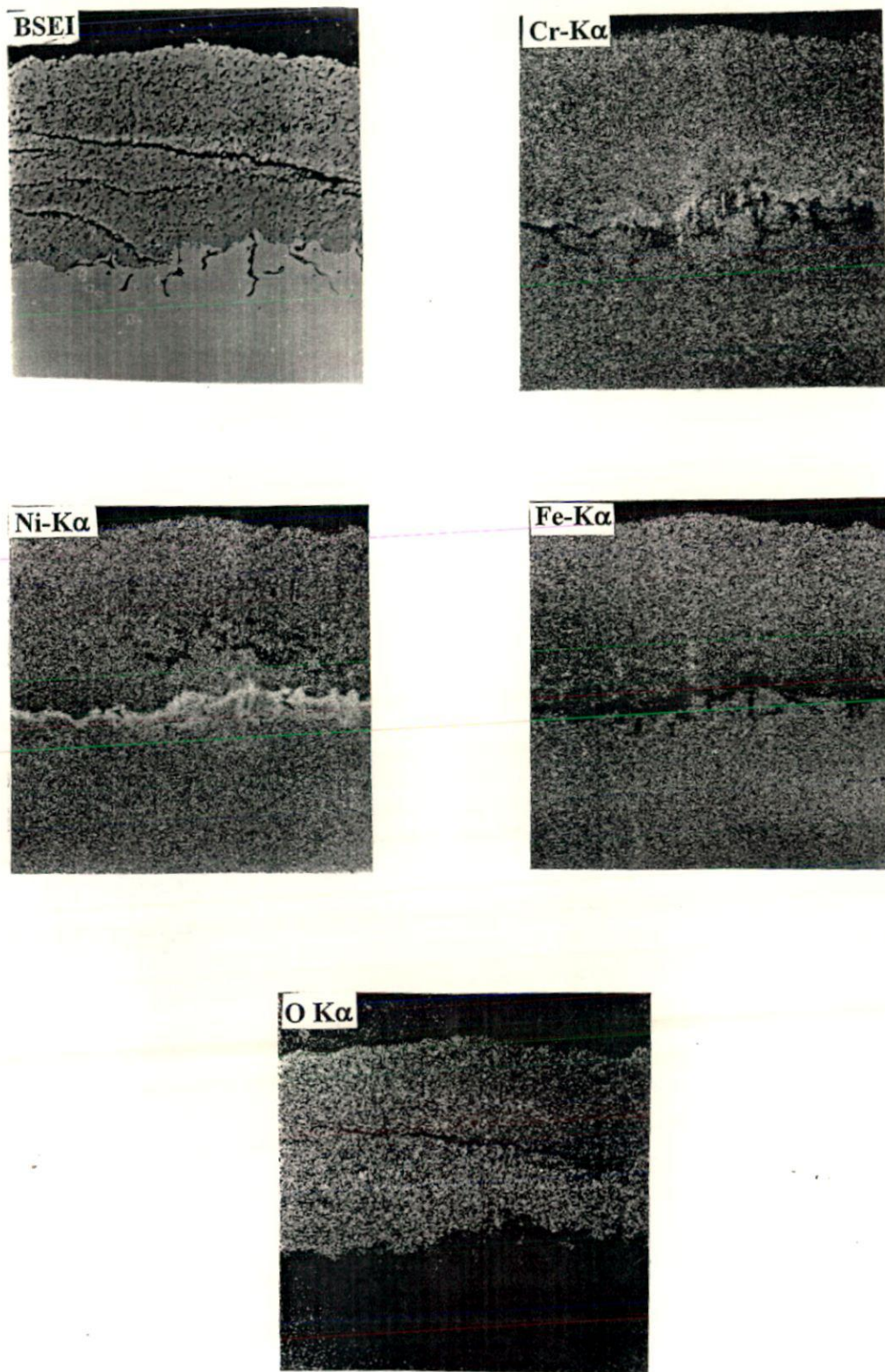
Fig. 5.6: BSEI and X-ray mapping of the cross section of alloy A (Superfer 800H) after cyclic hot corrosion at 900^0C in Na_2SO_4-60%V_2O_5.   (X 400)

Fig. 5.7:   BSEI and X-ray mapping of the cross section of alloy B (Superco 605) after cyclic hot corrosion at 900^0C in Na_2SO_4-60% V_2O_5.   (X 400)

Fig. 5.8: BSEI and X-ray mapping of the cross section of alloy C (Superni 75) after cyclic hot corrosion at 900^0C in Na_2SO_4-60% V_2O_5. (X 600)
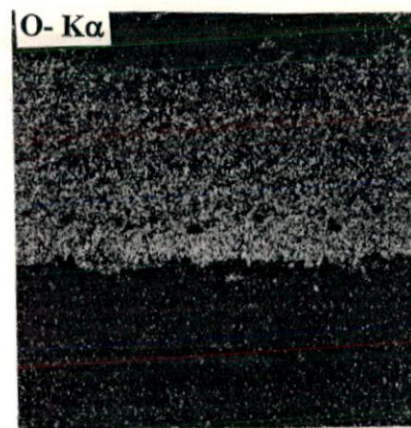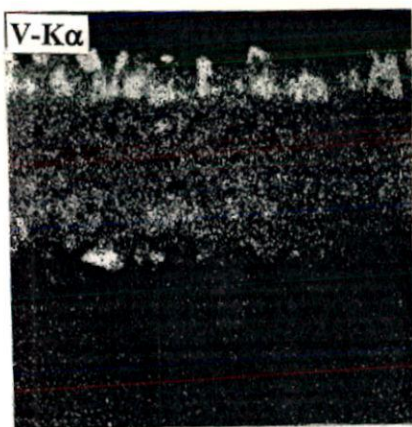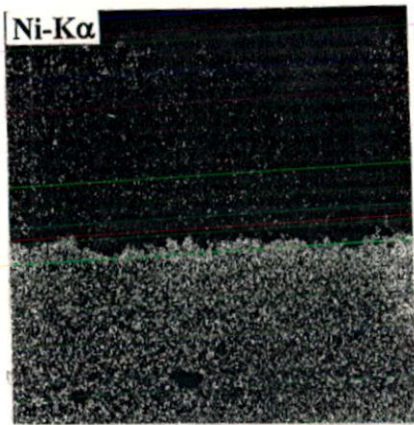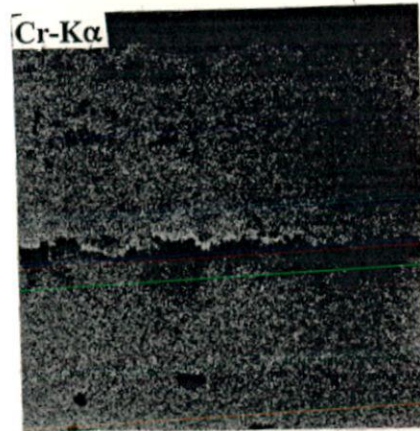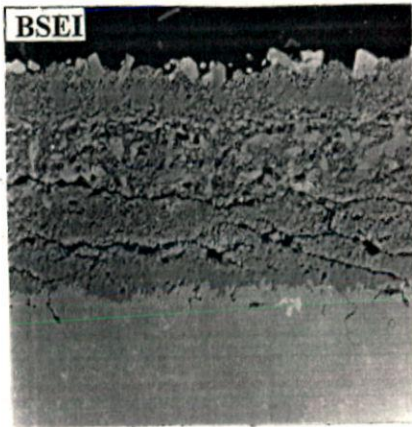
Fig. 5.9: BSEI and X-ray mapping of the cross section of alloy D (Superni 718) after cyclic hot corrosion at 900^0C in Na_2SO_4-60% V_2O_5. (X 400)
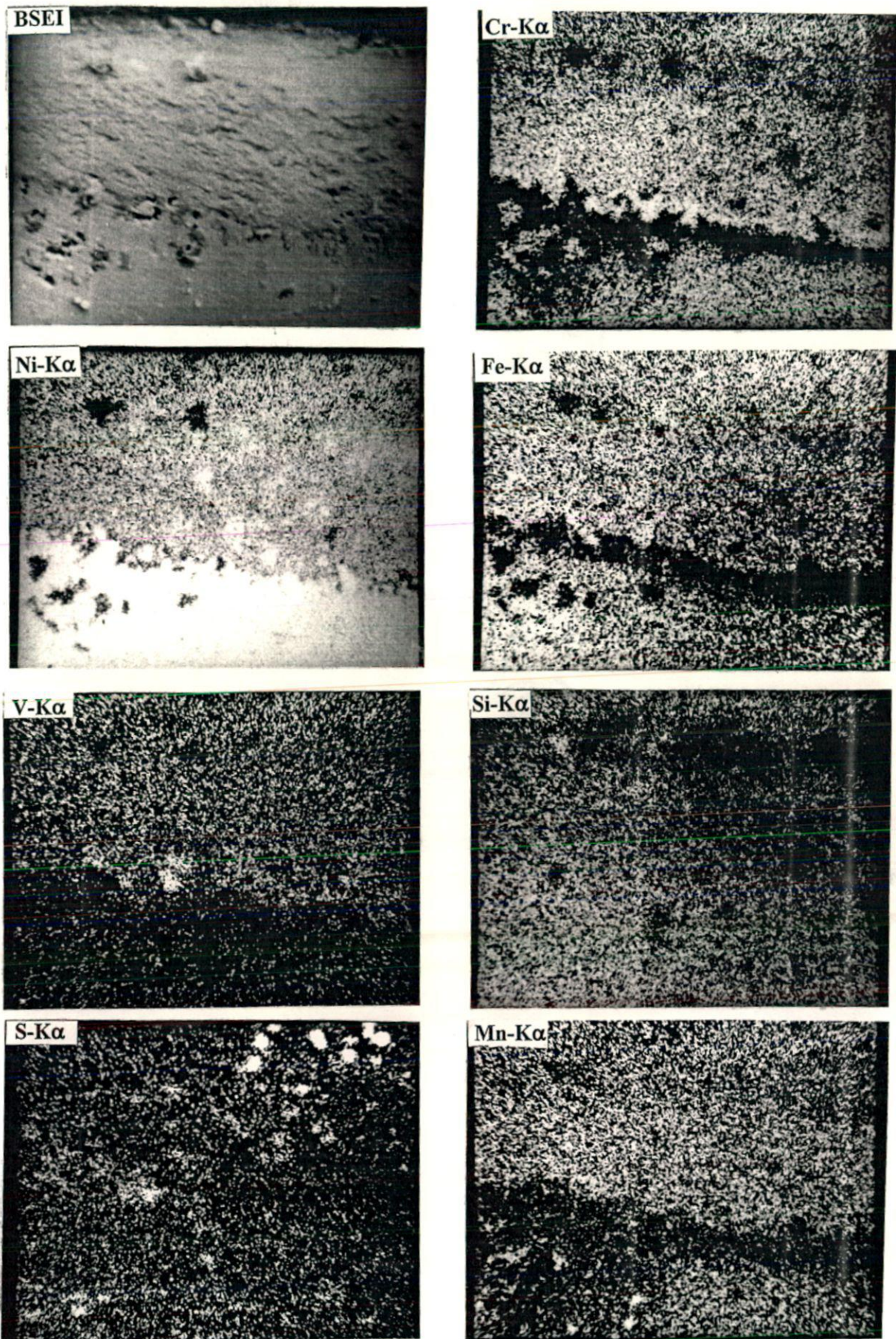
Fig. 5.10: BSEI and X-ray mapping of the cross section of alloy E (Superni 601) after cyclic hot corrosion at 900^0C in Na_2SO_4-60% V_2O_5. (X 600)

5.2 HOT CORROSION STUDIES IN Na_2SO_4-60%V_2O_5+MgO

5.2.1 Visual Observations

Macrographs for corroded specimens of alloys A, B, C, D & E after exposure for 50 cycles at 900^0C with Na_2SO_4-60% V_2O_5+ MgO coating in air are shown in Fig. A.1. The scale on the alloy A showed shinning black, yellow and lustrous mass. Spalling was observed after 25 cycles, loose non-adherent scale on the surface was visible after 31 cycles but this scale spalled off after 40 cycles so experimentation was stopped in this case assuming no salt for further reaction is present on the surface of the sample. Scale of the alloy B showed grey, black mass, spalling was noticed after 14 cycles. The scale of the alloy C showed black, yellowish mass, which looked adherent and compact and the scale for alloy D showed grey, reddish yellow and brown colored mass. Macrograph also indicates the regions where spalling occurred and fresh areas were exposed. In case of alloy E also the scale is brownish and black in appearance. The surface was rough and little spalling was noticed after 10 cycles.

5.2.2 Kinetic Data

Fig. 5.11, 5.12 and 5.13 show the plots drawn between weight change and time (number of cycles) for the alloys A, B, C, D & E. In these plots comparison is shown between wt. gain values obtained for these alloys with and without MgO. For alloy A, Fig. 5.11 thermogravemetric data is shown only up to 40 cycles as the scale was spalling off. From these plots it is evident that the corrosion is more in the case of Na_2SO_4-60%V_2O_5 and it has reduced considerably in the presence of MgO. Weight decrease is nearly 50% with MgO addition upto 30 cycles. Fig. 5.12, for alloy B shows an increase in weight gain up to 20 cycles and then the rate of weight gain decreases and this decrease may be attributed to thermal stresses induced spalling. The total wt. gain value decreases from 22 mg/cm^2 to 3.43 mg/cm^2 after 50 cycles indicating massive spalling & possible volatilization of reaction products.

Weight change plots shown in Fig. 5.13 for nickel base alloys C, D and E, a rapid increase in weight gain is indicated for alloy C during first 2 cycles after which rate of weight

gain is linear and the weight gain value is reduced from 7.61 mg/cm^2 to 4.86 mg/cm^2 with MgO after 50 cycles. Alloy D also shows a similar trend of rapid increase in weight gain during the first 2 cycles and then rate of weight gain is very slow but gradual increase is indicated. The total weight gain value decreases from 9.4 mg/cm^2 to 5.9 mg/cm^2. Plot for alloy E also shows a rapid increase in weight gain during the initial few cycles and then the rate of weight gain is nearly constant upto 30 cycles, which further increased gradually. But the total weight gain value decreased by nearly 35% in the presence of MgO after 50 cycles.

5.2.3 X-Ray Diffraction Analysis

The results of XRD analysis of the samples are presented in Tables A.4, A.5 and A.6 and XRD profiles shown in Fig. 5.14, 5.15 and 5.16. The main phases identified in the scale of alloy A were Fe_2O_3, FeS, Cr_2O_3, FeV_2O_4, $Mg_3V_2O_8$, and $NiCr_2O_4$. Whereas in the scales of alloy B Cr_2O_3, $Co_3V_2O_8$, NiO and CoV_3 were identified and scales of the alloy C contain $Ni(VO_3)_2$, Cr_2O_3, NiO, FeS, TiO_2, $Mg_3V_2O_8$ and $NiCr_2O_4$. The prominent phases identified in the scales of alloy D where mainly Cr_2O_3, $Ni(VO_3)_2$, FeS, NiO, $Mg_3V_2O_8$, FeV_2O_4, Fe_2O_3 and $NiCr_2O_4$ & in the scales of alloy E the main phases identified where Cr_2O_3, NiO, $Ni(VO_3)_2$, $Mg_3V_2O_8$, FeV_2O_4, FeS and $NiCr_2O_4$.

5.2.4 Measurement of scale thickness

The average scale thickness values measured for alloys A, B, C, D and E from their back scattered images shown in Fig. 5.17 are 33.3, 53.5, 15, 46 and 23.4 microns in Na_2SO_4–60% V_2O_5+MgO environment after exposure at 900^{0}C.

5.2.5 SEM, EDAX and EPMA Results

Fig.5.18 presents SEM micrographs for alloys A, B, C, D and E. SEM micrograph indicates formation of a massive scale in case of alloy A, Fig. 5.18 (a) and it also indicates tendency to spalling. In case of alloy B nodules are present in the scale and at some places spalling is indicated. SEM/ EDAX from the surface of the alloy C at areas 1, 2 & 3 as presented in

79

Fig. 5.18 (c) & Table A.29 revealed that the matrix consists of mainly Ni & Cr where Mg & V are also present. There is presence of other phases like Ni–rich phase containing mainly Cr & Ti. Sulphur is also indicated in the top of the scale. In case of alloy D, large size nodules are seen on top of the scale and the matrix is consisting of a crystalline phase and spalling is indicated. In case of alloy E also, the top of the scale is consisting of nodules.

EPMA for alloy A; Fig. 5.19 shows the formation of a duplex scale, outer scale being rich in oxides of V, Mg, Cr, S and Fe while the inner layer of scale is mainly Cr_2O_3. Sulphur is present in the scale as well as in the substrate, internal sulphidation is indicated. Mg, V and oxygen are co-existing in the scale. The region below the Cr rich layer is depleted of Cr but rich in Ni. The BSEI and X-ray maps of alloy B are shown in Fig.5.20. Medium size scale is indicated, there is a thin layer at the top and bottom of the scale which is rich in Ni. The scale is rich in Co, W, Ni and Cr. Mg and V are also present in the scale as revealed by their X-ray images. In case of alloy C a thin scale rich in Cr is present, Fig. 5.21. X-ray maps also show the presence of Ni, Fe, Mg and V in the scale. Ti and S are also indicated through out the scale. X-ray maps for alloy D, Fig. 5.22 show that the scale is rich in Cr, Fe, Ni, Mg and V. Ni is mainly present in the top layer where as inner layer is rich in Cr but the interface is depleted of Cr and rich in Ni. Magnesium and vanadium in this alloy are distributed through out the scale at same positions indicating formation of vanadates. EPMA for alloy E, Fig.5.23 shows a medium size scale and indicates grain boundary oxidation. The top scale is rich in Cr, Ni and Fe. Aluminum is present along the grain boundaries. V and S are concentrated in small areas in the scale.

Fig. 5.11: Weight change plots for the alloy A (Superfer 800H) after cyclic hot corrosion at 900°C in Na₂SO₄-60% V₂O₅ +MgO

Fig. 5.12: Weight change plot for the alloy B (Superco 605) after cyclic hot corrosion at 900°C in Na₂SO₄-60% V₂O₅+ MgO

Fig. 5.13: Weight change plots for the nickel base alloys: alloy C (Superni 75), alloy D (Superni 718) and alloy E (Superni 601) after cyclic hot corrosion at 900°C in Na_2SO_4-60% V_2O_5 + MgO.

Fig. 5.14: X-ray diffraction profile for alloy A (Superfer 800H) after cyclic hot corrosion at 900°C in Na_2SO_4-60% V_2O_5+ MgO. V_2O_5.

Fig. 5.15: X-ray diffraction profile for alloy B (Superco 605) after cyclic hot corrosion at 900°C in Na_2SO_4-60% V_2O_5 + MgO.

Fig. 5.16: X-ray diffraction profiles for the nickel base alloys: alloy C (Superni 75), alloy D (Superni 718) and alloy E (Superni 601) after cyclic hot corrosion at 900^0C in Na_2SO_4-60% V_2O_5 + MgO.
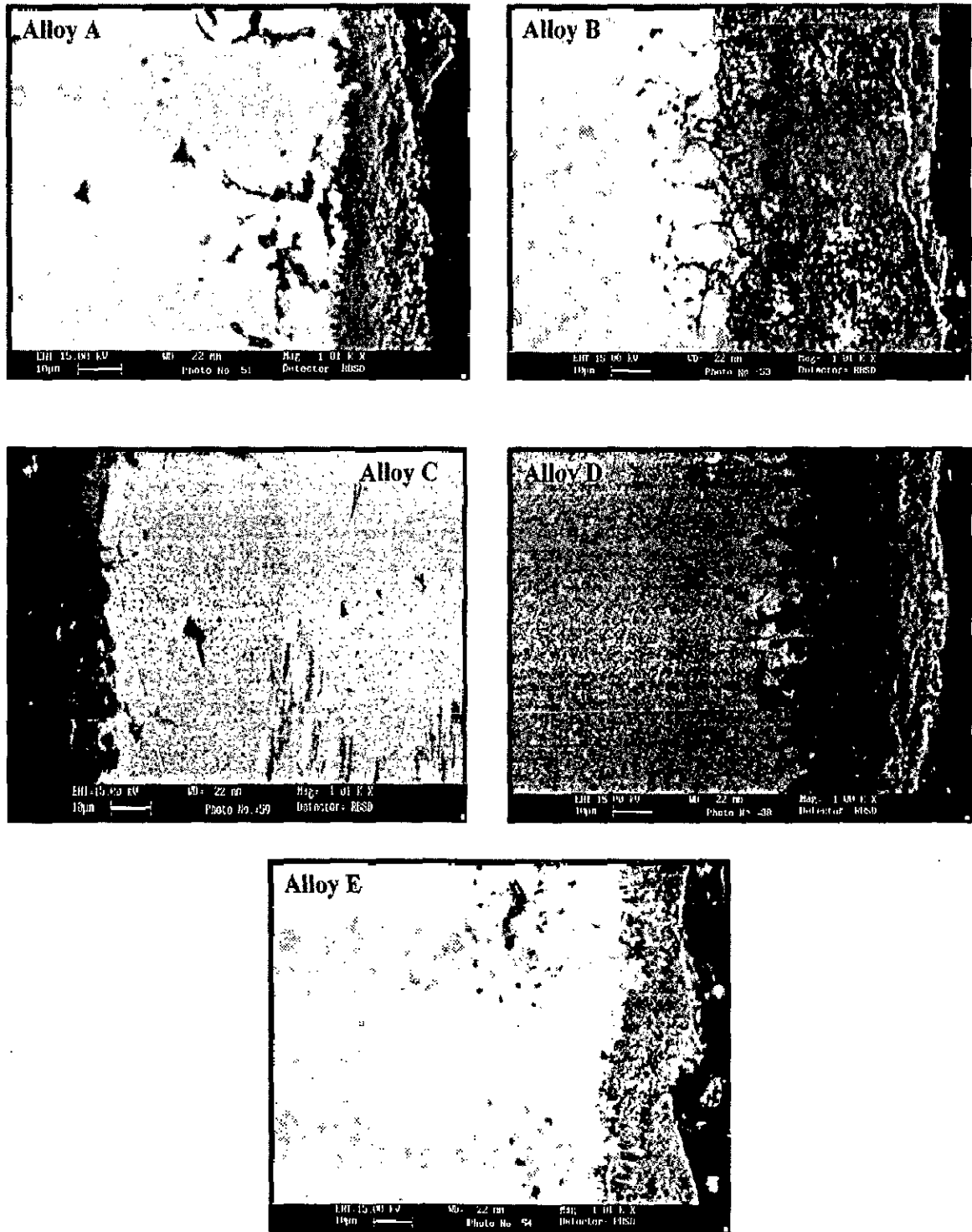
Fig . 5.17: BSE images of alloy A (Superfer 800H), alloy B (Superco 605), alloy C (Superni 75), alloy D (Superni 718) and alloy E (Superni 601) in Na$_2$SO$_4$-60%V$_2$O$_5$+MgO environment after exposure at 900^{0}C in cyclic conditions.
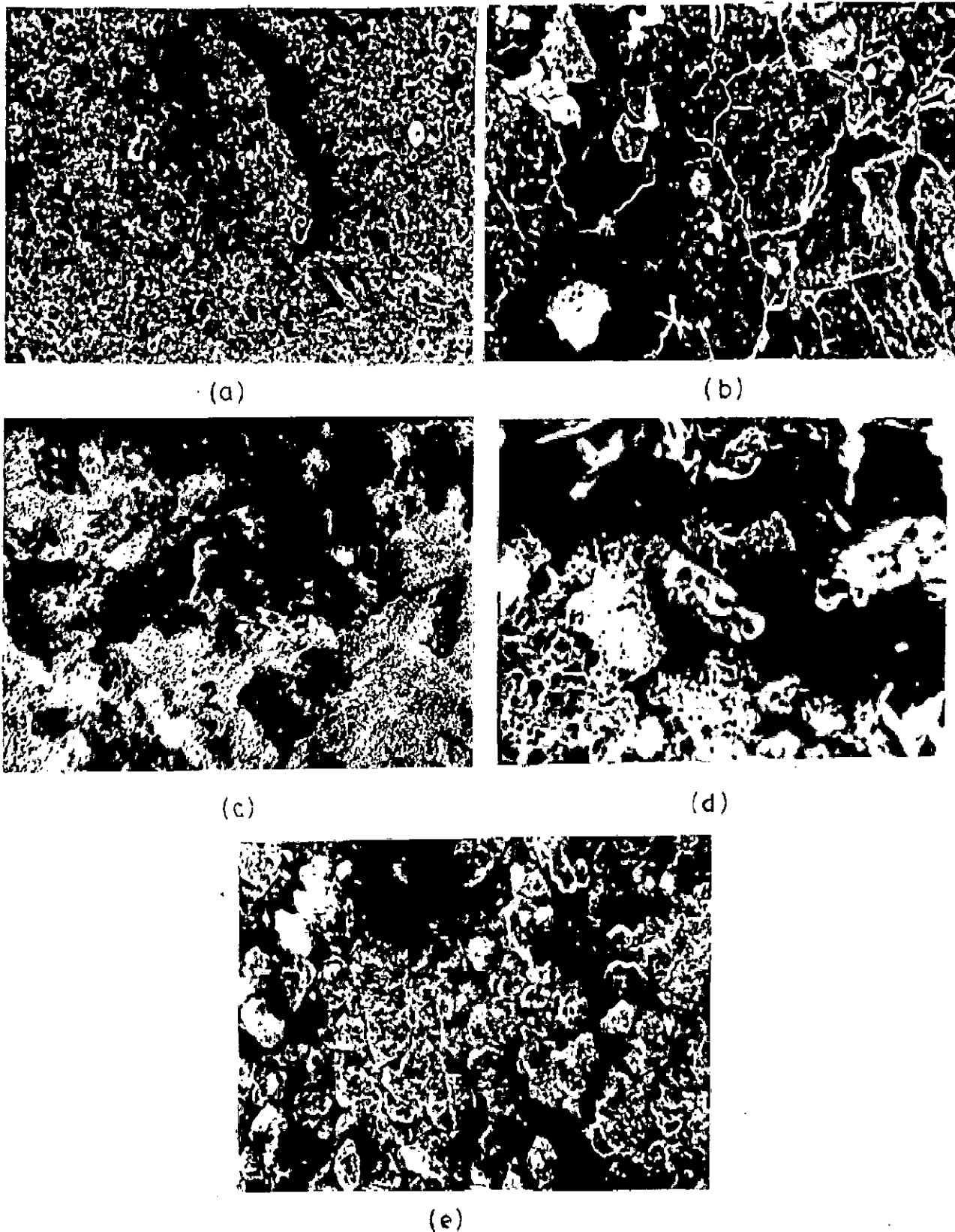
Fig. 5.18:   Scanning Electron Micrographs after cyclic hot corrosion in Na_2SO_4-60%V_2O_5
+ MgO of alloys:

a) Alloy A (Superfer 800H)   (X 640)

b) Alloy B (Superco 605)   (X 640)

c) Alloy C (Superni 75)   (X 400)

d) Alloy D (Superni 718)   (X 640)

e) Alloy E (Superni 601)   (X 640)

Fig. 5.19: BSEI and X-ray mapping of the cross section of alloy A (Superfer 800H) after cyclic hot corrosion at 900^0C in Na_2SO_4-60%V_2O_5+MgO. (X 400)

Fig. 5.20: BSEI and X-ray mapping of the cross section of alloy B (Superco 605) after cyclic hot corrosion at 900^0C in Na_2SO_4-60% V_2O_5 + MgO. (X 600)

Fig. 5.21: BSEI and X-ray mapping of the cross section of alloy C (Superni 75) after cyclic hot corrosion at 900^0C in Na_2SO_4-60%V_2O_5 + MgO   (X 600)

Fig. 5.22: BSEI and X-ray mapping of the cross section of alloy D (Superni 718) after cyclic hot corrosion at 900^0C I n Na_2SO_4-60% V_2O_5+ MgO. (X 400)

Fig. 5.23: BSEI and X-ray mapping of the cross section of alloy E (Superni 601) after cyclic hot corrosion at 900⁰C in Na_2SO_4-60%V_2O_5 + MgO. (X 800)

91

5.3 HOT CORROSION STUDIES IN Na$_2$SO$_4$-60%V$_2$O$_5$ +20%CaO

5.3.1 Visual Observations

In case of alloy A, the scale was dark grey in colour, adherent in nature, but had spalling tendency. The scale was steel grey, lustrous, shinning mass and adherent in nature for alloy B though macrograph showed the areas where the scale has spalled off and fresh surface got exposed. In case of alloy C, the scale appeared to be slightly yellow, present as dense patches on the surface indicating the presence of some unreacted salt on the specimen surface. In case of alloy D, the appearance of the scale was just similar to that for alloy B. It also indicated presence of unreacted salt on the surface and areas where coating has spalled off. Scale in case of alloy E was dark grey, compact and adherent. Fig. A.1 shows the macrographs for corroded specimens of alloys A, B, C, D & E after exposure for 50 cycles at 900^{0}C with Na$_2$SO$_4$-60%V$_2$O$_5$+20%CaO coating in air.

5.3.2 Kinetic Data

Figs. 5.24, 5.25 and 5.26 show the plots drawn between weight change and number of cycles for the specimens of alloys A, B, C, D & E after exposure for 50 cycles at 900^{0}C with Na$_2$SO$_4$–60%V$_2$O$_5$+20%CaO coating in air. The plot for alloy A shows a gradual increase in weight gain up to about 30 cycles and it remains nearly same up to 38 cycles after which there is a decrease in weight gain due to sudden sputtering of the scale and after that it continuously decreased down to 3.5 mg/cm^2. The maximum weight gain is slightly less than that in Na$_2$SO$_4$–60%V$_2$O$_5$ environment. Plot for alloy B, Fig. 5.25 shows a gradual increase up to 25 cycles and weight gain is about 15 mg/cm^2 but increase is very slow from 25th to 50th cycle and it is only 3 mg/cm^2. Over all weight gain is 18.5 mg/cm^2. In case of alloy C, rapid increase is noticed in the initial 2 cycles and then it is linear up to 12 cycles but increases marginally after that. Maximum weight gain is about 4 mg/cm^2. Plot for alloy D shows a parabolic nature in weight gain behaviour up to 20 cycles after which the curve shows

waviness upto 50 cycles. Over all weight gained is 2/3rd of that in $Na_2SO_4-60\%$ V_2O_5 environment. Alloy E showed the slow and gradual increase in weight gain /unit area. In this case weight gain is just half of that in $Na_2SO_4-60\%V_2O_5$ environment. The weight change trend for alloys C, D and E is presented in Fig 5.26.

5.3.3 X-Ray Diffraction Analysis

The prominent phases analysed in the corrosion product formed after application of $Na_2SO_4-60\%V_2O_5+20\%CaO$ and exposure at 900^0C are given in Tables A.7, A.8 and A.9 for Fe-base, Co-base and Ni-base alloys. Similarly their profiles are shown in Fig. 5.27, 5.28 and 5.29. Vanadates of Fe and Ca are identified in the scale along with oxides of Fe and Ni in alloy A. NiO and Cr_2O_3 have probably reacted to form spinel $NiCr_2O_4$ as it identifies the main peaks along with other possible phases Fe_2O_3, $Ca_3V_2O_8$, $NiFe_2O_4$, $(Cr,Fe)_2O_3$, FeS, Cr_2O_3 and FeV_2O_4. Alloy B indicated presence of $Co_3V_2O_8$, Cr_2O_3, NiO, $NiCo_2O_4$ and CoV_3 and scales of the alloy C contain Cr_2O_3, NiO, $Ni(VO_3)_2$, $Ca_3V_2O_8$ and $NiCr_2O_4$. The prominent phases identified in the scales of alloy D were mainly NiO, $(Cr,Fe)_2O_3$, Cr_2O_3, $Ni(VO_3)_2$ and $NiCr_2O_4$ & in the scales of alloy E the main phases identified were Cr_2O_3, $Ca_3V_2O_8$, NiO, $Ni(VO_3)_2$, $NiFe_2O_4$ and $NiCr_2O_4$.

5.3.4. Measurement of Scale Thickness

Average Scale thickness values as observed from back scattered images of alloys A, B, C, D and E, measured according to the micron scale shown in Fig. 5.30 are 41, 34, 9, 43 and 42 μm.

5.3.5. SEM, EDAX and EPMA Results

Fig. 5.31 (a, b, c, d and e) presents SEM micrographs for alloys A, B, C, D & E respectively with $Na_2SO_4-60\%V_2O_5+20\%CaO$ coating after exposure at 900^0C for 50 cycles in air.

SEM micrograph of the top scale in case of alloy A, Fig. 5.31 (a) shows a massive scale formation having nodules and intergranular cracks. In case of alloy B, Fig. 5.31 (b) scale seems to

be spongy with some porosity. In case of alloy C, the scale is consisting of nodules distributed in crystalline matrix. EDAX analysis of points 1, 2, 3 marked on the SEM image Fig.5.31 (c) presented in Table A.29 shows that the matrix is mainly Ni & Cr and nodules are rich in Ni, Cr, Ca and V. In case of alloy D, elongated phases are present in a crystalline matrix whereas in case of alloy E, there is a continuous scale with nodules present at some places and precipitation along the grain boundaries. Presence of pores in the scale is also visible.

Fig. 5.32, BSEI & X-ray maps for alloy A indicate formation of a thick duplex scale, the outer scale is rich in oxides of Ni, Cr & Fe while the inner scale is mainly Cr_2O_3. Cr- enriched layer is indicated just above the substrate where Ni & Fe are absent and this Cr is getting internally oxidised and layer is penetrating into the scale. Both Al & Si are also internally oxidised with chromium. Ca & V are present in the scale and they co-exist at the same spots and are of nearly the same concentration. Mn & S are coexisting along the interface. Ti is also concentrated in the substrate just below the interface and has also got oxidised.

In case of alloy B, EPMA Fig 5.33, indicates medium size scale. The scale is consisting of mainly Cr & Co and in the areas depleted of Cr; W is present in higher concentration. Nickel is also distributed uniformly in the scale. The scale substrate interface is even and no penetration of scale in the substrate is observed.

The BSEI and X-ray maps of alloy C, Fig. 5.34 show a very thin scale consisting of mainly Cr with some amount of Ni. Calcium is also present in the top of the scale and is coexisting with V. Ti is present in the scale distributed uniformly. S has been detected in minor amounts on top of the scale. No internal oxidation has been indicated. The interface between substrate and scale has a very thin scale rich in Cr where Ni is absent.

In case of alloy D, Fig. 5.35 EPMA indicates formation of medium size scale which basically consists of Ni, Cr & Fe. Area depleted of Ni & Fe just above the substrate has a thin irregular layer rich in Cr. Calcium & vanadium are present in the scale and are coexisting at same places The EDAX analysis of this alloy along the cross-section presented in Table 5.1 corresponding to the points shown on the BSEI of the cross-section, Fig. 5.37 also shows a single layer scale mainly consisting of Ni, Fe & Cr. The area in the scale just above the

substrate has higher amount of chromium. Vanadium & calcium are present throughout the scale. Titanium, aluminium, manganese and tantalum are also incorporated in the scale.

The EPMA for alloy E, Fig.5.36 indicates medium size scale rich in Cr and Fe containing some amount of Ni. The concentration of Ni at the scale substrate interface is high along a thin layer and Ni rich band is present where both Fe and Cr are absent. Above this, there is a Cr rich thin band. Ca and V are also indicated in the scale.

Fig. 5.24: Weight change plots for the alloy A (Superfer 800H) after cyclic hot corrosion at 900^0C in Na_2SO_4-60% V_2O_5 +CaO.

Fig. 5.25: Weight change plot for the alloy B (Superco 605) after cyclic hot corrosion at 900^0C in Na_2SO_4-60%V_2O_5+CaO.
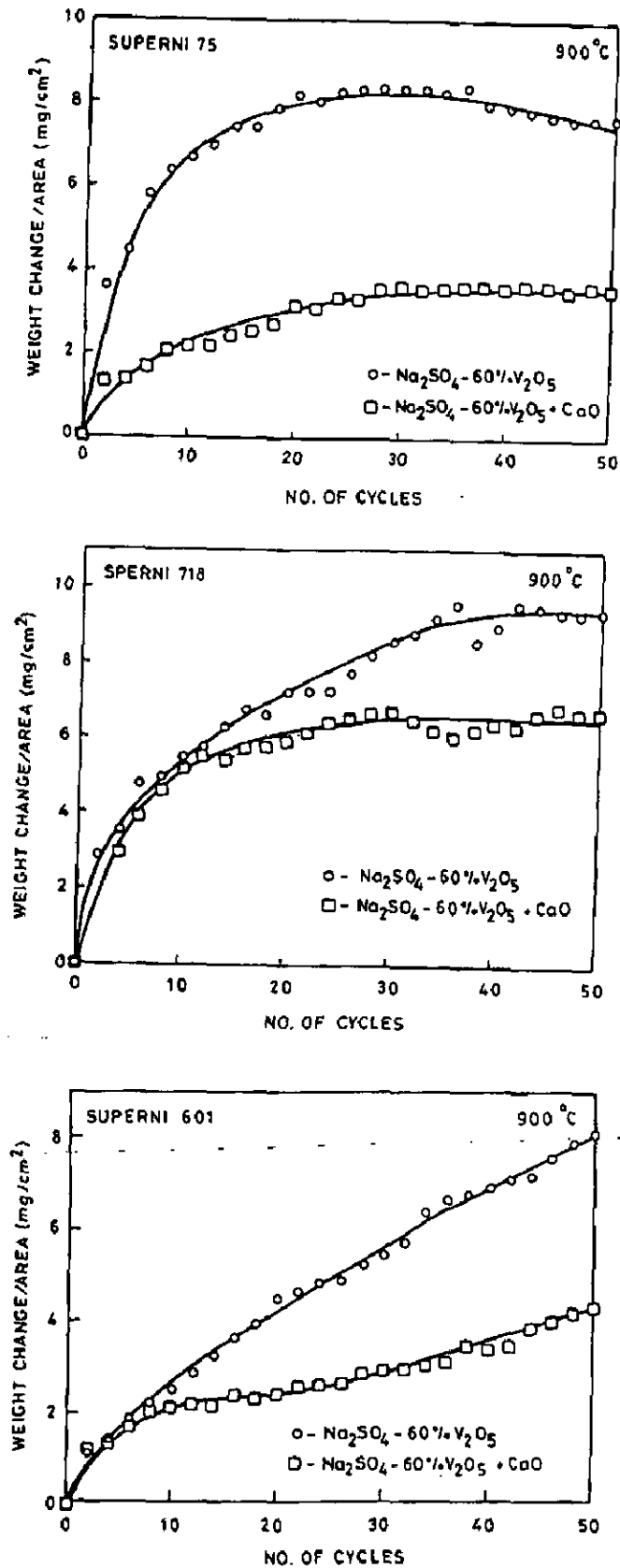
Fig. 5.26: Weight change plots for the nickel base alloys: alloy C (Superni 75), alloy D (Superni 718) and alloy E (Superni 601) after cyclic hot corrosion at 900°C in Na₂SO₄-60% V₂O₅ +CaO.
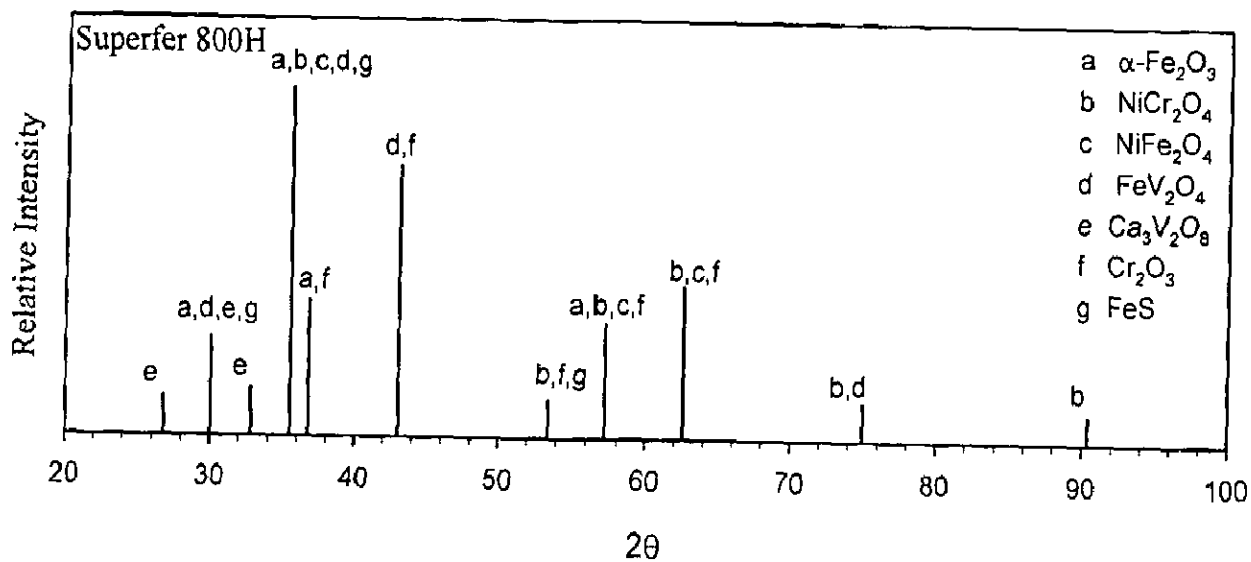
Na_2SO_4-60% V_2O_5 +CaO.

Fig. 5.27: X-ray diffraction profile for alloy A (Superfer 800H) after hot corrosion ay 900^0C in Na_2SO_4-60%V_2O_5+CaO.
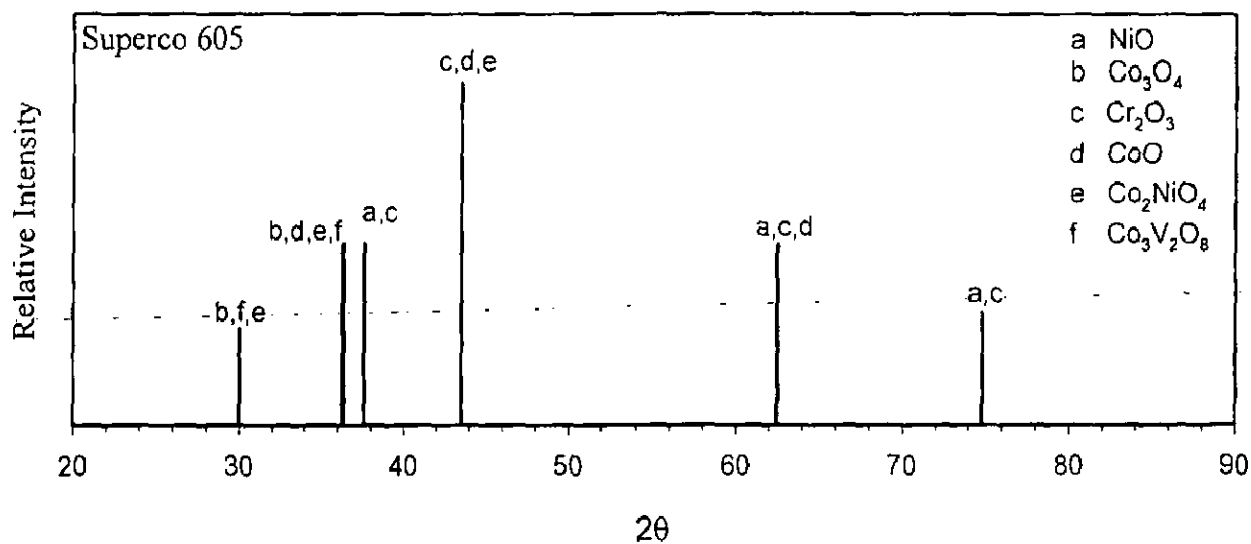
Fig. 5.28: X-ray diffraction profile for alloy B (Superco 605) after cyclic hot corrosion at 900^0C in Na_2SO_4-60%V_2O_5+CaO.
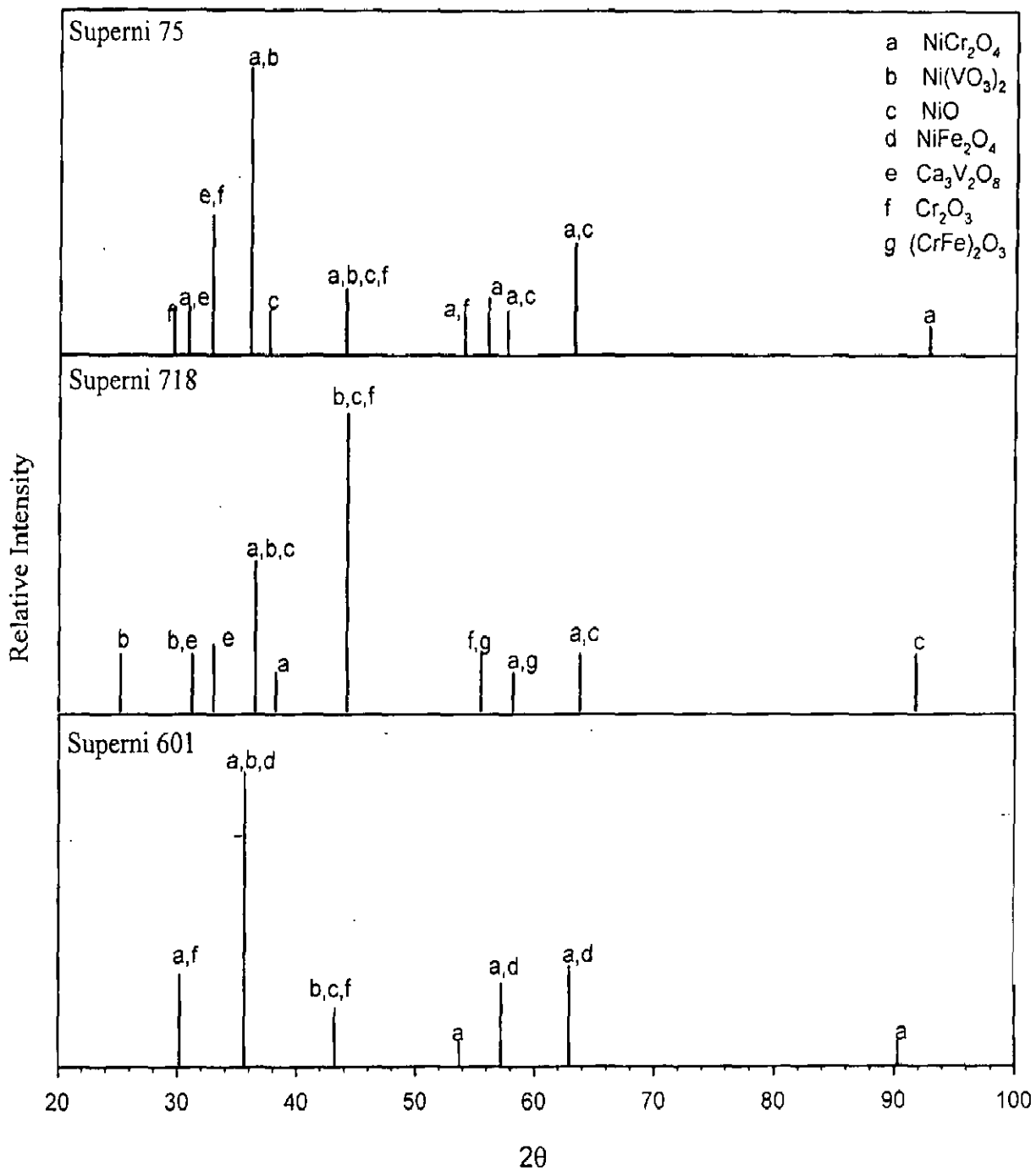
Fig. 5.29: X-ray diffraction profiles for the nickel base alloys: alloy C (Superni 75), alloy D (Superni 718) and alloy E (Superni 601) after cyclic hot corrosion at 900^0C in Na_2SO_4-60% V_2O_5 + CaO.
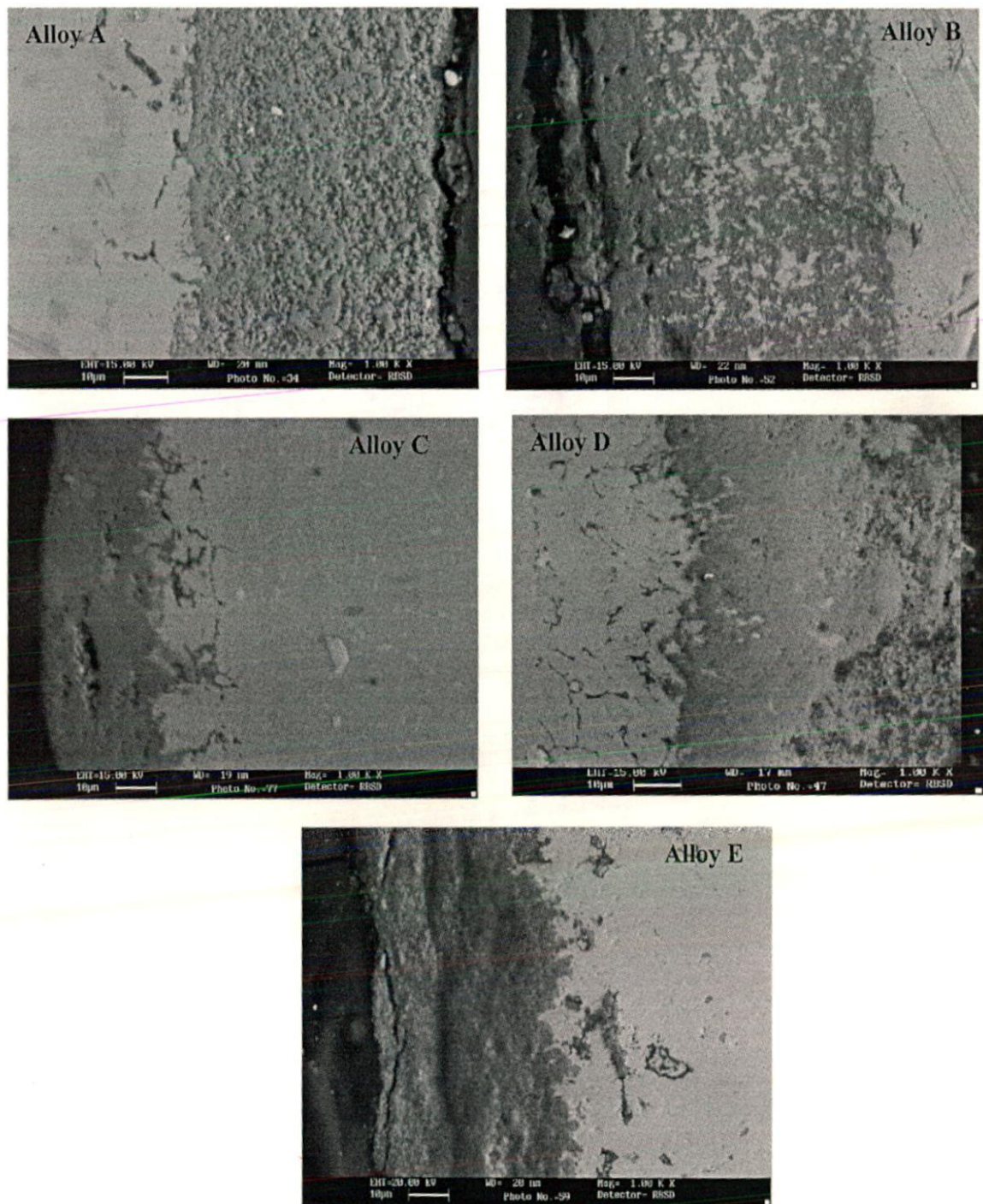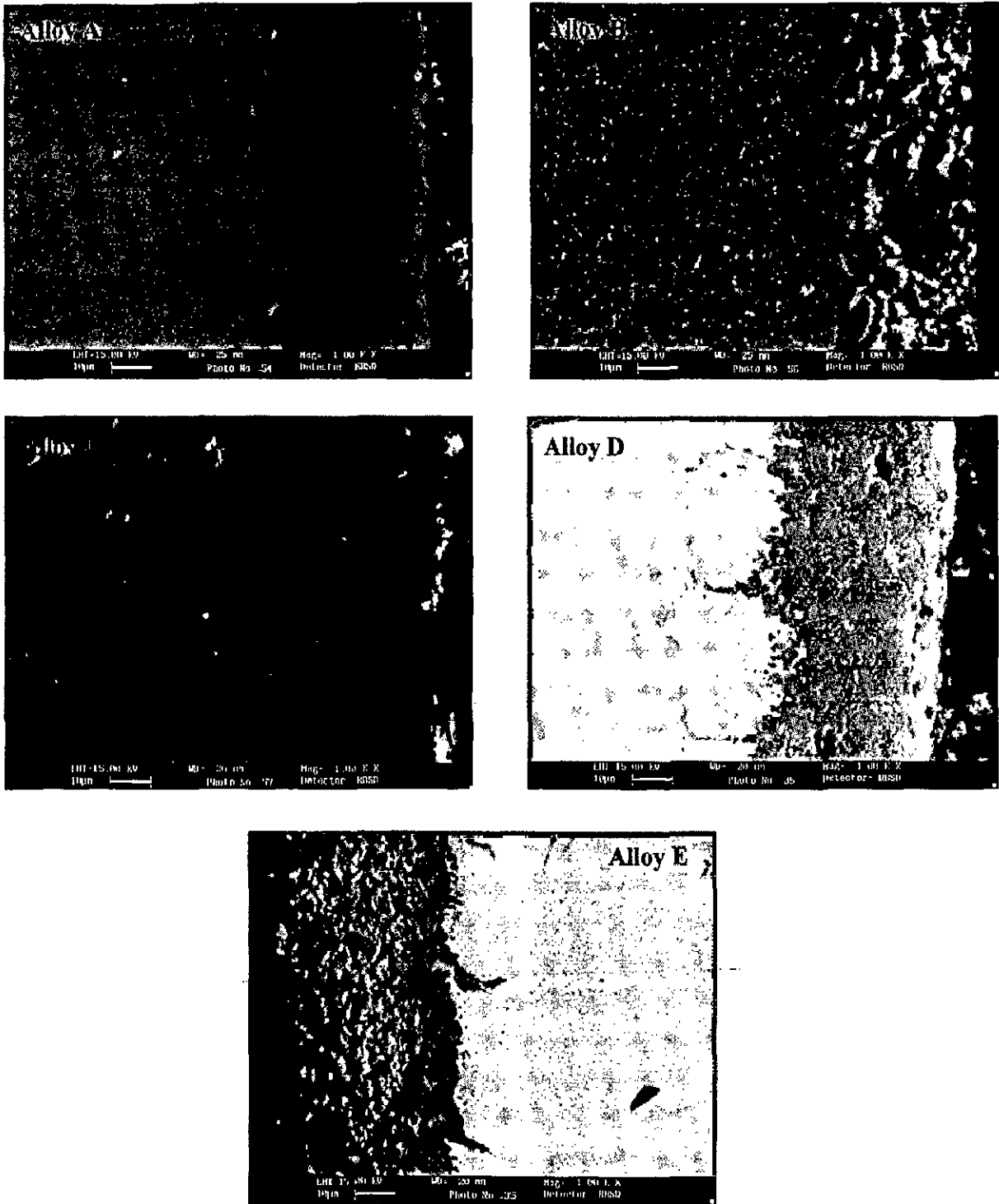
Fig. 5.30 : BSE images of alloy A (Superfer 800H), alloy B (Superco 605), alloy C (Superni 75), alloy D (Superni 718) and alloy E (Superni 601) in Na_2SO_4-60%V_2O_5 + CaO environment after exposure at 900^0C in cyclic conditions.
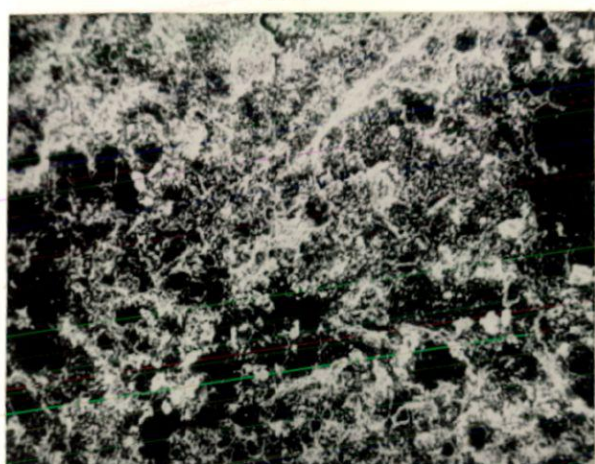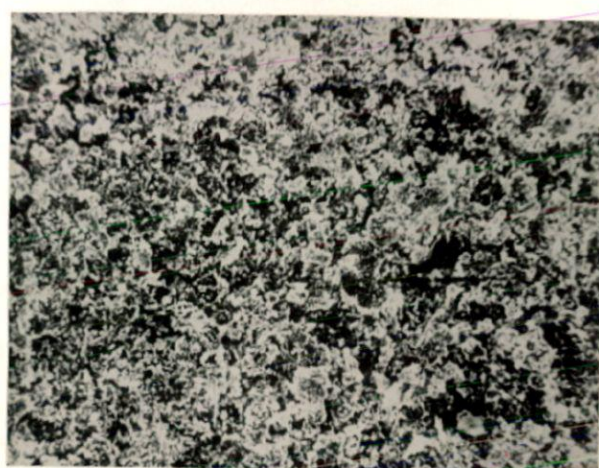
(a)

(b)

(c)

(d)

(e)
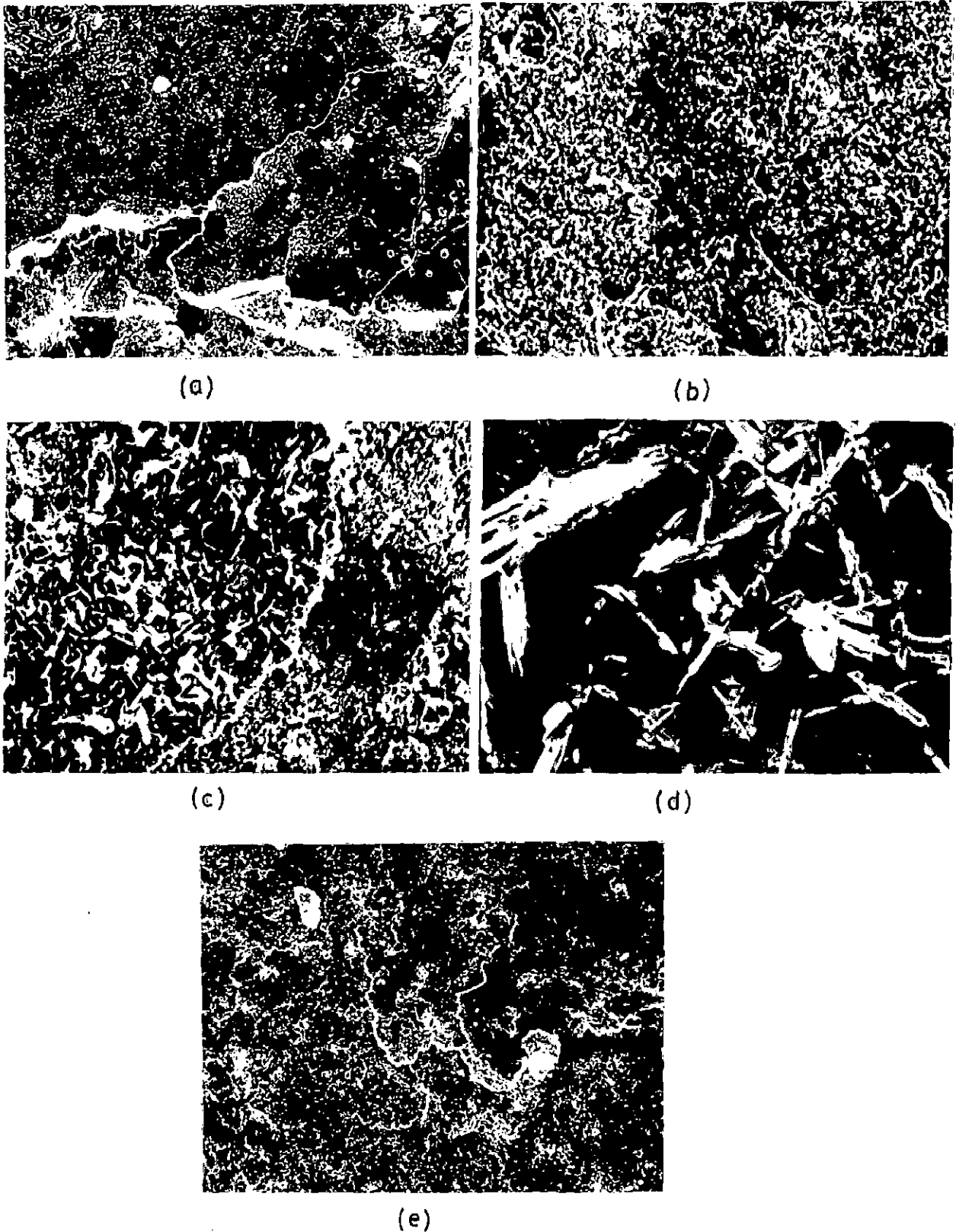
Fig. 5.31:   Scanning Electron Micrographs after cyclic hot corrosion in Na_2SO_4-60%V_2O_5 +CaO of alloys:

a) Alloy A (Superfer 800H)   (X 640)

b) Alloy B (Superco 605)   (X 640)

c) Alloy C (Superni 75)   (X 650)

d) Alloy D (Superni 718)   (X 640)

e) Alloy E (Superni 601)   (X 640)
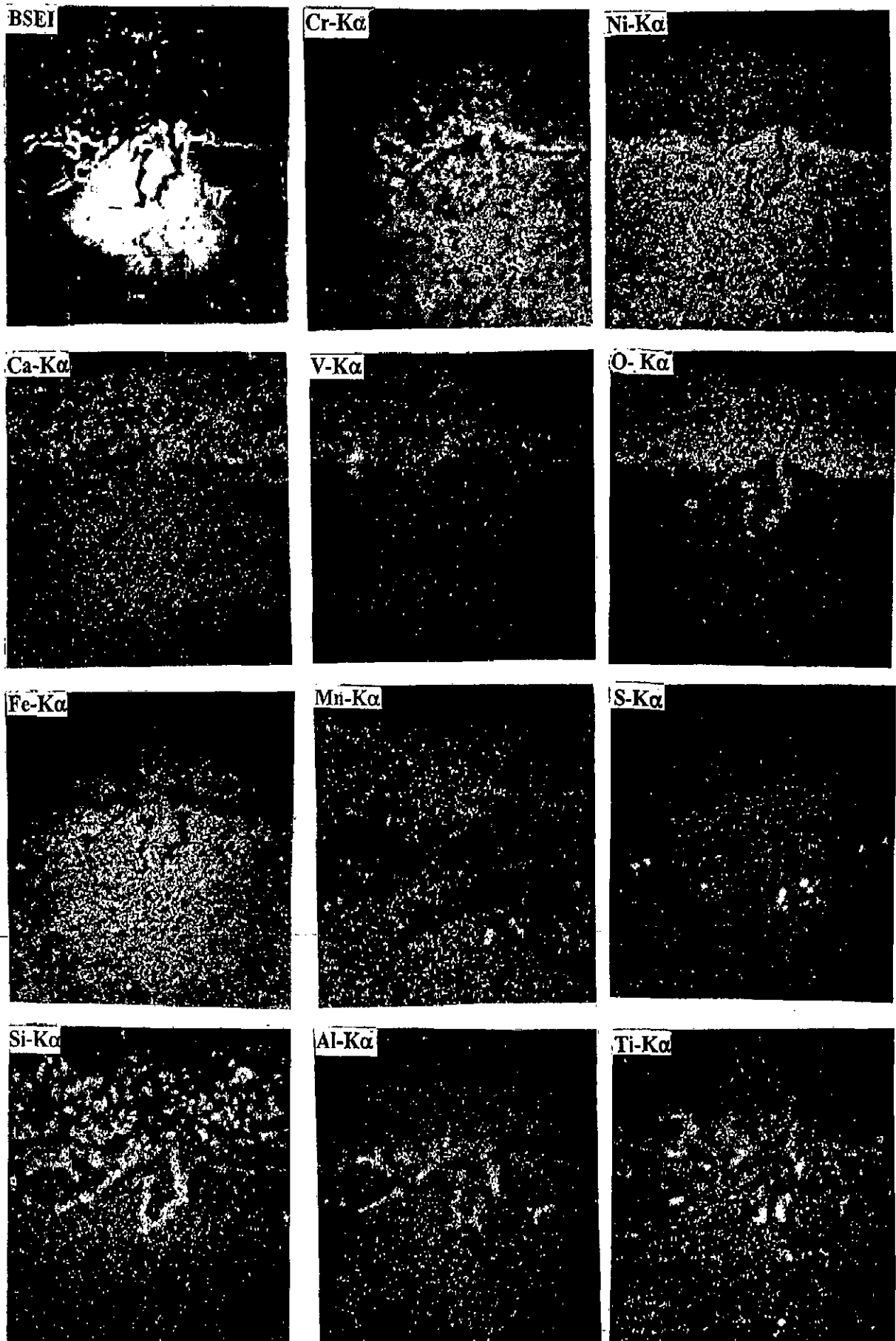
Fig. 5.32: BSEI and X-ray mapping of the cross-section of alloy A (Superfer 800H) after cyclic hot corrosion at 900^0C in Na_2SO_4-60% V_2O_5 + 20% CaO.   (X 400)

Fig. 5.33: BSEI and X-ray mapping of the cross-section of alloy B (Superco 605) after cyclic hot corrosion at $900^{0}C$ in Na_2SO_4-60% V_2O_5 + 20% CaO. (X 400)

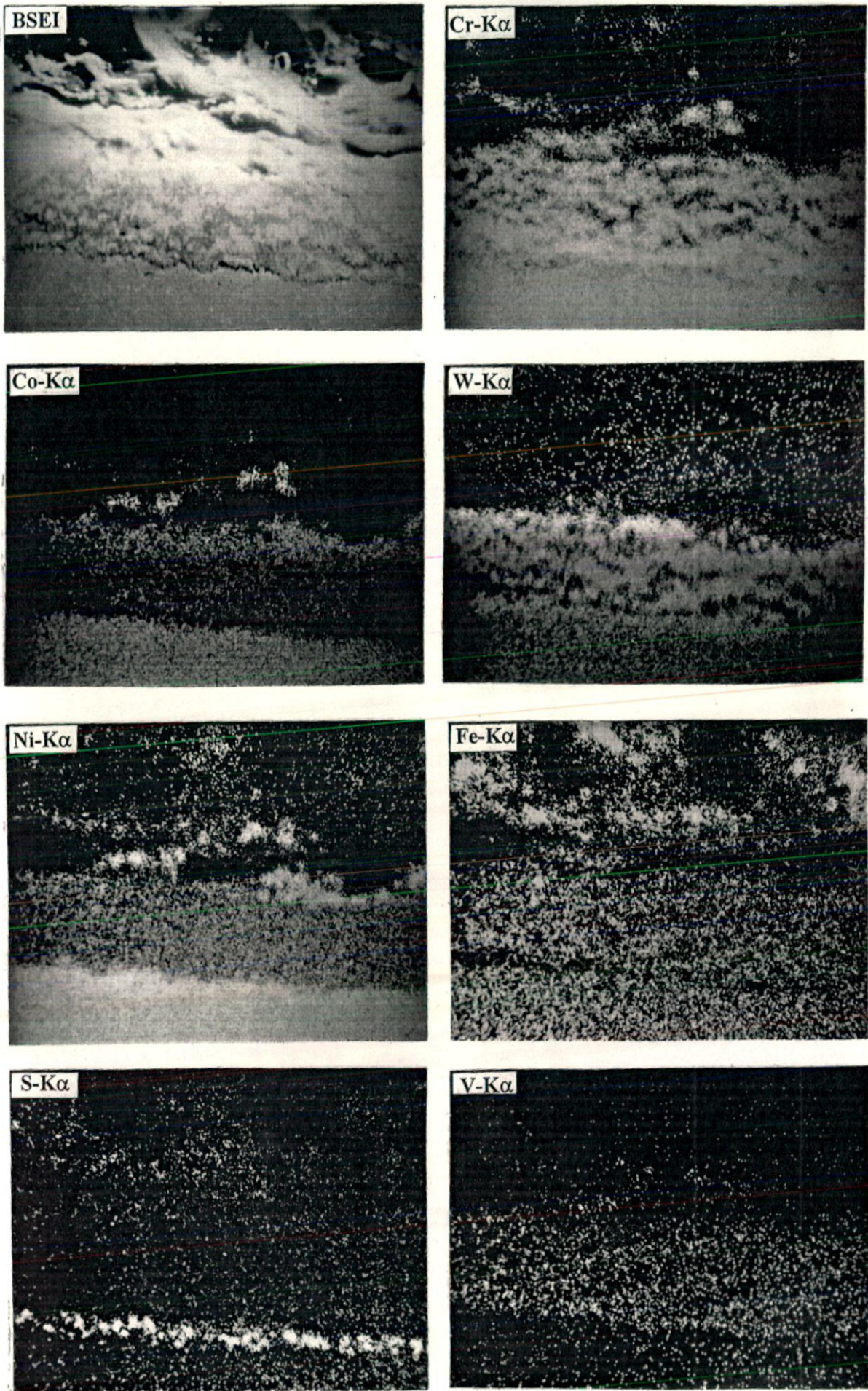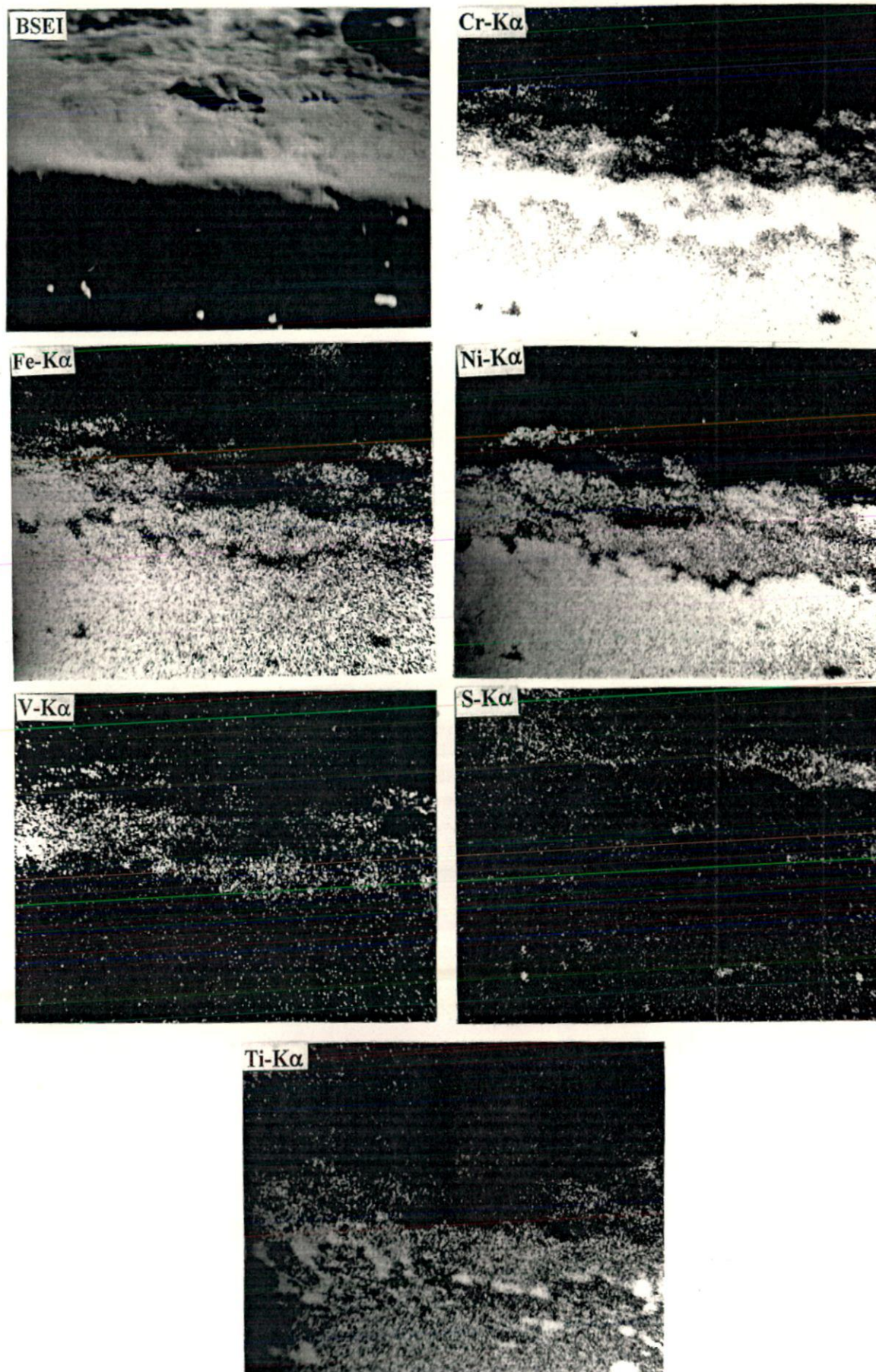**Fig. 5.34:** BSEI and X-ray mapping of the cross-section of alloy C (Superni 75) after cyclic hot corrosion at 900^0C in Na_2SO_4-60% V_2O_5 + 20% CaO. (X 800)

Fig. 5.35: BSEI and X-ray mapping of the cross-section of alloy D (Superni 718) after cyclic hot corrosion at 900^0C in Na_2SO_4-60% V_2O_5 + 20% CaO.   (X 600)

Fig. 5.36: BSEI and X-ray mapping of the cross-section of alloy E (Superni 601) after cyclic hot corrosion at 900^0C in Na_2SO_4-60% V_2O_5 + 20% CaO.　　(X 600)

# EDAX Analysis of Superni 718 in Na₂SO₄-60%V₂O₅+20%CaO along the Cross-Section after cyclic hot corrosion at 900°C
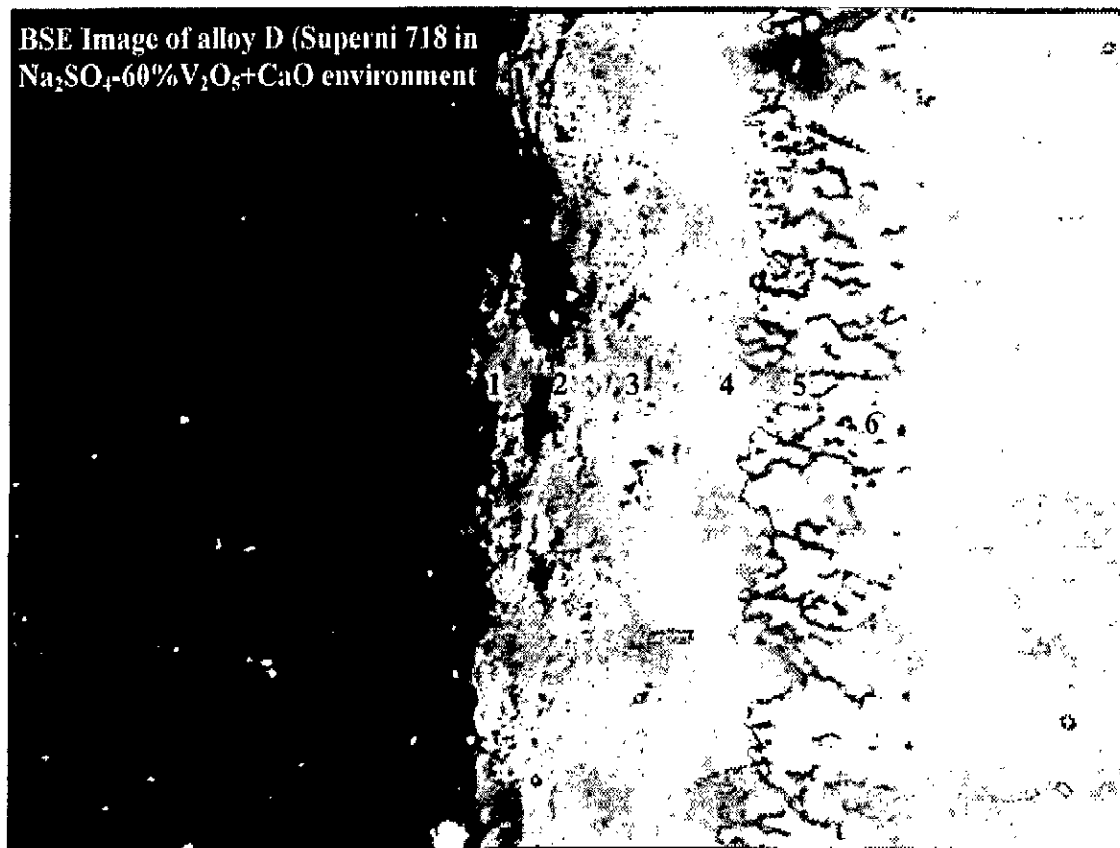
Fig. 5.37: Back Scattered Image of alloy D (Superni 718) after cyclic hot corrosion in Na_2SO_4-60%V_2O_5+ CaO at 900°C.

Table. 5.1: Wt % of elements corresponding to points marked on Fig. 5.37, BSE image of alloy D (Superni718).

Point of analysis	Weight % of element												
	O	Fe	Ni	Cr	Ti	Al	Mn	Si	Cu	Ca	Na	V	Ta
1	18.09	22.72	29.26	22.12	1.48	1.57	0.30	-	0.55	0.53	0.57	1.03	1.76
2	22.98	21.48	30.48	20.03	0.89	0.53	0.18	-	0.36	0.26	0.24	1.81	0.76
3	25.75	21.60	28.47	20.34	0.75	0.46	0.28	0.11	-	0.29	-	1.65	0.27
4	28.02	16.51	21.30	31.22	16.08	0.54	0.20	-	-	0.15	-	0.45	-
5	5.47	8.18	57.99	20.18	0.57	4.74	0.12	0.62	-	0.20	-	1.43	0.47
6	0.00	9.73	85.89	3.45	0.35	-	-	0.14	-	-	-	0.11	0.32

5.4 HOT CORROSION STUDIES IN Na$_2$SO$_4$- 60%V$_2$O$_5$+ 20%MnO$_2$

5.4.1 Visual Observations

Surface of the alloy A, showed the presence of a dark black adherent scale, but for alloy B, the scale was fragile and steel grey in colour. In case of alloy C, the scale was dense and compact, adherent slightly yellowish in colour, indicating presence of the salt film on the surface. Similarly in alloy D, the scale was again brownish yellow colored, compact mass, adherent in nature. Surface scale of alloy E was also slightly yellowish in colour indicating presence of unreacted salt though the salt film was present as small patches on the surface. The areas where salt had reacted or scale had spalled off were dark black in colour. These observations are shown in Fig. A.1

5.4.2 Kinetic Data

In case of alloy A, Fig. 5.38, an increase in weight gain up to 22 cycles and then spalling with simultaneous oxidation has been noticed. Over all weight gain is about 7.5 mg/cm^2. Where as in alloy B, the nature of rise in weight gain is nearly parabolic up to 30 cycles and after that it is nearly constant as shown in Fig. 5.39. Overall weight gain is about 3/4th of that without MnO$_2$ addition. Plot for Ni-base alloys, Fig. 5.40 indicates a slight change in wt. after an initial increase up to 20 cycles for alloy C. When a sudden rise is noticed at 22nd cycle and after that a gradual increase has been observed up to 50th cycle. Over all weight gain is about 6 mg/cm^2. Similar trend is seen in case of alloys D and E where the final weight gain is 7.8mg/cm^2 and 6.2 mg/cm^2 respectively.

5.4.3 X-Ray Diffraction Analysis

Tables A.10, A.11 and A.12 & Fig. 5.41, 5.42 and 5.43 present the X-ray diffraction data for alloys A, B, C, D & E exposed to Na$_2$SO$_4$-60% V$_2$O$_5$ +20% MnO$_2$ environment at 900^{0}C for 50 cycles in air. Main peak of FeV$_2$O$_4$ was identified indicating it to be major phase in case of alloy A, and the other possible phases identified were Fe$_2$O$_3$, FeS, Cr$_2$O$_3$, (Cr,Fe)$_2$O$_3$, NiCr$_2$O$_4$,

NiFe$_2$O$_4$, and NiCrMnO$_4$. Whereas in alloy B, the possible phases identified were Co$_3$O$_4$, Co$_3$V$_2$O$_8$, NiCo$_2$O$_4$, Cr$_2$O$_3$, Co$_2$MnO$_4$ (2CoO.MnO$_2$) and NiWO$_4$. Prominent phases identified in scales of nickel base alloys were NiO, NiS, NiCr$_2$O$_4$, Cr$_2$O$_3$ and spinels Ni(VO$_3$)$_2$, NiCrMnO$_4$ & NiMn$_2$O$_4$ for alloy C and Ni(VO$_3$)$_2$, NiO, NiCr$_2$O$_4$, Mn$_3$O$_4$, Cr$_2$O$_3$, and (Cr,Fe)$_2$O$_3$ in alloy D. Where as in alloy E, the main phases identified were Ni(VO$_3$)$_2$, NiO and Cr$_2$O$_3$ but other possible phases identified were NiCr$_2$O$_4$, FeV$_2$O$_4$,, NiMn$_2$O$_4$, Fe$_2$O$_3$ and (Cr,Fe)$_2$O$_3$.

5.4.4. Measurement of scale thickness

The average thickness values for scales of alloys A, B, C, D and E measured from back scattered images after exposure in Na$_2$SO$_4$-60%V$_2$O$_5$ +20%MnO$_2$ environment are 30, 53.5, 20.5, 33.3 and 44 μm respectively as per the micron scale shown in the Fig. 5.44.

5.4.5. SEM, EDAX and EPMA Results

Fig 5.45 (a, b, c, d and e) presents the SEM micrographs for alloys A, B, C, D and E respectively coated with Na$_2$SO$_4$-60%V$_2$O$_5$+20% MnO$_2$ after exposure for 50 cycles at 900^{0}C. The SEM micrograph of the surface of alloy A indicates a massive scale and shows certain areas where spalling has taken place. In case of alloy B, two distinct layers are seen; top layer indicates partial melting and the layer beneath indicates dense scale.

SEM of the alloy C shows presence of elongated crystals. In other areas, there is large sized crystal growth. In case of alloy D, there is a presence of large size nodules in the scale and the nodules are porous. In case of alloy E, the scale is sponge like and contains craters indicating volatilization of species.

The EPMA for alloy A, (Fig 5.46) indicates formation of a medium size scale which is mainly rich in iron at top. The layer just above the substrate is Cr-rich where Ni and Mn are absent. There is penetration of the scale into the substrate due to internal oxidation which mainly consists of chromium oxide. At the top of the scale there is Al and S. Titanium is also present in scale just above the substrate/scale interface.

In case of alloy B, (Fig. 5.47) EPMA indicates a thick scale which consists of mainly Co, Cr, W and little amount of Ni. W is distributed throughout the scale. There is a nickel rich sub scale present at the interface; sulphur is present in the outermost scale and also as a thin layer along the interface between the scale and the substrate. Wherever W is present, areas are depleted of Cr. Vanadium is present throughout the scale, S at the interface is co-existing with Mn thereby indicating formation of MnS. The EDAX analysis along cross-section of the same alloy (Fig. 5.51 and Table 5.2), indicates that the top scale is rich in Co, Cr and W. As we move inwards the amount of W goes an increasing whereas other constituents like Cr and Ni go on decreasing. At the alloy substrate interface the amount of W is less and the amount of Cr increases. Na, V & S as well as Mn are present along the cross-section of the scale.

BSEI and X-ray maps for alloy C are shown in Fig. 5.48. The scale is relatively thin and mainly consists of Cr with some amount of Ni and Ti. Layer just beneath the Cr rich scale is depleted of Cr and is rich is Ni. Vanadium & manganese are co-existing throughout the scale. The layer just above the Cr_2O_3 layer is rich in Fe. Titanium is also present in the scale. BSEI and X-ray maps for alloy D are shown in Fig. 5.49. A very thin uniform scale has formed. This scale mainly consists of Cr rich thin continuous scale at the scale/substrate interface. Above this thin scale, there is presence of Ni, Fe and Cr rich scale. Aluminium, manganese & vanadium are also present in the upper scale. At the interface, there is a high concentration of Ti, which is penetrating into the scale. BSEI and X-ray maps of alloy E, (Fig. 5.50) show that the internal oxidation product mainly consists of Cr and Mn oxides. Medium size scale is indicated, V is present throughout the scale and S is present at the top of the scale. Silicon is present at top of the scale in pockets.
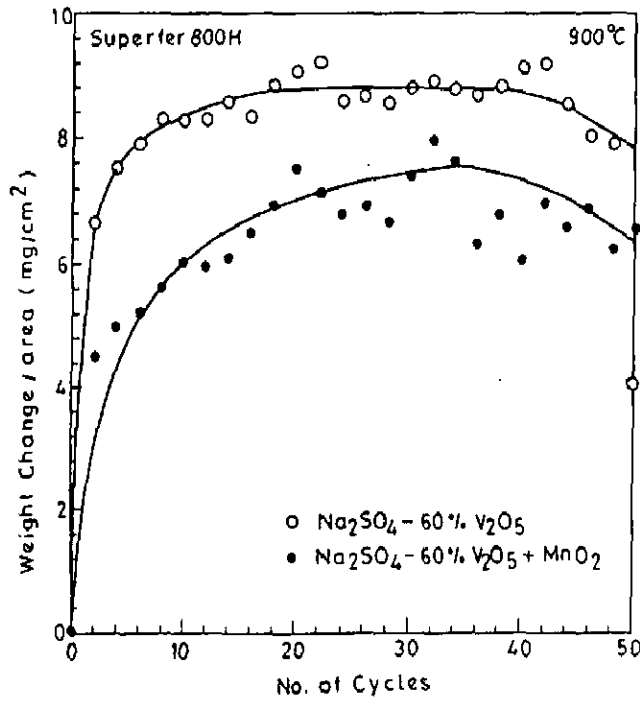
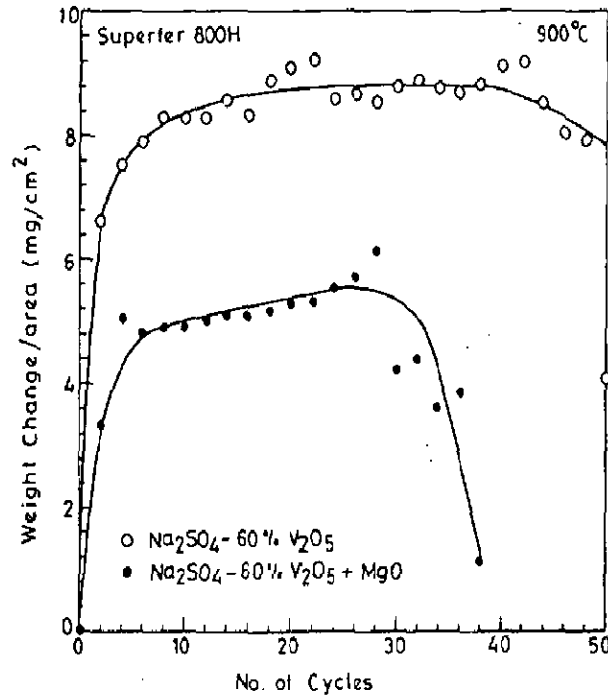**Fig. 5.38:** Weight change plot for alloy A (Superfer 800H) after cyclic hot corrosion at 900°C in Na_2SO_4-60% V_2O_5+20%MnO_2.
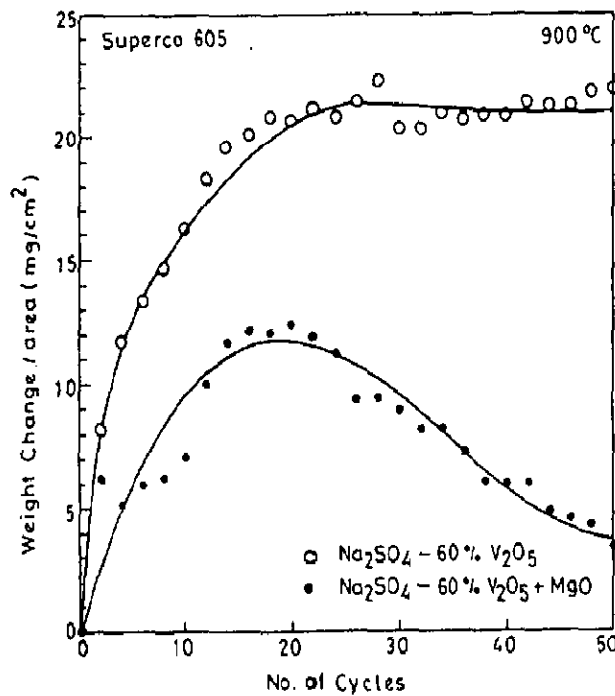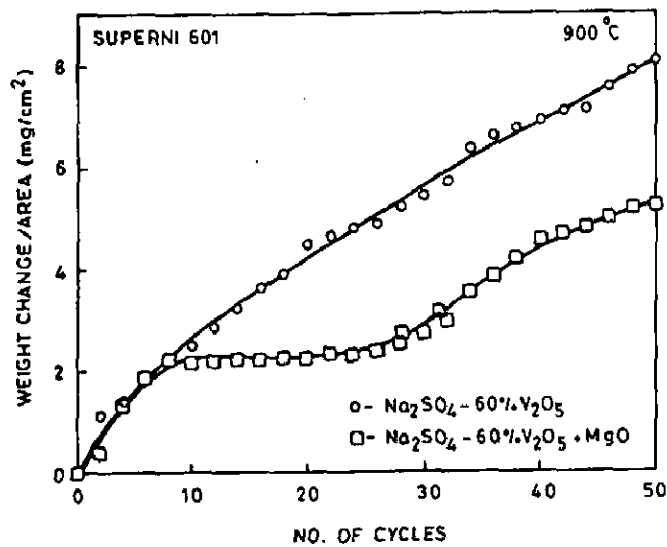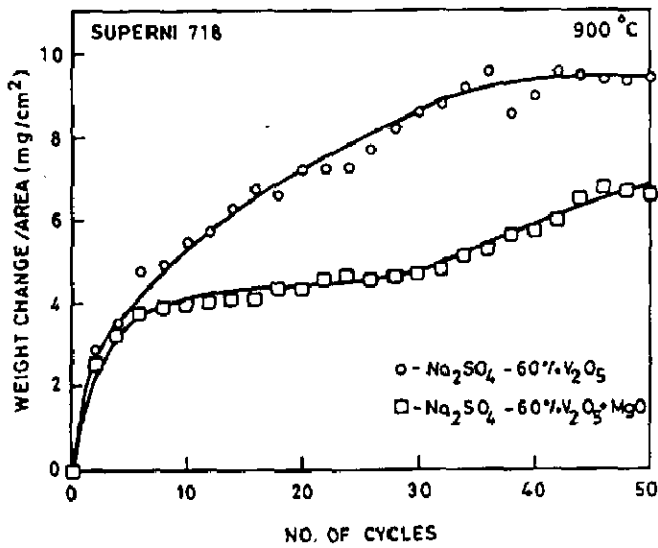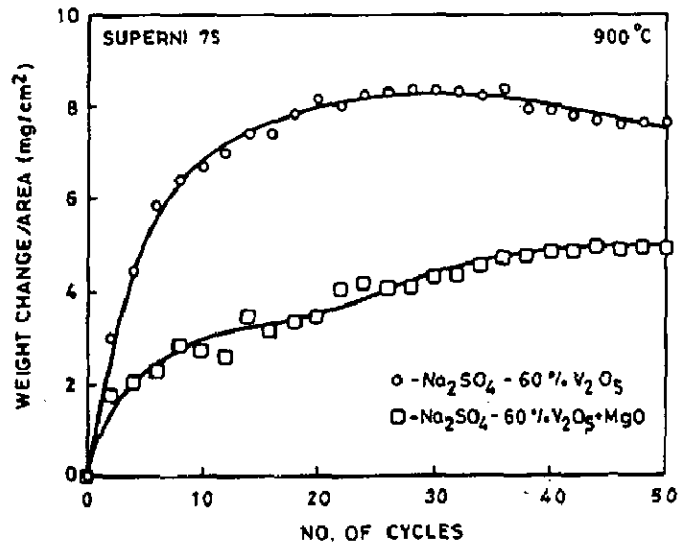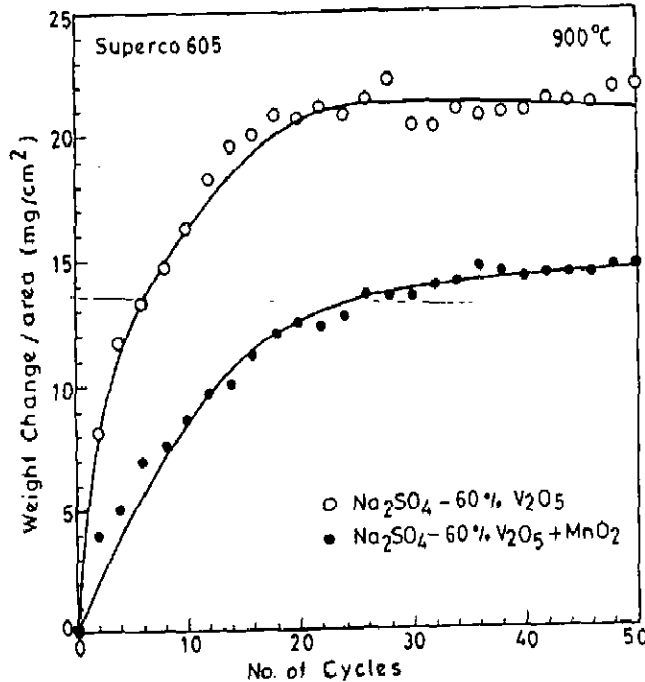

Fig. 5.39: Weight change plot for the alloy B (Superco 605) after cyclic hot corrosion at 900°C in Na_2SO_4-60% V_2O_5 +20% MnO_2.
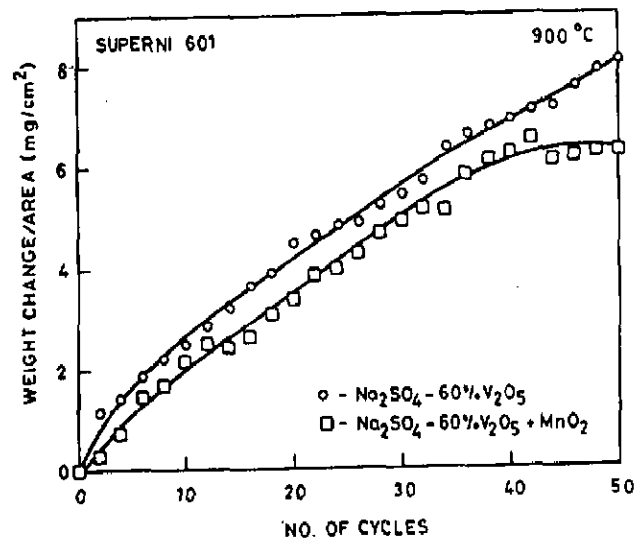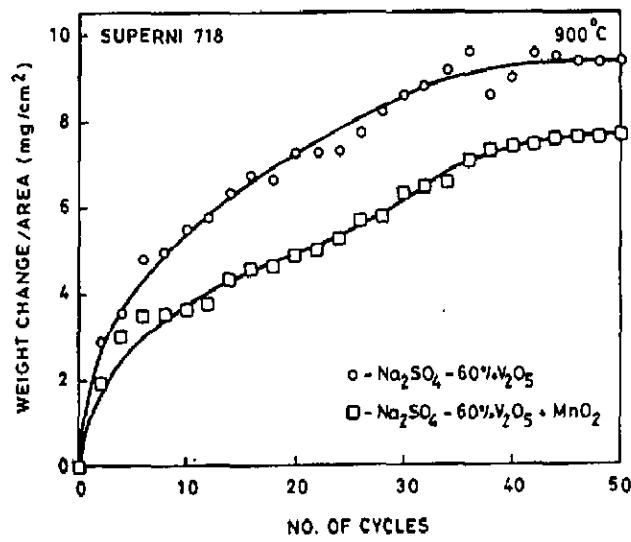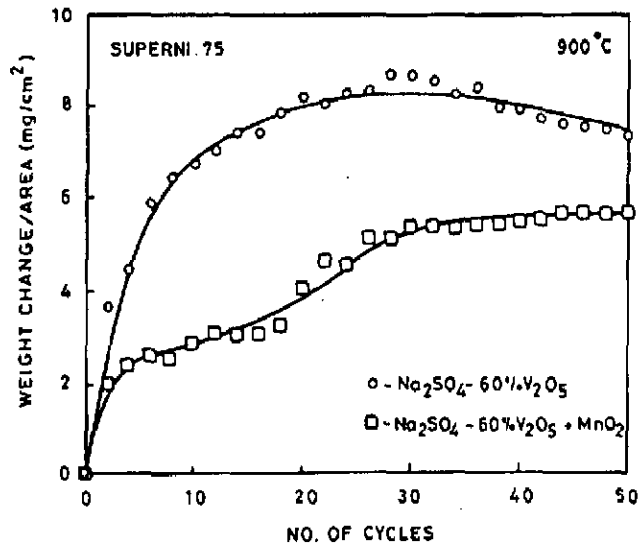
Fig. 5.40: Weight change plots for the nickel base alloys, alloy C (Superni 75), alloy D (Superni 718) and alloy E (Superni 601) after cyclic hot corrosion at 900°C in Na₂SO₄-60% V₂O₅ +20% MnO₂.
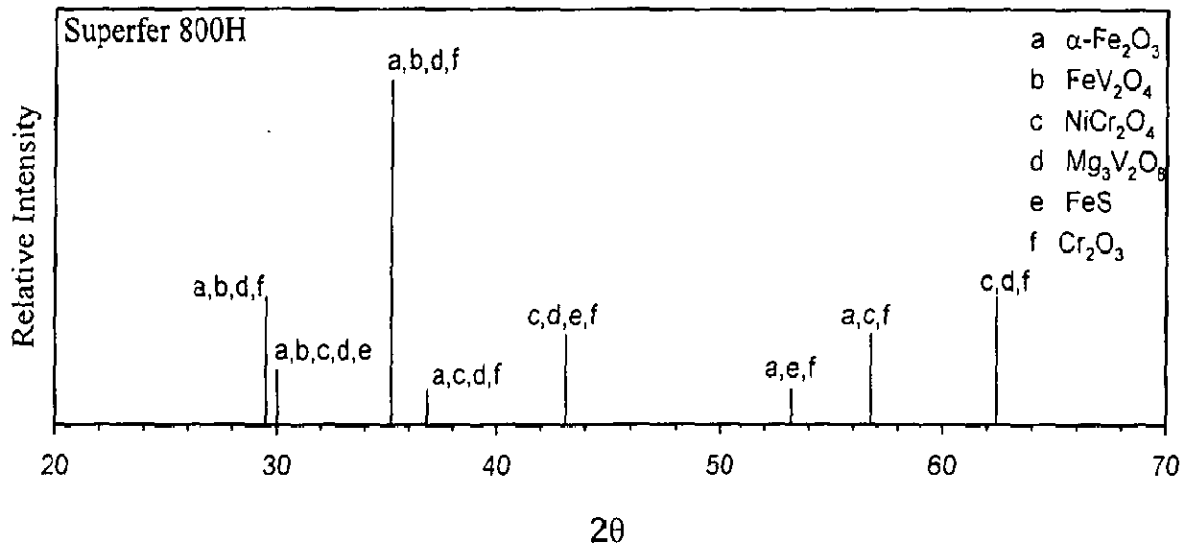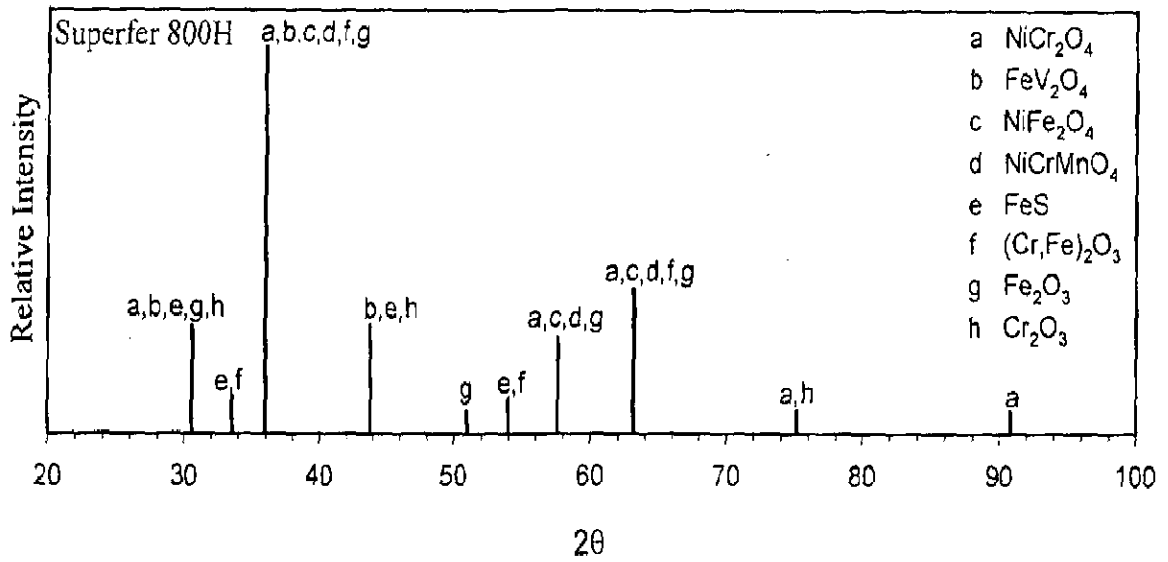
Fig. 5.41: X-ray diffraction profile for alloy A (Superfer 800H) after cyclic hot corrosion at 900^0C in Na_2SO_4-60% V_2O_5 +20% MnO_2.
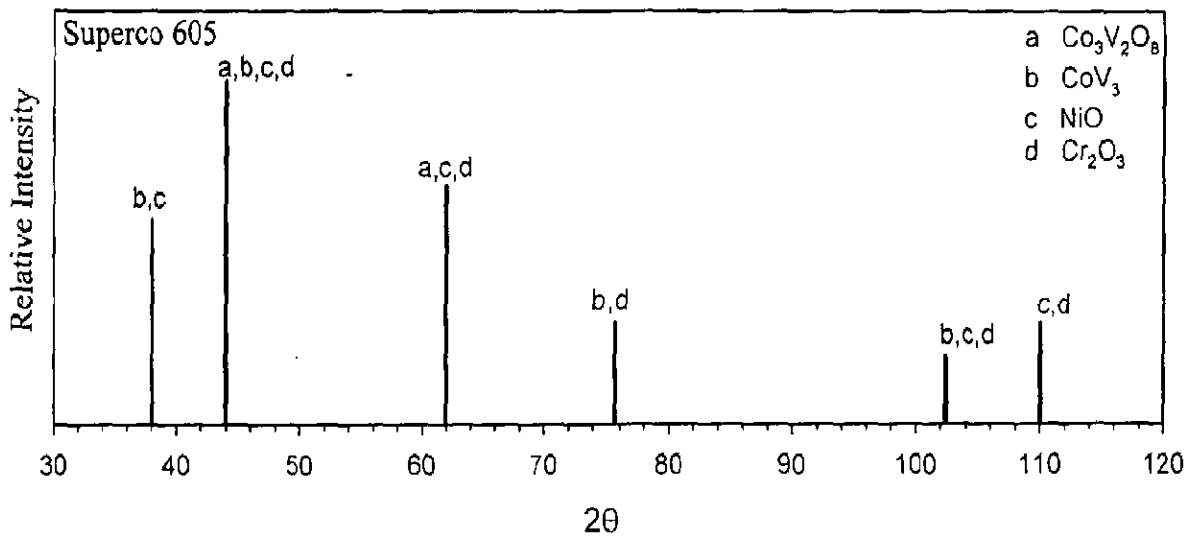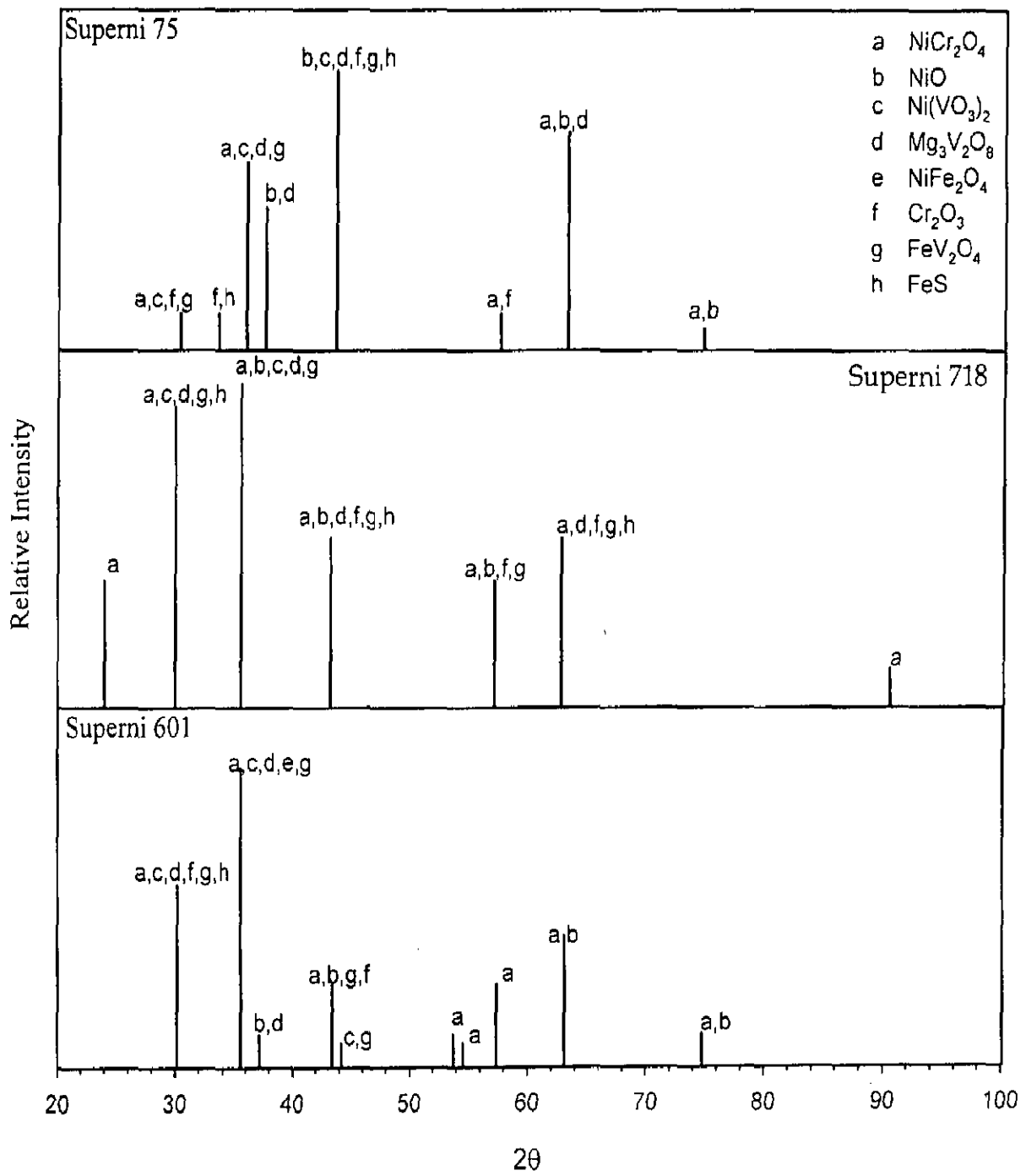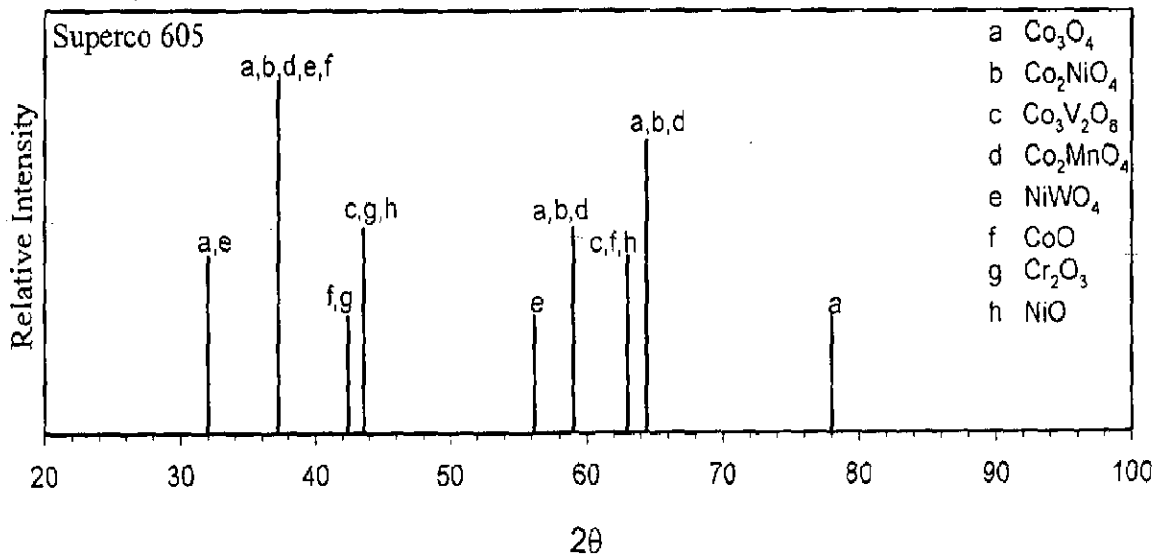

Fig. 5.42: X-ray diffraction profile for alloy B (Superco 605) after cyclic hot corrosion at 900^0C in Na_2SO_4-60% V_2O_5 +20% MnO_2.
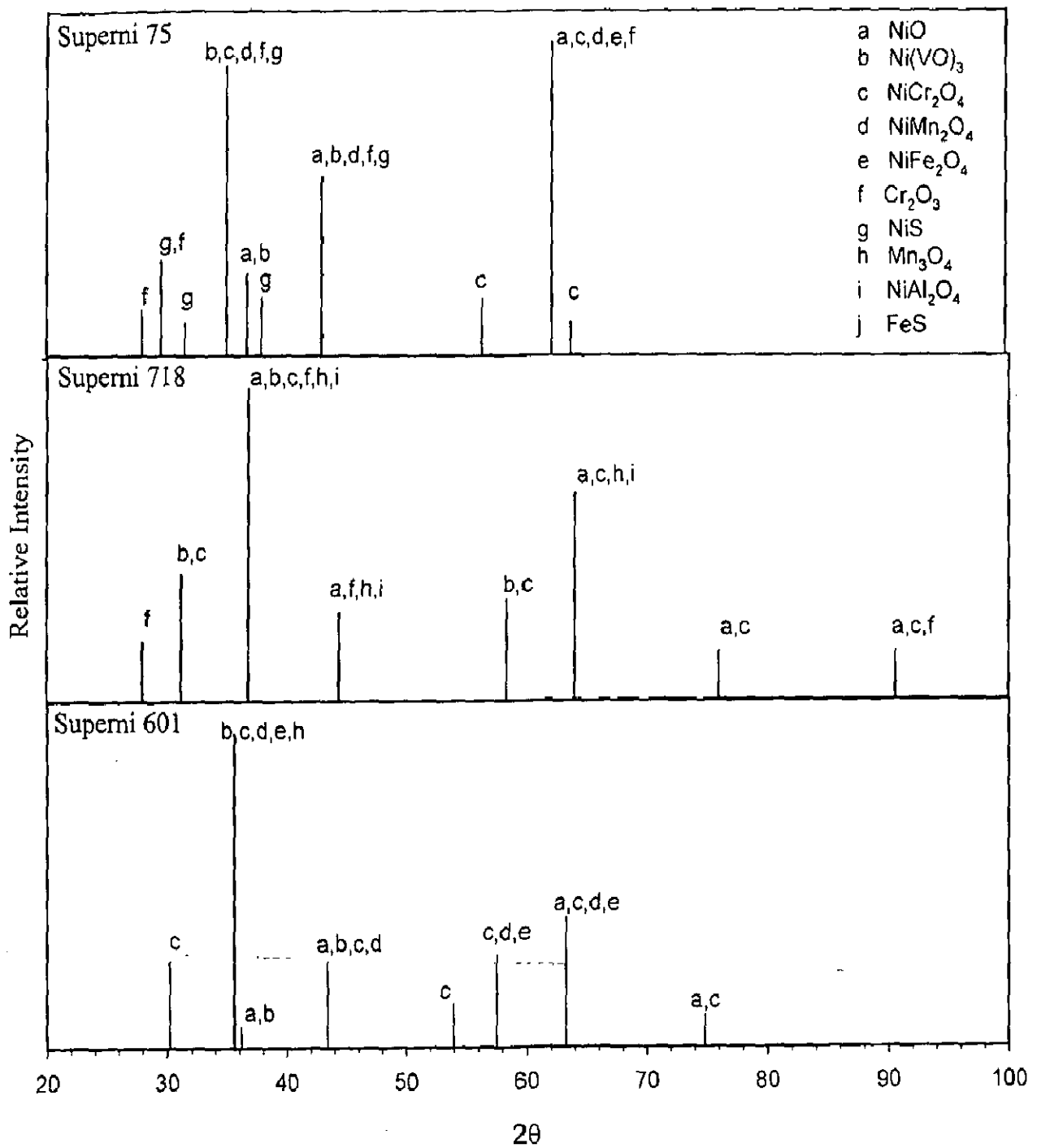
Fig. 5.43: X-ray diffraction profiles for the nickel base alloys: alloy C (Superni 75), alloy D (Superni 718) and alloy E (Superni 601) after cyclic hot corrosion at 900°C in Na₂SO₄-60% V₂O₅ +20% MnO₂.
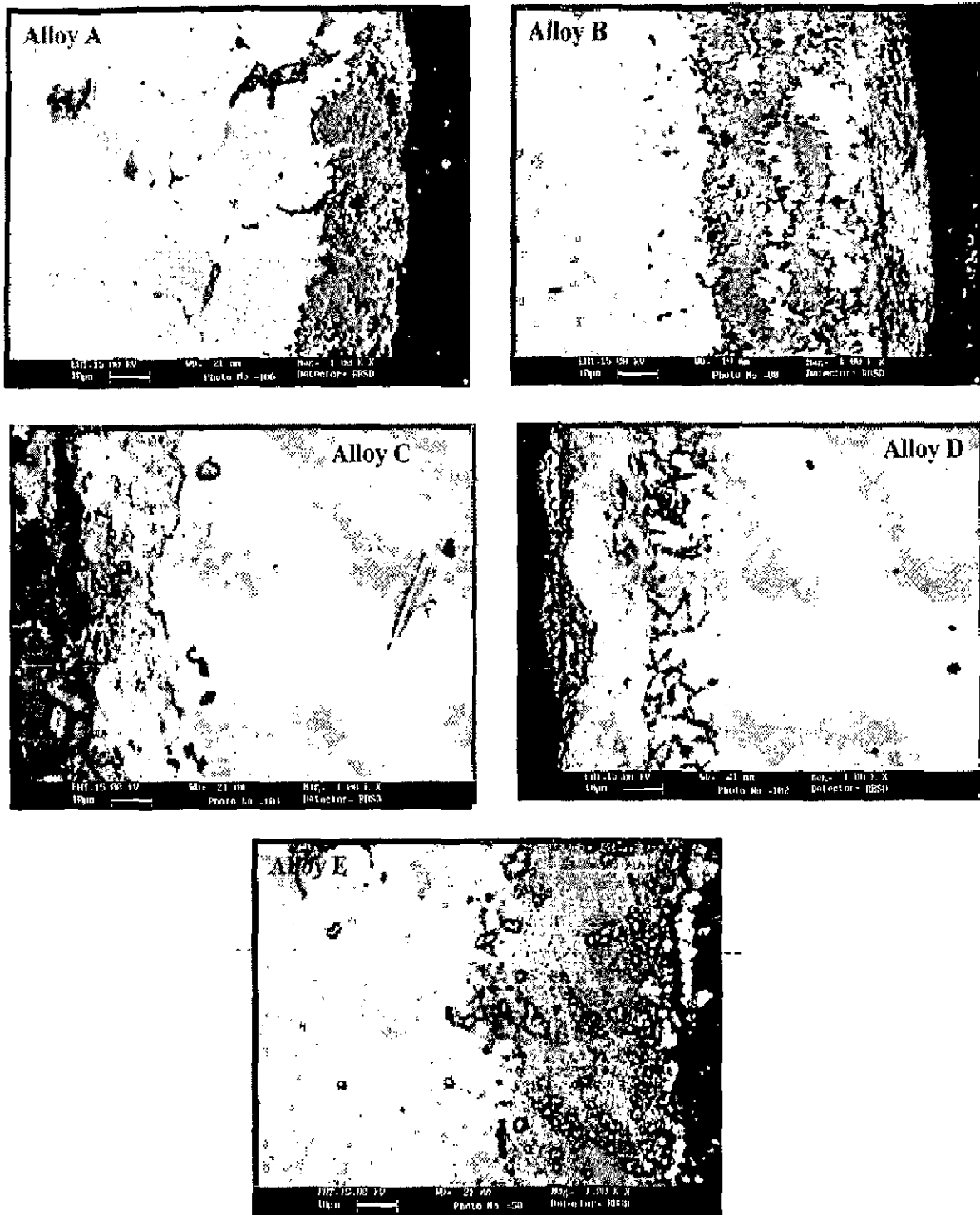
Fig. 5.44: BSE images of alloy A (Superfer 800H), alloy B (Superco 605), alloy C (Superni 75), alloy D (Superni 718) & alloy E (Superni 601) in Na_2SO_4-60%V_2O_5+20%MnO_2 environment after exposure at 900°C under Cyclic Conditions.

(a)

(b)

(c)

(d)

(e)
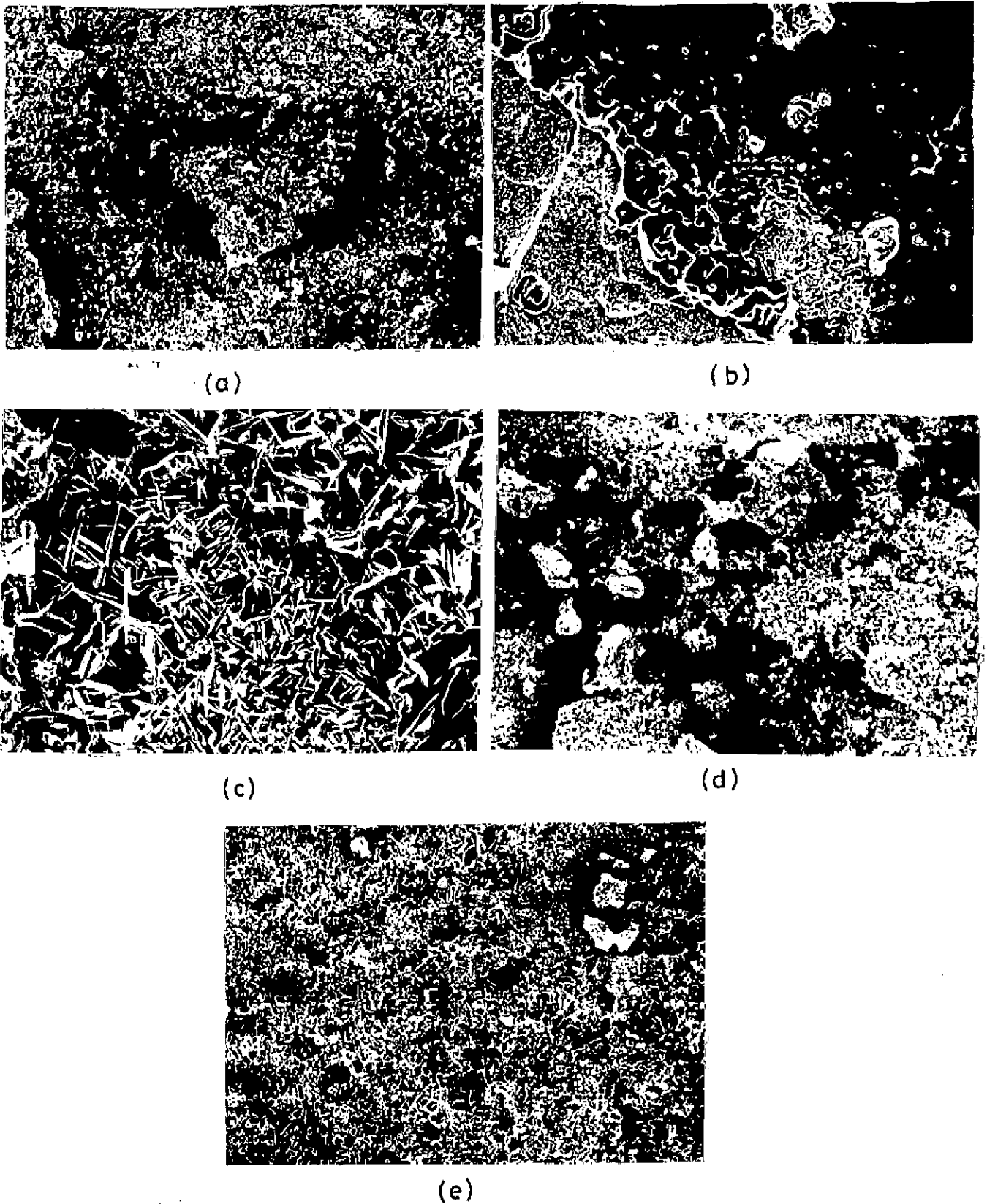
Fig. 5.45: Scanning Electron Micrographs after cyclic hot corrosion in Na_2SO_4-60%V_2O_5 +20% MnO_2 of alloys:

a) Alloy A (Superfer 800H)   (X 640)

b) Alloy B (Superco 605)   (X 640)

c) Alloy C (Superni 75)   (X 640)

d) Alloy D (Superni 718)   (X 640)

e) Alloy E (Superni 601)   (X 640)
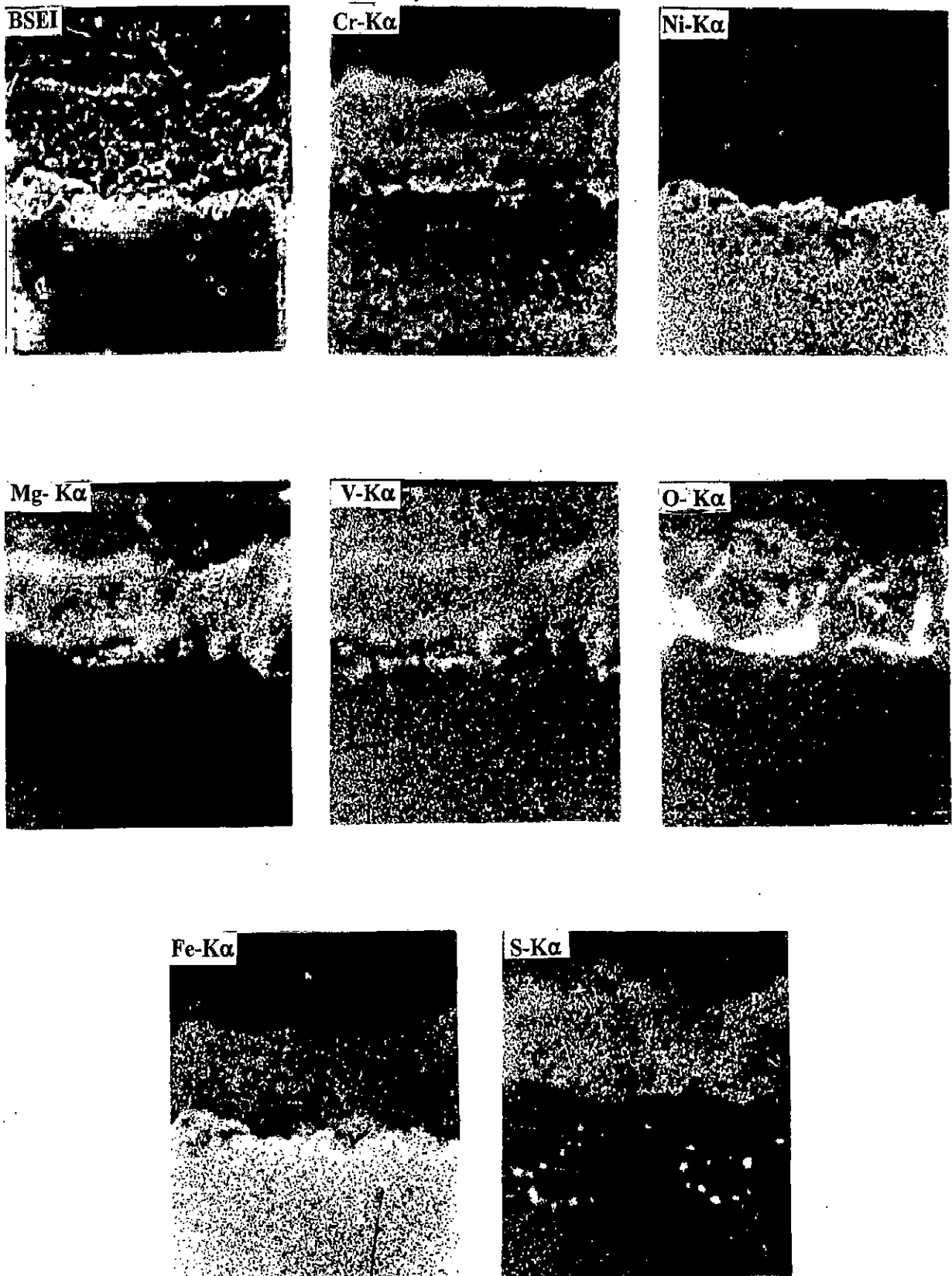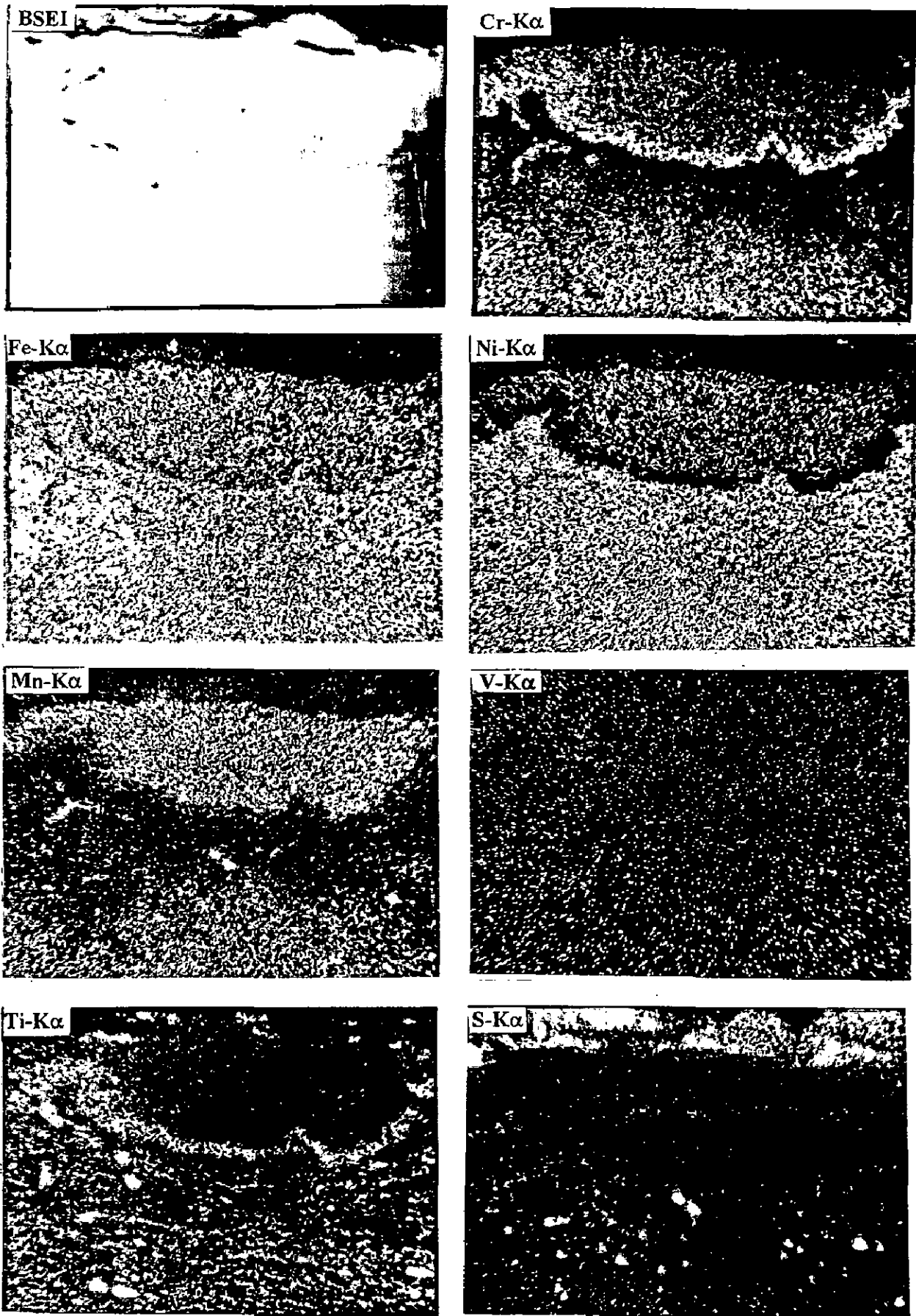
Fig. 5.46:   BSEI and X-ray mapping of the cross section of alloy A (Superfer 800H) after
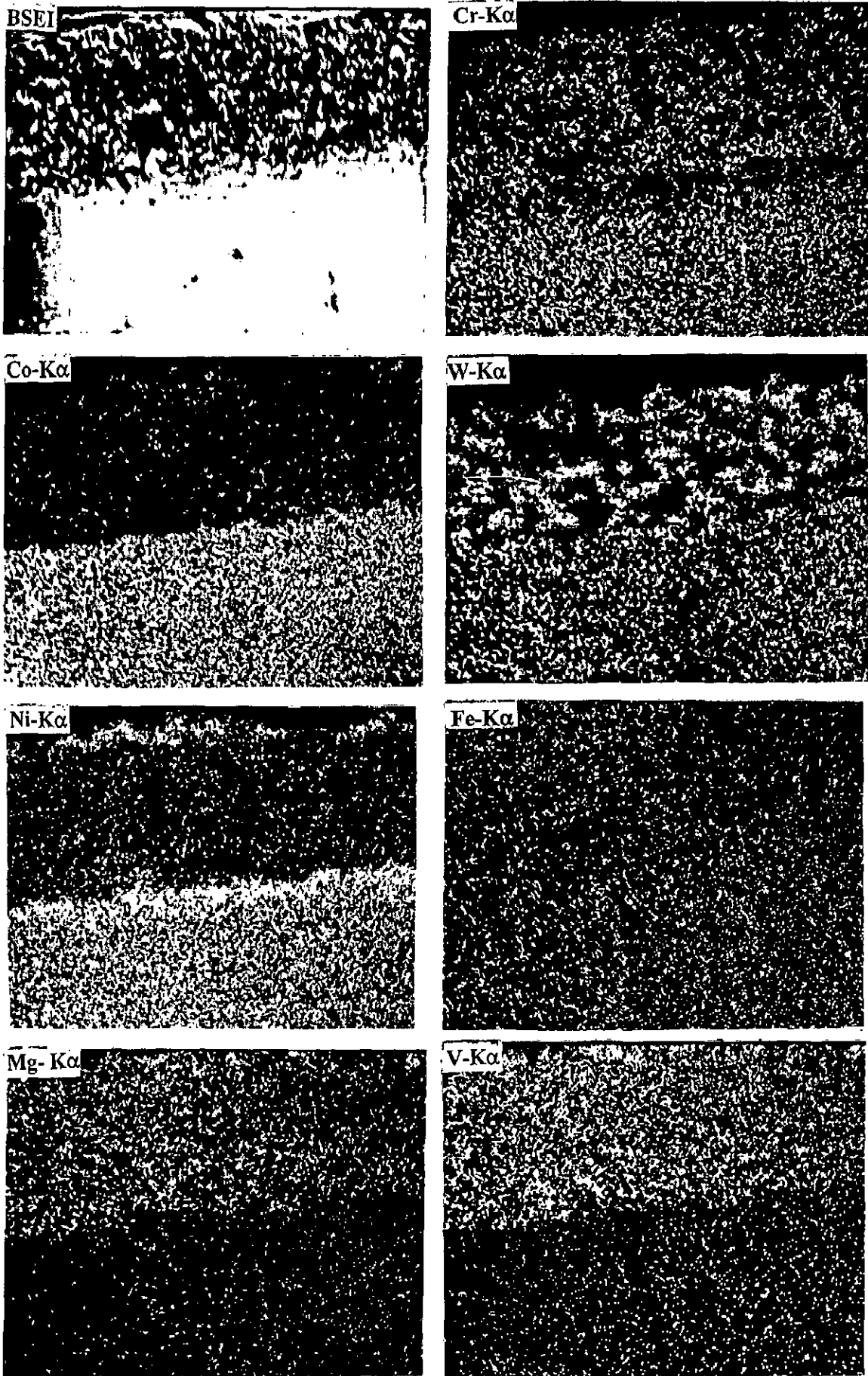cyclic hot corrosion at 900^0C in Na_2SO_4-60% V_2O_5+20% MnO_2 (X 800)
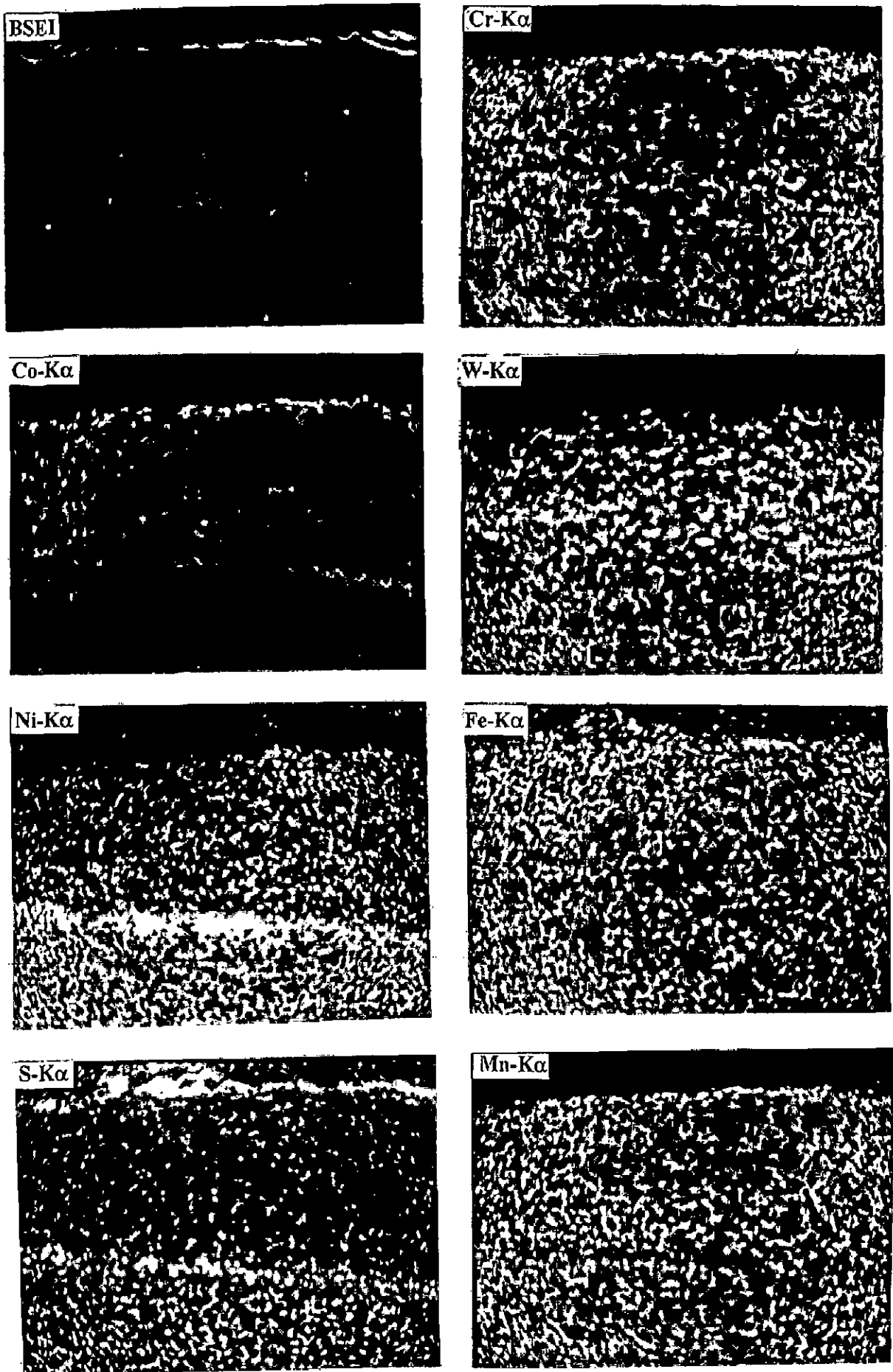
Fig. 5.47: BSEI and X-ray mapping of the cross section of alloy B (Superco 605) after cyclic hot corrosion at 900^0C in Na_2SO_4-60% V_2O_5+20% MnO_2. (X 400)
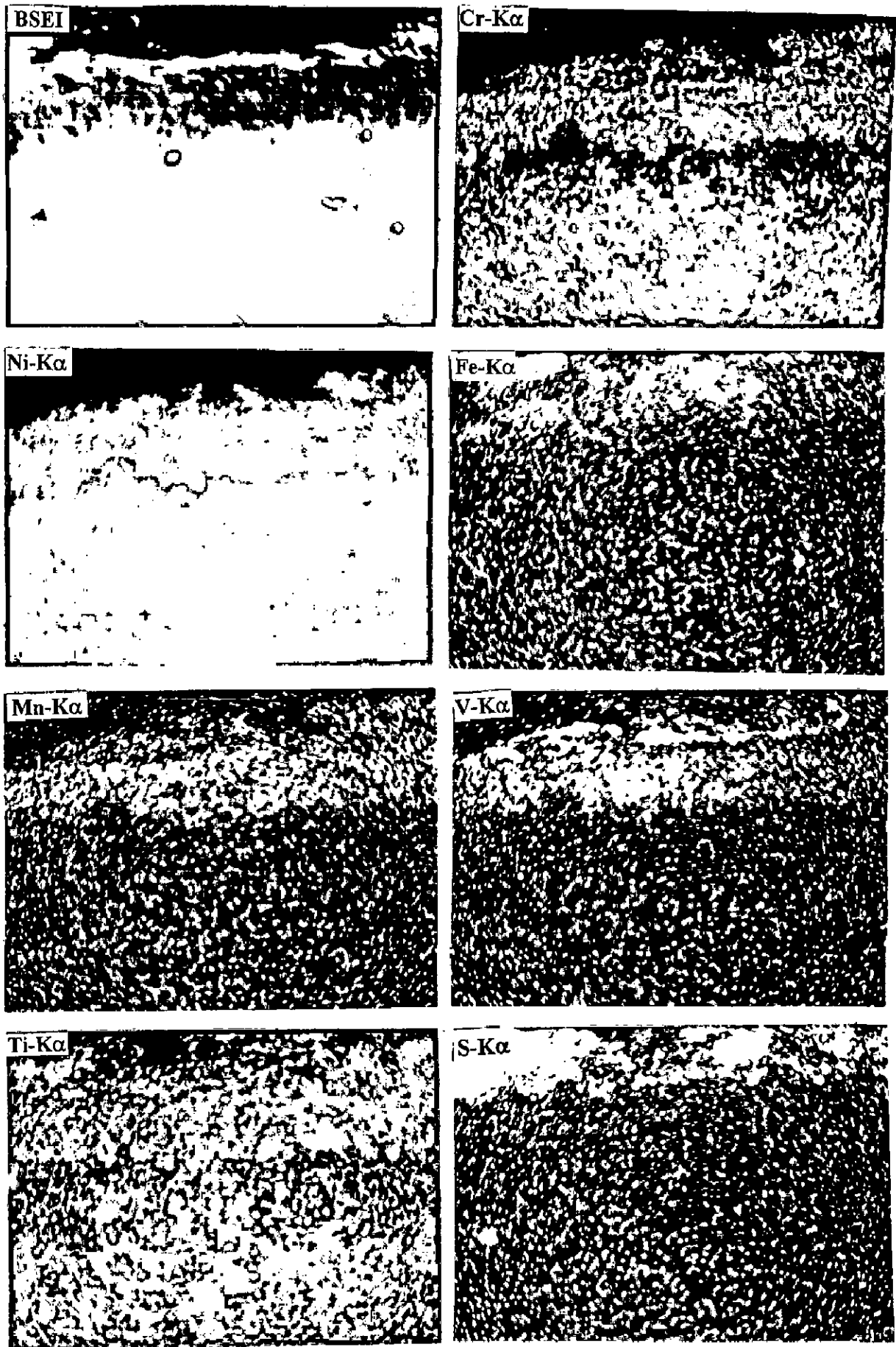
Fig. 5.48: BSEI and X-ray mapping of the cross section of alloy C (Superni 75) after cyclic hot corrosion at 900^0C in Na_2SO_4-60% V_2O_5 + MnO_2. (X 600)
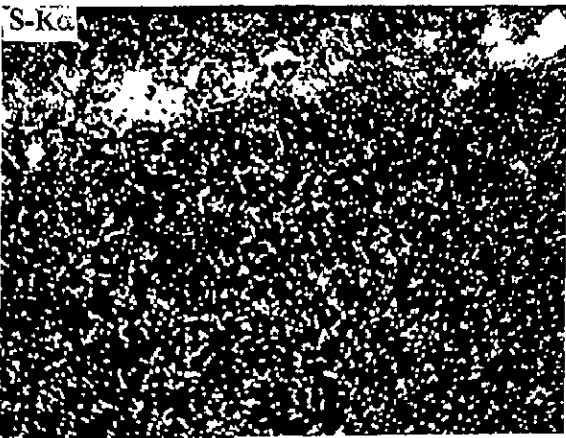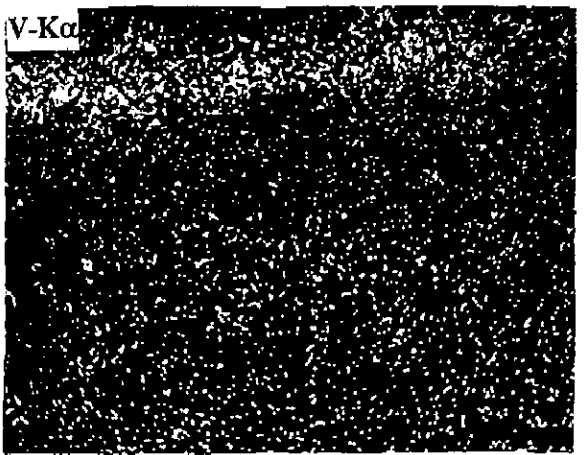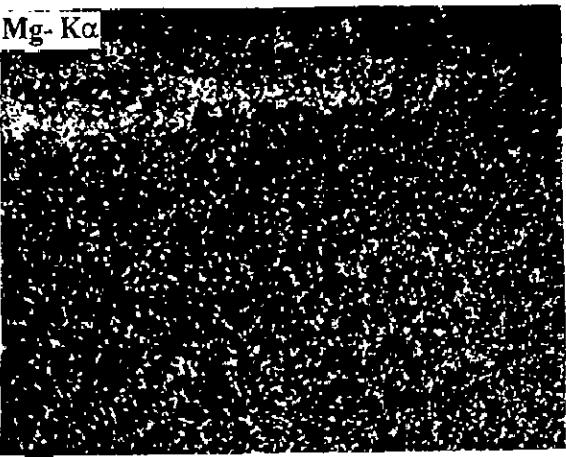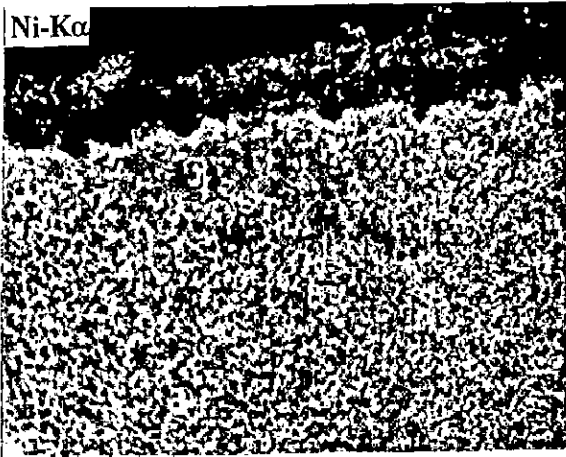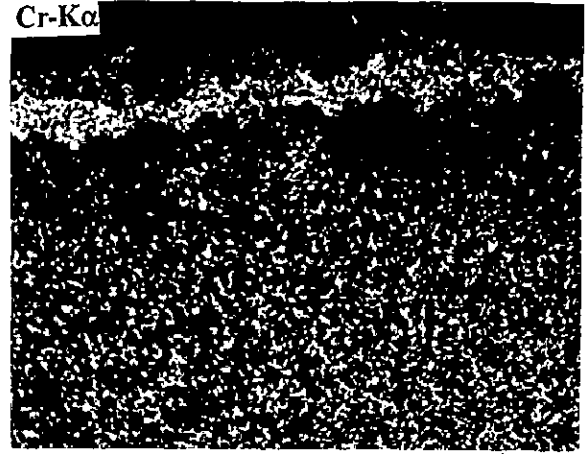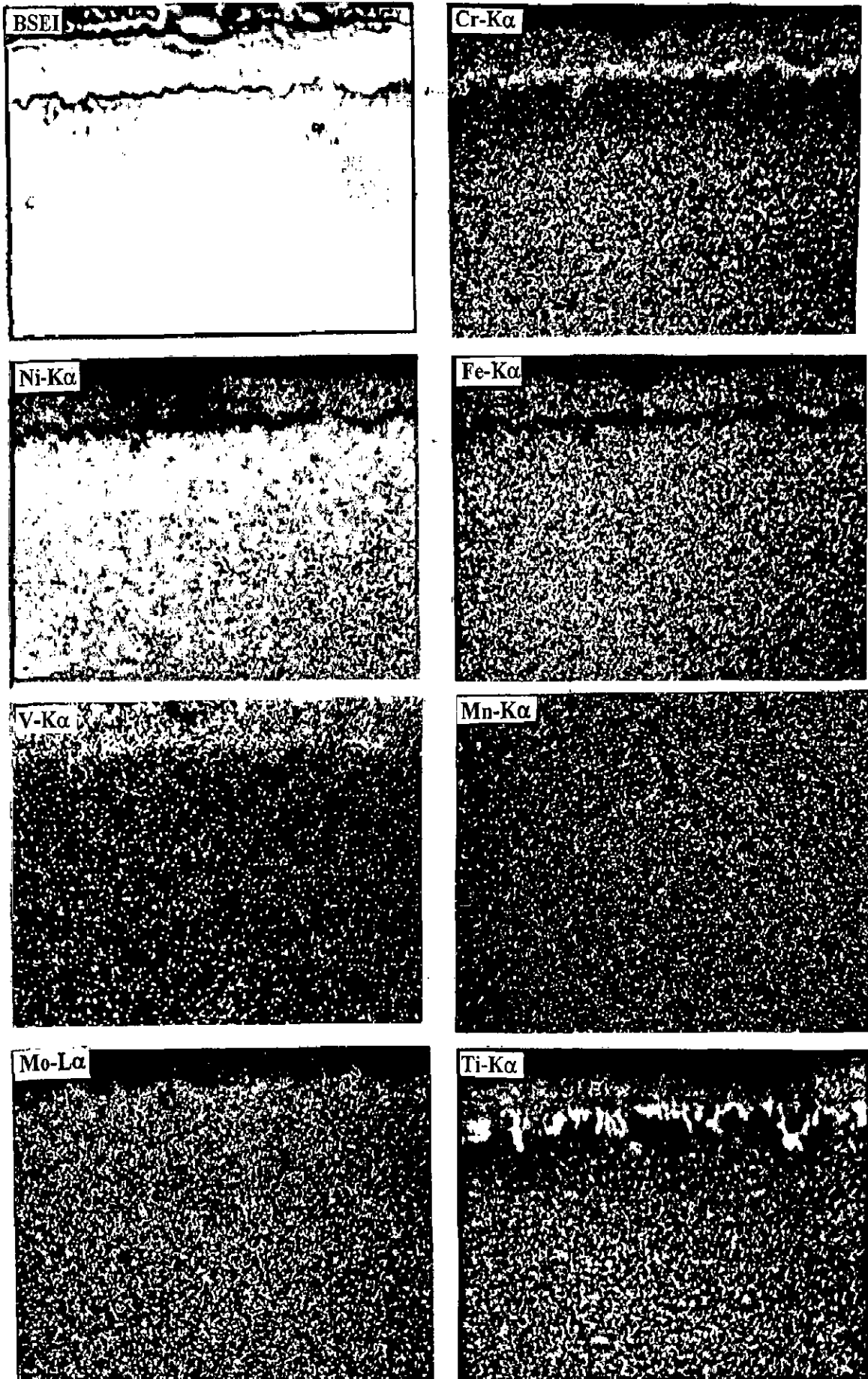
Fig. 5.49:   BSEI and X-ray mapping of the cross section of alloy D (Superni 718) after cyclic hot corrosion at 900^0C in Na_2SO_4-60% V_2O_5+20% MnO_2.   (X 600)

120
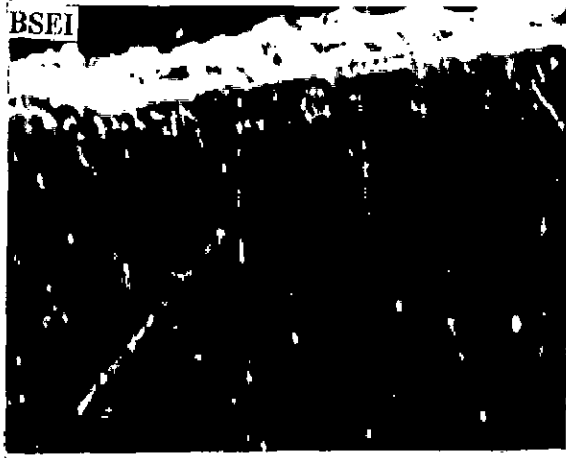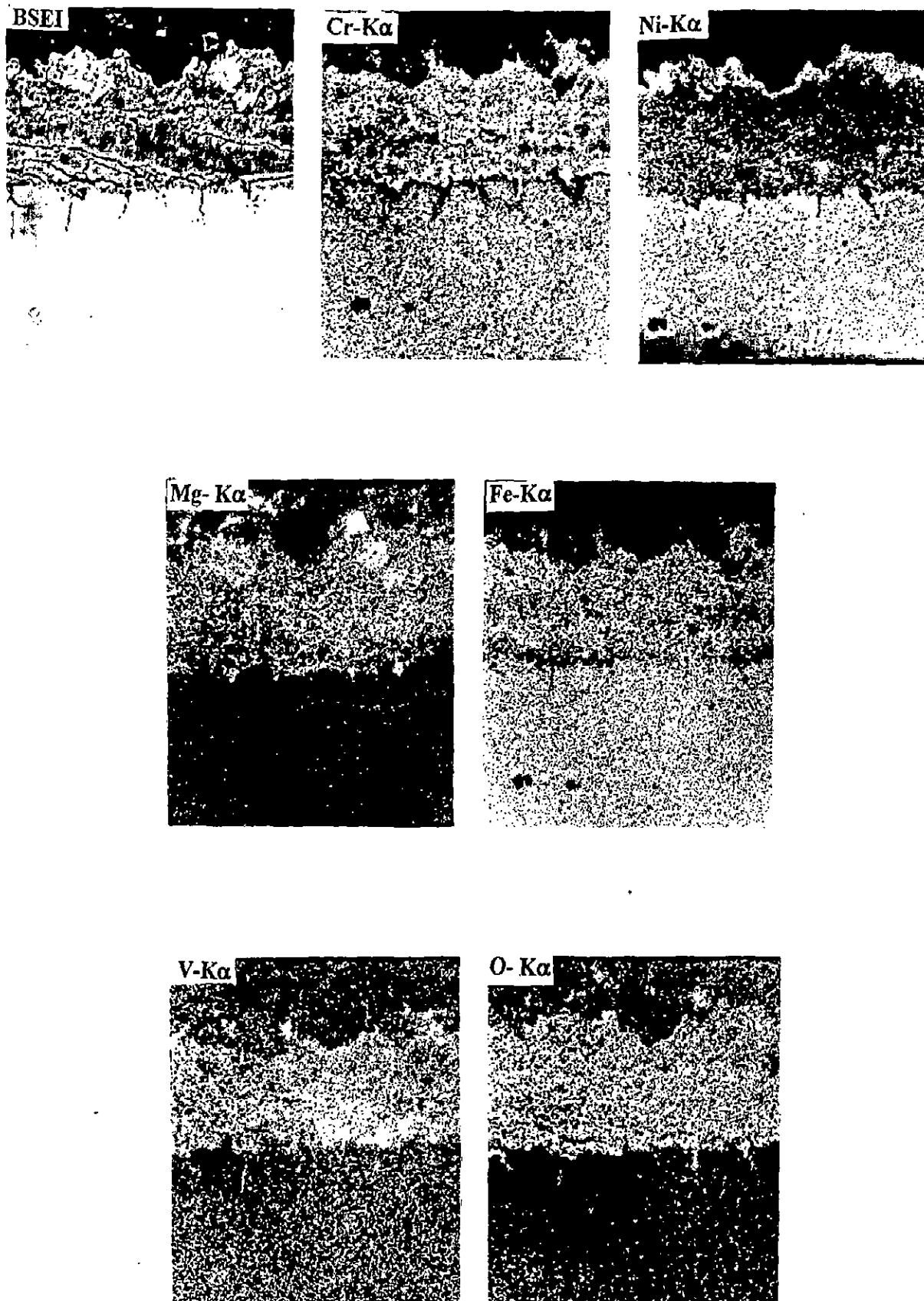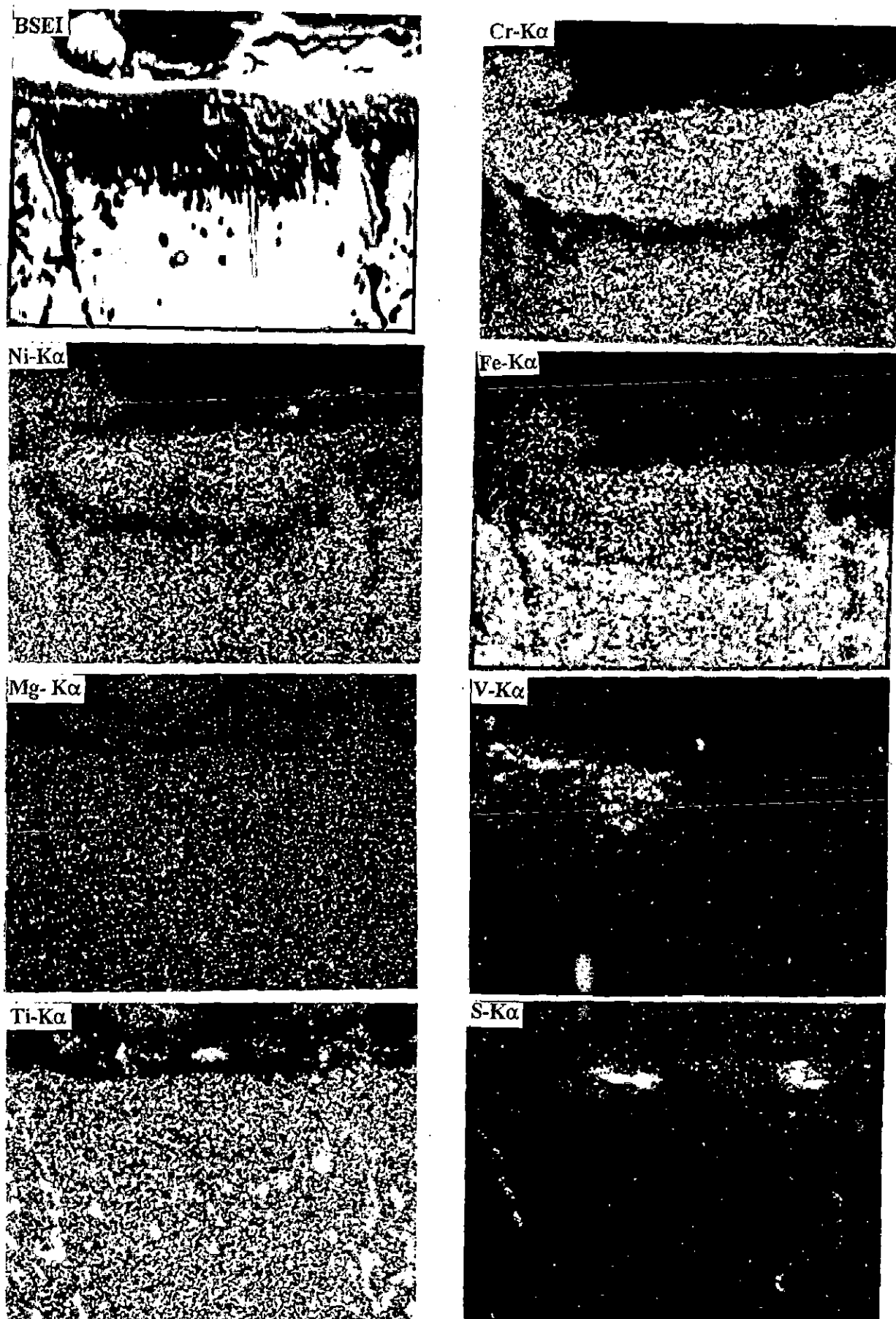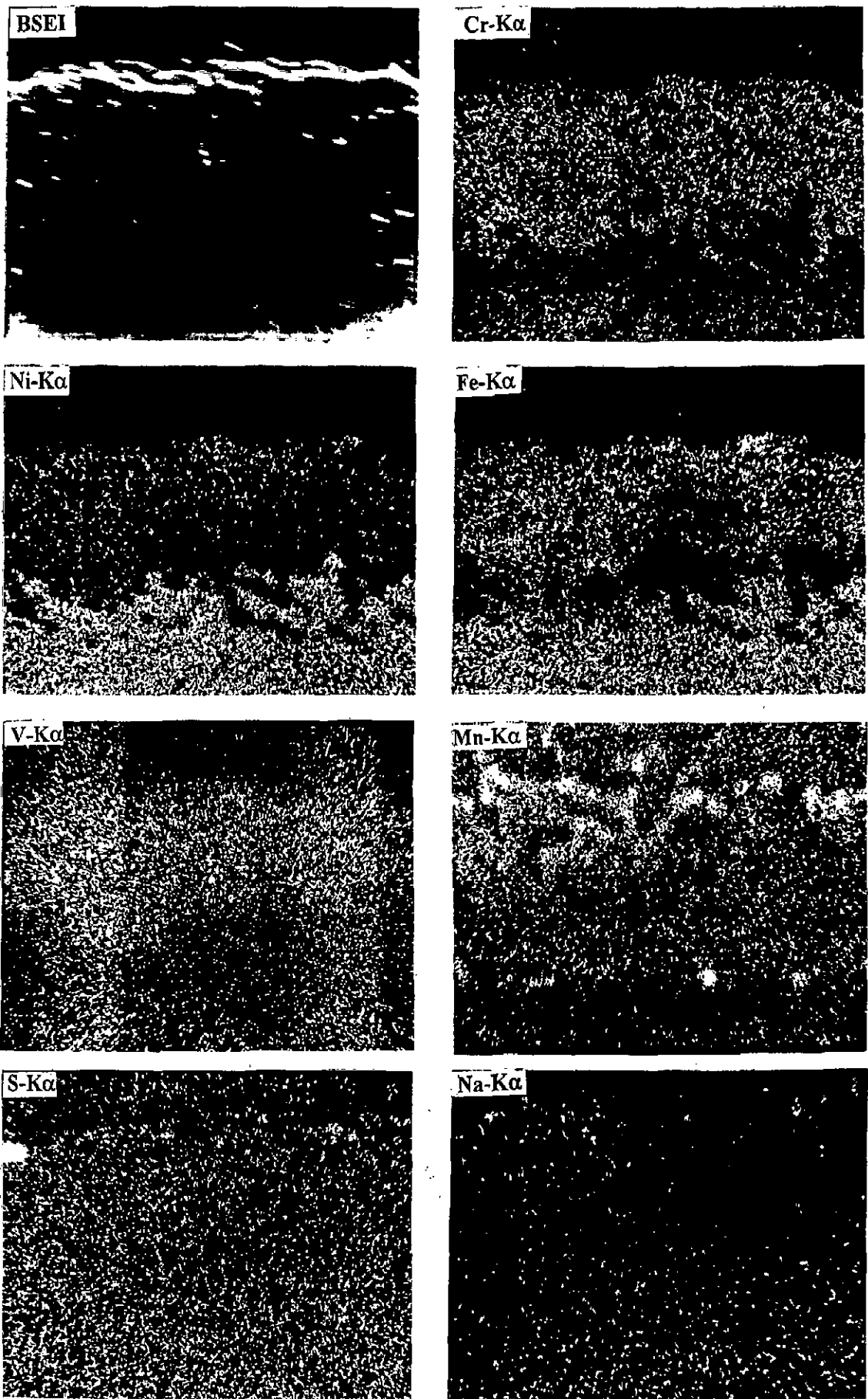
Fig. 5.50: BSEI and X-ray mapping of the cross section of alloy E (Superni 601) after cyclic hot corrosion at 900^0C in Na_2SO_4-60% V_2O_5+20% MnO_2. (X 600)

EDAX Analysis of alloy B (Superco 605) in Na₂SO₄-60%V₂O₅ + 20%MnO₂ along the Cross-Section after cyclic hot corrosion at 900°C

BSE Image of Alloy B (Superco 605) in Na₂SO₄-60%V₂O₅+20% MnO₂

Fig. 5.51 : Back Scattered Image of alloy B (Superco 605) after cyclic hot corrosion in Na₂SO₄-60%V₂O₅+ MnO₂ at 900°C.

Table. 5.2: Wt % of elements corresponding to points marked on Fig. 5.51, BSE image of alloy B (Superco 605).

Point of analysis	Weight % of element									
	O	Fe	Ni	Cr	Co	W	Mn	Na	V	S
1	29.05	0.95	3.38	18.87	26.04	19.95	-	0.07	0.85	0.06
2	32.16	0.95	2.68	16.77	23.58	21.42	1.23	0.10	0.97	011
3	30.80	0.58	3.16	10.47	19.18	34.34	0.45	0.10	0.11	0.07
4	31.03	0.48	3.78	10.02	18.87	34.31	0.49	0.16	-	0.00
5	31.08	0.53	3.39	17.49	25.35	25.51	0.55	0.13	1.03	0.01
6	7.39	1.20	9.46	17.80	47.00	15.50	1.46	-	0.17	-

5.5 HOT CORROSION STUDIES IN Na_2SO_4-60%V_2O_5 +10% $ZnSO_4$

5.5.1 Visual Observations

Fig. A.1 shows the macrographs for corroded specimens of alloys A, C, D & E after exposure for 50 cycles at 900^0C with Na_2SO_4-60%V_2O_5+10%$ZnSO_4$ coating in air. The surface scale is black in colour, rough, and spalled at many places in case of alloy A.

For alloy C the scale was dense and adherent but spalled off from most of the surface and remained intact along the edges, so the edges were yellowish in colour where as other areas looked dull black. The scale of alloy D & E was uneven and dark grey/black in colour. Spalling was observed during experimentation in both the cases.

5.5.2 Kinetic Data

The plots of weight gain vs number of cycles for the alloys A, C, D and E in Na_2SO_4-60%V_2O_5 + 10%$ZnSO_4$ coating at 900^0C in air for maximum up to 30 cycles has been shown in Figs. 5.52, 5.53, 5.54 and 5.55. In case of alloy B a very thick grey coloured scale was found in the first two cycles, which showed blister formation as well. Those blisters gave way & cracked and whole of the coating came out up to the 8th cycle. So no further experimentation could be carried on. Even in iron base alloy Superfer 800H (alloy A) and nickel base alloy Superni 718 (alloy D) sputtering and spalling of the scale started after 10 cycles because of which experimentation could be carried only up to 30 cycles. Plot for alloy A shows a rapid increase in the weight gain during first 10 cycles, maximum weight gain reaching up to ~8 mg/cm^2. For alloy C, the increase in weight is more during initial cycles and after 15 cycles it is nearly constant. The wt. gain seems nearly 60% of that without $ZnSO_4$ addition. In case of alloy D, there is a steady increase up to 10 cycles but spalling and wt. loss noticed during 10 to 12 cycles after which there is no appreciable change in wt. gain but alloy E behaved more or less like alloy C, there is a gradual increase in weight tending to be linear up to 22 cycles and change in weight is nearly same up to 25 cycles after which decrease in weight occurred due to the spalling of the scale and the weight gain after 30 cycles of exposure is 4 mg/cm^2.

5.5.3. X-ray diffraction analysis

XRD data is complied in Tables A.13 to A.16 and X-Ray diffraction profiles are shown in Figs. 5.56, 5.57, 5.58 and 5.59 for the alloys A, C, D and E respectively. The prominent phases identified on the corroded specimen of alloy A were Fe_2O_3, $ZnFeVO_4$, $ZnFe_2O_4$, $NiCr_2O_4$, $Ni\ Fe_2O_4$, FeS and Cr_2O_3. In Ni base alloy C, the main phase identified is NiO. The main phases identified in alloy D are Fe_2O_3, $NiCr_2O_4$, NiO and Cr_2O_3 whereas in case of alloy E the main phases are $ZnFe_2O_4$, $ZnFeVO_4$, $Ni(VO_3)_2$, $NiCr_2O_4$ and Cr_2O_3.

5.5.4. Measurement of scale Thickness

Scale thickness measured from the back scattered images given in Fig. 5.60 for alloys A, C, D and E coated with Na_2SO_4-60%V_2O_5+10%$ZnSO_4$ and exposed at 900^0C are 46.6, 34, 41.5 and 46 μm respectively after 30 cycles.

5.5.5. SEM, EDAX and EPMA Results

SEM analysis of the alloys A, C, D and E after exposure presented in Fig. 5.61 (a, b, c, d and e) of the surface indicates formation of continuous scale with pores in case of alloy A, crystalline structure is indicated in Fig. 5.61(b) for alloy C. EDAX of the surface of the scale for the same alloy C (Fig.5.61, c and Table A.29) indicates that mainly Ni is present in the scale with small amount of Cr, Zn and V. SEM of alloy D reveals a massive scale indicating spalling in some areas but for the alloy E, a crystalline growth at the top of the scale is noticed.

BSEI and X-ray images of alloy A coated with Na_2SO_4-60%V_2O_5+10%$ZnSO_4$ after hot corrosion shown in Fig. 5.62 indicates formation of medium size scale mainly consisting of an outer scale rich in Ni, Cr and Fe. This is followed by a thick middle scale, which again contains mainly chromium with Ni & Fe. The region between the top scale & the middle scale contains higher concentration of sulphur. Vanadium is present at the interface between the substrate and the scale. There is a thin layer rich in Ni present along the alloy/scale interface where concentration of V is also high indicating nickel vanadate formation. Aluminium is also present in high concentration along this region, incorporation of Mn and Ti is also indicated in the scale.

The EPMA analysis for Alloy C (Supermi 75) Fig. 5.63 indicates formation of medium size scale mainly containing Cr, Fe and Ni. The region just above the substrate has got Cr rich layer penetrating into the substrate. The V is seen throughout the scale. Internal oxidation of Ti is seen just below the scale. The EDAX analysis of this alloy along cross-section at different points in the scale presented in Fig. 5.66 and Table 5.3, indicates that top layer of the scale consists of mainly Ni with small amount of Cr and little amounts of Zn, Fe, Ti, S & V. As we go down the scale, the amount of Ni goes on decreasing and that of Cr goes on increasing. The amount of V & S also goes on decreasing and the amount of Ti increases up to one level. It further indicates that outer scale mainly contains Ni and the subscale above the substrate is rich in Cr.

X–ray images for alloy D, Fig. 5.64 indicate top layer of the scale being rich in Cr. Nickel and Fe are also present but the scale just below this is depleted in Cr. Along the internal grain boundaries, chromium has got oxidised where Ni & Fe are absent. V and Zn are indicated co-existing in same areas at the top of the scale. Oxidation of Al along the grain boundaries is indicated. Ti is present in the scale and at certain points it is in higher concentration.

The EPMA analysis of the corroded alloy E, Fig. 5.65 indicates formation of a medium sized scale which is mainly consisting of Ni, Cr and Fe. The concentration of the Cr along the interface between the substrate and the scale is slightly higher. The substrate is depleted in Cr & Fe and is rich in Nickel. The internal oxidation of Al is indicated. V is seen throughout the scale and at some points it is at higher concentration and co-existing with Zn.

Elemental EDAX analysis across the scale of alloy E (Fig. 5.67 and Table 5.4) indicates that the top scale is rich in Ni & Cr and the amount of Cr increases as we move downwards in the scale. Al is present throughout the scale but the intergranular region is mainly containing Al_2O_3. Amount of Zn goes on increasing as we travel down the scale. V is present throughout the scale and its amount also goes on increasing as we move down in the scale. S is also indicated in traces in the scale. Presence of oxygen indicates formation of mainly oxides throughout the scale.
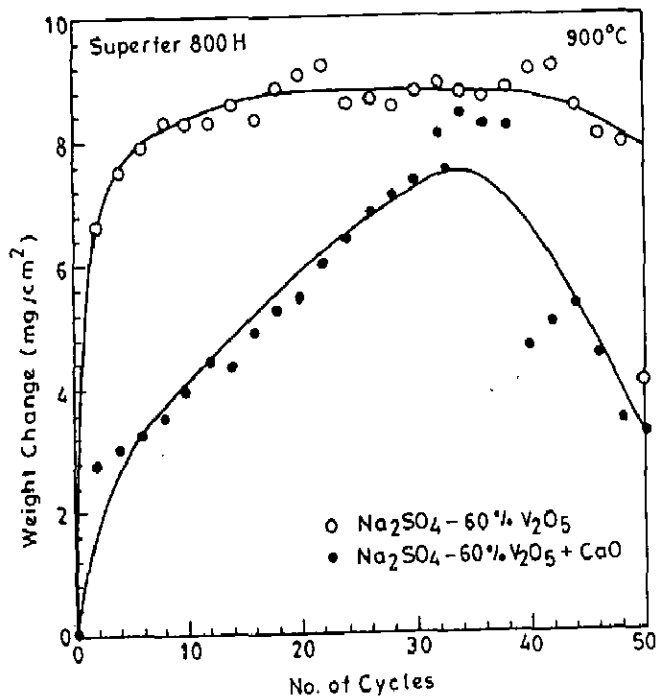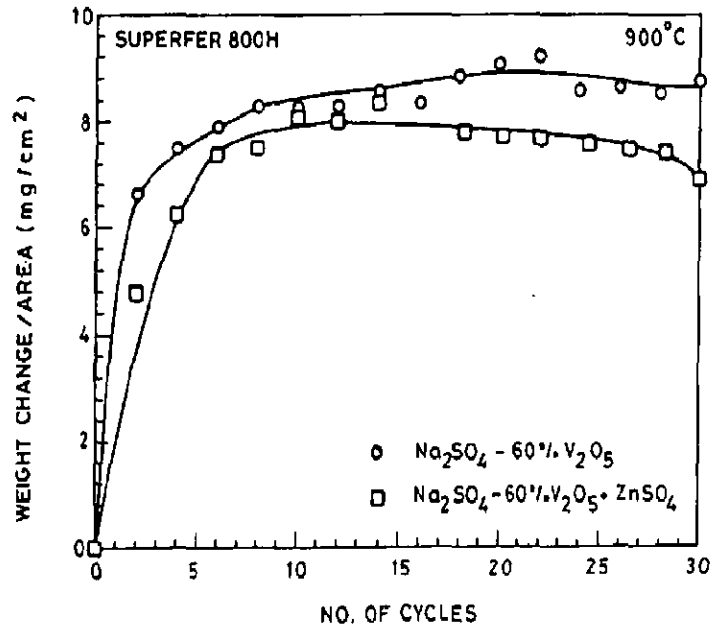
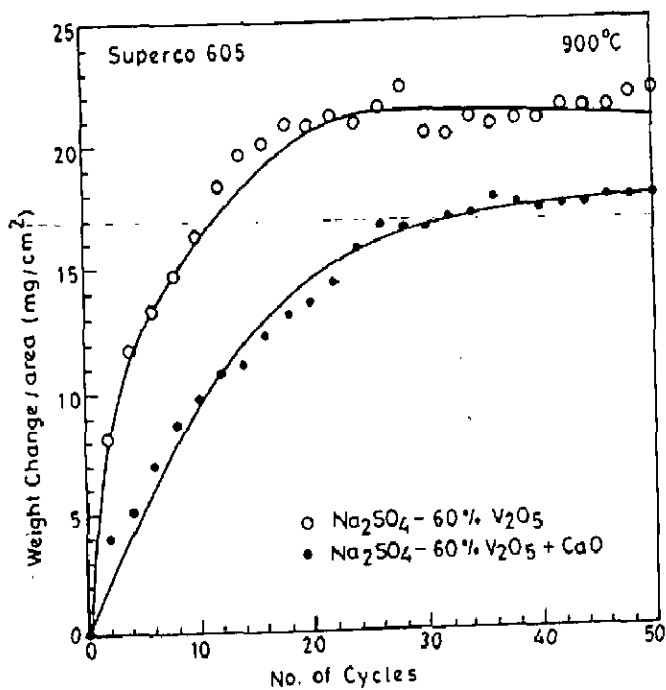**Fig. 5.52:** Weight change plot for the alloy A (Superfer 800H) after cyclic hot corrosion at 900⁰C in Na₂SO₄-60% V₂O₅ +ZnSO₄.
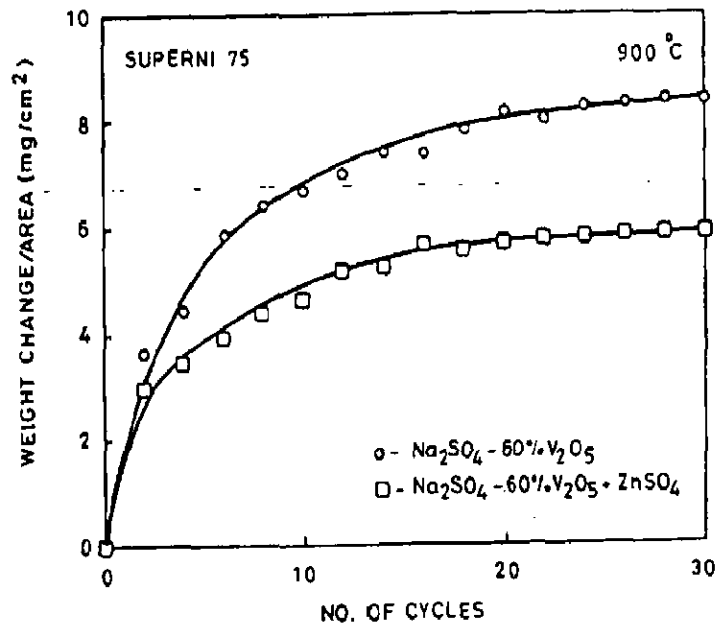
Fig. 5.53: Weight change plot for the alloy C (Superni 75) after cyclic hot corrosion at 900⁰C in Na₂SO₄-60% V₂O₅ + ZnSO₄.

126
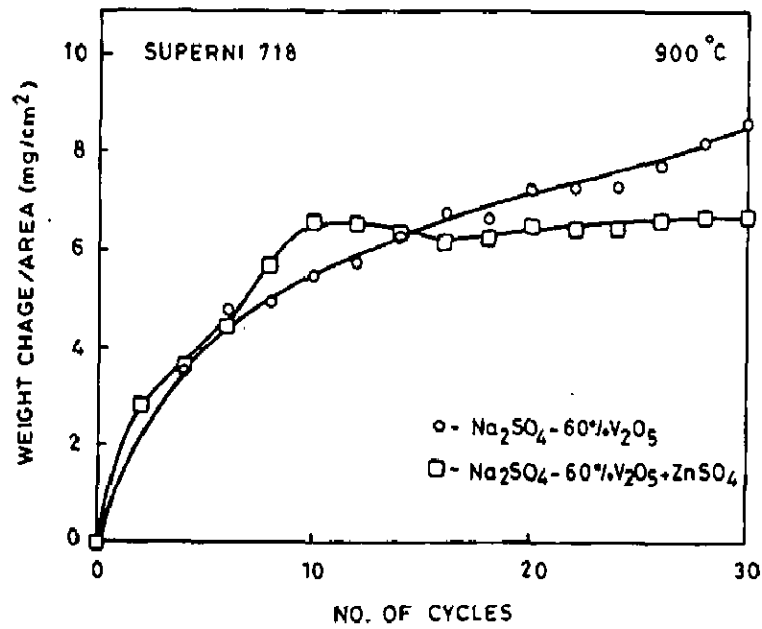
Fig. 5.54: Weight change plot for the alloy D (Superni 718) after cyclic hot corrosion at 900°C in Na$_2$SO$_4$-60% V$_2$O$_5$ + ZnSO$_4$.
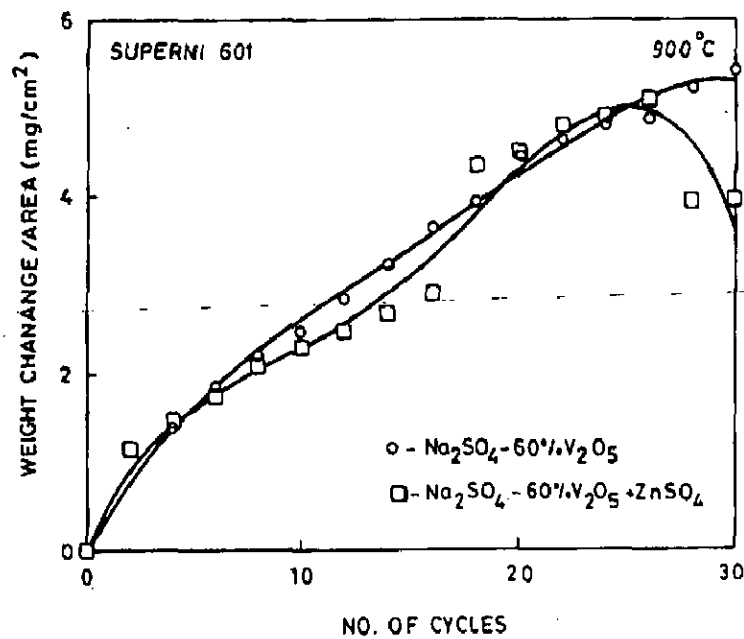
Fig. 5.55: Weight change plot for the alloy E (Superni 601) after cyclic hot corrosion at 900°C in Na$_2$SO$_4$-60% V$_2$O$_5$ + ZnSO$_4$.
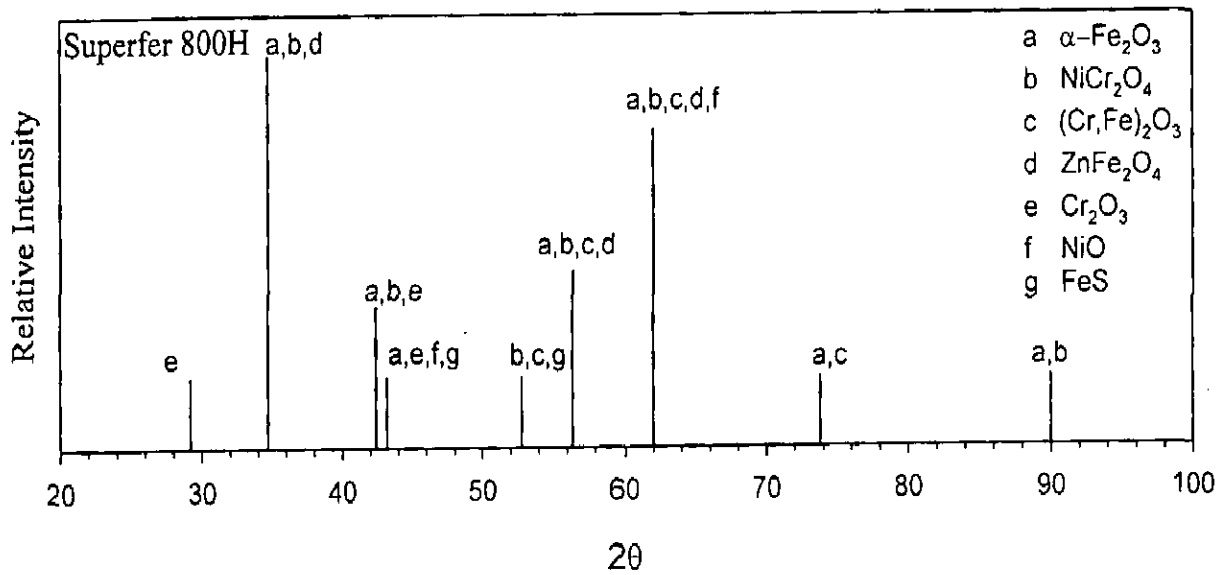
Fig. 5.56: X-ray diffraction profile for alloy A (Superfer 800H) after cyclic hot corrosion at 900°C in Na_2SO_4-60% V_2O_5+ $ZnSO_4$.
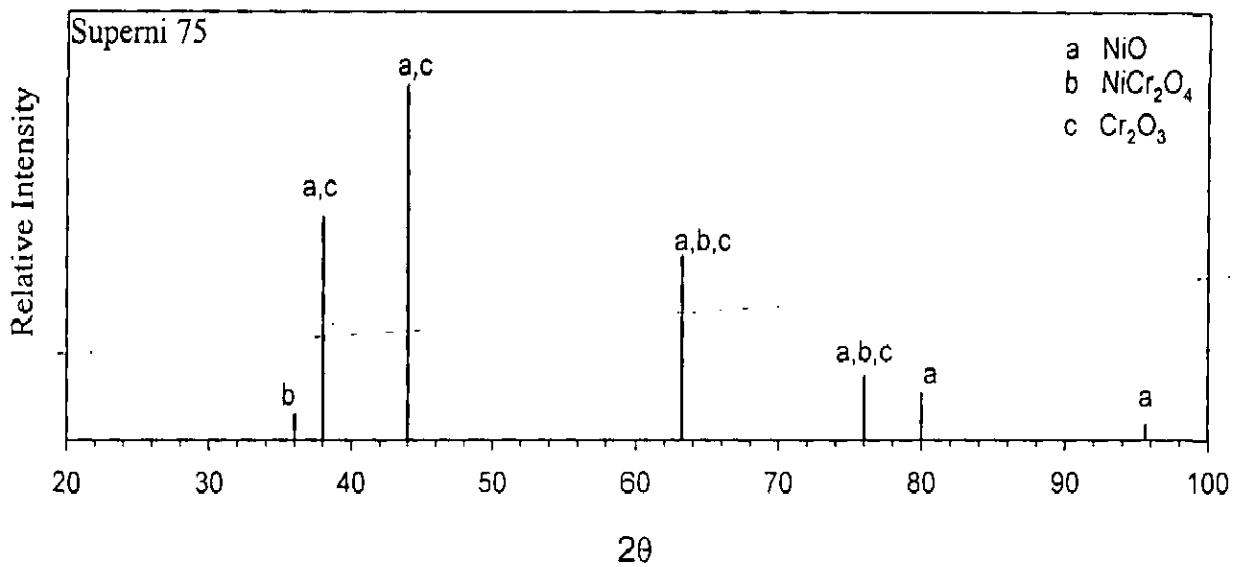
Fig. 5.57: X-ray diffraction profile for alloy C (Superni 75) after cyclic hot corrosion at 900°C in Na_2SO_4-60% V_2O_5+ $ZnSO_4$.

128
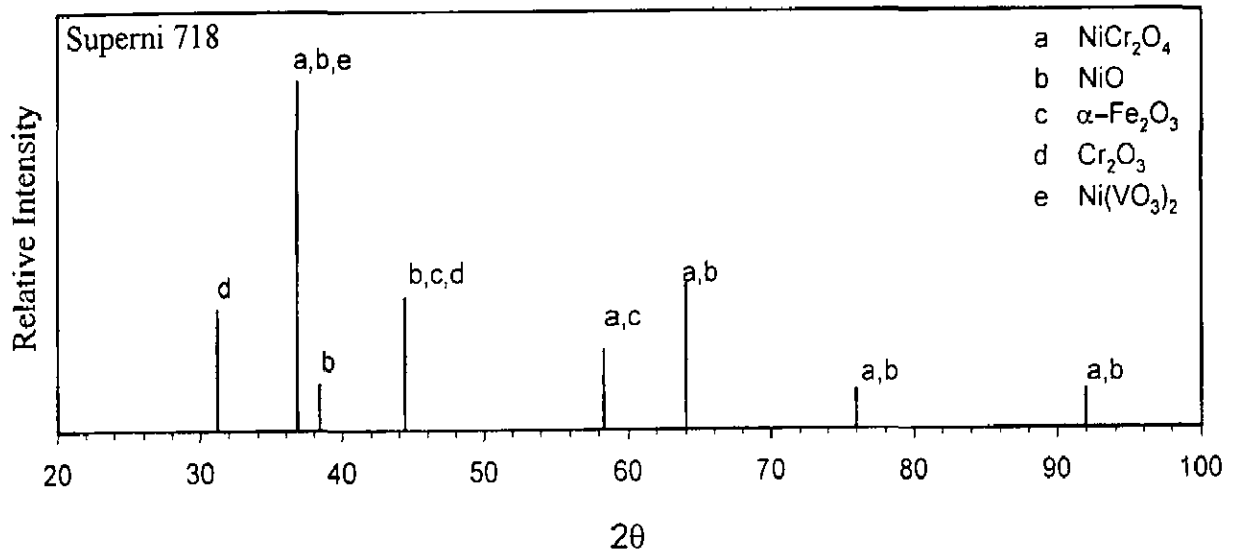
Fig. 5.58: X-ray diffraction profile for alloy D (Superni 718) after cyclic hot corrosion at 900^0C in Na_2SO_4-60% V_2O_5 + $ZnSO_4$.
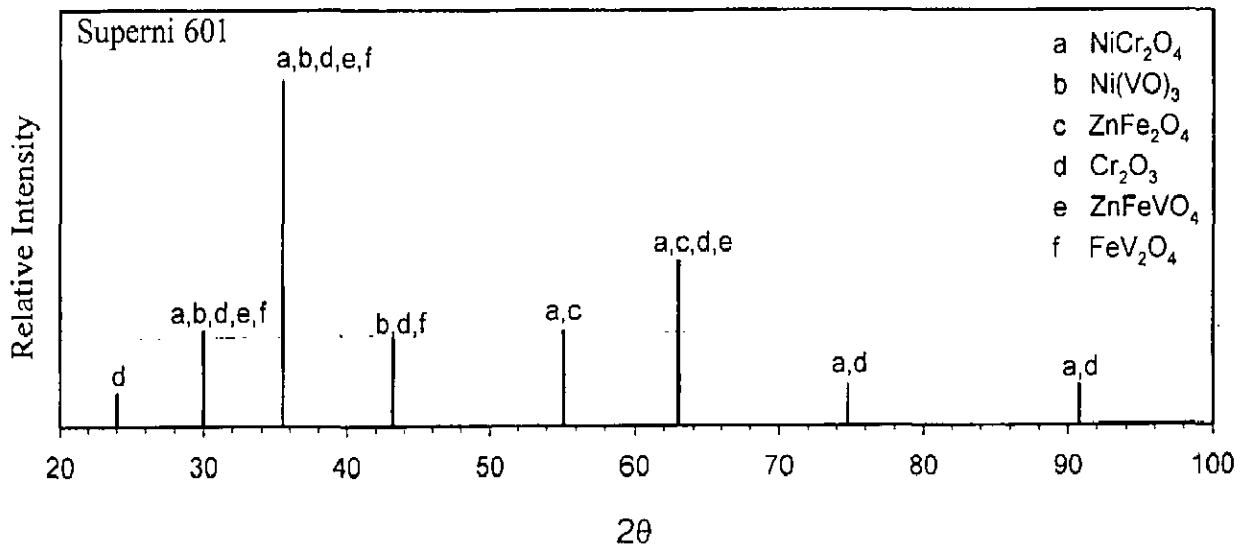
Fig. 5.59: X-ray diffraction profile for alloy E (Superni 601) after cyclic hot corrosion at 900^0C in Na_2SO_4-60% V_2O_5 + $ZnSO_4$.
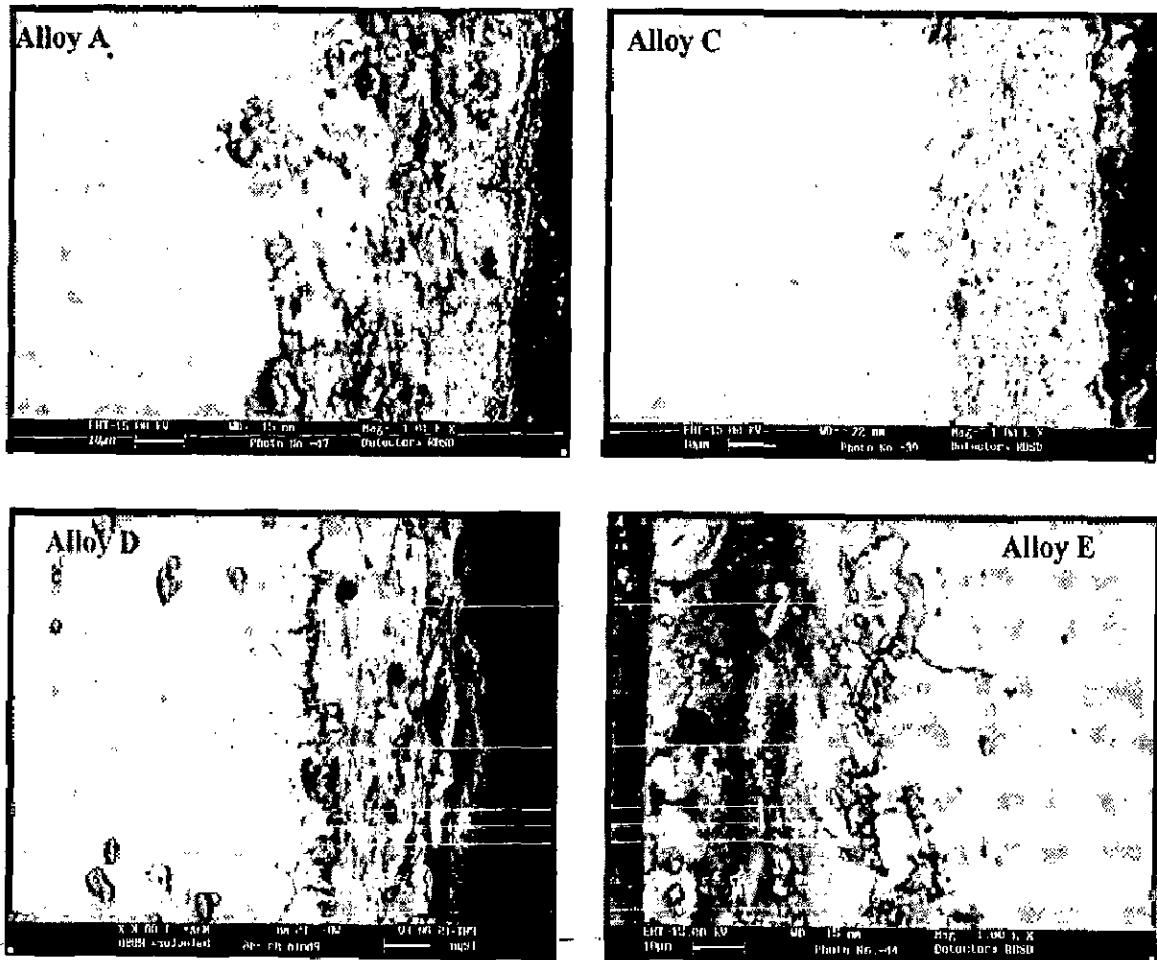
Fig . 5.60: BSE images of alloy A (Superfer 800H), alloy C (Superni 75), alloy D (Superni 718) and alloy E (Superni 601) in Na_2SO_4-60%V_2O_5 +10%$ZnSO_4$ environment after exposure at 900^{0}C in cyclic conditions.

(a)

(b)

(c)

(d)

(e)
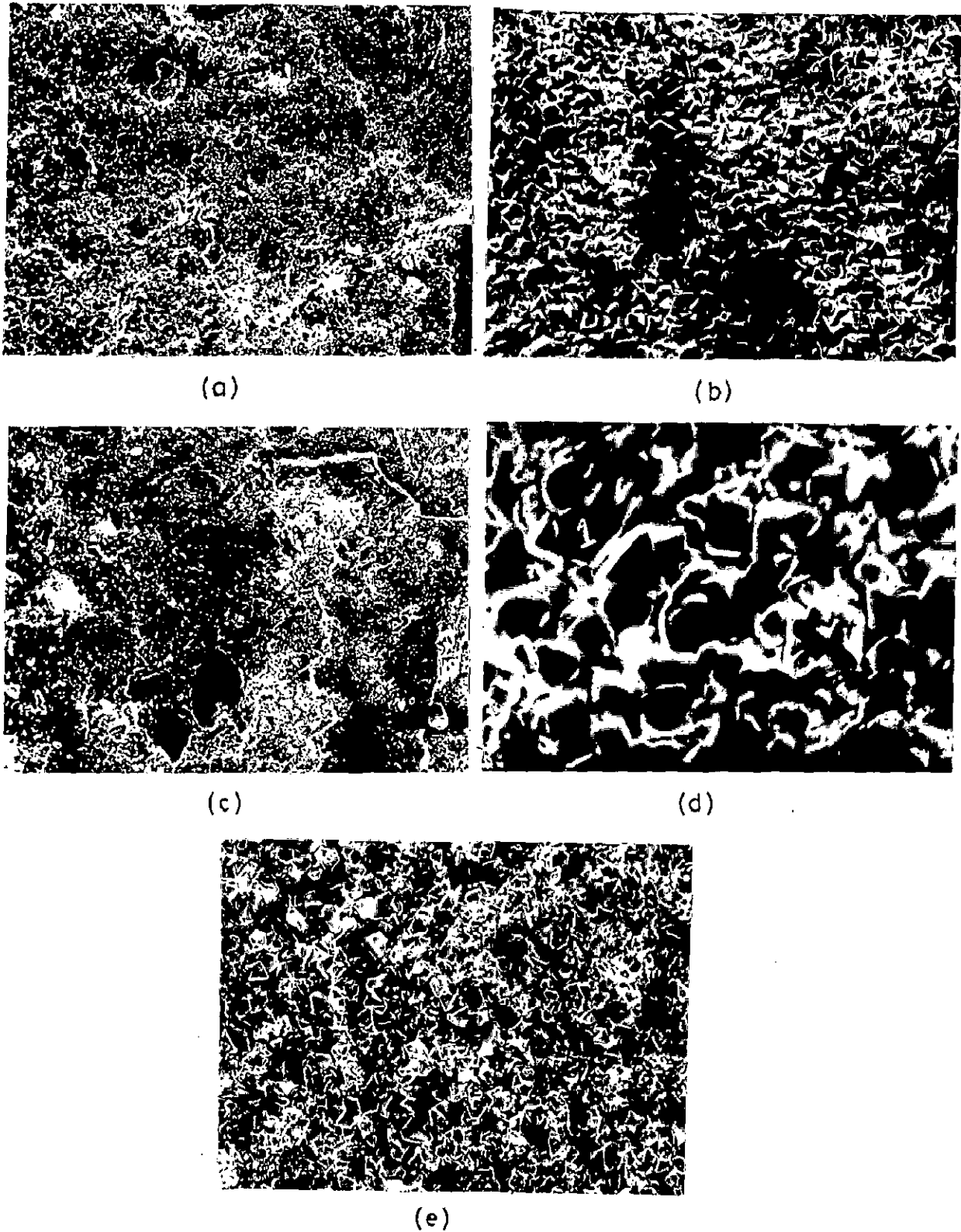
Fig. 5.61: Scanning Electron Micrographs after cyclic hot corrosion in Na_2SO_4-60%V_2O_5 +$ZnSO_4$ of alloys:

a) Alloy A (Superfer 800H) (X 640)
b) & c) Alloy C (Superni 75) (X 640) & (X 3000)
d) Alloy D (Superni 718) (X 640)
e) Alloy E (Superni 601) (X 640)
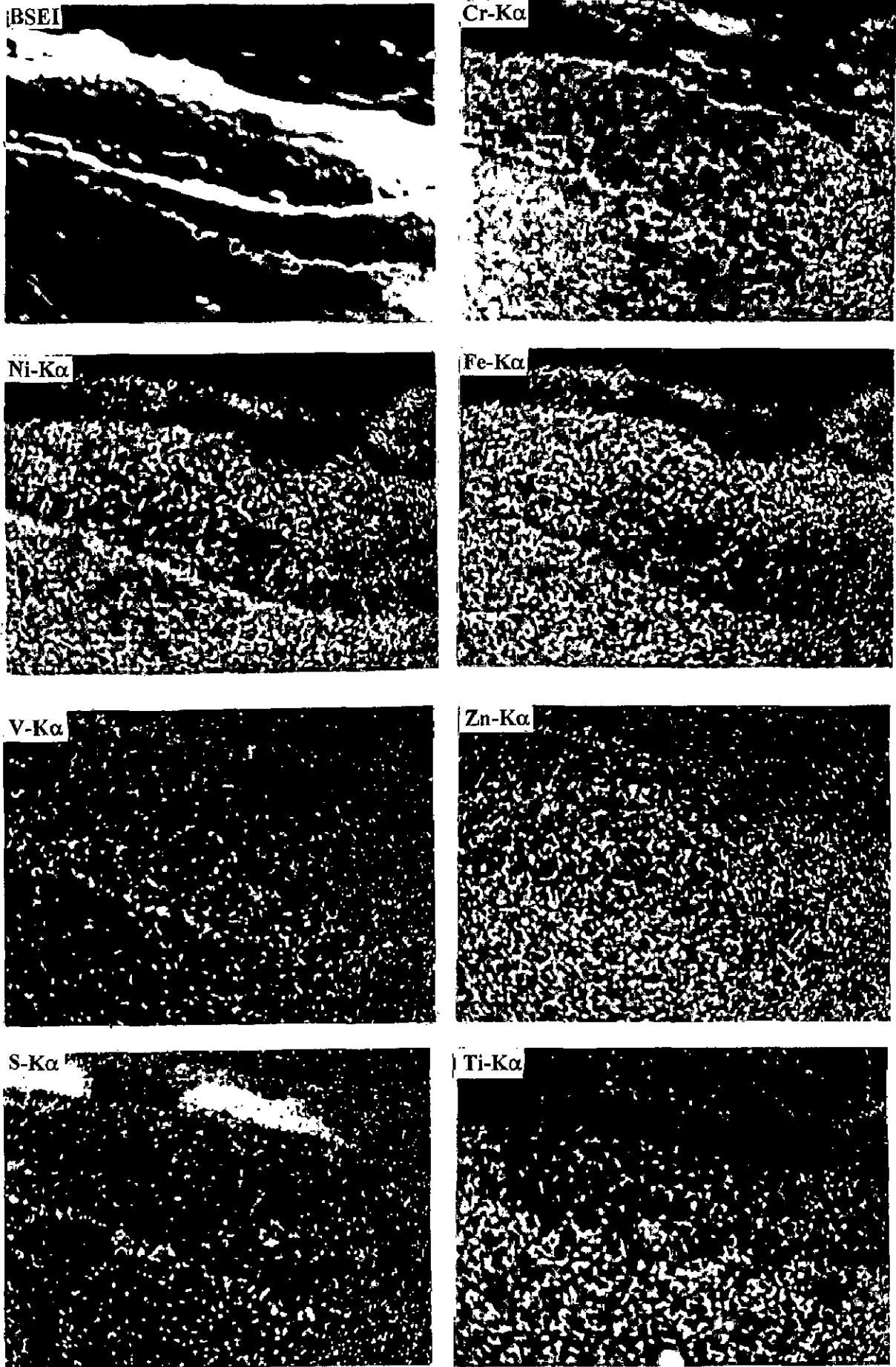
Fig. 5.62: BSEI and X-ray mapping of the cross section of alloy A (Superfer 800H) after cyclic hot corrosion at 900^0C in Na_2SO_4-60% V_2O_5+$ZnSO_4$ (X 600)
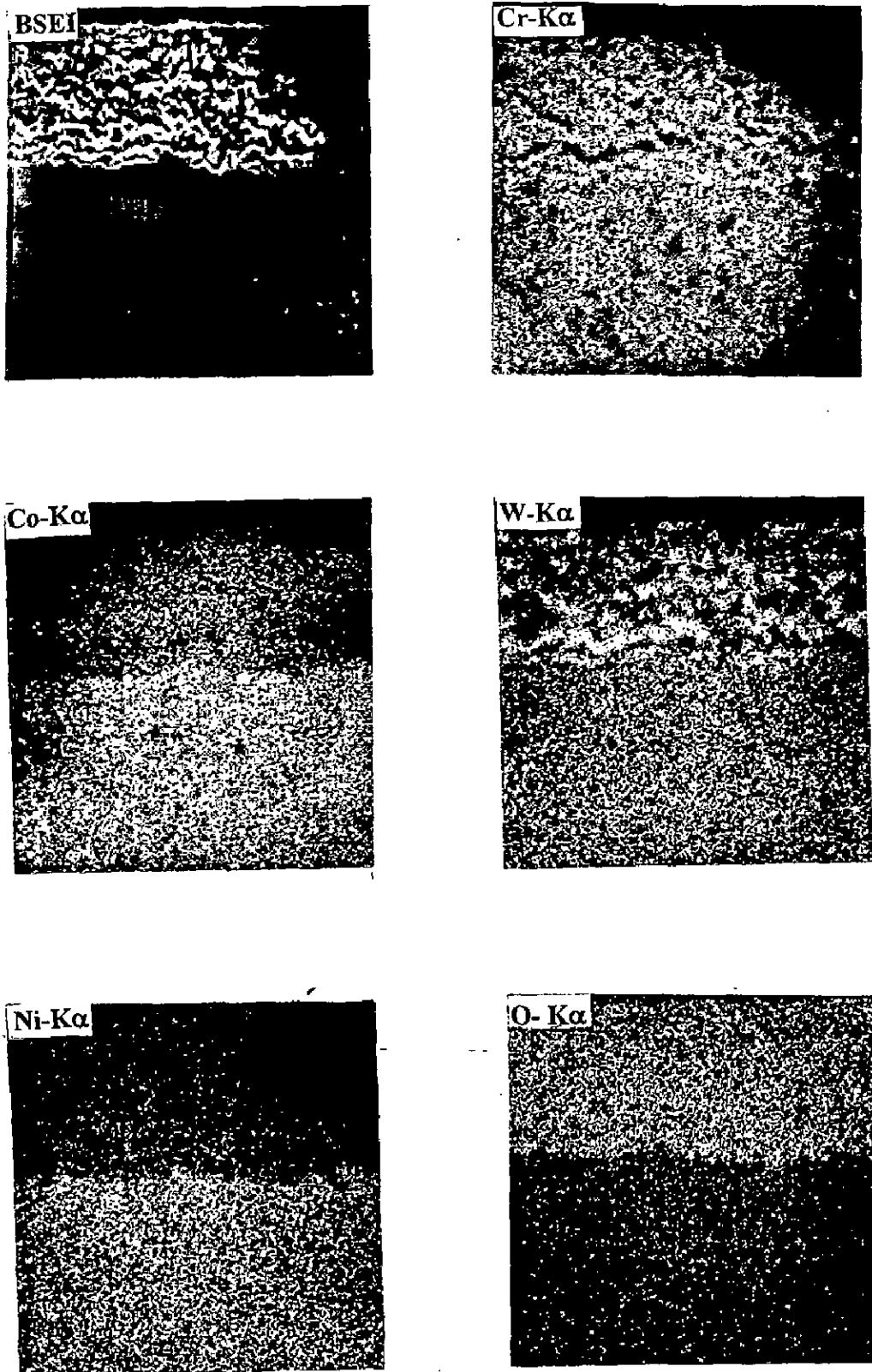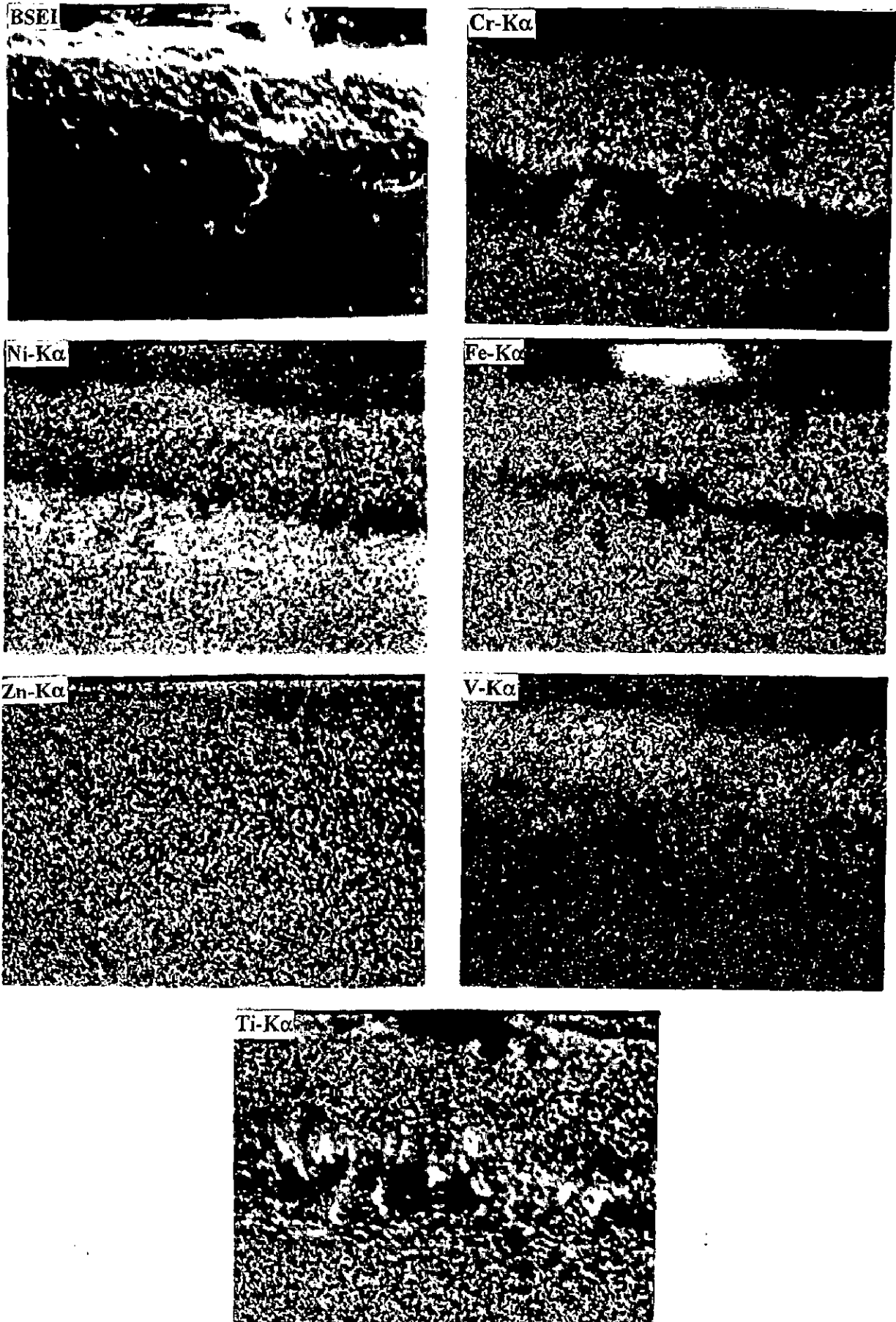
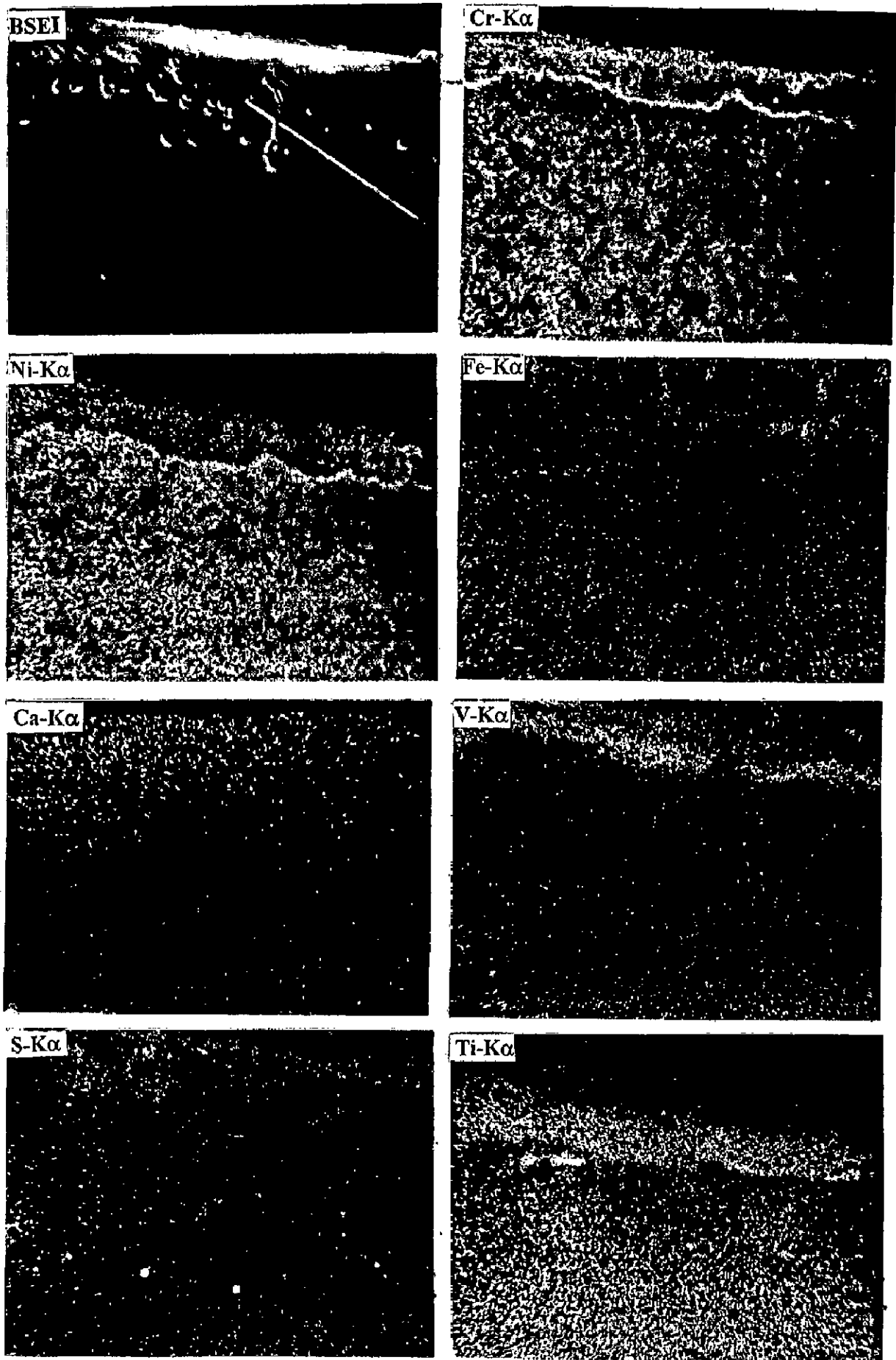**Fig. 5.63:** BSEI and X-ray mapping of the cross section of alloy C (Superni 75) after cyclic hot corrosion at 900^0C in Na_2SO_4-60% V_2O_5+$ZnSO_4$ (X 600)
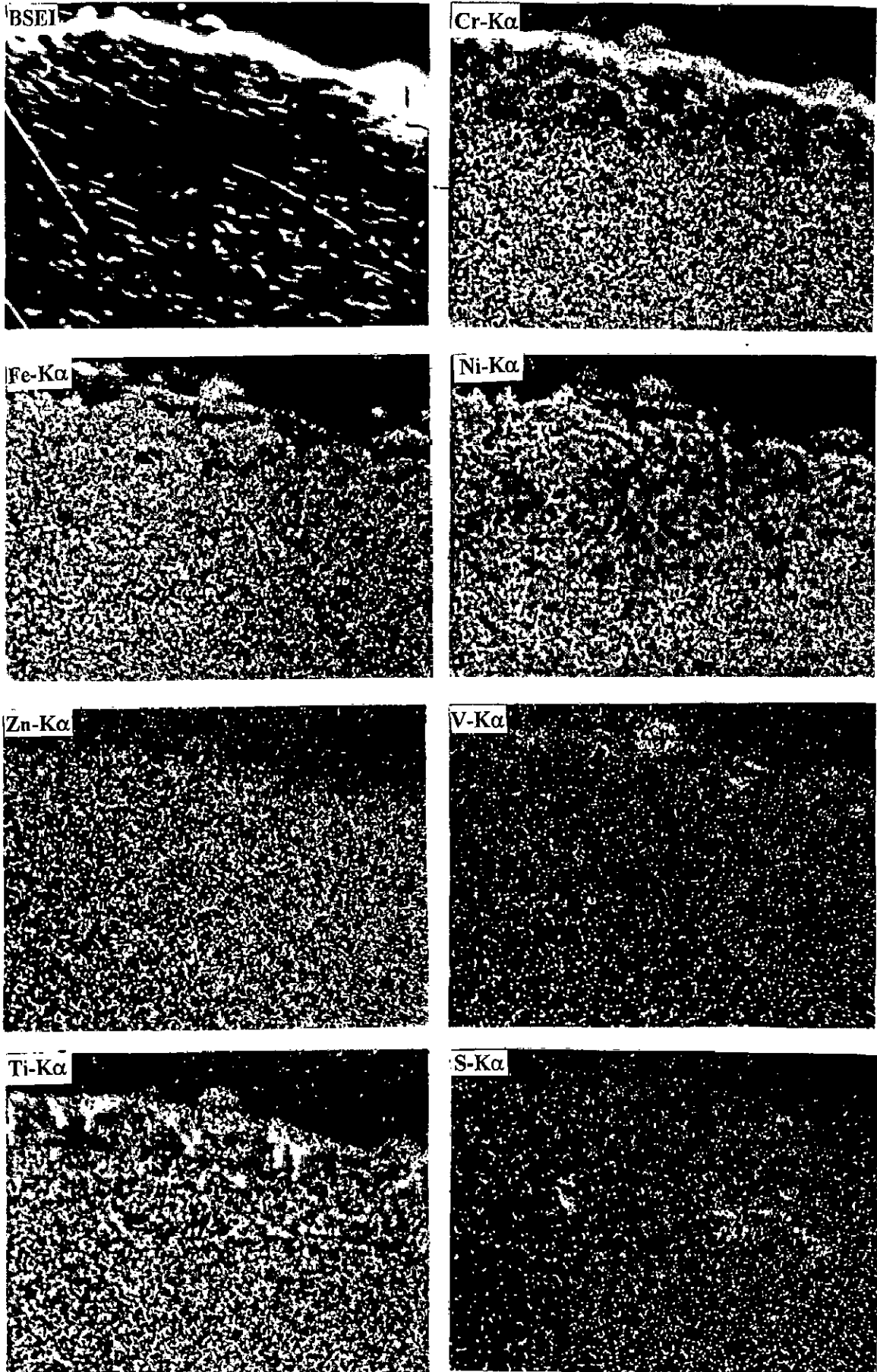
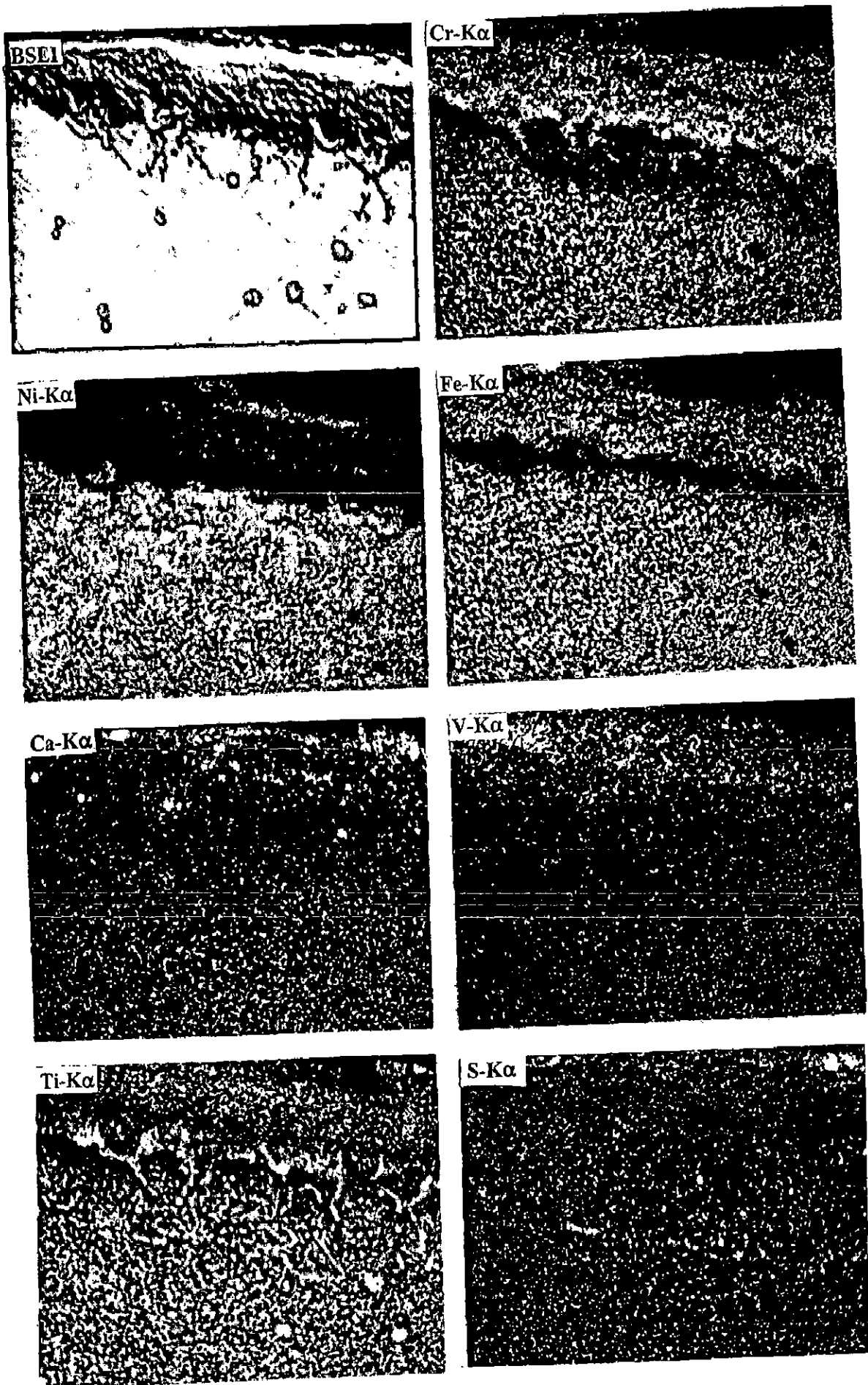**Fig. 5.64:** BSEI and X-ray mapping of the cross section of alloy D (Superni 718) after cyclic hot corrosion at 900^0C in Na_2SO_4-60% V_2O_5+$ZnSO_4$ (X 800)
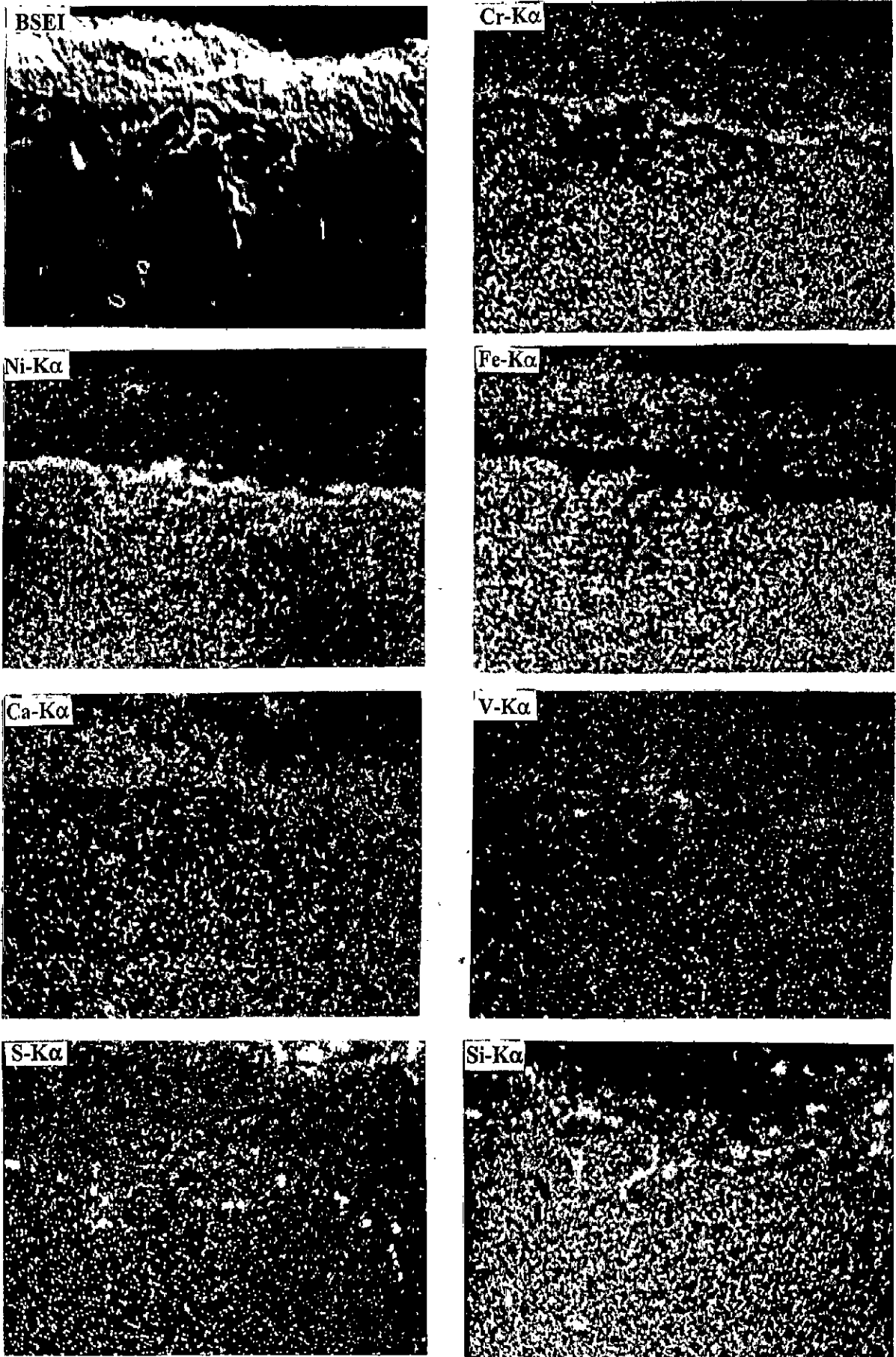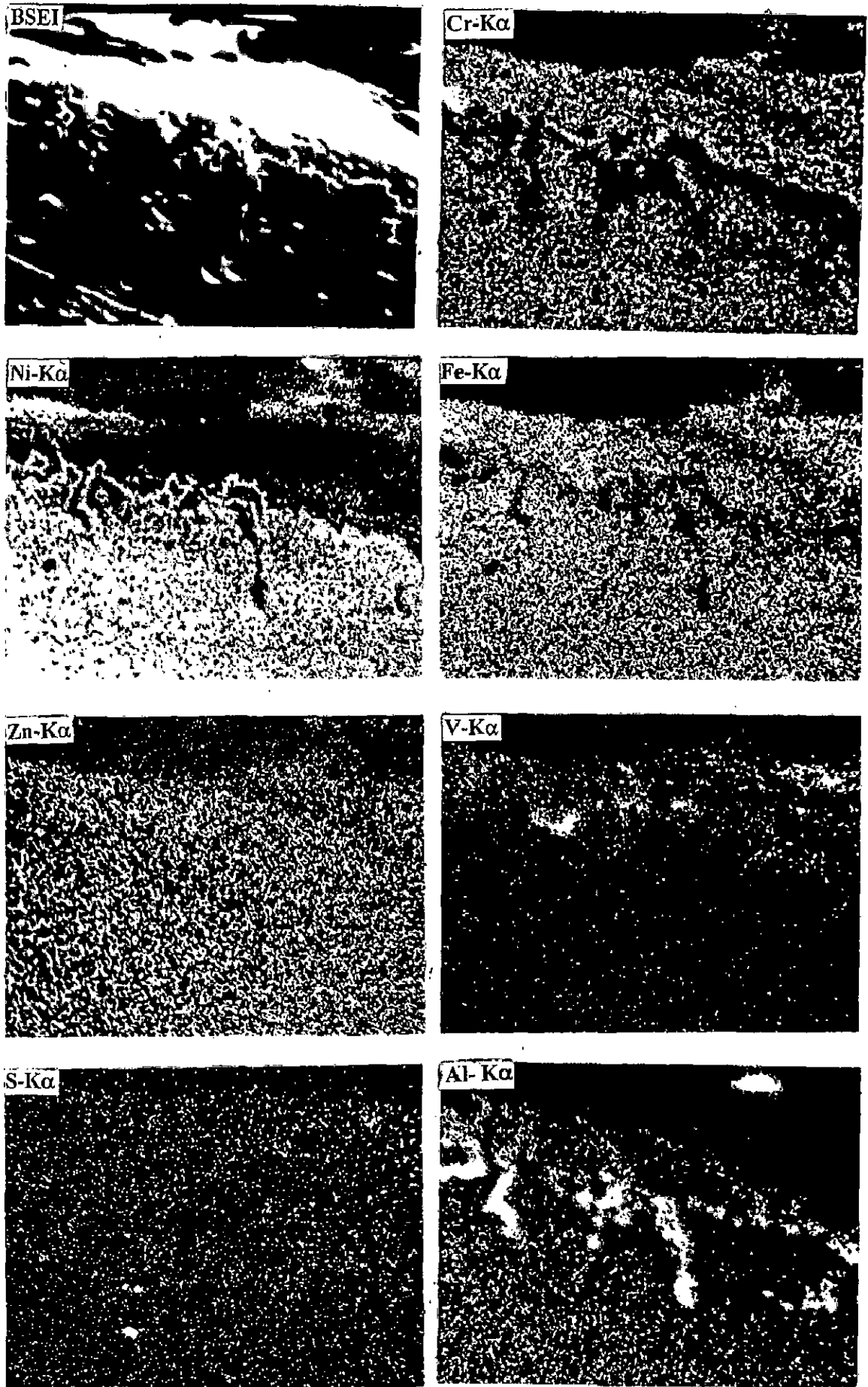
Fig. 5.65: BSEI and X-ray mapping of the cross section of alloy E (Superni 601) after cyclic hot corrosion at 900^0C in Na_2SO_4-60% V_2O_5+$ZnSO_4$ (X 800)

EDAX Analysis of Superni75 in Na$_2$SO$_4$-60%V$_2$O$_5$+ ZnSO$_4$ along the Cross-Section

BSE Image of alloy C in
Na$_2$SO$_4$-60%V$_2$O$_5$ +10%ZnSO$_4$
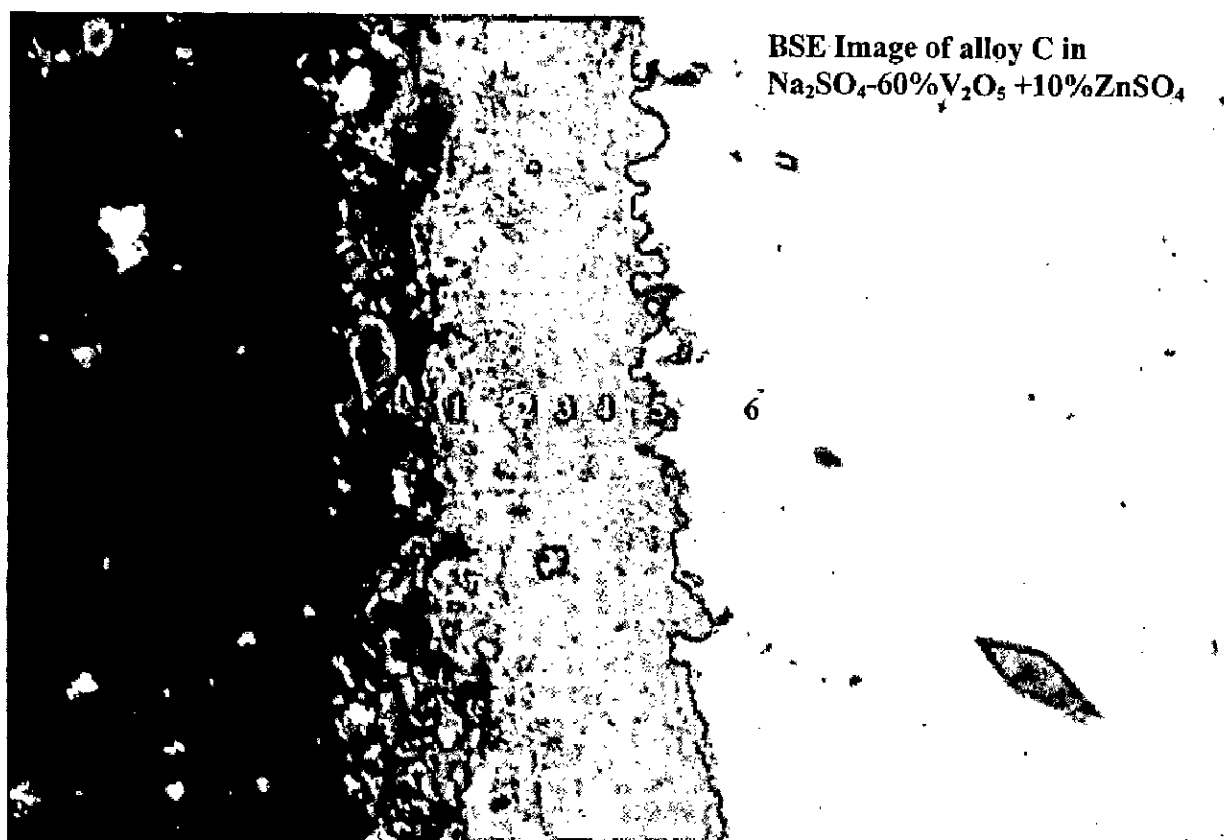
Fig. 5.66 : Back Scattered Image of alloy C (Superni 75) after cyclic hot corrosion in Na$_2$SO$_4$-60%V$_2$O$_5$+ ZnSO$_4$ at 900^{9}C.

Table. 5.3 : Wt. % of elements corresponding to points marked on Fig. 5.66, BSE image of alloy C (Superni75).

Point of analysis	Weight % of element							
	O	Fe	Ni	Cr	Zn	Ti	S	V
1	16.62	0.22	72.96	5.57	0.31	0.13	0.17	3.61
2	24.71	0.10	57.00	14.72	0.25	0.26	-	3.10
3	28.00	0.17	41.94	26.04	0.61	0.5	0.07	2.17
4	29.33	-	39.56	28.42	0.54	0.62	0.08	1.47
5	27.13	-	36.90	33.20	0.56	0.74	0.03	1.30
6	-	0.02	92.15	8.08	-	0.01	-	-

EDAX Analysis of Superni 601 in Na₂SO₄-60%V₂O₅+ ZnSO₄ along the Cross-Section
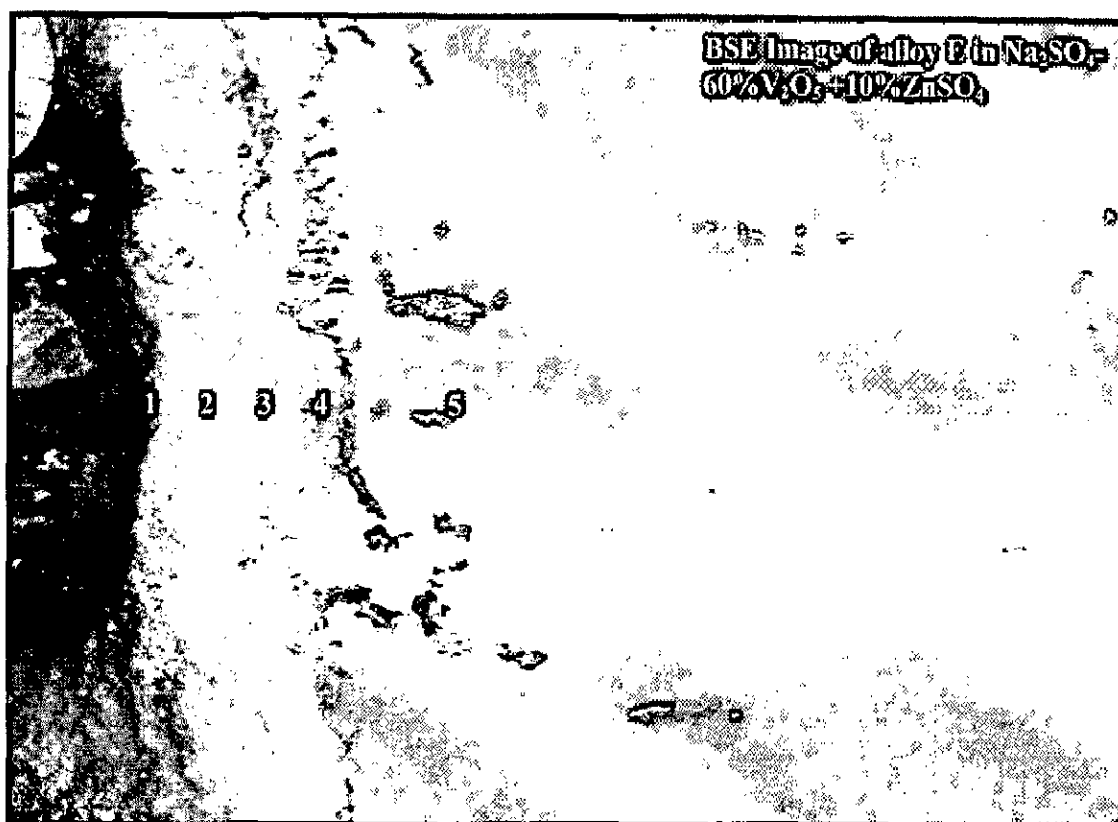
Fig. 5.67 : Back Scattered Image of alloy E (Superni 601) after cyclic hot corrosion in Na₂SO₄-60%V₂O₅+ ZnSO₄ at 900°C.

Table. 5.4 : Weight % of elements corresponding to points marked on Fig. 5.67, BSE image of alloy E (Superni 601).

Point of Analysis	Weight % of element											
	O	Fe	Ni	Cr	Al	Mn	Si	Cu	Zn	Na	V	S
1	28.60	9.5	32.93	22.15	1.13	1.25	0.63	-	0.48	-	3.12	-
2	33.48	8.27	29.97	21.52	0.99	1.04	0.46	-	0.53	-	2.52	0.08
3	32.85	8.06	30.42	18.93	1.47	1.08	0.74	0.16	0.54	1.00	4.58	0.12
4	34.65	7.61	29.10	19.64	1.73	0.90	0.70	0.15	0.38	0.89	4.31	-
5	3.63	11.06	59.39	22.42	1.79	0.78	0.60	-	-	-	0.13	-

5.6 HOT CORROSION STUDIES IN Na$_2$SO$_4$-60%V$_2$O$_5$ WITH SUPERFICIALLY APPLIED CeO$_2$

5.6.1 Visual Observations

Macrographs for corroded specimens of alloys A, B, C, D & E after exposure for 50 cycles at 900^{0}C in Na$_2$SO$_4$-60% V$_2$O$_5$ with superficially applied CeO$_2$ coating in air are shown in Fig. A.2.

The scale on the alloy A, showed a grey shinning scale. White coating was visible on the surface till 15th cycle after that colour changed to dark black and spalling started though the amount of the spalled scale was very less. The final scale on the alloy B showed black adherent lustrous mass although spalling was continuous after 25 cycles. In case of alloy C surface was dull, compact, with whitish & grey areas and black patches indicating the presence of unreacted thick salt film on the surface of the sample. Similar is the appearance in case of alloys D and E. Salt coating was visible on the surface but the amount of unreacted salt present on the surface of alloy D was comparatively less as compared to alloys C and E. In all the three alloys very little spallling was noticed.

5.6.2 Kinetic Data

Plot for alloy A, Fig. 5.68 shows an increase in weight gain up to 20 cycles and then decreasing trend observed up to 50th cycle. The maximum weight gain is about 7.8 mg/cm^2 but the final weight after 50 cycles decreased down to 5mg/cm^2. In case of alloy B, (Fig. 5.69) a similar trend is observed and in this case also weight increases up to 20th cycle and decreases gradually to about 5 mg/cm^2. But the maximum weight gain is 15 mg/cm^2. Fig. 5.70 shows the plots of weight change data for alloys C, D and E. In case of alloy C, a very slight change is noticed but it is evident from the figure that increasing trend is followed up to 20 cycles after that it remains nearly constant. Over all weight change is very less, just 1/4th of that without CeO$_2$. In case of alloy D, a gradual rise in weight gain up to 30 cycles is observed after which it starts decreasing. Maximum weight gain is about 6.5 mg/cm^2 which is 3/4th of

the one without CeO_2. In case of alloy E, there is a gradual increase in weight, though some spalling is indicated at 10th and 35th cycle & maximum change in weight is about 5 mg/cm^2.

5.6.3 X-Ray Diffraction Analysis

In case of alloy A coated with Ceria in Na_2SO_4–60%V_2O_5 environment the main peaks of FeS, Cr_2O_3 $NiCr_2O_4$, $NiFe_2O_4$, FeV_2O_4, Fe_2O_3 and $(Cr,Fe)_2O_3$ have been identified. In cobalt base alloy B the main peaks of $CoCr_2O_4$ and $NiCo_2O_4$ have been identified and other possible phases may be WO_3, $CoWO_4$, Co_3O_4, Cr_2O_3, $NiWO_4$ and $Co_3V_2O_8$. In Ni base alloy C (Supermi 75), the main phase identified is NiO. Where as CeO_2 may possibly be present along with other phases such as NiS, Cr_2O_3, $NiCr_2O_4$ and $Ni(VO_3)_2$. The prominent phases identified in alloy D are NiO, Cr_2O_3 and $NiCr_2O_4$ along with vanadates FeV_2O_4 and $Ni(VO_3)_2$. In case of alloy E, the main phases identified are $Ni(VO_3)_2$, NiO, $NiCr_2O_4$, FeS, FeV_2O_4 and Cr_2O_3. CeO_2 may possibly be present. The results of the XRD analysis are compiled in Tables A.17, A.18 and A.19 and presented in Fig. 5.71, 5.72 & 5.73.

5.6.4. Measurement of Scale Thickness

Average value of the scale thickness observed from the BSE images of alloys A, B, C, D & E shown in Fig. 5.74 are 50, 41.5, 25, 30 and 32 μm respectively

5.6.5. SEM, EDAX and EPMA Results

In case of alloy A Fig. 5.75 (a), there is massive scale showing craters and presence of some crystalline phases on the top surface of the scale. Surface EDAX of the same alloy Fig. 5.76 (a), Table 5.5, corresponding to different points on the scale surface indicates presence of Fe, Ni & Cr in the scale. Ceria is randomly distributed at some points in the scale. At area 2, where mainly ceria is present, Ni is absent. Fe and Cr are present in smaller amounts. In case of alloy B, SEM micrograph Fig. 5.75 (b) and The SEM/ EDAX analysis at the points marked on the Fig. 5.76 (b) corresponding to this alloy, given in Table 5.5, indicates formation of

nodules of Co-rich phase containing mainly Co, Cr and little amount of iron. V is present in the scale surface at all the points, with chromium and cobalt at point 1 & 3 whereas at point 2 45.72% V is present with 69.2% of ceria. SEM micrograph for alloy C, Fig 5.75 (c) shows that the scale is consisting of matrix having coarse grains with nodules present across the scale. Scanning Electron Micrograph of alloy D, Fig. 5.75 (d) indicates scale structure consisting of sponge like elongated phases. SEM/EDAX analysis of the alloy E given in Table 5.5 corresponding to points marked on the SEM image for this alloy in Fig. 5.76 (c) shows scale consisting of matrix containing Cr, Ni & Fe (point 2 & 3) and with nodules concentrated in some regions (point 1) which are basically Ni rich phase (Ni is 68.53%) containing vanadium (20.16%) & ceria (5.96%).

In case of alloy A, the EPMA results shown in Fig. 5.77 indicate formation of thick dense scale which mainly consists of Cr, Ni and some Fe. A thin layer above the interface is depleted in Ni & Cr but is rich in Fe, and in the areas depleted of Fe, silicon is present in higher concentration throughout the scale. The EDAX analysis of the alloy across the scale shown in Fig. 5.82 and Table 5.6 indicates outer scale rich in Fe and containing Cr & Ni. Ceria is indicated in traces near the substrate scale interface. Internal oxidation is indicated where mainly Ti is oxidised along the grain boundaries. V is present throughout the scale.

The EPMA analysis for alloy B, Fig. 5.78 indicates thick dense scale mainly consisting of Cr and Co. Ni is present in smaller amounts where Cr is absent, Co is present in high concentration throughout the scale. There is no internal oxidation indicated. There is a thin layer all along the alloy/scale interface rich in Nickel. Oxygen is present throughout the scale.

The EPMA of alloy C, Fig. 5.79 indicates formation of scale consisting of mainly Ni and Cr. There is indication of growth of Ni-Cr rich crystals, which suggests spinel formation. Ceria is present in high concentration in the scale and at same places, it is co-existing with V. Bottom of the scale contains mainly Cr & Ni. V is present in both the top & bottom layer.

EDAX analysis along cross-section of alloy C coated with ceria exposed to Na_2SO_4–60%V_2O_5 at 900^0C shown in Fig. 5.83 and Table 5.7 indicates presence of unreacted ceria on the top surface as point 1 shows presence of mainly Ce and oxygen. Vanadium is present all

along the cross-section. Inner scale contains mostly oxides of Ni and Cr. Ti is also present throughout the cross-section along with Ni, Cr and oxygen. Fe is present in the scale though in small amount.

The X-ray maps for alloy D (Fig. 5.80) reveals that the main scale is consisting of Fe, Cr and some Ni. Ti has got oxidised at points along the interface. Just above the interface, there is a thin layer rich in Cr where both Ni & Fe are absent followed by Ni rich scale. Silicon is also indicated in some areas in the scale. Al has got oxidised along the grain boundaries indicating internal oxidation.

The BSEI and X-ray maps for alloy E shown in Fig. 5.81 indicate medium size scale which is rich in Cr and contains Ni & Fe. V is present throughout the scale. There is internal oxidation along the grain boundaries near the interface between the scale and the substrate where Al has got oxidised.
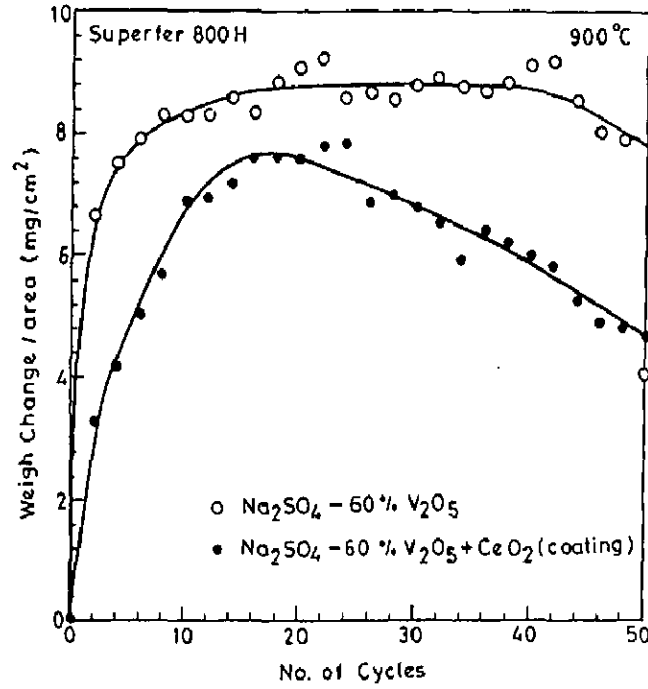
Fig. 5.68: Weight Change Plot for alloy A (Superfer 800H) after cyclic hot corrosion at 900°C in Na₂SO₄-60% V₂O₅ +CeO₂ Coating.
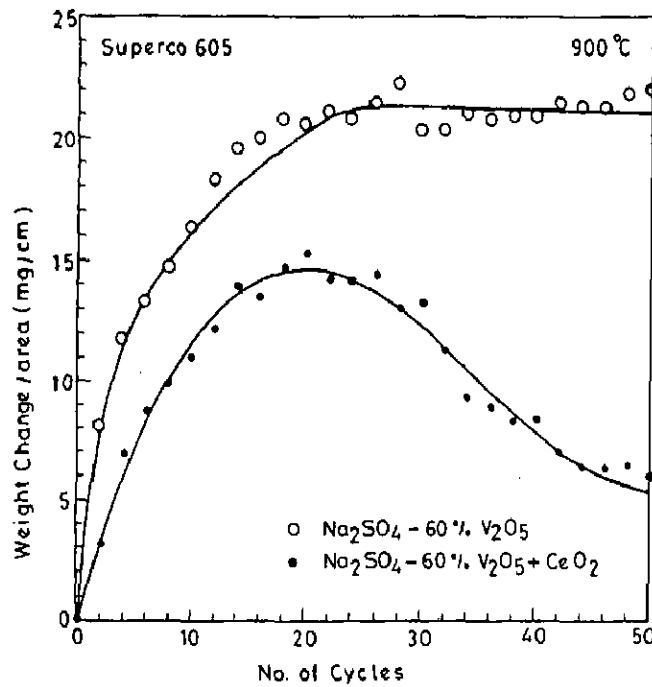
Fig. 5.69: Weight change plot for the alloy B (Superco 605) after cyclic hot corrosion at 900°C in Na₂SO₄-60% V₂O₅ + CeO₂ coating.
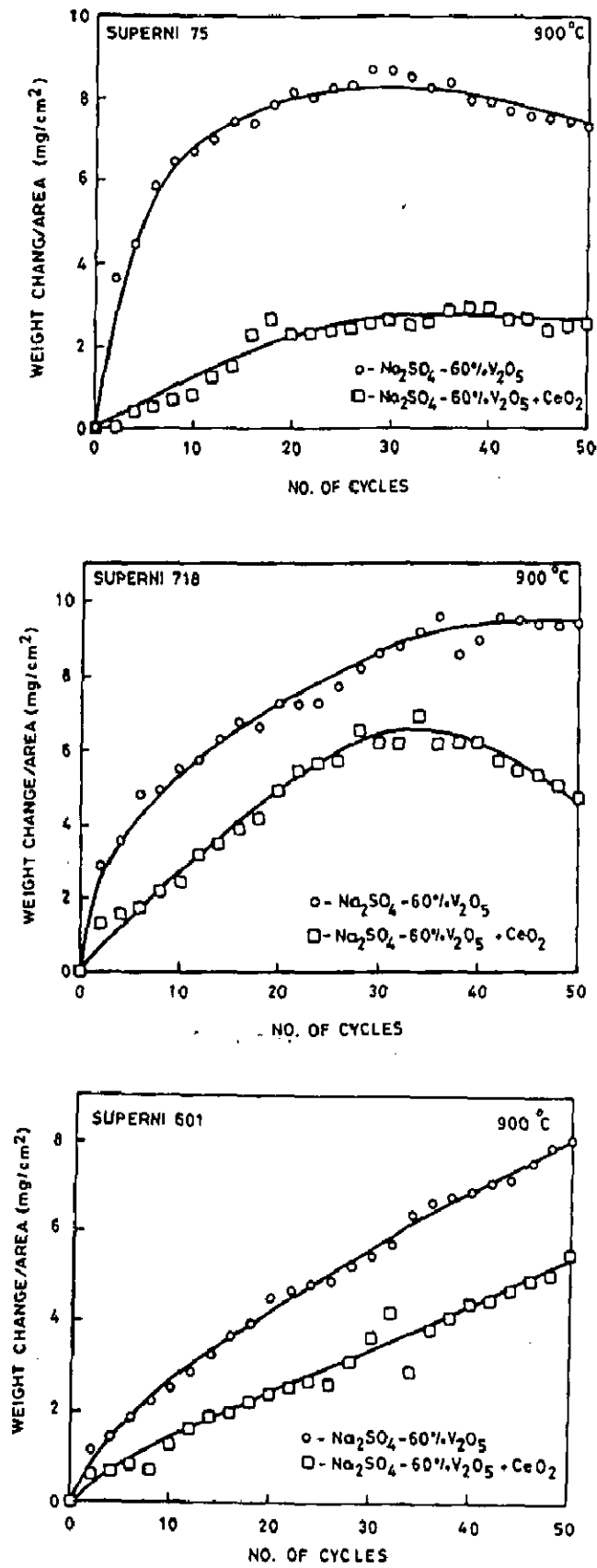
Fig. 5.70: Weight change plots for the nickel base alloys: alloy C (Superni 75), alloy D (Superni 718) and alloy E (Superni 601) after cyclic hot corrosion at $900^{0}C$ in Na_2SO_4-60% V_2O_5 + CeO_2 coating.
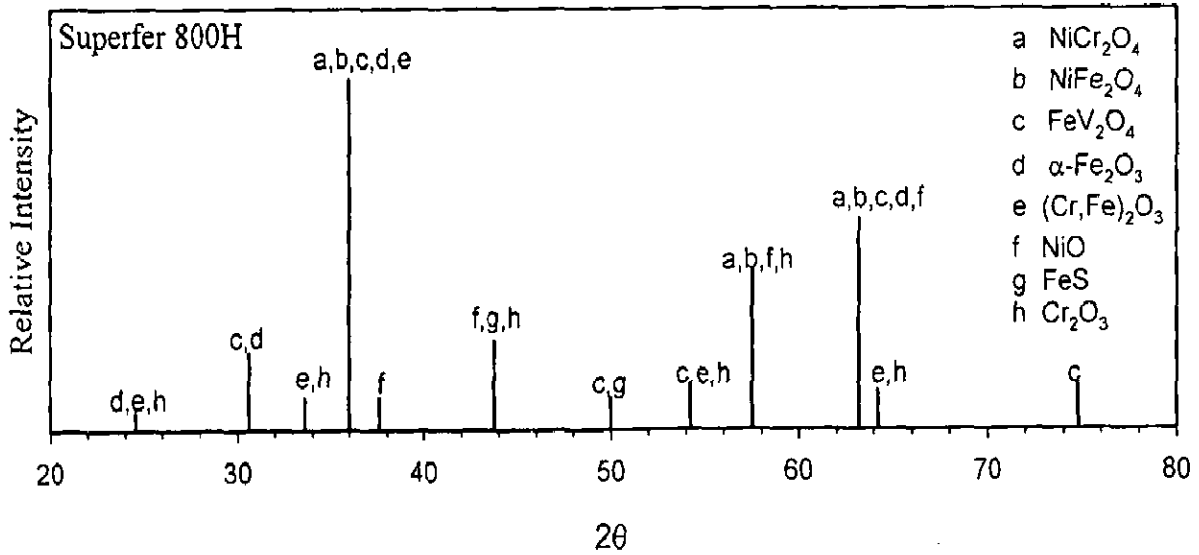
Fig. 5.72: X-ray diffraction profile for alloy A (Superfer 800H) after cyclic hot corrosion at 900^0C in Na_2SO_4-60% V_2O_5 + CeO_2 coating.
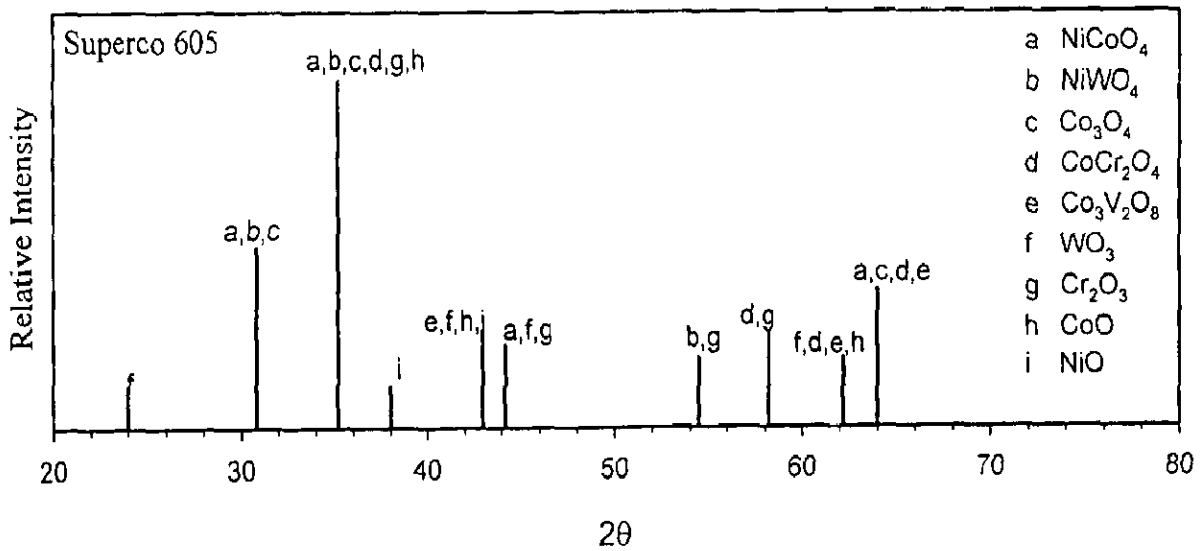
Fig. 5.71: X-ray diffraction profile for alloy A (Superfer 800H) after cyclic hot corrosion at 900^0C in Na_2SO_4-60% V_2O_5 + CeO_2 coating.

144
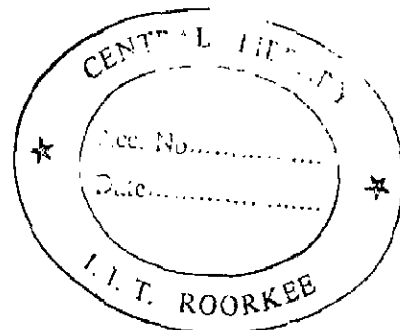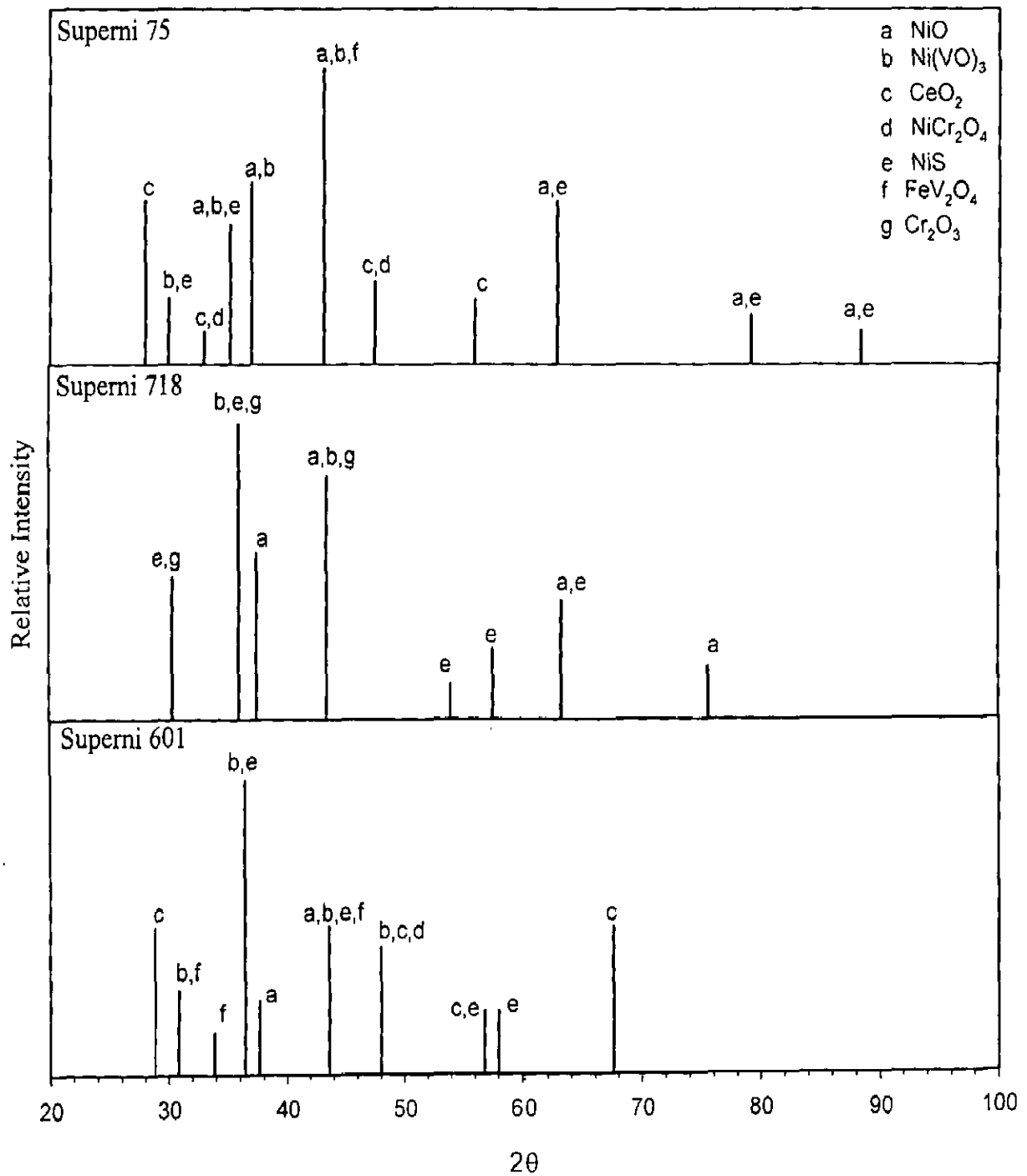
Fig. 5.73: X-ray diffraction profiles for the nickel base alloys: alloy C (Superni 75), alloy D (Superni 718) and alloy E (Superni 601) after cyclic hot corrosion at 900^0C in Na_2SO_4-60% V_2O_5 + CeO_2 coating.
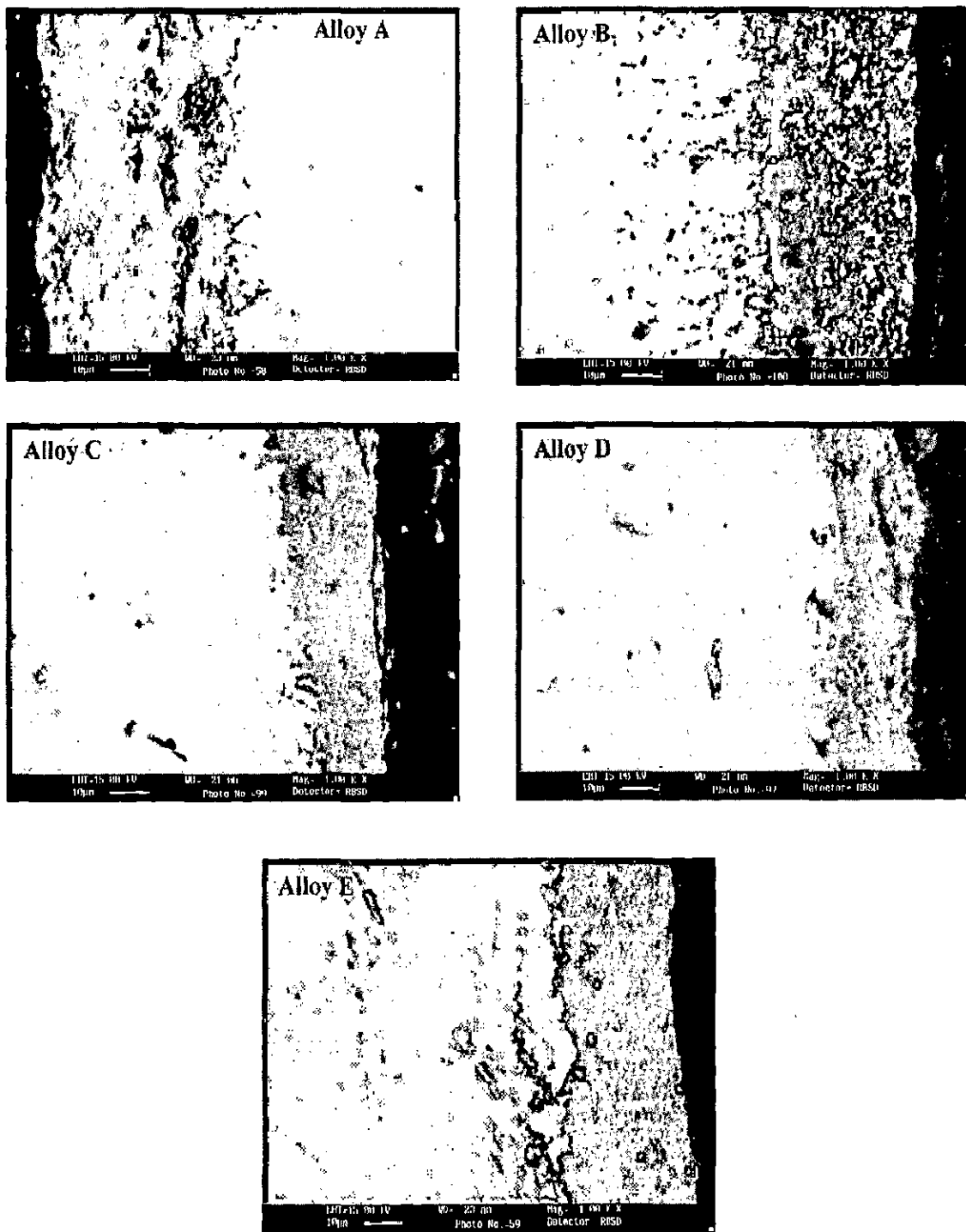
Fig. 5.74: BSE images of alloy A (Superfer 800H), alloy B (Superco 605), alloy C (Superni 75), alloy D (Superni 718) and alloy E (Superni 601) in Na_2SO_4-60%V_2O_5 + CeO_2 environment after exposure at 900^{0}C in cyclic conditions.
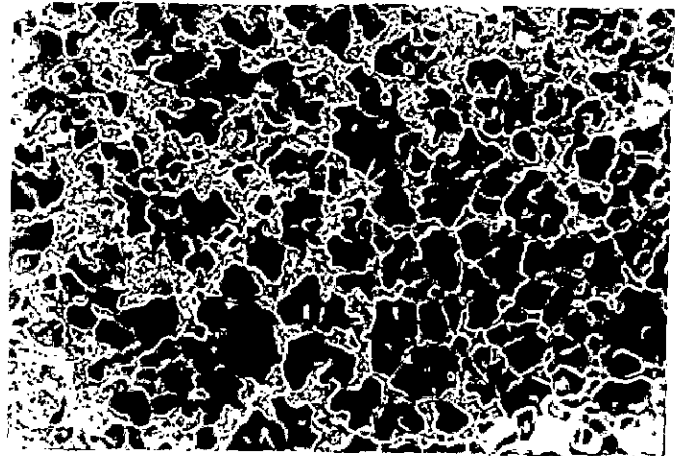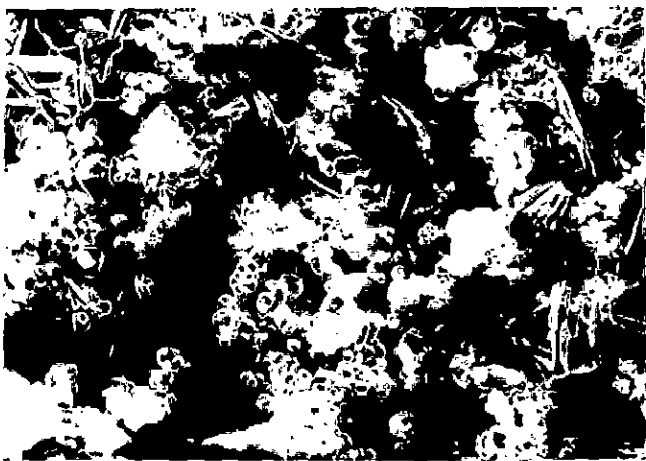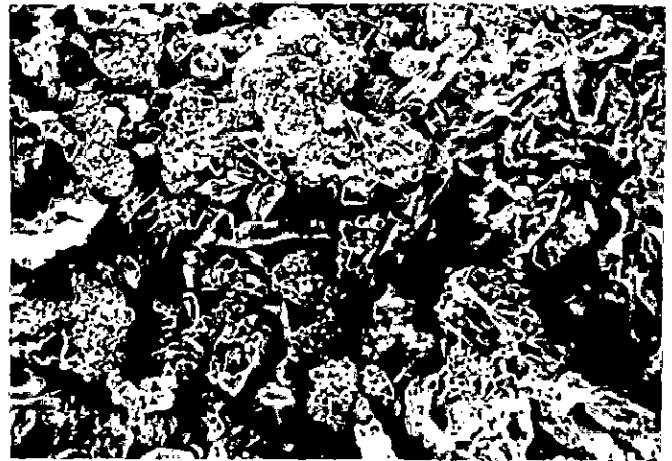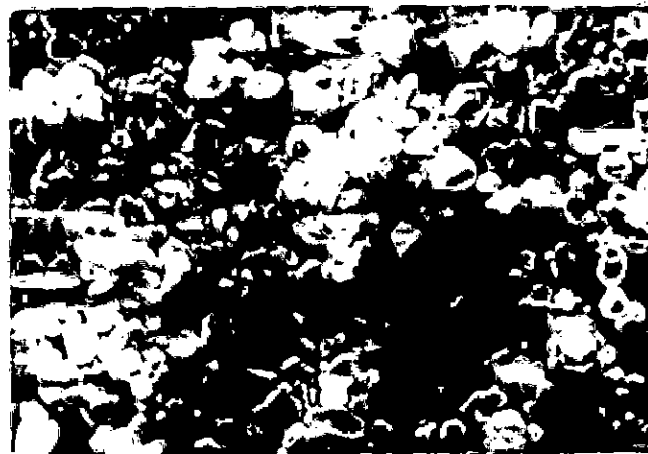
Fig. 5.75: Scanning Electron Micrographs after cyclic hot corrosion in Na_2SO_4-60%V_2O_5 + CeO_2 Coating of alloys:

a) Alloy A (Superfer 800H)   (640X)

b) Alloy B (Superco 605)   (640X)

c) Alloy C (Superni 75)   (640X)

d) Alloy D (Superni 718)   (640X)

e) Alloy E (Superni 601)   (640X)

(a)

(b)
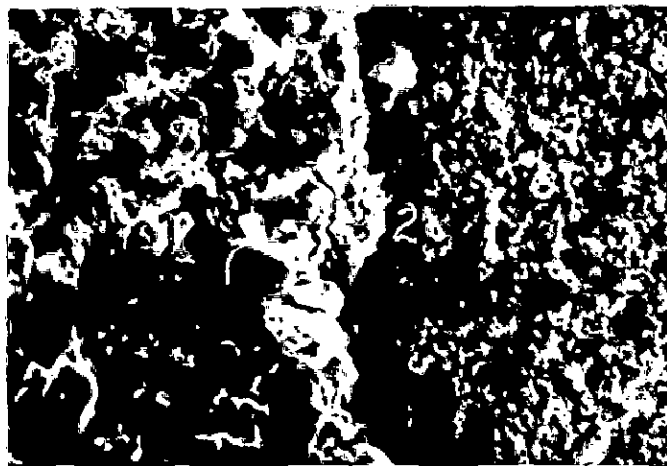
(c)

Fig. 5.76: Scanning Electron Micrographs showing points of surface EDAX analysis after cyclic hot corrosion in Na_2SO_4-60%V_2O_5+CeO_2 environment at 900^0C of alloys:

a) Alloy A (Superfer 800H)   (X 3000)

b) Alloy B (Superco 605)   (X 3000)

c) Alloy E (Superni 601)   (X 1000)

Table 5.5 : EDAX Analysis of surface scale of alloys: alloy A (Superfer 800H), alloy B (Superco 605) and alloy E (Superni 601) after cyclic hot corrosion in Na_2SO_4-60%V_2O_5+CeO_2 environment at 900°C showing elemental percentages corresponding to points marked on Fig. 5.76

Alloy Designation	Analysis Point	Element Wt.%													
		Fe	Cr	Ni	Co	W	Ti	Al	Mn	Si	Cu	Na	V	S	Ce
Alloy A (Superfer 800H)	1	63.77	32.85	1.10	-	-	0.09	0.34	1.99	0.21		-	0.22	-	-
	2	10.39	6.74	0.00			0.04	1.01	-	0.25		-	-	-	81.62
	3	46.16	30.18	14.78			0.01	0.55	4.87	0.35		0.57	2.20	-	0.37
	4	51.73	30.97	8.46			0.71	0.28	4.19	0.26		0.42	1.92	-	1.08
Alloy B (Superco 605)	1	1.71	37.36	4.71	48.64	1.77	-	-	3.88	-	-	0.09	1.22	-	1.11
	2	2.30	24.43	1.04	12.12	-	-	-	4.09	0.81	-	1.10	45.72	1.37	6.93
	3	3.78	50.59	4.32	23.71	-	-	-	13.39	-	-	0.58	2.41	-	1.62
Alloy E (Superni 601)	1	1.21	2.13	68.53	-	-	-	0.47	0.14	0.34	0.36	0.72	20.16	-	5.96
	2	14.33	37.90	37.93	-	-	-	0.35	2.14	0.04	-	0.24	6.15	-	2.21
	3	14.85	37.48	37.52	-	-	-	1.77	2.09	0.31	-	1.05	4.03	-	1.17
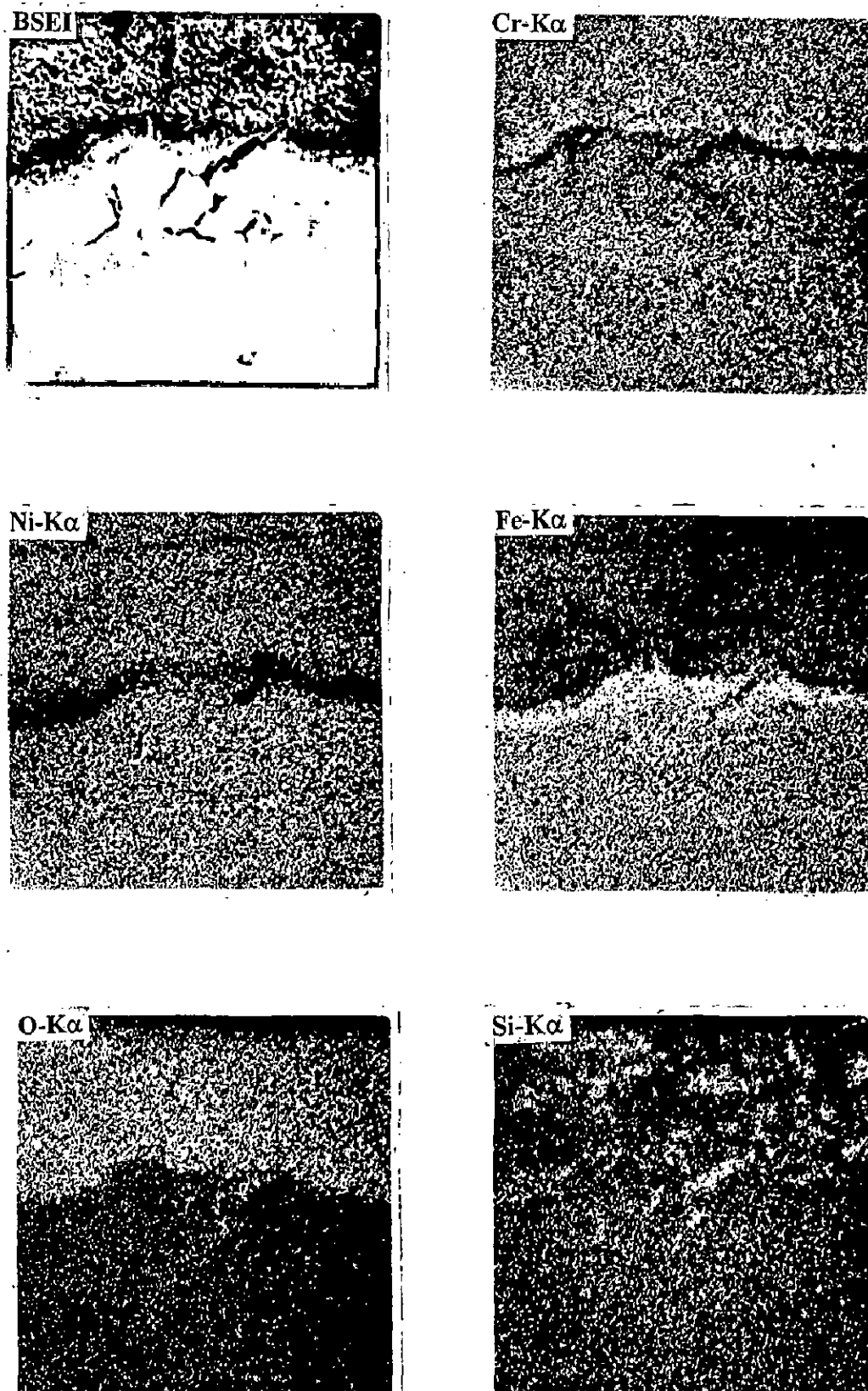
Fig. 5.77: BSEI and X-ray mapping of the cross section of alloy A (Superfer 800H) after cyclic hot corrosion at 900^0C in Na_2SO_4-60%V_2O_5+CeO_2 (X 400)
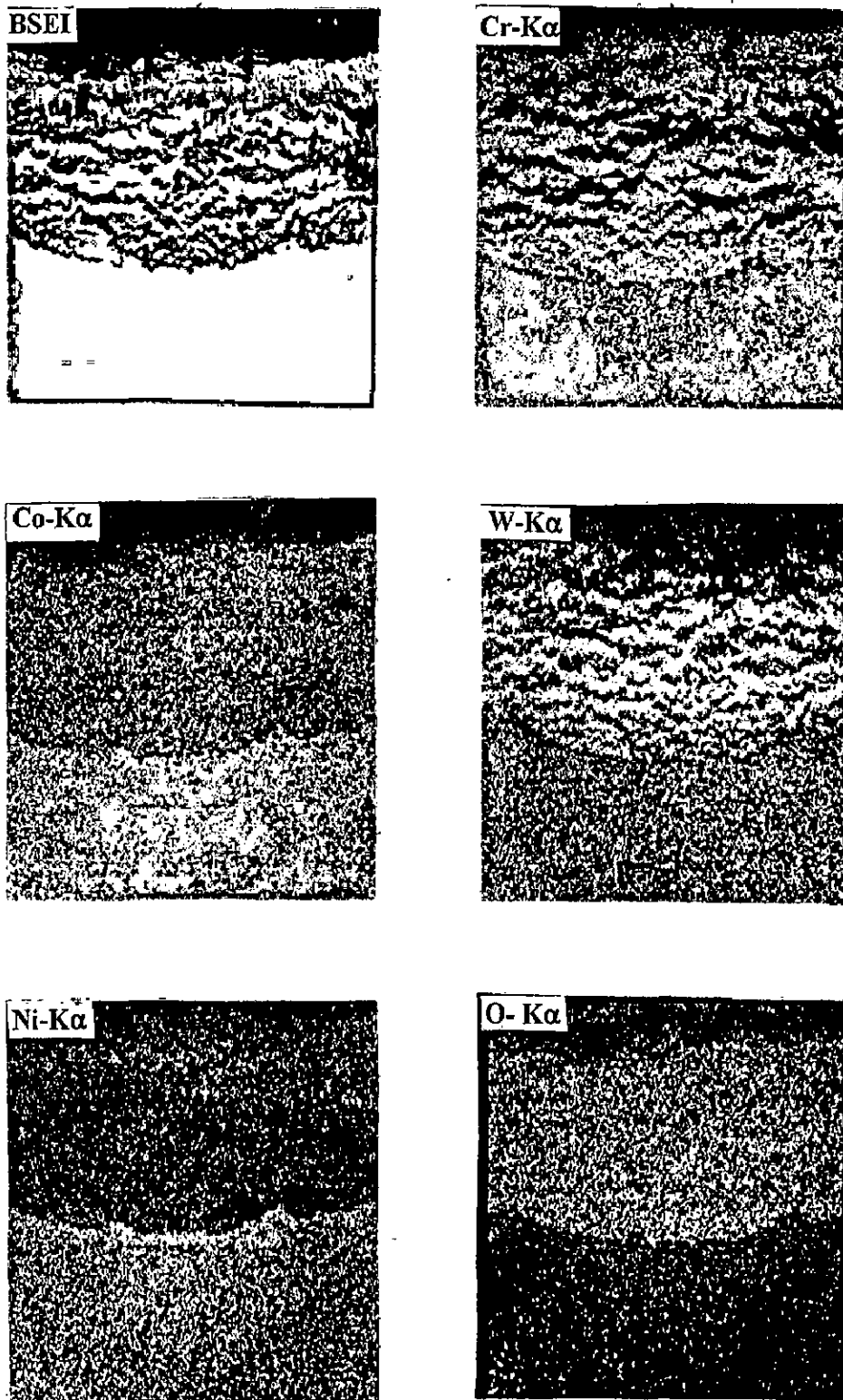
Fig. 5.78: BSEI and X-ray mapping of the cross section of alloy B (Superco 605) after cyclic hot corrosion at 900^0C in Na_2SO_4-60%V_2O_5+CeO_2 (X 400)
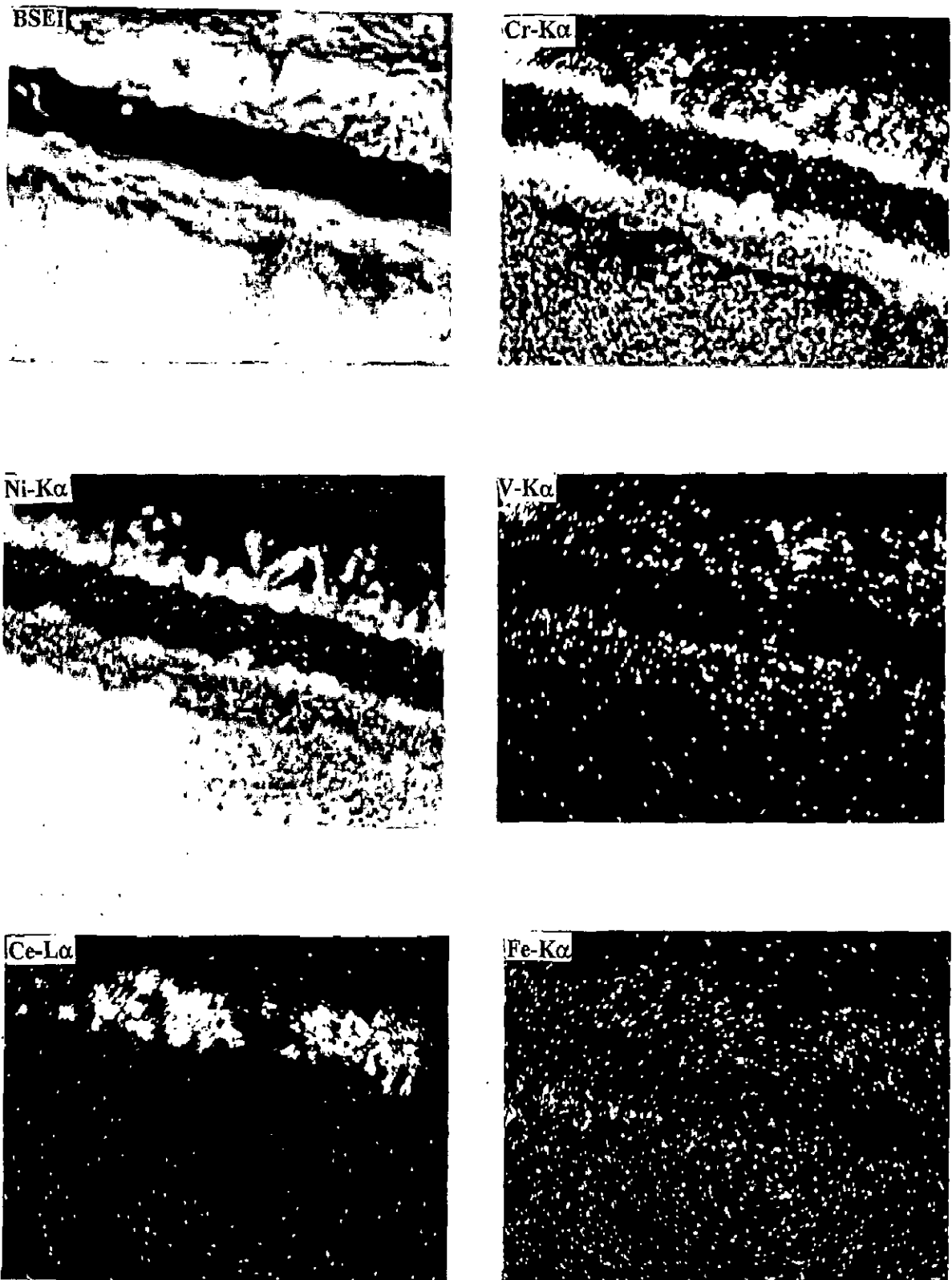
Fig. 5.79: BSEI and X-ray mapping of the cross section of alloy C (Superni 75) after cyclic hot corrosion at 900^0C in Na_2SO_4-$60\%V_2O_5$+CeO_2 (X 600)
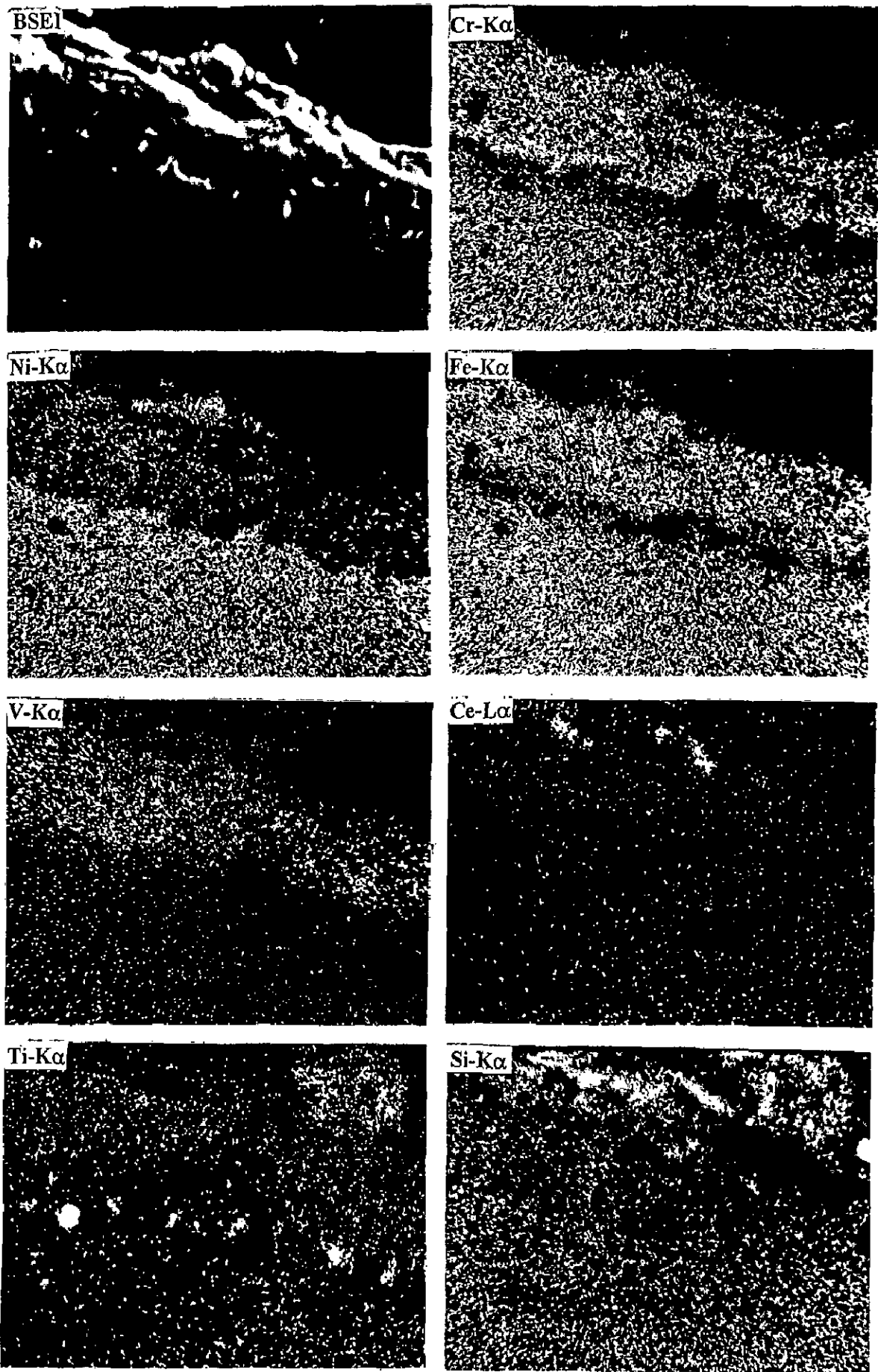
Fig. 5.80: BSEI and X-ray mapping of the cross section of alloy D (Superni 718) after cyclic hot corrosion at 900^0C in $Na_2SO_4\text{-}60\%V_2O_5\text{+}CeO_2$ (X 600)

Fig. 5.81: BSEI and X-ray mapping of the cross section of alloy E (Superni 601) after cyclic hot corrosion at 900^0C in Na_2SO_4-60%V_2O_5+CeO_2 (X 600)

Fig. 5.82 : Back scattered image of alloy A (Superfer 800H) after cyclic hot corrosion in Na₂SO₄-60%V₂O₅+ CeO₂ at 900°C.

Table. 5.6 : Wt. % of elements corresponding to points marked on Fig. 5.82, BSE image of alloy A (Superfer 800H).

Point of Analysis	Weight % of Elements										
	O	**Cr**	**Fe**	**Ni**	**Mn**	**Ti**	**Al**	**Si**	**V**	**Na**	**Ce**
1	35.09	16.47	32.90	13.06	1.05	0.50	0.22	0.68	0.18	-	-
2	32.00	15.10	30.94	17.65	1.52	0.27	0.13	1.48	1.58	-	-
3	31.99	19.41	35.75	9.86	0.68	0.49	0.11	0.25	0.97	0.05	-
4	31.18	23.26	31.82	11.39	0.50	0.54	-	0.31	0.53	-	0.06
5	24.39	18.16	23.13	15.27	0.81	10.19	2.65	4.50	0.25	0.01	-
6	0.00	12.14	41.55	43.63	0.34	0.78	0.11	0.75	0.09	-	0.06
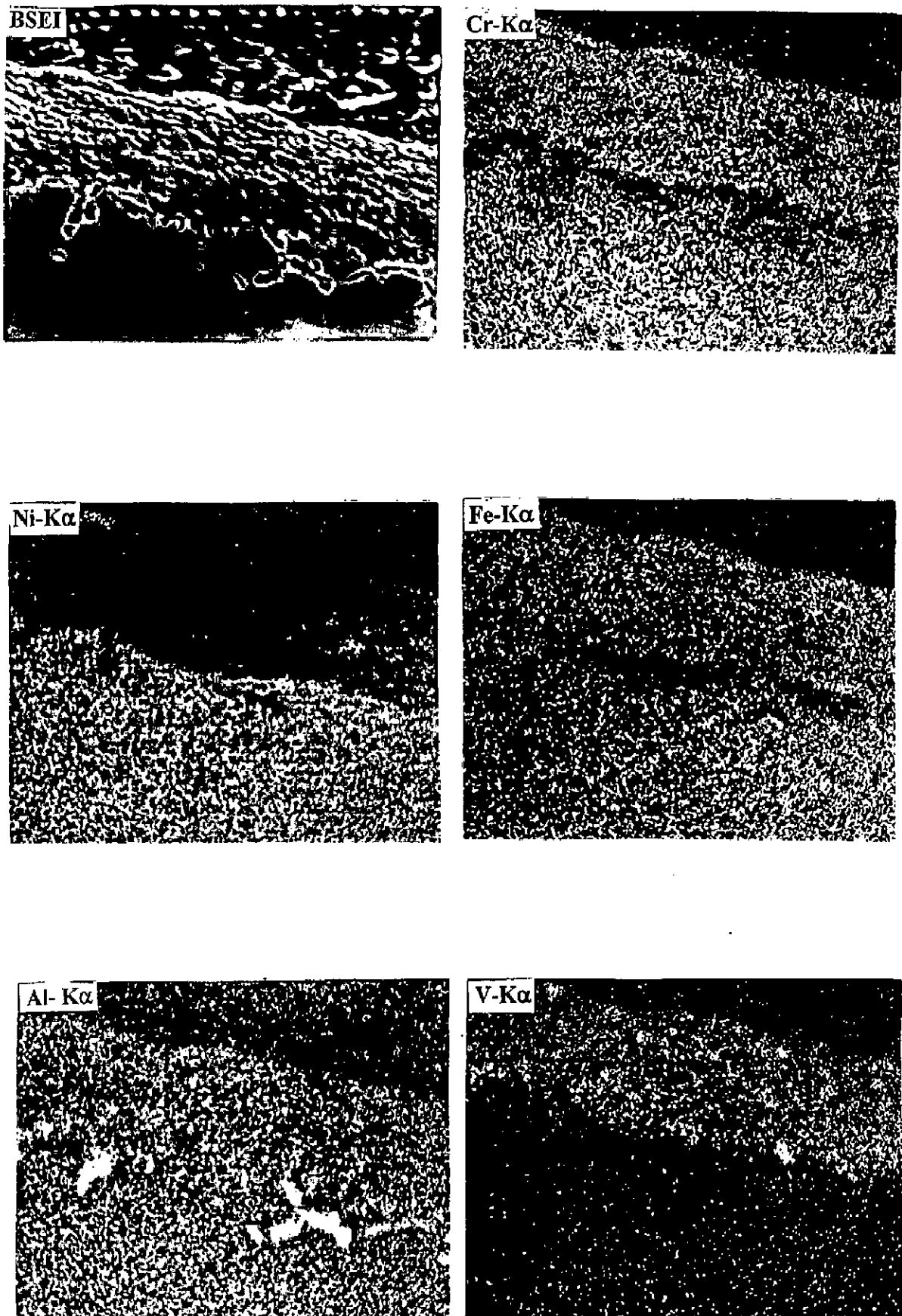
EDAX Analysis of alloy Superni 75 coated with CeO₂ in Na₂SO₄-60%V₂O₅ along the cross-section
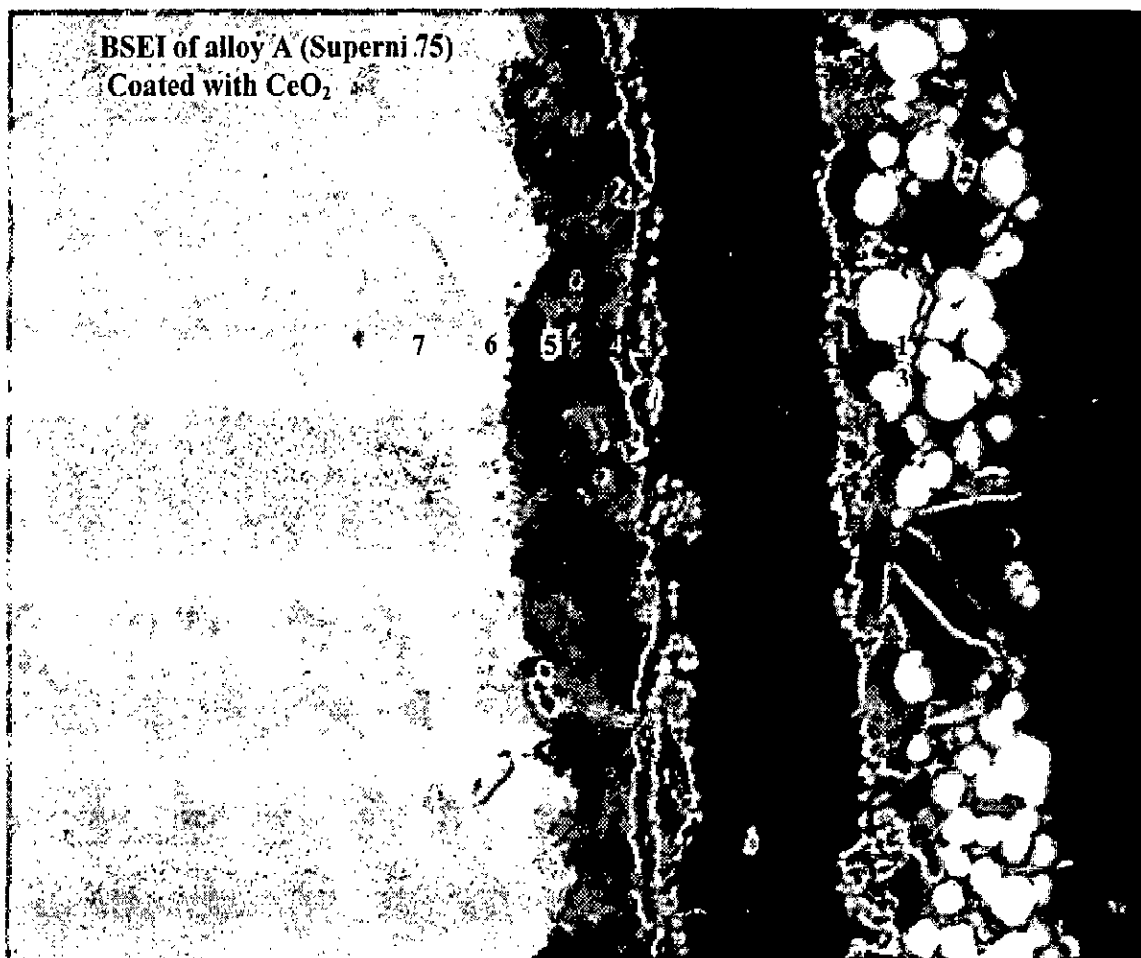
Fig. 5.83 : Back scattered image of alloy C (Superni 75) after cyclic hot corrosion in Na₂SO₄-60%V₂O₅+ CeO₂ at 900⁰C.

Table. 5.7 : Wt. % of elements corresponding to points marked on Fig. 5.83, BSE image of alloy C (Superni75).

Point of Analysis	Weight % of Elements						
	O	Cr	Fe	Ni	Ti	Ce	V
1	23.49	0.21	-	0.84	-	74.38	0.67
2	23.60	7.72	-	66.06	0.20	1.47	0.94
3	17.65	4.88	-	22.23	0.07	50.76	4.38
4	27.74	34.68	0.41	36.00	0.64	-	0.97
5	27.68	25.54	0.28	44.52	0.53	-	1.17
6	25.62	22.56	0.04	51.03	0.34	-	0.30
7	0.00	16.48	0.22	83.37	0.16	-	0.06

5.7 HOT CORROSION STUDIES IN Na_2SO_4-60%V_2O_5 WITH SUPERFICIALLY APPLIED Y_2O_3

5.7.1 Visual Observations

Macrographs for alloys A, B, C, D and E superficially coated with Y_2O_3 and exposed to Na_2SO_4–60%V_2O_5 at 900^0C are shown in Fig. A.2 after completion of 50 cycles. Alloy A, B, C & E showed the presence of unreacted salt on the surface. Scale on the surface of these alloys showed white and light yellow coloured mass, dull and adherent in nature. Spalling of the salt coating has been observed which was the least in alloy E. Whereas in case of D, the colour of top scale surface changed from yellow to black and no unreacted salt was visible.

5.7.2 Kinetic Data

Weight change data for alloys A, B, C, D and E is shown in Fig. 5.84 to 5.86. In case of alloy A, the rate of initial weight gain is slightly higher and the weight gain is nearly constant but substantially lower than that without Y_2O_3 coating. In case of alloy B, there is weight gain upto 18 cycles and then weight loss is observed. Where as after 30 cycles there is no appreciable change in weight gain upto 50 cycles. In case of alloy C, after faster rate of reaction in the initial few cycles, no appreciable increase in weight was observed between 5 to 30 cycles. A gradual decrease in weight is indicated between 30 to 50 cycles. In case of alloy D, the rate of weight gain is gradual and very slow from initial 2 cycles up to 45 cycles after which decrease in weight was noticed. In case of alloy E, after an initial gain in weight, no appriciable change in weight has been observed between 10 to 50 cycles.

5.7.3 X-Ray Diffraction Analysis

X-ray diffraction results (Table A.20 to A.22 and Fig. 5.87, 5.88 and 5.89) in general indicated the presence of oxides and vanadates. The prominent phases identified in alloy A are FeV_2O_4, $NiCr_2O_4$, FeS, CrS and Cr_2O_3. In case of alloy B, the phases identified in the

scales were $Co_3V_2O_8$, Cr_2O_3, $NiWO_4$, $NiCo_2O_4$, Co_3O_4, Cr_2O_3 and $CoCr_2O_4$. In case of nickel base alloy C, the main phases identified were $NiCr_2O_4$, NiO and Cr_2O_3 along with other possible phases $NiCr_2S_4$ NiS and Y_2O_3. The major phases present in the scales of alloy D have been identified as NiO and FeV_2O_4, Cr_2O_3, $Ni(VO_3)_2$, and $NiCr_2O_4$. The scale of alloy E. revealed the main peaks of $Ni(VO_3)_2$, $NiCr_2O_4$, NiO and Cr_2O_3 along with few peaks of Y_2O_3.

5.7.4 Measurement of Scale Thickness

Average values of the scale thickness observed from the BSE images of alloys A, B, C, D & E (Fig. 5.90) are ~20, 30, 16.5, 18.5 and 31 μm respectively. Alloy A has shown the least value in Na_2SO_4-60%V_2O_5 + Y_2O_3 in comparison to all other environments.

5.7.5 SEM, EDAX and EPMA Results

Fig. 5.91(a, b, c, d and e) presents SEM micrographs of alloys A, B, C, D & E. Micrograph for alloy A shows two regions, one showing the region where coating has fallen off and other shows the presence of salt crystals on the surface indicating presence of sulphurous compound. SEM of alloy B shows spongy scale with pores inside indicating perhaps the release of some gas or vapours. SEM of alloy C & E shows the presence of rod like crystalline structure again indicating presence of unreacted salt crystals on the surface. In case of alloy D, massive scale formation is noticed. EDAX analysis of the surface scale at areas marked on Fig. 5.91 (d) given in Table A.30 shows that the scale contains grains rich in nickel (point 3) surrounded by a phase which is rich in Fe. The scales of the alloy D mainly comprises of compounds of Fe, Ni & Cr. Other elements like Ti, Na, S & V are present at few locations.

EPMA analysis for the alloys A, B, C, D & E is given in Figs. 5.92 to 5.96. The BSE image of the alloy A (Fig.5.92) shows that a very thin scale is formed. X-ray image for Cr indicates the presence of a distinct chromium rich band which is continuous. Yttrium is present at top of the scale where both V & S are also present. MnS is present in the substrate and Si in the scale near the substrate. EDAX analysis of the same alloy along the cross-section

(Fig. 5.97 and Table 5.8) indicates that top scale contains small percentages of Fe, Ni & Cr. Higher percentages of Cr at points 2, 3 and 4 further indicate the presence of a thick continuous Cr-rich band. Y & V are present throughout the cross-section and almost at same locations along with Cr-band.

In case of alloy B, EPMA analysis (Fig. 5.93 and Fig. A.3) indicates presence of medium size scale which is rich in chromium and cobalt. W is present in high concentration in the scale. S has penetrated into the substrate. Scale just above the substrate is depleted in Cr and rich in Ni. Fe and V also exist in the scale.

In case of alloy C (Fig. 5.94), thin scale has formed. Top layer is containing mainly Cr with Ni and there is presence of vanadium and S along with Y. Sulphur is also present in the substrate and it is coexisting with Cr and Y.

The EPMA analysis of alloy D, (Fig. 5.95 and Fig. A.4) indicates medium size scale containing mainly Ni, Cr & Fe and the scale is continuous. Above this scale there is thin layer of S and at the substrate and scale interface, sulphur is distributed along the region and at these points Cr and Fe are absent. V is also present throughout the scale. Ta, Ti and Al are also indicated in the scale. EDAX analysis for the same alloy D along the cross-section is given in Table 5.9 corresponding to back scattered image (Fig. 5.98) at various points from surface to substrate. From this analysis it can be inferred that there is oxygen rich scale mainly containing Cr, Ni & Fe indicating formation of oxides and spinels. Vanadium is present in the outer scale. The internal oxidation has taken place and at these points there is presence of higher concentration of Al & Ti. Analysis at point 4 in the intergranular region indicates quite high wt. % of Ti and Al. Y has been spotted in uppermost region at point 1 only.

In case of alloy E, the EPMA analysis (Fig. 5.96) indicates presence of a very thin continuous Cr rich layer where both Ni & Fe are absent. Above this layer, there is presence of V & Y, indicating probable formation of YVO_4. S is present with Fe above this thin Cr layer at some points. The top scale could be containing Ni, Fe and Cr. The presence of S in Fe-rich areas containing both Cr and Ni indicates formation of sulphides.

159
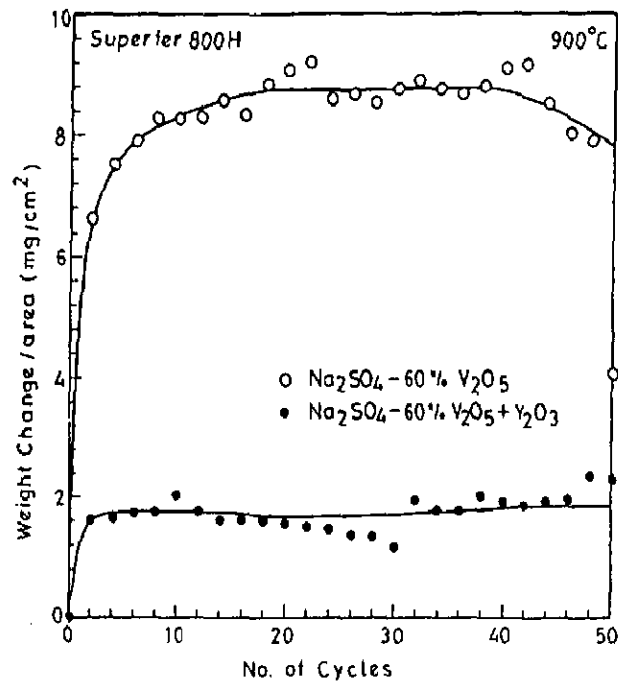
Fig. 5.84: Weight change plot for alloy A (Superfer 800H) after cyclic hot corrosion at 900⁰C in Na₂SO₄-60% V₂O₅ +Y₂O₃ coating.
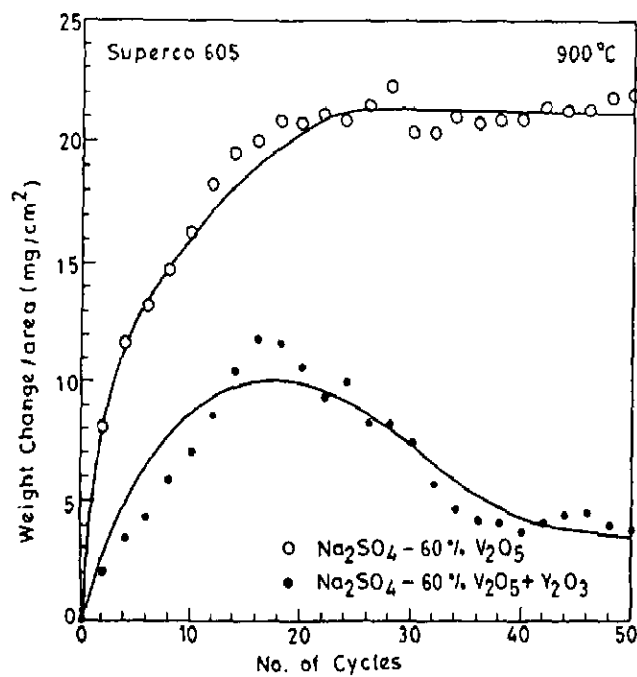
Fig. 5.85: Weight change plot for the alloy B (Superco 605) after cyclic hot corrosion at 900⁰C in Na₂SO₄-60% V₂O₅ + Y₂O₃ coating.

160

Fig. 5.86: Weight change plots for the nickel base alloys, alloy C (Superni 75), alloy D (Superni 718) and alloy E (Superni 601) after cyclic hot corrosion at 900°C in Na₂SO₄-60% V₂O₅ + Y₂O₃ coating.

Superfer 800H

a Fe$_2$O$_3$
b Cr$_2$O$_3$
c FeV$_2$O$_4$
d CrS
e NiCr$_2$S$_4$
f NiCr$_2$O$_4$
g Y$_2$O$_3$

Relative Intensity

b

b,e,f

b,f

a,b   c,d   d,e   e,g   d,g   e,g   a,b,c,f

20   30   40   50   60   70   80

2θ

Fig. 5.88:   X-ray diffraction profile for alloy A (Superfer 800H) after cyclic hot corrosion at 900^{0}C in Na$_2$SO$_4$-60% V$_2$O$_5$ +Y$_2$O$_3$ coating.

Superco 605

a NiWO$_4$
b NiCo$_2$O$_4$
c Co$_3$O$_4$
d Cr$_2$O$_3$
e CoCr$_2$O$_4$

Relative Intensity

a,b,c

a,b,c

d

a,d,e   b,c,d,e   b,c,d,e

0

20   30   40   50   60   70   80

2θ
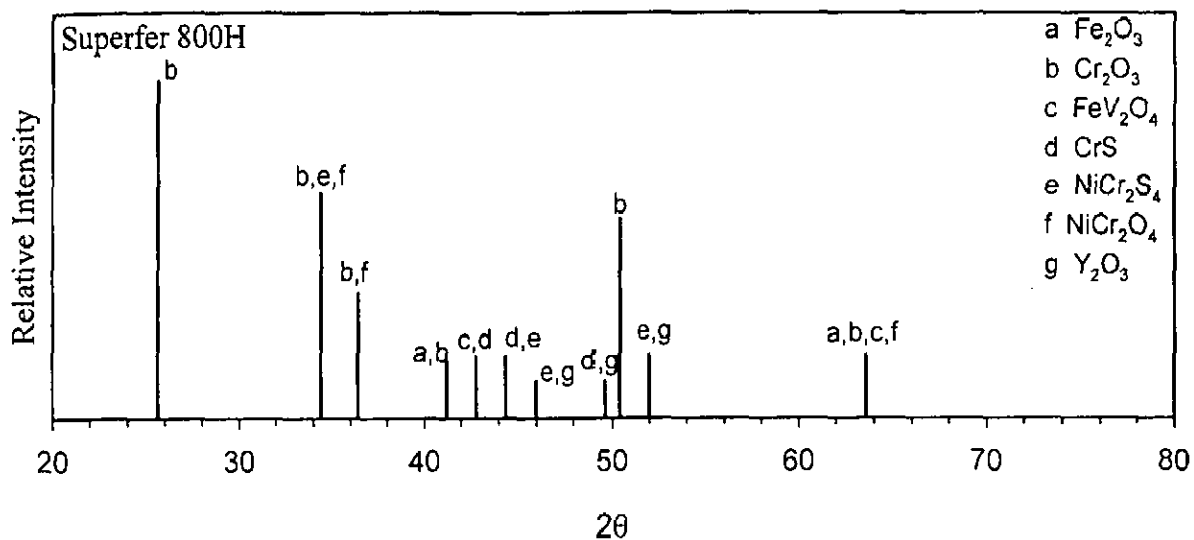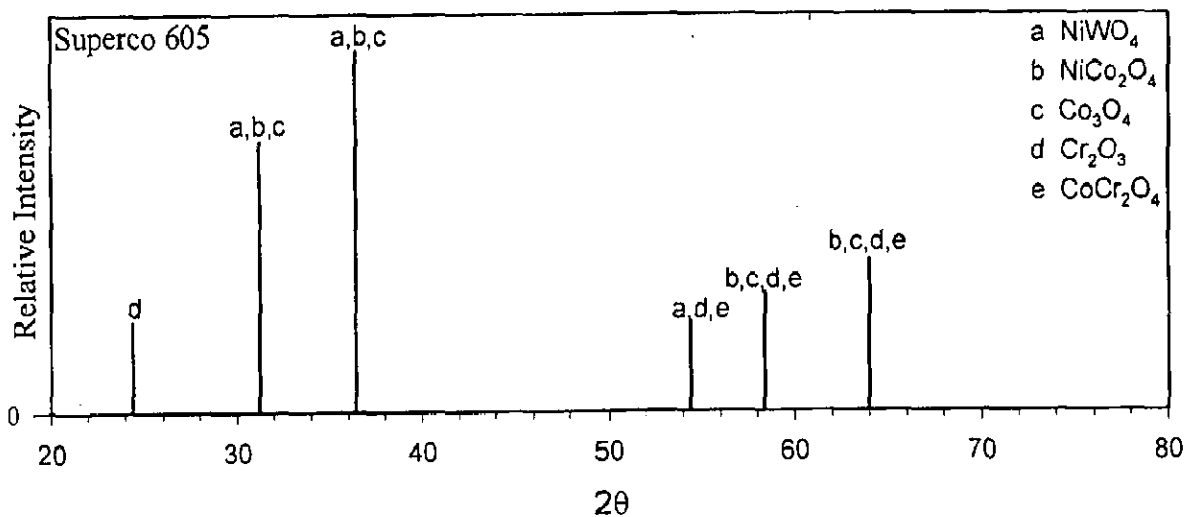
Fig. 5.87:   X-ray diffraction profile for alloy B (Superco 605) after cyclic hot corrosion at 900^{0}C in Na$_2$SO$_4$-60% V$_2$O$_5$ + Y$_2$O$_3$ coating.

162

Fig. 5.89: X-ray diffraction profiles for the nickel base alloys: alloy C (Superni 75), alloy D (Superni 718) and alloy E (Superni 601) after cyclic hot corrosion at 900^0C in Na_2SO_4-60% V_2O_5 + Y_2O_3 coating.
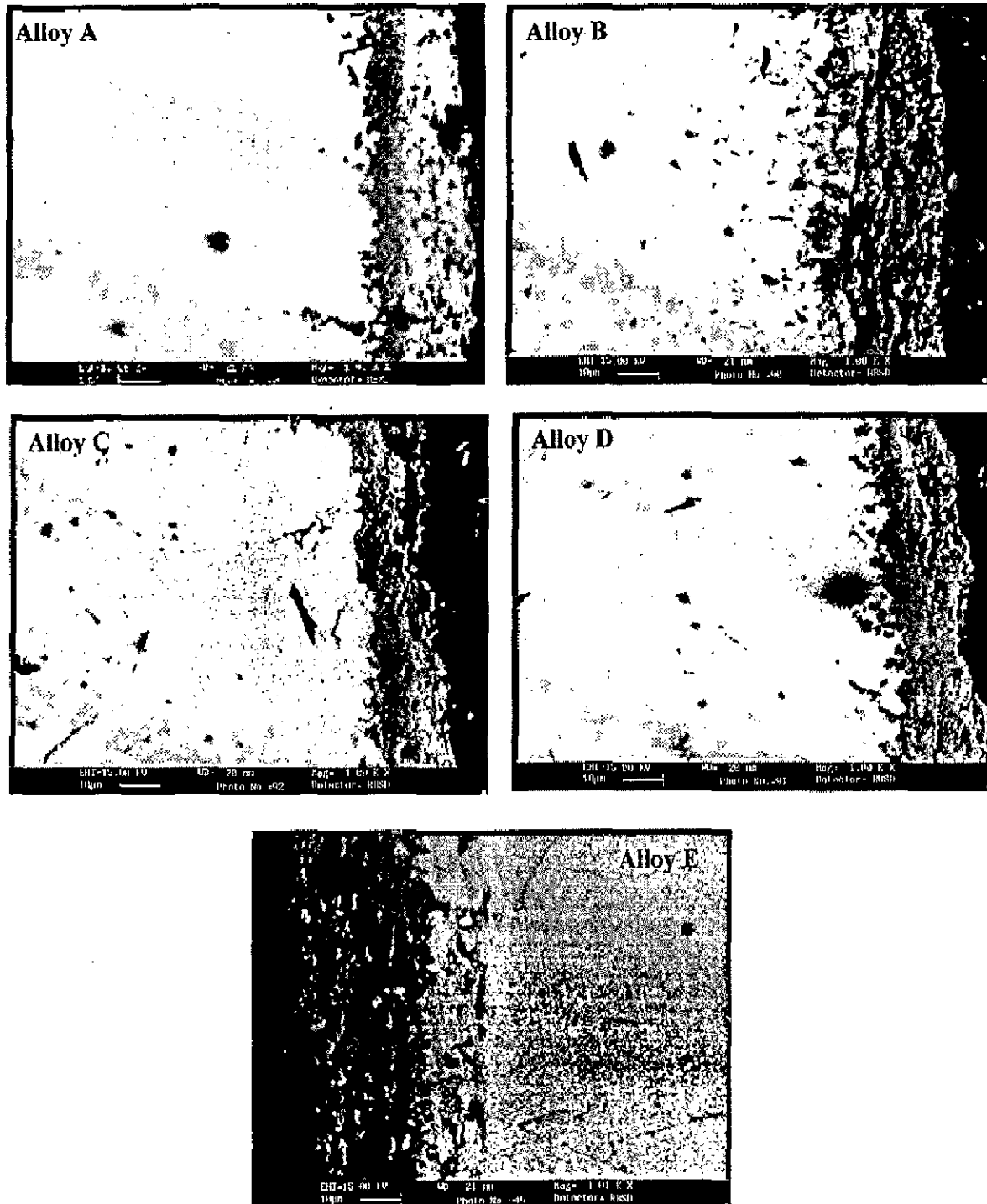
Fig. 5.90: BSE images of alloy A (Superfer 800H), alloy B (Superco 605), alloy C (Superni 75), alloy D (Superni 718) and alloy E (Superni 601) in Na_2SO_4-60%V_2O_5 + Y_2O_3 environment after exposure at 900°C in cyclic conditions.
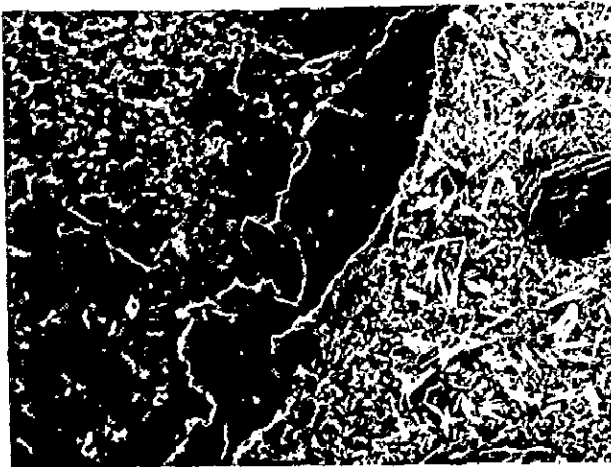
(a)
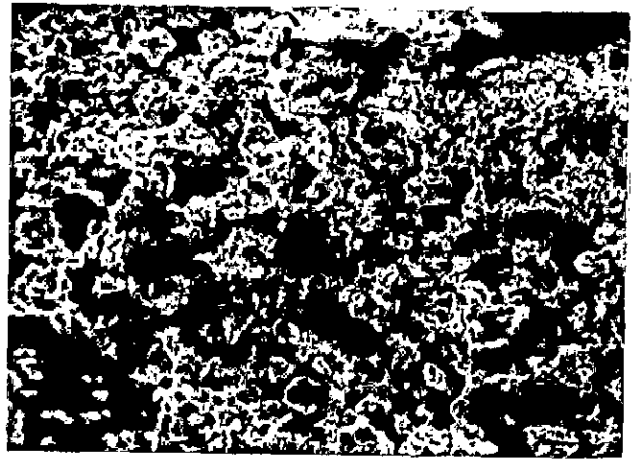
(b)

(c)

(d)
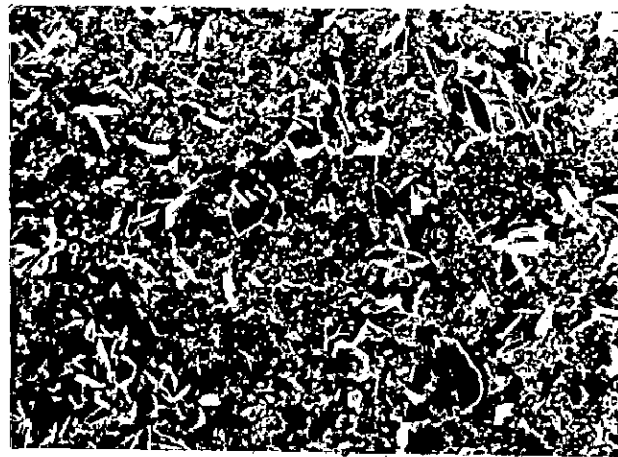
(e)

Fig. 5.91 :   Scanning Electron Micrographs after cyclic hot corrosion in Na_2SO_4-60%V_2O_5
+Y_2O_3 coating at 900°C of alloys:

a) Alloy A (Superfer 800H)   (X 640)

b) Alloy B (Superco 605)   (X 640)

c) Alloy C (Superni 75)   (X 640)

d) Alloy D (Superni 718)   (X 650)

e) Alloy E (Superni 601)   (X 640)
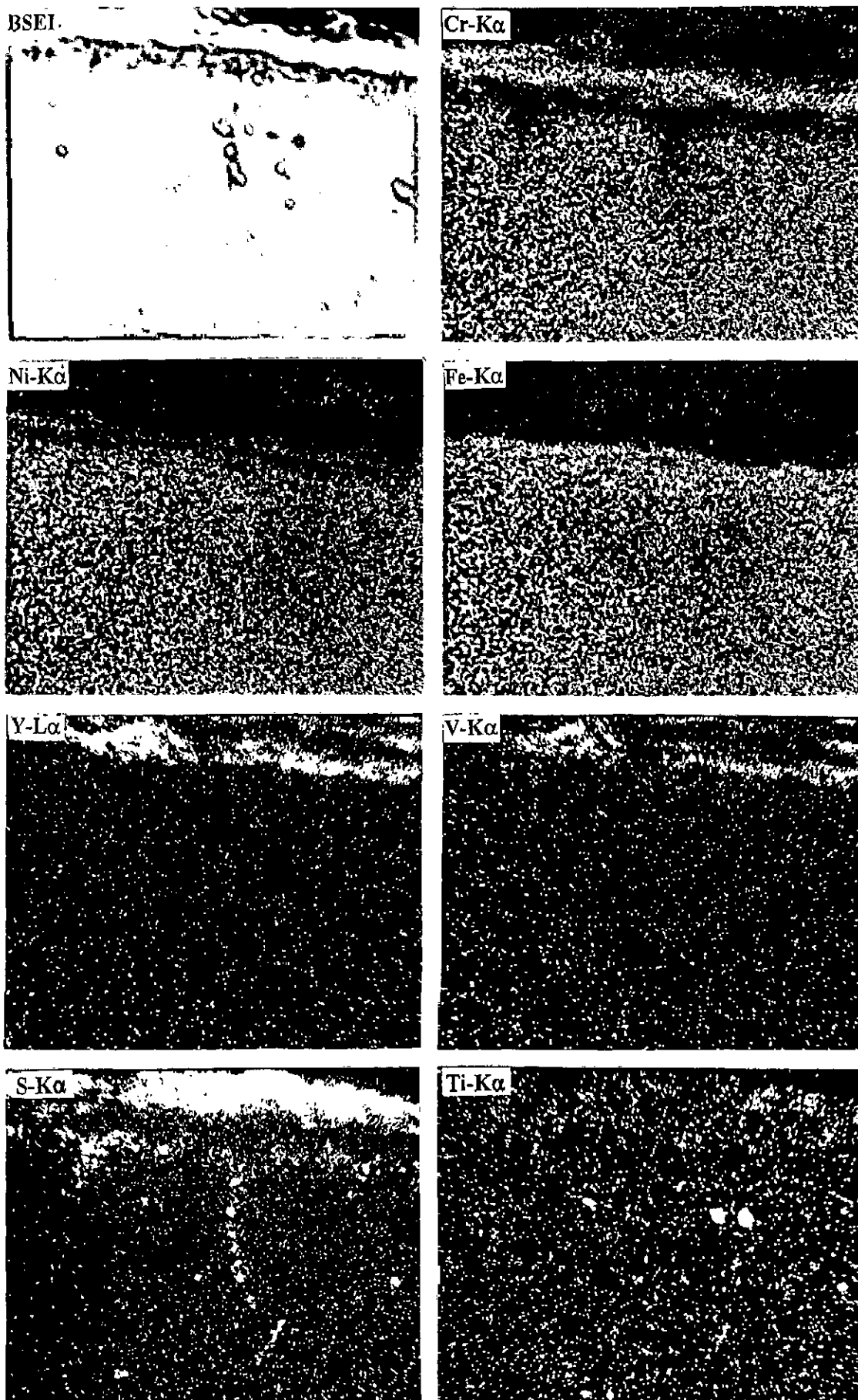
Fig. 5.92: BSEI and X-ray mapping of the cross-section of alloy A (Superfer 800H) after cyclic hot corrosion at 900^0C in Na_2SO_4-60%V_2O_5+Y_2O_3. (X 800)
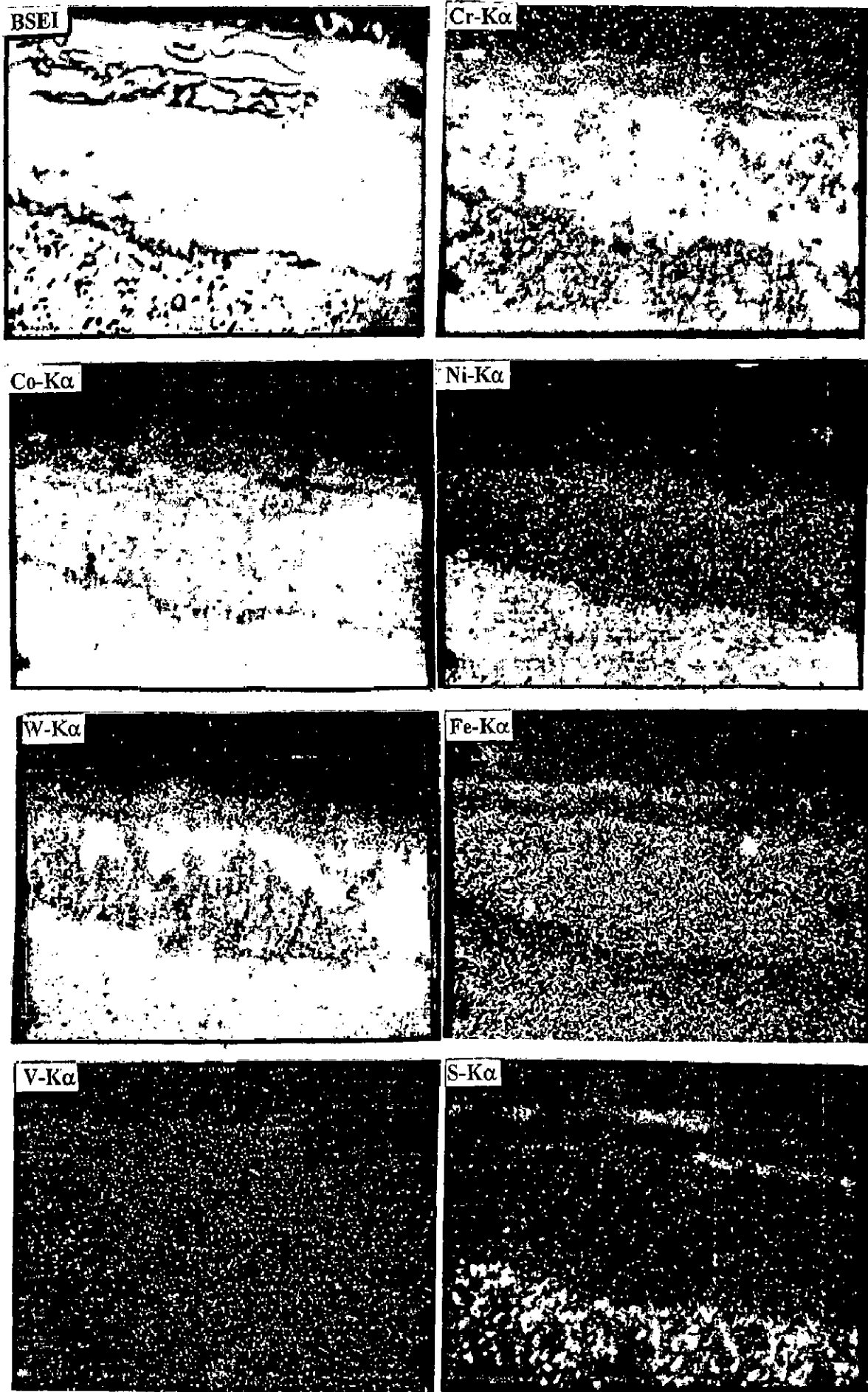
Fig. 5.93: BSEI and X-ray mapping of the cross section of alloy B (Superco 605) after cyclic hot corrosion at 900^0C in Na_2SO_4-60%V_2O_5+Y_2O_3. (X 800)
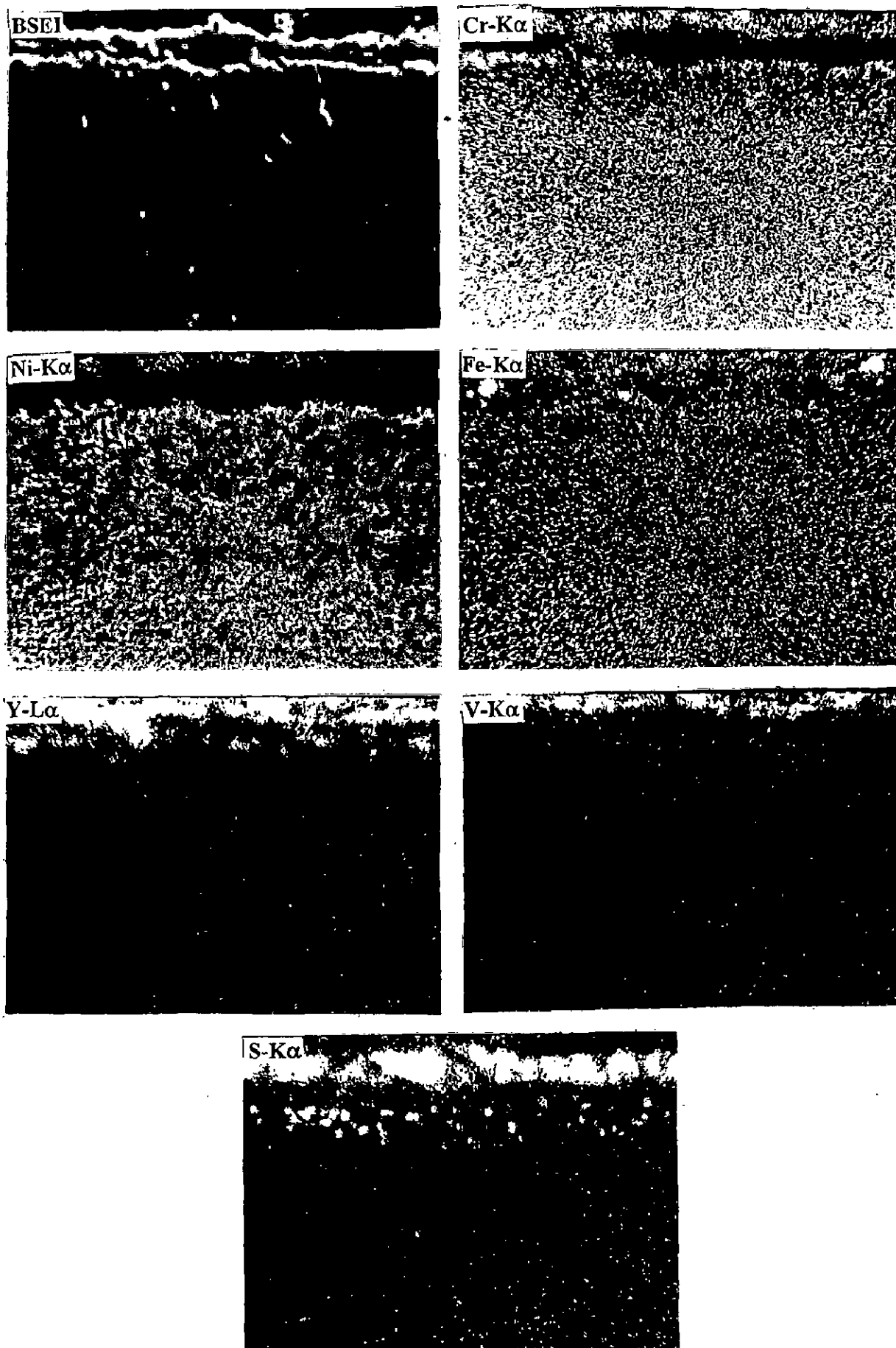
Fig. 5.94: BSEI and X-ray mapping of the cross section of alloy C (Superni 75) after cyclic hot corrosion at 900°C in Na_2SO_4-60%V_2O_5+Y_2O_3. (X 800)
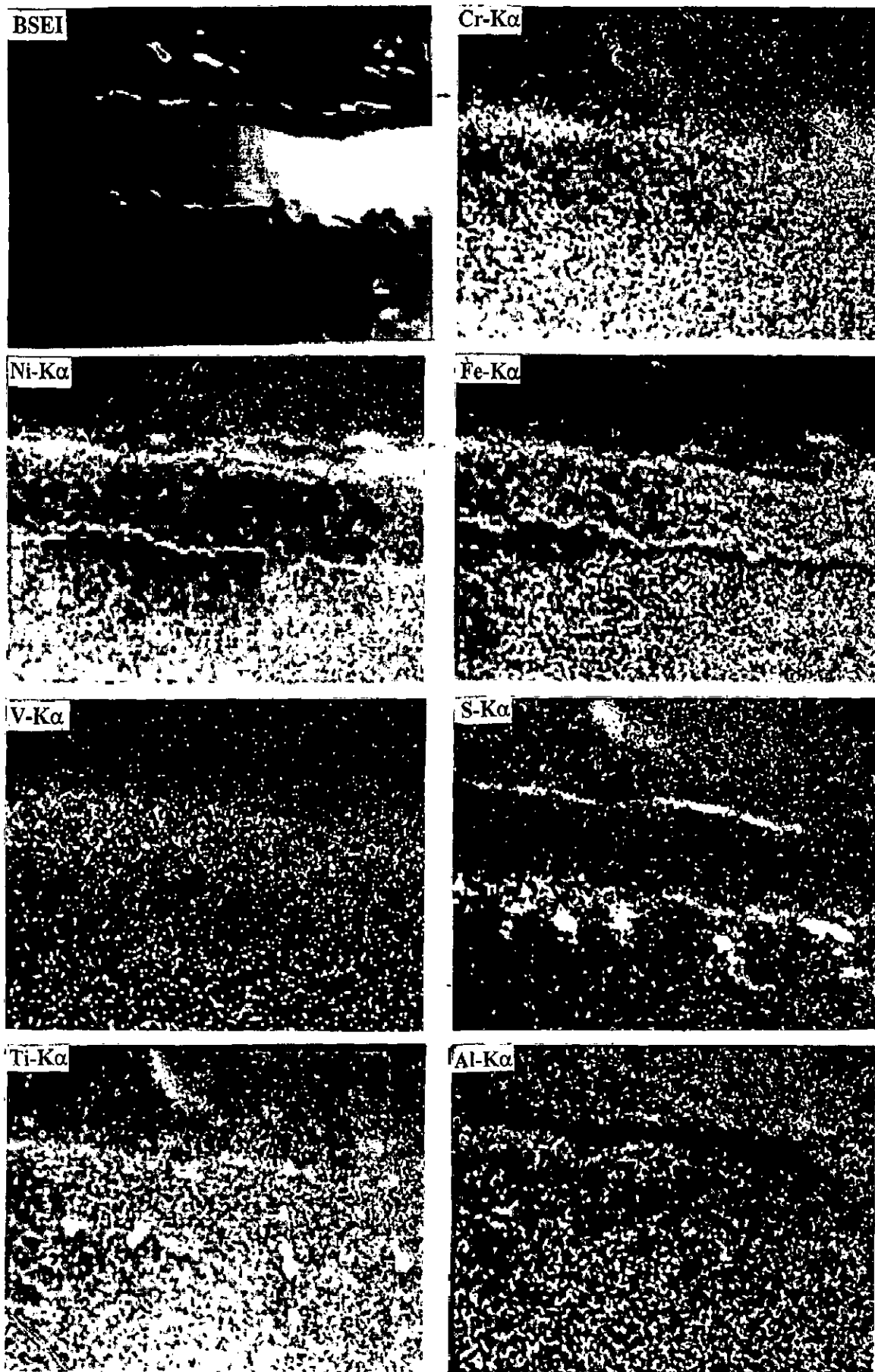
Fig. 5.95:   BSEI and X-ray mapping of the cross section of alloy D (Superni 718) after cyclic hot corrosion at 900^0C in $Na_2SO_4-60\%V_2O_5+Y_2O_3$.   (X 800)
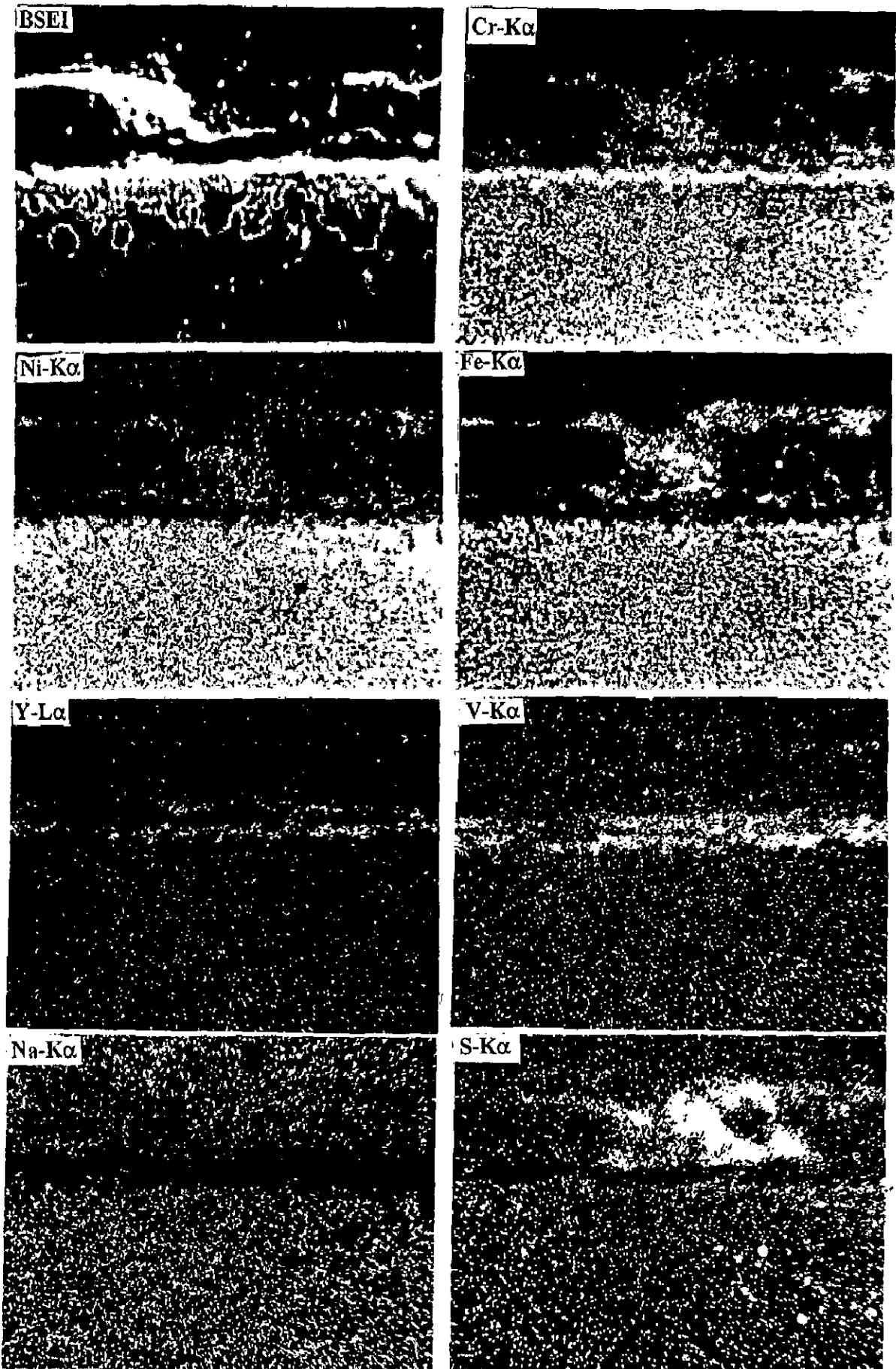
Fig. 5.96: BSEI and X-ray mapping of the cross section of alloy E (Superni 601) after cyclic hot corrosion at 900°C in Na_2SO_4-60%V_2O_5+Y_2O_3. (X 600)

EDAX Analysis of alloy A (Superfer 800H) in Na₂SO₄-60%V₂O₅+Y₂O₃ along the Cross-Section

$EDAX\ Analysis\ of\ alloy\ A\ (Superfer\ 800H)\ in\ Na_2SO_4\text{-}60\%V_2O_5+Y_2O_3$ along the Cross-Section

Fig. 5.97 :   Back Scattered Image of Alloy A (Superfer 800H) after cyclic hot corrosion in Na₂SO₄-60%V₂O₅+ Y₂O₃ at 900°C.

$Na_2SO_4\text{-}60\%V_2O_5+ Y_2O_3$ at 900^0C.

Table. 5.8 :   EDAX analysis for Alloy A (Superfer 800H) coated with Y_2O_3 in $Na_2SO_4\text{-}60\%V_2O_5$ at different positions along the cross-section corresponding to Fig. 5.97.

Point of Analysis	Weight % of Elements											
	O	Fe	Cr	Ni	Y	V	Ti	Mn	Si	Al	Na	S
1	27.9	42.04	20.32	1.13	2.95	1.64	1.15	2.86	0.34	0.19	-	-
2	36.94	21.03	27.79	1.14	5.31	3.53	0.62	2.52	0.74	0.20	0.12	0.07
3	34.71	23.46	36.25	1.15	0.24	0.59	0.72	1.95	0.76	0.12	0.10	-
4	25.45	20.30	30.12	17.50	-	0.13	1.55	0.43	3.37	0.65	-	0.50
5	0.00	45.02	18.92	33.50	-	-	0.22	1.22	1.06	0.27	-	-

EDAX Analysis of alloy D (Superni 718) in Na$_2$SO$_4$-60%V$_2$O$_5$+Y$_2$O$_3$ along the Cross-Section

Fig. 5.98 : Back Scattered Image of alloy D (Superni 718) after cyclic hot corrosion in Na$_2$SO$_4$-60%V$_2$O$_5$+ Y$_2$O$_3$ at 900°C.

Table. 5.9 : EDAX analysis for alloy D (Superni 718) coated with Y$_2$O$_3$ in Na$_2$SO$_4$-60%V$_2$O$_5$ at different positions along the cross-section corresponding to Fig. 5.98.

Point of Analysis	Weight % of element													
	O	Fe	Ni	Cr	Ti	Al	Mo	Mn	Si	Cu	Y	V	S	Ta
1	6.94	21.50	53.16	13.57	0.99	1.30	-	0.09	0.90	0.18	0.38	0.60	0.49	0.05
2	9.76	17.00	44.70	24.54	1.02	0.48	-	-	1.13	0.12	-	0.46	0.84	-
3	26.5	13.38	20.70	34.91	3.29	1.24	-	0.30	-	-	-	0.33	-	0.36
4	14.02	13.95	53.12	13.19	2.82	2.23	-	-	0.16	-	-	-	0.17	-
5	0.70	17.03	70.11	9.70	0.47	0.35	0.66	0.27	0.23	-	-	-	0.45	-

5.8 HOT CORROSION STUDIES IN Na$_2$SO$_4$-60%V$_2$O$_5$ WITH SUPERFICIALLY APPLIED SnO$_2$

5. 8. 1 Visual Observations

Macrographs of the corroded specimens of alloys A, B, C, D and E after exposure for 50 cycles in Na$_2$SO$_4$-60%V$_2$O$_5$ with a superficial coating of SnO$_2$ are shown in Fig. A.2. The reaction product present on the surface of alloys A, C & E was reddish in colour showing the presence of unreacted salt though it had fallen off at some places mainly on the edges. The scale of the alloy B & D was black in colour. Colour of the sample B changed to greyish black and showed smooth and adherent scale after Ist cycle. Sputtering of the scale was observed in the 3rd cycle with some spalling tendency in the subsequent cycles.

5.8.2 Kinetic Data

Fig. 5.99-5.101 show the plots drawn between weight change and time (No. of Cycles) for alloys A, B, C, D and E. In case of alloy A, there is decrease in the weight gain with SnO$_2$ coating. Initial weight gain with SnO$_2$ coating is nearly half as compared to one without SnO$_2$ coating. In the initial cycles weight tends to become nearly constant but abruptly increases after 10 cycles and then becomes nearly constant.

In case of alloy B, with application of SnO$_2$ layer the rate of weight gain is much less and maximum weight gain is achieved at 20 cycles, which is approximately less than half of that without SnO$_2$ coating. Alloy C shows similar trend as in alloy A & B but the overall weight gain upto about 20 cycles is 1/3rd of that of alloy B with the application of SnO$_2$. The overall weight gain after 50 cycles is nearly 65% of that without SnO$_2$ coating.

In case of alloy D, in general the weight gain is less than that without SnO$_2$ coating but the behaviour is erratic. Overall weight gain is around 8 mg/cm^2 that is about 80% of the one without SnO$_2$. In case of alloy E, the initial weight gain upto 14 cycles is nearly same but in

case of SnO_2 coating the weight becomes constant after that and there is slight decrease with the increase in number of cycles whereas after 40 cycles slight increase is indicated.

5.8.3 X-Ray Diffraction Analysis

X-ray diffraction results (Table A.23 to A.25 and Fig. 5.102 to 5.104) in general indicated the presence of oxides and vanadates. The prominent phases identified in alloy A were Fe_2O_3, FeV_2O_4, $NiCr_2O_4$, $NiFe_2O_4$, Cr_2O_3, FeS, $(Cr,Fe)_2O_3$ and SnO_2. In case of alloy B, the phases identified in the scales were Cr_2O_3, Co_3O_4, $NiCo_2O_4$, $Co_3V_2O_8$, $NiWO_4$ and NiO. In case of nickel base alloy C, the main phases identified were SnO_2, Cr_2O_3 and NiO, whereas in alloy D, $Ni(VO_3)_2$, $NiCr_2O_4$, Cr_2O_3, FeV_2O_4 and NiO were detected. The scale of alloy E revealed the presence of SnO_2, $NiCr_2O_4$, Cr_2O_3, FeV_2O_4 and NiO as the possible phases. All major peaks of SnO_2 could be identified in alloys A, C and E

5.8.4 Measurement of scale Thickness

Average values of the scale thickness observed from the BSE images of alloys A, B, C, D & E (Fig. 5.105) are 32, 52, 34, 18 and 50 μm respectively

5.8.5. SEM, EDAX and EPMA Results

Fig. 5.106 presents the SEM micrograph of alloys A, B, C, D & E. In case of alloys A, C & E one can observe crystalline growth at the top surface of the scale which indicates the presence of SnO_2 that can be clearly seen at higher magnification (3.27 KX) in case of alloy E in form of cuboids as shown in Fig. 5.106 (e & f). The alloy B indicates a massive scale with intergranular cracks and irregular shaped craters in the scale indicating escaping of gas or vapours. Whereas in alloy D, there is a continuous dense layer showing spalling in some regions.

The EPMA of the alloy A, Fig. 5.107 indicates formation of thick scale consisting of mainly Fe & Cr and presence of Fe, Ni and Cr together at two pockets indicating formation of spinels. There is a presence of Sn in higher concentration in the scale and Sn is coexisting with V at some places. There is a thin continuous layer just above the substrate which is rich in Ni

and this area is depleted of Fe and Cr. Internal oxidation of Cr is indicated penetrating into the substrate. In case of alloy A, coated with SnO_2, EDAX analysis (Fig 5.112 and Table 5.10) across the scale indicates the formation of a scale in which the top layer mainly consists of Fe, Ni and Cr. Small amounts of Sn ,V and Na are also present in the scale. Internal oxidation is indicated.

In case of alloy B (Fig. 5.108), the scale is mainly consisting of higher concentration of Cr and Co. Co is uniformly present throughout the scale. In the areas depleted of Cr, W is present. There is a sub layer which is continuous and rich in Cr. S is indicated at the top of the scale and also sulphide specs are seen near the substrate/scale interface. The EDAX analysis of alloy B (Fig. 5.113 and Table 5.11) indicates that top layer is rich in W and Co whereas Fe & Ni are also present in very small concentration. The amount of Cr increases as one moves into the subscale. Presence of Sn is also indicated in the scale. In the upper region of the scale a very small amount of V is also indicated. S is present in traces in the scale. The oxygen is present throughout the scale indicating mainly formation of oxides and spinels.

EPMA analysis of alloy C (Fig. 5.109) indicates that the scale is of medium thickness and consists of mainly chromium with lesser amount of Ni and pockets of Fe rich areas. Sn is present in the higher concentrations at the top of the scale whereas V is present in the main scale. Ti is present throughout the scale and pockets of S rich areas are also indicated.

The EPMA analysis of alloy D indicates formation of relatively thinner scale as shown in Fig. 5.110. Scale is rich in Cr and contains Ni both distributed uniformly. There is a thin Mo rich subscale in which both Ni and Cr are absent. There is presence of Al at the top of the scale. S is also present on top of the scale as well as in the substrate. Al & S are co-existing in some of the areas at the top. Ti is also present along with S and internal oxidation has taken place. Internal oxidation of Mo and Ti is observed.

EPMA of alloy E, Fig. 5.111 indicates that scale is thick and uniform. There is presence of Sn on the surface. Thick scale is basically rich in nickel at the top surface. Fe, Cr and Ni are present in the scale. V is present in the scale along the substrate scale interface in high concentration but there is no internal oxidation.
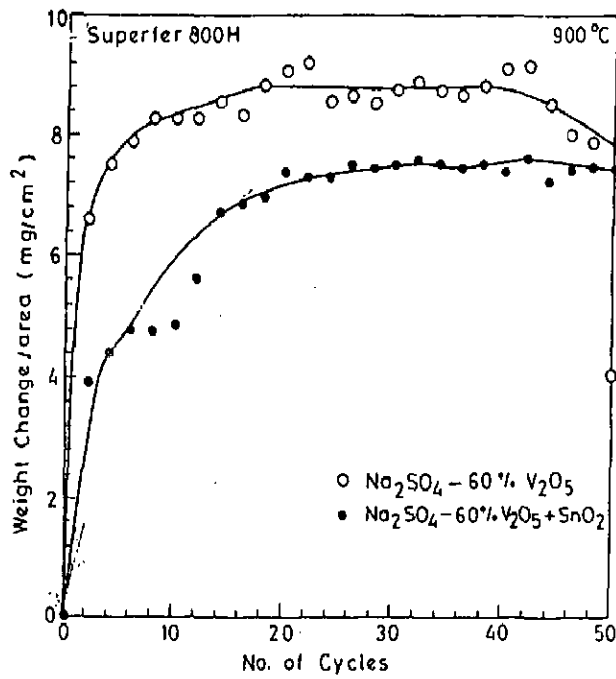
Fig. 5.99: Weight change plot for alloy A (Superfer 800H) after cyclic hot corrosion at 900°C in Na₂SO₄-60% V₂O₅ + SnO₂ coating.
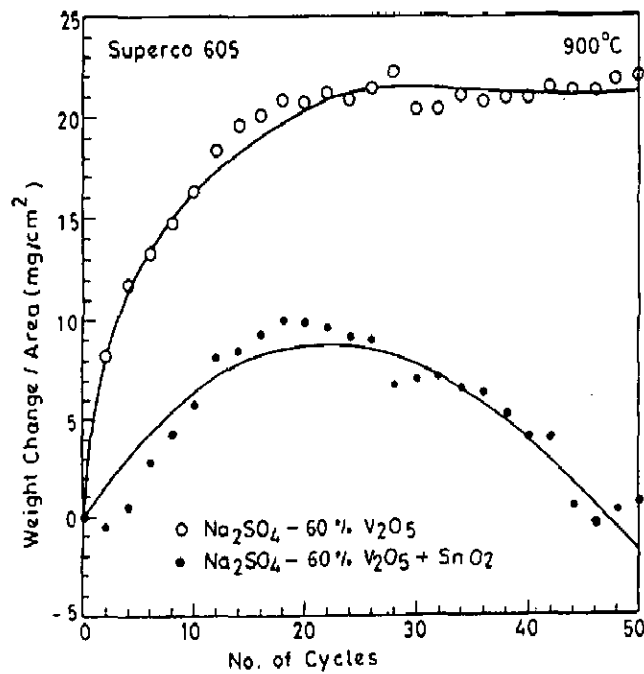
Fig. 5.100: Weight change plot for the alloy B (Superco 605) after cyclic hot corrosion at 900°C in Na₂SO₄-60% V₂O₅ + SnO₂ coating.

176
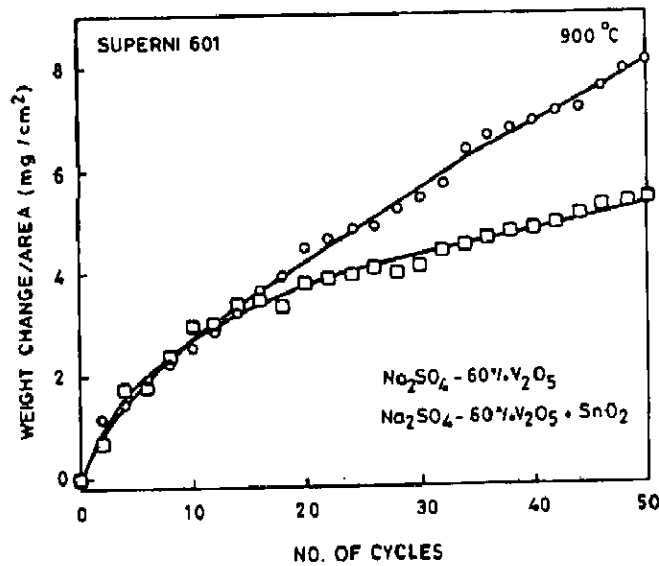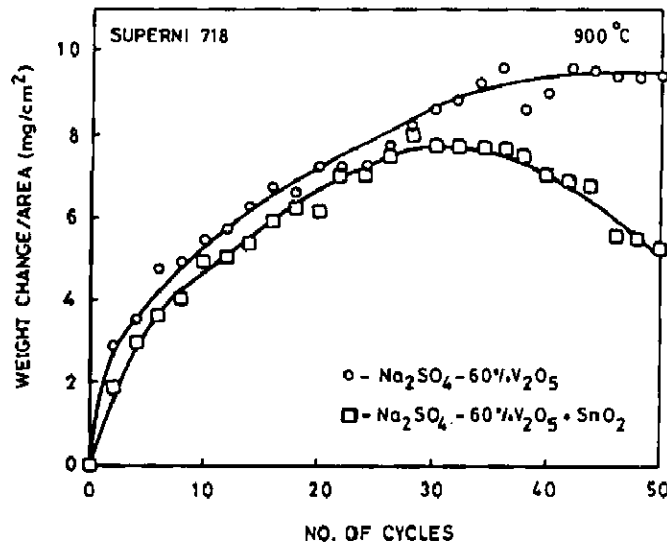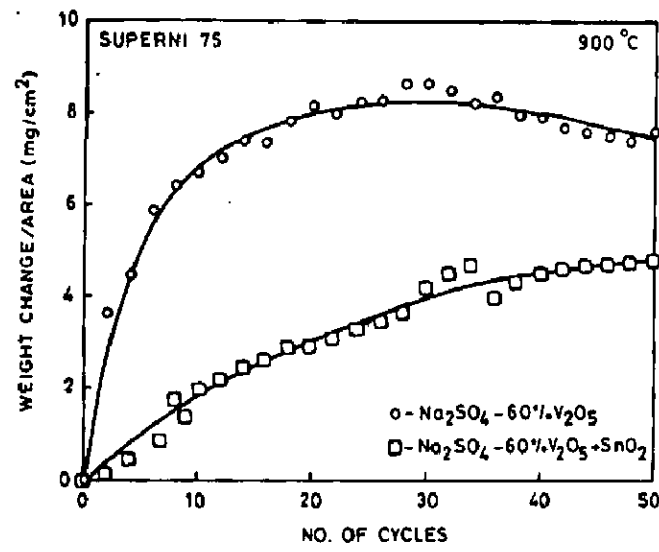
Fig. 5.101: Weight change plots for the nickel base alloys: alloy C (Superni 75), alloy D (Superni 718) and alloy E (Superni 601) after cyclic hot corrosion at 900^0C in Na_2SO_4-60% V_2O_5 + SnO_2 coating.
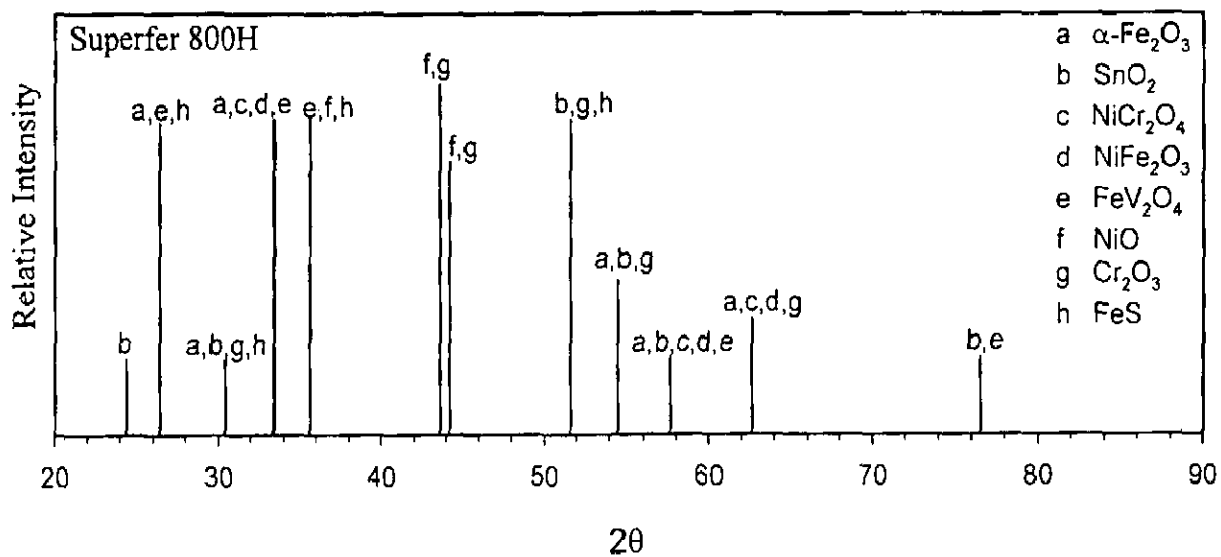
Fig. 5.102: X-ray diffraction profile for alloy A (Superfer 800H) after cyclic hot corrosion at 900^0C in Na_2SO_4-60% V_2O_5 + SnO_2 coating.
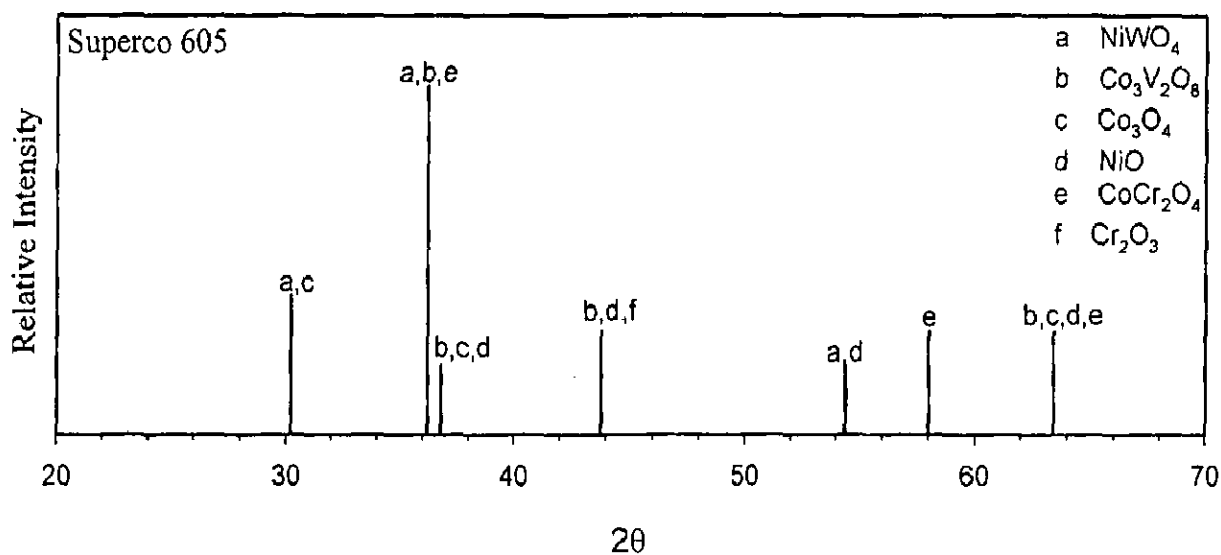
Fig. 5.103: X-ray diffraction profile for alloy B (Superco 605) after cyclic hot corrosion at 900^0C in Na_2SO_4-60% V_2O_5 + SnO_2 coating.
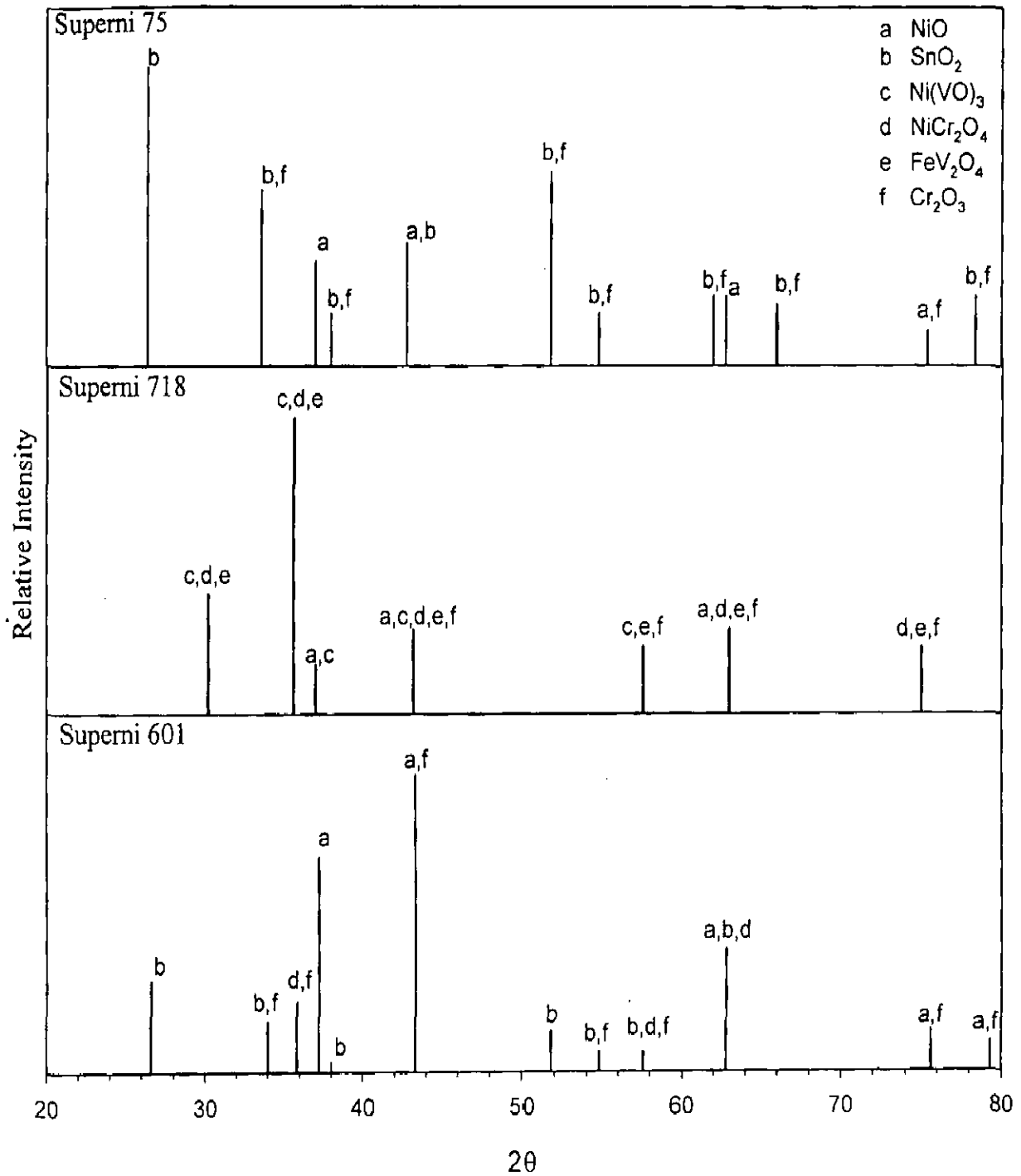
Fig. 5.104: X-ray diffraction profiles for the nickel base alloys: alloy C (Superni 75), alloy D (Superni 718) and alloy E (Superni 601) after cyclic hot corrosion at 900^0C in Na_2SO_4-60% V_2O_5 + SnO_2 coating.
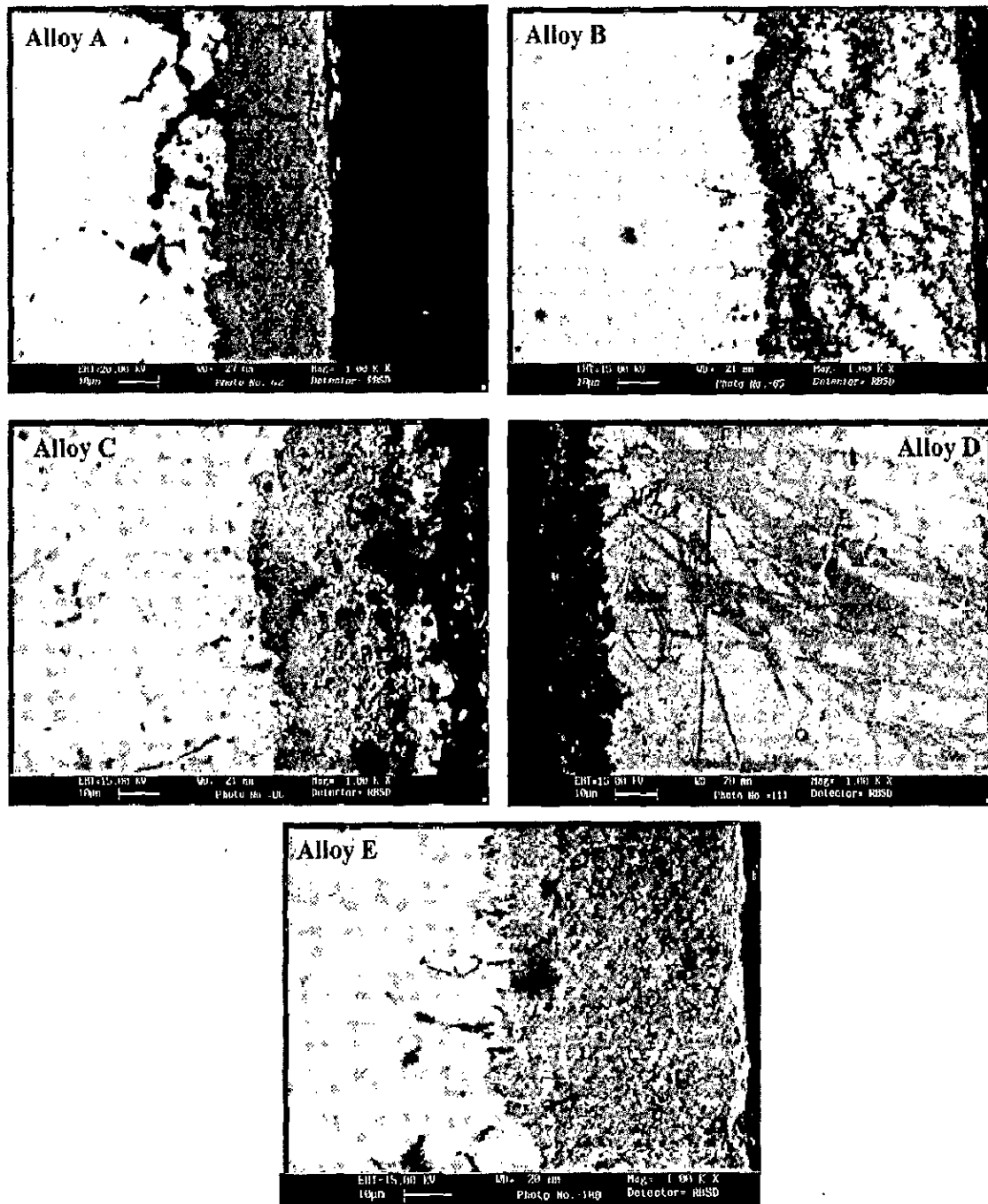
Fig. 5.105 :   BSE images of alloy A (Superfer 800H), alloy B (Superco 605), alloy C (Superni 75), alloy D (Superni 718) and alloy E (Superni 601) in Na_2SO_4-60%V_2O_5 + SnO_2 environment after exposure at 900°C in Cyclic Conditions.

(a)

(b)

(c)

(d)

(e)

(f)
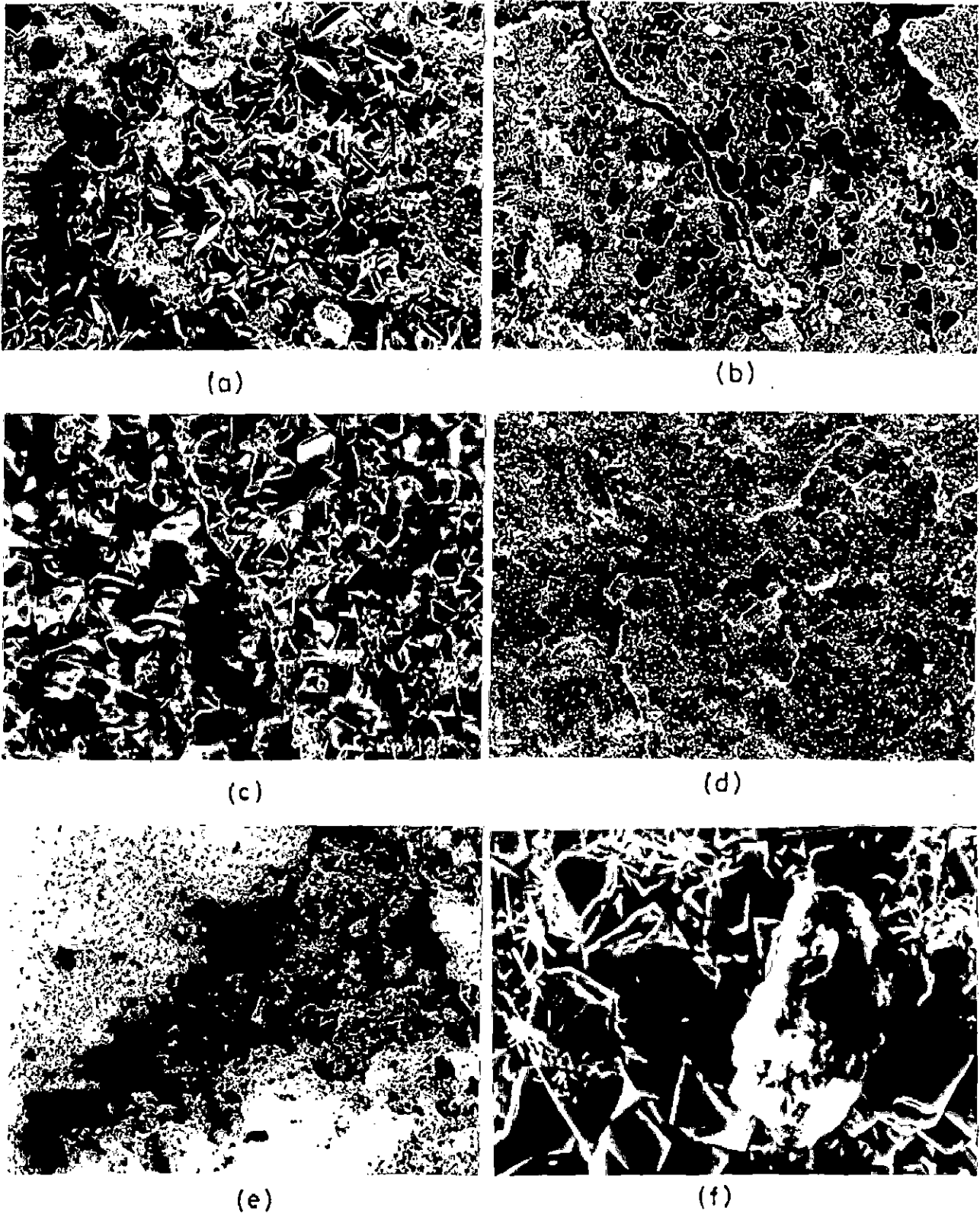
Fig. 5.106: Scanning Electron Micrographs after cyclic hot corrosion in Na_2SO_4-60%V_2O_5 +SnO_2 of alloys:

a) Alloy A (Superfer 800H)	(X 640)
b) Alloy B (Superco 605)	(X 640)
c) Alloy C (Superni 75)	(X 640)
d) Alloy D (Superni 718)	(X 640)
e) & f) Alloy E (Superni 601)	(X 420 & 3.27 KX)
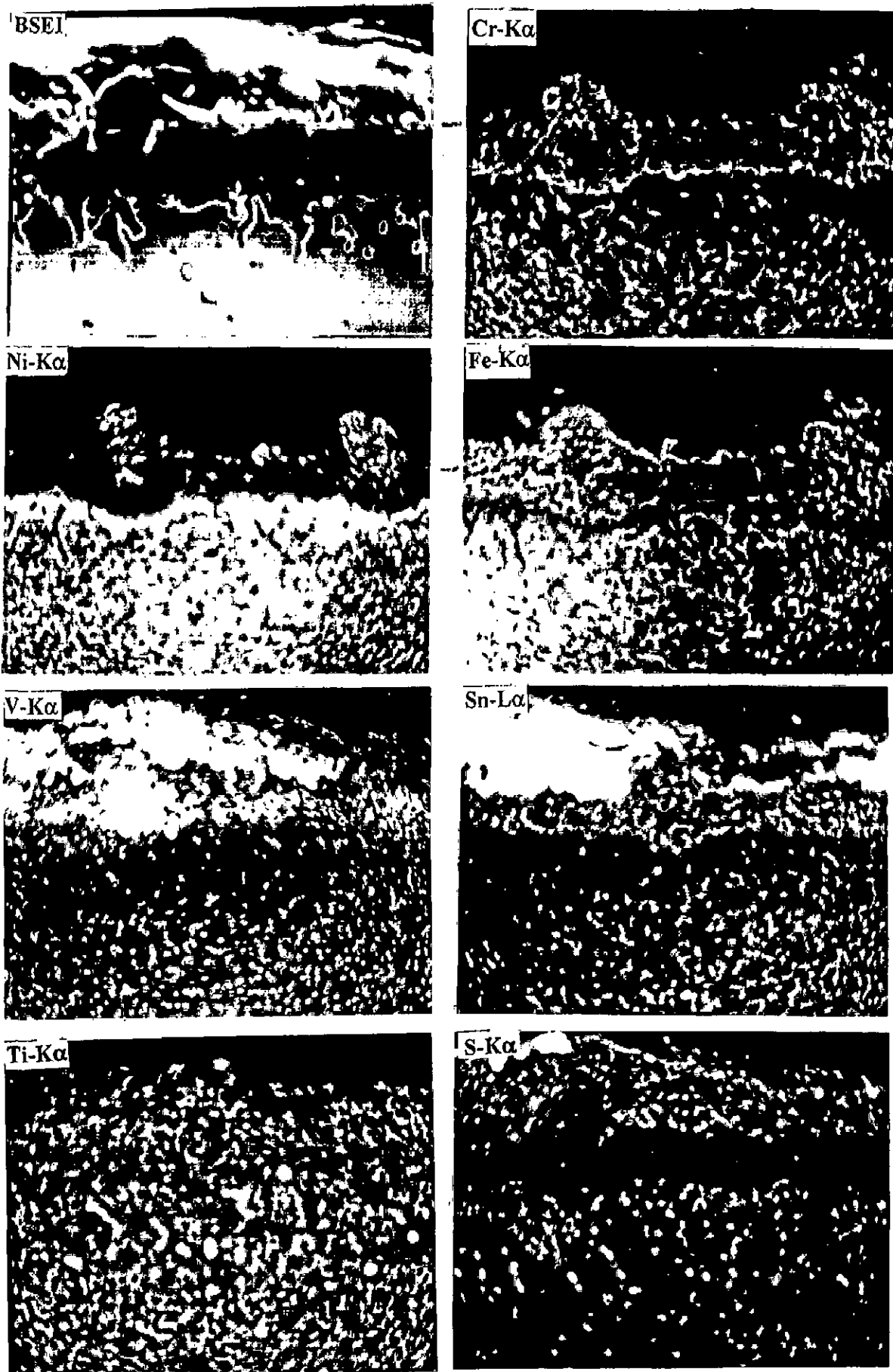
Fig. 5.107: BSEI and X-ray mapping of the cross section of alloy A (Superfer 800H) after cyclic hot corrosion at 900^0C in Na_2SO_4-60% V_2O_5 +SnO_2. (X 400)

182
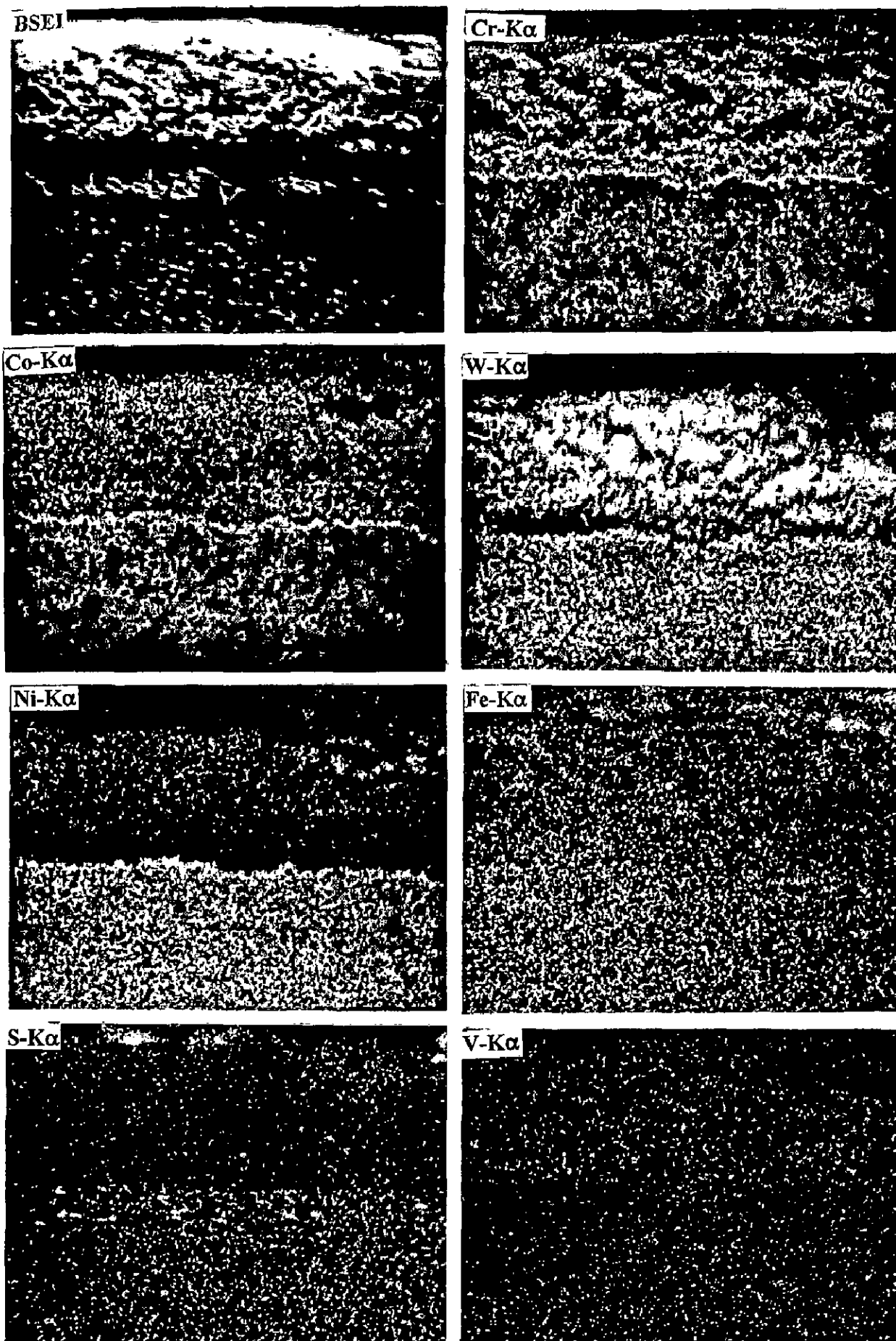
Fig. 5.108: BSEI and X-ray mapping of the cross section of alloy B (Superco 605) after cyclic hot corrosion at 900^0C in Na_2SO_4-60% V_2O_5 + SnO_2 (X 600)
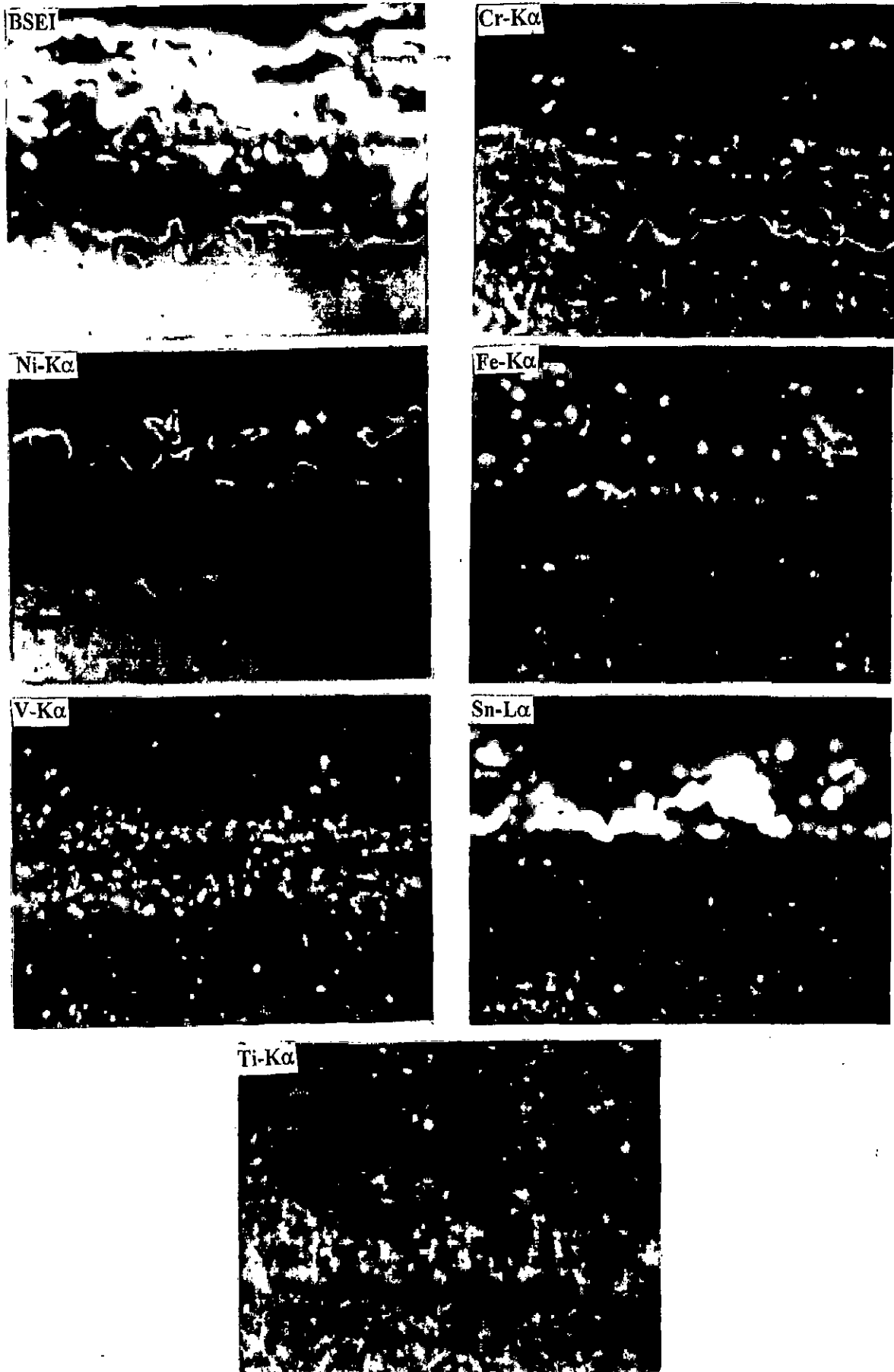
Fig. 5.109:   BSEI and X-ray mapping of the cross section of alloy C (Superni 75) after cyclic hot corrosion at 900^0C in Na_2SO_4-60% V_2O_5 + SnO_2.   (X 600)
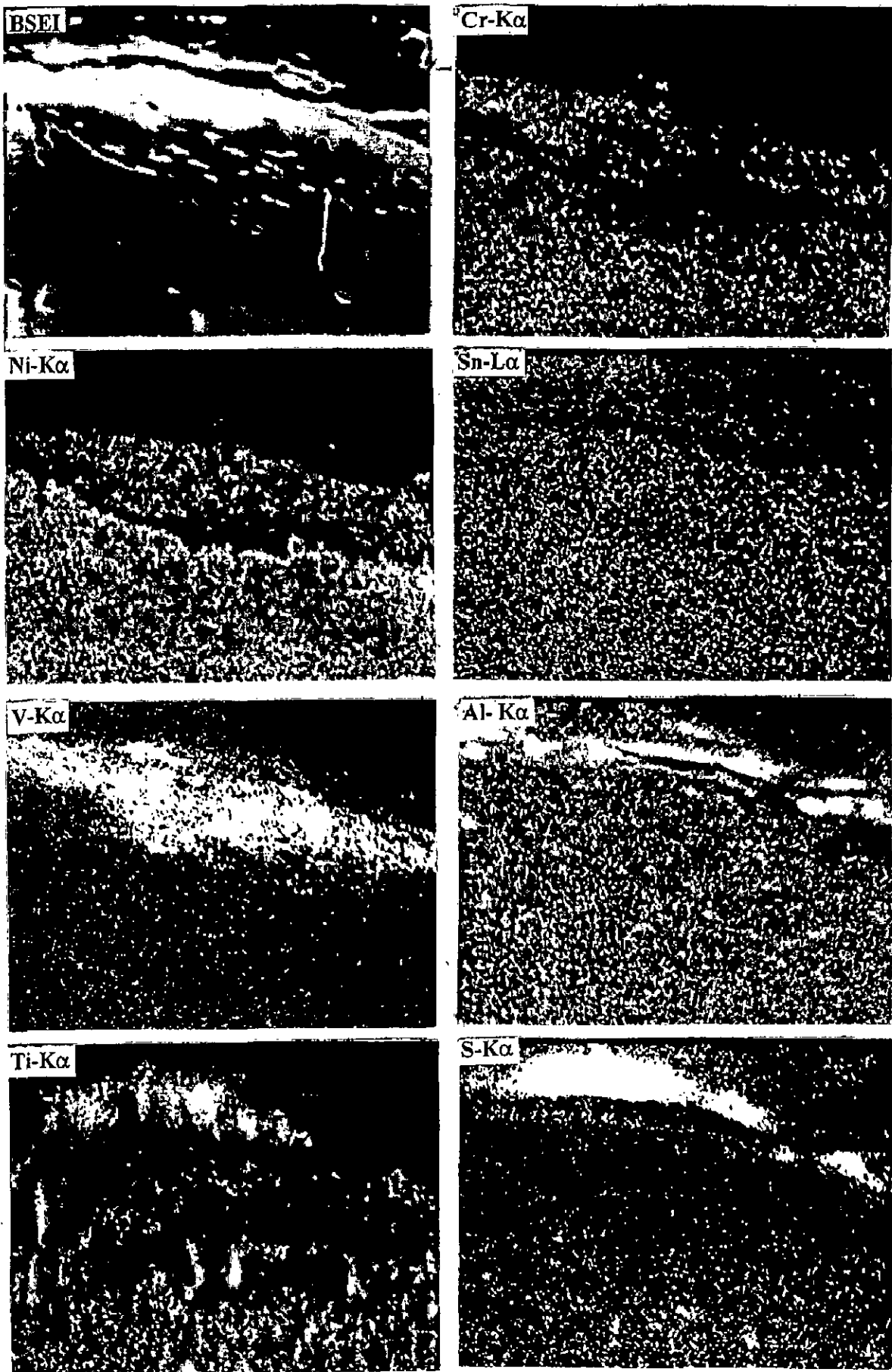
Fig. 5.110: BSEI and X-ray mapping of the cross section of alloy D (Superni 718)after cyclic hot corrosion at 900^0C in Na_2SO_4-60% V_2O_5 + SnO_2. (X 1000)
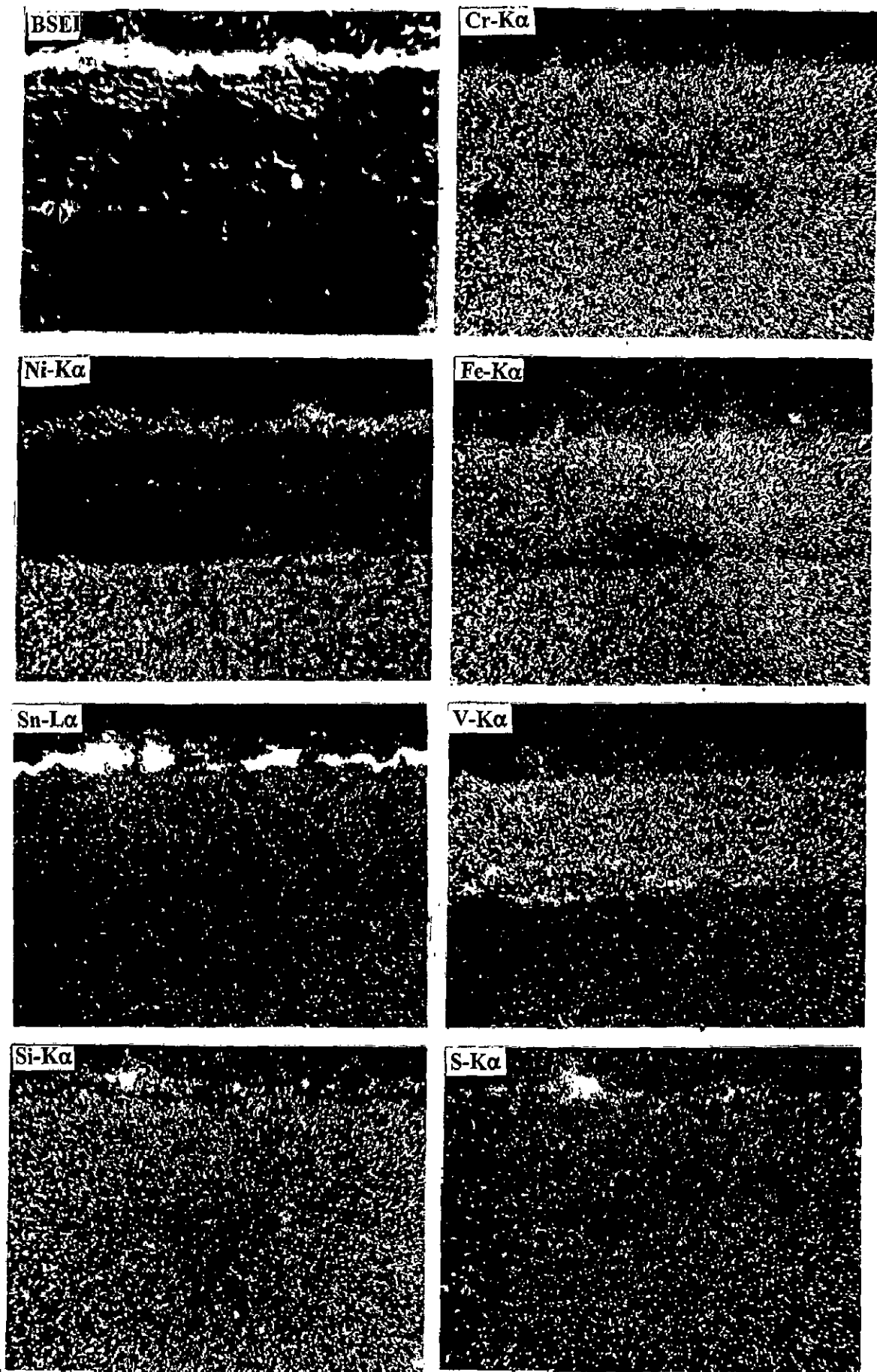
Fig. 5.111: BSEI and X-ray mapping of the cross section of alloy E (Superni 601)after cyclic hot corrosion at 900^0C in Na_2SO_4-60% V_2O_5 + SnO_2. (X 400)

EDAX Analysis of alloy A (Superfer 800H) in Na_2SO_4-60%V_2O_5+SnO_2 along the Cross-Section
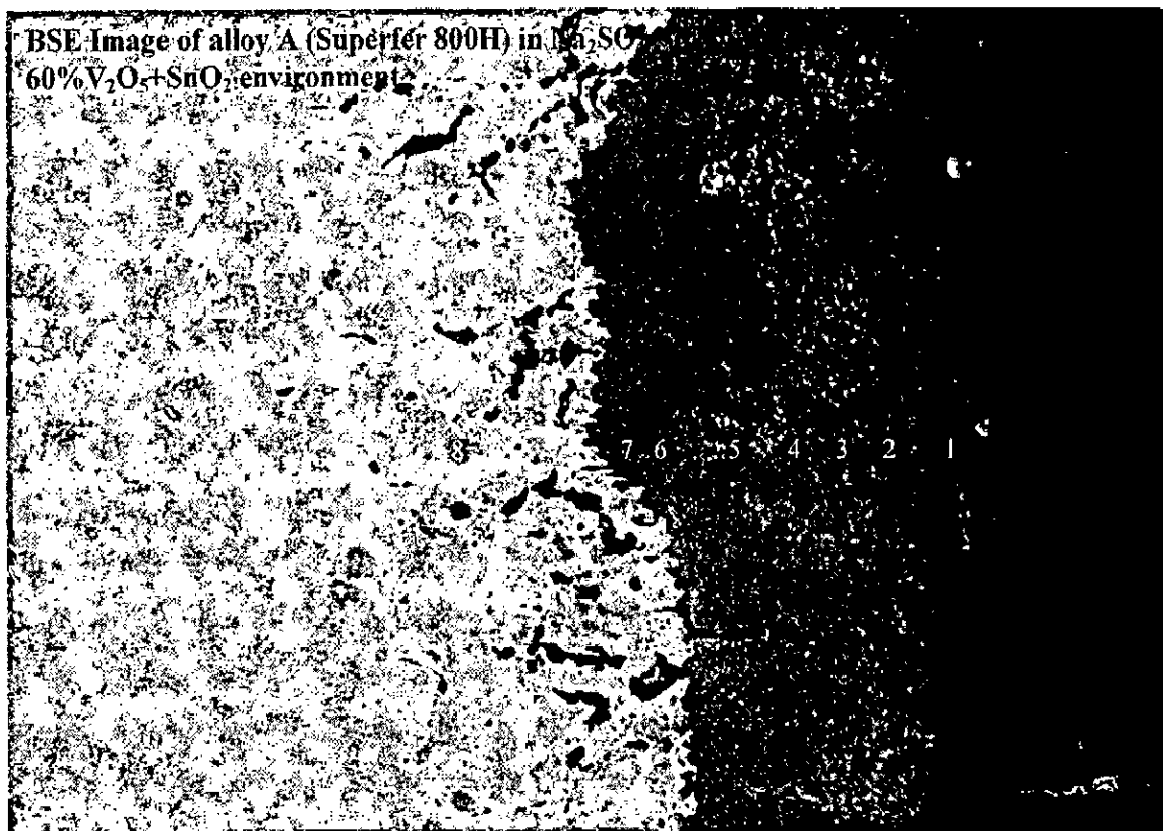
Fig. 5.112 : Back Scattered Image of Alloy A (Superfer 800H) after cyclic hot corrosion in Na_2SO_4-60%V_2O_5+ SnO_2 at 900^0C.

Table : 5.10 EDAX analysis for alloy Superfer 800H coated with SnO_2 in Na_2SO_4-60%V_2O_5 at different positions along the cross-section corresponding to Fig. 5.112.

Point of Analysis	Weight % of Elements											
	O	Fe	Cr	Ni	Al	Ti	Mn	Si	V	Na	Sn	S
1	14.24	36.03	19.27	13.07	2.57	0.80	2.97	4.75	0.74	-	4.89	0.63
2	32.08	28.61	16.61	14.05	-	0.31	2.80	1.25	2.72	0.89	0.64	-
3	34.23	33.08	17.82	4.2	0.43	0.49	1.34	1.39	3.59	2.08	1.19	0.15
4	41.29	29.82	16.23	5.47	0.22	0.17	1.58	0.66	2.28	1.13	0.99	0.12
5	36.39	31.17	18.61	8.32	0.38	0.28	2.33	0.65	1.35	0.01	0.46	0.03
6	35.18	32.05	24.80	3.12	0.32	0.40	0.96	0.47	1.46	0.40	0.80	-
7	20.98	15.89	26.13	34.81	0.12	0.36	0.32	0.86	0.25	-	0.11	0.14
8	2.45	39.16	16.63	39.56	0.16	0.32	0.87	0.79	-	-	-	0.03

EDAX Analysis of alloy B (Superco 605) in Na_2SO_4-60%V_2O_5+Y_2O_3 along the Cross-Section
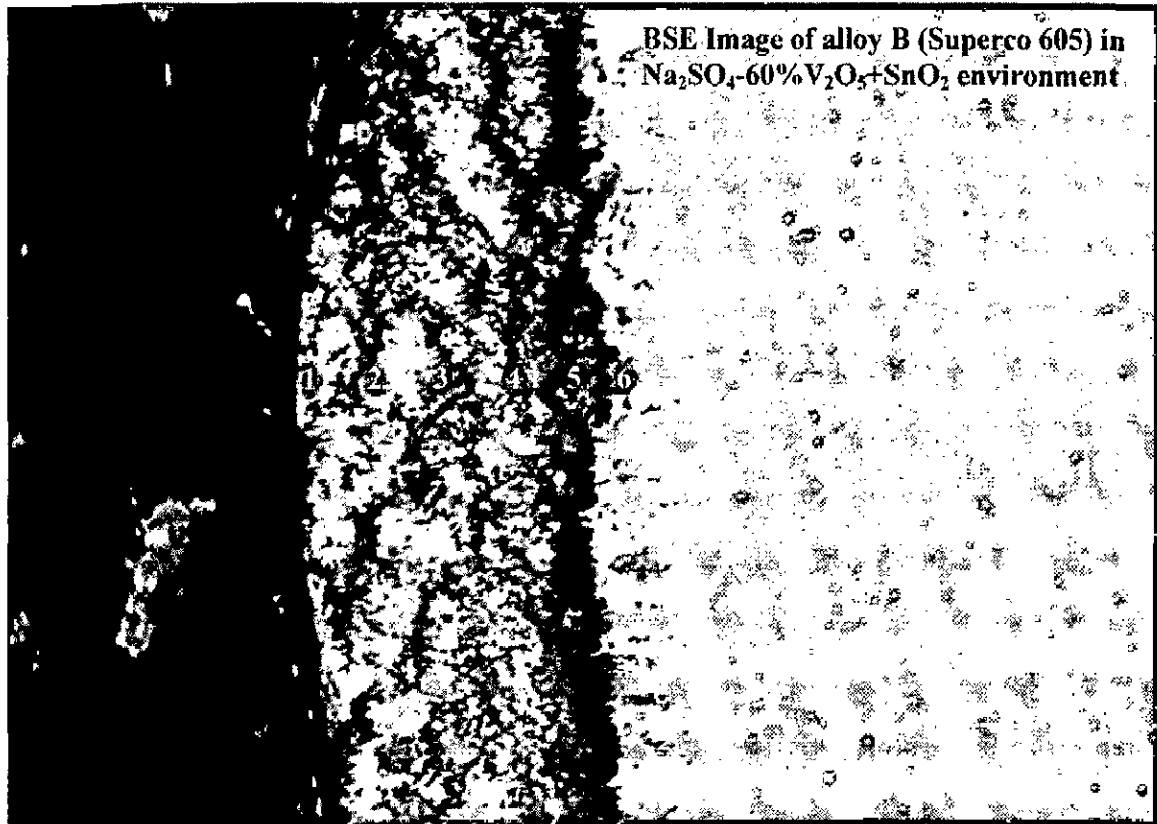
Fig. 5.113 : Back Scattered Image of Alloy B (Superco 605) after cyclic hot corrosion in Na_2SO_4-60%V_2O_5+ SnO_2 at 900^0C.

Table 5.11: EDAX analysis for alloy B (Superco 605) coated with SnO_2 in Na_2SO_4-60%V_2O_5 at different positions along the cross-section corresponding to Fig. 5.113.

Point of analysis	Weight% of elements										
	O	Fe	Ni	Cr	Co	W	Sn	Mn	Na	V	S
1	28.77	0.73	2.94	13.20	24.71	28.62	-	0.83	0.11	0.31	0.08
2	30.04	0.57	3.07	14.05	23.31	27.79	-	0.86	0.15	0.24	-
3	31.30	0.42	3.03	12.76	21.26	30.48	0.19	0.69	0.09	0.35	-
4	33.73	0.99	2.03	30.33	26.16	4.26	0.26	1.75	0.04	0.37	0.02
5	21.92	0.77	5.57	26.70	29.02	8.52	-	0.42	-	0.21	0.06
6	11.66	0.96	11.07	11.56	48.76	14.84	0.12	0.82	-	0.03	0.05

5.9 HOT CORROSION STUDIES IN Na$_2$SO$_4$-60%V$_2$O$_5$ WITH SUPERFICIALLY APPLIED ZrO$_2$

5.9.1 Visual Observations

Unreacted salt having yellowish red colour was present in patches on the surface of alloys A, C & D. Salt coating was more compact and adherent in alloys C & D as compared to alloy A which is visible from the macrographs shown in Fig. A.2 for superficially coated alloys. The scale in case of alloy A was non-adherent, shinning and black in colour. Very little spalling and scaling was observed in alloys C & D. Alloy B showed the formation of thick black scale with sputtering and spalling behaviour. Scale of alloy E was also black and thin in appearance, but it was adherent having little spalling tendency.

5.9.2 Kinetic Data

The weight change data for the alloys A, B, C, D & E with and without ZrO$_2$ coating when exposed to Na$_2$SO$_4$-60%V$_2$O$_5$ at 900^{0}C under cyclic conditions is plotted in Fig. 5.114 to 5.116. In case of alloy A, it can be inferred that ZrO$_2$ coating leads to decrease in the weight gain and the maximum weight gain at about 30 cycles is 80% of that without inhibitor. In case of alloy B, there is a steep rise in weight in the first two cycles and then there is a gradual increase in weight and the curve is leveling off as the no. of cycles is increasing.

In case of alloy C, the extent of weight gain is very less as compared to alloy A. After initial 2 cycles, the weight gain is very marginal and it shows a decreasing trend after 30 cycles. The alloy C with ZrO$_2$ coating shows nearly 1/4th of weight gain as compared to one without ZrO$_2$ coating. In case of alloy D again, the weight gain with ZrO$_2$ coating is significantly less as compared to one without ZrO$_2$. The maximum weight gain is decreased to less than half with ZrO$_2$. After 30 cycles, unlike the trend of

steep rise in case of main alloy, there is much smaller weight gain and that remains more or less constant upto 50 cycles. In case of alloy E, there is a decrease in weight gain with application of ZrO_2 coating but here there is marginal increase in weight during the initial cycles, then there is a gradual increase in weight up to 50 cycles. The maximum weight gain is decreased to half with application of ZrO_2.

5.9.3 X-Ray Diffraction Analysis

X-ray diffraction results compiled in Tables A.26 to A.28 and Fig. 5.117 to 5.119 in general indicated the presence of oxides and vanadates. The prominent phases identified in alloy A are Fe_2O_3, FeV_2O_4, $NiFe_2O_4$, Cr_2O_3, NiO, $(Cr,Fe)_2O_3$ and $NiCr_2O_4$. In case of alloy B, the phases identified in the scales were Co_3O_4, $Co_3V_2O_8$, Co_2NiO_4, $CoCr_2O_4$, Cr_2O_3 CoO and $NiWO_4$. In case of nickel base alloy C, the main phases identified were Cr_2O_3 & $NiCr_2O_4$ whereas in alloy D, Cr_2O_3, $Ni(VO_3)_2$, $NiCr_2O_4$ and NiO were analyzed. The scale of alloy E revealed the presence of $NiCr_2O_4$, FeV_2O_4, NiO, Cr_2O_3 and Fe_2O_3 as the possible phases. Peaks of ZrO_2 in alloys A, D and E could also be identified.

5.9.4 Measurement of Scale Thickness

Average value of the scale thickness observed from the BSE images of alloys A, B, C, D & E, measured from Fig. 5.120 are 43, 58, 17.5, 33 and 44 µm respectively. Alloy C has shown a very thin scale after 50 cycles.

5.9.5 SEM, EDAX and EPMA Results

Fig. 5.121(a, b, c, d, e & f) presents the Scanning Electron Micrographs for alloys A, B, C, D and E respectively after exposure to Na_2SO_4–60% V_2O_5 at 900^0C coated with ZrO_2. SEM micrograph in case of alloy A shows mixture of crystalline and globular structures whereas in case of alloy B indicates transgranular cracks and granular

190

structure indicating some porosity in the grains. In case of alloy C (Fig. 5.121 c) shows a dense scale with large size nodules. In case of alloy D, there is presence of sulphide crystals and nodules Fig. 5.121(d) which at higher magnification (Fig. 5.121, e) shows the crystal growth with directionality indicating oxidation of intermetallic phases. In case of alloy E, the scale is consisting of mainly two phases, nodular phase dispersed in a matrix.

Fig. 5.122 to 5.126 presents BSEI and X-ray maps for alloys A, B, C, D and E with ZrO_2 coating exposed to Na_2SO_4–60%V_2O_5 at 900°C for 50 cycles. EPMA micrographs for alloy A indicate formation of relatively thick scale which is mainly consisting of Cr, Ni and Fe. Vanadium & zirconium are also present in the scale. The interface between the scale and the substrate is depleted of Cr and there is a Ni rich thin layer. Al & Ti are also present in the scale. The EDAX analysis across the scale for alloy A (Fig. 5.127 & Table 5.12) indicates that the outer scale is rich in iron and contains Cr, Ni and Zr with V & S. As we proceed inwards it remains basically Fe rich scale and V is seen across the scale. S also penetrates up to the substrate. Internal oxidation is indicated and the oxides so formed are mainly of Cr, Si, Fe & Ni.

In case of alloy B, the scale is thicker and has distinct layers. Top scale is rich in chromium & Co followed by middle scale, which is rich in W and where W is present Co, is absent. Nickel is also present in the upper layer and areas rich in Ni are depleted of Cr. The SEM/ EDAX analysis of alloy B, (Fig. 5.128 & Table 5.13) shows a top scale mainly rich in Co, Cr and W. There is a middle layer which is rich in mainly W & Co. Zr is indicated in the scale in the top and middle area and has also penetrated into the alloy. S & V are also present in the scale.

In the alloy C, a very thin scale is formed which is mainly consisting of chromium or Iron as observed from BSE Image. Elemental X-ray maps indicate, where Cr is depleted iron is present. Sulphur and iron are co-existing on the top of the scale indicating sulphide formation. V is incorporated in the scale. Small amount of zirconium is also present in the scale. EDAX analysis of alloy C (Fig. 5.129 and Table 5.14)

indicates that the top layer is mainly containing oxides of Cr & Ni and their content increases in the lower layer. Zr is also present is the scale along with V & S. Ti has also been incorporated in the scale.

In case of alloy D, EPMA indicates that the scale is slightly thicker as compared to alloy C and consists of mainly Cr with small amount of Nickel. Top scale is rich in Fe and these areas are depleted of Ni and Cr. V and Zr are present in high concentration on the top of the scale. Mo rich area is indicated in substrate just below the scale/substrate interface. Ti is also observed in the scale. SEM/ EDAX analysis across the alloy D (Fig. 5.130 and Table 5.15) shows that the top scale is mainly consisting of Ni & Cr. Their extent is more or less same throughout the cross-section of scale. Ti, Al, Si, Zr, Na & V are present throughout the scale.

BSEI and X-ray maps for alloy E show a single layer scale rich in Cr & Fe and containing Zr & V. S is present on top of the scale. Al is present near the alloy interface between substrate and the scale. Internal oxidation is indicated and internal oxides are mainly rich in Cr & Al.
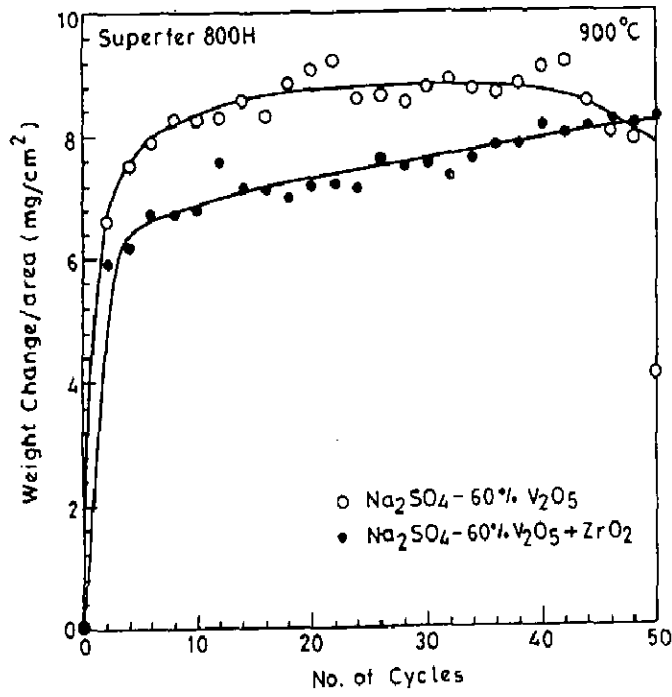
Fig. 5.114: Weight change plot for alloy A (Superfer 800H) after cyclic hot corrosion at 900^{0}C in Na$_2$SO$_4$-60% V$_2$O$_5$ +ZrO$_2$ coating.
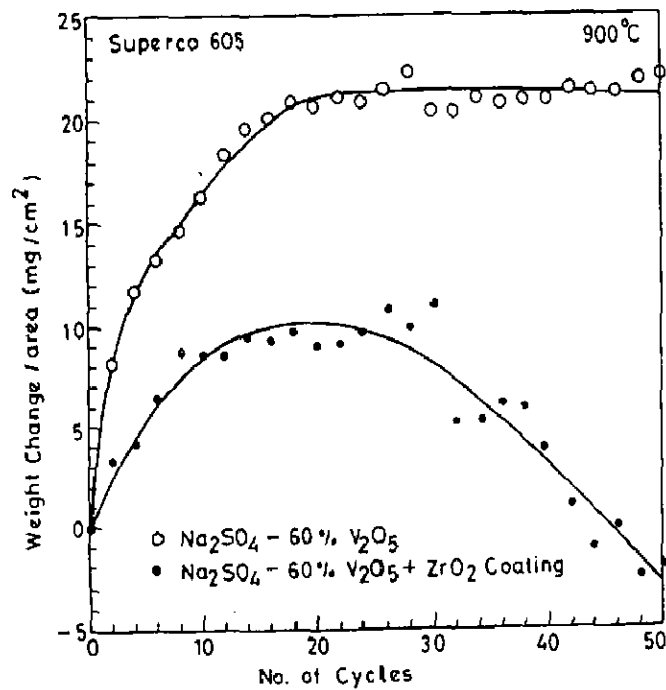
Fig. 5.115: Weight change plot for the alloy B (Superco 605) after cyclic hot corrosion at 900^{0}C in Na$_2$SO$_4$-60% V$_2$O$_5$ + ZrO$_2$ coating.
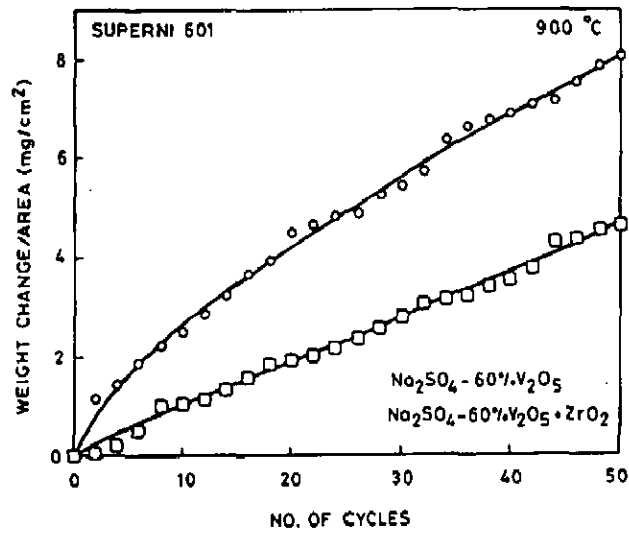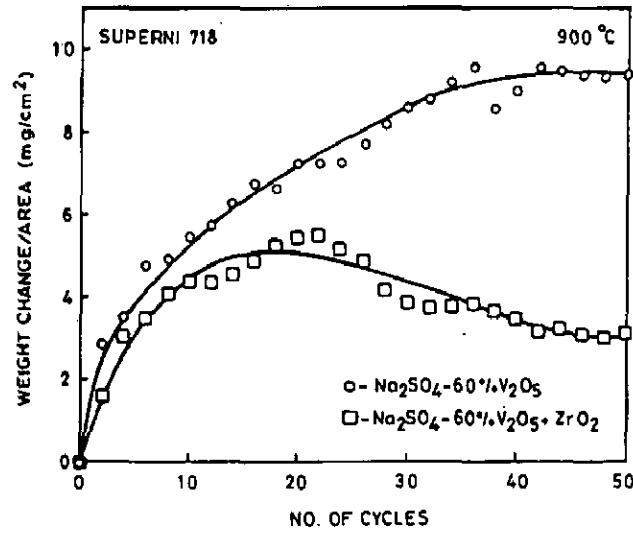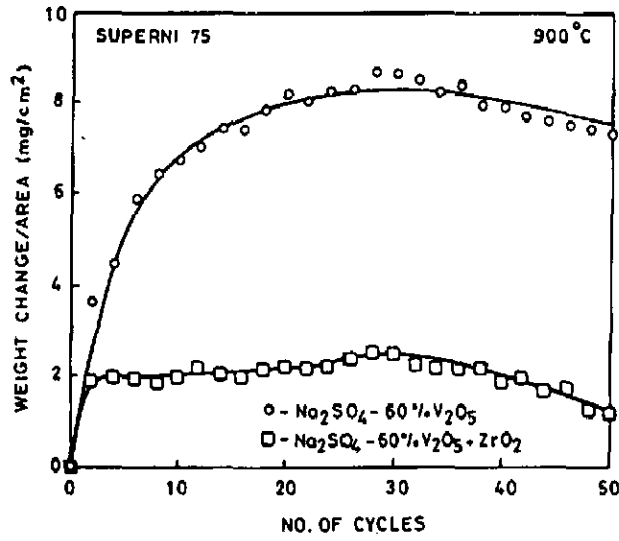
Fig. 5.116: Weight change plots for the nickel base alloys, alloy C (Superni 75), alloy D (Superni 718) and alloy E (Superni 601) after cyclic hot corrosion at 900°C in Na_2SO_4-60% V_2O_5 + ZrO_2 coating.
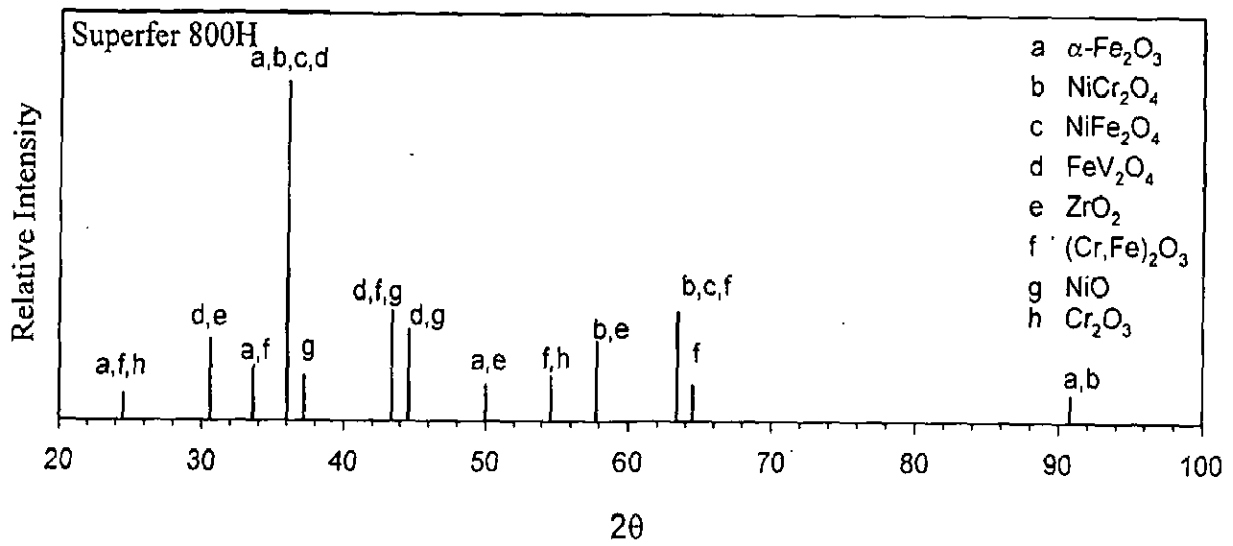
Fig. 5.117: X-ray diffraction profile for alloy A (Superfer 800H) after cyclic hot corrosion at 900^0C in Na_2SO_4-60% V_2O_5 + ZrO_2.
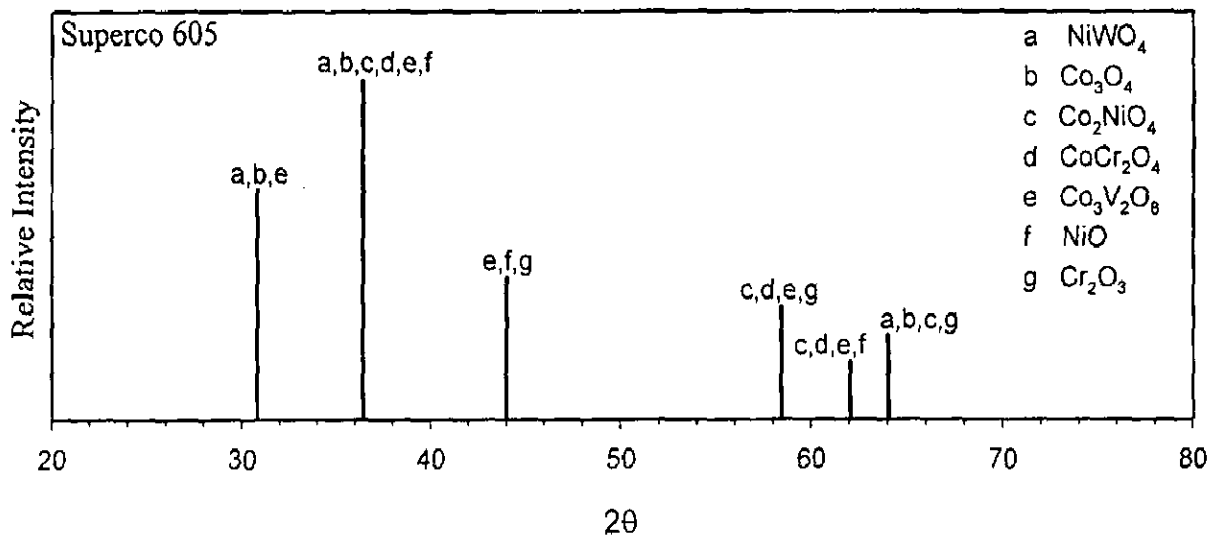
Fig. 5.118: X-ray diffraction profile for alloy B (Superco 605) after cyclic hot corrosion at 900^0C in Na_2SO_4-60% V_2O_5 + ZrO_2 coating.
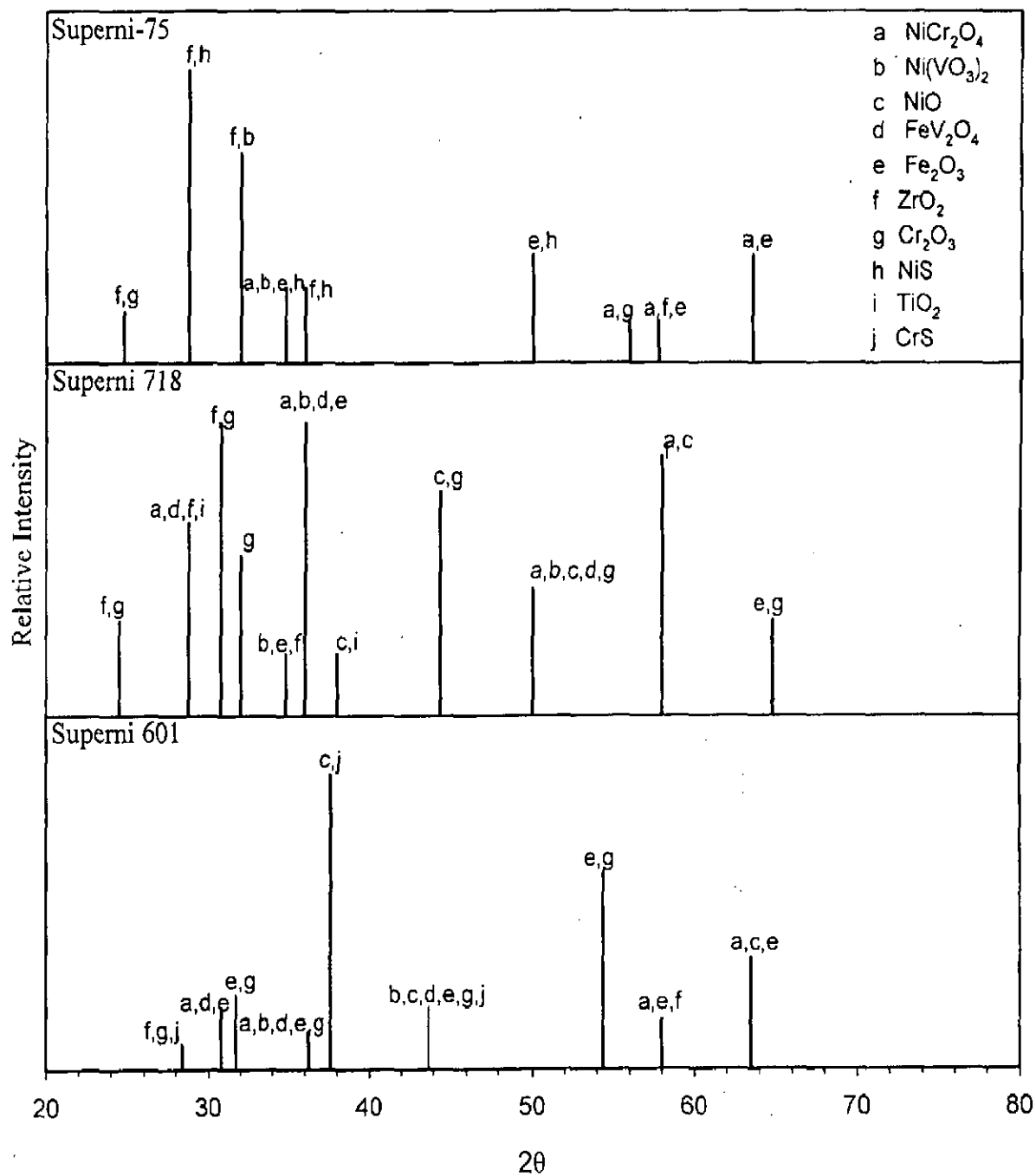
Fig. 5.119: X-ray diffraction profiles for the nickel base alloys: alloy C (Superni 75), alloy D (Superni 718) and alloy E (Superni 601) after cyclic hot corrosion at 900^0C in Na_2SO_4-60% V_2O_5 + ZrO_2 coating.
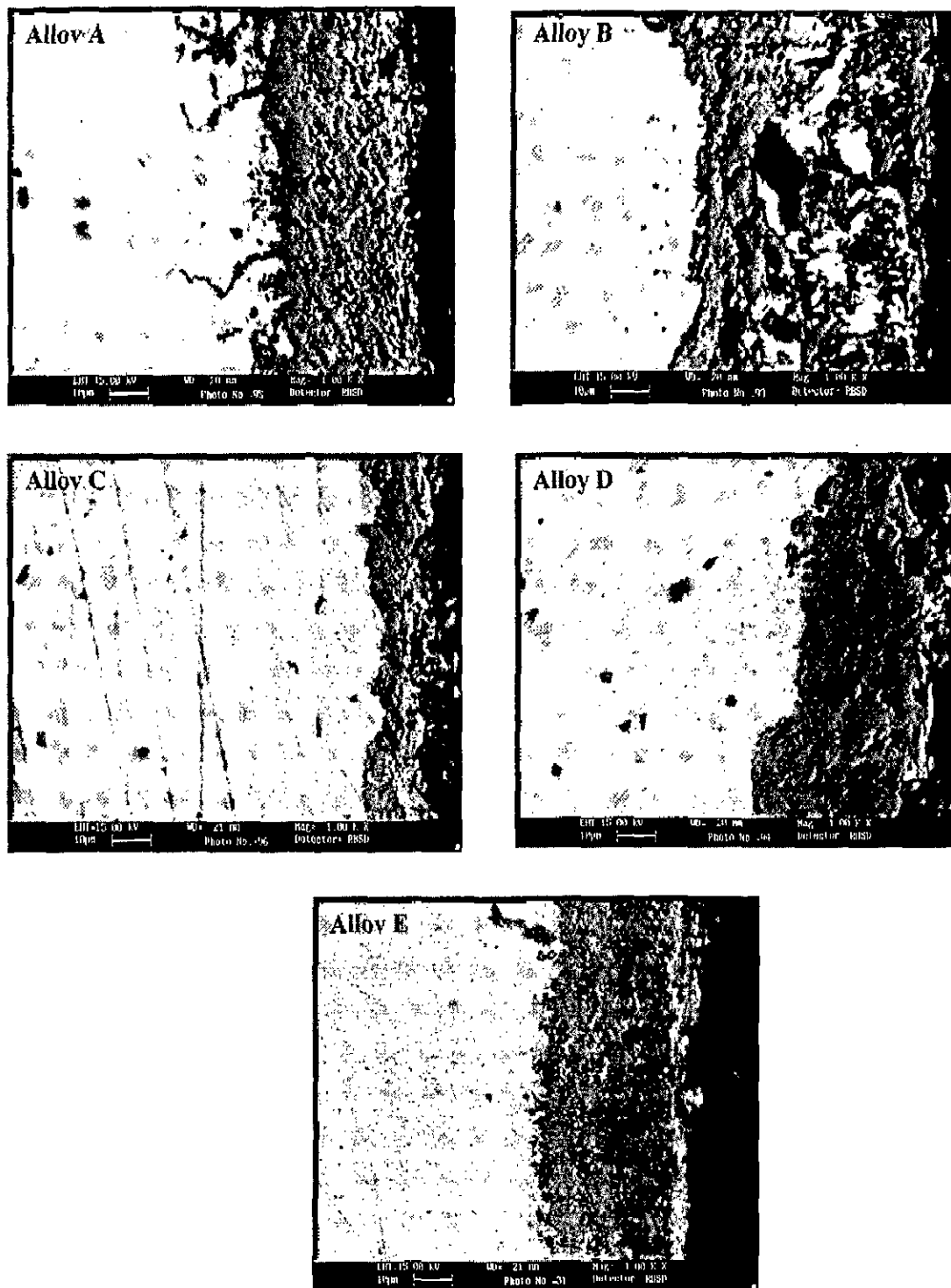
Fig. 5.120: BSE images of alloy A (Superfer 800H), alloy B (Superco 605), alloy C (Superni 75), alloy D (Superni 718) & alloy E (Superni 601) in Na$_2$SO$_4$-60%V$_2$O$_5$+ZrO$_2$ environment after exposure at 900^{0}C under cyclic conditions.
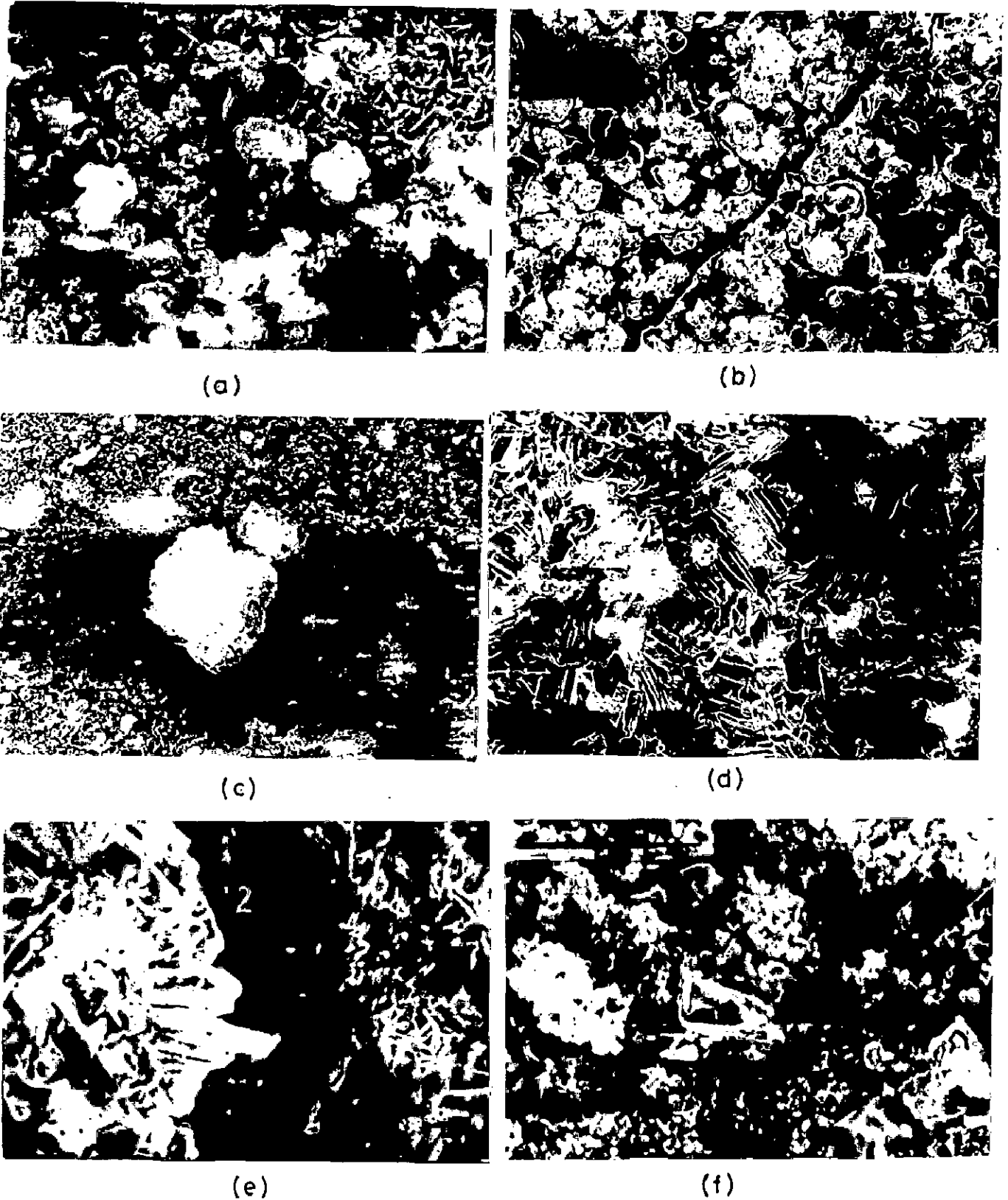
Fig. 5.121: Scanning Electron Micrographs after cyclic hot corrosion in Na_2SO_4-60%V_2O_5 +ZrO_2 coating at 900^0C of alloys:

a) Alloy A (Superfer 800H)   (X 640)

b) Alloy B (Superco 605)   (X 640)

c) Alloy C (Superni 75)   (X 640)

d) & e) Alloy D (Superni 718)   (X 640) & (X 1200)

f) Alloy E (Superni 601)   (X 640)

198
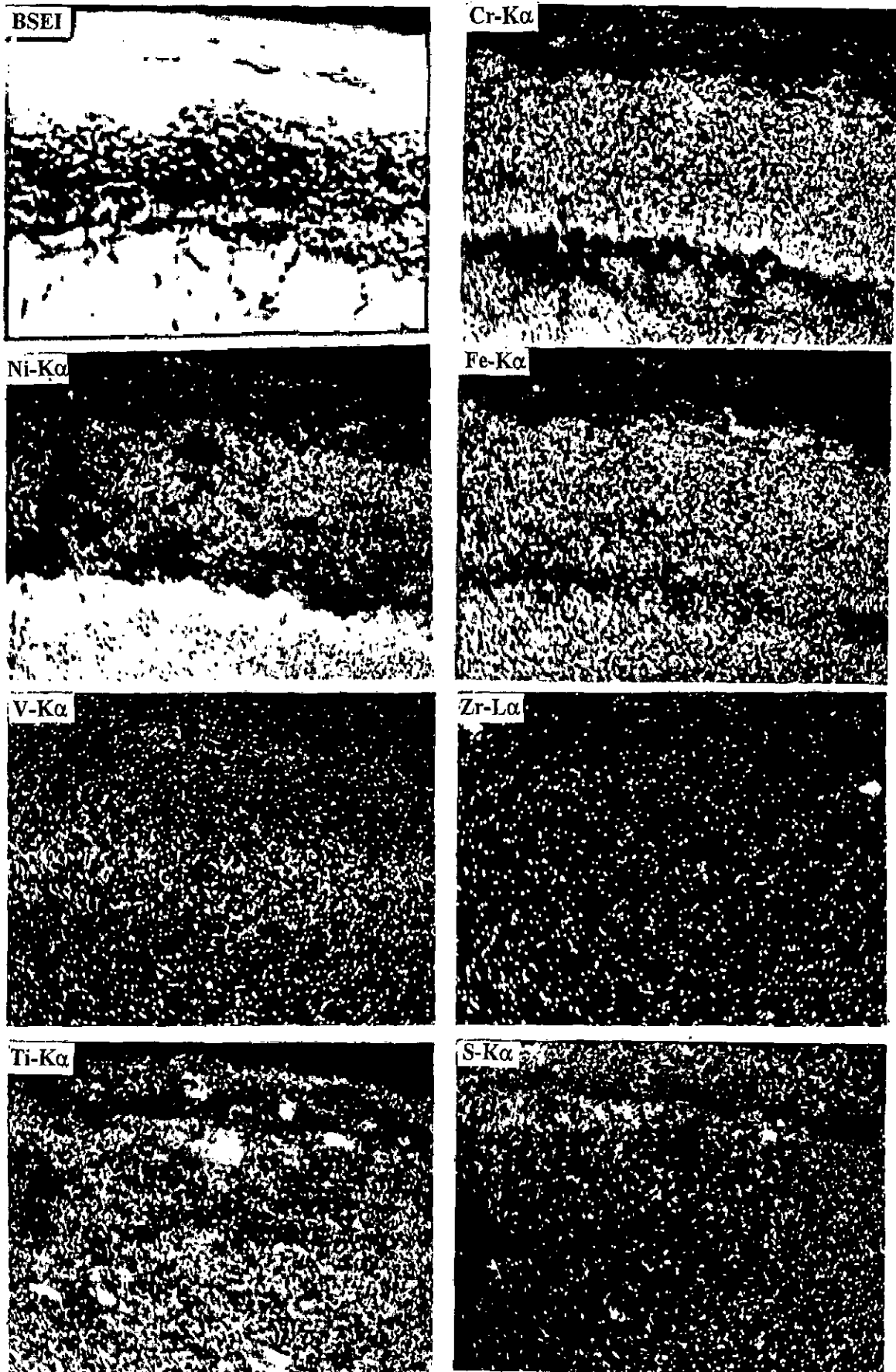
Fig. 5.122: BSEI and X-ray mapping of the cross-section of alloy A (Superfer 800H) after cyclic hot corrosion at 900^0C in Na_2SO_4-60%V_2O_5+ZrO_2.   (X 600)
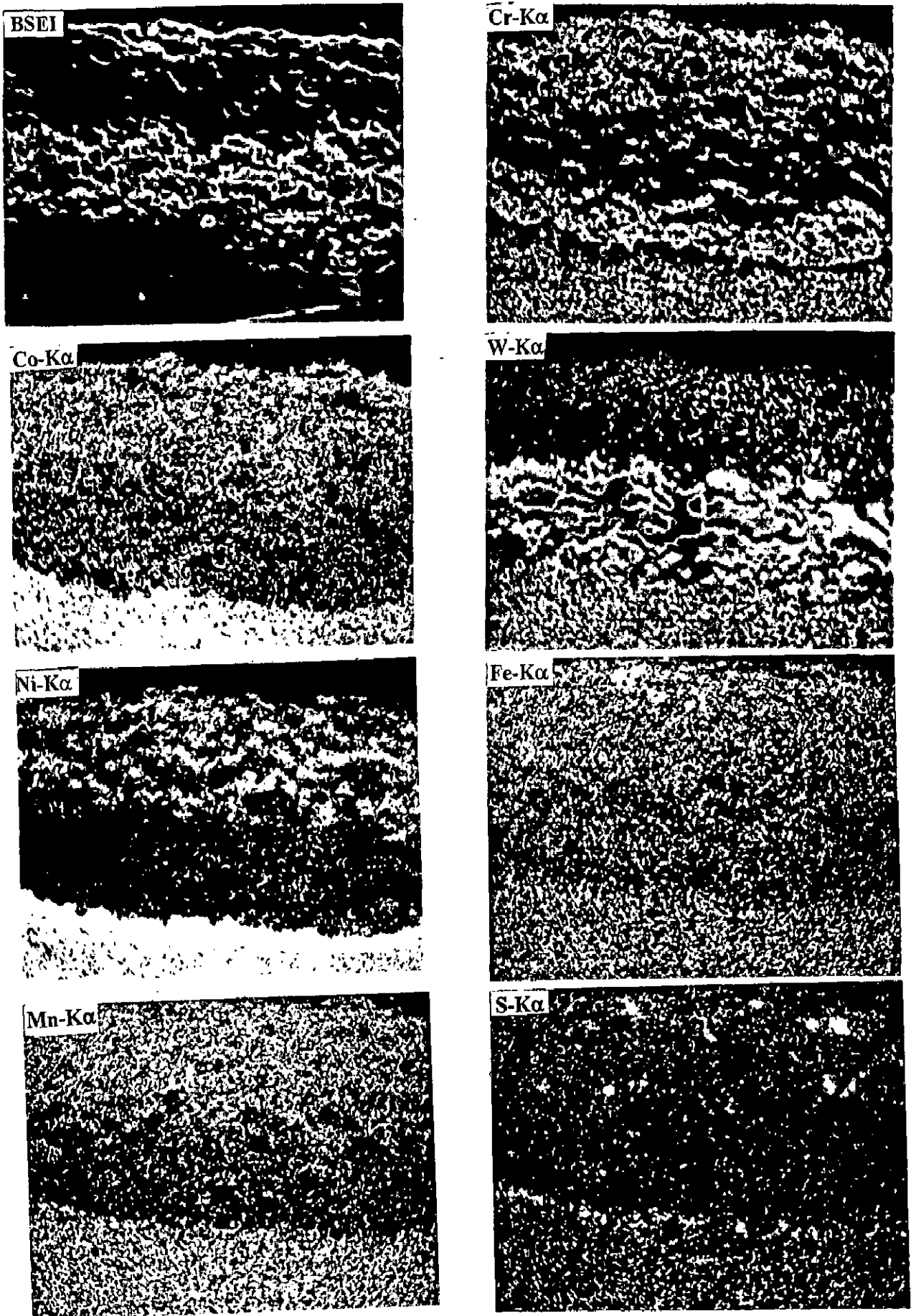
Fig. 5.123: BSEI and X-ray mapping of the cross section of alloy B (Superco 605) after cyclic hot corrosion at 900^0C in Na_2SO_4-60%V_2O_5+ZrO_2. (X 600)
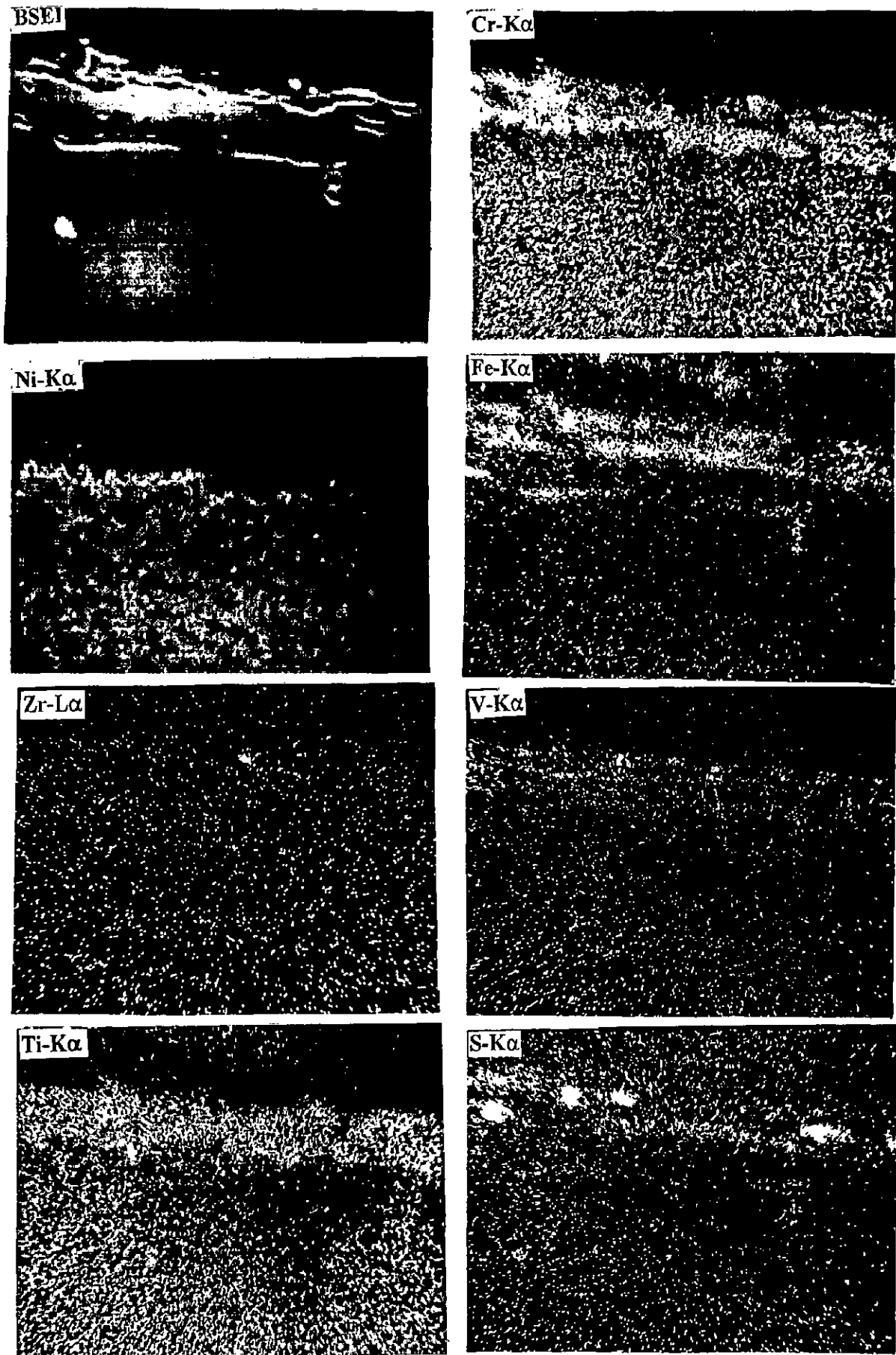
Fig. 5.124: BSEI and X-ray mapping of the cross section of alloy C (Superni 75) after cyclic hot corrosion at 900^0C in Na_2SO_4-60%V_2O_5+ZrO_2 (X1000)
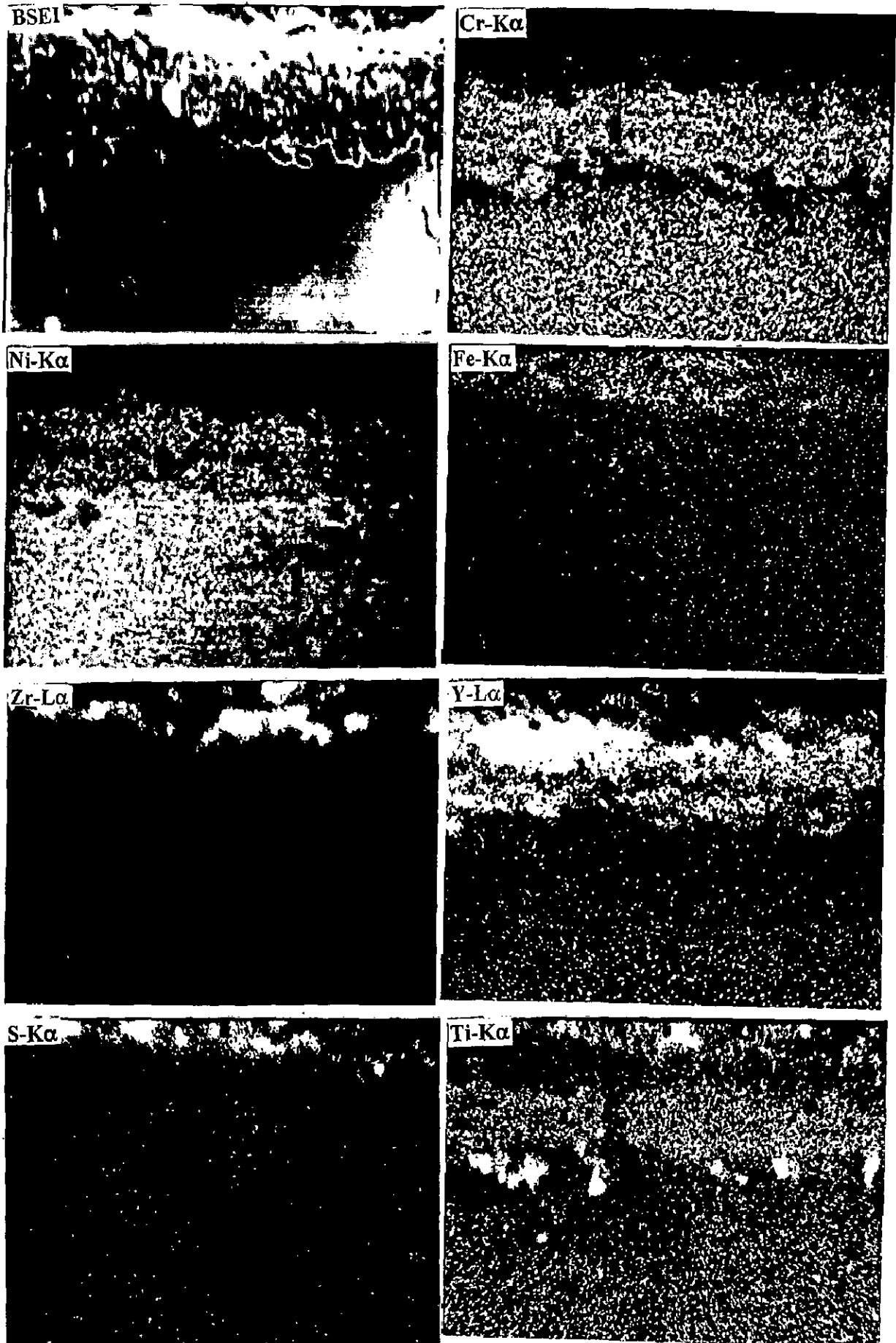
Fig. 5.125: BSEI and X-ray mapping of the cross section of alloy D (Superni 718) after cyclic hot corrosion at 900^0C in Na_2SO_4-60%V_2O_5+ZrO_2. (X 800)
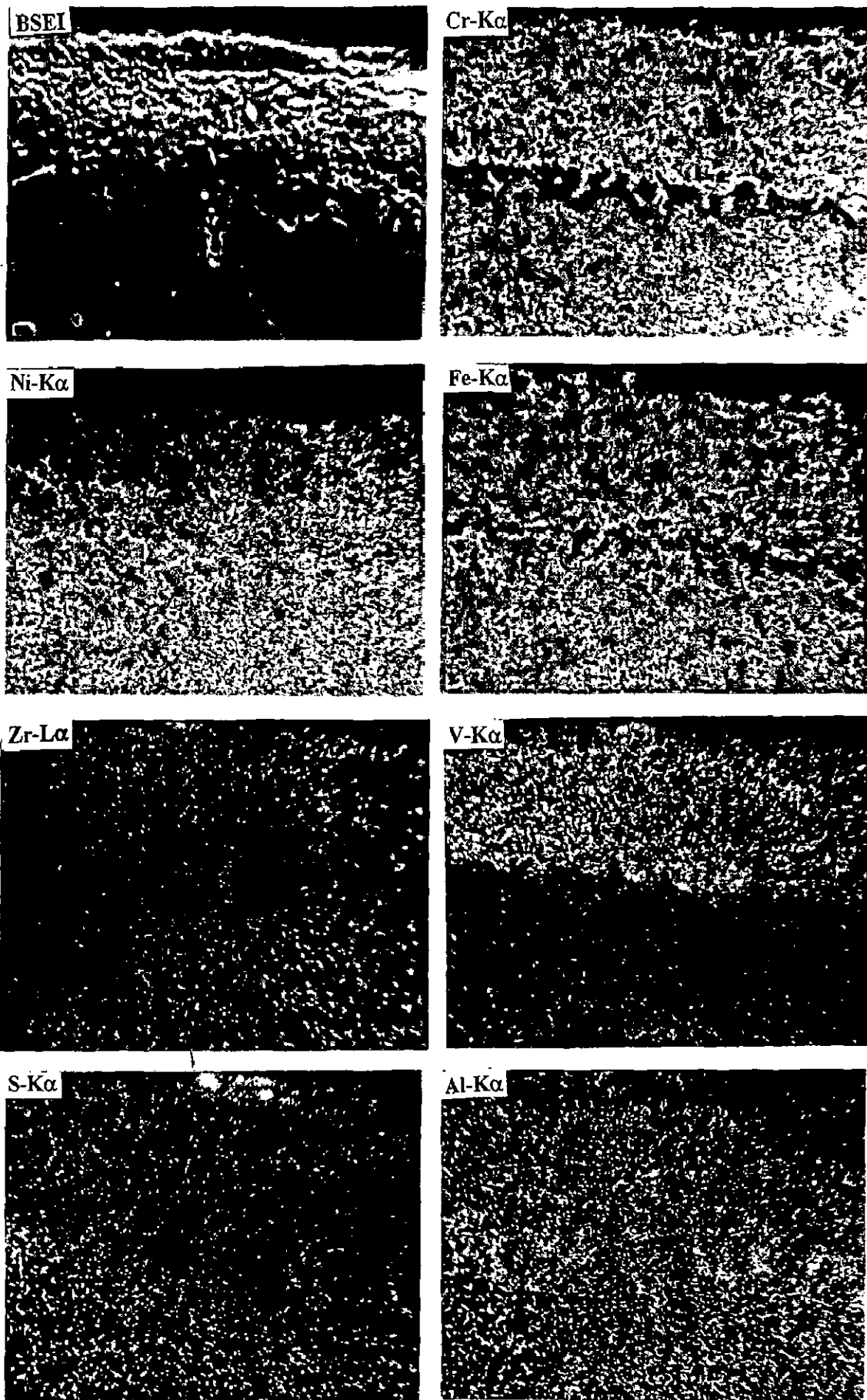
Fig. 5.126: BSEI and X-ray mapping of the cross section of alloy E (Superni 601) after cyclic hot corrosion at 900^0C in Na_2SO_4-60%V_2O_5+ZrO_2. (X 600)
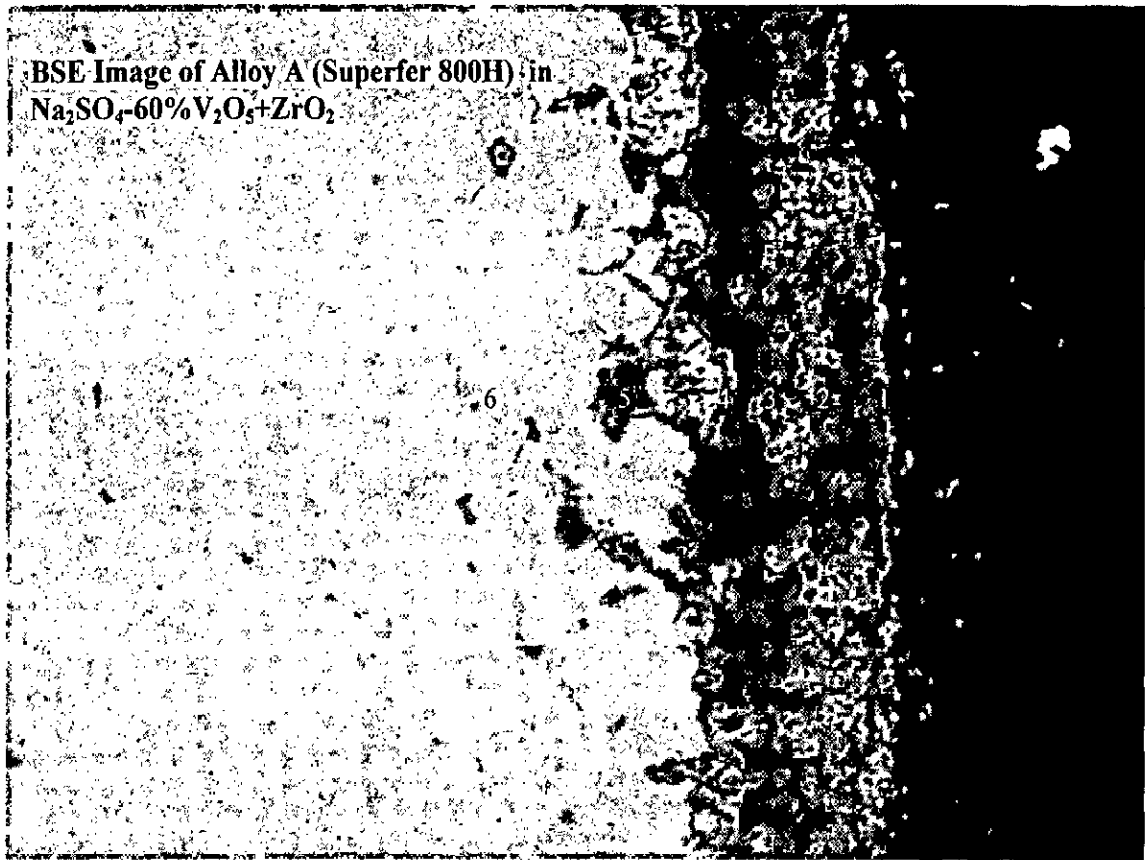
Fig. 5.127 : Back scattered image of alloy A (Superfer 800H) after cyclic hot corrosion in Na$_2$SO$_4$-60%V$_2$O$_5$+ ZrO$_2$ at 900^{0}C.

Table 5.12 : EDAX analysis for alloy A (Superfer 800H) coated with ZrO$_2$ in Na$_2$SO$_4$-60%V$_2$O$_5$ at different positions along the cross-section corresponding to Fig. 5.127.

Point of Analysis	Weight % of Element											
	O	Fe	Ni	Cr	Ti	Al	Mn	Si	Zr	Na	V	S
1	30.55	38.46	7.19	18.98	0.35	0.20	1.51	0.40	0.27	-	0.59	0.08
2	20.44	49.65	5.36	20.75	0.56	0.37	1.12	0.57	-	-	0.61	0.09
3	29.52	34.08	18.31	13.86	0.05	0.27	2.29	0.32	0.06	-	0.85	0.10
4	30.67	31.57	20.12	13.13	0.08	0.19	2.22	0.25	0.11	-	0.64	0.11
5	14.21	13.77	20.88	41.07	1.18	1.35	0.53	5.18	-	-	1.61	0.10
6	0.00	45.99	38.70	13.49	0.31	0.23	0.19	1.14	0.23	-	-	0.08
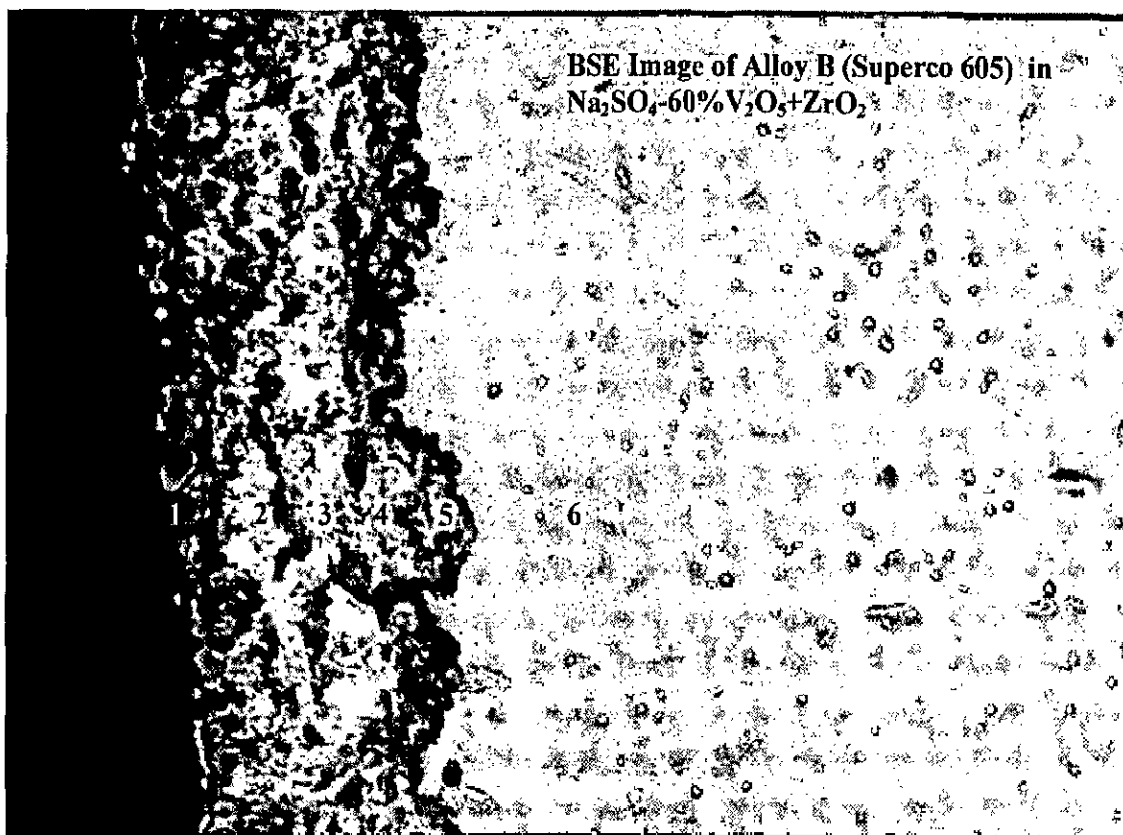
Fig. 5.128 :   Back scattered image of alloy B (Superco 605) after cyclic hot corrosion in Na$_2$SO$_4$-60%V$_2$O$_5$+ ZrO$_2$ at 900^{0}C.

Table 5.13 :   EDAX analysis for alloy B (Superco 605) coated with ZrO$_2$ in Na$_2$SO$_4$-60%V$_2$O$_5$ at different positions along the cross -section corresponding to Fig. 5.128.

Point of analysis	Weight% of element											
	O	Fe	Ni	Cr	Co	W	Zr	Mn	Si	Na	V	S
1	35.08	2.5	4.00	19.93	27.35	8.57	0.12	1.32	0.30	0.79	0.59	0.12
2	33.90	1.28	2.51	16.95	24.44	18.35	-	1.00	-	0.18	0.49	0.04
3	32.92	-	2.61	2.82	15.32	46.06	-	0.23	-	0.35	0.03	0.18
4	33.05	0.52	2.89	10.34	18.05	34.19	0.15	0.32	-	0.40	0.30	0.14
5	33.74	0.30	2.55	21.60	19.39	21.34	-	0.49	-	-	0.31	0.21
6	0.78	1.15	15.00	16.83	49.18	15.22	0.27	1.11	-	-	0.12	0.25
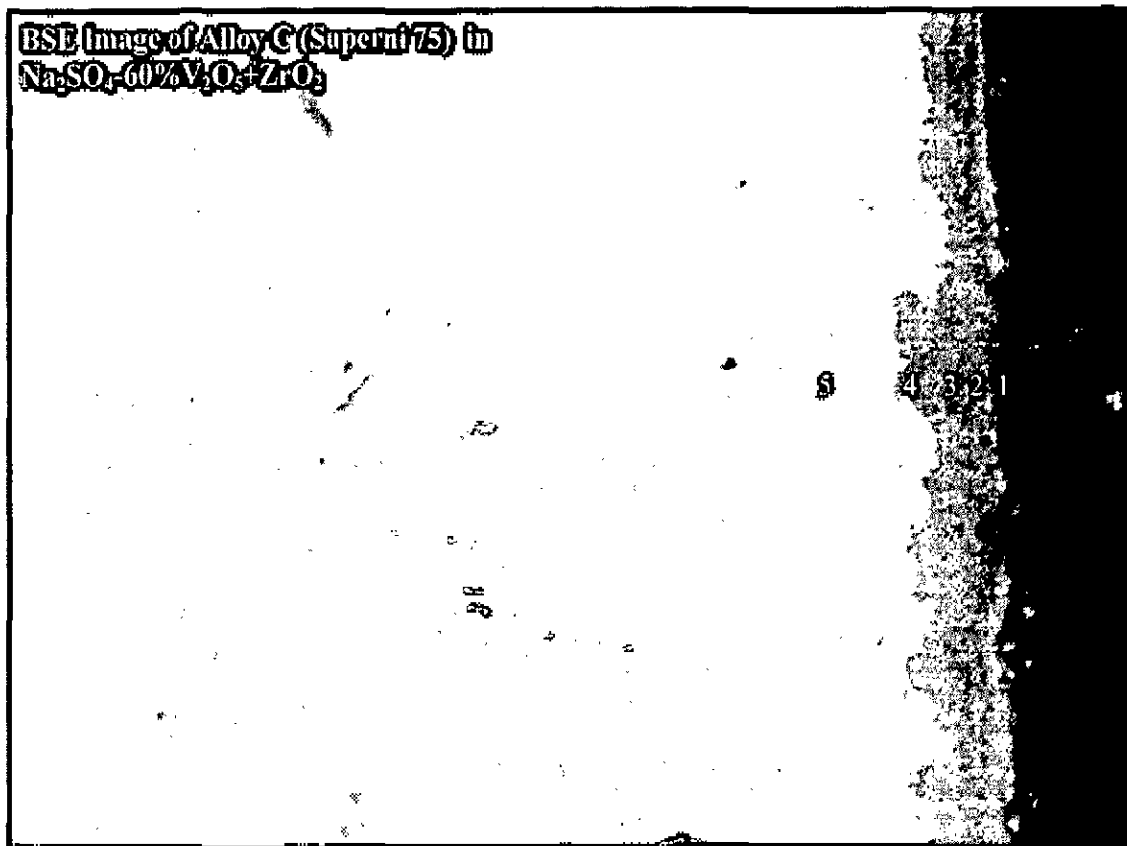
Fig. 5.129 : Back scattered image of alloy C (Superni 75) after cyclic hot corrosion in Na$_2$SO$_4$-60%V$_2$O$_5$+ ZrO$_2$ at 900^{0}C.

Table 5.14 : EDAX analysis for alloy C (Superni 75) coated with ZrO$_2$ in Na$_2$SO$_4$-60%V$_2$O$_5$ at different positions along the cross-section corresponding to Fig. 5.129.

Point of analysis	Weight % of element							
	O	Fe	Ni	Cr	Zr	V	S	Ti
1	35.41	-	26.91	33.70	0.41	-	2.26	1.02
2	19.66	0.92	35.99	39.22	0.34	3.08	0.14	0.62
3	27.71	0.12	30.32	40.39	-	2.35	-	0.93
4	22.13	0.10	44.05	27.43	0.30	5.55	0.10	0.36
5	0.00	0.02	83.91	15.49	0.11	0.11	0.04	0.27

BSE Image of Alloy D (Superni 718) in
Na$_2$SO$_4$-60%V$_2$O$_5$+ZrO$_2$

5   4   3   2   1
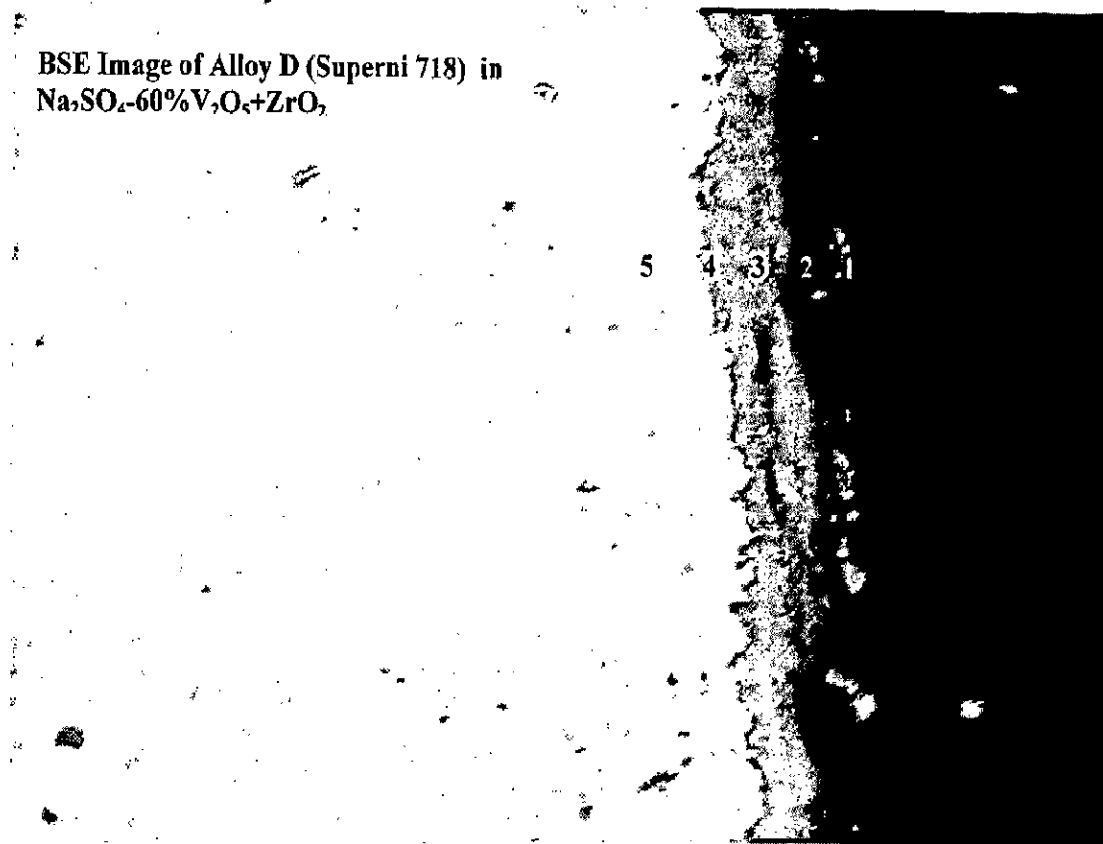
Fig. 5.130 : Back scattered image of alloy D (Superni 718) after cyclic hot corrosion in Na$_2$SO$_4$-60%V$_2$O$_5$+ ZrO$_2$ at 900^{0}C.

Table 5.15 : EDAX analysis for alloy D (Superni 718) coated with ZrO$_2$ in Na$_2$SO$_4$-60%V$_2$O$_5$ at different positions along the cross -section corresponding to Fig. 5.130.

Point of Analysis	Weight % of element													
	O	Fe	Ni	Cr	Ti	Al	Mo	Mn	Si	Cu	Zr	Na	V	S
1	31.37	0.50	30.15	32.64	0.88	0.37	0.32	0.06	0.44	0.06	0.22	0.11	2.65	-
2	30.59	9.84	30.375	32.29	0.96	0.28	-	0.69	0.28	0.28	0.25	0.25	3.26	0.08
3	27.59	0.22	32.71	31.46	1.01	0.19	-	-	0.31	0.22	0.35	0.64	3.71	0.06
4	36.45	0.31	27.13	31.95	1.08	0.25	-	0.34	0.26	0.28	0.18	0.45	2.30	-
5	-	-	86.69	15.00	0.13	0.33	0.06	0.10	0.16	-	-	-	0.06	0.02

CHAPTER 6

DISCUSSION

The results of the present investigation on the role of additives on hot corrosion of superalloys in Na_2SO_4-V_2O_5 environment at 900^0C under cyclic conditions have been discussed in this chapter. The superalloys A, B, C, D and E are Fe-base, Co-base and Ni-base alloys respectively. For finding out the effect of additives, these alloys were subjected to molten salt corrosion in most aggressive eutectic composition of $60\%V_2O_5$ and $40\%Na_2SO_4$ mixture. Consequently the additives were either mixed with this mixture or applied superficially on the surface and were subjected to cyclic corrosion in the above environment. From the thermogravemetric studies, it has been observed that maximum weight gain was mostly observed around 30 cycles in nearly all cases of hot corrosion runs with and without inhibitors. Hence the results of weight change have been discussed for 30 cycles and scale morphology, thickness, XRD, EDAX and EPMA for the total hot corrosion run of 50 cycles. The results have been compiled in Table A.31, showing the thickness of the scales, weight change after 30 cycles, probable phases identified by XRD formed and main features of SEM, EPMA and EDAX to facilitate the more meaningful discussion. Histograms have been plotted for the weight change for all the alloys with and without inhibitors presented in Fig. 6.1, 6.2, 6.3, 6.4 and 6.5. It will be relevant first to discuss the effect of Na_2SO_4-$60\%V_2O_5$ mixture on the superalloys A, B, C, D and E and it is followed by discussion on the effect of inhibitors mixed or applied superficially.

6.1 HOT CORROSION STUDIES IN Na_2SO_4-$60\%V_2O_5$

In this environment the maximum weight gain was observed in case of alloy B and minimum for alloy C. The sequence of hot corrosion rate based on weight gain after 30 cycles is as follows: Alloy B > Alloy A > Alloy D > Alloy E > Alloy C

The superior resistance of Ni-base alloys to the given environment is perhaps due to the formation of protective layer of Cr_2O_3 and formation of nickel vanadate. The same has been reported by Kerby and wilson (1973) in their study on Ni and Fe- base alloy in Na_2SO_4- V_2O_5.

Otereo et al (1987) have tried to explain the increase in corrosion rate in the initial stages to the higher fluidity of molten salt mixture in case of their study on hot corrosion of IN-657. They have concluded that molten salt acts as oxygen carrier, which leads to both increase in diffusion and transport phenomenon. The protective scale is destroyed or eliminated by molten salts and consequently the metal surface is exposed to direct action of aggressive environment. The molten salt also provides rapid diffusion paths for reactant species.

In case of alloy A, a thick multilayered scale is formed. There is a thin Ni rich continuous layer just above the substrate. Over this there is a Cr-rich layer and top scale consists of Cr, Ni and Fe. Main phases identified are α-Fe_2O_3 and spinels of NiO with Cr_2O_3 and Fe_2O_3. Formation of FeV_2O_4 has also been confirmed. Schematic illustration of some of the main aspects of reactions occurring in alloy A (Superfer 800H) are shown in Fig. 6.6

At temperature of reaction i.e. 900^0C, the Na_2SO_4- 60% V_2O_5 will combine and form $NaVO_3$ having a melting point of 610^0C as proposed by Kolta et al (1972) and this $NaVO_3$ acts as a catalyst and also serve as a oxygen carrier to the metal.

$$Na_2SO_4 + V_2O_5 = 2NaVO_3\,(l) + SO_2 + \frac{1}{2}\,O_2$$
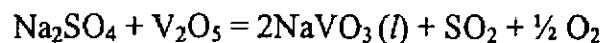
Chromium having higher affinity for oxygen to form Cr_2O_3 so in the earliest stages of hot corrosion, there is a fast increase in weight as observed upto 4 cycles.

$$2Cr + \frac{3}{2}\,O_2 \;\rightarrow\; Cr_2O_3$$
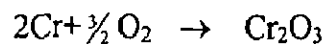
Further the oxidation of Fe and Ni will take place to form Fe_2O_3 and NiO as per the

following reactions:
$$2Fe + \frac{3}{2}\,O_2 \;\rightarrow\; Fe_2O_3$$

$$Ni + \frac{1}{2}\,O_2 \;\rightarrow\; NiO$$
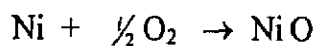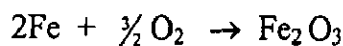
This is confirmed by presence of Fe, Ni and Cr oxides in the outer layer of the scale from the X-Ray maps where as Cr_2O_3 is present at alloy scale interface, which acts as a barrier but this layer, is not continuous and so it has permitted the transport of species.

NiO and Fe_2O_3 so formed combined with the Cr_2O_3 giving rise to formation of spinels $NiCr_2O_4$ and $FeCr_2O_4$ as per the following reactions:

$$NiO + Cr_2O_3 \rightarrow NiCr_2O_4$$

$$FeO + Cr_2O_3 \rightarrow FeCr_2O_4$$

$$NiO + Fe_2O_3 \rightarrow NiFe_2O_4$$
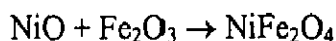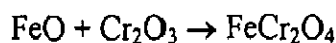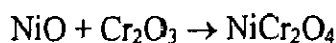
Kumar et al (1996) have ascribed slower increase in weight gain after initial rise to formation of Cr_2O_3 in their studies on Inconel 625.

Sierstein and Kofstad (1987) as well as Swaminathan et al (1993) have suggested simultaneous growth of oxides and their dissolution in molten salt as per following reaction:

$$Cr_2O_3 + 4NaVO_3 \rightarrow 2Na_2CrO_4(l) + V_2O_5 + O_2$$

Fryburg et al (1984) have suggested that this Na_2CrO_4 gets evaporated as a gas.

Fe oxide combines with $NaVO_3$ to form FeV_2O_4 as per the following reaction

$$2\,NaVO_3 + FeO \rightarrow FeV_2O_4 + Na_2O + O_2$$
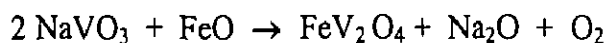
which has also been identified in the present study.

Malik et al (1984) have also reported the presence of this spinel in their study on 18:8 stainless steel in $Na_2SO_4-NaVO_3$ environment at 850 and 1000^0C.

The horizontal cracks have been observed as can be seen in the BSEI of the sample, Fig.5.6 and further spalling has been indicated. Spalling can be attributed to severe strain developed because of Fe_2O_3 precipitation from liquid phase and inter diffusion of intermediate layers of iron oxide as has been suggested by Sachs (1958).

The presence of three different phases in a thin layer would impose severe strain on the film which may result in cracking and exfoliation of the scale. The cracks may have allowed the aggressive liquid phase to reach the metal substrate. According to Sachs this mechanism is more applicable for Fe-base alloys which are susceptible to catastrophic oxidation instead of Ni and Co-base alloys where the scaling is not so fast. (Sachs, 1958)

The alloy B showed maximum weight gain and it is obvious from the thick scale revealed by EPMA. The scale is multilayered consisting of Fe rich scale containing Ni, Cr and

Co at the top followed by a thick scale where Fe, Co, Cr & W are co-existing. Scale just above the interface is mainly Cr rich. MnS is indicated just at the interface between the scale and substrate. Vanadium is seen in the scale indicating formation of vanadates. The thicker scale has formed due to oxidation of Co, W, Cr and Ni. Some of these oxides might be inducing acidic fluxing thereby destroying the protective properties. The spalling observed might also be contributing to continuation of corrosion till the end of the test. Probable mechanism of corrosion has been shown in Fig. 6.7

This tendency of the spalling has also been explained by Kofstad (1990) as a result of predominance of cationic diffusion in the growth of scales where no oxide is formed at or near the external surface and voids and porosity gradually develop at or near the metal scale interface due to the reduced volume of metal and lack of sufficient plastic deformation of scale. This leads to reduction in adherence as well as coherency of the scale thereby increasing tendency of spalling.

In case of alloy C the maximum weight gain is the least and the phases identified are NiO, Ni(VO$_3$)$_2$, NiCr$_2$O$_4$ and Cr$_2$O$_3$.There is a presence of thin continuous Cr$_2$O$_3$ layer just above the substrate which may be contributing to better resistance offered to hot corrosion by not allowing through it any transport.

In case of alloy D, there is a gradual increase in weight and the maximum weight gain is around 8.6 mg/cm^2. In this case there is presence of thin NiO layer just above the substrate. Above this thin NiO layer there is a continuous thin layer of Cr$_2$O$_3$, rest of the upper scale contains oxides of V, Cr, Fe & Ni. Spinels NiCr$_2$O$_4$ and Ni(VO$_3$)$_2$ are mainly present in the scale and have been identified by XRD. Slightly higher corrosion rate in case of alloy D might be partly attributed to the presence of 3% Mo in the alloy. This Mo may form oxides and sodium molybedate as suggested by Pettit and Meier (1984); Fryburg et al (1984) and Misra (1986 A and B). The porosity observed in the scale might also be contributed by escaping of these gases and volatile compounds.

In case of alloy E, the weight change is only 5.43mg/cm^2 after 30 cycles indicating that it offers better corrosion resistance as compared to alloy D. However the scale is thick

and in the scale Ni, Cr, Fe, V and Mn are present. The scale just above the substrate is rich in Ni where both Cr and Fe are absent. Presence of V in the scale indicates formation of vanadates. XRD confirmed the formation of FeV_2O_4 and $Ni(VO_3)_2$. Other phases identified are NiO, α-Fe_2O_3, Cr_2O_3, $NiCr_2O_4$ and $NiFe_2O_4$. There is a thin irregular Cr-rich layer present just above the Ni rich layer at the alloy/scale interface indicating diffusion of Cr from the substrate into the scale and enrichment of Ni near the substrate. Ni-rich pockets are also seen in the bulk scale. Fig 6.8 (a, b and c) show the possible corrosion mechanism in alloy C (Superni 75), alloy D (Superni 718) and alloy E (Superni 601).

6.2 HOT CORROSION STUDIES IN Na_2SO_4-60%V_2O_5 + MgO

Under the above conditions weight gain for alloy A after 4th cycle is negligible. Maximum weight gain is nearly 60% of the weight gain without MgO addition. The scale thickness also indicates that the MgO addition has reduced it to nearly half (62.5 to 33.3µ). So MgO is effective in reducing the hot corrosion in case of the alloy A (Superfer 800 H). The MgO reacts with SO_3 formed due to dissociation of Na_2SO_4 of the salt mixture and this reaction with MgO i.e. inhibitor results to form $MgSO_4$. Further V_2O_5 of the mixture prefers to react with $MgSO_4$, thereby forming Mg-vanadate which is solid at the temperature of reaction i.e. at 900^0C.

The formation of Mg-vanadate has been reported by Rhys Jones et al (1983) and Fichera et al (1987) as already discussed in Chapter 2 (sub chapter 2.9) on literature review. The formation of Mg-vanadate has been confirmed by X-ray diffraction.

Formation of Mg-vanadate is further confirmed from X-ray maps of EPMA in alloy A, (Fig.5.19) where Mg and V are co-existing in the top scale. There is a thin Cr_2O_3 layer just above the substrate and this Cr_2O_3 layer is also responsible for further stopping the continuous transport of cations and anions and thereby bringing the reaction to standstill. Above this Cr_2O_3 layer, there is presence of Fe, Ni, Cr & V, which may be due to the formation of spinels

NiCr$_2$O$_4$ and NiFe$_2$O$_4$. Schematic drawing showing the probable hot corrosion mechanism is shown in Fig. 6.9 (a).

The maximum weight gain for alloy B as indicated in the weight change plot is 33% less than the weight gain without any inhibitor. This is also obvious from the decrease in scale thickness. A medium size scale is formed as compared to a thick multilayer scale in case of where no MgO has been incorporated. Co, Cr, Mg and V are present throughout the scale and thin Ni rich layer is formed at the top of the scale and at the interface. W is present as islands, which are depleted of Cr. Magnesium and Vanadium are co-existing in the scale which is an indication of the formation of Mg-vanadates and that is probably responsible for the decreased rate of corrosion. These observations indicate that MgO addition is very beneficial in reducing corrosion rate. Due to unrestricted diffusion of oxygen ions to the metal surface, Cr formed Cr$_2$O$_3$ due to its high thermodynamic stability. Cr$_2$O$_3$ formation at the initial stage of the corrosion reaction may be the reason for rapid increase in weight gain during the first two cycles of the test, and the development of the continuous film might have reduced the corrosion rate (wt. gain rate) after 2nd cycle as the oxidation now proceeded by diffusion of oxygen to the metal/oxide interface through the oxide layer. Luthra (1982) has made similar reporting in his studies on Co-Cr alloys in Na$_2$SO$_4$.

Luthra and Shores (1980) after hot corrosion studies on Ni-30 Cr and Co-30 Cr alloys by pure Na$_2$SO$_4$ have mentioned that the rapid attack of oxygen at the beginning of the oxidation would be accompanied by the formation of nuclei of cobalt and chromium oxides. Ni, CO and W present in the alloy B in high concentration also might have reacted to form their respective oxides as

$$Ni + 1/2\ O_2 \rightarrow NiO$$

$$W + 3/2\ O_2 \rightarrow WO_3$$

$$Co + 3/2\ O_2 \rightarrow CoO_3$$
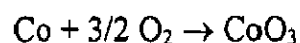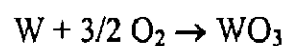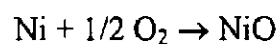
Cr$_2$O$_3$ scale then might have been basically fluxed with Na$_2$SO$_4$ to form Na$_2$CrO$_4$ as

$$Cr_2O_3 + 3/2\ O_2 + 2\ Na_2SO_4\ (l) \rightarrow 2\ Na_2CrO_4\ (l) + 2SO_3\ (g)$$
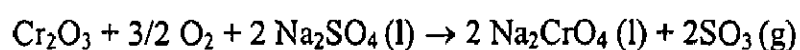
Later Na_2CrO_4 evaporated (Fryburg et al, 1984)

$$Na_2CrO_4 \text{ (l)} \rightarrow Na_2CrO_4 \text{ (g)}$$
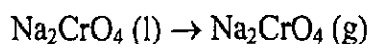
Due to this reaction Cr_2O_3 layer no longer remains protective and further degradation of the alloy B takes place. Even if Cr_2O_3 is formed, it may break down on long time exposure or thermal cycling as reported by Nagarajan et al (1982 B).

MgO addition decreased the total wt. gain value from 8.34 mg/cm^2 to 4.27 mg/cm^2, thickness of the scale also got reduced from 38.5 to 15μm in case of alloy C. Thus it can be inferred from these observations that MgO addition has a beneficial effect in reducing corrosion and this may be attributed to the inherent corrosion resistance property of the alloy C towards vanadic corrosion by formation of a thick protective Cr_2O_3 scale on its surface and also due to the formation of $Mg_3V_2O_8$ (m.p. 1190^{0}C) which remained solid during experimentation formed as a result of ratio of 3:1 as V_2O_5 has higher affinity for MgO in comparison to Na_2SO_4. EPMA and surface EDAX of the alloy C revealed that the matrix mainly consists of Ni and Cr as well as Mg and V are co-existing. S is also indicated on the top of the scale indicating formation of sulphides. XRD identified the presence of phases like Cr_2O_3, $Mg_3V_2O_8$, NiO, $NiCr_2O_4$, FeS and $Ni(VO_3)_2$.

The weight change plot for Ni base alloy D, Superni 718 after exposure at 900^{0}C with Na_2SO_4-60%V_2O_5 + MgO coating shows that corrosion rate is fast during the initial 2 cycles and then the rate decreases. Thickness of the scale formed on the alloy surface also reduced from 57.5 to 48μm. These observations suggest that MgO addition has some beneficial effect in reducing the corrosiveness of the environment. The mechanism is basically the same as explained for alloys A, B and C i.e. in place of a liquid $NaVO_3$ (m.p. 610^{0}C), a solid magnesium orthovanadate is formed as in this case also EPMA identified the presence of Mg and V in the scale as could be seen in Fig.5.22. XRD identified the formation of NiO, Cr_2O_3, $NiCr_2O_4$, $NiFe_2O_4$ and $Mg_3V_2O_8$ as the possible phases. Cracking of the scale and its spallation was observed during experimentation due to which fresh areas might have been exposed to corrosive environment. Spalled regions are clearly visible from the macrographs.

The weight change plot for alloy E shows the similar trend as for alloys C & D. There is increase in weight during the initial 2 to 4 cycles and then it becomes slow and linear. MgO addition in this case also seems to be helpful in reducing the severity of corrosion in Na_2SO_4-$60\%V_2O_5$ environment as scale thickness is also reduced from 52 to 23.4μm. In this case also Cr_2O_3 might have formed in the initial stages of exposure and helped in the reduction of the corrosion rate. Internal oxidation and sulphidation have been observed. SEM micrograph shows that the scale consists of coarse rounded particles like nodules, which indicate the formation of spinels. Some big particles and cavities in between are also present which make the scale porous. XRD identified the formation of oxides NiO, Fe_2O_3, Cr_2O_3; spinels $NiFe_2O_4$, $NiCr_2O_4$ and vanadates FeV_2O_4, $Ni(VO_3)_2$, $Mg_3V_2O_5$. EPMA X-ray maps (Fig.5.25) revealed the presence of Ni, Cr and Fe in the top scale with V & S. Mg is also indicated but its concentration is comparatively less. Cr is present in high concentration just above the alloy substrate to form a protective Cr_2O_3 layer. The oxides of Ni, Cr and Fe are uniformly distributed throughout the scale. Ti and Cr have got I along the grain boundaries thus indicating internal oxidation.

6.3 HOT CORROSION STUDIES IN Na_2SO_4-$60\%V_2O_5$+$20\%CaO$

Weight change after 30 cycles is 7.34 mg/cm^2 for alloy A in Na_2SO_4-$60\%V_2O_5$+CaO and scale thickness is 41μm measured after the corrosion run. Inhibiting behaviour in presence of CaO addition might be due to the formation of protective uniform chromium enriched band present throughout the scale and also formation of Ca-vanadate, $Ca_3V_2O_8$ has already been explained by the authors in one of their publication (Gitanjaly et al, 2002). EPMA maps shows presence of Ca and V along with oxygen at the same place in the scale. XRD identified the formation of such phases as Cr_2O_3, Fe_2O_3, FeV_2O_4, $NiFe_2O_4$ $NiCr_2O_4$, NiO, FeS and $Ca_3V_2O_8$. Oxidation and sulphidation have been the two main processes occurring during the corrosion phenomenon. Mn & S co-exist near the substrate thereby

indicating the MnS formation. Si & Al have got oxidised along the grain boundaries. Possible mechanism is shown schematically in Fig. 6.9 (b).

For alloy B, the weight gain value decreases from 22 mg/cm^2 to 16.3 mg/cm^2. after CaO addition. Thickness of the scale formed on the alloy surface also decreased from 78μm to 34μm. These observations suggest that CaO addition has a beneficial effect in reducing the corrosiveness of the environment for this alloy also. The elements Co, Ni, Cr & W present in the alloy oxidised during the corrosion process and later their spinel formation might have taken place to form $NiCo_2O_4$, $CO_3V_2O_8$, $CoCr_2O_4$, Cr_2O_3, NiO identified by XRD. X-ray maps indicate scale to be rich in Cr_2O_3 and the inner layer is mainly Cr_2O_3. Once the continuous layer of Cr_2O_3 has formed, further corrosion was not possible hence there has been decrease in the rate of corrosion. Thus presence of Cr_2O_3 is basically responsible for the decrease in the corrosion rate and no internal oxidation could take place.

In alloy C, the scale formed is very thin, just about 9μm and this thin scale mainly comprises of oxides of Ni & Cr as revealed by EPMA micrographs (Fig.5.34). Ca & V are co-existing in the scale. Interface between substrate and scale has a very thin scale rich in Cr and is depleted of Ni. The weight change is just 50% of that in Na_2SO_4-60%V_2O_5 environment. Thus incorporating 20% CaO is very beneficial in reducing the extent of corrosion in alloy C (Supermi 75). This decrease may be attributed to the formation of $Ca_3V_2O_8$ and rich chromia layer existing at the interface. Similar results have been reported by Kumar et al (1996) in their study on superalloy Supermi 75 with $CaSO_4$ as an inhibitor in Na_2SO_4-60%V_2O_5. Probable corrosion mechanism for alloys B and C, using CaO as an inhibitor in Na_2SO_4-60%V_2O_5 environment is shown schematically in Fig.6.10 a & b respectively.

In alloys D & E, again there is reduction in weight gain and scale thickness, indicating that there is reduction in corrosiveness of the environment. The mechanism by which the extent of corrosion decreases is similar to alloys A & C because EPMA indicates presence of Ca in the scale along with V and chromium appears to have concentrated near the alloy/oxide interface. Internal oxidation is indicated in both the alloys. Ti rich subscale appears to have

extended as stringers into the underlying alloy along the grain boundaries in alloy D and Si is present along the grain boundaries in alloy E. XRD has identified the presence of phases $Ni(VO_3)_2$, $NiCr_2O_4$, NiO and Cr_2O_3 in alloy D and similar phases like $Ni(VO_3)_2$, $Ca_3V_2O_8$, $NiCr_2O_4$, $NiFe_2O_4$, NiO and Cr_2O_3 in alloy E.

6.4 HOT CORROSION STUDIES IN Na_2SO_4-60%V_2O_5+20%MnO_2

A few manganese-based additives are also effective in preventing oil ash corrosion. Mn reacts with V in the fuel and thereby prevents it from reacting with Na to produce corrosive sodium vanadates as stated by Paul & Seeley (1991). Reduction in weight and scale thickness of all the alloys confirms the inhibiting effect of the MnO_2 addition. Weight change after 30 cycles with MnO_2 addition is 7.37, 13.47, 5.35, 6.28 and 4.93 mg/cm^2 which is about 16, 33.8, 36, 28 and 9.2 percent less than the weight gain values in the environment without MnO_2 for alloys A, B, C, D and E, indicating that MnO_2 may be useful as an inhibitor of hot corrosion in this aggressive environment.

Reduction in the scale thickness in case of alloys A, B, C, D, & E from 62.5, 78, 38.5, 57.5 and 52 microns to 30, 53.5, 20.5, 33.3 & 44 μm with addition of MnO_2 to Na_2SO_4-60%V_2O_5, has been observed further confirming that MnO_2 is helping in reducing the aggressiveness of the Na_2SO_4-60%V_2O_5. In case of alloy A the scale mainly contains Fe & Ni along with some amount of Cr and Mn. Cr-rich irregular shaped continuous thin band is present just above the interface. Ti is also co-existing with Cr in this band. S is present on top of the scale and in the substrate concentrated at few spots. Formation of compounds Fe_2O_3, FeV_2O_4, Cr_2O_3, FeS, $NiCr_2O_4$ and spinels of Fe, Ni, Mn and Cr have been identified. Presence of continuous Cr_2O_3 layer might be contributing to less aggressive attack. Beneficial effect of MnO_2 additive has been reported by Thilkan et al (1969 B) while they studied the effect of additives on oil ash corrosion of stainless steel in 90%V_2O_5-10% Na_2SO_4.

In case of alloy B, a thick scale has formed which mainly contains Cr & Co, W & Ni and Fe & Mn. Scale is triplex, the upper layer is rich in chromium, middle layer is mainly containing W rich phases. Most of the areas rich in tungsten are depleted of Cr. There is a nickel rich layer at the interface. Ingress of S and V is indicated by the EDAX analysis along the cross-section (Fig. 5.51 and Table 5.2) upto the substrate. Nickel sulphide and manganese sulphide formation is indicated from the elemental X-ray micrographs at the interface which is a clear indication that salt has penetrated through the pores and cavities formed due to the spallation of the oxide scale. But XRD identified the presence of spinels and oxides like $NiCo_2O_4$, Cr_2O_3, $Co_3V_2O_8$, Co_3O_4, Co_2MnO_4 ($2CoO.MnO_2$) and $NiWO_4$. Formation of phases $Co_3V_2O_8$ and $NiCo_2O_4$ has been reported by Jones and Williams (1987).

In case of alloys C & D, Cr is present throughout the scale, but in alloy D it is also present as a rich thin continuous band at the interface depleted of both Fe and Ni and this Cr_2O_3 layer is perhaps helping in reducing the rate of corrosion. In the scale of alloy C, manganese, iron, nickel and vanadium exist together indicating formation of vanadates. Substrate below the scale is depleted of Cr and scale is rich in Cr. S is present in the top most regions indicating formation of suphides. XRD identified the $Ni(VO_3)_2$, $NiCr_2O_4$, Cr_2O_3, NiS, NiO, FeS and $NiMn_2O_4$. Inhibiting effect in alloy C is due to high concentration of Cr in the scale and formation of vanadates and spinels.

In case of alloy D, above the Cr rich layer, Fe, V, Al and Ni are distributed throughout the scale and Ti has got oxidised along the interface providing pegs and interlocking the scale with the substrate. Mn and V are co-existing in the scale. XRD identified the formation of Cr_2O_3, $NiCr_2O_4$, $NiAl_2O_4$, Mn_3O_4 and mainly $Ni(VO_3)_2$. Continuous Cr rich layer just above the interface may be contributing to protection in alloy D.

Ni, Cr, Mn & V are coexisting in the scales of alloy E as revealed by EPMA (Fig. 5.50) so thereby indicating nickel vanadate. Formation of vanadates of Ni and Fe and their spinels have been identified through X-ray diffraction analysis. Thus probable mechanism of inhibition may be attributed to formation of vanadates mostly $Ni(VO_3)_2$ and spinels in alloy E.

The lesser weight gain in case of nickel base alloys may be further contribution of nickel vanadates. Swaminathan et al (1992) have reported that the rapid increase in weight at the initial hours is due to the ease in diffusion of Ni and oxygen ions in the molten vanadium pentoxide (Ni interstitial compound). Once the compact, solid vanadate layer is formed the short circuit diffusion paths are blocked and diffusion becomes difficult for the oxygen ions towards the metal surface. After a certain time the solidification of vanadate in the short circuit paths occur and the solid vanadate layer gets compact and decreases the diffusion of ions. Consequently, the oxidation rate falls with time; hence the weight gain gets slowed down with time.

6.5 HOT CORROSION STUDIES IN Na$_2$SO$_4$-60%V$_2$O$_5$+10%ZnSO$_4$

Weight change after 30 cycles with ZnSO$_4$ addition is 7.6, 6.39, 6.69 and 3.96 mg/cm^2 which is about 12, 23, 22 and 27 percent less than the weight gain values in the environment without ZnSO$_4$ for alloys A, C, D and E. In alloys C, D and E, effect is nearly same.

Scale mainly consists of an upper layer rich in Ni, Cr and Fe followed by a thick layer which contains mainly chromium along with Ni & Fe in alloy A (Fig. 5.62). The region between the top layer & the thick middle layer contains higher concentration of sulphur. Vanadium is present at the interface between the substrate and the scale thus indicating ingress of S and V through the scale resulting in the formation of vanadates and sulphides. There is a thin layer rich in Ni and in this region concentration of V is also high indicating formation of Ni(VO$_3$)$_2$. But XRD identified mainly the formation of oxides of Fe, Cr & Ni, their spinels (Cr,Fe)$_2$O$_3$, NiCr$_2$O$_4$ & ZnFe$_2$O$_4$ and FeS.

In case of alloy C, scale mainly contains Cr, Fe and Ni. The region just above the substrate has got Cr rich layer penetrating into the substrate. The V is seen throughout the scale. Internal oxidation of Ti is seen just below the scale. The EDAX analysis also indicates that top layer mainly contains Ni. Analysis at points 1 and 2 on the scale surface Fig. 5.61 (b)

and Table A.29 have shown the presence of mainly Ni and it has also been confirmed from the EDAX analysis along cross-section (Fig. 5.66 and Table 5.3). XRD analysis confirmed the presence of NiO, Cr_2O_3 and $NiCr_2O_4$ in the scale. Presence of chromia rich scale could be a reason for lowering the corrosion rate.

In alloy D also, presence of thin Cr_2O_3 layer just above the substrate could be contributing to lowering the corrosion rate similar to alloy C. V and Zn are indicated co-existing in same areas at the top of the scale from their respective X-ray images shown in Fig. 5.64. XRD identified the peaks of NiO, $NiCr_2O_4$, $Ni(VO_3)_2$, Fe_2O_3 and Cr_2O_3.

In alloy E, the concentration of the Cr along the interface between substrate and scale is slightly higher which is seen from the EDAX analysis across the scale (Fig. 5.67 and Table 5.4). EPMA X-ray maps also reveal irregular Cr-rich layer just above the substrate, which is not continuous. V is present throughout the scale and its amount also goes on increasing as we move down in the scale. Amount of Zn also goes on increasing as we travel down the scale indicated from the elemental EDAX analysis. Al is present in high concentration along the intergranular region thus indicating internal oxidation. Presence of oxygen indicates formation of mainly oxides throughout the scale. XRD detected the peaks of $NiCr_2O_4$, Cr_2O_3, $Ni(VO_3)_2$ and spinels of Zn, Fe and V such as $ZnFe_2O_4$ and $ZnFeVO_4$ along with the formation of vanadates. Thus the possible reason for the 27% decrease in weight change could be contribution of thin Cr_2O_3 layer near the substrate and formation of vanadates.

6.6 HOT CORROSION STUDIES IN Na_2SO_4-60% V_2O_5 WITH SUPERFICIALLY APPLIED CeO_2

In case of CeO_2 coated samples a thick scale is indicated in alloys A & B where as it is of medium size in alloys C, D & E. The scale thickness values are 50, 41.5, 25, 30 and 32μm in case of alloys A, B, C, D & E respectively. But there is an indication of reduction in the rate of corrosion for all the alloys. Weight gain has also decreased to some extent in all the alloys. This decrease is 23% in alloy A, 35% in alloy B, 68% in alloy C, 28% in alloy D and

by 33% in case of alloy E. Thus it can be inferred that ceria is effective in case of all the alloys and in alloy C it is most effective.

A thick dense scale mainly containing Cr, Ni and Fe is indicated in alloy A (Fig.5.77). There is penetration of the scale into the substrate where mainly Si is getting oxidised along the grain boundaries. Such finding has also been reported by Roy et al (1995) in their study on superficially ceria coated AISI-347 grade stainless steel. Internal oxidation of silicon along the alloy grain boundaries and formation of such phases have been reported by them. They have observed Si concentrated at the alloy/oxide interface and Si-rich subscale well extended as stringers into the underlying alloy along the grain boundaries.

X-ray diffraction pattern from the outer surface of the scale formed reveals the formation of $NiCr_2O_4$, FeV_2O_4, Fe_2O_3, Cr_2O_3 and $(Cr,Fe)_2O_3$. EDAX of the surface and cross-section has indicated the presence of ceria in the scale, even though EPMA failed to detect it probably due to its low concentration. The inhibiting effect of superficially applied CeO_2 in the aggressive environment of Na_2SO_4-60%V_2O_5 may be due to the presence of ceria in the scale and a thin continuous layer of Cr_2O_3 present at the margin of the scale abounding the substrate impeding the transport of species.

In case of alloy B, maximum weight change is nearly 1/3rd of that without ceria in Na_2SO_4-60%V_2O_5. Cobalt, tungsten and chromium are seen in the scale. But W is mainly present in form of elongated streaks where Cr is absent, which indicates a stepwise formation of scale where first Cr gets oxidised and in the Cr depleted area below it concentration of W increases and so W gets oxidised and then just beneath this concentration of Cr increases and so it gets oxidised and Cr_2O_3 so formed may be responsible for lowering the extent of corrosion. X-ray diffraction profiles also indicate the presence of $CoCr_2O_4$, $NiCo_2O_4$, Co_2O_3, Co_3O_4, Cr_2O_3 and $NiWO_4$ compounds on the surface scale after hot corrosion run.

Macrographs show the presence of salt coating on the surface of the alloys C, D & E. This is more intact in case of alloys C and E. In alloys C, D and E, thick Cr_2O_3 continuous layer has been observed in EPMA, which is perhaps contributing to decreased corrosion rates. The formation of $CeVO_4$ may be suggested at places where Ce and V are co-existing.

Presence of CeO_2 in case of alloys C & E is indicated from the XRD analysis. Formation of $CeVO_4$ is also established from the EPMA micrographs in case of alloys C & E. Thus presence of CeO_2 on the surface and possibly formation of $CeVO_4$ may be contributing to the reduction of corrosion attack in alloys C, D and E. Reidy and Jones (1995) have proposed that ceria (CeO_2) is chemically inert to the molten $NaVO_3$-SO_3 system at 1073K for SO_3 partial pressure upto 3×10^{-6} atm. But at higher SO_3 partial pressure CeO_2 with V_2O_5 components of the melt react to form $CeVO_4$. Conditions of reaction are mentioned in Table 2.3 as reported by Jones et al (1986). Further Ecer et al (1982) in their study have reported that the rates of oxidation of both the Ni- and Fe-base alloys were markedly reduced by the superficial application of CeO_2 powder on the alloy surface and it also improved the scale adherence and resulted in marked changes in the oxidation morphology. Seal et al (1994) and (2001) have also reported that superficially applied CeO_2 not only reduced the rates of scale growth for all the three varieties of steel but also imparted improved scale adhesion to the respective alloy substrates. Similar reporting has also been made by Mitra et al (1993) in their study on superficially applied CeO_2 coating on 304 stainless steel. They proposed that such improvement could be due to the change in mechanism of scale growth from the scale/gas interface to the alloy/scale interface and faster attainment of steady state Cr_2O_3-rich scale along with complex spinel formation. Schematic representation of the corrosion mechanism for superficially coated ceria in case of alloy C is shown in Fig. 6.11.

6.7 HOT CORROSION STUDIES IN Na_2SO_4-60%-V_2O_5 WITH SUPERFICIALLY APPLIED Y_2O_3

With application of Y_2O_3 superficial coating weight gain values have decreased to 1.15, 7.40, 3.39, 5.13 and 1.43 mg/cm^2 i.e by 86.88% in alloy A, 63.6% in alloy B, 38.5% in alloy C, 40.2% in alloy D and 73.66% in alloy E after exposure of 30 cycles at 900^{0}C. The scale thickness after 50 cycles is the least in case of alloy A which is nearly ~20μ of all the

coatings applied to Superfer 800H. This thin scale is rich in Cr; where Y and V are co-existing, thereby indicating formation of YVO_4 which is clearly indicated in the X-ray images and further confirmed by the EDAX of the SEM (BSEI) of the cross-section.

Alloy B has shown the formation of medium size scale (30 μm) rich in Cr and Co. Scale thickness is less than half of that without Y_2O_3 barrier coating. X-ray analysis identified the main phases $CoCr_2O_4$, Cr_2O_3, Co_3O_4, $NiCo_2O_4$ and $NiWO_4$. Hou and stringer (1987) have reported that surface coated oxides reduced the oxidation rate of Co-25wt.% Cr to different degrees and found CaO being the most effective and Y_2O_3 & La_2O_3 better than CeO_2 and ZrO_2.They even reported the formation of phases $CoCr_2O_4$ and CoO during oxidation studies of Co-25wt.% Cr.

In case of alloy C again a very thin scale is observed about 16.5μ in size and contains mainly Cr and Ni. Y is present as a thin layer along with V & S on the top of the scale. X-ray diffraction analysis has identified the presence of $NiCr_2O_4$, Cr_2O_3, NiO, TiO_2 and Y_2O_3 on the scale surface.

X-ray mapping (Fig.5.95) has revealed that the scale formed in alloy D is rich in Ni, Cr and Fe. Y is present in pockets on top scale. EDAX analysis for alloy D at various points from surface to substrate has also indicated the presence of Ni, Cr & Fe in the scale and Al & Ti in the intergranular region in substrate and Y in the uppermost region. Ti, Na, S & V are also present at few locations (Fig. 5.98 and Table 5.9) corresponding to back scattered image. Surface analysis has further confirmed that scale is mainly consisting of compounds of Fe, Ni & Cr. Very little spalling is noticed in all the alloys which is obvious from the macrographs of the sample showing the presence of unreacted salt coating on the surface of the samples in case of alloys A, B, C and E. In case of sample E, the unreacted salt coating is more uniform and intact. Ce and Y confer resistance to spalling and are often applied as a superficial coating, or ion implanted as reported by Hocking (1993). The scale thickness values measured after the experimentation in their decreasing order follows the trend as:

Alloy C < Alloy D < Alloy A < Alloy B and Alloy E.

Protection is provided by continuous Cr_2O_3 layer and YVO_4 which is solid at 1860^0C. YVO_4 might have formed as revealed by EPMA where both V and Y exist together at same points in alloys A and E which is having m.p. of 1860^0C. So it would be a solid phase developed at the 900^0C and that may be the reason for the inhibiting behaviour observed with Y_2O_3 coating in Na_2SO_4-60%V_2O_5 environment. Formation of YVO_4 in presence of $NaVO_3$ has been confirmed by Jones et al, 1985 & 1986 (Table 2.3). Possible mechanism of corrosion in alloys A (Superfer 800H) and C (Superni 75) is shown in Fig.6.12 a & b respectively.

Yedong and Stott (1994) have reported that establishment of a chromia scale can be promoted effectively by the presence of an Y_2O_3 film on Ni-15Cr alloy and at least locally on Ni-10 Cr. On the basis of their elemental distribution analysis, they concluded that the scale formed on the alloy coated with Y_2O_3 was consisting of mainly of fine-grained chromia. Details had been discussed earlier (2.16 of chapter 2). They proposed that selective oxidation is promoted by application of Y_2O_3 and leads to formation of Cr_2O_3 layer and probably this is the reason for presence of a chromia rich continuous scale formed on alloy A in Na_2SO_4-60%V_2O_5+Y_2O_3 environment.

Stringer et al have postulated on the basis of their study on high temperature oxidation of Ni-20Cr alloys containing dispersed oxide phases that dispersed particles act as heterogeneous nucleation sites for oxide grains thereby reducing the inter nuclear distance, which allows more rapid formation of a continuous chromia film and produces a linear oxide grain size (Hou and Stringer, 1986).

6.8 HOT CORROSION STUDIES IN Na_2SO_4-60%-V_2O_5 WITH SUPERFICIALLY APPLIED SnO_2

In case of SnO_2 superficially coated samples a thick scale is formed in alloys A, B & E whereas medium size scale is observed in case of alloys C & D. Weight change is 7.26, 6.96, 4.21, 7.13 and 3.70 mg/cm^2 respectively after 30 cycles with SnO_2 application. Percentage decrease in weight gain in alloys A, B, C, D and E is 17.2, 66, 50, 17 and 32 percent

respectively. SnO_2 has been indicated in the corrosion product as unreacted oxide by both XRD and SEM-EDAX analysis of the scale in alloys A, C & E. The effectiveness of the SnO_2 therefore may not be due to the formation of Sn-vanadate. It may perhaps be due to its non-reactive nature with the corroding species. Jones (1993) in their study on reaction of SnO_2 with vanadate-sulphate melts concluded that tin-oxide is inert to chemical reaction with $NaVO_3$ at 700^0C & 800^0C and suggested that SnO_2 may be potentially useful as a material for protection against molten vanadate-sulphate hot corrosion at moderate temperatures. SnO_2 (m.p. 1630^0C) although not reacting but might have allowed transport of the oxidizing species through the pores and cracks developed in the SnO_2 layer. So in most of the cases scale has developed below the SnO_2 layer. But average scale thickness in all alloys is lower than that in Na_2SO_4-V_2O_5 environment. X-ray diffraction has also identified the presence of SnO_2 in alloys A, C and E on the scale surface. In case of alloy A, thick scale formed is duplex in nature upper layer rich in Sn and the lower mainly containing Fe and Cr as revealed by their respective X-ray images (Fig. 5.107). Formation of spinels of Fe, Ni, and Cr in the scale is indicated in two pockets in the scale. There is a presence of thin Cr-rich continuous band above the substrate. Presence of SnO_2 is even obvious from the crystalline growth observed by the SEM analysis of the top surface of the scale, which has been further confirmed from the XRD analysis. Presence of this refractory SnO_2 in the scale is possibly helpful in decreasing the rate of corrosion. In alloy B, Cr that is present in the top layer in W depleted areas and a band type Cr rich thick layer present above the substrate may be contributing factors in lowering the corrosion rate of alloy B in SnO_2 presence. Presence of MnS is indicated at the interface between the substrate and scale.

In case of alloy C, SEM (BSEI) of the sample along alloy/scale cross-section indicate the formation of medium size scale and elemental X-ray mapping reveals that the scale is mainly containing Cr and lesser amount of Ni. Sn is present in higher concentration at top of the scale where as V is present in the main scale indicating formation of nickel vanadates. Presence of higher percentage of Cr in the scale and the SnO_2 on the top surface may be the possible factors for decrease in the corrosion rate. In alloy D, the weight gain in the sample

with SnO_2 coating is little lower than without SnO_2 coating (19%) after 30 cycles which is possibly due to the oxidation occurred via transport of species from across the coating and formation of loose, nonadherent, porous scale formed as spalling is indicated in wt. change plot. Spalling of the applied SnO_2 coating could be seen in the macrographs (Fig. A.2). In case of alloy E, the average value of scale thickness is slightly less than one without SnO_2 coating but no internal oxidation is observed. SnO_2 is present on the top of the scale and no reaction seems to have occurred with V as it is mainly present in the main scale. XRD also confirmed the presence of SnO_2 in the scale. SnO_2 layer is not continuous and the gaps have allowed the reacting species to react with the alloy. Possible mode of corrosion for alloys A (Superfer 800H) and E (Superni 601) coated with SnO_2 and exposed to Na_2SO_4-60%V_2O_5 environment are shown in Fig. 6.13 a & b.

6.9 HOT CORROSION STUDIES IN Na_2SO_4-60%. V_2O_5 WITH SUPERFICIALLY APPLIED ZrO_2

With ZrO_2 superficial coating also, overall weight gain is less in case of alloys A, B, C, D & E as observed after 30 cycles. ZrO_2 is not much effective in alloy A as weight gain is only 10.72 percent less than the alloy without ZrO_2 coating. In alloys B, D and E decrease in weight gain is nearly same and is nearly half of that of the weight gain without ZrO_2 coating. Where as in alloy C this decrease in weight is maximum about 70%. Thick scale formed in alloy A is rich in Cr, Ni, Fe & V. Zr has been detected at few spots in the scale by EDAX analysis of the cross-section of the sample (Fig. 5.127 & Table 5.12). Absence of protective continuous chromia layer and presence of less protective NiO is the main reason for more corrosion rate in alloy A.

Similar can be reason for thicker scale in alloy B where scale is multilayered, top layer is rich in Cr, Ni & Co followed by middle layer, which is rich in W and Cr where W is present Co, is absent. Cr in very high concentration is present just above the interface and in the

substrate there is a Ni-rich layer. The areas rich in Ni are depleted of Cr as indicated by EPMA and EDAX along the cross-section. It is probable that the oxides initially formed went away from the substrate (Saxena, 1986) and they might have formed spinels of Ni, Co and W. EDAX analysis has shown the presence of Zr in the scale in the top and middle area and has also penetrated into the alloy. S & V are also present in the scale. Schematic representation of the corrosion mechanism in alloy B is shown in Fig. 6.14(a).

Molten salt might have reached the substrate through the openings in ZrO_2 superficial coating where it reacted with the metal. The alternating expansion and contraction in the coating might have led to the development of high thermal stresses which later caused the spalling of the coating and thereby enhanced the further oxidation of the substrate. Similar penetration of molten Na_2SO_4 through pores and cracks has been reported by Chen et al (1993) while studying the degradation of plasma-sprayed zirconia coatings on stainless steel during their hot corrosion test.

Alloy/scale cross-section as viewed in the SEM (BSEI) for ZrO_2 coated alloys C and D reveals the formation of a thin oxide scale. The protectiveness to hot corrosion of alloys C and D may be attributed to formation of spinels, vanadates, presence of unreacted ZrO_2 and presence of chromia rich layer above the substrate. In case of alloy C, the dense scale formed is mainly containing oxides of Cr & Ni and their content increases in the lower layer of the scale. Zr is also present in the scale as well as V & S. Ti has also been incorporated in the scale (Fig. 5.129 and Table 5.14). Presence of these elements in the scale is revealed by their corresponding X-ray images (Fig. 5.124).

Similarly in alloy D also the top scale is mainly consisting of Ni & Cr. Their extent is more or less same throughout the cross-section of scale which suggests the formation to a large extent of $NiCr_2O_4$ in both the alloys and that has been confirmed by XRD. Fe, Ti, Al, Si, Zr, Na & V are present throughout the scale revealed by EDAX analysis of the scale along the cross-section (Fig. 5.130 and Table 5.15). It is possible that ZrV_2O_7 may have formed as Zr, V and Oxygen are present in the scale at same areas as observed from the EDAX analysis and further supported by the EPMA X-ray mapping (Fig. 5.125). The conditions of formation of ZrV_2O_7

are given in Table 2.3. The extent of the beneficial effect greatly depends on the integrity of the applied oxide coatings. The most dense and continuous coatings seem to be the most effective as reported by Hou and Stringer (1987) and it can also be a reason for the reduced corrosion in alloys C, D and E since applied coating after the experimentation has been found to be mostly intact in these alloys. According to them applied coatings can act as a semi-blocking layer and reduce the oxidation rate or even locally promote Cr_2O_3 formation. Possible corrosion mechanism in alloy D (Superni 718) coated with ZrO_2 is shown in Fig 6.14(b).

SEM (BSEI) micrograph for alloy E coated with Na_2SO_4-60% V_2O_5 + ZrO_2 reveals the formation of a single layer scale with prominent internal oxidation along the grain boundaries of the substrate alloy. Presence of Ni, Cr and Fe along with V, Al and S in the scale is evident from their corresponding X-ray images. The scale is rich in Cr & Fe. Incorporation of vanadium indicates formation of vanadates and spinels. FeV_2O_4, $NiCr_2O_4$, NiO, Fe_2O_3 and Cr_2O_3 have been detected by the X-ray diffraction analysis. Chromium and aluminum have oxidised along the grain boundaries in the substrate. X-ray map for Zr has shown that it is present on top of the scale at two spots having very low concentration. The reactive element is present mostly at the outer surface of the oxide scale has been revealed in case of alloys C & D also and this observation agrees with the findings of Hou and Stringer (1987). They investigated the beneficial effects of surface–applied nitrate converted CaO, CeO_2, Y_2O_3, La_2O_3, HfO_2 and ZrO_2 on the oxidation behaviour of Co- and Ni- base alloys at 1000 and 1100^0C. They further reported that oxide adhesion promoted by this superficial treatment is remarkable.
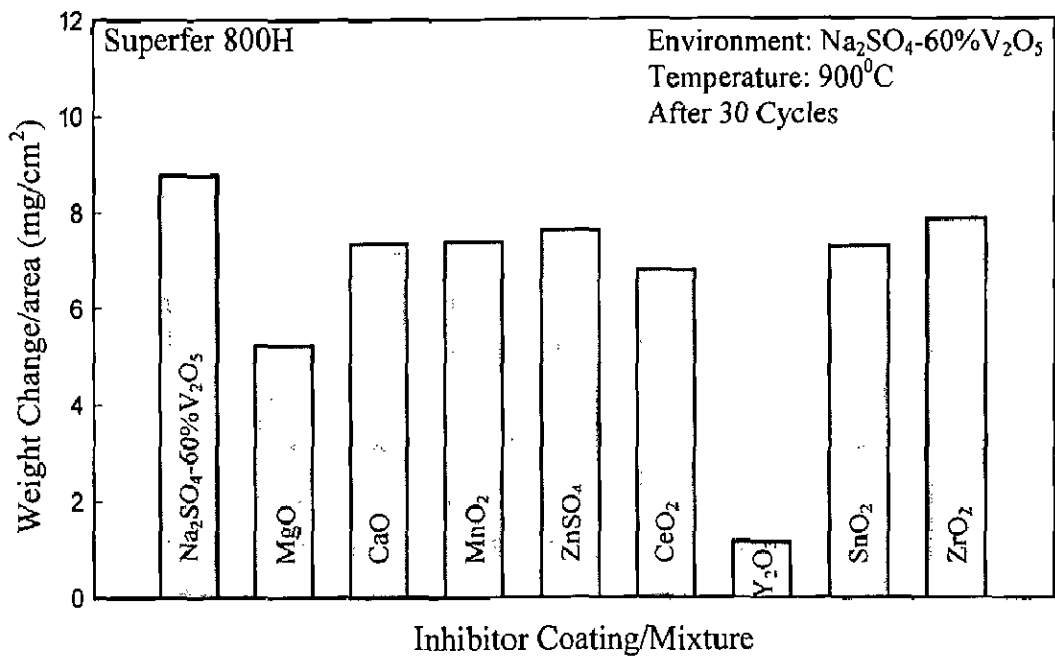
Fig. 6.1 : Weight change plot for alloy A (Superfer 800H) with different inhibitors applied (mixture/coating) in Na_2SO_4-60%V_2O_5 environment after exposure for 30 cycles at 900°C.
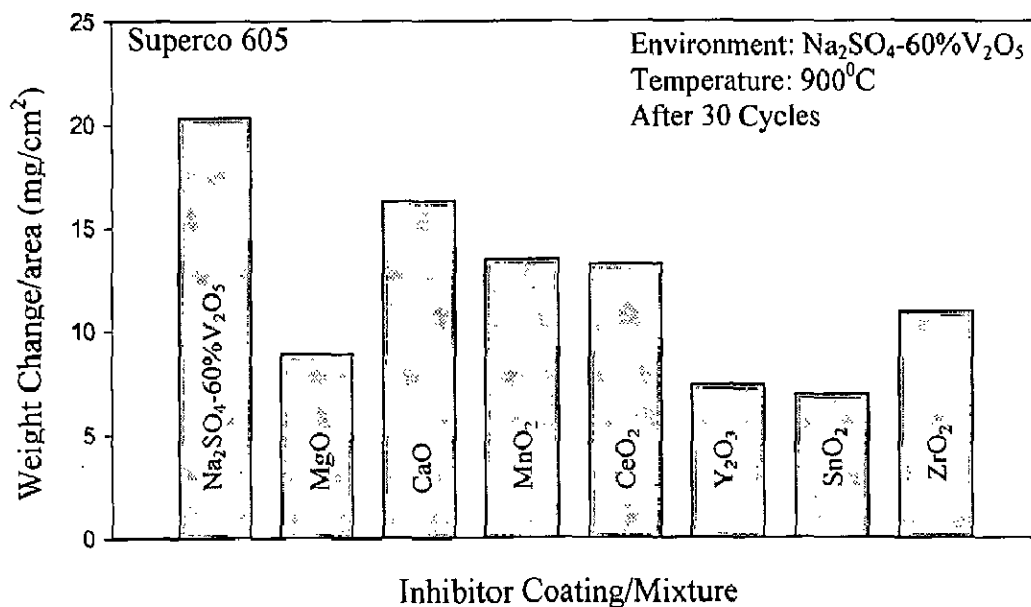
Fig. 6.2 : Weight change plot for alloy B (Superco 605) with different inhibitors applied (mixture/coating) in Na_2SO_4-60%V_2O_5 environment after exposure for 30 cycles at 900°C.
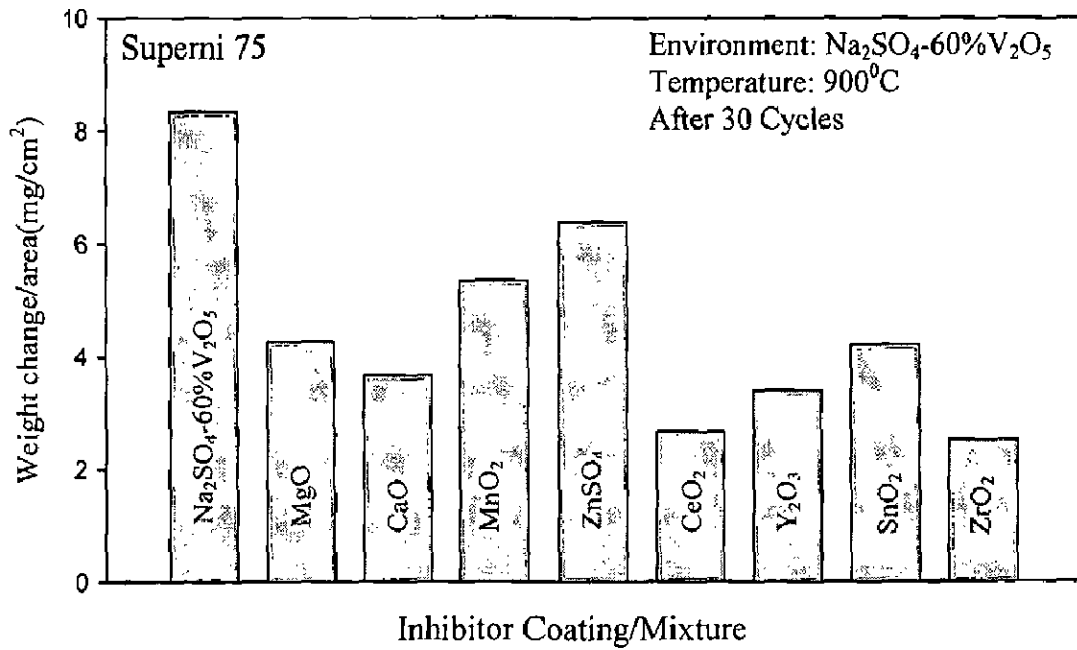
Fig. 6.3 : Weight change plot for alloy C (Superni 75) with different inhibitors applied (mixture/coating) in Na_2SO_4-60%V_2O_5 environment after exposure for 30 cycles at 900^0C.
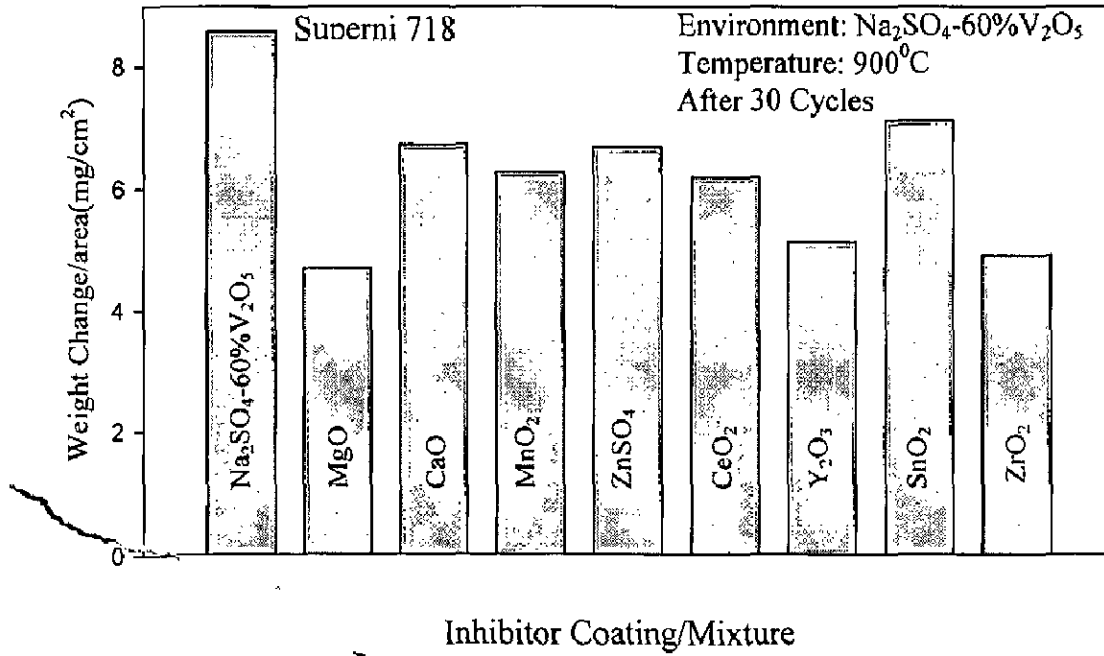
Fig. 6.4 : Weight change plot for alloy D (Superni 718) with different inhibitors applied (mixture/coating) in Na_2SO_4-60%V_2O_5 environment after exposure for 30 cycles at 900^0C.
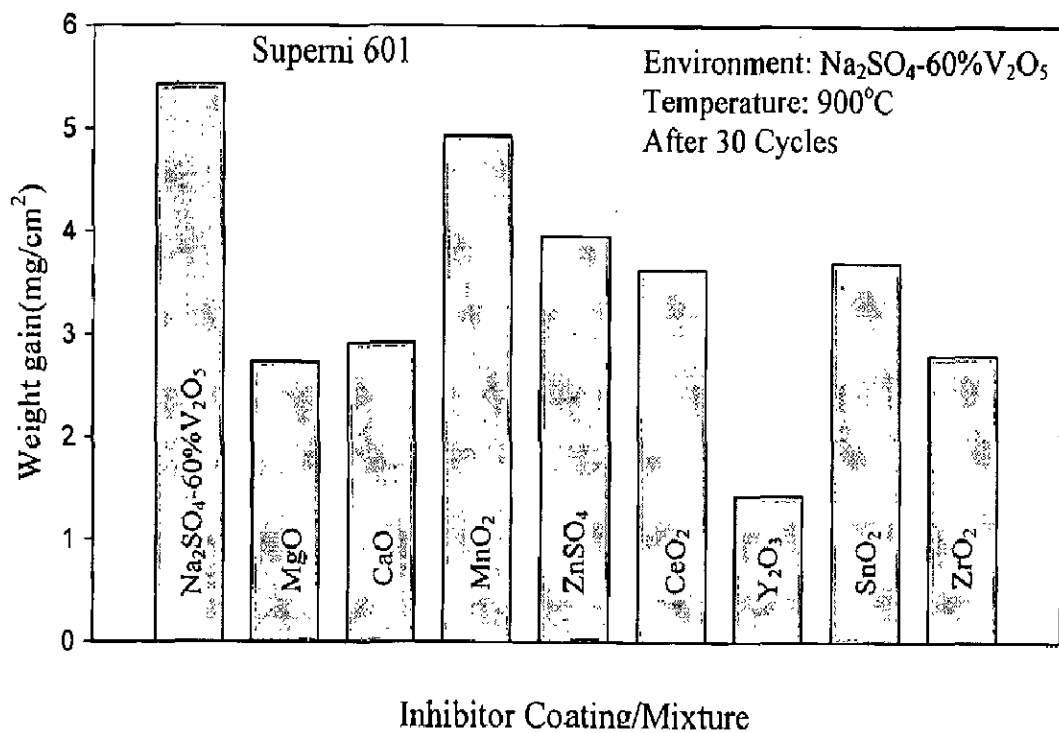
Fig. 6.5 : Weight change plot for alloy E (Superni 601) with different inhibitors applied (mixture/coating) in Na_2SO_4-60%V_2O_5 environment after exposure for 30 cycles at 900^0C.

Air

Na_2SO_4 - 60% V_2O_5

Superfer 800H

Air

Liquid $NaVO_3$

$O^{2-}\downarrow$

↑ ↑ ↑
Fe Cr Ni

Oxygen adsorption

Air
Liquid $NaVO_3$

| Fe_2O_3 | | Cr_2O_3 | | NiO |

↑ ↑ ↑
Fe^{3+} Cr^{3+} Ni^{2+}

Oxide Nucleation
& growth

Liquid $NaVO_3$

$\downarrow O^{2-}$

Vanadates, oxides & spinels

Scale growth &
Internal oxidation

Crack on Scale
surface

Air
$O^{2-}\downarrow$

Spinels Oxides
and vanadates

FeV$_2$O$_7$,NiCr$_2$O$_4$, Fe$_2$O$_3$

Cr_2O_3 rich layer

NiO rich & Fe-depleted
region

↓
Internal Oxidation

Substrate
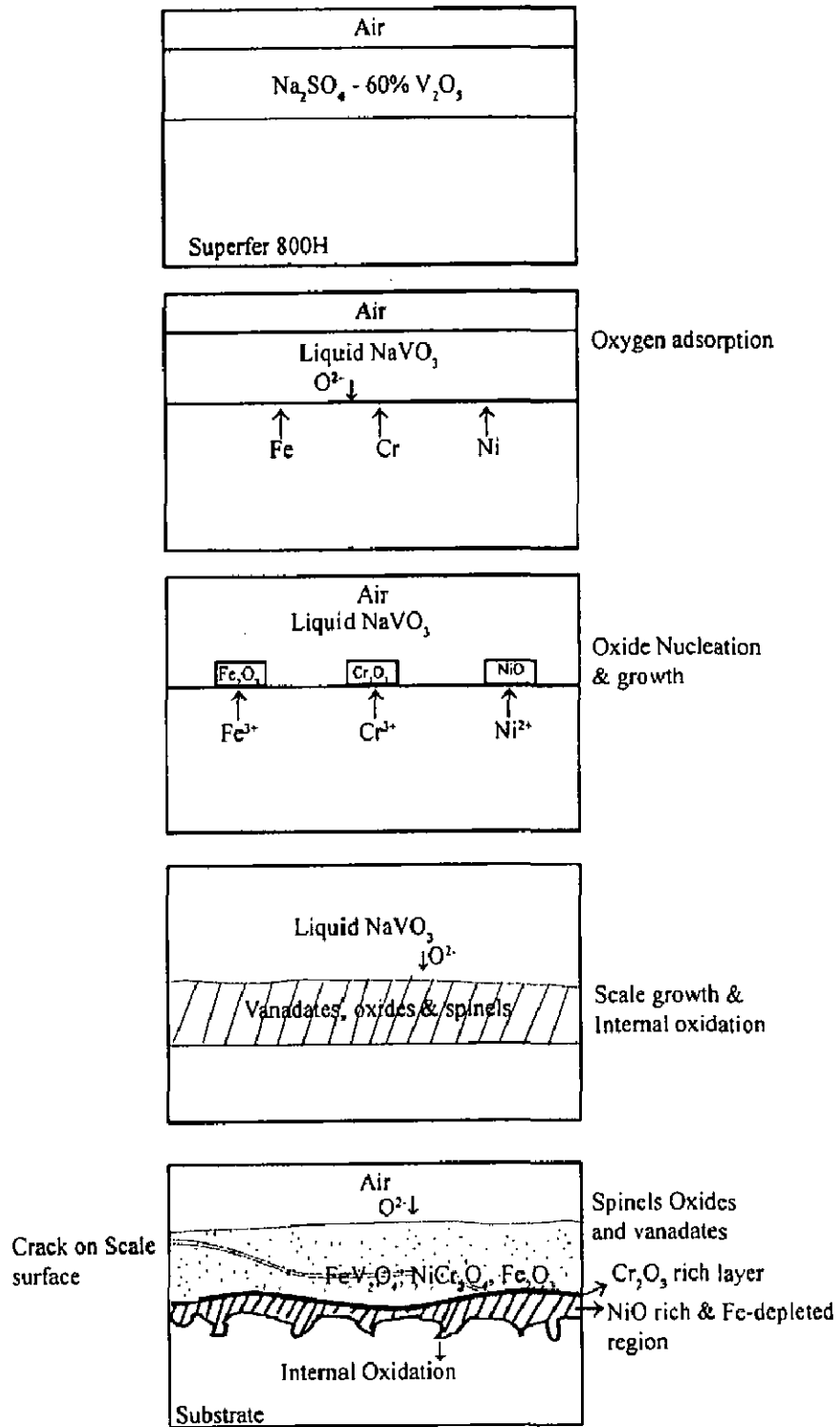
Fig. 6.6 : Schematic illustration of some of the main aspects of the corrosion mechanism occuring in alloy A (Superfer 800H) in Na_2SO_4-60% V_2O_5 after exposure for 50 cycles at 900°C.

233
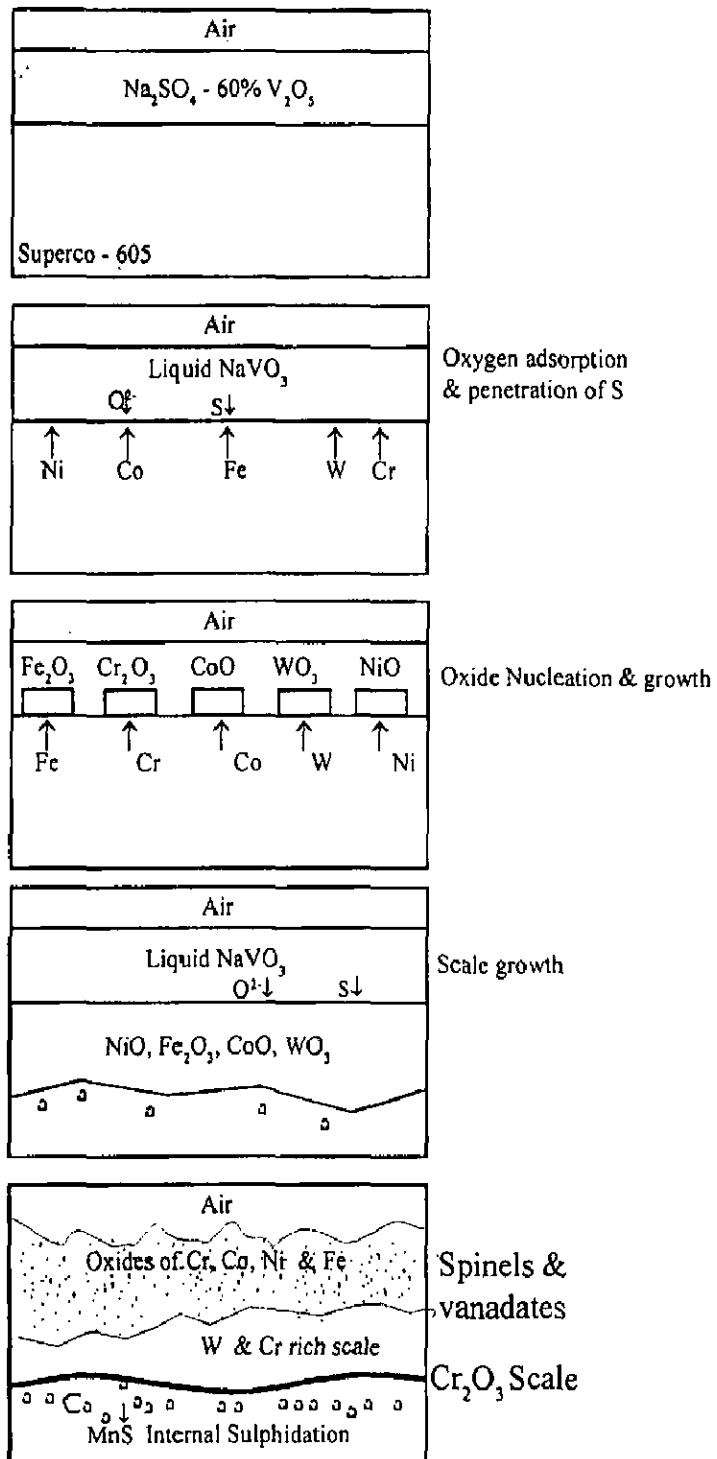
Fig. 6.7 : Schematic illustration of some of the main aspects of the corrosion mechanism occuring in alloy B (Superfer 605) in Na_2SO_4-60% V_2O_5 after exposure for 50 cycles at 900°C.

234
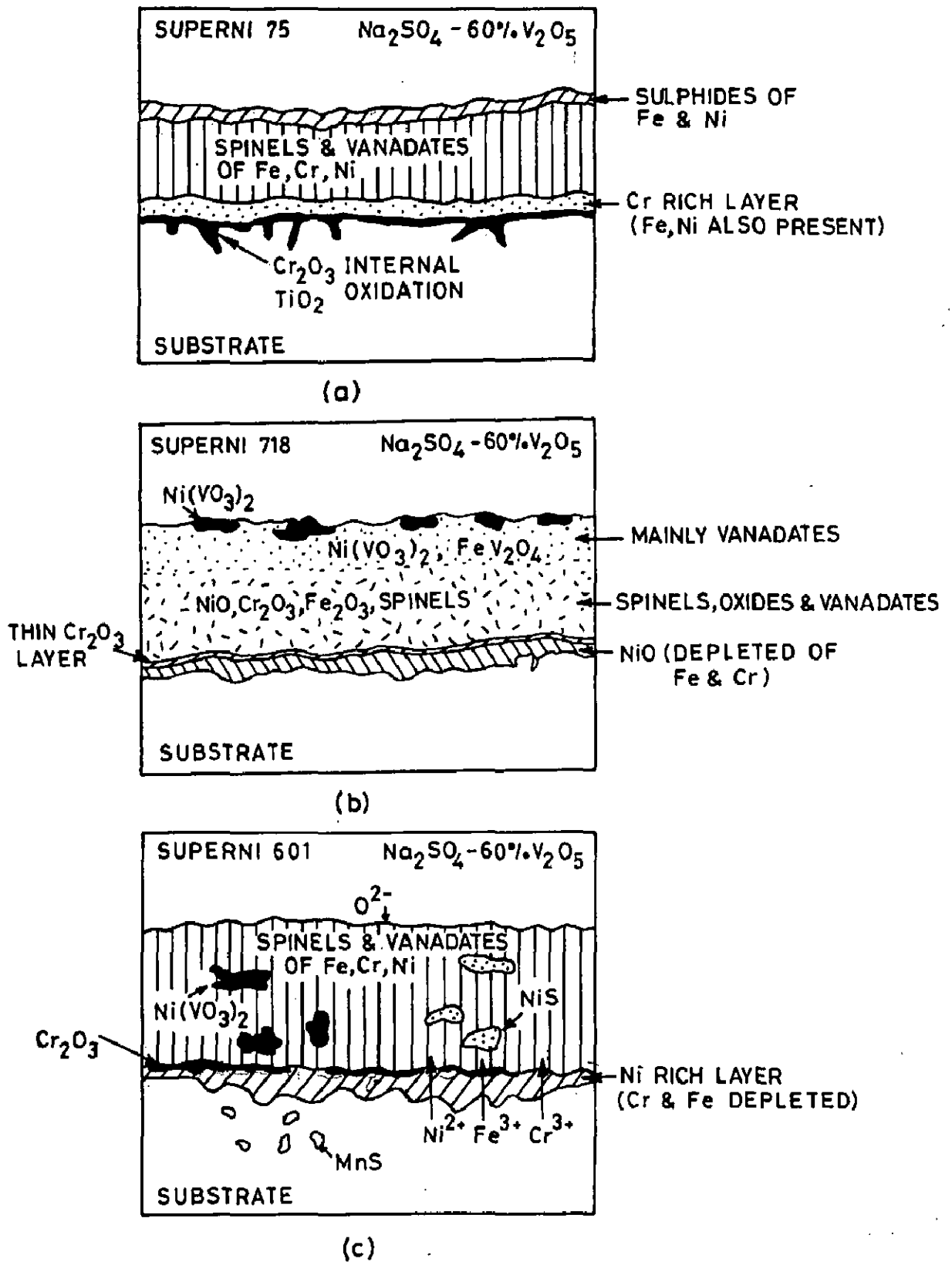
Fig. 6.8: Schematic diagram showing probable hot corrosion mechanism in Na₂SO₄-60%V₂O₅ after exposure for 50 cycles at 900°C for alloys:

(a) Alloy C (Superni 75)

(b) Alloy D (Superni 718)

(c) Alloy E (Superni 601)

235
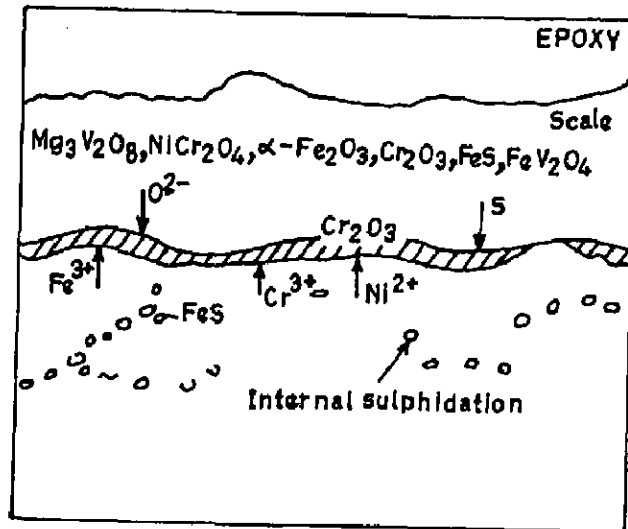
(a)
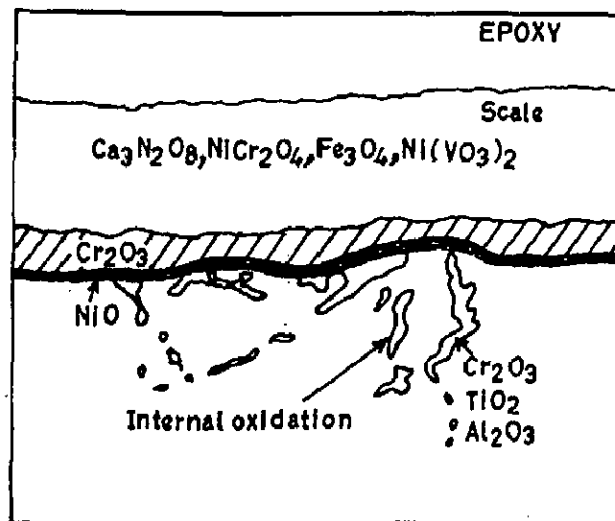
(b)

Fig. 6.9: Schematic diagram showing probable hot corrosion mechanism for alloy A (Superfer 800H) after exposure for 50 cycles at 900^0C in :

(a) Na_2SO_4-60%V_2O_5+MgO

(b) Na_2SO_4-60%V_2O_5+CaO

SUPERCO 605 $Na_2SO_4 - 60\%V_2O_5 + CaO$

O^{2-}

OXIDES

Cr_2O_3, Co_3O_4, WO_3

W RICH PHASE

Cr_2O_3

Ni - RICH LAYER

Co^{2+} Cr^{3+} W^{6+} Ni^{2+}

SUBSTRATE

(a)

SUPERNI 75 $Na_2SO_4 - 60\%V_2O_5 + CaO$

Fe_2O_3

OXIDE SCALE $Ca_3V_2O_8, NiO, Cr_2O_3, NiCr_2O_4, Ni(VO_3)_2, TiO_2$

Cr_2O_3

NiO

SUBSTRATE
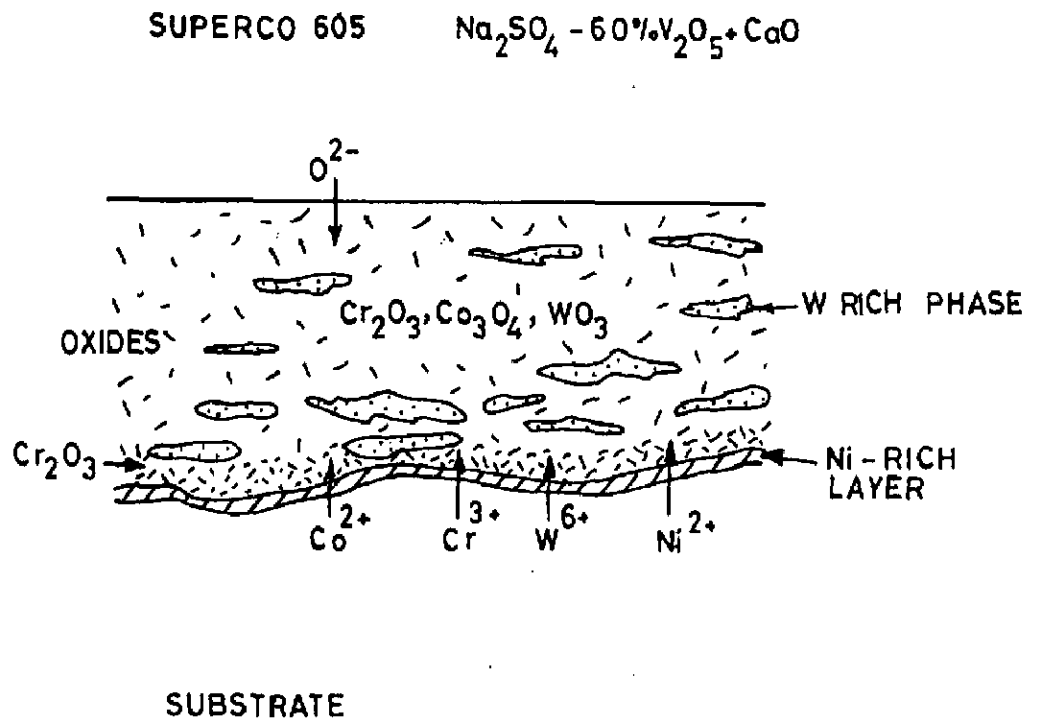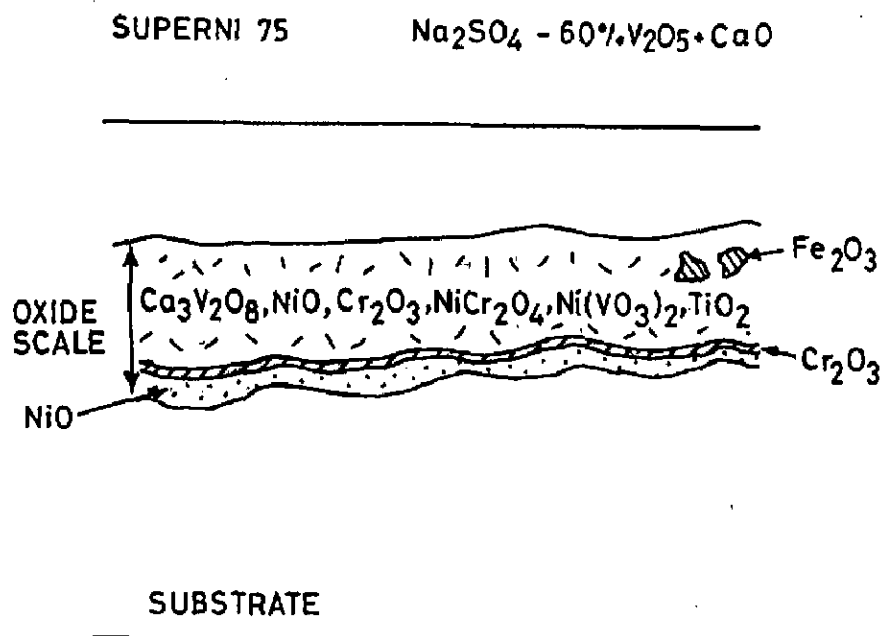
(b)

Fig. 6.10:   Schematic diagram showing probable hot corrosion mechanism in Na_2SO_4-60%V_2O_5+20%CaO after exposure for 50 cycles at 900^{0}C for alloys:

(a) Alloy B (Superco 605)

(b) Alloy C (Superni 75)

SUPERNI 75 $Na_2SO_4 - 60\%V_2O_5 + CeO_2$

SPINELS OF
Ni & Cr

CeVO$_4$

CeO$_2$

CeO$_2$ &
CeVO$_4$

NiO & Cr$_2$O$_3$

DETACHMENT OF SCALE

O^{2-}

$NiO, Cr_2O_3, NiCr_2O_4, Ni(VO_3)_2$

Ni^{2+} Cr^{3+}

SUBSTRATE
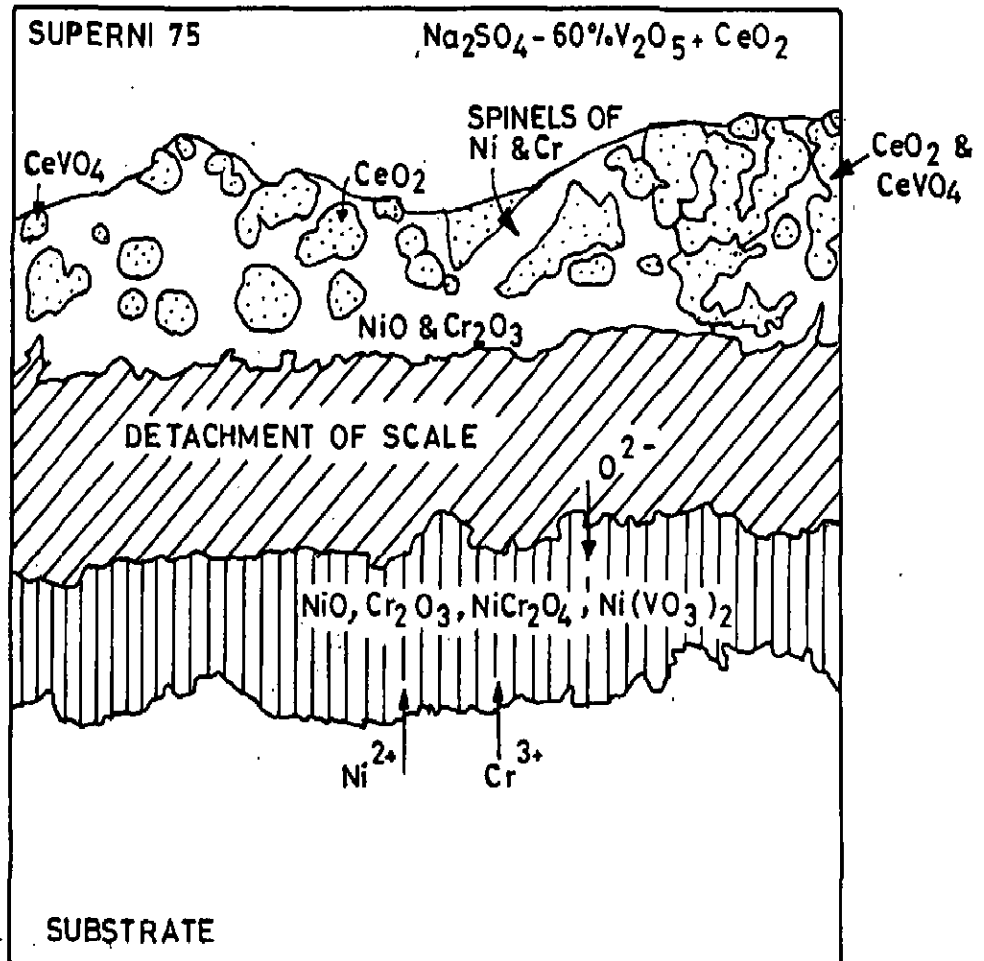
Fig. 6.11:   Schematic representation of the corrosion mechanism in alloy C (Superni 75) with superficially coated ceria after exposure for 50 cycles in Na$_2$SO$_4$-60%V$_2$O$_5$ at 900^{0}C.
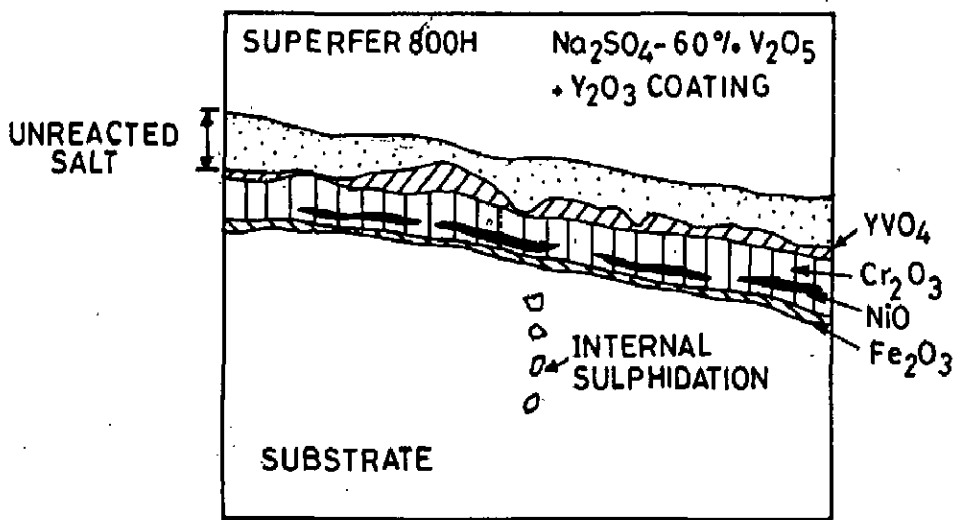
(a)
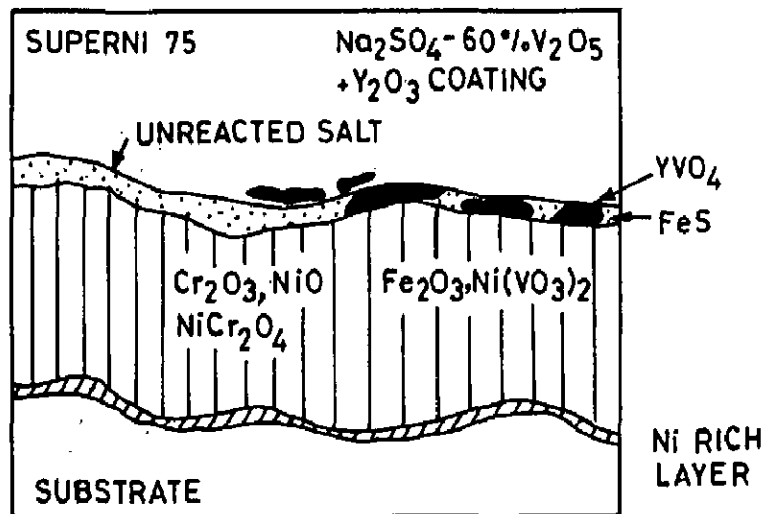
(b)

Fig. 6.12: Schematic diagram showing probable mechanism of hot corrosion with superficially coated Y_2O_3 in Na_2SO_4-60%V_2O_5 environment at 900^0C for:

(a) Alloy A (Superfer 800H)

(b) Alloy C (Superni 75)

SUPERFER 800H $Na_2SO_4 - 60\% V_2O_5 + SnO_2$

SnO₂

UNREACTED SALT

SPINELS OF Fe,Ni,Cr

SPINELS OF Fe,Ni,Cr

$FeV_2O_4, Fe_2O_3, Cr_2O_3$

Cr RICH LAYER

Ni RICH LAYER

Cr_2O_3 INTERNAL OXIDATION

TiO_2

INTERNAL SULPHIDATION

SUBSTRATE

(a)

SUPERNI 601 $Na_2SO_4 - 60\% V_2O_5 + SnO_2$

SnO_2

NiO

OXIDES AND VANADATES OF Fe,Ni AND Cr

Ni RICH ZONE

SUBSTRATE
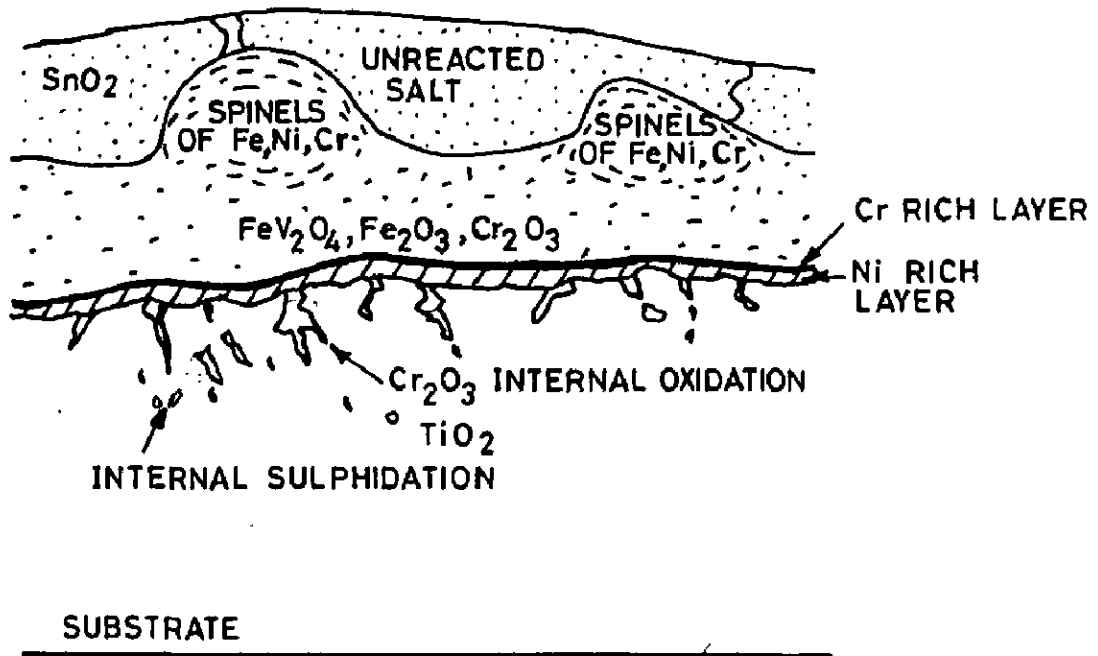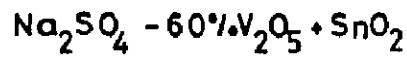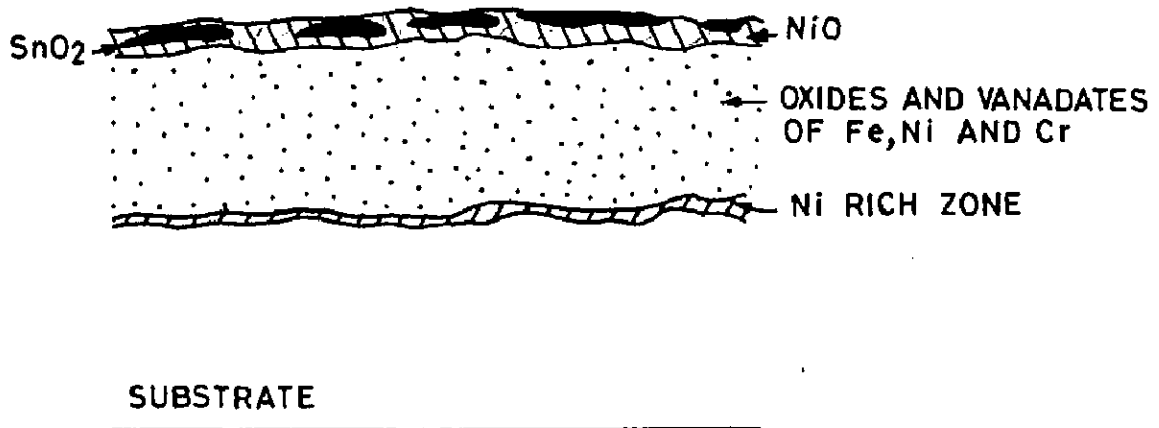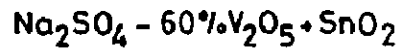
(b)

Fig. 6.13:   Schematic diagram showing development of scale below the superficially coated SnO_2 after exposure in Na_2SO_4-60%V_2O_5 environment for 50 cycles at 900^0C of:

(a) Alloy A (Superfer 800H)

(b) Alloy E (Superni 601)

240
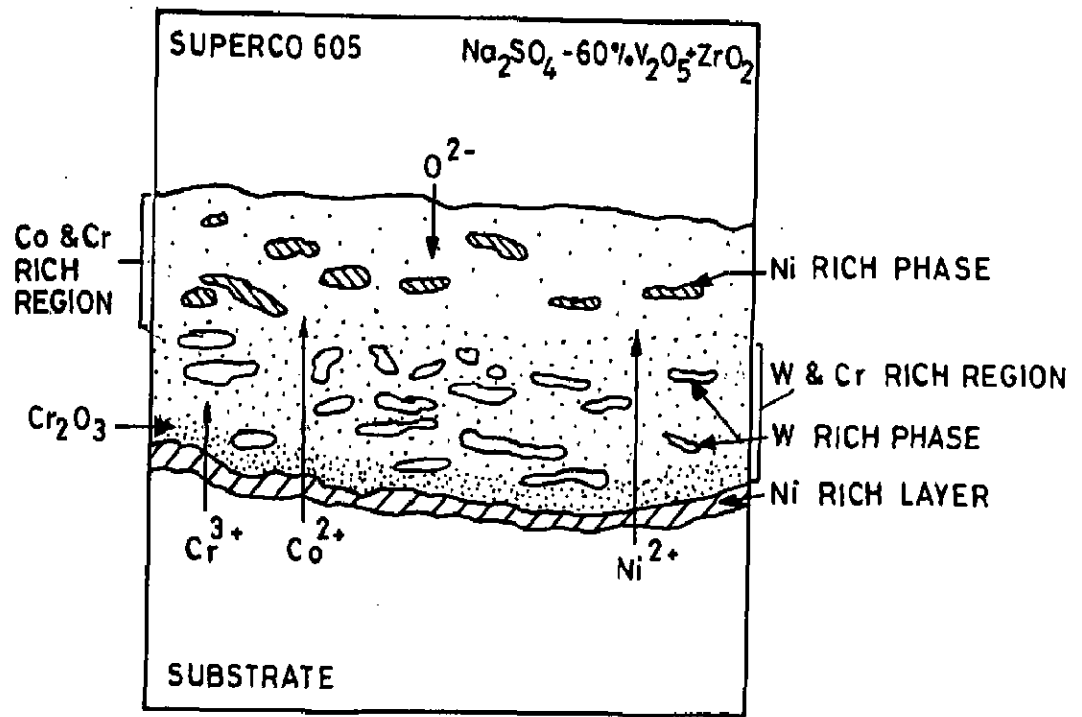
(a)
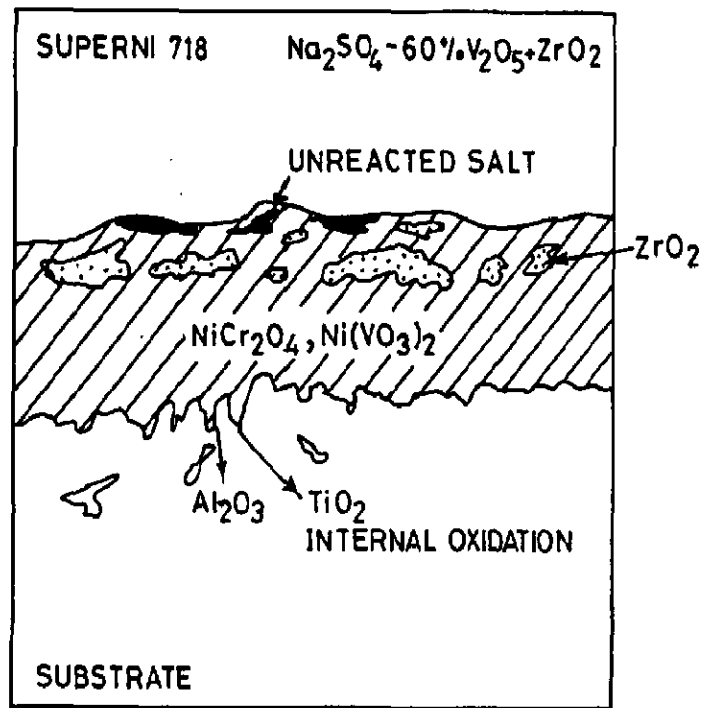
(b)

Fig. 6.14: Schematic representation of the corrosion mechanism with superficially coated ZrO_2 in Na_2SO_4-60%V_2O_5 environment after exposure for 50 cycles at 900^{0}C :
(a) Alloy B (Superco 605)
(b) Alloy D (Superni 718)

CHAPTER 7

CONCLUSIONS

In case of superalloys A (Superfer 800H), B (Superco 605), C (Supermi 75), D (Supermi 718) & E (Supermi 601), the application of inhibitor as a coating /mixture leads to a decrease in overall maximum weight gain (around 30 cycles) as upto 30 cycles there is maximum weight gain in nearly all cases and afterwards there is a weight loss which is contributed by various factors like spalling, volatilization of phases and other complex factors. Scale thickness values (after 50 cycles) indicate that these inhibitors are effective in providing protection to the alloys in aggressive environment of Na_2SO_4-60%V_2O_5.

1. On the basis of the total weight gain measurements (around 30 Cycles), as shown in Fig. 7.1, following conclusions can be drawn:-

    i. In Na_2SO_4-60%V_2O_5, the corrosion rate is significant and follows the trend

    Alloy B> Alloy A > Alloy D > Alloy E > Alloy C

    ii. Addition of MgO in the ratio of 3:1 is effective in all the alloys and the maximum weight gain is nearly half of that of the base alloy without the MgO addition.

    iii. CaO is nearly as effective as MgO in case of alloy E and provides still better protection in alloy C, where as it is having lesser inhibiting effect in case of alloys A, B and D.

    iv. MnO_2 is most effective in alloy D and in other alloys the effect is nearly same as that with CaO. It is least effective in case of alloy E.

    v. $ZnSO_4$ in case of alloy B led to extensive spalling and experimentation had to be terminated. In case of alloy A, it has very less inhibiting effect where as in other alloys C, D & E it has nearly similar extent of beneficial effect.

vi. CeO_2 is most effective in case of alloy C where it has reduced the weight gain to about $1/3^{rd}$. In other alloys the extent of inhibition is nearly same.

vii. Y_2O_3 is most effective in inhibiting corrosion by Na_2SO_4-60%V_2O_5 in all the alloys and it is found to be most beneficial in case of alloy A. Comparatively in alloy D, it is less effective.

viii. SnO_2 is most effective in alloy B whereas in other alloys, the extent of inhibiting effect is similar except in alloy A, Superfer 800H, where it is least effective.

ix. ZrO_2 is most effective in alloy C whereas in alloys E, D and B, inhibiting effect is nearly similar and it is marginally effective in case of alloy A.

2. The addition of MgO as an inhibitor in the ratio 3: MgO :: 1 : V_2O_5 to Na_2SO_4-60%V_2O_5 environment reduced the rate of corrosion of all the alloys at 900^0C. The inhibiting behavior of MgO is due to the formation of $Mg_3V_2O_8$ (m.p. 1190^0C), which has been confirmed by the XRD and EPMA elemental analysis which indicates co-existence of Mg and Vanadium. $Mg_3V_2O_8$ formed is in the solid form at the test temperature so it has contributed to decrease in the corrosion rate. There is indication of Cr-rich band at the alloy/scale interface, which may also be contributing to the lesser extent of reaction. This Cr has come from the substrate that is indicated from the chromium-depleted area at the top of the substrate.

3. CaO is found to be most effective in case of alloy C where scale thickness is around $1/4^{th}$ of that without inhibitor, which is due to the contribution of a distinct continuous Cr_2O_3 layer and formation of solid calcium vanadate. In alloy D, there is further penetration of the scale into the substrate. Presence of continuous layer of Cr_2O_3 at the interface between the scale and the substrate and formation of calcium vanadate similar to Mg-vanadate may be the reason for inhibiting behaviour in alloys A, C, D and E identified by XRD and EPMA. Marginal reduction in alloy B may be due to inner Cr_2O_3 layer. Calcium vanadate could not be detected by XRD.

4. Reduction in weight and scale thickness of all the alloys confirms the inhibiting effect of the MnO_2 additions. In alloy A, Cr- rich continuous scale at the interface may be

contributing to lesser extent. In Alloy B, there is triplex scale, upper layer is Cr-rich, middle layer is containing W and Ni and bottom layer is Ni-rich. There is a presence of MnS just below the interface indicating ingress of S which is further confirmed by EDAX. In alloys C, D and E, there is indication of formation of vanadates and a Cr-rich layer just above the interface. In case of alloy D, presence of a typical Cr-rich continuous band may be contributing to lesser extent of attack. Ti is present along the interface, which might be helping in interlocking the scale to the substrate.

5. $ZnSO_4$ addition has shown very marginal effect on the reduction in corrosion rate for all the alloys. In case of alloys A, C and D, Cr_2O_3 layer has formed just above the substrate but internal oxidation is indicated. In alloy A (Superfer 800H) Al has got oxidised at the interface and in alloy C, (Superni 75) Ti has internally oxidised along the grain boundaries. In case of alloy D (Superni 718), both Al and Ti have oxidised where as in alloy E (Superni 601), there is a thin Cr-rich irregular layer just above the substrate, which is not continuous, and perhaps it is not able to provide protection leading to internal oxidation. Scale penetrates into the substrate where Al has got internally oxidised.

6. In case of superficially coated ceria, the main reasons for reducing the attack of corrosive environment in alloys C, D and E may be the presence of unreacted CeO_2 on the surface. Presence of Cr_2O_3 layer in the scale and very high concentrated Cr_2O_3 thin layer above the substrate /scale interface may also be a contributing factor for the protection of these alloys. CeO_2 coated alloy B i.e. Superco 605 gave the thinnest scale. Presence of Cr_2O_3 thin layer near the substrate may be contributing to lowering of the extent of corrosion. Ceria has been identified on the top of the scale in alloys A, B and E by SEM/EDAX analysis. The presence of this ceria might have also led to better adhesion of the scale and affected the scale growth mechanism. Internal oxidation of silicon in alloy A has been observed by EPMA and these internal oxide stringers may be contributing to better adhesion of the scale. Similar observation has also been reported by Roy et al (1995). The formation of $CeVO_4$ could not be confirmed by XRD whereas both Ce & V are co-existing in the scale of all the alloys.

7. Y_2O_3 superficial coating has decreased the reaction rate of Na_2SO_4-$60\%V_2O_5$ environment for all the alloys and has been observed to be most effective in alloy A. In case of alloys A & E, Y & V are co-existing in EPMA elemental X-ray images but XRD does not confirm the formation of YVO_4. This phase if formed has a melting point of 1810^0C, so it would be a solid phase developed at the 900^0C and could be one of the contributing factor for the inhibiting behaviour observed with Y_2O_3 coating in Na_2SO_4-$60\%V_2O_5$ environment. Jones et al (1986) have also observed the formation of YVO_4 and have opined that it was not generally possible to identify reaction co-products by X-ray diffraction. There is distinct presence of Cr_2O_3 rich layer as a band just above the substrate/scale interface in alloys A & E. Whereas Cr_2O_3 is present with Fe and Ni in the scales of alloys C & D and in Co-base alloy co-existing with Co, W, Fe and small percentage of Ni. Y_2O_3 seems to be contributing to better adhesion of the scale as least spalling is noticed in all the alloys with Y_2O_3 as inhibitor. Further applied coating is observed to be intact in most of the areas for all the alloys except alloy D. But EDAX analysis of alloy D revealed the presence of Y on the top of the scale. There is ingress of S to the substrate in all the alloys. Unreacted salt is also indicated at the top of the scale in alloys A, B, C and E.

8. SnO_2 is effective in reducing the scale thickness to nearly half for alloys A & C where as for alloys B & D effect is similar but it has failed to provide any protection in case of alloy E (Superni 601) and led to slightly thicker scale. The effectiveness of the SnO_2 is perhaps due to its non-reactive nature with the corroding species and high melting point (1630^0C). The better inhibiting behaviour in case of alloy B, may also be ascribed to band type Cr rich thick layer present just above the substrate. In case of alloy E i.e Superni 601, unreacted SnO_2 is present on the top of the scale even after the reaction but this layer is not continuous and scale has developed beneath it. This scale mostly consists of Cr, Fe, Ni and V and it gives indication of formation of vanadates. Vanadates of Fe and Ni have been identified by XRD other than formation of $NiCr_2O_4$, Cr_2O_3 rich band above the substrate is not observed.

9. Superficial application of ZrO_2 has probably improved the adherence of scale in alloys C and D, indicated by minimum spalling and presence of unreacted Na_2SO_4-V_2O_5 on the surface. Zr and V co-exist in the scales of alloys C and D as indicated by EPMA and EDAX but formation of ZrV_2O_7 is not confirmed by XRD. Cr rich layer is present in both the alloys, which may also be contributing to reduced reaction rates. Alloy A (Superfer 800H) developed a thick scale, which mainly consisted of Fe, Cr and Ni. Cr has diffused from the substrate to form chromium oxide layer leading to enrichment of nickel in the substrate. There is indication of internal oxidation. In alloy B, outer scale consists of Cr, Co and Ni where as inner scale is rich in tungsten and chromium. There is a Cr rich layer just above the interface and in the substrate there is a Ni-rich layer. In case of alloy E a single layer scale with prominent internal oxidation along the grain boundaries of the substrate alloy is indicated. Presence of Ni, Cr and Fe along with V, Al and S in the scale is evident from their corresponding X-ray images and EDAX analysis. The scale is rich in Cr & Fe. FeV_2O_4, $NiCr_2O_4$, NiO, Fe_2O_3 and Cr_2O_3 have been detected by the X-ray diffraction analysis. Chromium and aluminum have oxidised along the grain boundaries. X-ray mapping for Zr has shown that it is present on top of the scale at two spots having very low concentration.

10. Among the superalloys, alloy C i.e. Superni 75 gave the best resistance to attack by Na_2SO_4-60%V_2O_5 and nearly all the inhibitors specially MgO, CaO, CeO_2, SnO_2, ZrO_2, and Y_2O_3 are the most effective for inhibiting the hot corrosion in the above environment. The Superco-605 has been found to have least resistance to the given environment and also inhibiting effect is comparatively less in case of all inhibitors used. In case of $ZnSO_4$ it was deleterious and led to vigorous attack even in the initial stage of hot corrosion and led to the stoppage of the experimentation.

11. In Co-base alloy internal oxidation has not been observed in almost all the environments but the scale formed shows distinct layers such as Cr-rich, Ni-rich and W-rich areas. W rich areas are present as elongated streaks mostly as a middle layer as revealed by EPMA micrographs of Co-base alloys in various environments.

12. Hot corrosion products observed in the scale of these alloys are mostly oxides of the elements present in the alloy. Internal oxides mainly indicated oxides of Ti and Al in alloy A, Ti along grain boundaries in alloy C and again Ti and Al in alloys D and E. Internal sulphidation of Mn is indicated in alloys A and B as Mn and S are present together as revealed by EPMA.

13. Oxides of Fe, Ni and Co react with Cr_2O_3 to form spinels of composition MCr_2O_4. As XRD identified the formation of such phases e.g $FeCr_2O_4$, $NiFe_2O_4$, $NiCr_2O_4$ and $CoCr_2O_4$ in Fe, Ni and Co-base alloys respectively.

14. Most beneficial effect of superficial coatings of CeO_2, Y_2O_3, SnO_2 and ZrO_2 is the considerable improvement in scale adherence to alloy substrate as minimum spalling was observed with these coatings and even the coating remained intact in most of superficially coated samples which has been confirmed from visual observations and optical macrographs.

15. All the Ni-base alloys have shown superior corrosion resistance as compared to Fe- and Co base alloys because these alloys form larger amount of refractory nickel vanadate, $Ni(VO_3)_2$ which acts as a diffusion barrier for the oxidizing species as reported by Seierstein and Kofstad, 1987. Formation of $Ni(VO_3)_2$ has been identified by XRD and even revealed by EPMA.

16. As could be seen from the EPMA micrographs, the presence of continuous Cr_2O_3 layer at the substrate /scale interface is predominantly seen in most of the alloys where weight gain and scale thickness has been very less. In all the cases where continuous Cr_2O_3 layer has formed, there is depletion of chromium in the substrate which indicates the outward transport of Cr. This Cr_2O_3 layer further stops the movement of cations /anions thereby inhibiting the further reaction.
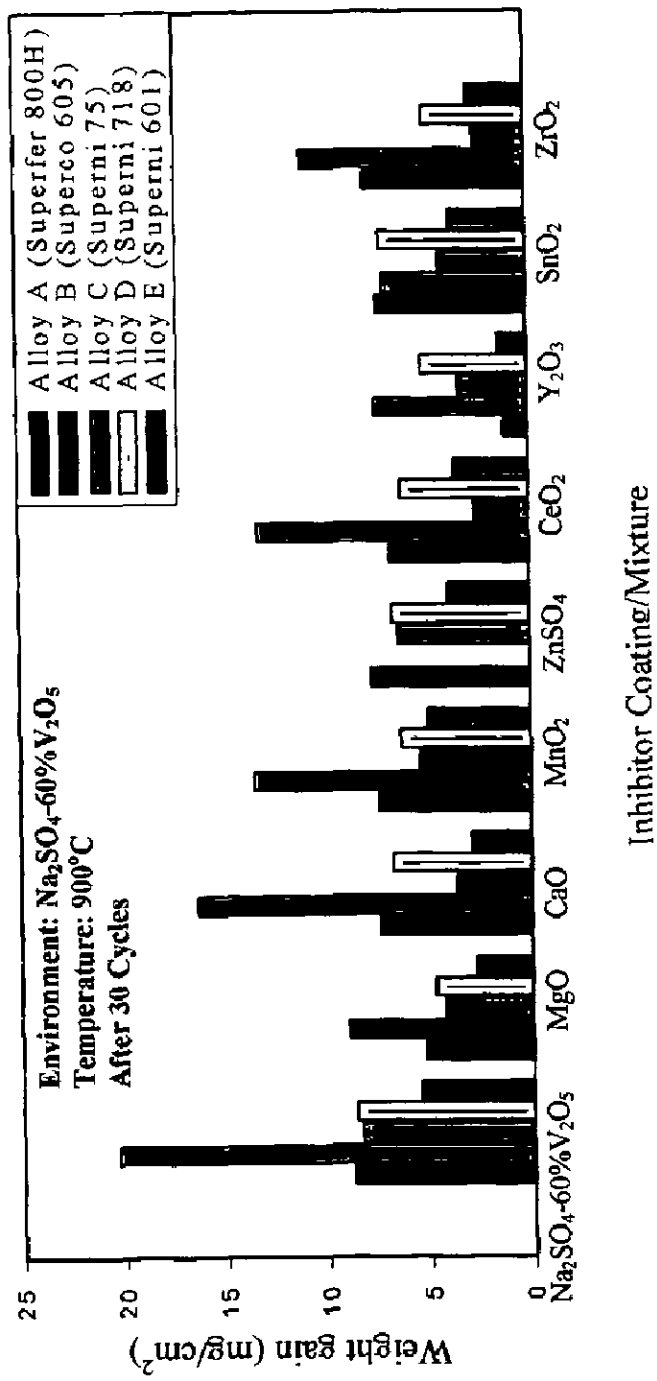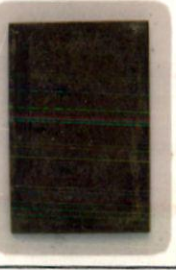
Fig. 7.1 : Weight Change plot for alloys : alloy A (Superfer 800H), alloy B (Suuperco 605), alloy C (Superni 75), Alloy D (Superni 718) and alloy E(Superni 601) after exposure for 30 cycles in salt mixtures and superficially applied coatings at 900°C.
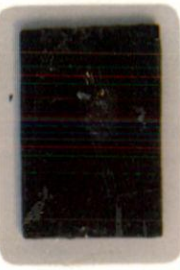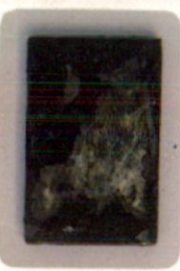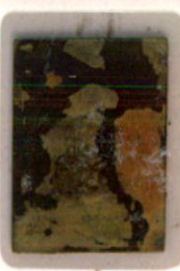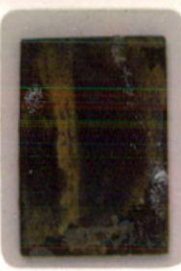
SUGGESTIONS FOR FUTURE WORK

1. Hot corrosion tests with inhibitor coatings in burner rig set up as well as in actual industrial environment for longer duration preferably 1000 hours should be carried out to predict the performance of inhibitors in actual service conditions.

2. It is important to investigate the mode of application of these inhibitors on the boiler tubes in the areas prone to molten salt corrosion.

3. Detailed study can be made with one alloy and one type of inhibitor exposed to aggressive environment for different lengths of time so that progressive development of the scale can be studied and mechanism of transport of species and gradual development of the scale can be understood.

4. Hot stage microscopy can also be used to follow the development of the scale throughout the hot corrosion run.

5. To have better insight into the behaviour of superficially applied oxides and mixed in aggressive environment, reactions between oxides and Na_2SO_4-V_2O_5 should be studied in more detail.

6. Effect of adding 10wt.% $ZnSO_4$ to Na_2SO_4-60%V_2O_5 on Co-base superalloy should be studied in detail to understand the mechanism of sputtering and spalling of the scale.

7. An insight into cost effectiveness of applying the inhibitors is needed.

8. Effect of other oxides like BaO, In_2O_3, Cr_2O_3, Al_2O_3, PbO etc. should also be tried.

Environment	ALLOY A	ALLOY B	ALLOY C	ALLOY D	ALLOY E
Na_2SO_4-60%V_2O_5					
Na_2SO_4-60%V_2O_5 +MgO (MgO:V_2O_5::3:1)					
Na_2SO_4-60%V_2O_5 +20% CaO					
Na_2SO_4-60%V_2O_5 +20% MnO_2					
Na_2SO_4-60%V_2O_5 +10% $ZnSO_4$					

Fig.A.1:   Macrographs of alloy A (Superfer 800H), alloy B(Superco 605) , alloy C (Superni 75), alloy D (Superni 718) and alloy E (Superni 601) exposed to different salt mixtures after exposure at 900^0C for 50 cycles.

Environment	ALLOY A	ALLOY B	ALLOY C	ALLOY D	ALLOY E
Na_2SO_4-60%V_2O_5 +CeO_2 Coating					
Na_2SO_4-60%V_2O_5 +Y_2O_3 Coating					
Na_2SO_4-60%V_2O_5 + SnO_2 Coating					
Na_2SO_4-60%V_2O_5 +ZrO_2 Coating					

Fig.A.2: Macrographs of alloy A (Superfer 800H), alloy B(Superco 605) , alloy C (Superni 75), alloy D (Superni 718) and alloy E (Superni 601) with superficially applied oxides (CeO_2, Y_2O_3, SnO_2 and ZrO_2) and then exposed to Na_2SO_4-60%V_2O_5 at 900^0C for 50 cycles.
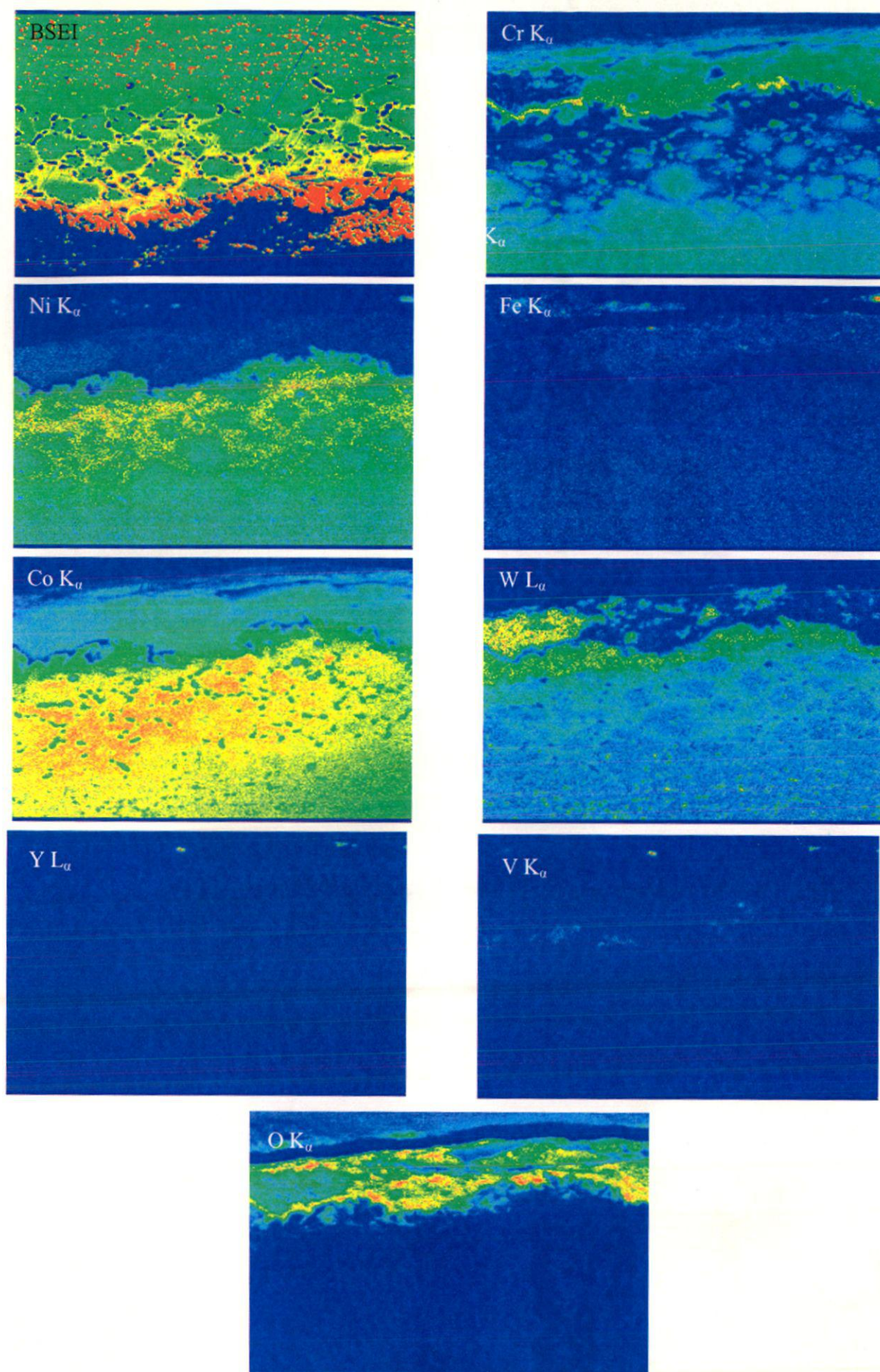
Fig. A.3: BSEI and X-ray mapping of the cross section of alloy B (Superco 605) after cyclic hot corrosion at 900^0C in Na_2SO_4-60% V_2O_5 + Y_2O_3. (X 1600)
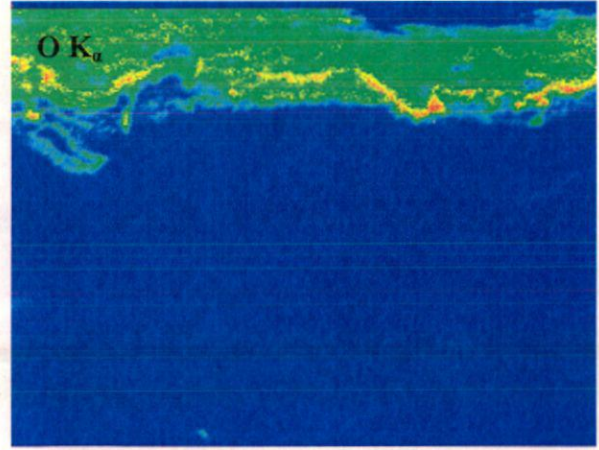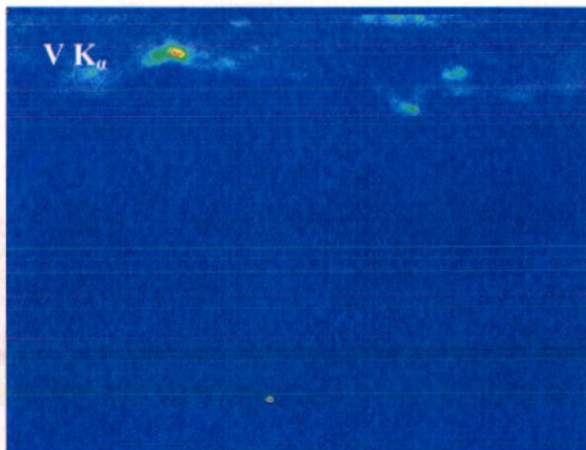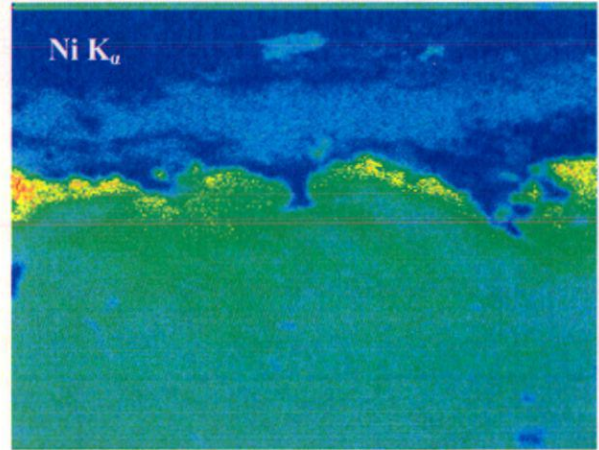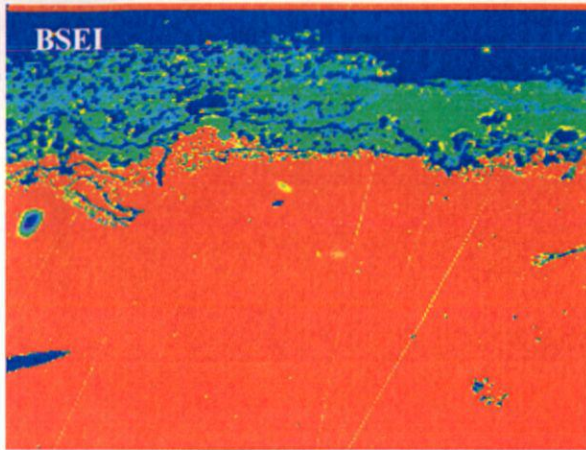
Fig. A.4:   BSEI and X-ray mapping of the cross section of alloy D (Superni 718) after cyclic hot corrosion at 900^0C in Na_2SO_4-60% V_2O_5 + Y_2O_3. (X 800)
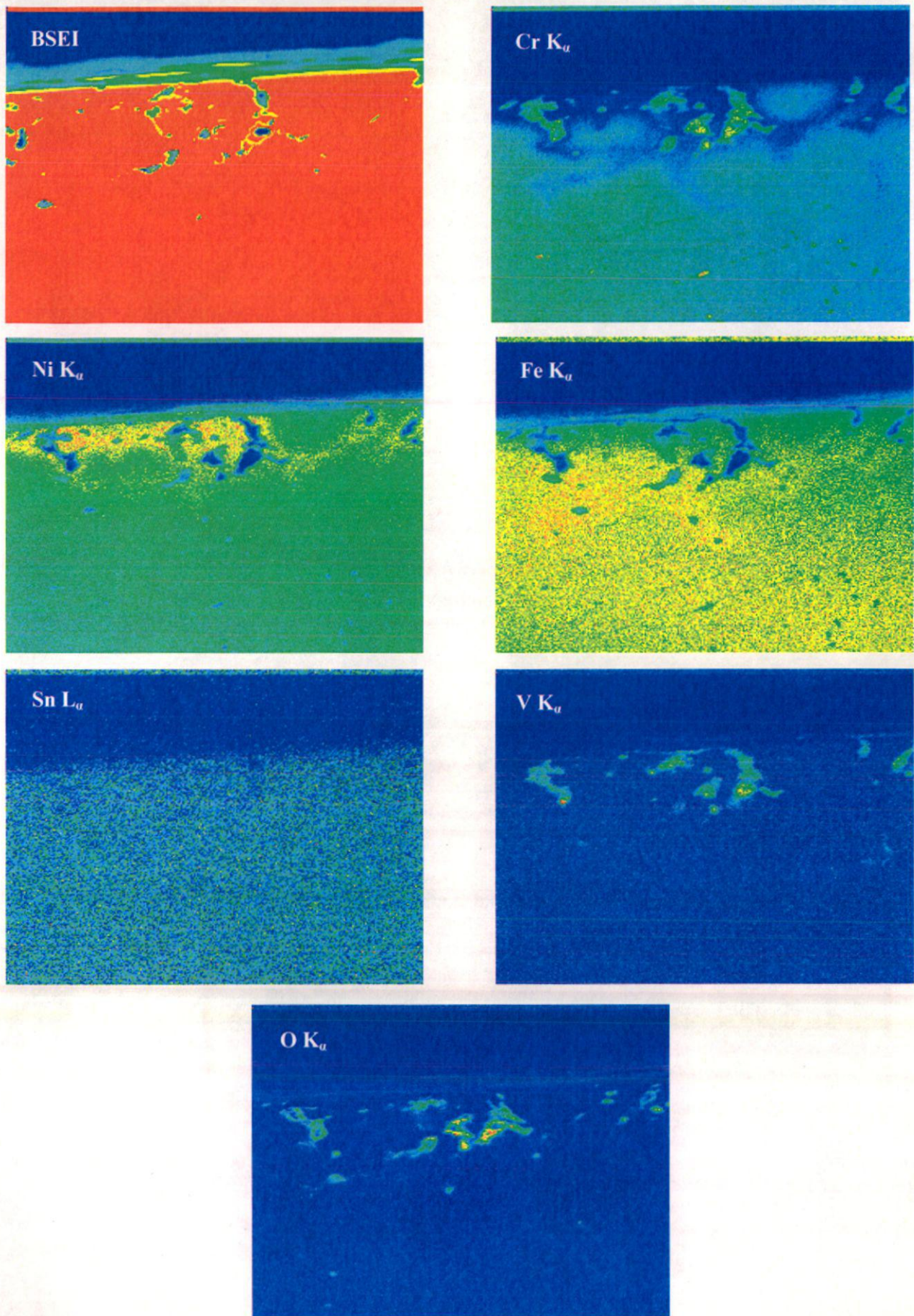
Fig. A.5: BSEI and X-ray mapping of the cross section of alloy A (Superfer 800H) after cyclic hot corrosion at 900^0C in Na_2SO_4-$60\%V_2O_5$+SnO_2 (X 1250)
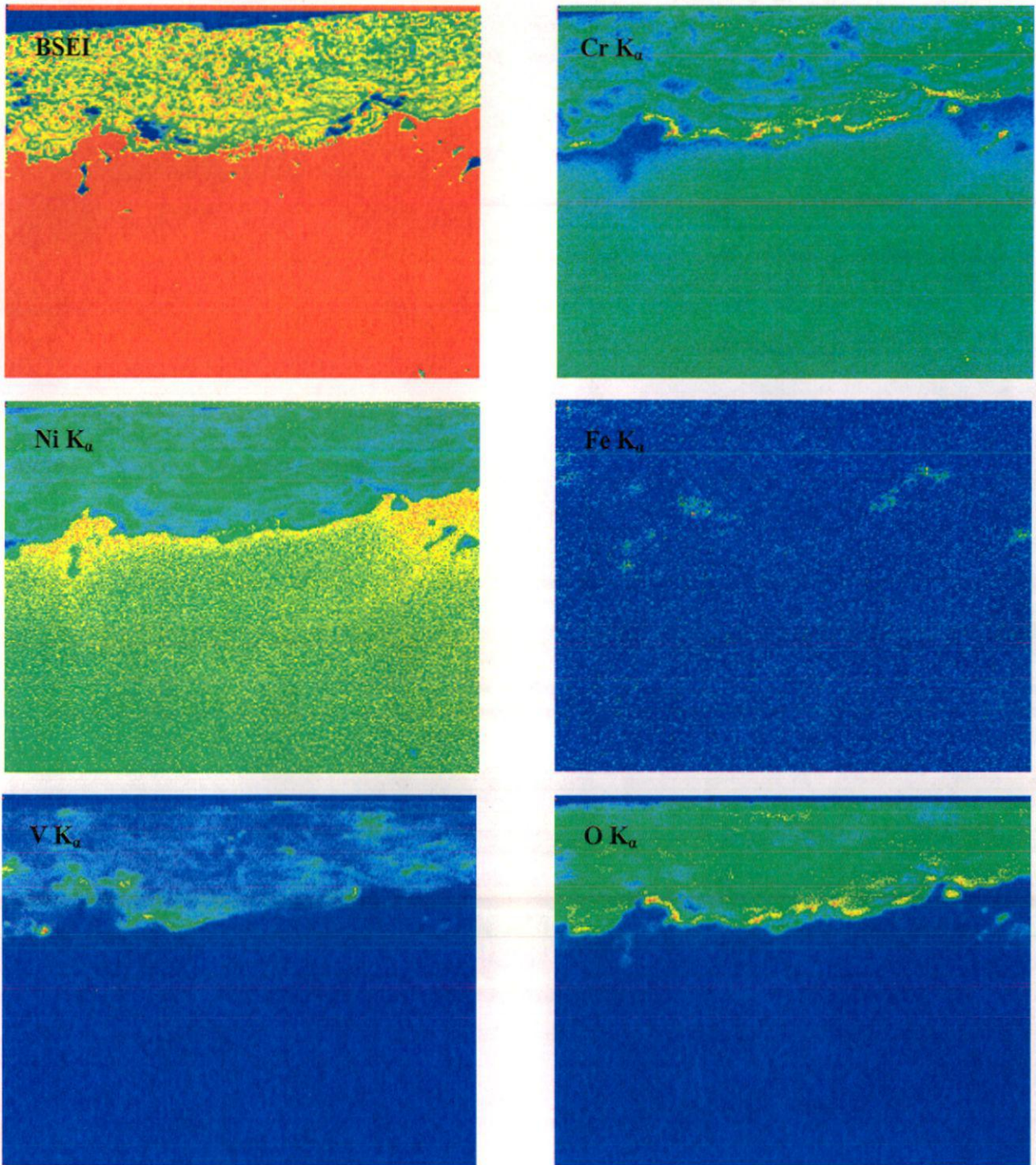
Fig. A.6: BSEI and X-ray mapping of the cross section of alloy C (Superni 75) after cyclic hot corrosion at 900^0C in Na_2SO_4-60% V_2O_5 + SnO_2. (X 1600)
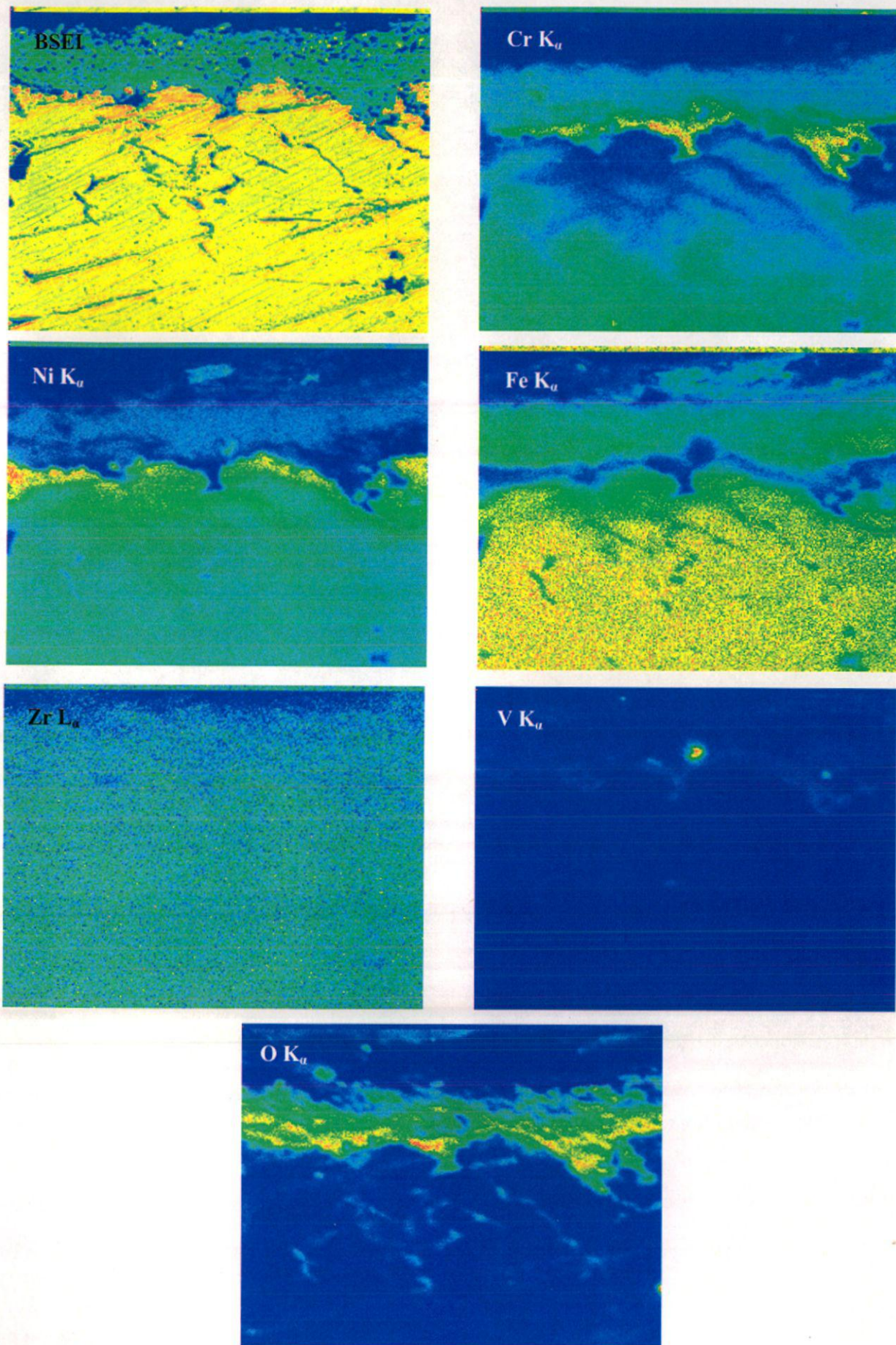
Fig. A.7   BSEI and X-ray mapping of the cross section of alloy A (Superfer 800H) after cyclic hot corrosion at 900^0C in Na_2SO_4-60% V_2O_5 +ZrO_2 (X 1600)
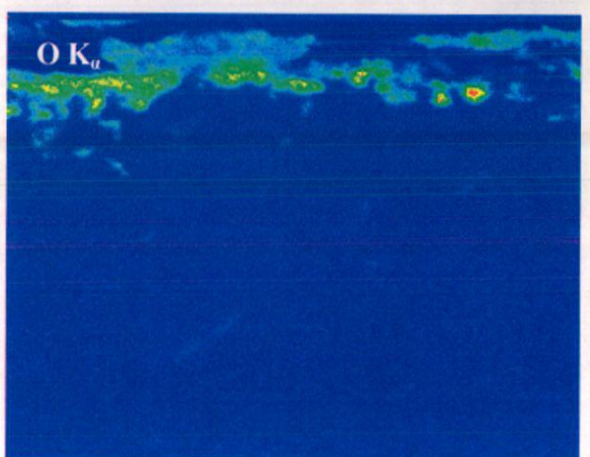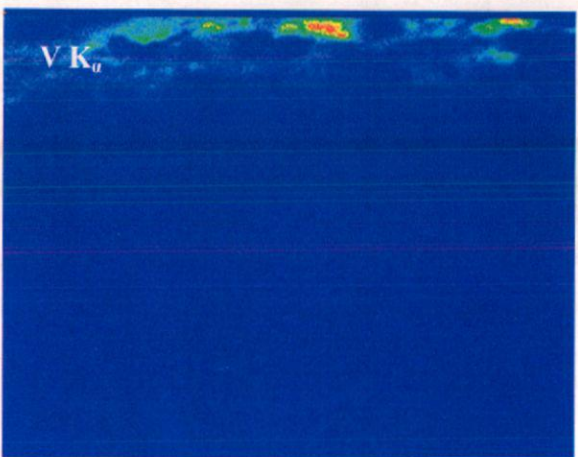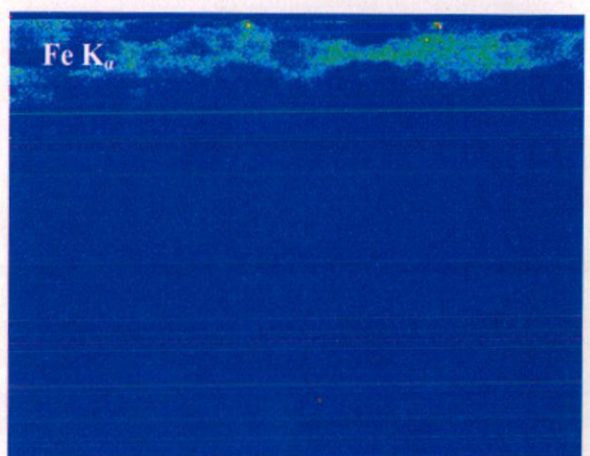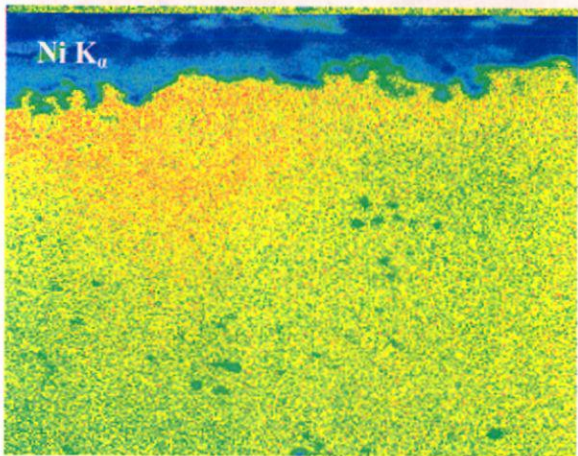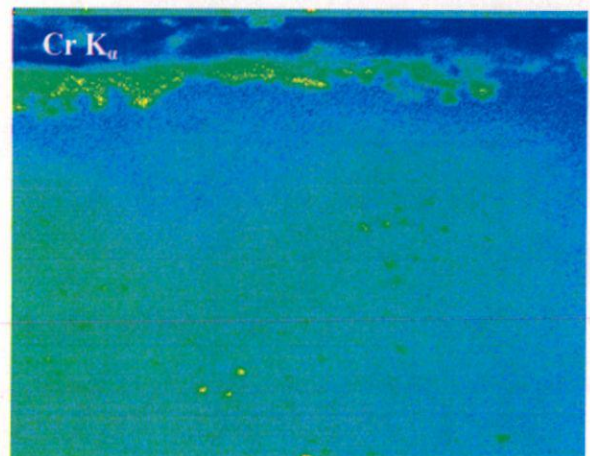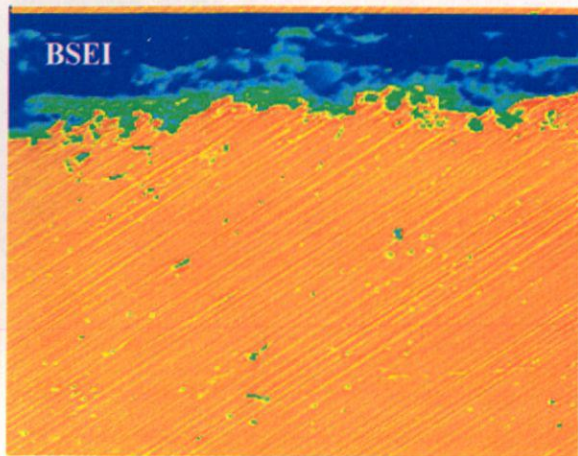
Fig. A.8: BSEI and X-ray mapping of the cross section of alloy C (Superni 75) after cyclic hot corrosion at 900^0C in Na_2SO_4-60% V_2O_5 + ZrO_2. (X 1600)

Table A.1: XRD Analysis for Alloy A (Superfer 800H) After Exposure for 50 Cycles at 900^0C in Na_2SO_4-60%V_2O_5.

S.No.	"d" Values	Phases Identified
1	2.9558	FeV_2O_4,$NiCr_2O_4$
2	2.5257	α-Fe_2O_3, FeV_2O_4, $NiCr_2O_4$, $NiFe_2O_4$,Cr_2O_3
3	2.1103	α-Fe_2O_3, FeV_2O_4
4	1.7137	α-Fe_2O_3, FeV_2O_4
5	1.6189	FeV_2O_4, $NiCr_2O_4$, $NiFe_2O_4$, Cr_2O_3
6	1.4864	α-Fe_2O_3, $NiCr_2O_4$, $NiFe_2O_4$, Cr_2O_3
7	1.2765	α-Fe_2O_3, Cr_2O_3
8	1.0870	α-Fe_2O_3, Cr_2O_3

Table A.2: XRD Analysis for Alloy B (Superco 605) After Hot Corrosion for 50 Cycles at 900^0C in Na_2SO_4-60%V_2O_5.

S.No.	"d" Values	Phases Identified
1	3.7035	Cr_2O_3
2	2.8996	$NiWO_4$, $NiCo_2O_4$, Co_3O_4
3	2.4785	$NiWO_4$, Cr_2O_3, $NiCo_2O_4$, $CoCr_2O_4$
4	2.4267	CoO, Co_3O_4, NiO
5	2.1009	CoO,Cr_2O_3, $Co_3V_2O_8$, NiO
6	2.0555	$Co_3V_2O_8$, CoO, Cr_2O_3
7	1.6732	$NiWO_4$, WO_3
8	1.5808	$CoCr_2O_4$
9	1.4907	CoO, $CoCr_2O_4$, NiO
10	1.4530	CoO, $Co_3V_2O_8$, Co_3O_4, $NiCo_2O_4$

Table A.3: XRD Analysis for Nickel Base Alloys: Alloy C (Superni 75), Alloy D (Superni 718) & Alloy E (Superni 601) After Exposure for 50 Cycles at 900^0C in Na_2SO_4-$60\%V_2O_5$.

S. No.	Alloy	"d" values	Phases Identified
1		2.9088	$Ni(VO_3)_2$, $NiCr_2O_4$
2		2.4785	$NiCr_2O_4$,$NiFe_2O_4$,$Ni(VO_3)_2$, Cr_2O_3
3		2.3893	NiO
4	Alloy C	2.0734	$Ni(VO_3)_2$, Cr_2O_3
5	(Superni 75)	1.6903	$NiFe_2O_4$, $Ni(VO_3)_2$, Cr_2O_3
6		1.5933	$NiFe_2O_4$, $NiCr_2O_4$, Cr_2O_3,
7		1.4695	$NiCr_2O_4$, Cr_2O_3, NiO
8		1.2606	$NiCr_2O_4$, NiO, Cr_2O_3
9		1.0768	$NiCr_2O_4$, Cr_2O_3
1		3.7035	$(Cr,Fe)_2O_3$
2		2.8996	$Ni(VO_3)_2$, α-Fe_2O_3, FeV_2O_4
3		2.4785	NiO, $NiCr_2O_4$, α-Fe_2O_3, $Ni(VO_3)_2$, Cr_2O_3
4		2.4267	NiO, $Ni(VO_3)_2$
5	Alloy D	2.1009	NiO,Cr_2O_3
6	(Superni 718)	2.0555	NiO, $NiCr_2O_4$,FeV_2O_4
7		1.6732	$NiCr_2O_4$,FeV_2O_4, $(Cr,Fe)_2O_3$, α-Fe_2O_3
8		1.5808	$NiCr_2O_4$,FeV_2O_4, Cr_2O_3
9		1.4907	$(Cr,Fe)_2O_3$,NiO,$NiCr_2O_4$, Cr_2O_3
10		1.4531	NiO, FeV_2O_4, α-Fe_2O_3, Cr_2O_3
1		2.9368	$NiCr_2O_4$,FeV_2O_4, α-Fe_2O_3
2		2.5052	$Ni(VO_3)_2$, $NiCr_2O_4$, $NiFe_2O_4$, FeV_2O_4, Cr_2O_3
3		2.4016	NiO
4		2.0779	$Ni(VO_3)_2$,NiO, FeV_2O_4, Cr_2O_3
5		1.6961	$NiCr_2O_4$ $Ni(VO_3)_2$, $(Cr,Fe)_2O_3$
6	Alloy E	1.6009	$NiCr_2O_4$, $NiFe_2O_4$, $(Cr,Fe)_2O_3$, Cr_2O_3
7	(Superni 601)	1.4674	$NiCr_2O_4$, $NiFe_2O_4$, FeV_2O_4, NiO, Cr_2O_3
8		1.2648	$NiCr_2O_4$,NiO, $(Cr,Fe)_2O_3$, FeV_2O_4, Cr_2O_3
9		1.0796	$NiCr_2O_4$, Cr_2O_3

Table A.4: XRD Analysis for Alloy A (Superfer 800H) After Exposure for 40 Cycles at 900^0C in Na_2SO_4-60%V_2O_5+MgO.

S.No.	"d" Values	Phase Identified
1	4.8161	$Mg_3V_2O_8$, $NiCr_2O_4$
2	3.0143	Fe_2O_3,$Mg_3V_2O_8$, FeV_2O_4, Cr_2O_3
3	2.9750	Fe_2O_3, $Mg_3V_2O_8$,FeV_2O_4,FeS, $NiCr_2O_4$,
4	2.5465	Cr_2O_3, FeV_2O_4, Fe_3O_4, $Mg_3V_2O_8$
5	2.4394	Fe_2O_3,$NiCr_2O_4$, $Mg_3V_2O_8$, Cr_2O_3
6	2.0963	$NiCr_2O_4$, $Mg_3V_2O_8$,FeS, Cr_2O_3
7	1.7196	Fe_2O_3, Cr_2O_3, FeS
8	1.6189	Fe_2O_3, Cr_2O_3, $NiCr_2O_4$
9	1.4864	$Mg_3V_2O_8$, Cr_2O_3, $NiCr_2O_4$

Table A.5: XRD Analysis for Alloy B (Superco 605) After Exposure for 50 Cycles at 900^0C in Na_2SO_4-60%V_2O_5+MgO.

S.No.	"d" Values	Phase Identified
1	2.3651	CoV_3, NiO
2	2.0555	Cr_2O_3, $Co_3V_2O_8$, NiO, CoV_3
3	1.4737	NiO, $Co_3V_2O_8$, Cr_2O_3
4	1.2563	Cr_2O_3, CoV_3
5	0.9882	NiO,CoV_3, Cr_2O_3
6	0.9400	NiO, Cr_2O_3

Table A.6: XRD Analysis for Nickel Base Alloys: Alloy C (Superni 75), Alloy D (Superni 718) & Alloy E (Superni 601) After Exposure for 50 Cycles at 900^0C in Na_2SO_4-60%V_2O_5+MgO.

S. No.	Alloy	"d" values	Phase Identified
1		2.9368	$NiCr_2O_4$, $Ni(VO_3)_2$, Cr_2O_3
2		2.6641	FeS, Cr_2O_3
3		2.4918	$Ni(VO_3)_2$, $NiCr_2O_4$, $Mg_3V_2O_8$,TiO_2
4	Alloy C	2.3893	NiO, $Mg_3V_2O_8$
5	(Superni 75)	2.0734	$Ni(VO_3)_2$,NiO, $Mg_3V_2O_8$, FeS,Cr_2O_3 $NiCr_2O_4$,
6		1.5983	Cr_2O_3, $NiCr_2O_4$
7		1.4695	$NiCr_2O_4$, $Mg_3V_2O_8$, NiO
8		1.2677	$NiCr_2O_4$,NiO
1		3.7035	$NiCr_2O_4$
2		2.9751	$Ni(VO_3)_2$, $NiCr_2O_4$, $Mg_3V_2O_8$, FeV_2O_4, FeS
3	Alloy D	2.5052	$NiCr_2O_4$, $Mg_3V_2O_8$,FeV_2O_4,NiO, $Ni(VO_3)_2$
4	Superni 718	2.0917	$NiCr_2O_4$, $Mg_3V_2O_8$,,NiO, FeV_2O_4, FeS,Cr_2O_3
5		1.6085	$NiCr_2O_4$,NiO, FeV_2O_4, α-Fe_2O_3, Cr_2O_3
6		1.4779	$NiCr_2O_4$, α-Fe_2O_3, $Mg_3V_2O_8$, FeV_2O_4,Cr_2O_3, NiO
1		2.9558	Cr_2O_3, $Ni(VO_3)_2$, FeV_2O_4, $Mg_3V_2O_8$, $NiCr_2O_4$, FeS
2		2.5188	$NiFe_2O_4$, $Ni(VO_3)_2$, $NiCr_2O_4$, FeV_2O_4, $Mg_3V_2O_8$
3	Alloy E	2.4267	NiO, $Mg_3V_2O_8$,
4	Superni 601	2.0825	Cr_2O_3, NiO, $Mg_3V_2O_8$, $Ni(VO_3)_2$,FeV_2O_4,FeS
5		1.6034	Cr_2O_3, NiO, $NiCr_2O_4$, $NiFe_2O_4$, FeV_2O_4
6		1.4716	NiO, $Mg_3V_2O_8$, $NiCr_2O_4$, $NiFe_2O_4$

Table A.7: XRD Analysis for Alloy A (Superfer 800H) After Exposure for 50 Cycles at 900^0C in Na_2SO_4- 60%V_2O_5 +20%CaO.

S. No.	"d" Values	Phases Identified
1	4.9222	$Ca_3V_2O_8$
2	2.9751	$Ca_3V_2O_8,\alpha-Fe_2O_3$, FeV_2O_4,FeS
3	2.6874	$Ca_3V_2O_8$, $(Cr,Fe)_2O_3$
4	2.5257	$\alpha-Fe_2O_3$, FeV_2O_4,$NiCr_2O_4$, $NiFe_2O_4$, FeS
5	2.4394	$\alpha-Fe_2O_3$, Cr_2O_3
6	2.1009	FeV_2O_4, Cr_2O_3
7	1.7137	$NiCr_2O_4$, $(Cr,Fe)_2O_3$, Cr_2O_3, FeS
8	1.6086	$\alpha-Fe_2O_3$, $NiCr_2O_4$, $NiFe_2O_4$, Cr_2O_3
9	1.4821	$NiCr_2O_4$, $NiFe_2O_4$, Cr_2O_3
10	1.2649	$NiCr_2O_4$, FeV_2O_4

Table A.8 XRD Analysis for Alloy B (Superco 605) After Exposure for 50 Cycles at 900^0C in Na_2SO_4- 60%V_2O_5 +20%CaO.

S. No.	"d" Values	Phases Identified
1	2.9750	$Co_3V_2O_8$
2	2.47186	$Co_3V_2O_8$, NiO, Cr_2O_3, $NiCo_2O_4$
3	2.38933	Cr_2O_3, NiO, CoV_3
4	2.07795	CoV_3, Cr_2O_3
5	1.48214	Cr_2O_3, NiO, $NiCo_2O_4$, $Co_3V_2O_8$
6	1.26775	Cr_2O_3, NiO, CoV_3

Table A.9   XRD Analysis for Nickel Base Alloys: Alloy C (Superni 75), Alloy D (Superni 718) & Alloy E (Superni 601) After Exposure for 50 Cycles at 900^0C in Na_2SO_4–60%V_2O_5+20%CaO.

S. No.	Alloy	"d" Values	Phases Identified
1		3.0143	Cr_2O_3, $Ni(VO_3)_2$
2		2.8995	$NiCr_2O_4$, $Ni(VO_3)_2$, $Ca_3V_2O_8$
3		2.7272	Cr_2O_3, $Ni(VO_3)_2$, $Ca_3V_2O_8$
4		2.4918	$NiCr_2O_4$, $Ni(VO_3)_2$, TiO_2, Cr_2O_3
5		2.3893	NiO
6		2.0555	Cr_2O_3, $NiCr_2O_4$, NiO, $Ni(VO_3)_2$
7	Alloy C	1.6961	Cr_2O_3, $NiCr_2O_4$, TiO_2
8	(Superni 75)	1.6401	$NiCr_2O_4$
9		1.5983	$NiCr_2O_4$, NiO, Cr_2O_3
10		1.4695	$NiCr_2O_4$, NiO, Cr_2O_3
11		1.0593	$NiCr_2O_4$, NiO
1		3.5298	$Ni(VO_3)_2$
2		2.8633	$Ni(VO_3)_2$
3		2.4588	$Ni(VO_3)_2$, $NiCr_2O_4$, NiO, Cr_2O_3, TiO_2
4		2.3532	$NiCr_2O_4$
5		2.0466	NiO, $Ni(VO_3)_2$, Cr_2O_3
6		1.6537	Cr_2O_3, $NiCr_2O_4$, TiO_2, $(Cr,Fe)_2O_3$
7	Alloy D	1.8533	$NiCr_2O_4$, $Ni(VO_3)_2$, Cr_2O_3, $(Cr,Fe)_2O_3$
8	(Superni 718)	1.4571	$NiCr_2O_4$, NiO, Cr_2O_3
9		1.4331	NiO
10		1.0722	NiO
11		0.9579	NiO
1		4.8688	Cr_2O_3, $NiCr_2O_4$, $Ca_3V_2O_8$
2		2.9558	$NiCr_2O_4$, $Ca_3V_2O_8$
3		2.7039	$Ca_3V_2O_8$, Cr_2O_3
4		2.5188	$NiCr_2O_4$, $Ni(VO_3)_2$, $NiFe_2O_4$
5	Alloy E	2.0917	NiO, Cr_2O_3, $Ni(VO_3)_2$
6	(Superni 601)	1.7048	$NiCr_2O_4$, Cr_2O_3, $Ni(VO_3)_2$
7		1.6085	$NiCr_2O_4$, $NiFe_2O_4$
8		1.4758	$NiCr_2O_4$, $NiFe_2O_4$, NiO
9		1.0861	$NiCr_2O_4$, NiO

Table A.10: XRD Analysis for Alloy A (Superfer 800H) After Exposure for 50 Cycles at 900^0C in $Na_2SO_4\text{-}60\%V_2O_5\text{+}20\%MnO_2$.

S. No.	"d" Values	Phase Identified
1	4.7647	FeV_2O_4, $NiCr_2O_4$
2	2.9180	FeV_2O_4, Fe_2O_3, FeS, Cr_2O_3, $NiCr_2O_4$
3	2.6563	FeS, $(Cr,Fe)_2O_3$, Cr_2O_3
4	2.4917	FeV_2O_4, $NiCr_2O_4$, $NiFe_2O_4$, $NiCrMnO_4$, Fe_2O_3,
5	2.0644	FeV_2O_4, FeS, Cr_2O_3
6	1.7885	Fe_2O_3
7	1.6960	FeS, $(Cr,Fe)_2O_3$
8	1.5932	$NiCr_2O_4$, $NiFe_2O_4$, $NiCrMnO_4$, Fe_2O_3
9	1.4695	$NiCr_2O_4$, $NiFe_2O_4$, $NiCrMnO_4$, Fe_2O_3, Cr_2O_3
10	1.2619	$NiCr_2O_4$, Cr_2O_3
11	1.0832	$NiCr_2O_4$

Table A.11: XRD Analysis for Alloy B (Superco 605) After Exposure for 50 Cycles at 900^0C in $Na_2SO_4\text{-}60\%V_2O_5\text{+}20\%MnO_2$.

S. No.	"d" Values	Phase Identified
1	2.8406	Co_3O_4, $NiWO_4$, CO_2NiO_4
2	2.4141	Co_3O_4, CO_2NiO_4, CoO, $NiWO_4$
3	2.1290	CoO, Cr_2O_3 Co_2MnO_4
4	2.0734	$CO_3V_2O_8$, Cr_2O_3, NiO
5	1.6348	$NiWO_4$, Cr_2O_3, $CO_3V_2O_8$
6	1.5637	Co_3O_4, Co_2MnO_4
7	1.4737	$CO_3V_2O_8$, CoO, Cr_2O_3
8	1.4410	Co_3O_4, CO_2NiO_4, Co_2MnO_4
9	1.2235	Co_3O_4, Cr_2O_3

Table A.12: XRD Analysis for Nickel Base Alloys: Alloy C (Superni 75), Alloy D (Superni 718) & Alloy E (Superni 601) After Exposure for 50 Cycles at 900^0C in Na_2SO_4-60%V_2O_5+20%MnO_2.

S. No.	Alloys	"d" Values	Phase Identified
1		3.1390	Cr_2O_3
2	Alloy C	2.9751	Cr_2O_3, NiS
3	(Superni 75)	2.7935	NiS, Mn_3O_4
4		2.5257	$NiCr_2O_4$, $Ni(VO_3)_2$, NiS, $NiCrMn_2O_4$, Mn_3O_4
5		2.4141	Cr_2O_3
6		2.3414	NiO, $Ni(VO_3)_2$
7		2.0779	NiS
8		1.6137	NiO, $Ni(VO_3)_2$, Cr_2O_3, $NiCrMn_2O_4$
9		1.4779	$NiCr_2O_4$, NiO, $NiCrMn_2O_4$, Mn_3O_4, Cr_2O_3
1		3.1828	Cr_2O_3
2	Alloy D	2.9558	$NiCr_2O_4$, $Ni(VO_3)_2$,
3	Superni 718	2.4394	$NiCr_2O_4$, NiO, $Ni(VO_3)_2$, $NiAl_2O_4$
4		2.0379	NiO, Mn_3O_4, Cr_2O_3, $NiAl_2O_4$
5		1.5783	$NiCr_2O_4$, $Ni(VO_3)_2$, Mn_3O_4, Cr_2O_3
6		1.4531	$NiCr_2O_4$, NiO, Mn_3O_4, Cr_2O_3, $NiAl_2O_4$
7		1.2648	$NiCr_2O_4$, NiO
8		1.0870	$NiCr_2O_4$, NiO
1		2.9558	$NiCr_2O_4$
2	Alloy E	2.5188	$NiCr_2O_4$, $NiFe_2O_4$, $Ni(VO)_3$, $NiCrMn_2O_4$, Mn_3O_4
3	Superni 601	2.4784	NiO, $Ni(VO)_3$, α-Fe_2O_3, Mn_3O_4
4		2.0825	NiO, $NiCr_2O_4$, $Ni(VO)_3$, $NiCrMn_2O_4$, Cr_2O_3
5		1.6960	$NiCr_2O_4$, Cr_2O_3
6		1.5983	$NiCr_2O_4$, $NiFe_2O_4$, $NiCrMn_2O_4$, α-Fe_2O_3, Cr_2O_3
7		1.4674	$NiCr_2O_4$, $NiFe_2O_4$, NiO, Mn_3O_4, Cr_2O_3
8		1.2677	$NiCr_2O_4$, NiO

Table A.13: XRD Analysis for Alloy A (Superfer 800H) After Exposure for 30 Cycles at 900°C in Na_2SO_4-60%V_2O_5+10%$ZnSO_4$.

S.No.	"d" Values	Phases Identified
1	3.0547	Cr_2O_3
2	2.5800	α-Fe_2O_3, $ZnFe_2O_4$, $NiCr_2O_4$, $NiFe_2O_4$
3	2.1293	α-Fe_2O_3, (Cr, Fe)$_2O_3$, FeV_2O_4
4	2.0917	Cr_2O_3, α-Fe_2O_3, FeV_2O_4, NiO, FeS,
5	1.7317	(Cr, Fe)$_2O_3$, FeV_2O_4, $NiCr_2O_4$, $NiFe_2O_4$
6	1.6294	α-Fe_2O_3, (Cr, Fe)$_2O_3$, $NiFe_2O_4$, $NiCr_2O_4$, $ZnFe_2O_4$
7	1.4950	α-Fe_2O_3, (Cr, Fe)$_2O_3$, NiO. $ZnFe_2O_4$
8	1.2824	α-Fe_2O_3, (Cr, Fe)$_2O_3$, FeS
9	1.0889	NiO, FeS, $NiCr_2O_4$

Table A.14: XRD Analysis for Alloy C (Superni 75) After Exposure for 30 Cycles at 900°C in Na_2SO_4-60%V_2O_5+10% $ZnSO_4$.

S.No.	"d" Values	Phases Identified
1	2.3651	NiO
2	2.0555	NiO, Cr_2O_3, $NiCr_2O_4$, FeV_2O_4
3	1.4612	NiO, Cr_2O_3, $NiCr_2O_4$
4	1.2507	NiO, Cr_2O_3, $NiCr_2O_4$
5	1.1979	NiO, Cr_2O_3
6	0.9548	NiO, Cr_2O_3
7	0.9315	NiO, Cr_2O_3

Table A.15: XRD Analysis for Alloy D (Superni 718) After Exposure for 30 Cycles at 900^{0}C in Na_2SO_4-60%V_2O_5+10% $ZnSO_4$.

S.No.	"d" Values	Phases Identified
1	2.8633	Cr_2O_3
2	2.4494	NiO, $NiCr_2O_4$, $Ni(VO_3)_2$
3	2.3414	NiO
4	2.0379	Cr_2O_3, NiO, Fe_2O_3, $Ni(VO_3)_2$
5	1.5783	$NiCr_2O_4$, Fe_2O_3
6	1.4531	$NiCr_2O_4$, NiO
7	1.2507	$NiCr_2O_4$, NiO
8	1.0704	$NiCr_2O_4$, NiO

Table A.16: XRD Analysis for Alloy E (Superni 601) After Exposure for 30 Cycles at 900^{0}C in Na_2SO_4-60%V_2O_5+10% $ZnSO_4$.

S.No.	"d" Values	Phases Identified
1	3.7035	Cr_2O_3
2	2.9751	$NiCr_2O_4$, $Ni(VO_3)_2$, Cr_2O_3, $ZnFeVO_4$
3	2.5257	$Ni(VO_3)_2$, Cr_2O_3, $NiCr_2O_4$
4	2.0917	$Ni(VO_3)_2$, Cr_2O_3, NiO
5	1.6620	$NiCr_2O_4$, $ZnFeVO_4$
6	1.4737	$NiCr_2O_4$, Cr_2O_3, $ZnFeVO_4$, NiO
7	1.2677	$NiCr_2O_4$, Cr_2O_3, NiO
8	1.0814	$NiCr_2O_4$, Cr_2O_3, NiO

Table A.17: XRD Analysis for Alloy A (Superfer 800H) After Exposure for 50 Cycles at 900^0C in Na_2SO_4-60%V_2O_5+CeO_2 Coating.

S.No.	"d" Values	Phases Identified
1	3.6145	αFe_2O_3, $(Cr, Fe)_2O_3$, Cr_2O_3
2	2.9181	FeV_2O_4, Fe_2O_3, FeS
3	2.6641	$(Cr, Fe)_2O_3$, Cr_2O_3, FeS
4	2.4918	$NiCr_2O_4$, $NiFe_2O_4$, FeV_2O_4, Fe_2O_3, $(Cr, Fe)_2O_3$
5	2.3893	NiO
6	2.0644	FeS, NiO, Cr_2O_3
7	1.8220	FeV_2O_4, $(Cr, Fe)_2O_3$
8	1.6903	$(Cr, Fe)_2O_3$, FeV_2O_4, FeS
9	1.6009	$NiCr_2O_4$, $NiFe_2O_4$, $(Cr, Fe)_2O_3$, Fe_2O_3, Cr_2O_3
10	1.4695	$NiCr_2O_4$, $NiFe_2O_4$, FeV_2O_4, Fe_2O_3, Cr_2O_3
11	1.4490	$(Cr, Fe)_2O_3$
12	1.2677	FeV_2O_4

Table A.18: XRD Analysis for Alloy B (Superco 605) After Exposure for 50 Cycles at 900^0C in Na_2SO_4-60%V_2O_5+CeO_2 Coating.

S.No.	"d" Values	Phases Identified
1	3.7035	WO_3, $CoWO_4$
2	2.8996	Co_3O_4, $NiCo_2O_4$, $NiWO_4$, $CoWO_4$
3	2.4785	$NiCo_2O_4$, $NiWO_4$, Co_3O_4, $CoCr_2O_4$, CoO, Cr_2O_3
4	2.3651	NiO
5	2.1009	$Co_3V_2O_8$, WO_3, CoO, NiO
6	2.04665	$NiCo_2O_4$, WO_3, Cr_2O_3, NiO
7	1.6817	$NiWO_4$,
8	1.5833	Co_2O_3, $CoCr_2O_4$, Cr_2O_3
9	1.4907	WO_3, $CoCr_2O_4$, CoO
10	1.4530	$NiCo_2O_4$, Co_3O_4, Cr_2O_3

Table A.19: XRD Analysis for Nickel Base Alloys: Alloy C (Superni 75), Alloy D (Superni 718) & Alloy E (Superni 601) After Exposure for 50 Cycles at 900^0C in Na_2SO_4-60%V_2O_5+CeO_2 Coating.

S. No.	Alloys	"d" Values	Phase Identified
1		3.1828	CeO_2
2	Alloy C	2.9751	$Ni(VO_3)_2$, NiS
3	(Superni 75)	2.7111	CeO_2, $CeVO_4$, Cr_2O_3
4		2.5465	$Ni(VO_3)_2$, $NiCr_2O_4$, NiO, NiS
5		2.4267	NiO, $Ni(VO_3)_2$, Cr_2O_3
6		2.0917	NiO, $Ni(VO_3)_2$, Cr_2O_3
7		1.9119	CeO_2, $CeVO_4$, NiS
8		1.6401	CeO_2, Cr_2O_3
9		1.4779	NiO, $NiCr_2O_4$, Cr_2O_3
10		1.2080	$NiCr_2O_4$, NiO, Cr_2O_3
11		1.1045	$NiCr_2O_4$, NiO
1		2.9368	$NiCr_2O_4$, FeV_2O_4
2	Alloy D	2.4918	$NiCr_2O_4$, $Ni(VO_3)_2$, FeV_2O_4, Cr_2O_3
3	Superni 718	2.3955	NiO
4		2.0779	NiO, $Ni(VO_3)_2$, FeV_2O_4, Cr_2O_3
5		1.6961	$NiCr_2O_4$, Cr_2O_3,
6		1.5983	$NiCr_2O_4$, Cr_2O_3
7		1.4695	$NiCr_2O_4$, NiO, Cr_2O_3,
8		1.2563	NiO, Cr_2O_3
1		3.0962	CeO_2
2	Alloy E	2.8996	$Ni(VO_3)_2$, FeV_2O_4
3	Superni 601	2.6487	FeS, Cr_2O_3
4		2.4653	$Ni(VO_3)_2$, $NiCr_2O_4$, FeV_2O_4, Cr_2O_3
5		2.3893	NiO
6		2.0734	$Ni(VO_3)_2$, NiO, $NiCr_2O_4$, FeS, FeV_2O_4, Cr_2O_3
7		1.8931	$Ni(VO_3)_2$, CeO_2, $CeVO_4$
8		1.6189	CeO_2, $NiCr_2O_4$
9		1.5883	$NiCr_2O_4$, Cr_2O_3
10		1.3841	CeO_2

Table A.20: XRD Analysis for Alloy A (Superfer 800H) After Exposure for 50 Cycles at 900^{0}C in Na$_2$SO$_4$-60%V$_2$O$_5$+Y$_2$O$_3$ Coating

S. No.	"d" Values	Phases Identified
1	3.4755	CrY$_2$S$_4$, TiO$_2$, Cr$_2$O$_3$
2	2.6039	YVO4, Cr$_2$O$_3$, FeS, Cr$_2$S$_3$
3	2.4653	Cr$_2$O$_3$, NiCr$_2$O$_4$
4	2.1885	Fe$_2$O$_3$, Cr$_2$O$_3$
5	2.1103	FeV$_2$O$_4$
6	2.0379	Fe$_2$O$_3$, Cr$_2$O$_3$, FeS, Cr$_2$S$_3$
7	1.9771	Y$_2$O$_3$
8	1.8357	Y$_2$O$_3$, Fe$_2$O$_3$, YVO$_4$, Cr$_2$O$_3$,CrS
9	1.8085	YVO$_4$, Cr$_2$O$_3$
10	1.7565	FeS, Y$_2$O$_3$, Cr$_2$S$_3$
11	1.4612	FeV$_2$O$_4$, Fe$_2$O$_3$, Cr$_2$O$_3$, NiCr$_2$O$_4$

Table A.21: XRD Analysis for Alloy B (Superco-605) After Exposure for 50 Cycles at 900^{0}C in Na$_2$SO$_4$-60%V$_2$O$_5$+Y$_2$O$_3$ Coating.

S. No.	"d" Values	Phases Identified
1	3.6437	WO$_3$, Cr$_2$O$_3$
2	2.8633	NiWO$_4$, NiCo$_2$O$_4$, Co$_3$O$_4$
3	2.4653	NiWO$_4$, NiCo$_2$O$_4$, Co$_3$O$_4$
4	1.6845	NiWO$_4$, WO$_3$, Cr$_2$O$_3$, CoCr$_2$O$_4$
5	1.5783	NiCo$_2$O$_4$, Co$_3$O$_4$, Cr$_2$O$_3$, CoCr$_2$O$_4$
6	1.4530	NiCo$_2$O$_4$, Co$_3$O$_4$, Cr$_2$O$_3$, CoCr$_2$O$_4$

Table A.22: XRD Analysis for Nickel Base Alloys: Alloy C (Superni 75), Alloy D (Superni 718) & Alloy E (Superni 601) After Exposure for 50 Cycles at 900^0C in Na_2SO_4-60%V_2O_5+Y_2O_3 Coating.

S. No.	Alloy	"d" Values	Phases Identified
1		3.4755	TiO_2, CrY_2S_4, Cr_2O_3
2		2.8996	Y_2O_3, TiO_2
3	Alloy C	2.6336	YVO_4, Y_2O_3, $NiCr_2O_4$,Cr_2O_3, $NiCr_2S_4$
4	(Superni 75)	2.4918	$NiCr_2O_4$, Cr_2O_3, NiS, $Ni(VO_3)_2$, TiO_2
5		2.3893	NiO
6		2.1919	$NiCr_2O_4$, TiO_2, Y_2O_3
7		2.0734	$NiCr_2S_4$, NiO, Cr_2O_3, $Ni(VO_3)_2$, $NiCr_2O_4$
8		1.8639	Y_2O_3, NiS
9		1.8219	YVO_4, NiS, Cr_2O_3
10		1.7692	YVO_4, Y_2O_3, $NiCr_2S_4$, Cr_2O_3
11		1.5783	Y_2O_3, NiO, Cr_2O_3
12		1.4695	NiO, Cr_2O_3
1		2.8633	$NiCr_2O_4$, FeV_2O_4, Y_2O_3
2		2.4523	$NiCr_2O_4$, FeV_2O_4, Cr_2O_3, $Ni(VO_3)_2$
3		2.3651	NiO
4	Alloy D	2.0555	NiO, FeV_2O_4, Cr_2O_3, $Ni(VO_3)_2$
5	(Superni 718)	1.5783	$NiCr_2O_4$, FeV_2O_4, Cr_2O_3, Y_2O_3
6		1.4531	$NiCr_2O_4$, FeV_2O_4, NiO, Cr_2O_3
7		1.2507	$NiCr_2O_4$, FeV_2O_4, Cr_2O_3
8		1.0686	$NiCr_2O_4$, Cr_2O_3
1	Alloy E	3.0973	$Ni(VO_3)_2$, Y_2O_3, Cr_2O_3
2	(Superni 601)	2.5843	$Ni(VO_3)_2$, Cr_2O_3
3		2.4653	$Ni(VO_3)_2$, $NiCr_2O_4$, NiO, Cr_2O_3
4		2.0037	$Ni(VO_3)_2$ $NiCr_2O_4$, NiO, Cr_2O_3
5		1.7951	$Ni(VO_3)_2$, Y_2O_3, YVO_4
6		1.7440	$Ni(VO_3)_2$, Cr_2O_3, Y_2O_3
7		1.2507	$NiCr_2O_4$, Cr_2O_3

Table A.23: XRD Analysis of Alloy A (Superfer 800H) After Exposure for 50 Cycles at 900^{0}C in Na$_2$SO$_4$-60%V$_2$O$_5$+SnO$_2$ Coating.

S.No.	"d" Values	Phases Identified
1	3.3720	SnO$_2$
2	2.9368	Fe$_2$O$_3$, FeV$_2$O$_4$, FeS
3	2.6796	SnO$_2$, Fe$_2$O$_3$, Cr$_2$O$_3$, FeS, (Cr,Fe)$_2$O$_3$
4	2.5188	Fe$_2$O$_3$, FeV$_2$O$_4$, NiCr$_2$O$_4$, NiFe$_2$O$_4$
5	2.0734	FeV$_2$O$_4$, FeS, (Cr,Fe)$_2$O$_3$
6	2.0461	Cr$_2$O$_3$, NiO
7	1.7692	SnO$_2$, Cr$_2$O$_3$, FeS, (Cr,Fe)$_2$O$_3$
8	1.6817	Fe$_2$O$_3$, SnO$_2$, Cr$_2$O$_3$, (Cr,Fe)$_2$O$_3$
9	1.5983	Fe$_2$O$_3$, FeV$_2$O$_4$, SnO$_2$, Cr$_2$O$_3$, FeS, NiCr$_2$O$_4$, NiFe$_2$O$_4$
10	1.4821	Fe$_2$O$_3$, Cr$_2$O$_3$, NiCr$_2$O$_4$, NiFe$_2$O$_4$, (Cr,Fe)$_2$O$_3$
11	1.2444	FeV$_2$O$_4$, SnO$_2$, Cr$_2$O$_3$

Table A.24: XRD After Alloy B (Superco 605) After Exposure for 50 Cycles at 900^{0}C in Na$_2$SO$_4$-60%V$_2$O$_5$+SnO$_2$ Coating.

S.No.	"d" Values	Phases Identified
1	2.8996	NiWO$_4$, Co$_3$O$_4$, NiCo$_2$O$_4$
2	2.4785	NiWO$_4$, Co$_3$V$_2$O$_8$, CoCr$_2$O$_4$
3	2.4394	Co$_3$V$_2$O$_8$, NiO, Co$_3$O$_4$, NiCo$_2$O$_4$
4	2.0644	NiO, Co$_3$V$_2$O$_8$
5	1.6845	NiWO$_4$, NiO
6	1.5882	CoCr$_2$O$_4$
7	1.4653	NiO, Co$_3$V$_2$O$_8$,CoCr$_2$O$_4$, Co$_3$O$_4$, NiCo$_2$O$_4$

Table A.25: XRD Analysis for Nickel Base Alloys: Alloy C (Superni 75), alloy D (Superni 718) & Alloy E (Superni 601) After Exposure for 50 Cycles at 900^{0}C in Na_2SO_4-60%V_2O_5+SnO_2 Coating.

S. No.	Alloys	"d" Values	Phase Identified
1		3.3720	SnO_2
2		2.6641	SnO_2, Cr_2O_3
3		2.4267	NiO
4	Alloy C	2.3651	SnO_2, Cr_2O_3, NiO
5	(Superni 75)	2.1103	SnO_2, NiO
6		1.7692	SnO_2, Cr_2O_3
7		1.6732	SnO_2, Cr_2O_3
8		1.4950	SnO_2, Cr_2O_3
9		1.4779	NiO
10		1.4138	SnO_2, Cr_2O_3
11		1.2591	NiO, Cr_2O_3
12		1.2183	SnO_2, Cr_2O_3
1		2.9558	$Ni(VO_3)_2$, $NiCr_2O_4$, FeV_2O_4
2	Alloy D	2.5188	$Ni(VO_3)_2$, $NiCr_2O_4$, FeV_2O_4
3	Superni 718	2.4267	$Ni(VO_3)_2$, NiO
4		2.0917	$Ni(VO_3)_2$, NiO, $NiCr_2O_4$, FeV_2O_4, Cr_2O_3
5		1.5983	$Ni(VO_3)_2$, $NiCr_2O_4$, Cr_2O_3
6		1.4737	NiO, $NiCr_2O_4$, FeV_2O_4, Cr_2O_3
7		1.2649	$NiCr_2O_4$, FeV_2O_4, Cr_2O_3
1		3.3471	SnO_2
2		2.6336	SnO_2, Cr_2O_3, $(Cr,Fe)_2O_3$
3		2.4985	$NiCr_2O_4$, Cr_2O_3, $NiFe_2O_4$
4	Alloy E	2.4141	NiO
5	Superni 601	2.3651	SnO_2
6		2.0871	NiO, Cr_2O_3, $(Cr,Fe)_2O_3$
7		1.7628	SnO_2, $(Cr,Fe)_2O_3$
8		1.6732	SnO_2, $(Cr,Fe)_2O_3$
9		1.5983	SnO_2, $NiCr_2O_4$, Cr_2O_3, $NiFe_2O_4$
10		1.4779	SnO_2, NiO, $NiCr_2O_4$, $NiFe_2O_4$, $(Cr,Fe)_2O_3$
11		1.2563	NiO, Cr_2O_3
12		1.2067	NiO, Cr_2O_3

Table A.26: XRD Analysis for Alloy A (Superfer 800H) After Exposure for 50 Cycles at 900^{0}C in Na$_2$SO$_4$-60%V$_2$O$_5$+ZrO$_2$ Coating.

S.No.	"d" Values	Phases Identified
1	3.6290	Fe$_2$O$_3$, (Cr,Fe)$_2$O$_3$, Cr$_2$O$_3$
2	2.9180	FeV$_2$O$_4$, ZrO$_2$
3	2.6641	(Cr,Fe)$_2$O$_3$, Fe$_2$O$_3$, Cr$_2$O$_3$
4	2.4918	FeV$_2$O$_4$, Fe$_2$O$_3$, NiFe$_2$O$_3$, NiCr$_2$O$_4$
5	2.4141	NiO
6	2.0825	FeV$_2$O$_4$, (Cr,Fe)$_2$O$_3$, NiO, Cr$_2$O$_3$
7	2.0292	FeV$_2$O$_4$, NiO
8	1.8220	Fe$_2$O$_3$, ZrO$_2$
9	1.7565	(Cr,Fe)$_2$O$_3$, Cr$_2$O$_3$
10	1.6788	FeV$_2$O$_4$, (Cr,Fe)$_2$O$_3$, Fe$_2$O$_3$, Cr$_2$O$_3$
11	1.5933	FeV$_2$O$_4$, NiFe$_2$O$_3$, NiCr$_2$O$_4$, Cr$_2$O$_3$, ZrO$_2$
12	1.4653	FeV$_2$O$_4$, (Cr,Fe)$_2$O$_3$, Fe$_2$O$_3$, NiO, NiFe$_2$O$_3$, NiCr$_2$O$_4$
13	1.4430	(Cr,Fe)$_2$O$_3$
14	1.0814	Fe$_2$O$_3$, NiCr$_2$O$_4$

Table A.27: XRD After Alloy B (Superco 605) After Exposure for 50 Cycles at 900^{0}C in Na$_2$SO$_4$-60%V$_2$O$_5$+ZrO$_2$ Coating.

S.No.	"d" Values	Phases Identified
1	2.8996	Co$_3$O$_4$, NiWO$_4$, Co$_3$V$_2$O$_8$
2	2.4653	Co$_2$NiO$_4$, Co$_3$O$_4$, NiWO$_4$, NiO, CoCr$_2$O$_4$, Co$_3$V$_2$O$_8$
3	2.0555	Cr$_2$O$_3$, NiO, Co$_3$V$_2$O$_8$
4	1.5783	Co$_2$NiO$_4$, CoCr$_2$O$_4$, Cr$_2$O$_3$, Co$_3$V$_2$O$_8$
5	1.4950	NiO, CoCr$_2$O$_4$, CoO, Cr$_2$O$_3$, Co$_3$V$_2$O$_8$
6	1.4530	Co$_3$O$_4$, Co$_2$NiO$_4$, NiWO$_4$, Cr$_2$O$_3$

Table A.28: XRD Analysis for Nickel Base Alloys: Alloy C (Superni 75), Alloy D (Superni 718) & Alloy E (Superni 601) After Exposure for 50 Cycles at 900^{0}C in Na_2SO_4-60%V_2O_5+ZrO_2 Coating.

S. No.	Alloys	"d" Values	Phase Identified
1		3.0962	ZrO_2, Cr_2O_3
2	Alloy C	2.7935	ZrO_2, Cr_2O_3, NiS
3	(Superni 75)	2.5749	ZrO_2, Cr_2O_3, $Ni(VO_3)_2$
4		2.4918	Cr_2O_3, $NiCr_2O_4$, NiS, Fe_2O_3, $Ni(VO_3)_2$
5		1.8220	ZrO_2, NiS
6		1.795	Fe_2O_3, NiS, ZrO_2
7		1.6401	$NiCr_2O_4$, Cr_2O_3
8		1.5933	ZrO_2, $NiCr_2O_4$, Fe_2O_3
9		1.4612	$NiCr_2O_4$, Cr_2O_3
1		3.6290	Fe_2O_3, Cr_2O_3
2	Alloy D	3.0962	ZrO_2, Cr_2O_3
3	(Superni 718)	2.8996	Fe_2O_3, TiO_2, ZrO_2, FeV_2O_4
4		2.7935	ZrO_2, Cr_2O_3
5		2.5749	$Ni(VO_3)_2$, ZrO_2, Fe_2O_3
6		2.4918	$NiCr_2O_4$, $Ni(VO_3)_2$, NiO, Fe_2O_3, FeV_2O_4
7		2.3651	NiO, TiO_2
9		2.0379	$Ni(VO_3)_2$, NiO, FeV_2O_4
10		1.4654	$NiCr_2O_4$, NiO
11		1.4370	$NiCr_2O_4$, NiO, Cr_2O_3, Fe_2O_3
1		3.1389	ZrO_2, Cr_2O_3,CrS
2	Alloy E	2.8996	ZrO_2, FeV_2O_4, Fe_2O_3
3	(Superni 601)	2.8193	Cr_2O_3
4		2.4785	$NiCr_2O_4$, FeV_2O_4, Fe_2O_3, $Ni(VO_3)_2$, Cr_2O_3
5		2.3893	Cr_2O_3, NiO, CrS
6		2.0689	Cr_2O_3, FeV_2O_4, NiO, $Ni(VO_3)_2$, CrS, Fe_2O_3
7		1.6845	Cr_2O_3, $(Cr,Fe)_2O_3$, Fe_2O_3
8		1.5883	ZrO_2, $NiCr_2O_4$, Cr_2O_3, Fe_2O_3, $(Cr,Fe)_2O_3$
9		1.4633	$NiCr_2O_4$ Cr_2O_3, NiO

Table: A.29: EDAX analysis of surface of alloy C (Superni 75) in different environments after cyclic hot corrosion at 900°C

Environment	Point of Analysis	Element %										
		Fe	Ni	Cr	Ti	Mg	Ca	Zn	Y	Na	V	S
Na₂SO₄-60%V₂O₅+MgO	1	22.70	55.27	18.94	0.07	4.46	-	-	-	-	1.14	0.20
	2	1.40	65.56	26.76	0.91	4.84	-	-	-	-	1.32	0.23
	3	0.99	67.11	24.69	1.12	6.02	-	-	-	-	1.36	0.18
Na₂SO₄-60%V₂O₅+CaO	1	0.95	66.17	17.63	0.56	-	-	-	-	-	15.63	-
	2	2.49	68.91	18.46	0.27	-	0.48	-	-	-	10.87	0.01
	3	10.62	42.34	41.47	2.02	-	6.10	-	-	-	8.53	1.15
Na₂SO₄-60%V₂O₅+ZnSO₄	1	-	100.19	2.83	-	-	-	1.37	-	-	0.37	0.02
	2	-	99.76	2.47	0.05	-	-	-	-	-	0.69	-

Table: A.30: EDAX analysis of surface of alloy D (Superni 718) in different environments after cyclic hot corrosion at 900°C

Enviroment	Point of Analysis	Element %										
		Fe	Ni	Cr	Ti	Al	Si	Zr	Y	Na	V	S
Na₂SO₄-60%V₂O₅+ZrO₂	1	0.06	60.59	2.78	0.12	0.86	0.30	0.45		1.96	35.63	1.18
	2	0.73	41.77	55.16	0.58	0.18	0.04	0.18		1.66	3.81	0.08
	3	0.68	61.30	24.62	0.32	0.83	0.31	0.41		2.22	11.60	0.24
Na₂SO₄-60%V₂O₅+Y₂O₃	1	19.41	63.57	18.40	0.92	-	-	-		2.74	-	0.24
	2	31.74	46.37	28.72	3.15					-	0.59	-
	3	16.83	76.93	11.08	0.81					-	0.18	0.39

Table A.31: SUMMARY OF RESULTS

* (After 30 Cycles) mg/cm²   † (After 50 cycles in most of the alloys) μm

Environment	Alloy	*Weight Change	†Scale Thickness	XRD	SEM/EDAX/EPMA
Na₂SO₄-60%V₂O₅	A	8.77	62.5	α-Fe₂O₃, FeV₂O₄, NiCr₂O₄, NiFe₂O₄, Cr₂O₃	Cavities visible on the surface showing spalled regions. Thick scale having horizontal cracks. Top layer rich in Ni & Fe. Discontinuous Cr rich layer present near the scale/substrate interface. A nickel rich continuous layer present just above the substrate.
	B	20.34	78	NiWO₄, Cr₂O₃, NiCo₂O₄, CoCr₂O₄, Co₃O₄, NiO, CoO, Co₃V₂O₈	A thick multilayer scale is formed, consisting of Fe and Ni-rich scale at the top, which also contains Co and Cr. A thick layer having W follows it, containing Fe and Cr. But the areas rich in W are depleted of Cr. Cr rich sub scale is present just above the interface. Vanadium is distributed throughout the scale. Higher concentration of S is indicated just above the substrate where Mn is also present in higher concentration indicating. MnS formation, just below a tungsten rich scale.
	C	8.34	38.5	NiCr₂O₄, NiO, NiFe₂O₄, Ni(VO₃)₂, Cr₂O₃	Medium size scale, Cr rich layer present near the substrate, V is present throughout the scale. Ti present as a thin irregular layer above the substrate and S at the top. Cr-rich layer just above the substrate. In this area Ni and Fe are also occurring with Cr. V is also indicated in the scale and V is occurring in the layer, just above the substrate where Ni, Fe and Cr are present.
	D	8.58	57	NiO, NiCr₂O₄, α-Fe₂O₃, Ni(VO₃)₂, Cr₂O₃, FeV₂O₄, (Cr,Fe)₂O₃	Crystalline growth on the top surface is seen in SEM micrograph. Outer layer is rich in oxides of Cr & Ni. Inner layer is mainly Cr₂O₃. NiO present at interface between scale and the substrate.
	E	5.43	52	Ni(VO₃)₂, NiCr₂O₄, NiFe₂O₄, FeV₂O₄, Cr₂O₃, NiO, FeS	SEM indicates fine-grained dense scale with longitudinal cracks. EPMA reveals thick scale containing Fe, Cr and Ni. Top layer is rich in Fe, middle layer contains more of Cr. The inner layer is rich in Ni depleted of Fe and Cr. Ni is concentrated at few spots in the scale. V is present throughout the scale but more near the substrate. Internal sulphidation is indicated.
Na₂SO₄-60%V₂O₅ +MgO	A	5.21	33.3	Cr₂O₃, Fe₂O₃, Mg₃V₂O₈, FeV₂O₄, FeS, NiCr₂O₄	SEM indicates formation of a massive scale EPMA shows duplex scale, outer layer being rich in oxides of V, Mg, Cr, S and Fe while the inner layer is mainly Cr₂O₃. S is present in the scale as well as in the substrate, internal Sulphidation is indicated. Mg, V and oxygen are co-existing in the scale.

	Phases	Observations
B 8.92 53.5	Cr_2O_3, $Co_3V_2O_8$, NiO, Cr_2O_3, CoV_3	Nodule formation and spalling tendency revealed by SEM analysis. The scale is rich in Co, W, Ni and Cr. Mg and V are also present in the scale. Thin Ni rich layer is present on the top and bottom of the scale.
C 4.27 15	FeS, Cr_2O_3, NiO $Ni(VO_3)_2$, $NiCr_2O_4$, $Mg_3V_2O_8$, TiO_2	Thin scale rich in Cr has formed Ni, Fe, Mg and V are revealed by corresponding X-ray images in the top of the scale also. Ti and S are also present through out the scale. Sulphur is indicated in the top of the scale also. EDAX from the surface of the alloy C at areas 1, 2 & 3 revealed that the matrix consists of mainly Ni & Cr where Mg & V are also present
D 4.70 46	$NiCr_2O_4$, NiO $Mg_3V_2O_8$, FeV_2O_4, Cr_2O_3, $Ni(VO_3)_2$, α-Fe_2O_3, FeS	Large size nodules are seen on top of the scale. Crystalline phase and spalling is indicated. Scale is rich in Cr, Fe, Ni Mg and V. Ni is mainly present in the top layer where as inner layer is rich in Cr but the interface is depleted of Cr and rich in Ni. Magnesium and vanadium are distributed through out the scale at same positions indicating formation of vanadates.
E 2.73 23.4	Cr_2O_3, $Ni(VO_3)_2$, FeV_2O_4, $Mg_3V_2O_8$, $NiCr_2O_4$, $NiFe_2O_4$, FeS, NiO	SEM reveals the presence of nodules in the surface scale. BSEI and X-ray maps show the formation of a medium size scale and grain boundary oxidation X-ray maps indicate that V and S are concentrated in small areas in the scale. The top scale is rich in Cr, Ni and Fe. Aluminum is present along the grain boundaries.
Na₂SO₄-60%V₂O₅+CaO A 7.34 41	$Ca_3V_2O_8$, $(Cr,Fe)_2O_3$, α-Fe_2O_3, FeV_2O_4, $NiCr_2O_4$, FeS, $NiFe_2O_4$, Cr_2O_3	SEM shows a massive scale with nodules and intergranular cracks. Thick duplex scale with Ni, Cr & Fe present in the outer layer and mainly Cr_2O_3 in the inner layer is revealed by X-ray images. Cr- enriched layer is just above the substrate where Ni & Fe are absent. Al & Si are internally oxidized with chromium. Ca & V are present in the scale at the same spots indicating Ca-vanadate formation. Mn & S are coexisting along the interface.
B 16.30 34	$Co_3V_2O_8$, NiO, Cr_2O_3, CoV_3	Scale is spongy & having some porosity. The scale is consisting of mainly Cr & Co. W Ni is distributed uniformly in the areas depleted of Cr. Ni is present in higher concentration in the areas depleted of Cr. Ni is distributed uniformly in the scale. The scale substrate interface is even and no penetration of scale in the substrate is observed.
C 3.66 9	$NiCr_2O_4$, NiO $Ni(VO_3)_2$, TiO_2, Cr_2O_3, $Ca_3V_2O_8$	Scale consists of nodules distributed in crystalline matrix. EDAX indicated that nodules are rich in Ni, Cr, Ca and V. BSEI and X-ray maps of alloy C, show a very thin scale consisting of mainly Cr with some amount of Ni. Calcium is present in the scale and is coexisting with V. Ti is also present in the scale distributed uniformly. S has been detected in minor amounts on top of the scale. No internal oxidation has been indicated.

278

				Phases	Description
	D	6.73	43	Cr_2O_3, $NiCr_2O_4$, TiO_2, $(Cr,Fe)_2O_3$ NiO, $Ni(VO_3)_2$.	Elongated phases dispersed in a crystalline matrix are present. Medium size scale consists of Ni, Cr & Fe. An area depleted of Ni & Fe just above the substrate has a thin irregular layer rich in Cr. Ca & V are coexisting in the scale. EDAX analysis also confirmed that scale mainly consists of Ni, Fe & Cr. The scale just above the substrate has higher amount of Chromium. Vanadium & Calcium are present throughout the scale. Ti, Al, Mn and Ta have also been indicated in the scale.
	E	2.92	42	$NiCr_2O_4$, NiO, Cr_2O_3, $Ni(VO_3)_2$, $NiFe_2O_4$, $Ca_3V_2O_8$ FeV_2O_4, Fe_2O_3,	Continuous scale with nodules and precipitation along the grain boundaries. Pores also visible in the scale. Medium size scale rich in Cr and Fe and some amount of Ni has formed after exposure. Scale substrate is rich in Ni where both Fe and Cr are absent. Above this, there is a Cr rich thin band. Ca and V are also indicated in the scale.
Na_2SO_4-$60\%V_2O_5$ +MnO2	A	7.37	30	FeV_2O_4 Fe_2O_3, FeS, $NiCr_2O_4$, $NiFe_2O_4$, and $NiCrMnO_4$	SEM indicated massive scale formation. The EPMA indicates formation of a medium size scale, which is mainly rich in iron at top. Al and S are also present in the outer scale. The scale just above the substrate is Cr-rich where Ni and Mn are absent. Penetration of the scale into the substrate due to internal oxidation of Cr is indicated. Ti is also present in scale just above the substrate/scale interface.
	B	13.47	53.5	Co_3O_4, $Co_3V_2O_8$, $NiCo_2O_4$, Cr_2O_3, CoO, $NiWO_4$, Co_2MnO_4	Two distinct layers are seen in SEM, upper layer indicates partial melting and the inner scale is dense. EPMA indicated thick scale consisting of mainly W, Cr, Fe and little amount of Ni. Wherever W is present, areas are depleted of Cr. There is a Nickel rich layer at the interface; S is present in the outermost scale and also as a thin layer along the interface between the scale and the substrate. MnS is located near the interface. The EDAX analysis also revealed the presence of Co, Cr and W in the outermost scale. At the alloy/substrate interface the amount of W is less and the amount of Cr is higher. Presence of Na, V & S as well as Mn is indicated along the cross-section of the scale.
	C	5.35	20.5	$NiCr_2O_4$, $Ni(VO_3)_2$, NiS, $NiCrMnO_4$, NiO, Mn_3O_4, Cr_2O_3, Fe_2O_3	There is a large sized crystal growth in alloy C. The scale is relatively thin and mainly consists of Cr with some amount of Ni and Ti. Layer beneath the Cr rich scale is enriched with Ni and depleted of Cr. Mn and V are co-existing throughout the scale. Outer scale above the Cr_2O_3 scale is rich in Fe.
	D	6.28	33.3	$NiCr_2O_4$, NiO, $Ni(VO_3)_2$, Mn_3O_4, Cr_2O_3, $NiAl_2O_4$	Large size nodules have been observed in the scale by SEM. Cr rich thin continuous scale at the scale/substrate interface indicated by EPMA. Above this thin scale, there is presence of Ni, Fe and Cr rich scale. Al, Mn & V are also present in the outerscale. At the interface, there is a high concentration of Ti, which is penetrating into the scale.

Condition	Sample			Phases	Observations
	E	4.93	44	NiCr$_2$O$_4$, Cr$_2$O$_3$, Ni(VO$_3$)$_2$, NiO NiCrMn$_2$O$_4$, Mn$_3$O$_4$ NiFe$_2$O$_4$, α-Fe$_2$O$_3$	SEM revealed sponge like scale and that contains craters. EPMA shows formation of a medium size scale. V is present throughout the scale and S is present at the top of the scale. Silicon is present at top of the scale in pockets. Internal oxidation involves mainly oxides of Cr and Mn.
Na$_2$SO$_4$-60%V$_2$O$_5$+ZnSO$_4$	A	7.6	46.6	α-Fe$_2$O$_3$, NiCr$_2$O$_4$, (Cr, Fe)$_2$O$_3$, NiO NiFe$_2$O$_4$, ZnFe$_2$O$_4$ FeV$_2$O$_4$ & FeS	Formation of continuous scale with pores is seen in SEM analysis. Upper layer is rich in Ni, Cr and Fe, followed by a thick layer, which again contains mainly chromium with Ni & Fe. Ingress of S and V through the scale is observed. There is a thin layer rich in Ni and in this region concentration of V is also high indicating formation of Ni(VO$_3$)$_2$.
	C	6.39	34	Main peaks of NiO and few of Cr$_2$O$_3$ & NiCr$_2$O$_4$	Crystalline structure is indicated. EDAX of the top scale shows the presence of mainly Ni and small amount of Cr, Zn & V in the scale. EPMA also indicated that scale mainly contains Cr, Fe and Ni. The region just above the substrate has got Cr rich layer penetrating into the substrate. The V is seen throughout the scale. Internal oxidation of Ti is seen just below the scale.
	D	6.69	41.5	NiCr$_2$O$_4$, Ni(VO$_3$)$_2$, NiO, Ni(VO$_3$)$_2$ and Cr$_2$O$_3$.	Massive scale & spalling indicated. EPMA reveals the presence of a thin Cr$_2$O$_3$ layer just above the substrate. V and Zn are indicated co-existing. Outer scale is rich in Cr. Ni and Fe are also present but the scale just below this is depleted in Cr. Internal oxidation of Al & Ti along the grain boundaries is indicated.
	E	3.96	46	NiCr$_2$O$_4$, Cr$_2$O$_3$, NiO, Ni(VO$_3$)$_2$ and ZnFeVO$_4$	Crystalline growth at the top of the scale is noticed. Irregular Cr-rich layer is present just above the substrate The substrate is depleted in Cr & Fe and is rich in nickel. The internal oxidation of Al is indicated. V is seen co-existing with Zn. Elemental EDAX analysis across the scale of alloy E also indicates that the top scale is rich in Ni & Cr. The amount of Cr increases as we move downwards in the scale. Al is present throughout the scale.
Na$_2$SO$_4$-60%V$_2$O$_5$+CeO$_2$	A	6.78	50	NiCr$_2$O$_4$, Cr$_2$O$_3$, NiFe$_2$O$_4$, FeS, FeV$_2$O$_4$, Fe$_2$O$_3$ and (Cr,Fe)$_2$O$_3$	Massive scale showing craters and presence of some crystalline phases are revealed by SEM. EDAX of surface scale showed presence of Fe, Ni & Cr. Ceria is randomly distributed at some points in the scale. EDAX of cross-section also revealed that top scale is rich in Fe containing Cr & Ni. Ceria is indicated in traces. EPMA showed thin continuous layer of Cr$_2$O$_3$ present at the margin of the scale. Scale mainly consists of Cr, Ni and some Fe. Si has got oxidized along the grain boundaries.

			Phases	Description
B	13.23	41.5	$NiCo_2O_4$, $NiWO_4$, Co_3O_4, $CoCr_2O_4$, CoO, Cr_2O_3, NiO	Surface EDAX indicates nodules of Co-rich phase containing mainly Co, Cr and little amount of ceria etc. V is seen at some places in the matrix present in large concentration with ceria. EPMA revealed thick dense scale mainly consisting of Cr and Co. Co is present in high concentration throughout the scale and internal oxidation indicated.
C	2.66	25	NiO, FeS, $NiCr_2O_4$ $Ni(VO_3)_2$ and CeO_2	SEM micrograph for alloy C shows that the scale is consisting of matrix having coarse grains with nodules present across the scale. EPMA reveals growth of Ni-Cr rich crystals indicating spinel formation. Ceria is present in high concentration in the scale and at same places, it is co-existing with V indicating probable formation of $CeVO_4$.
D	6.20	30	$NiCr_2O_4$, Fe_2O_3 $Ni(VO_3)_2$, NiO	Scale structure consists of sponge like elongated phases. It mainly comprises of Fe, Cr and some nickel. Corresponding X-ray image indicates internal oxidation of Ti at points along the interface. A thin layer rich in Cr is present above the substrate where both Ni & Fe are absent followed by enrichment of Ni in the substrate. Silicon is also indicated in some areas in the scale. Al has got oxidized along the grain boundaries indicating internal oxidation.
E	3.63	32	$Ni(VO_3)_2$, NiO, $NiCr_2O_4$, FeS, FeV_2O_4, and Cr_2O_3	Scale consists of matrix containing Cr, Ni and Fe with nodules which are basically Ni-rich phase containing V & ceria. EPMA also indicates medium sized scale which is rich in Cr and contains Ni & Fe. V is present throughout the scale. There is internal oxidation along the grain boundaries near the interface between the scale and the substrate where Al has got oxidized.
Na₂SO₄-60%V₂O₅ +Y₂O₃ A	1.15	20	FeV_2O_4, Fe_2O_3, Cr_2O_3, FeS, CrS, Y_2O_3	SEM shows presence of sulphurous compound. Thin scale is formed and it is a rich band of Cr, which is continuous. Presence of unreacted salt is indicated on surface of the sample. MnS is present in the substrate. Y is co-exiting with V in the scale, indicating possible formation of YVO_4.
B	7.40	30	$Co_3V_2O_8$, Cr_2O_3, $NiWO_4$, $NiCo_2O_4$, Co_3O_4, Cr_2O_3 and $CoCr_2O_4$	Spongy scale observed from SEM micrograph having pores indicating release of some gas or vapours. EPMA shows that scale is rich in chromium and cobalt. EDAX of the cross-section revealed presence of Y in the scale at some spots where V is also present in higher concentration indicating formation of YVO_4. Scale just above the substrate is depletd in Cr.
C	3.39	16.5	$NiCr_2O_4$, NiO, NiS, Cr_2O_3, $NiCr_2S_4$, TiO_2 and Y_2O_3	Unreacted salt crystals indicated by SEM. A thin scale is observed and contains mainly Cr and Ni. Y is present as a thin layer along with V & S on the top of the scale.

				Compounds	Description
	D	5.13	18.5	$NiCr_2O_4$, FeV_2O_4, Cr_2O_3, $Ni(VO_3)_2$, NiO	SEM reveals massive scale formation. Scale formed is rich in Ni, Cr and Fe. Y is present in pockets in top scale. EDAX analysis at various points from surface to substrate has also indicated the presence of Ni, Cr & Fe in the scale and Al & Ti in the intergranular region in substrate and Y in the uppermost region. Ti, Na, S & V are also present at few locations. Surface analysis has further confirmed that scale is mainly consisting of compounds of Fe, Ni & Cr. Very little spalling is noticed in all the alloys.
	E	1.43	31	$Ni(VO_3)_2$, $NiCr_2O_4$, NiO, Cr_2O_3, Y_2O_3	Unreacted salt crystals indicated by SEM. The top scale contains small percentages of Fe, Ni & Cr followed by a thick continuous Cr-rich band. Y & V are present throughout the X-section and almost at same locations along with Cr-band. Probable formation of YVO_4 is indicated.
Na_2SO_4-60%V_2O_5+SnO_2	A	7.26	32	Fe_2O_3, FeV_2O_4, $NiCr_2O_4$, $NiFe_2O_4$ Cr_2O_3, FeS, $(Cr,Fe)_2O_3$ and SnO_2	Thick scale has formed and on the top of this scale, unreacted SnO_2 is seen. Scale mainly contains Ef &Cr as revealed by their respective X-ray images. There is a presence of thin Cr-rich continuous band above the substrate. Presence of SnO_2 is even obvious from the crystalline growth observed by the SEM analysis of the top surface of the scale. Presence of this refractory SnO_2 on the scale is possibly helpful in decreasing the rate of corrosion
	B	6.96	52	Co_2O_3, Co_3O_4, $Co_3V_2O_8$, $CoCr_2O_4$, $NiCr_2O_4$, $NiWO_4$	SEM indicates a massive scale with intergranular cracks and irregular shaped craters in the scale. Medium size scale has formed mainly consisting of Co. Cr that is present in the top layer in W depleted areas and a band type Cr rich thick layer present above the substrate. S is indicated at the top of the scale and sulphide specs seen near interface. Presence of MnS is indicated at the interface between the substrate and scale.
	C	4.21	34	SnO_2, Cr_2O_3 and NiO	SEM indicates crystalline phase indicating SnO_2 presence on the surface. Elemental X-ray mapping reveals that the scale is mainly containing Cr and lesser amount of Ni. Sn is present in higher concentration at top of the scale where as V is present in the main scale indicating formation of nickel vanadates.
	D	7.13	18	$Ni(VO_3)_2$, $NiCr_2O_4$, Cr_2O_3, FeV_2O_4 and NiO, Fe_2O_3	SEM showed presence of continuous dense layer having spalling tendency. BESI revealed the formation of a thin scale rich in chromium and contains Ni distributed uniformly. There is thin Mo rich layer in which both Ni and Cr are absent. Al & S are co-existing in some of the areas on the top. Internal oxidation of Mo and Ti is observed.

E		3.70	50	SnO₂, NiCr₂O₄, Cr₂O₃, FeV₂O₄ and NiO, NiFe₂O₄, Ni(VO₃)₂	Crystalline growth at the top surface of the scale indicates the presence of SnO_2. SnO_2 is present on the top of the scale and no reaction seems to have occurred with V as it is mainly present in the main scale. Sn is present on the surface. Thick scale is basically rich in Ni near oxide/air interface. Fe, Cr and Ni are present in the main scale. V is present along Scale/substrate interface. No internal oxidation indicated.
A	Na₂SO₄-60%V₂O₅ +ZrO₂	7.83	43	Fe₂O₃, ZrO₂, FeV₂O₄, NiFe₂O₄, Cr₂O₃, NiO, (Cr,Fe)₂O₃, NiCr₂O₄ and	Crystalline and globular structure is being revealed by SEM. EDAX showed that scale is rich in iron and contains Cr, Ni and Zr with V & S. As we proceed inwards it remains basically Fe rich scale and V is seen across the scale. S also penetrates up to the substrate. Internal oxidation is indicated. EPMA confirms the presence of Cr, Ni, & Fe in the scale. V & Zr are also present in the scale. Ni enrichment indicated along the alloy/scale interface. Al & Ti are also there in the scale.
B		10.94	58	CO₃O₄, CO₃V₂O₈, Co₂NiO₄, CoCr₂O₄ and NiWO₄	Transgranular cracks and granular structure indicating some porosity in the grains is observed in the scanning electron micrograph. BSEI and X-ray images showed the formation of a thick scale having distinct layers. Top layer is rich in chromium & Co followed by middle layer, rich in W and where W is present Co, is absent. Inner layer is Cr rich. Nickel is also present in the upper layer and areas rich in Ni are depleted of Cr.
C		2.51	17.5	ZrO₂, Cr₂O₃ & NiCr₂O₄	A dense scale with large size nodules, which on higher magnification show the crystal growth with directionality indicating oxidation of inter-metallic phases. EPMA shows a very thin scale mainly consisting of chromium and iron and some patches with higher concentration of S. V is incorporated in the scale as well as small amount of Zirconium.
D		4.91	33	Cr₂O₃, ZrO₂ Ni(VO₃) NiCr₂O₄, .NiO	Presence of sulphide crystals and nodules is indicated on scale surface. Scale consists of mainly Cr with small amount of nickel. Top scale is rich in Fe and these areas are depleted of Ni and Cr. V and Zr are present in substrate just below the scale/substrate interface. Ti is also observed in the scale. SEM/ EDAX analysis also revealed that the top scale is mainly consisting of Ni & Cr.
E		2.80	44	NiCr₂O₄, FeV₂O₄, NiO, Cr₂O₃ and Fe₂O₃, ZrO₂ and CrS	Macrographs reveal the presence of nodules in the matrix. Single layer scale rich in Cr & Fe and containing Ni and V has been observed. S is present on top of the scale. Al is present along the interface between substrate and the scale. Internal oxidation is indicated and internal oxides are mainly rich in Cr & Al.

Table A. 32 : Summary of hot corrosion of Fe-, Ni- & Co- base alloys in Na$_2$SO$_4$ and combustion gas environments

Material	Environment	Behaviour/Mechanism
Pure Iron	Na$_2$SO$_4$ 600 and 800°C SO$_3$-SO$_2$-O$_2$ mixed atmospheres.	Accelerated phenomenon observed has been attributed to the formation of a liquid sulphate phase. At the same time, the formation of FeSO$_4$ in Na$_2$SO$_4$ occurred. The initially solid phase became liquid when the iron sulphate concentration reached a critical value. Once the salt layer was completely liquid, SO$_3$ migrated inwards from the gas/salt interface. (Nanni et al, 1987)
Pure Iron	Na$_2$SO$_4$ deposits simulated combustion gas containing SO$_3$ at 600-800°C	The accelerated reaction observed in the presence of Na$_2$SO$_4$ deposits was attributed to the formation of a liquid salt solution between Na$_2$SO$_4$ and the sulphates of the corroded metal with the production of duplex scales consisting of a mixture of metal oxides and sulphides. (Gesmundu & Viani, 1988)
High Purity Iron	Gas mixture O$_2$ + 4% SO$_2$/SO$_3$ 500-800°C.	The reaction rate increased with increasing temperature in the range 500-640°C, but at around 640°C the rate constant drops by about an order of magnitude and then increased with increasing temperature. At lower temperatures, iron sulphate is formed on the surface and inner layer of the scale is mainly Fe$_2$O$_3$, Fe$_3$O$_4$ and Fe$_{1-y}$O (depending on the temperature) and Fe$_{1-x}$S. The sulphide phase is distributed as a three-dimensional network in the inner layer of the scale and it serves as a path for rapid outward diffusion of iron, thereby producing the rapid reaction rate. At higher temperatures the scale has the same composition as that of iron oxidised in oxygen, i.e. Fe$_2$O$_3$, Fe$_3$O$_4$ and Fe$_{1-y}$O. (Holt and Kofstad, 1989)
Pure Iron	Na$_2$SO$_4$ deposit, O$_2$-rich atmospheres containing SO$_2$-SO$_3$ at 650 –700°C	The accelerated oxidation of pure iron beneath Na$_2$SO$_4$ deposit is believed to be induced by the formation of eutectic melt of Na$_2$SO$_4$ -iron sulphate. The growth of oxide has been reported to predominate although fluxing contributed a little to the corrosion.
Fe-Al Alloys	-Do-	In alloys containing Al, fluxing proceeds at a considerable rate in the early stages due to the different oxygen pressure at the oxide/melt interface. Reduction of SO$_3$ released SO$_2$, which caused the formation of sulphides in the scale. Sulphides were supposed to contribute considerably to the acceleration due to their high defect concentration. (Shi et al, 1993)

Material	Conditions	Observations
Pure Iron	Na$_2$SO$_4$ deposits in Oxygen at 750^{0}C	The accelerated oxidation was attributed to the formation of abundant sulphide which was observed to be having highly defected lattice and allowed rapid diffusion of iron ions. It had most of the characteristics of low-temperature hot corrosion except that it occurred under basic conditions developed by the removal of sulphur from the sulphate deposits instead of usual acidic conditions. (Shi, 1993)
-Do-		He has also reported the possibilities of a Na$_2$SO$_4$-Na$_2$O eutectic melt developing on metals coated with Na$_2$SO$_4$ in O$_2$/Air at intermediate temperatures in another study. In iron based alloys when Al or Cr content is so low that it can not form protective Al$_2$O$_3$ or Cr$_2$O$_3$ film, Na$_2$SO$_4$-Na$_2$O melt emerges and causes accelerated oxidation. (Shi, 1995)
Pure Iron	Na$_2$SO$_4$, Na$_2$SO$_4$+NaCl, Na$_2$SO$_4$+V$_2$O$_5$, combustion gas at 600^{0}C	Iron suffered low temperature hot corrosion in the presence of salt deposits at 600^{0}C. The additions of NaCl and V$_2$O$_5$ to Na$_2$SO$_4$ changed the corrosion kinetics significantly and modified the scale structure.(Lingchuan, et al1996)
Pure Iron & Fe-5Cr Alloy	Na$_2$SO$_4$ at 1 atmosphere of oxygen at 900^{0}C	Pure iron did not undergo accelerated oxidation, which has been attributed to the thickening of the scale too rapidly for sulphur to penetrate the oxide and interact directly with the metal. Authors further reported an immediate acceleration in oxidation rate of Fe-5Cr alloy in the presence of Na$_2$SO$_4$ deposits this was attributed to sulphide formation mechanism which initially restricted spinel formation. (Trafford & Whittle, 1980 A).
Fe-13Cr Alloy	-Do-	In their another study conducted on Fe-13% Cr alloy under similar conditions, Na$_2$SO$_4$ coating markedly enhanced the oxidation rate and resulted in the formation of thick, compact and stratified scales. They postulated that formation of sulphides in the alloy substrate and mechanical failure of scale are responsible for the enhanced oxidation. (Trafford & Whittle, 1980 B)
18:8 Austenitic Steel	Na$_2$SO$_4$ and Na$_2$SO$_4$+ NiSO$_4$, Na$_2$SO$_4$+ CoSO4 and Cr$_2$(SO$_4$)$_3$, (NH$_4$)$_3$MoO$_4$, NaVO$_3$ or Na$_2$WO$_4$ 650 to 1000^{0}C in air	Steels coated with a mixture of Na$_2$SO$_4$+ NiSO$_4$ and Na$_2$SO$_4$+ CoSO$_4$ showed higher corrosion rates than either the Na$_2$SO$_4$ or transition metal sulphate coated at 650^{0}C,this has been attributed to formation of low temperature eutectics. At 1000^{0}C, except the Cr$_2$(SO$_4$)$_3$ or CoSO$_4$ coated steel, the steel coated with all other salts e.g. NaVO$_3$, Na$_2$WO$_4$ or (NH$_4$)$_3$MoO$_4$, has much higher corrosion rates than the Na$_2$SO$_4$ coated steel. The decomposition of these salts into volatile oxides e.g. WO$_3$, V$_2$O$_5$ or MoO$_3$ has been reported to be the sole reason for catastrophic oxidation. (Malik et al, 1984)

Material	Environment	Findings
Steel SS 110, AISI 303 and 18 Cr-8 Ni	Ash residues from coals of Indian origin at 650 and 1000°C	Ash was non-aggressive at low temperatures of 650 and 850°C due to its inability to form alkali trisulphates. At temperatures of 900 and 1000°C the coal ash showed corrosivity as a result of combined sulphidation and molten alkali sulphate attack. The high ash with higher SiO_2 content was invariably more aggressive than the low ash which contained more silicates. (Malik and Ahmad, 1984)
Ferritic Steel	Na_2SO_4 in combustion gas 600-800°C	Accelerated corrosion rate is related to the formation of a liquid layer by dissolution of metal sulphates in Na_2SO_4. Metal sulphides are formed in the inner scale region and partial scale dissolution in the salt occurs due to the presence of liquid layer. Precipitation of solid particles in the liquid results in a porous non-protective layer. (Gesmundu and Nanni)
Ferritic Steels containing Cr, Al & Ti	Fused salt mixture containing Na_2SO_4 at 927°C and gas mixture CO, CO_2, CH_4, H_2O, H_2 and H_2S at 600°C	The presence of Ti with 12 % Cr and 3% Al increases the proportion of Fe which diffuses to the outer layer of the scale. The excellent behaviour of steels at temperatures above 600°C is explained by the increase of Al diffusion coefficient with temperature. (Coze et al, 1989)
AISI 304 Steel	$Na_2SO_4 + Fe(SO_4)_3$	The inner layers of the scales contained Cr_2S_3 followed by a thick but discontinuous layer of FeS. The middle layer forming bulk of the scale seemed to contain Na_2CrO_4, $NaFeO_4$ and $NaNiO_4$ while the outer layer composed of Fe_2O_3. The cracking of the scale has been attributed to these fluxing products and to the evolution of gases. (Misbahul Amin, 1994)
Low Alloy Steel High Alloy Steel	NaCl or fly ash at 500°C, 600°C & 700°C	The chlorides reacted with the scale forming $FeCl_2$ (s) at the scale/metal interface, evaporation of $FeCl_2$ (g) and its oxidation to Fe_2O_3 at the scale surface, chlorine partially returning to the scale. This resulted in porous non- protective scale and active oxidation. (Grabke et al, 1995)
Austenitic Stainless Steel	Molten Alkali Sulphate deposits 850°C	The formation of $(Na, K)_3Fe(SO_4)_3$ was found to be responsible for the accelerated corrosion of the steel in a mixture of $Na_2SO_4+K_2SO_4$. $Na_2SO_4+CaSO_4$ or $CaSO_4+K_2SO_4$ formed low melting eutectics, which first attacked the protective chromia scales followed by the formation of iron trisulphate as well as fluxing products. (Amin, 1996)
9Cr-Mo Steels (T91 & EM12)	Synthetic environments related coal-fired boilers 460-800°C	The corrosion kinetics of both steels in air was reported to follow a cubic rate law. They further observed that a maximum corrosion rate was at approximately 600°C. At the same temperature, this maximum was observed for specimens oxidized with an ash deposit enriched in alkali salts. The rates of corrosion increased when temperature approached 800°C which has been attributed to the melting of alkali silicates. (Colot et al,1997)

286

Material	Conditions	Observations
304 Stainless Steel	Thin films (1mm) of molten sulphate synthetic flue gas, 650°C upto 2000 h analyzed at 200h intervals	The concentration of elements Fe, Cr and Ni entering the melt after the initial attack remained essentially constant for around 800 h, after which spallation of the protective Cr_2O_3 layer and rapid attack occurred over the next 400 h, by which time the protective layer had reformed. The pre-carburised coupons produced a several-fold increase in Fe, Cr and Ni concentrations in the melt over the pre-oxidized coupons. Stop-start corrosion mechanism confirmed that increased corrosion can take place if superheater and reheater tubes made of 304 stainless steel are subjected to reducing conditions during a failed start up procedure or subsequently. (Griffiths and Phillips, 2001)
Alloy 800H	SO_2-O_2, 750°C and 850°C	Protective chromia scale developed on the alloy in the early stages cracked and spalled in quite a short time period. This led to the growth of iron and nickel sulphides beneath the chromia layer, causing more chromia spallation. (Xu et al, 1994)
Fe-, Ni- and Co-base Superalloys	Combustion gases and Na_2SO_4 600°C and above	Mo delayed the initiation of hot corrosion attack because the formation of MoO_3 inhibited the formation of oxide ions in the melt. Ta did not produce deleterious effect, due to the formation of high melting sodium tantalate by avoiding sodium molybedate formation. Nb adversely affected hot corrosion resistance but enough data is not available for its reasoning. W, Mo and V are also harmful as their oxides induced acidic fluxing. Cr and Al produced beneficial effects by formation of protective oxide on alloy surfaces. (Pettit & Meier, 1984)
Fe-, Ni- and Co-base Alloys	SO_2, SO_3 & O_2 atmospheres	It has been reviewed that the lowest sulphur pressure required to form FeS is p_{s_2} =2.25 x 10^{-11} atmosphere whereas oxygen pressure p_{o_2} = 4.49 x 10^{-13} atmosphere. The condition for S diffusion across the oxide layer is p_{s_2} (gas/ MO) > p_{s_2} (MO/M). S transport through oxide may result in sulphide formation at the scale/metal interface or within the oxide. (Stroosnijder and Quadakkers, 1986)
Fe_3Al-5Cr	Air and 1% SO_2-air 605°C and 800°C	Hot Corrosion of iron aluminide was significantly more severe than oxidation and mixed oxidation-sulphidation which they attributed to the formation of aluminium sulphide at the interface of metal-salt and faster diffusion of oxygen through the molten salt covering the specimen surface. (Lee and Lin, 1999)

287

Material	Conditions	Observations
Binary Iron Aluminide (Fe₃Al)	Na_2SO_4 (2.5±0.2 mg/mm²) in pure oxygen 1100 K, 1225 K and 1330K	The faster kinetics observed in the initial stages of oxidation have been related to the formation of θ-Al_2O_3 and slower kinetics in the later stages of oxidation to the formation of α-Al_2O_3. The overall rate of hot corrosion was higher than that of oxidation at all temperatures. The presence of α-Fe_2O_3 in addition to alumina was indicated by XRD. Cross-sectional microscopy revealed that the metal-scale interfaces were pitted in hot corrosion conditions and the pits contained aluminium sulphide. Sulphides were also detected along grain boundaries in the intermetallic near the scale-metal interface. (Das et al, 2002).
Pure Nickel	Na_2SO_4-$CaSO_4$ salt mixtures at 900°C in purified oxygen	For salt mixtures containing 80% or more of $CaSO_4$, the sulphide layer was found to be virtually absent and sulphide particles were dispersed in the oxide layer. The authors concluded that the sulphur diffusing through the initial oxide was totally consumed by nickel sulphide (Ni_3S_2) formation within the oxide layer and did not reach the Ni-NiO interface. (Arbab & Shatynski, 1985)
Pure Nickel	Molten Na_2SO_4 at 900°C under SO_3 + SO_2 + O_2 gas mixture & SO_2 and O_2 atmospheres	The corrosion loss in mixed atmosphere containing SO_3 is reported to be larger than those observed in pure SO_2 and O_2 atmospheres. The corrosion loss was found to correspond to the thickness of the oxide layers. High corrosion losses have been attributed to the fact that SO_3 strongly acts as an oxidizing agent for the corrosion process. (Motihara, et al 1991)
Pure Nickel Udimet 700	Na_2SO_4 in a high velocity burner rig, 900°C -Do-	Corrosion of Ni in the burner rig produced a relatively compact NiO scale along with some internal grain boundary corrosion. Corrosion of Udimet 700 was observed to occur in two stages. During the first stage, the corrosion proceeded by the reaction of Cr_2O_3 scale with the Na_2SO_4 and evaporation of the Na_2CrO_4 reaction product from the surface of the corroding sample. Cr depletion in the alloy occurred and sulphide particles were formed in the Cr depletion zone. Extensive sulphidation occurred during the second stage of corrosion and a thick scale formed. (Misra, 1987)
Nickel	Thin fused Na_2SO_4 film in an SO_2-O_2 gas atmosphere at 900°C	Chromate anion suppressed the sulphidation of Ni probably by precipitating solid Cr_2O_3 from the melt. Vanadate anions enhanced the onset of the hot corrosion and sulphidation probably via rapid dissolution of the protective oxide scale at cracks/defects or grain boundaries. (Otuska & Rapp, 1990)
B-1900	Na_2SO_4	Na_2SO_4 interacted with the alloy to form sodium and sulphur compounds, rapid removal of sulphur from the Na_2SO_4 by unretarded diffusion of sulphur and precipitation of Cr-rich sulphide phases promoted the formation of Na_2O. The catastrophic oxidation observed during sulphidation was due to interactions between Na_2O and the substrate. (Bornstein and Decresente, 1970)

Alloy	Conditions	Observations
Nickel-base Alloys	Na_2SO_4 1 atm oxygen 650 to 1000°C	Authors observed that catastrophic or self-sustaining rapid oxidation can occur in alloys which contain Mo, W or V because solutions of oxides of these elements with Na_2SO_4 decrease the oxide ion activity of the molten salts, producing melts which are acidic fluxes for oxide scales. The accelerated oxidation type of attack was observed with most alloys which did not contain Mo, W or V was more severe than normal oxidation but much less than catastrophic oxidation. (Goebel, et al 1973)
Ni-Cr and Ni-Al Alloys	Na_2SO_4 with addition of 1% PbO at 900°C	1% PbO to Na_2SO_4 resulted in large increase in the rate of hot corrosion of Ni-Cr alloys at 900°C this is ascribed to the formation of $PbCrO_4$ which is soluble in molten Na_2SO_4 and became more significant with increasing Cr content in the alloy. Catastrophic corrosion resulted with alloys containing 10-15% Cr. The Na_2SO_4 induced hot corrosion of Ni-30Al was also enhanced by the addition of PbO to the salt. This is attributed to the formation of a soluble complex PbO. Al_2O_3. (Chatterji et al, 1975)
Ni-15Cr-Mo alloys	Na_2SO_4 coating for 24 hr at 900°C	Authors concluded that greater the Cr content, the greater is the resistance to hot corrosion. For the complex alloys acid fluxing seemed to be a more probable process than basic fluxing. The breakaway to catastrophic attack was clearly related to Mo content. For Ni-15%Cr to 25%Cr, threshold amount of Mo is 3-4% below which catastrophic attack is not encountered. Above 3-4% Mo catastrophic attack was encountered. (Peters, Whittle & Stringer, 1976)
Ni-23.1 Nb-4.4Al and Ni-19.7Nb-6.0 Cr-2.5Al	Na_2SO_4 coating Dean rig test at 900°C and 1100°C	Below the outer layer, mainly of $NiNb_2O_6$, high proportion of Al_2O_3 has been reported to be present. Internal oxidation of the metal producing Al_2O_3 and Cr_2O_3 is believed to occur before the development of external Al_2O_3 layer. In some isolated regions the alloy was found to be much more severely attacked, the pit contained $NiNb_2O_6$, $NbCrO_4$ and Ni. At 1100°C, more uniform corrosion is reported, the outer layer was mainly $NiCr_2O_4$ and beneath it a layer of Cr_2O_3 containing particles of $NbCrO_4$ was observed. Internal oxides were mainly Al_2O_3 and there were massive Ni-rich sulphides ahead of oxidation front. (Johnson et al, 1978)
Ni-30Cr and Co-30Cr	Na_2SO_4, 600-900°C, accelerated oxidation tests	The rapid rate of attack is explained on the basis of sulphation of the transient surface oxides (Ni or Co oxides) and the dissolution of these transition metal sulphates into Na_2SO_4 to yield a liquid phase. (Luthra and Shores, 1980)
Nimonic 105	Na_2SO_4, NaCl and mixtures of the two 900°C, in air & O_2+SO_2/SO_3	Pure Na_2SO_4 in air did not seem to be very corrosive towards Nimonic 105. SO_3 pressures below 5×10^{-3} did not affect the electrokinetic behaviour, but pressures greater than 5×10^{-3} atmospheres produced higher corrosion rates which may be attributed to the acid fluxing by the sulphate melt. Addition of NaCl to the molten Na_2SO_4 resulted in increased dissolution of Nimonic 105. (Sequeira and Hocking, 1981)

Ni-base Superalloys, B-1900 and NASA-TRW IVA	Na_2SO_4 salt deposit at 900°C in pure O_2	After an induction period of little corrosion, local basic fluxing attack of the Cr_2O_3/Al_2O_3 scale spreaded to cover the surface and generated catastrophic linear kinetics. *During catastrophic attack of B-1900, the sulphate ions reacted to release SO_2 and formed sulphides in the alloy and salt was converted to Na_2MoO_4.* (Fryburg et al, 1982)
Nickel-200, Rene-80 and CoCrAlY Coating	$NiSO_4$-Na_2SO_4 at 750°C	Little corrosion was reported when solid solution mixed sulphates formed on the metal surface, but severe corrosion occurred when molten sulphates were formed. In nickel-200, *corrosion proceeded by liquid Ni_3S_2-Ni formation below the surface oxide.* No discernible sulphide was produced with Rene-80 and CoCrAlY which gave the characteristic LTHC morphology. Ternary Ni, Co, Na-sulphates were detected in the CoCrAlY corrosion. (Jones and Godmski, 1982)
B-1900 Superalloy	10% Na_2SO_4-90% $CaSO_4$ at 900°C in air for 6, 12 and 24 h of exposure	The addition of $CaSO_4$ has been observed to reduce dramatically the magnitude of Na_2SO_4-induced hot corrosion of the alloy at 900°C. Trace quantity of PbO impurity in coal caused catastrophic corrosion owing to severe grain boundary attack. (Stewart & Shatynski, 1982)
Ni base Alloys (Nimonic Alloys)	Na_2SO_4 with and without $NiSO_4$, $CoSO_4$ and $Cr_2(SO_4)_3$, air, 650-1000°C	Lower oxidation rates upto 800°C are attributed to scale morphology consisting of inner scale of Cr_2O_3 acting as protective oxide film and external scales of NiO. This morphology is maintained at higher temperature. The formation of transition metal oxide film upto 800°C or a mixed oxide film at higher temperatures has been reported the main reason for lower oxidation rates. (Malik and Ahmad 1983)
IN738 Pre-oxidized	Na_2SO_4 975°C in oxygen	During an induction period of 55 hrs first Cr_2O_3 and then TiO_2 were dissolved as basic solutes in Na_2SO_4. There after the oxidation of Mo and W formed liquid Na_2 (MoO_4, WO_4), which served as a flux for the acidic dissolution of Cr_2O_3 and Al_2O_3. The beneficial effect of Ta with respect to hot corrosion attack is explained on the basis of the ability of the Ta_2O_5 to tie up the Na_2O and prevent the formation of a molten Na_2MoO_4 phase. ΔG is reported to be more negative for formation of $NaTaO_3$ than Na_2MoO_4. (Fryburg et al, 1984)
Ni-base Superalloys containing Mo	Na_2SO_4 in O_2, 750-950°C and in $O_2 + SO_2$ at 950°C	The alloys underwent catastrophic corrosion, which has been reported to be associated with the formation of Na_2MoO_4-MoO_3 melt. It is suggested that rapid corrosion occurs by dissolution of Ni at the melt-alloy/oxide interface and formation of NiO at the melt-gas interface. (Misra, 1986 A) Catastrophic corrosion was observed for lower SO_2 levels (<0.24%), and a highly porous scale was developed in Udimet 700 at 950°C. This catastrophic corrosion was observed to be associated with the presence of MoO_3 in the melt along with Na_2SO_4 and Na_2MoO_4. (Misra, 1986 B)

290

Material	Environment	Remarks
Ni and Ni-base Alloy EI 867 with the Aluminide and Cr-Al Diffusion Coatings	Pure Na$_2$SO$_4$	Low alloyed aluminide and Cr-Al coatings showed very poor resistance to oxidation. After 24 hrs, these had been almost completely removed. Modification of highly alloyed aluminide coatings with Cr resulted in uniform and relatively slow degradation of the coating. Cr enriched zone is supposed to act as a barrier to the oxidation of refractory metals such as Mo, W and V thus preventing the onset of catastrophic corrosion. (Godlewski and Godlewska, 1987)
IN 738 Superalloy, Ni-22Cr, Ni-20Cr-3Al and Ni-20Cr-4Mo	In SO$_2$ / O$_2$ atmosphere at 700 and 900°C.	Al improved the corrosion resistance at 700°C. Mo had a detrimental effect on the corrosion rate due to the volatile MoO$_3$. At 900°C IN 738 and at 700°C Ni-20Cr-Al improved to be the best. In the first stage, initial oxide layer was built up immediately, in the second stage external oxide layers and sulpliide areas were built up whereas in the third stage, internal sulphide structure was developed. (Sidky and Hocking, 1987A & B)
Ni-16Cr-2Nb, IN 738, Ni-16Cr and Superalloy 537	Na$_2$SO$_4$ 900 and 1000°C	Na$_2$SO$_4$ coated coupons of Ni-16Cr-2Nb and Ni-16Cr developed dense, protective oxide scales and exhibited good hot corrosion resistance. Alloys 537 and IN 738 experienced a shift from basic fluxing to acidic fluxing and as the temperature was increased, the rate of attack increased significantly. (Zho et al, 1987)
Ni- base Alloys	Na$_2$SO$_4$(s) and NaCl(s) in air 850 and 1000°C	Cr$_2$O$_3$ formers were found to be more aggressively attacked by NaCl than Na$_2$SO$_4$. An increase in the amount of NaCl in the Na$_2$SO$_4$-NaCl mixture greatly enhanced their corrosion rates. Weight losses observed during the hot corrosion have been attributed to several factors viz. formation of volatile chromate, chlorides and gaseous SO$_2$/SO$_3$. (Malik et al, 1988)
Ni-base Superalloys	Na$_2$SO$_4$ in air 704 & 900°C	The alloys showed high wt. loss at 900°C. Thick corrosion products formed on the alloys were stated to be composed of oxides near the gas interface and of sulphides adjacent to the unaffected substrate. At 704°C more severe attack was reported when 45 mole % MgSO$_4$ was added to Na$_2$SO$_4$. Addition of SO$_3$ to gas mixture containing oxygen at 704°C caused severe corrosion of many alloys. (Levy et al 1989)
Pure Nickel Inconel 600 Incoloy 825	Molten Na$_2$SO$_4$ deposit oxidizing gaseous environments (Ar + 300 ppm O$_2$) and Ar+1%O$_2$ 940°C	Pure nickel showed enhanced oxidation in Ar +1% O$_2$ with Na$_2$SO$_4$ deposit of 5mg/cm^2. Inconel 600 is able to form a protective layer of chromia in Ar +1% O$_2$ with or without a thin layer of Na$_2$SO$_4$. But Incoloy 825 was not able to form chromia in Ar +1% O$_2$ with or without Na$_2$SO$_4$ which was attributed to the formation of nickel and chromium molybedates due to 3.22% Mo present in the alloy. When O$_2$ content is only 300ppm, sodium sulphate layer strongly enhanced the corrosion of Inconel 600 and Incoloy 825 but no attack was detected on pure nickel. (Santorelli et al, 1989)

291

Alloy	Conditions	Observations
Nimonic-75	90% Na_2SO_4 and 10% NaCl 700-1000°C in welded and unwelded conditions.	While the oxidation attack increased with temperature, the hot corrosion attack dropped in the higher ranges of temperature. This is attributed to vaporization of the salt mixture. The weight gain due to oxidation and hot corrosion followed a power function the exposure time. (Sreenivas and Radhakrishnan, 1998)
CM 247 LC Superalloy	Na_2SO_4 and Na_2SO_4+NaCl mixtures 900°C	It was observed that bare CM 247 LC was severely corroded in just 4 hr, while it was completely consumed in 70 hr when tested in 90%Na_2SO_4+10%NaCl at 900°C. The results showed that a chloride containing melt is more corrosive than pure sodium sulphate. (Gurrappa, 1999)
Fe- and Ni-base Commercial Wrought Alloys	Burner rig test Two fuel sulphur contents (0.4 and 1.0 wt%) and synthetic sea salt 900°C	Ni-base alloys tested exhibited superior hot corrosion resistance over the Fe-base alloys. When exposed to a 1000-hour test with the injection of 50 ppm salt, the Fe content of a Ni-22Cr-18 Fe-9Mo alloy appeared to be detrimental to the hot corrosion resistance of this alloy when compared to a Ni-22 Cr-9Mo alloy. The W content in a Ni-22 Cr-14 W alloy did not show a detrimental affect on the hot corrosion resistance of this material. Also, Fe-base alloys containing less than 25 wt% Cr did not perform well in a 500-hour test burning fuel containing 1.0 wt% sulphur and 50 ppm salt injected into the combustion zone. Reasons for the performance of the alloys are suggested to be the 'quality' or protectiveness of the oxide scale grown on a given alloy. (Harper, Barnes and Regan, 1999)
Ni-base Superalloys containing Re and Ta and Mar-M247 alloy	Mach 0.3 Burner rig at 900°C for 300 1-hr cycles	The hot corrosion behaviour of all four new alloys containing same Al level as in Mar-M247 but decreased Cr and Co and increased strengthening elements (Re and Ta) was superior to that of the Mar-M247 alloy. The Mar-M247 alloy began to lose weight almost immediately whereas the other four alloys appeared to undergo an incubation period of 50-150 1-hr cycles. Cross-sectional microstructures showed regions of rampant corrosion attack (propagation stage) in all five alloys after 300 1-hr cycles. This rampant corrosion morphology was similar for each of the alloys with Ni and Cr sulphides located in an inner subscale region. From the observed morphology, the attack was suggested a classic 'Type I', or high temperature, hot corrosion attack. (Nesbitt et al, 2001)
Co-base Alloys HA 188 and S-57 under Cyclic Condition	Sea salt + Na_2SO_4 at 900-1000°C for 100h by Burner rig test.	An outer porous scale of CoO and Cr_2O_3 was observed on alloy S-57 and the thickness was more at 1000°C than that at 900°C. Most of the outer scale spalled upon thermal cycling. Beneath the porous scale was a dense scale consisting of spinels probably $CoCr_2O_4.25CoAl_{20}O_4$. The internal corrosion zone was reported to be consisting of Al and S. (Santaro, 1979)

Material	Environment	Remarks
Cobalt	SO_2 atmosphere, 800-1000°C	Reaction of cobalt with SO_2 at 800-1000°C generally leads to simultaneous oxide formation and sulphurization. At sufficiently high temperatures around 1000°C, and reduced SO_2 pressure, CoO was the only reaction product observed. (Holthe and Kofstad, 1980)
Co-Cr, Co-Cr-Ta and Co-Cr-Ti Alloys	Dry air containing vapours of Na_2SO_4, $Na_2SO_4+Na_2O$ and Na_2SO_4+NaCl 900°C in a Dean'rig	Basic salt was more aggressive to binary Co-Cr alloys, suggesting basic fluxing mechanism. Presence of Ta and Ti content was high enough to produce second phases in the alloys, preferential attack along the phase boundaries occurred. The presence of NaCl in the salt greatly enhanced the attack by cracking the outer oxide scale and by forming volatile compounds. (Nagarajan, Stringer and Whittle, 1982 A)
Co-Cr-Al Alloys	-Do-	The presence of small amounts of Al in Cr_2O_3 forming alloys had relatively little effect. Chromium contents of 20% and above showed excellent hot corrosion resistance to both Na_2SO_4 and the basic salt. Remained unattacked even 20 days of exposure. Presence of NaCl was always detrimental, leading to scale fracture and enhancing internal sulphidation. (Nagarajan, Stringer and Whittle, 1982 B)
Co-Cr-Mo Alloys	-Do-	Presence of Mo in general caused accelerated and sometimes catastrophic corrosion. The influence of 2.5% Mo addition was observed to be minimum. The presence of 10% Mo in the CoO forming alloys caused acidic fluxing in the pure Na_2SO_4. The higher Cr (20 and 25%) containing alloys suffer accelerated and sometimes catastrophic corrosion in all the environments which has been they have reported due to the formation of volatile and low-melting oxides of Mo. (Nagarajan, Stringer and Whittle, 1982 C)
Co-Cr, Co-Al and Co-Cr-Al Alloys.	Na_2SO_4 600 to 750°C in O_2-SO_2-SO_3	Co-Cr and Co-Cr-Al alloys reacted non-uniformly, usually in the form of pits and Co-Al alloys suffered broad frontal attack. Under all conditions, a thin sulphur-rich band containing sulphides was observed at the alloy/scale interface and cobalt dissolved near the interface and formed Co_3O_4 /or $CoSO_4$ (S). (Luthra, 1982)
Co-Cr, Co-Al and Co-Cr-Al Alloys	Na_2SO_4, in O_2-0.15% (SO_2+SO_3) at 750°C.	Accelerated oxidation tests at 750°C showed that the corrosion resistance of binary Co-Cr and Co-Al alloys increases with the Cr and Al content of alloys. This protection is offered by the rapid growth of $CoCr_2O_4/Cr_2O_3$ and $CoAl_2O_4/Al_2O_3$ oxides in comparison to CoO and Co_3O_4. At high enough Cr ($\geq 40\%$) and Al ($\geq 15\%$) concentrations, the growth rates are so fast that liquid does not even form consequently the corrosion rates are very low. Tests on Co-Cr-Al alloys indicated that simultaneous presence of Cr and Al is deleterious to the resistance against low temperature hot corrosion. (Luthra, 1985)

Co-Cr Alloys containing about 37.5 wt. % Cr	Na$_2$SO$_4$	Corrosion was caused by the formation of Na$_2$SO$_4$-CoSO$_4$ eutectic (melting point 575°C). However, the presence of Al possibly interfered with the formation of CoCr$_2$O$_4$ and Cr$_2$O$_3$. Addition of small amount of reactive element such as Y or Hf to Co-37.5 to 50 wt% Cr alloy had been shown to promote scale adhesion. (Luthra & Leblanc, 1987)
CoCrAlY Alloy	MgSO$_4$ - Na$_2$SO$_4$ melts 973 K (eutectic m.p.)	The presence of MgSO$_4$ in Na$_2$SO$_4$ affected the chemistry of corrosion behaviour of sulphate melt in relation to the LTHC of CoCrAlY alloy. Less sulphation of Co$_3$O$_4$ by SO$_3$ was found with 50 m/o of MgSO$_4$ - Na$_2$SO$_4$ than with pure Na$_2$SO$_4$ and there was less corrosion in SO$_3$ for CoCrAlY coupons coated with 50 m/o of MgSO$_4$ - Na$_2$SO$_4$. Corrosion initially observed was found to be controlled by sulphidation/dissolution of cobalt oxide from the CoCrAlY surface- a process that MgSO$_4$ inhibits. At a later stage, the corrosion rate was believed to be controlled by involving S rich phases at the corrosion front. (Jones and Williams, 1986)
Aluminide coated Co-base Superalloy (DZ40M)	Air, isothermal & cyclic oxidation at 1000°C	Coating degradation primarily resulted from Al-depleting to heal the oxide scale on the outer surface during the cyclic oxidation, unlike that primarily from inward Al diffusion to the substrate during isothermal process. Ti increased the degradation of the present coating during high-temperature oxidation. (Liu et al, 2001)

Interactions of metal oxides such as Co$_3$O$_4$, NiO, Al$_2$O$_3$, Cr$_2$O$_3$, Fe$_2$O$_3$ and SiO$_2$ with Na$_2$SO$_4$ at 1100 &1200K resulted in reaction products having three phase structure Viz.Na$_2$O.M$_2$O$_2$.M$_2$O$_x$ and metal sulphide and /or metal sulphate. It was proposed that the formation of Na$_2$O.M$_2$O$_x$ depended on the solid-state solubility of metal oxide in the molten salt at high temperatures. Under limited solubility conditions Na$_2$O.M$_2$O$_x$ was invariably formed, but as soon as this condition was relaxed the oxide M$_2$O$_x$ precipitation occurred and formed a separate phase. Decrease in wt. loss value with increasing Na$_2$SO$_4$ has been attributed to binding of sulphur in the form of metal sulphide or metal sulphate. (Mobin et al, 1996)

REFERENCES

1. Almeraya, F., Martinez-Villafane, A., Gaona, C., Romero, M.A. and Malo, J.M., (1998 A), "Hot Corrosion of the Steel SA213-T22 and SA213-TP347H in 80% V_2O_5-20% Na_2SO_4 Mixture," *Revista de Metalurgia*, Vol. 34, No. 1, pp. 11-17.

2. Almeraya-Calderon, F., Mertinez-Villafane, A. and Gonzalez Rodriguez, J.G., (1998 B), "Electrochemical Studies of Hot Corrosion of Type 347H Stainless Steel," *British Corros. J.*, Vol. 33, No. 4, pp. 288-91.

3. Amin, M.M, (1994), "Oxidation behaviour of AISI-304 steel in the presence of Na_2SO_4 and $Fe_2(SO_4)_3$ at 973K, *Thin Solid Films*, 237, pp. 172-74.

4. Amin, M.M, (1996), "Hot Corrosion of Austenitic Steel in Molten Alkali Sulphate deposits at 850^0C," *Practical Metallography*, Vol. 33, No. 5, pp.256-63.

5. Arbab, M. and Shatynski, S.R., (1985), "Hot Corrosion of Nickel in Na_2SO_4-$CaSO_4$ Mixtures," *J.Electrochem. Soc.*, Vol. 132, No. 9, pp. 2264-28.

6. Barbooti, M.M., Al-Madfai, S.H. and Nassouri, H.J., (1988), "Thermomechanical Studies on Hot Ash Corrosion of Stainless Steel 304 and Inhibition by Magnesium Sulphate," *Thermochimica. Acta*, 126, pp. 43-49.

7. Beltran, A.M. and Shores, D.A., (1972), "*Hot Corrosion Ch. 11*," *The Superalloys*, Eds. Sims, C.T. and Hagel, W.C., Wiley Publ., John Wiley and Sons, N. Y.

8. Bhaskar Natarajan, (August, 2001), Special Feature: Energy Conservation and Environment, *Frontline* Magazine, pp. 109.

9. Blaustein, E., of Pentol GmbH, D-7858 Weil a/Rhein, West Germany,"Technical Evaluation of Magnesia's Influence on Fireside Deposits, Combustion and Emissions on Oil-Fired Boilers"-*A Report*.

10. Bornstein, N.S. and DeCrescente, M.A., (1969), *Trans. AIME*, No.245, pp. 583.

11. Bornstein, N.S. and DeCrescente, M.A., (1970), "The Role of Sodium and Sulfur in the Accelerated Oxidation Phenomena-Sulphidation," *Corrosion*, Vol. 26, No. 7, pp. 209-14.

12. Bornstein, N.S. and DeCrescente, M.A., (1971), *Met. Trans.*, No.2, pp. 2875.

13. Bornstein, N.S. and DeCrescente, M.A., (1972), "Interaction Between Vanadium in Gas Turbine Fuels and Sufidation attack," *Corrosion*, Vol. 28, pp. 264.

14. Bornstein, N.S., DeCrescente, M.A. and Roth, H.A., (1973), "The Relationship Between Relative Oxide Ion Content of Na_2SO_4, the Presence of Liquid Metal Oxides and Sulfidation Attack," *Metall. Trans.*, Vol. 4, pp. 1799-1810.

15. Bornstein, N.S., DeCrescente, M.A. and Roth, H.A., (1975), "Effect of Vanadium and Sodium Compound on the Accelerated Oxidation of Nickel Base Alloys," *Proc. of Conf. On Gas Turbine Mater. in the Marine Environment, MMIC-75-27*, Columbus, Ohio, USA, pp. 115-60.

16. Castello, P., Stott, F.H. and Gesmundo, F., (1999), "Yttrium-Promoted Selective Oxidation of Aluminium in the Oxidation at 1100^0C of an Eutectic $Ni-Al-Cr_3C_2$ Alloy," *Corrosion Science*, Vol. 41, pp. 901-18.

17. Chatterji, D., Mckee, D.W., Romeo, G. and Spacil, H.S., (1975), "The Effects of Lead on the Hot Corrosion of Nickel-Base Alloys," *J. Electrochem. Soc.*, Vol. 122, No. 7, pp. 941-51.

18. Chen, H.C; Liu, Z.Y. and Chuang, Y.C., (1993), "Degradation of Plasma-Sprayed Alumina and Zirconia Coatings on Stainless Steel during Thermal Cycling and Hot Corrosion," *Thin Solid Films*, Vol. 223, No. 1, pp. 56-64.

19. Chengbo Xiao and Yafang Han, (1999), "Effect of Yttrium on Diffusion Layer of Ni-Al-Mo-B alloy IC6 during High Temperature Oxidation Process," *Scripta Metallurgica*, Vol. 41, No. 11, pp. 1217-21.

20. Clark, G.M. and Morley, R., (1976), "A Study of the $MgO-V_2O_5$ System," *Journal of Solid State Chemistry*, Vol. 16, pp. 429-435.

21. Colot, D., Petelot, D., Hoch, P. and Beranger, G., (1997), "Mechanisms of hot Corrosion in Coal Fired Boilers Gas T91 and EM12 Steels," *Materials Science Forum*, Vol.251-254, No. part 2, pp. 641-48.

22. Coze, L. J., Franzoni, U., Cayla, O., Devisme, A. and Lefort, A., (1989), "The Development of High-Temperature Corrosion-resistant Aluminium-containing Ferritic Steels," *Mater. Science and Engineering*, A.120, pp. 293-300.

23. Cuevas-Arteaga, C., Porcayo-Calderon, J., Izquierdo, G., Martinez-Villafane, A. and Gonzalez-Rodriguez, J.G., (2001), "Study of Hot Corrosion of Alloy 800 using Linear Polarization Resistance and Weight Loss Measurement," *Materials Science and Technology*, 17, (7), pp. 880-85.

24. Das, D., Balasubramaniam, R. and Mungole, M.N., (2002), "Hot Corrosion of Fe_3Al," *Journal of Materials Science*, Vol. 37, No. 6, pp. 1135-42.

25. Deadmore, D.L. and Lowell, C.E., (1978), *Rep. TM 78966*, (NASA Lewis Research Center, Cleveland, OH).

26. Deanhardt, M.L. and Stern, K.H., (1982), "Solubility of Yttrium Oxide in Na_2SO_4 and NaCl Melts," *J. Electrochem. Soc.: Electrrochemical Science and Technology*, Vol. 129, No. 10, pp. 2228-32.

27. Deb, D., Iyer, S. R. and Radhakrishnan, V.M., (1996), "A Comparative Study of Oxidation and Hot Corrosion of A Cast Nickel base Superalloy in Different Corrosive Environment," *Mater. Letters*, Vol. 29, pp. 19-23.

28. Dooley, R. B. and Wilson, J. R., (1975), "The Corrosion of A 50Cr-50Ni Alloy in Liquid Vanadate Systems in the Temperature Range 750-950^0C," *Transactions of the ASME*, July, pp. 422-28.

29. Ecer, G.M., Singh, R.B. and Meier, G.H., (1982), "The Influence of Superficially Applied Oxide Powders on the High-Temperature Oxidation Behavior of Cr_2O_3 Forming Alloys," *Oxidation of Metals*, Vol. 18, No. 1/2, pp. 55-81.

30. Fairman, L., (1962), "Technical Note: Mechanism of Accelerated Oxidation by Vanadium-Containing Fuel Ash," *Corros. Sc.*, Vol. 2, pp. 293-96.

31. Fichera, M., Leonardi, R. and Farina C.A, (1987), "Fuel Ash Corrosion and its Prevention with MgO Addition," *Electrochem. Acta*, Vol. 32, No. 6, pp. 955-60.

32. Foggo G., Nordman D. B. and Jones R.L., (1984), "Inhibition of Low Temperature Hot Corrosion by Zn, Na Mixed Sulphates," *J. Electrochem. Soc.*, Vol. 131, No.3, pp. 515-22.

33. Fryburg, G.C., Kohl, F.J., Stearns, C.A. and Fielder, W.L., (1982), "Chemical Reactions Involved in the Initiation of Hot Corrosion of B-1900 and NASA-TRW VIA,"*J. Electrochem. Soc.*, Vol. 129, No. 3, pp. 571-85.

34. Fryburg, G.C., Kohl, F.J. and Stearns, C.A., (1984), "Chemical Reactions Involved in the Initiation of Hot Corrosion of IN-738," *J. Electrochem. Soc.*, Vol. 131, No. 12, pp. 2985-96.

35. Gesmundo, F. and Nanni, P., "Low Temperature Hot Corrosion of Two Low-Chromium Commercial Steels," Instituto Chimica Fisica Applicata Dei Materiali, Genova (Italia), pp. 54 ter-1 to 54 ter-6.

36. Gesmundo, F. and Viani, F., (1988), "The Mechanism of Low-Temperature Corrosion of Pure Iron and Manganese At 600-800°C," *Materials Chemistry and Physics*, 20, pp.513-28.

37. Gitanjaly, Prakash, S. and Singh, S., (2002), "Effects of MgO and CaO on Hot Corrosion of Fe-base Superalloy Superfer 800H in Na_2SO_4-60%V_2O_5 Environment," *British Corrosion Journal*, Vol. 37, No. 1, pp. 56-62.

38. Godlewski, K. and Godlewska, E., (1987), "The Effect of Chromium on the Corrosion Resistance of Aluminide Coatings on Nickel and Nickel-based Substrates," *Materials Science and Engineering*, 88, pp. 103-109.

39. Goebel, J. A. and Pettit, F. S., (1970), Met. Trans., 1, pp. 1943.

40. Goebel, J. A., Pettit, F. S. and Goward, G. W., (1973), "Mechanisms for the Hot Corrosion of Nickel-Base Alloys," *Metallurgical Transactions*, Vol. 4, pp. 261-75.

41. Grabke, H.J., Reese, E. and Spiegel, M., (1995), "The Effects of Chlorides, Hydrogen Chloride and Sulfur Dioxide in the Oxidation of Steels below Deposits," *Corrosion Science*, Vol. 37, No. 7. pp. 1023-43.

42. Griffiths, T.R. and Phillips, N.J., (2001), "Thin Film Hot Corrosion Studies of Oxidised and Carburised 304 Stainless Steel," *Materials Science Forum*, Vol. 369-372, No. 1, pp.109-16.

43. Gupta, D.K. and Rapp, R.A., (1980), "The Solubilities of NiO, Co₃O₄ and Ternary Oxides in Fused Na₂SO₄ at 1200 K," *J. Electrochem Soc. Solid State Sc. Technol.*, Vol. 127, No. 10, pp. 2194-2203.

44. Gurrappa, I., (1999), "Hot corrosion Behaviour of CM 247 LC alloy in Na₂SO₄ and NaCl Environments" *Oxidation of Metals*, Vol. 51, No. 5, pp. 353-382.

45. Hancock, P.J., Hancock H.A., Caley, W.F. and Hollingshead R.S., (1989), "A Review of Recent Studies of the Role of Zinc as an Inhibitor of Hot Corrosion from Molten Sulphates," *Material Sci. & Engg.*, A120, pp. 313-18.

46. Hancock, P.J., (1988), *M.A.Sc. Thesis*, Technical University of Nova Scotia, Halifax, NS, Canada.

47. Hancock H.A., Caley, W.F. and Hollingshead R.S., (1985), *Mater. Sc. Monogr.* A, 28, pp. 157-65.

48. Hancock, P., (1987), "Vanadic and Chloride Attack of Superalloys," *Materials Sc. Tech.*, Vol. 3, pp. 536-44.

49. Harlow, W.F., (1944), *Proc. Inst. Mech. Engrs.* (London), 151, pp. 293.

50. Harper, M.A., Barnes, J.E. and Regan, C., (1999), "Hot Corrosion Burner Rig Testing of various Commercial Alloys," *Conference: Corrosion 99*, San Antonio, TX, USA, 25-30 April.

51. Harris, G.T., Child, H.C. and Kerr, J.A., (1955), "Effect of the Composition of Gas-Turbine Alloys on Resistance to Scaling and to Vanadium Pentaoxide Attack," *Journal of the Iron and Steel Institute*, Vol. 179, pp. 342-47.

52. Hocking, M.G., (1993), "Hot Corrosion of Coatings for Superalloys," *I.O.M. Conference*.

53. Suito, H. and Gaskell, D.R., (1971), "The Thermodynamics of Melts in the System VO₂-V₂O₅," *Metall. Trans.*, Vol. 2, pp. 3299-3303.

54. Hollingshead, R.S., (1980), *Canadian Armed Forces Rep. 80.2*, (Defence Research Establishment Atlantic, Dartmouth, NS, Canada).

55. Holt, A. and Kofstad, P., (1989), "High Temperature Corrosion of Iron in O₂ + 4% SO₂/SO₃ at 500-800°C," *Mater. Sc. Engg.*, Vol. A120, pp. 101-104.

56. Holthe, K. and Kofstad, P., (1980), "High Temperature Corrosion of Cobalt in SO_2," *Corrosion Science*, Vol. 20, pp. 919-36.

57. Hou, P.Y. and Stringer, J., (1987), "Effect of Surface-Applied Reactive Metal Oxides on the High Temperature Oxidation of Alloys," *Materials Science and Engineering*, 87, pp. 295-302.

58. Hou, P.Y. and Stringer, J., (1989), "Effect of Surface-Applied Reactive Element Oxides on the Oxidation of Binary Alloys Containing Cr,"*Materials Science and Engineering*, 87, pp. 295-302.

59. Hwang, Y.S. and Rapp, R.A., (1989), "Thermochemistry and Solubilities of Oxides in Sodium Sulphate-Vanadate Solutions," *Corrosion.*, Vol. 45, No. 11, pp. 933-36.

60. Iyer, K.J.L., Iyer, S.R. and Radhakrishnan, V.M., (1987 A), "High Temperature Attack of Nimonic 80A by Vanadium," *Prakt. Metallography*, 24, pp. 165-174.

61. Iyer, S.R., Iyer, K.J.L. and Radhakrishnan, V.M., (1987 B), "Hot Corrosion Cracking of Nimonic 80A," *High Temperature Technology*, Vol. 5, No. 3, pp. 145-150.

62. Iyer, S.R., Iyer, K.J.L. and Radhakrishnan, V.M., (1987 C), "High Temperature Corrosion of a Ni-Base Superalloy by Vanadium," *Proc. of 10th ICMC, Madras, India*, Vol. IV, pp. 3665-70.

63. Johnson, D.M., Whittle, D.P. and Stringer, J., (1978), The Hot Corrosion of Directionally solidified Ni-Cr-Nb-Al ($\gamma_r - \delta$) Eutectic Alloys," *Oxidation of Metals*, Vol. 12, No. 3, pp. 273-91.

64. Jones, R.L. (1988) "Low-Quality Fuel Problems with advanced engine materials," *High Temp. Technol*, 6, 187.

65. Jones, R.L., (1990), "Oxide Acid-Base Reactions in Ceramic Corrosion," *High Temperature Science,* Vol. 27, pp. 369-79.

66. Jones, R.L., (1991) "Oxide Acid-Base Reactions Relating to the Inhibition of Vanadium Attack on REY Zeolite Catalysts," *Journal of Catalysis* 129, pp. 269-74.

67. Jones, R.L., (1992), "Thermogravimetric Study of the 800^{0}C Reaction of Zirconia Stabilizing Oxides with SO_3-$NaVO_3$," *Journal of The Electrochem Society*, Vol.139, No.10, pp. 2794-99.

68. Jones R.L., (1993), "Resistance of Tin Dioxide to Chemical Reaction with Vandate-Sulphate Melts," *J. Am. Ceramic Soc.*, Vol. 76, No. 6, pp. 1635-37.

69. Jones, R.L., and Gadomski, S.T., (1982), "Reactions of $SO_2(SO_3)$ with NiO-Na_2SO_4 in Nickel-Sodium Mixed Sulphate Formation and Low Temperature Hot Corrosion," *J. Electrochem Soc.*, Vol.129, No. 7, pp. 1613-18.

70. Jones, R.L., and Williams, C.E., (1987), "Hot Corrosion of Co-Cr-Al-Y by Molten Sulfate-Vanadate Deposits," *Mater. Sci. Eng.*, 87, pp. 353-60.

71. Jones, R.L. and Williams, C.E., (1986), "Mixed $MgSO_4$-Na_2SO_4 Effects in the 973K Hot Corrosion of CoCrAlY," *J. of Electrochem. Society* (Solid State Science and Technology), Vol. 133, No. 1, pp. 217-23.

72. Jones, R.L. and Williams, C.E. and Jones, S.R., (1986), "Reaction of Vanadium Compounds with Ceramic Oxides," *J. of Electrochem. Society*: Solid State Science and Technology, Vol. 133, No. 1, pp. 227-30.

73. Jones, R.L. and Williams, C.E. and Jones, S.R., (1985),"Sulfation of CeO_2 and ZrO_2 Relating to Hot Corrosion," *J. of Electrochem. Society*: Solid State Science and Technology, Vol. 132, No. 6, pp. 1498-1501.

74. Jose, P.D, Gupta, D.K and Rapp, R.A, (1985), "Solubility of α-Al_2O_3 in Fused Na_2SO_4 at 1200K," *J. of Electrochem. Society*, Vol.132, No. 3, pp. 735-37.

75. Kanary, L.E., Caley, W.F., Hancock, H.A. and Hollingshead, R.S., (1987), *Mater. Sc. Technol.*, 3, pp. 571-575.

76. Keck, J.W : *Am. Soc.* Mech. Engrs. Paper 62-WA-99.

77. Kerby, R.C. and Wilson, J.R., (1972), "Electrical Conduction Properties of Liquid Vanadates. II. The Sodium Vanadates," *Canadian Journal of Chemistry*, Vol. 58, pp 2871-76.

78. Kerby, R.C. and Wilson, J.R.,(1973), "Corrosion of Metals by Liquid Vanadium Pentaoxide and the Sodium vanadates," *Trans ASME*, Jan., 36-44.

79. Khanna, A.S., Wasserfuhr, C., Quadakkers, W.J. and Nickel, H., (1989), "Addition of Yttrium, Cerium and Hafnium to Combat the Deleterious Effect of Sulphur Impurity during Oxidation of an Ni-Cr-Al Alloy," *Materials Science and Engineering*, A120, pp.185-91.

80. Khanna, A.S. and Jha, S.K, (1998), "Degradation of Materials under Hot Corrosion Conditions," *Trans. Indian Inst. Met.*, Vol. 51, No. 5, pp. 279-90.

81. Kofstad, P., (1988) *"High Temperature Corrosion"* per Kofstad, Elsevier Applied Science, London & New York, Chapter 14, pp. 465.

82. Kofstad, P., (1990), "High Temperature Corrosion of Metals," *Microscopy of Oxidation.* (Proc. Conf.) LONDON, pp. 1-9.

83. Kolta, G.A., Hewaidy, I.F. and Felix, N.S., (1972), "Reactions Between Sodium Sulphate and Vanadium Pentoxide," *Thermochim. Acta*, Vol. 4, pp. 151-64.

84. Krasil'nikov, V.N., Glazyrin, M.P., Palkin, A.P., Perelyaeva, L.A. and Ivakin, A.A., (1987), "The $Na_2O-V_2O_5-SO_3$ System," *Russian Journal of Inorganic Chemistry*, 32, (3), pp. 425-428.

85. Kuiry, S.C., Seal, S., Bose, S.K. and Roy, S. K., (1994), "Effect of Surface Preparation on the High-Temperature Oxidation Behaviour of AISI 316 Stainless Steel," *ISIJ Int.*, Vol. 34, No. 7, pp. 599-606.

86. Kumar, A., Tiwari, S.N. & Prakash, S., (1996), "The Role of Inhibitors on Hot Corrosion Behavior of Superni 75 in $Na_2SO_4-V_2O_5$ Environment Under Cyclic conditions," *National Seminar on Surface Engineering*, Institution of Engineers, Jaipur.

87. Kumar, L., Venkataramani, M., Sundararaman, M., Mukhopadhyay, P. and Garg, S.P, (1996), "Studies on the oxidation Behaviour of Inconel 625 between 873 and 1523 K," *Oxidation of Metals,* Vol.45, Nos.1/2, pp. 221-44.

88. Lambert, P., Champagne, B. and Arseneault, B., (1991), "Oxidation and Hot Corrosion in $Na_2SO_4-10\%V_2O_5$ of Ni-17Cr-6Al-0.5Y and Ni-16Cr-5.7Al-0.47Y-5Si, MCrAlY alloys at 700^0C," *Canadian Metallurgical Quarterly*, Vol. 30, No. 2, pp. 125-30. ·

89. Lees, D.G., (1987), "On the Reasons for the Effects of Dispersions of Stable Oxides and Additions of Reactive Elements on the Adhesion and Growth-Mechanisms of Chromia and Alumina Scales-The "Sulphur Effect," *Oxidation of Metals*, Vol. 27, Nos. 1/2, pp. 75-81.

90. Lagrange, M.H., Huntz, A.M. and Davidson, J.H., (1984), "The influence of Y, Zr or Ti Additions on the High Temperature Oxidation Resistance of Fe-Ni-Cr-Al Alloys of Variable Purity," *Corrosion Science*, Vol. 24, No. 7, pp. 613-27.

91. Lee, W.H. and Lin, R.Y., (1999), "Oxidation, Sulphidation and Hot Corrosion of Intermetallic Compound Fe_3Al at 605^0C to 800^0C," *Materl. Chem. and Phy*, Vol. 58, No. 3, pp. 231-42.

92. Levy, M., Huie, R. and Pettit, F., (1989), "Oxidation and Hot Corrosion of Some Advanced Superalloys at 1300 to 2000^0F (704 to 1093^0C)," *Corrosion*, Vol. 45, No. 8, pp. 661-74.

93. Lingchuan L., Li. R. Zhu and Gesmundo, F., (Dec.,1996), "Hot Corrosion of Iron in the presence of Salt Mixture Deposit containing NaCl and V_2O_5 at 600^0C," *Journal of Mateials Science and Technology*, Vol. 12, No. 6, Dec., pp. 445-451.

94. Liu, P. S., Liang, K. M., Zhou, H. Y., Gu, S. R., Sun, X. F., Guan, H. R., Jin, T. and Yang, K. N., (2001), "Cyclic Oxidation Behavior of Aluminide Coatings on the Co-Base Superalloy DZ40M," *Surf. Coat. Tech.*, Vol. 145, pp. 75-79.

95. Longa-Nava and Takemoto, M. (1992), "High-Temperature Corrosion of Laser–Glazed Alloys in Na_2SO_4-V_2O_5," *Corrosion*, Vol. 48. pp.599.

96. Longa-Nava, K., Zhang, Y.S., Takemoto, M. and Rapp, R.A., (1996), "Hot Corrosion of Nickel-Chromium and Nickel-Chromium-Aluminum Thermal-Spray Coatings by Sodium Sulfate-Sodium Metavanadate Salt," *Corrosion*, Vol. 52, No. 9, pp. 680-88.

97. Luthra, K.L. and Shores, D.A., (1980), "Mechanism of Na_2SO_4 Induced Corrosion at 600-900 ^0C," *J. Electrochem. Soc.*, Vol. 127, No. 10, pp. 2202-10.

98. Luthra, K.L., (1982), "Low Temperature Hot Corrosion of Cobalt-Base Alloys: Part I. Morphology of the Reaction Product," *Metallurgical Transactions A*, Vol. 13A, October, pp.1843-52.

99. Luthra, K.L. and Spacil, H.S., (1982), "Impurity Deposits in Gas Turbines from Fuels Containing Sodium and Vanadium," *J. Electrochem Soc.*, Vol.129, No. 3, pp. 649-56.

100. Luthra, K.L., (1985), "Kinetics of the Low Temperature Hot Corrosion of Co-Cr-Al Alloys," *J. Electrochem. Soc.*, Vol. 132, No. 6, pp. 1293-98.

101. Luthra, K. L. and Leblanc O. H., (1987), "Low Temperature Hot Corrosion of Co-Cr-Al Alloys," *Mater. Sci. Engg.*, Vol. 87, pp. 329-35.

102. Maclsaac, L.M., Caley, W.F., Hancock, H.A. and Hollingshead, R.S., (1988), *Mater. Sci. Technol.*, No.4, pp. 1035-1038.

103. Malik, A.U. and Ahmad, S., (1983), "Na_2SO_4-Induced Corrosion of Some Nimonic Alloys at 650 to 1000^0C," *Metallkunde*, Vol. 74, No. 12, pp. 819-24.

104. Malik, A.U., Amin, M.M. and P. Ahmad, S., (1984), "Hot Corrosion Behaviour of 18Cr-8Ni Austenitic Steel in Presence of Na_2SO_4 and Transition Metal Salts," *Transactions of the Japan institute of Metals*, Vol. 25, No. 3, pp. 168-78.

105. Malik, A. U and Ahmad, S., (1984), High Temperature Technol, Vol. 2, No. 4, pp. 217-223.

106. Malik, A.U. and Mobin, M., (1987), "Studies on Some Solid State Reactions Relevant to Hot Corrosion," *Proc. of 10th ICMC, Madras, India*, Vol. IV, pp. 3345-65.

107. Malik, A.U., Asrar, N., Ahmad, S. and Siddiqi, N. A., (1988) "Hot Corrosion Behaviour of Some Industrially Important Nickel-base Alloys in Presence of Na_2SO_4 (S) and NaCl (S)," *Metallkunde*, Vol. 79, No.5, pp. 285-95.

108. Misra, A.K., (1986 A), "Mechanism of Na_2SO_4-Induced Corrosion of Molybdenum Containing Nickel-Based Superalloys at High Temperatures-I," *J. Electrochem. Soc.*, Vol. 133 No. 5, pp. 1029-37.

109. Misra, A.K., (1986 B), "Mechanism of Na_2SO_4-Induced Corrosion of Molybdenum Containing Nickel-Based Superalloys at High Temperatures-II," *J. Electrochem. Soc.*, Vol. 133 No. 5, pp. 1038-42.

110. Misra, A.K., (1987), "Na_2SO_4-Induced Corrosion of Pure Nickel and Superalloy Udimet 700 in a High Velocity Burner Rig at 900^0C," *Corrosion-NACE*, Vol. 43, No. 7, pp. 440-49.

111. Mitra, S.K., Roy, S.K. and Bose, S.K., (1993), "Influence of Superficial Coating of CeO_2 Oxidation Behavior of AISI 304 Stainless Steel," *Oxidation of Metals*, Vol. 39, Nos. 3/4, pp.221-29.

112. Mobin, M., Malik, A.U., Ahmad, S., Hasan, S.K. and Ajmal, M., (1996), "Studies on the Interactions of Metal Oxides and Na_2SO_4 at 1100 and 1200 K in Oxygen," *Bull. Mater. Sc.*, Vol. 19, No. 5, pp. 807-21.

113. Motoi Hara, Toshio Hisaichi, K Itoh and Y.Shinata, (1991), *Journal Japan Institute of Metals*, 55(11), pp. 1207-1215.

114. Nagarajan, V., Stringer, J. and Whittle, D.P., (1982 A), "The Hot Corrosion of Cobalt-Base Alloys in a Modified Dean's Rig-I. Co-Cr, Co-Cr-Ta and Co-Cr-Ti Alloys," *Corrosion Science*, Vol. 22, No. 5, pp. 407-27.

115. Nagarajan, V., Stringer, J. and Whittle, D.P., (1982 B), "The Hot Corrosion of Cobalt-Base Alloys in a Modified Dean's Rig-II. Co-Cr-Al Alloys," *Corrosion Science*, Vol. 22, No. 5, pp. 429-39.

116. Nagarajan, V., Stringer, J. and Whittle, D.P., (1982 C), "The Hot Corrosion of Cobalt-Base Alloys in a Modified Dean's Rig-III. Co-Cr-Mo Alloys," *Corrosion Science*, Vol. 22, No. 5, pp. 441-453.

117. Nanni, P., Buscaglia, V., Asmundis, C.D. and Roy, S.K., (1987), "Sodium Sulphate Induced Hot Corrosion of Pure Fe, Mn and Cr in Combustion Gas," *Proc. of 10th ICMC, Madras, India*, Vol. IV, pp. 3413-22.

118. Nesbitt, J.A., Harris, K., Helmink, R. and Erickson, G., (11-16 Mar. 2001), "Burner Rig Hot Corrosion of Five Ni-base Alloys including Mar-M247," *Conference: Corrosion/2001*, Houston, TX, USA, ,

119. Niles, W.D. and Sanders, H.R.,(1962), "Reactions of Magnesium with Inorganic Consituents of Heavy Fuel Oil and Characteristics of Compounds Formed," *Transactions of the ASME, Journal of Engineering for Power*, April, pp. 178-86.

120. Otero, E., Merino, M.C., Pardo, A., Biezma, M.V. and Buitrago, G., (1987), "Study on Corrosion Products of IN657 Alloy in Molten Salts," *Proc. of 10th ICMC, Madras, India*, Vol. IV, pp. 3583-91.

121. Otero, E., Pardo, A., Hernaez, J. and Perez, F.J., (1990), "The Hot Corrosion of IN-657 Superalloys in Na_2SO_4-V_2O_5 Melt Eutectic," *Corros. Sc.*, Vol. 30, pp. 677-83.

122. Otsuka, N. and Rapp, R.A., (1990), "Effects of Chromate and Vanadate Anions on the Hot Corrosion of Preoxidized Ni by a Thin Fused Na_2SO_4 Film at 900^0C," *J. Electrochem. Soc.*, Vol. 137, No. 1, pp. 53-60.

123. Pandey, J.L, Prakash, S. and Mehta, M.L, (1987), "Effect of Zirconium on Isothermal and Cyclic Oxidation of Fe-15wt.%Cr-4wt.%Al Alloy in the Temperature Range of 1000-1300^0C," *Proc. of 10th ICMC, Madras, India*, Vol. IV, pp. 3507-3521.

124. Pantony, D.A. and Vasu, K. I., (1968 A), "Studies in the Corrosion of Metals under Melts-1. Theoretical Survey of Fire-Side Corrosion of Boilers and Gas-Turbines in the Presence of Vanadium Pentoxide," *J. Inorg. Nucl. Chem.*, Vol. 30, pp. 423-32.

125. Pantony, D.A. and Vasu, K.I., (1968 B), "Studies in the Corrosion of Metals under Melts-III," *J.Inorg. Nucl. Chem.*, Vol. 10, pp. 755-79.

126. Paul, L.D. and Seeley, R.R., (1991), "Oil Ash Corrosion- A Review of Utility Boiler Experience," *Corrosion*, Vol. 47, No. 2, pp. 152-59.

127. Peters, K.R., Whittle, D. P. and Stringer, J., (1976), "Oxidation and Hot Corrosion of Nickel-Based Alloys Containing Molybdenum," *Corros. Sci.*, Vol. 16, (1976), pp. 791-804.

128. Pettit, F.S. and Giggins, C.S., (1987), "Hot Corrosion, Ch. 12," *Superalloys II*, Eds. Sims, C.T., Stollof, N.S. and Hagel, W.C., Wiley Publ., N. Y.

129. Pettit, F.S. and Meier, G.H., (1984), "Oxidation and Hot corrosion of Superalloys," Superalloys (1984), M. Gell, C.S. Kartovich, R.H. Bricknel, W.B. Kent, J.F. Radovich (Eds.), *The Met. Soc. of AIME*, Warrendale, Pensylvania, pp. 651-687.

130. Prakash, S. and Tewari, V.K., (June 23-July 7, 1992), "High Temperature oxidation of Metals and Alloys, *Q.I.P. Short Term Course Proceedings*, university of Roorkee, Roorkee.

131. Rapp, R.A., (1986), "Chemistry and Electrochemistry of the Hot Corrosion of Metals," *Corros.*, Vol. 42, No. 10, pp. 568-77.

132. Rapp, R.A., (1990), "Hot Corrosion of Materials," *Pure & Appl. Chem.*, Vol. 62, No. 1. pp. 113-22.

133. Rapp, R.A., (2002), "Hot Corrosion of Materials: A Fluxing Mechanism," *Corros. Sci*, Vol. 44, No. 2, pp. 209-21.

134. Rapp, R.A. and Goto, K.S., (1981), "The Hot Corrosion of Metals by Molten Salts," *Symposium on Fused Salts*, J. Braunstein and J. R. Selman (Eds.), The Electrochemical Society, Pennington, N. J., pp.159.

135. Rapp, R.A and Zhang, Y.S., (December, 1994), "Hot Corrosion of Materials: Fundamental Studies," *JOM*, pp. 47-55.

136. Reese, J.R., Jonakin, J and Caracristi, V.Z., (1964), *Combustion*, Nov., 36, pp. 29.

137. Reid, W.T. (ed.), (1971), *External Corrosion and Deposits-Boiler and Gas Turbines*, American Elsevier, New York, Chapter 7, "Additives",

138. Reidy, R.F. and Jones, R.L., (1995), "Thermogravimetric Analysis of the Reaction of CeO_2 with the $NaVO_3$-SO_3 System," *J. Electrochem. Soc.*, Vol. 142, No. 4, pp. 1352-56.

139. Rhys-Jones T.N., Nicholls, J.R. and Hancock, P., (1983), "Effects of SO_2/SO_3 on the Efficiency with which MgO Inhibits Vanadic Corrosion in Residual Fuel Fired Gas Turbines," *Corrosion Science*, Vol. 23, No. 2, pp. 139-49.

140. Roy, S.K., Bottino, C., Rakesh, V.R., Kuiry, S.C. and Bose, S.K., (1995), "Improved High Temperature Oxidation Behaviour of AISI 347 Grade Stainless Steel by Superficial Coating of CeO_2," *ISIJ* Int., Vol. 35, No. 4, pp. 433-42.

141. Sachs, K., (1958), "Accelerated High Temperature Oxidation due to Vanadium Pentoxide," *Metallurgia*, Apr., pp. 167-73.

142. Santoro, G.J., (1979), "Hot Corrosion of Four Superalloys: HA-188, S-57, IN-617 and TD-NiCrAl," *Oxidation of Metals*, Vol. 13, No. 5, pp. 405-35.

143. Santorelli, R., Sivieri, E. and Reggiani, R.C., (1989), "High-Temperature Corrosion of Several Commercial Fe-Cr-Ni Alloys Under a Molten Sodium Sulphate Deposit in Oxidizing Gaseous Environments," *Materials Science and Engineering*, A120, pp. 283-91.

144. Saxena Deepak, (1986), "Effect of Zr and Y Addition on High Temperature Sulphidation Behaviour of Fe-15Cr-4Al," *Ph.D. Thesis*, Met. and Mat. Engg. Deptt., UOR, Roorkee, India.

145. Seal, S., Bose, S. K. and Roy, S. K., (1994), "Improvement in the Oxidation Behaviour of Austenitic Stainless Steels by Superficially Applied, Cerium Oxide Coatings," *Oxidation of Metals*, Vol. 41, Nos. 1/2, pp. 139-78.

146. Seal, S., Roy, S.K., Bose, S.K. and Kuiry, S.C., (2001), "Ceria-Based High- Temperature Coatings for Oxidation Prevention," *JOM-e*, No.1.

147. Seiersten, M. and Kofstad, P., (1987), "The Effect of SO_3 on Vanadate-Induced Hot Corrosion," *High Temp. Tech.*, Vol. 5, No. 3, pp. 115-22.

148. Sequeira, C.A.C. and Hocking, M.G., (1981), "Hot Corrosion of Nimonic 105 in Sodium Sulfate-Sodium Chloride Melts," *Corrosion*, Vol. 37, No. 7, pp. 392-406.

149. Sharma, R.N., (1996), "Hot Corrosion Behaviour of Iron- and Nickel-Base Superalloys in Salt Environments at Elevated Temperatures," *Ph. D. Thesis*, Met. and Mat. Engg. Deptt., UOR, Roorkee, India.

150. Shi, L., Zhang, Y. and Shih,, S., (1993), "The Low Temperature Hot corrosion of Iron and Iron-Aluminium Alloys," *Corrosion Sci.*, Vol. 33, No, 9, pp.1427-38.

151. Shi, L., (1993), "Accelerated Oxidation of Iron Induced by Na_2SO_4 Deposits in Oxygen at 750^0C- A New Type Low-Temperature Hot Corrosion," *Oxidation of Metals*, Vol. 40, Nos. 1/2, pp. 197-211.

152. Shi, L., (1995), "On the Possibility of a Na_2SO_4-Na_2O Eutectic Melt Developing on Metals Coated with Na_2SO_4 Deposit in Oxygen/Air at Intermediate Temperatures," *Corros. Sc.*, Vol. 37, No. 8, pp. 1281-87.

153. Shores, D.A. and Luthra, K.L., (1980), "Na_2SO_4 Induced Corrosion of Ni- and Co-base Alloys at Intermediate Temperatures," *Conf. Proceedings of TMS, K. Natesan, The Metallurgical Soc.*, pp. 86-102.

154. Shores, D.A., (1981), "New Perspectives on Hot Corrosion Mechanisms," *High Temperature Corrosion, R.A. Rapp (Ed.), NACE*, Houston, Texas, pp. 1-12.

155. Sidky, P.S. and Hocking, M.G., (1987 A), "The Hot Corrosion of Ni-Based Ternary Alloys and Superalloys for Application in Gas Turbines Employing Residual Fuels," *Corrosion Science*, Vol. 27, No. 5, pp. 499-530.

156. Sidky, P.S. and Hocking, M.G., (1987 B), "The Hot Corrosion of Ni-Based Ternary Alloys and Superalloys for Gas Turbine Applications-II. The Mechanism of Corrosion in SO_2/O_2 atmospheres," *Corrosion Science*, Vol. 27, No. 2, pp. 205-14.

157. Smeggil, J.G, (1987), "Some Comments on the Role of Yttrium in Protective Oxide Scale Adherence," *Materials Science and Engineering*, Vol. 87, pp. 261-67.

158. Sreenivas, K.S. and Radhakrishnan, V.M., (1998), "Oxidation and Hot Corrosion Behaviour of Nimonic 75 Superalloy," *Indian Journal of Engineering and Materials Science*, Vol. 5, No. 5, pp. 295-301.

159. Strawbridge, A. and Rapp, R.A., (1994), "The Role of Reactive Elements on Scale Growth in High Temperature Oxidation of Pure Nickel, Iron, Cobalt and Copper," *J. Electrochem. Soc.*, Vol. 141, No. 7, pp. 1905-114.

160. Stewart, S.F.C. and Shatynski, S.R., (1982), "Hot Corrosion of B-1900 Superalloy by Simulated Fludized Bed Coal Combustor Deposits," *Oxidation of Metals*, Vol.18, No. 3/4, pp. 163-85.

161. Stott, F.H., Wood, G.C. and Stringer, J., (1995), "The Influence of Alloying Elements on the Development and Maintenance of Protective Scales," *Oxidation of Metals*, Vol.44, Nos.1/2, pp.113-45.

162. Stringer J., (1977), "Hot Corrosion of High Temperature alloys," *Ann. Rev. Mater. Sci.* 7, 477.

163. Stroosnijder, M.F. and Quadakkers, W.J., (1986), "Review of High Temperature Corrosion of Metals and Alloys in Sulphidizing/Oxidizing Environments I. Corrosion of Metals," *High Temperature Technology*, Vol. 4, No.2, pp.83-95.   -   -   -   -   -   -   -

164. Stroud, W.F. and Rapp, R.A., (1978), *High Temperature Metal Halide Chemistry, Electrochemical Society*, Pennington, NJ, pp. 574-594.

165. Swaminathan, J. and Raghavan, S., (1992), Effect of Vanadic Corrosion on Creep-Rupture Properties of Superni-600 at 650-750^{0}C," *Materials at High Temperatures*, Vol. 10, No. 4, pp. 242-50.

166. Swaminathan, J. and Raghavan, S., (1994), "Vanadic Hot Corrosion-Creep Interaction of Superni-C 276 in the Temperature Range 650-750^{0}C," *High Temp. Mater. Processes*, Vol. 13, No. 4, pp. 277-97.

167. Swaminathan, J., Raghavan, S. and Iyer, S.R., (1993), "Studies on the Hot Corrosion of Some Nickel-Base Superalloys by Vanadium Pentoxide," *Trans. IIM*, Vol. 46, No. 3, pp. 175-81.   ·

168. Tewari, S.N. and Prakash, S., (1996), "Hot Corrosion Behaviour of an Iron-Base Superalloy in Salt Environment at Elevated Temperatures," *Proc. of Symp. on Metals and Materials Research, IIT, Madras*, 4-5th July, pp. 107-17.

169. Tewari, S.N. and Prakash, S., (1997A), "Studies on the Hot Corrosion Behaviour of Some Superalloys in Na_2SO_4-V_2O_5," *Proc. of SOLCEC, Kalpakkam*, India, 22-24th Jan., Paper C33.

170. Tewari, S.N. and Prakash, S., (1998), "Literature Review-Magnesium Oxide as Inhibitor of Hot Oil Ash Corrosion", *Materials Science and Technology*, Vol. 14, pp. 467-72.

171. Tewari, S. N., (1997 B), "Investigations on Hot Corrosion of Some Fe-, Ni- and Co-Base Superalloy in Na_2SO_4-V_2O_5 Environment under Cyclic Conditions," *Ph. D. Thesis*, Met. and Mat. Engg. Deptt., UOR, Roorkee, India.

172. Thilakan, H.R., Lahiri, A.K. and Banerjee, T., (1967), "Studies on the Resistance of Alloy Steels against Oil Ash Corrosion-Part I," *NML Technical Journal*, May, pp. 20-25.

173. Thilkan, H.R., Lahiri, A.K. and Banerjee, T., (1969), "Studies on the Resistance of Alloy Steels against oil Ash Corrosion-Part II," *NML Technical Journal*, February, pp.12-16.

174. Trafford, D.N.H. and Whittle, D.P., (1980 A), "The Salt Induced Corrosion Behaviour of Fe-Cr Alloys at Elevated Temperatures-I. Alloys Dilute in Chromium," *Corrosion Science*, Vol. 20, pp. 497-507.

175. Trafford, D.N.H. and Whittle, D.P., (1980 B), "The Salt Induced Corrosion Behaviour of Fe-Cr Alloys at Elevated Temperatures-II. Alloys Rich in Chromium," *Corrosion Science*, Vol. 20, pp. 509-30.

176. Valdes, C.J., Dooley, R.B. and Wilson, J.R., (1973), "The Corrosion of A.I.S.I 446 Stainless Steel in Molten Vanadates in the Temperature Range 700-900^{0}C," *Report Defence Research Board Canada*, Grant No. 7535-14.

177. Weinbruch, S., Anastassiadis, A., Ortner, H.M., Martinz, H.P. and Wilhartitz, P., (1999), "On the Mechanism of High-Temperature Oxidation of ODS Superalloys: Significance of Yttrium Depletion Within the Oxide Scales," *Oxidation of Metals*, Vol. 51, No. 1/2, pp. 111.

178. Whittle, D.P., (1972), "High Temperature Oxidation of Superalloys," *Oxid. Met.*, 1, pp. 172.

179. Xu, H., Hocking, M.G. and Sidky, P.S., (1994), "Sulphidation-Oxidation Behavior of Alloy 800H in SO_2-O_2 and H_2-H_2S-CO-CO_2 Atmospheres," *Oxid. Met.*, Vol. 41, Nos. 1/2, pp. 81-101.

180. Yedong, H. and Stott F.H., (1994), "The Selective Oxidation of Ni-15%Cr and Ni-10%Cr Alloys Promoted by Surface Applied Thin Oxide Films," *Corrosion Science*, Vol. 36, No. 11, pp. 1869-84.

181. Yedong, H. and Stott, F.H, (1996), "The Effects of Thin Surface-Applied Oxide Coating Films on the Selective Oxidation of Alloys," *Corrosion Science*, Vol. 38, No. 11, pp. 1853-68.

182. Zhang, Y.S. and Rapp, R.A., (1985), "Solubility of α-Fe_2O_3 in Fused Na_2SO_4 at 1200K," *J. of Electrochem. Society.* Vol.132, No. 3, pp. 734-735.

183. Zhang, Y.S., (1986), "Solubilities of Cr_2O_3 in Fused Na_2SO_4 at 1200K," *J. of Electrochem. Society,* Vol.133, No. 3, pp. 655-57.

184. Zhang, Y.S. and Rapp, R.A., (1987), "Solubilities of CeO_2, HfO_2 and Y_2O_3 in Fused Na_2SO_4-30 mol% $NaVO_3$ and CeO_2 in Pure Na_2SO_4 at 900^0C," *Corrosion*, Vol. 43, No. 6, pp. 348-52.

185. Zhang, Y.S. and Rapp, R.A., (1994), "Solubility of CeO_2 in Molten Na_2SO_4-10 mol% $NaVO_3$ Salt Solution at 900^0C," *Proceedings of the Ninth International Symposium on Molten Salts, Electrochem. Soc.*, May 1994.

186. Zho, Y., Zhu, R. and Guo, M., (1987), "Hot Corrosion of Some Nickel-Base Superalloys Containing Niobium," *Corrosion-NACE*, Vol. 43, No. 1, pp.51-55.